

ABSTRACT

ELDEEB, HADIR MAHMOUD AHMED MAHMOUD. Modeling Tensile Behavior of 3D Orthogonal Woven Composites from High Performance Natural Fibers. (Under the direction of Dr. Abdel-Fattah Seyam).

Over the past few decades, ecological concerns resulted in an interest in using natural fibers such as flax and hemp in composite materials. Although, natural fibers have comparable mechanical properties to glass fibers, involving them in composites is challenging because of the inherent variability in their mechanical and physical properties. This variability is an obstacle in manufacturing due to the difficulty of predicting the properties of the composite without the need of manufacturing it. Modeling the mechanical behavior of 3D orthogonal woven (3DOW) composites from natural fibers is very beneficial in characterizing the composite material with a minimal need for multiple trials and coupon testing.

From the literature review, it was found that most of the previous modeling of the mechanical behavior of 3DOW composites focused on linear elastic region only ignoring the plastic region. In addition, most of the work done was limited to plain jammed structures and few researchers dealt with limited number of weaves. Additionally, the previous work done on natural fiber surface treatment mostly focused on the small amount of fibers and few researches addressed 2D fabrics.

In this work, a generalized model to predict the entire tensile load-extension of 3DOW composites from natural spun yarns (flax and hemp) was developed. This model was verified experimentally through producing composites with different fabric architectures such as the number of Y- yarn layers, the weave pattern and the Z- to Y-yarns ratio. The results showed a general good agreement between the theoretical and experimental curves.

The model was applied on 3DOW composites from preforms from as supplied yarns and yarns with enhanced surface treatment to reveal the effect of treatment on the model prediction. The results indicated better agreement between the theoretical and the experimental curves from bleached yarns than that from as supplied yarns.

A numerical parametric study was performed to expose the architecture potential of 3DOW preforms. Composite panels were produced using 3D orthogonal weaving technology and infused using Vacuum Assisted Resin Transfer Molding (VARTM) process. Different 3DOW composites were tested for tensile, impact (Tup and Charpy) and compression properties to empathize their failure mechanisms in terms of structural parameters. A full study of the effect of composite thickness, weave design and the contribution of Z-binders was investigated. The study concluded that the number of Y-yarn layers had the most significant effect on the mechanical behavior of composites.

The properties of composites from natural fibers (flax and hemp) were compared to composites from glass fibers. Composites from natural fibers showed lower tensile stress compared to glass composites due to the low fiber volume fraction of samples from natural fibers, however specific modulus was found to be comparable. In case of impact properties, composites from natural fibers showed equivalent specific impact properties compared to that from glass composites.

© Copyright 2020 by Hadir Mahmoud Ahmed Mahmoud Eldeeb

All Rights Reserved

Modeling Tensile Behavior of 3D Orthogonal Woven Composites from High Performance
Natural Fibers

by
Hadir Mahmoud Ahmed Mahmoud Eldeeb

A dissertation submitted to the Graduate Faculty of
North Carolina State University
in partial fulfillment of the
requirements for the degree of
Doctor of Philosophy

Fiber and Polymer Science

Raleigh, North Carolina
2020

APPROVED BY:

Dr. Abdel-Fattah Seyam
Committee Chair

Dr. Peter Hauser

Dr. Mohamed Bourham

Dr. Trevor Little

DEDICATION

This work is dictated to my parents for always believing in me and providing abundant motivation during my academic journey and beyond.

BIOGRAPHY

Hadir Eldeeb was born in Mansoura, Egypt in 1991. She earned her B.Sc. from Textile Engineering Department, Faculty of Engineering, Mansoura University, Egypt with a 1st class honor. After graduation Hadir worked for three months in terry towel mill as a quality engineer followed by a one year working in Egypt Tailoring Company as a production and quality engineer. Hadir then joined Mansoura University to work for two years as a teaching and research assistant. In 2016, Hadir received a provost fellowship to join a Ph.D. in Fiber and Polymer Science Program at Wilson College of Textiles, North Carolina State University, US. She is planning to join the textile industry in the US after graduation.

ACKNOWLEDGMENTS

I am grateful to Dr. Seyam for his continuous encouragement and guidance throughout Ph.D. study and beyond, in addition to his support whenever needed as a father while I am away from my family. I would like to extend to Dr. Peter Hauser, Dr. Mohamed Bourham and Dr. Trevor Little for guidance and support as a great advisory committee.

I greatly appreciate the help I got from Dr. Mohamed Midani in developing the model. Thanks to my friends and colleagues Dr. Anuradha Gupta, Dr. Betsy Claunch and I am grateful to Dr. Rahul Vallabh for his discussions and opinions. I would like to thank Divya, Margaret, Candace, Anna and Olivia for their assistance in my research. Special thanks to Tri Vu, Jeff Krauss and Teresa white for their technical support.

Distinct thanks to Dr. Ebraheem Shady and Dr. Mohamed Eldessouki for their encouragement to travel and study abroad, I am now obtaining my Ph.D. degree because of their believe in my ability to do this from the beginning.

Thanks to my friend Nawal for supporting me all time. Thanks to my childhood friends Eman, Maha and Heba and to my friends who became a family for me here Manal, Zahra, Nur, Walaa, Sara, Mariam, Marwa, Shimaa, Israa, Naglaa, Nawal and Eman. Special thanks to Dina and her husband Dr. Mohamed Ramadan and their children Mohmoud and Jojo for their kind and generous support from my first day in the US as a family.

I am grateful to my parents and sister and brother Shosho and Ahmed for their encouragement and support throughout my life. Thanks to my uncles and aunts specially my uncles Ali, Osama, Maher, Mohamed and my aunt Betty and their families.

TABLE OF CONTENTS

LIST OF TABLES	x
LIST OF FIGURES	xvii
1. INTRODUCTION	1
1.1. Definition of Composites	1
1.2. Classification of Composites.....	2
1.3. Green Composites	3
1.4. Preforms of Green Composites	4
1.5. Natural Fibers.....	6
1.6. Morphology of Flax Stem	7
1.7. Lignocellulosic Structures.....	9
1.8. Chemical and Mechanical Structure of Cellulose	10
2. LITERATURE REVIEW	12
2.1. Geometrical Modeling.....	12
2.2. Fiber Surface Treatments	21
2.2.1. Mechanical Treatments.....	22
2.2.2. Physical Treatment	23
2.2.2.1. Plasma Treatment (17)	24
2.2.3. Solvent Extraction.....	28
2.2.4. Thermal Treatment.....	29
2.2.5. Steam Explosion	29
2.2.3. Chemical Treatment	30
2.2.3.1. Alkaline Treatment.....	30

2.2.3.2.	Coupling Agents.....	38
2.2.3.3.	Bleaching.....	40
2.2.3.4.	Peroxide.....	44
2.2.3.5.	Nanoparticles Treatments.....	46
2.2.4.	Comparison of Different Surface Treatments	48
2.3.	Properties of Green Composites.....	53
2.3.1.	Physical Properties.....	53
2.3.2.	Mechanical Properties.....	56
3.	OBJECTIVES.....	67
4.	EXPERIMENTAL.....	69
4.1.	Materials.....	69
4.1.1.	Fibers.....	69
4.1.2.	Resin and Curing Agent.....	70
4.2.	Experimental Design	73
4.2.1.	Design of Experiment A	74
4.2.2.	Design of Experiment B.....	74
4.3.	Preforms Formation.....	75
4.4.	Resin Infusion	77
4.5.	Testing and Evaluation.....	78
4.5.1.	Fiber Testing	78
4.5.2.	Yarn Testing.....	81
4.5.3.	Composite Testing	86
4.5.4.	Resin Tensile Properties	94

4.5.5. Statistical Analysis.....	95
5. RESULTS AND DISCUSSION.....	96
5.1. Results of Fiber Testing	96
5.1.1. Fiber Linear Density	96
5.1.2. Fiber Tensile Properties	97
5.2. Results of Yarn Testing.....	100
5.3. Results of Composite Testing	102
5.3.1. Experimental Design A.....	102
5.3.2. Experimental Design B	154
6. GENERALIZED MODEL AND EXPERIMENTAL VERIFICATION FOR THE LOAD- EXTENSION BEHAVIOR OF 3DOW COMPOSITES	171
6.1. Generalized Load-Extension Model of 3DOW Preforms	171
6.1.1. Nomenclature	173
6.1.2. Assumptions and a Generalized Model of Any Weave	175
6.1.3. Load-Extension Properties of X, Y and Z-yarns	180
6.1.4. Volume Fraction of Yarns and Matrix Components.....	181
6.1.5. The Load-Extension Properties of General 3DOW Preform Under Biaxial Loading.....	181
6.2. Experimental Data	183
6.2.1. Load-Extension Curves of Natural Fibers and Yarns	184
6.2.2. Load-Extension Curve of Vinylester Resin	188
6.3. Model Verification	190
7. OVERALL CONCLUSION AND SUGGESTION FOR FUTURE WORK	196

REFERENCES	200
APPENDICES	210
Appendix A	211
A.1. Results of Fiber Denier Measurements	211
A.2. Results of Fiber Tensile Properties	214
A.3. Load-Extension Curves of Hemp and Flax Fibers	218
A.4. Linear Density and Tensile Properties of Hemp and Flax Yarns.....	220
A.5. Load-Extension Curves of Hemp and Flax Yarns.....	228
A.6. Regression Equation, Upper and Lower Limits of Load-Extension Curves of Hemp and Flax Yarns	230
Appendix B	236
B.1. Experimental vs. Model Tensile Load-Elongation Curves of 3DOW Composites from Flax Fibers Based on the Tensile Properties of the Yarn.....	236
B.2. Experimental vs. Model Tensile Load-Elongation Curves of 3DOW Composites from Hemp Fibers Based on the Tensile Properties of the Yarn	259
B.3. Experimental vs. Model Tensile Load-Elongation Curves of 3DOW Composites from Flax Fibers Based on the Tensile Properties of the Single Fiber	287
B.4. Numerical Example of Calculating Load-Extension Curve of 3DOW Composites	307
Appendix C	312
C.1. Load-Elongation Curves of 3DOW Composites of Tensile Test- Experimental Design A	312
C.2. Load-Elongation Curves of 3DOW Composites of Tensile Test- Experimental Design B	330

C.3. Force-Displacement Curves of 3DOW Composites of Tup Impact Test- Experimental Design A.....	335
C.4. Force-Displacement Curves of 3DOW Composites of Tup Impact Test- Experimental Design B.....	345
C.5. Typical Compression Curves of 3DOW Composites of Test- Experimental Design A ..	350
C.6. Typical Compression Curves of 3DOW Composites of Test- Experimental Design B..	362
Appendix D	365
D.1. Statistical Analysis of Experimental Design A	366
D.1.1. Tensile Test	366
D.1.2. Tup Impact	390
D.1.3. Charpy Impact	402
D.1.4. Compression Test	426
D.2. Statistical Analysis of Experimental Design B	442
D.2.1. Tensile Test	442
D.2.2. Tup Impact	450
D.2.3. Charpy Impact	458
D.2.4. Compression Test	466

LIST OF TABLES

Table 1.	Natural fiber constituents, adapted from (13)	10
Table 2.	Fiber mechanical properties, adapted from (12)	11
Table 3.	Tensile Properties Comparison (43).....	34
Table 4.	Constituent analysis of untreated and alkaline treated flax fibers (45).....	38
Table 5.	Diffusion, sorption and permeability coefficients for flax/epoxy composite (48).....	43
Table 6.	Fabric basis weight of the twill 2/2 fabrics used for the preparation of the composites (48)	44
Table 7.	Mechanical properties of PLA and PLA-based composites, adapted from (52).....	51
Table 8.	Mechanical properties of treated sisal fiber-reinforced polyester composites, adapted from (53).....	52
Table 9.	Diffusion, sorption and permeability coefficient for treated sisal/polyester composites at different temperatures (53).....	55
Table 10.	The mechanical properties of flax/PLA and Cordenka/PLA composites (59)	56
Table 11.	Mechanical properties of UD-flax specimen (61).....	57
Table 12.	Mechanical properties of the 2d-flax specimen (61).....	58
Table 13.	Compressive properties of UD composites with different natural fibers with a fiber volume fraction of 40% (64)	63
Table 14.	Comparison of tensile and compressive properties for flax and bamboo UD composites with equal fiber volume fractions of 40% (64)	63
Table 15.	Specifications of warp, weft and binder yarns	70
Table 16.	Typical properties of the liquid Derakane® 8084 Vinylester resin	71
Table 17.	Typical properties of the cured Derakane® 8084 Vinylester resin.....	72

Table 18.	Typical properties of the initiator NOROX® MEKP-925H	73
Table 19.	The infusion parameters	73
Table 20.	Variables and their levels of design of experiment A	74
Table 21.	Design of experiment B	75
Table 22.	The testing parameters of yarn tensile properties using the MTS Q Test machine ...	82
Table 23.	Theoretical and experimental FVF of samples- Experimental design A	89
Table 24.	Theoretical and experimental FVF of samples- experimental design B	90
Table 25.	Average linear density and tensile properties of 150 single fibers of each fiber type.....	99
Table 26.	Average linear density and tensile properties of yarns measured at 2.54 cm gauge length.....	101
Table 27.	Samples ID of experimental design A and their variable parameters	103
Table 28.	Results of tensile test in the warp (Y-yarn) direction- experimental design A.....	106
Table 29.	Results of tensile test in the weft (X-yarn) direction- experimental design A.....	107
Table 30.	Comparison of the tensile properties of composites from glass, flax and hemp fibers.....	119
Table 31.	Average Tup impact data- experimental design A.....	121
Table 32.	Comparison of Tup impact properties of composites from glass, flax and hemp fibers.....	132
Table 33.	Charpy impact results in the warp direction- experimental design A.....	133
Table 34.	Charpy impact results in the weft direction- experimental design A.....	134
Table 35.	Comparison of Charpy impact properties of composites from glass, flax and hemp fibers	143

Table 36.	Compression test results – Warp direction	145
Table 37.	Compression test results – Weft direction	146
Table 38.	Variable used in experimental design B.....	155
Table 39.	Results of tensile test in the weft (X-yarn) direction- experimental design B	156
Table 40.	The Tup impact test results- experimental design B.....	161
Table 41.	Charpy impact results in the weft direction- experimental design B	165
Table 42.	Compression test results in the weft direction – experimental design B	168
Table 43.	Minimum number of samples of fiber denier	214
Table 44.	Minimum number of samples of fiber tenacity	215
Table 45.	Minimum number of samples of yarns' tensile properties of 2.54 cm gauge length.....	224
Table 46.	Structure of Sample Preform.....	307
Table 47.	Predicted force of 3DOW composites in the X- and Y-directions.....	311
Table 48.	Nomenclature of variables used in statistical analysis.....	365
Table 49.	ANOVA Results- Tensile (Warp)- Peak load	366
Table 50.	ANOVA Results – Tensile (Warp)- Peak stress	369
Table 51.	ANOVA Results – Tensile (Warp)- Tensile Load Normalized by Preform Areal Density	372
Table 52.	ANOVA Results – Tensile (Warp)- Tensile Load Normalized by Composite Areal Density	375
Table 53.	ANOVA Results- Tensile (Weft)- Peak load.....	378
Table 54.	ANOVA Results – Tensile (Weft)- Peak stress	381
Table 55.	ANOVA Results – Tensile (Weft)- Tensile Load Normalized by Preform Areal	

	Density	384
Table 56.	ANOVA Results – Tensile (Weft)- Tensile Load Normalized by Composite Areal Density	387
Table 57.	ANOVA Results – Tup impact- Impact Energy	390
Table 58.	ANOVA Results – Tup impact- Impact Energy Normalized by Thickness	393
Table 59.	ANOVA Results – Tup impact- Impact Energy Normalized by Preform Areal Density	396
Table 60.	ANOVA Results – Tup impact- Impact Energy Normalized by Composite Areal Density	399
Table 61.	ANOVA Results – Tup impact (Warp) - Impact Energy.....	402
Table 62.	ANOVA Results – Tup impact (Warp) - Impact Energy Normalized by Thickness	405
Table 63.	ANOVA Results – Tup impact (Warp) - Impact Energy Normalized by Preform Areal Density	408
Table 64.	ANOVA Results – Tup impact (Warp) - Impact Energy Normalized by Composite Areal Density	411
Table 65.	ANOVA Results – Tup impact (Weft) - Impact Energy	414
Table 66.	ANOVA Results – Tup impact (Weft) - Impact Energy Normalized by Thickness	417
Table 67.	ANOVA Results – Tup impact (Weft) - Impact Energy Normalized by Preform Areal Density	420
Table 68.	ANOVA Results – Tup impact (Weft) - Impact Energy Normalized by Composite Areal Density	423

Table 69.	ANOVA Results- Compression (Warp)- Peak load	426
Table 70.	ANOVA Results – Compression (Warp)- Peak stress	428
Table 71.	ANOVA Results – Compression (Warp)- Compression Load Normalized by Preform Areal Density	430
Table 72.	ANOVA Results – Compression (Warp)- Compression Load Normalized by Composite Areal Density	432
Table 73.	ANOVA Results- Compression (Weft)- Peak load	434
Table 74.	ANOVA Results – Compression (Weft)- Peak stress	436
Table 75.	ANOVA Results – Compression (Weft)- Compression Load Normalized by Preform Areal Density	438
Table 76.	ANOVA Results – Compression (Weft)- Compression Load Normalized by Composite Areal Density	440
Table 77.	ANOVA Results- Tensile (Weft)- Effect of X-yarn type on Peak load	442
Table 78.	ANOVA Results- Tensile (Weft)- Effect of X-yarn type on Peak stress	444
Table 79.	ANOVA Results- Tensile (Weft)- Effect of X-yarn type on Peak load Normalized by Preform Areal Density	446
Table 80.	ANOVA Results- Tensile (Weft)- Effect of X-yarn type on Peak load Normalized by Composite Areal Density	448
Table 81.	ANOVA Results – Tup impact- Effect of X-yarn type on Impact Energy	450
Table 82.	ANOVA Results – Tup impact- Effect of X-yarn type on Impact Energy Normalized by Thickness	452
Table 83.	ANOVA Results – Tup impact- Effect of X-yarn type on Impact Energy Normalized by Preform Areal Density	454

Table 84.	ANOVA Results – Tup impact- Effect of X-yarn type on Impact Energy	
	Normalized by Composite Areal Density	456
Table 85.	ANOVA Results – Charpy impact- Effect of X-yarn type on Impact Energy.....	458
Table 86.	ANOVA Results – Charpy impact- Effect of X-yarn type on Impact Energy	
	Normalized by Thickness.....	460
Table 87.	ANOVA Results – Charpy impact- Effect of X-yarn type on Impact Energy	
	Normalized by Preform Areal Density	462
Table 88.	ANOVA Results – Charpy impact- Effect of X-yarn type on Impact Energy	
	Normalized by Composite Areal Density	464
Table 89.	ANOVA Results- Compression (Weft)- Effect of X-yarn type on Compression	
	Load Peak load	466
Table 90.	ANOVA Results- Compression (Weft)- Effect of X-yarn type on Peak stress	468
Table 91.	ANOVA Results- Compression (Weft)- Effect of X-yarn type Peak load	
	Normalized by Preform Areal Density	470
Table 92.	ANOVA Results- Compression (Weft)- Effect of X-yarn type Peak load	
	Normalized by Composite Areal Density	472

LIST OF FIGURES

Figure 1.	Schematic of composite material (6).....	2
Figure 2.	Classification of composite material (3)	3
Figure 3.	Applications of green composites (8-11)	4
Figure 4.	Preforms of green composites; (a) 2D structures, (b) 3D structures (8-10).....	5
Figure 5.	Classification of natural fibers, adapted from (1,13)	7
Figure 6.	Bundle of flax fibers; (a) Stem cross-section, (b) Elementary flax fiber, adapted from (16,17)	9
Figure 7.	The molecular structure of cellulose (13)	11
Figure 8.	The straight-line segments of a unit structure of plain weave (20).....	13
Figure 9.	A repeat of one yarn structure in the warp direction (21)	14
Figure 10.	Structure within one repeat along the warp yarn axis (21)	14
Figure 11.	A 3D orthogonal weaving unit cell (22)	15
Figure 12.	Infinitesimal volume element in the 3D anisotropic space (22)	15
Figure 13.	A schematic diagram of (a) X-model, (b) Y-model, and (c) Z-model (23)	16
Figure 14.	A schematic diagram for a unit cell of 3DOW composite (24)	17
Figure 15.	3DOW composite with its Representative unit cell (RUC) (25).....	18
Figure 16.	The four constituent layers in the 3D woven composite (25)	18
Figure 17.	3DOW preform (jammed and non-jammed structures) (26).....	20
Figure 18.	SEM images of cotton fiber (a) before extension; (b) at 3.8% extension; (c) at 6.4% extension; (d) fracture at 7.4% extension (note rupture near left end) (30)..	23
Figure 19.	SEM images of flax fibers (a) Untreated, (b) Plasma treated (32).....	25
Figure 20.	SEM images of fractured flax/PET composite (a) Untreated flax fibers, (b)	

	Plasma treated (32).....	25
Figure 21.	Values of tensile modulus E, breaking strength (σ), and breaking strain (ϵ %) of dry composites: (a) flax/ UPR composite, (b) flax/ UPR composite plasma treated, (c) (flax/PET)/ UPR composite, (d) (flax/PET)/ UPR composite plasma treated, (e) flax/ UPR composite autoclave treated, (f) flax/ UPR composite autoclave plasma treated (32).....	26
Figure 22.	Tensile strength values of flax fiber-reinforced polyester composites (33).....	27
Figure 23.	Flexural strength values of flax fiber-reinforced polyester composites (33)	27
Figure 24.	The schematic representation of the fiber contents before and after alkaline treatment (40)	31
Figure 25.	The infrared spectra of untreated and treated hemp fibers.....	33
Figure 26.	Schematic diagram of VARTM method (44)	35
Figure 27.	Tensile properties and fiber contents of flax fiber composites (44)	36
Figure 28.	Tensile properties and fiber contents of hemp fiber composites (44).....	36
Figure 29.	Fracture surfaces of hemp fiber composites; (a) untreated and (b) PVA 5 wt. % (44)	37
Figure 30.	SEM images of flax fiber; (a) untreated; (b) alkaline treated, adapted from (45) .	38
Figure 31.	Schematic representation of the interphases formed on the henequen fibers; (a) untreated, (b) alkaline treated, (c) alkaline treated followed by a silane treatment (47)	40
Figure 32.	Fiber volume fractions of hot platen press and autoclave prepared composites (48)	42
Figure 33.	Tensile strength of hot platen press and autoclave prepared composites (48)	42

Figure 34.	Influence of pretreatments on the effective yarn strength (48)	43
Figure 35.	FTIR spectra of UHMWPE fibers (49)	45
Figure 36.	SEM micrographs of (a) untreated fiber, (b) treated fiber (49).....	45
Figure 37.	Stress-strain curves of NR and 2 wt. % UHMWPE fibers/NR composites (49) ...	46
Figure 38.	SEM images of fractured surface: (a) UHMWPE fibers/NR composites, (b) treated UHMWPE fibers/NR composites, adapted from (49)	46
Figure 39.	Stress –deformation curves of (a) untreated, (b) alkali treated fiber reinforced composites, adapted from (50).....	47
Figure 40.	FTIR spectra of (a) raw kenaf, and (b) alkali-treated kenaf fibers (41)	49
Figure 41.	Storage modulus of PLA and PLA-based composites: (a) neat PLA, (b) composite with untreated fiber, (c) composite with fiber treated by alkali, (d) composite with fiber treated by silane 1, and (e) composite with fiber treated by silane 2, adapted from (52)	50
Figure 42.	Flexural properties of neat PLA and PLA-based composites, adapted from (52) .	50
Figure 43.	Impact properties of treated and untreated sisal/polyester composites (53)	53
Figure 44.	The comparison of Young’s modulus E of the composite between theoretical and experimental results (55)	54
Figure 45.	Comparison of the tensile strength of kenaf/PP composites to other natural fiber composites (62).....	59
Figure 46.	Comparison of flexural strength of kenaf/PP composites to other natural fiber composites (62)	59
Figure 47.	Comparison of the specific modulus of various fibers (62)	60
Figure 48.	Compressive strength of alkalized treatment of natural fiber reinforced	

	laminate samples (63)	61
Figure 49.	Tensile strength of alkalized treatment of natural fiber reinforced laminate samples (63)	61
Figure 50.	Bending strength of alkalized treatment of natural fiber reinforced laminate samples (63)	62
Figure 51.	Impact strength of alkalized treatment of natural fiber reinforced laminate samples (63)	62
Figure 52.	Air cooling: (a) PLA/flax/PLA stack; (b) microdroplet, adapted from (65).....	65
Figure 53.	1°C/min: (a) PLA/flax/PLA stack; (b) microdroplet, adapted from (65).....	66
Figure 54.	(a) view of the 3D weaving loom, (b) multi-insertion of weft yarns	76
Figure 55.	Denting Plan.....	77
Figure 56.	(a) VacMobiles® vacuum pump, (b) A schematic diagram of the VARTM technique	78
Figure 57.	(a) An extracted fiber with a pre-tension at the end, (b) The Vibromat instrument.....	79
Figure 58.	Cardboard frame used in single fiber tensile testing preparation.....	80
Figure 59.	Cardboard frame inside the grips of the MTS Q Test machine	81
Figure 60.	(a) Skein winder, (b) A scale.....	81
Figure 61.	Yarn Twistmeter.....	82
Figure 62.	(a) Sizing winder (b) Size box contains solution with a red dye	84
Figure 63.	Steps of preparing yarn samples for the confocal: (a) Tools used to prepare the yarn cross-section (b) The sized yarn surrounded by synthetic fibers and squeezed through the foam.....	85

Figure 64.	Slices of foam with sized yarn surrounded by synthetic fibers.....	85
Figure 65.	Yarn cross-section captured by the confocal	86
Figure 66.	Cutting plan.....	87
Figure 67.	Composite panel (a) after waterjet cutting and (b) after removing specimens	87
Figure 68.	Density Kit	88
Figure 69.	MTS Servo-hydraulic 370 load frame.....	91
Figure 70.	Instron impact testing equipment, (a) drop tower impact CEAST 9350, and (b) pendulum impactor II.....	93
Figure 71.	(a) CLC fixture, (b) A compression specimen fixed between CLC fixture (c) Composite specimens before and after compression	94
Figure 72.	Frequency distribution of denier of bleached flax fibers	97
Figure 73.	A specimen fixed in the MTS Load Frame along with tested specimens	105
Figure 74.	Main effect of layers on tensile load	109
Figure 75.	Main effect of layers on tensile load normalized by preform areal density	110
Figure 76.	Main effect of layers on tensile load normalized by composite areal density	110
Figure 77.	Main effect of layers on tensile strain	111
Figure 78.	Main effect of layers on tensile stress	111
Figure 79.	Main effect of weave on tensile load	113
Figure 80.	Main effect of weave on tensile load normalized by preform areal density	113
Figure 81.	Main effect of weave on tensile load normalized by composite areal density.....	114
Figure 82.	Main effect of weave on tensile strain	114
Figure 83.	Main effect of weave on tensile stress	115
Figure 84.	Main effect of Z: Y ratio on tensile load.....	116

Figure 85.	Main effect of Z: Y ratio on tensile load normalized by preform areal density...	116
Figure 86.	Main effect of Z: Y ratio on tensile load normalized by composite areal density	117
Figure 87.	Main effect of Z: Y ratio on tensile strain.....	117
Figure 88.	Main effect of Z: Y ratio on tensile stress.....	118
Figure 89.	Specimen after Tup impact test (a) Front view, (b) Back view, and (c) Side view	120
Figure 90.	Main effect of layers on peak force.....	123
Figure 91.	Main effect of layers on impact energy.....	123
Figure 92.	Main effect of layers on impact energy normalized by composite thickness	124
Figure 93.	Main effect of layers on impact energy normalized by preform areal density	124
Figure 94.	Main effect of layers on impact energy normalized by composite areal density .	125
Figure 95.	Main effect of weave on peak force	126
Figure 96.	Main effect of weave on impact energy	126
Figure 97.	Main effect of weave on impact energy normalized by composite thickness.....	127
Figure 98.	Main effect of weave on impact energy normalized by preform areal density....	127
Figure 99.	Main effect of weave on impact energy normalized by composite areal density	128
Figure 100.	Main effect of Z: Y-yarn ratio on peak force	129
Figure 101.	Main effect of Z: Y-yarn ratio on impact energy	129
Figure 102.	Main effect of Z: Y-yarn ratio on impact energy normalized by composite thickness.....	130
Figure 103.	Main effect of Z: Y-yarn ratio on impact energy normalized by preform areal	

	density	130
Figure 104.	Main effect of Z: Y-yarn ratio on impact energy normalized by composite areal density	131
Figure 105.	(a) Type of breaks in Charpy (b) Specimens showing complete and hinge break.....	135
Figure 106.	Main effect of layers on energy absorbed	136
Figure 107.	Main effect of layers on energy absorbed normalized by composite thickness...	136
Figure 108.	Main effect of layers on energy absorbed normalized by preform areal density.	137
Figure 109.	Main effect of layers on energy absorbed normalized by composite areal density	137
Figure 110.	Main effect of weave on energy absorbed	138
Figure 111.	Main effect of weave on energy absorbed normalized by composite thickness ..	139
Figure 112.	Main effect of weave on energy absorbed normalized by preform areal density	139
Figure 113.	Main effect of weave on energy absorbed normalized by composite areal density	140
Figure 114.	Main effect of Z: Y-yarn ratio on absorbed energy	141
Figure 115.	Main effect of Z: Y-yarn ratio on absorbed energy normalized by composite thickness.....	141
Figure 116.	Main effect of Z: Y-yarn ratio on absorbed energy normalized by preform areal Density.....	142
Figure 117.	Main effect of Z: Y ratio on absorbed energy normalized by composite areal density	142

Figure 118.	Compression specimens before and after testing	144
Figure 119.	Main effect of layers on the compression peak load	147
Figure 120.	Main effect of layers on the compression stress	148
Figure 121.	Main effect of layers on the normalized compression peak load by preform areal density	148
Figure 122.	Main effect of layers on the normalized compression peak load by composite areal density	149
Figure 123.	Main effect of weave on the compression peak load	150
Figure 124.	Main effect of weave on the compression stress	151
Figure 125.	Main effect of weave on the normalized compression peak load by preform areal density	151
Figure 126.	Main effect of weave on the normalized compression peak load by composite areal density	151
Figure 127.	Main effect of Z: Y-yarn ratio on the compression peak load	152
Figure 128.	Main effect of Z: Y-yarn ratio on the compression stress	153
Figure 129.	Main effect of Z: Y-yarn ratio on the normalized compression peak load by preform areal density	153
Figure 130.	Main effect of Z: Y-yarn ratio on the normalized compression peak load by composite areal density	154
Figure 131.	Effect of filling yarn type on tensile load	158
Figure 132.	Effect of filling yarn type on tensile load normalized by preform areal density .	158
Figure 133.	Effect of filling yarn type on tensile load normalized by composite areal density	159

Figure 134.	Effect of filling yarn type on tensile strain.....	159
Figure 135.	effect of filling yarn type on tensile stress	160
Figure 136.	Effect of filling yarn type on peak force	162
Figure 137.	Effect of filling yarn type on impact energy	162
Figure 138.	Effect of filling yarn type on impact energy normalized by composite thickness	163
Figure 139.	Effect of filling yarn type on impact energy normalized by preform areal density	163
Figure 140.	Effect of filling yarn type on impact energy normalized by composite areal density	164
Figure 141.	Effect of filling yarn type on energy absorbed.....	166
Figure 142.	Effect of filling yarn type on absorbed energy normalized by composite thickness	166
Figure 143.	Effect of filling yarn type on absorbed energy normalized by preform areal density	167
Figure 144.	Effect of filling yarn type on absorbed energy normalized by composite areal density	167
Figure 145.	Effect of filling yarn type on the compression peak load	169
Figure 146.	Effect of filling yarn type on the compression stress	169
Figure 147.	Effect of filling yarn type on the compression peak load normalized by preform areal density.....	170
Figure 148.	Effect of filling yarn type on the compression peak load normalized by composite areal density	170

Figure 149.	Ince's generalized 3D woven preform geometry of non-jammed structure for circular yarns cross-section (26)	172
Figure 150.	A unit at weave intersection in the deformed state used by Kawabata (20)	173
Figure 151.	The dimensions of the thickness (a) and width (b) of a specimen after tensile testing	177
Figure 152.	A schematic diagram of a generalized repeat of the 3DOW preform, including hybrid yarns.....	178
Figure 153.	X-yarn cross section of a general weave repeat, X-yarns are in red, Y-yarns are in blue, and Z-yarns are in gray.....	179
Figure 154.	Effect of stress-elongation characteristics on blend strength (73)	183
Figure 155.	Summary of the input and output parameters of the generalized model.....	184
Figure 156.	Load-extension curves of (a) 119 hemp fibers taken from yarns, (b) 121 bleached flax fibers taken from yarns	185
Figure 157.	Load-extension curves of (a) 17 samples of hemp X-yarn, (b) 30 samples of bleached flax X-yarn	187
Figure 158.	Breaking modes of pure resin tensile test	188
Figure 159.	Load-extension curves of 5 pure resin specimens.....	189
Figure 160.	The experimental data, regression equation and the upper and lower limits of a flax X-yarn	190
Figure 161.	Experimental vs. model tensile load-elongation for 6 Y-yarn layers 3DOW plain weave and 1:1 Z to Y-yarn ratio from bleached flax fibers (a) X-direction, (b) Y-direction	192
Figure 162.	Experimental vs. model tensile load-elongation for 6 Y-yarn layers 3DOW	

	plain weave and 1:1 Z to Y-yarn ratio from bleached flax fibers (a)	
	X-direction, (b) Y-direction	194
Figure 163.	Average denier of 150 single fibers of each fiber type	211
Figure 164.	Frequency distribution of fiber denier (a) Bleached flax, (b) Grey flax, (c)	
	BHS (Bleached High Strength) flax, (d) HS (High Strength) flax and (e)	
	Hemp	214
Figure 165.	Single fiber tenacity	214
Figure 166.	Specific strength of single fibers.....	215
Figure 167.	Breaking elongation of single fibers	216
Figure 168.	Single fiber initial modulus	216
Figure 169.	Specific initial modulus of single fibers.....	217
Figure 170.	Secant modulus at 10% breaking load of single fibers	217
Figure 171.	Specific secant modulus at 10% breaking load of single fibers.....	218
Figure 172.	Load-Extension curves of (a) 119 hemp fibers, (b) 121 bleached flax fiber, (c)	
	124 flax fibers, (d) 116 high strength bleached flax fibers, and (e) 125 high	
	strength flax fibers.....	219
Figure 173.	Linear density of flax and hemp yarns	220
Figure 174.	Yarn tenacity of 25.4 cm gauge length	220
Figure 175.	Yarn specific strength of 25.4 cm gauge length.....	221
Figure 176.	Yarn elongation of 25.4 cm gauge length	221
Figure 177.	Yarn initial modulus of 25.4 cm gauge length.....	222
Figure 178.	Yarn specific initial modulus of 25.4 cm gauge length	222
Figure 179.	Yarn tenacity of 2.54 cm gauge length	223

Figure 180.	Yarn specific strength of 2.54 cm gauge length.....	223
Figure 181.	Yarn elongation of 2.54 cm gauge length	225
Figure 182.	Yarn initial modulus of 2.54 cm gauge length.....	225
Figure 183.	Yarn specific initial modulus of 2.54 cm gauge length	226
Figure 184.	Yarn twist (twist/ m)	226
Figure 185.	Yarn twist multiplier	227
Figure 186.	Load-extension curves of (a) hemp X-yarns, (b) hemp Y-yarns, (c) hemp Z-yarns, (d) bleached flax X-yarns, (e) bleached flax Y-yarns, (f) bleached flax Z-yarns, (g) flax X-yarns, (h) flax Y-yarns, (i) bleached high strength flax X-yarns, (j) high strength flax X-yarns	229
Figure 187.	Regression equation, upper and lower limits of load-extension curves of (a) hemp X-yarns, (b) hemp Y-yarns, (c) hemp Z-yarns, (d) bleached flax X-yarns, (e) bleached flax Y-yarns, (f) bleached flax Z-yarns, (g) flax X-yarns, (h) flax-Y-yarns, (i) bleached high strength flax yarns, (j) high strength flax yarns	234
Figure 188.	Experimental vs. model tensile load-elongation curves of 3 Y-yarn layers 3DOW composites from bleached flax in the X- and Y-directions (a) plain and 1:1 Z to Y-yarn ratio, (b) 2x2 warp rib and 1:1 Z to Y-yarn ratio, (c) 3x3 warp rib and 1:1 Z to Y-yarn ratio, (d) plain and 1:3 Z to Y-yarn ratio, (e) 2x2 warp rib and 1:3 Z to Y-yarn ratio, (f) 3x3 warp rib and 1:3 Z to Y-yarn ratio...	242
Figure 189.	Experimental vs. model tensile load-elongation curves of 6 Y-yarn layers 3DOW composites from bleached flax in the X- and Y-directions (a) plain and 1:1 Z to Y-yarn ratio, (b) 2x2 warp rib and 1:1 Z to Y-yarn ratio, (c) 3x3	

warp rib and 1:1 Z to Y-yarn ratio, (d) plain and 1:3 Z to Y-yarn ratio, (e) 2x2
warp rib and 1:3 Z to Y-yarn ratio, (f) 3x3 warp rib and 1:3 Z to Y-yarn ratio...249

Figure 190. Experimental vs. model tensile load-elongation curves of 9 Y-yarn layers
3DOW composites from bleached flax in the X- and Y-directions (a) plain
and 1:1 Z to Y-yarn ratio, (b) 2x2 warp rib and 1:1 Z to Y-yarn ratio, (c) 3x3
warp rib and 1:1 Z to Y-yarn ratio, (d) plain and 1:3 Z to Y-yarn ratio, (e) 2x2
warp rib and 1:3 Z to Y-yarn ratio, (f) 3x3 warp rib and 1:3 Z to Y-yarn ratio...255

Figure 191. Experimental vs. model tensile load-elongation curves of 3 and 6 Y-yarn
layers 3DOW composites of plain weave and 1:1 Z to Y-yarn ratio (a) grey
flax X-yarns, (b) HS flax X-yarns and (c) BHS flax X-yarns in the X-
direction.....259

Figure 192. Experimental vs. model tensile load-elongation curves of 3 Y-yarn layers
3DOW composites from Hemp in the X- and Y-directions (a) plain and 1:1 Z
to Y-yarn ratio, (b) 2x2 warp rib and 1:1 Z to Y-yarn ratio, (c) 3x3 warp rib
and 1:1 Z to Y-yarn ratio, (d) plain and 1:2 Z to Y-yarn ratio, (e) 2x2 warp rib
and 1:2 Z to Y-yarn ratio, (f) 3x3 warp rib and 1:2 Z to Y-yarn ratio (g) plain
and 1:3 Z to Y-yarn ratio, (h) 2x2 warp rib and 1:3 Z to Y-yarn ratio, (i) 3x3
warp rib and 1:3 Z to Y-yarn ratio268

Figure 193. Experimental vs. model tensile load-elongation curves of 6 Y-yarn layers
3DOW composites from Hemp in the X- and Y-directions (a) plain and 1:1 Z
to Y-yarn ratio, (b) 2x2 warp rib and 1:1 Z to Y-yarn ratio, (c) 3x3 warp rib
and 1:1 Z to Y-yarn ratio, (d) plain and 1:2 Z to Y-yarn ratio, (e) 2x2 warp rib
and 1:2 Z to Y-yarn ratio, (f) 3x3 warp rib and 1:2 Z to Y-yarn ratio (g) plain

and 1:3 Z to Y-yarn ratio, (h) 2x2 warp rib and 1:3 Z to Y-yarn ratio, (i) 3x3
warp rib and 1:3 Z to Y-yarn ratio278

Figure 194. Experimental vs. model tensile load-elongation curves of 9 Y-yarn layers
3DOW composites from Hemp in the X- and Y-directions (a) plain and 1:1
Z to Y-yarn ratio, (b) 2x2 warp rib and 1:1 Z to Y-yarn ratio, (c) 3x3 warp rib
and 1:1 Z to Y-yarn ratio, (d) plain and 1:2 Z to Y-yarn ratio, (e) 2x2 warp rib
and 1:2 Z to Y-yarn ratio, (f) 3x3 warp rib and 1:2 Z to Y-yarn ratio (g) plain
and 1:3 Z to Y-yarn ratio, (h) 2x2 warp rib and 1:3 Z to Y-yarn ratio, (i) 3x3
warp rib and 1:3 Z to Y-yarn ratio287

Figure 195. Experimental vs. model tensile load-elongation curves of 3 Y-yarn layers
3DOW composites from Flax in the X- and Y-directions (a) plain and 1:1 Z to
Y-yarn ratio, (b) 2x2 warp rib and 1:1 Z to Y-yarn ratio, (c) 3x3 warp rib and
1:1 Z to Y-yarn ratio, (d) plain and 1:3 Z to Y-yarn ratio, (e) 2x2 warp rib and
1:3 Z to Y-yarn ratio, (f) 3x3 warp rib and 1:3 Z to Y-yarn ratio294

Figure 196. Experimental vs. model tensile load-elongation curves of 6 Y-yarn layers
3DOW composites from Flax in the X- and Y-directions (a) plain and 1:1 Z to
Y-yarn ratio, (b) 2x2 warp rib and 1:1 Z to Y-yarn ratio, (c) 3x3 warp rib and
1:1 Z to Y-yarn ratio, (d) plain and 1:3 Z to Y-yarn ratio, (e) 2x2 warp rib and
1:3 Z to Y-yarn ratio, (f) 3x3 warp rib and 1:3 Z to Y-yarn300

Figure 197. Experimental vs. model tensile load-elongation curves of 9 Y-yarn layers
3DOW composites from Flax in the X- and Y-directions (a) plain and 1:1 Z to
Y-yarn ratio, (b) 2x2 warp rib and 1:1 Z to Y-yarn ratio, (c) 3x3 warp rib and
1:1 Z to Y-yarn ratio, (d) plain and 1:3 Z to Y-yarn ratio, (e) 2x2 warp rib and

1:3 Z to Y-yarn ratio, (f) 3x3 warp rib and 1:3 Z to Y-yarn ratio307

Figure 198. Load- extension curves of 3 Y-yarn layers 3DOW composites in the Y-yarn (warp) and X-yarn (filling) (a) plain and 1:1 Z to Y-yarn ratio, (b) 2x2 warp rib and 1:1 Z to Y-yarn ratio, (c) 3x3 warp rib and 1:1 Z to Y-yarn ratio, (d) plain and 1:3 Z to Y-yarn ratio, (e) 2x2 warp rib and 1:3 Z to Y-yarn ratio, (f) 3x3 warp rib and 1:3 Z to Y-yarn ratio317

Figure 199. Load- extension curves of 6 Y-yarn layers 3DOW composites in the Y-yarn (warp) and X-yarn (filling) (a) plain and 1:1 Z to Y-yarn ratio, (b) 2x2 warp rib and 1:1 Z to Y-yarn ratio, (c) 3x3 warp rib and 1:1 Z to Y-yarn ratio, (d) plain and 1:3 Z to Y-yarn ratio, (e) 2x2 warp rib and 1:3 Z to Y-yarn ratio, (f) 3x3 warp rib and 1:3 Z to Y-yarn ratio323

Figure 200. Load- extension curves of 9 Y-yarn layers 3DOW composites in the Y-yarn (warp) and X-yarn (filling) (a) plain and 1:1 Z to Y-yarn ratio, (b) 2x2 warp rib and 1:1 Z to Y-yarn ratio, (c) 3x3 warp rib and 1:1 Z to Y-yarn ratio, (d) plain and 1:3 Z to Y-yarn ratio, (e) 2x2 warp rib and 1:3 Z to Y-yarn ratio, (f) 3x3 warp rib and 1:3 Z to Y-yarn ratio329

Figure 201. Load- extension curves of 3 Y-yarn layers 3DOW composites in the X-yarn (filling) (a) bleached flax yarns, (b) BHS flax yarns, (c) HS flax yarns and (d) grey flax yarns.....332

Figure 202. Load- extension curves of 6 Y-yarn layers 3DOW composites in the X-yarn (filling) (a) bleached flax yarns, (b) BHS flax yarns, (c) HS flax yarns and (d) grey flax yarns.....334

Figure 203. Force- displacement curves of 3 Y-yarn layers 3DOW composites (a) plain

and 1:1 Z to Y-yarn ratio, (b) 2x2 warp rib and 1:1 Z to Y-yarn ratio, (c) 3x3 warp rib and 1:1 Z to Y-yarn ratio, (d) plain and 1:3 Z to Y-yarn ratio, (e) 2x2 warp rib and 1:3 Z to Y-yarn ratio, (f) 3x3 warp rib and 1:3 Z to Y-yarn ratio...338

Figure 204. Force- displacement curves of 6 Y-yarn layers 3DOW composites (a) plain and 1:1 Z to Y-yarn ratio, (b) 2x2 warp rib and 1:1 Z to Y-yarn ratio, (c) 3x3 warp rib and 1:1 Z to Y-yarn ratio, (d) plain and 1:3 Z to Y-yarn ratio, (e) 2x2 warp rib and 1:3 Z to Y-yarn ratio, (f) 3x3 warp rib and 1:3 Z to Y-yarn ratio...341

Figure 205. Force- displacement curves of 9 Y-yarn layers 3DOW composites (a) plain and 1:1 Z to Y-yarn ratio, (b) 2x2 warp rib and 1:1 Z to Y-yarn ratio, (c) 3x3 warp rib and 1:1 Z to Y-yarn ratio, (d) plain and 1:3 Z to Y-yarn ratio, (e) 2x2 warp rib and 1:3 Z to Y-yarn ratio, (f) 3x3 warp rib and 1:3 Z to Y-yarn ratio...345

Figure 206. Force- displacement curves of 3 Y-yarn layers 3DOW composites in the X-yarn (filling) (a) bleached flax yarns, (b) BHS flax yarns, (c) HS flax yarns and (d) grey flax yarns347

Figure 207. Force- displacement curves of 6 Y-yarn layers 3DOW composites in the X-yarn (filling) (a) bleached flax yarns, (b) BHS flax yarns, (c) HS flax yarns and (d) grey flax yarns349

Figure 208. Typical compression curves of 6 Y-yarn layers 3DOW composites (a) plain and 1:1 Z to Y-yarn ratio, (b) 2x2 warp rib and 1:1 Z to Y-yarn ratio, (c) 3x3 warp rib and 1:1 Z to Y-yarn ratio, (d) plain and 1:3 Z to Y-yarn ratio, (e) 2x2 warp rib and 1:3 Z to Y-yarn ratio, (f) 3x3 warp rib and 1:3 Z to Y-yarn ratio...355

Figure 209. Typical compression curves of 9 Y-yarn layers 3DOW composites (a) plain and 1:1 Z to Y-yarn ratio, (b) 2x2 warp rib and 1:1 Z to Y-yarn ratio, (c) 3x3

warp rib and 1:1 Z to Y-yarn ratio, (d) plain and 1:3 Z to Y-yarn ratio, (e) 2x2

warp rib and 1:3 Z to Y-yarn ratio, (f) 3x3 warp rib and 1:3 Z to Y-yarn ratio...361

Figure 210.	Force- displacement curves of 6 Y-yarn layers 3DOW composites in the X-yarn (filling) (a) bleached flax yarns, (b) BHS flax yarns, (c) HS flax yarns and (d) grey flax yarns	364
Figure 211.	Tukey HSD- Tensile (Warp)- Effect of Layers on Tensile Load.....	367
Figure 212.	Tukey HSD- Tensile (Warp)- Effect of weave on Tensile Load	368
Figure 213.	Tukey HSD- Tensile (Warp)- Effect of layers on Tensile stress	370
Figure 214.	Tukey HSD- Tensile (Warp)- Effect of weave on Tensile stress.....	371
Figure 215.	Tukey HSD- Tensile (Warp)- Effect of layers on Tensile Load Normalized by Preform Areal Density	373
Figure 216.	Tukey HSD- Tensile (Warp)- Effect of weave on Tensile Load Normalized by Preform Areal Density	374
Figure 217.	Tukey HSD- Tensile (Warp)- Effect of layers on Tensile Load Normalized by Composite Areal Density	376
Figure 218.	Tukey HSD- Tensile (Warp)- Effect of weave on Tensile Load Normalized by Composite Areal Density	377
Figure 219.	Tukey HSD- Tensile (Weft)- Effect of Layers on Tensile Load	379
Figure 220.	Tukey HSD- Tensile (Weft)- Effect of weave on Tensile Load	380
Figure 221.	Tukey HSD- Tensile (Weft)- Effect of layers on Tensile stress	382
Figure 222.	Tukey HSD- Tensile (Weft)- Effect of weave on Tensile stress	383
Figure 223.	Tukey HSD- Tensile (Weft)- Effect of layers on Tensile Load Normalized by Preform Areal Density	385

Figure 224.	Tukey HSD- Tensile (Weft)- Effect of weave on Tensile Load Normalized by Preform Areal Density	386
Figure 225.	Tukey HSD- Tensile (Weft)- Effect of layers on Tensile Load Normalized by Composite Areal Density	388
Figure 226.	Tukey HSD- Tensile (Weft)- Effect of weave on Tensile Load Normalized by Composite Areal Density	389
Figure 227.	Tukey HSD- Tup impact- Effect of Layers on Impact Energy	391
Figure 228.	Tukey HSD- Tup impact- Effect of Weave on Impact Energy	392
Figure 229.	Tukey HSD- Tup impact- Effect of Layers on Impact Energy Normalized by Thickness	394
Figure 230.	Tukey HSD- Tup impact- Effect of Weave on Impact Energy Normalized by Thickness	395
Figure 231.	Tukey HSD- Tup impact- Effect of Layers on Impact Energy Normalized by Preform Areal Density	397
Figure 232.	Tukey HSD- Tup impact- Effect of Weave on Impact Energy Normalized by Preform Areal Density	398
Figure 233.	Tukey HSD- Tup impact- Effect of Layers on Impact Energy Normalized by Composite Areal Density	400
Figure 234.	Tukey HSD- Tup impact- Effect of Weave on Impact Energy Normalized by Composite Areal Density	401
Figure 235.	Tukey HSD- Tup impact (Warp) - Effect of Layers on Impact Energy	403
Figure 236.	Tukey HSD- Tup impact (Warp) - Effect of Weave on Impact Energy	404
Figure 237.	Tukey HSD- Tup impact (Warp) - Effect of Layers on Impact Energy	

	Normalized by Thickness.....	406
Figure 238.	Tukey HSD- Tup impact (Warp) - Effect of Weave on Impact Energy	
	Normalized by Thickness.....	407
Figure 239.	Tukey HSD- Tup impact (Warp) - Effect of Layers on Impact Energy	
	Normalized by Preform Areal Density	409
Figure 240.	Tukey HSD- Tup impact (Warp) - Effect of Weave on Impact Energy	
	Normalized by Preform Areal Density	410
Figure 241.	Tukey HSD- Tup impact (Warp) - Effect of Layers on Impact Energy	
	Normalized by Composite Areal Density	412
Figure 242.	Tukey HSD- Tup impact (Warp) - Effect of Weave on Impact Energy	
	Normalized by Composite Areal Density	413
Figure 243.	Tukey HSD- Tup impact (Weft) - Effect of Layers on Impact Energy	415
Figure 244.	Tukey HSD- Tup impact (Weft) - Effect of Weave on Impact Energy	416
Figure 245.	Tukey HSD- Tup impact (Weft) - Effect of Layers on Impact Energy	
	Normalized by Thickness.....	418
Figure 246.	Tukey HSD- Tup impact (Weft) - Effect of Weave on Impact Energy	
	Normalized by Thickness.....	419
Figure 247.	Tukey HSD- Tup impact (Weft) - Effect of Layers on Impact Energy	
	Normalized by Preform Areal Density	421
Figure 248.	Tukey HSD- Tup impact (Weft) - Effect of Weave on Impact Energy	
	Normalized by Preform Areal Density	422
Figure 249.	Tukey HSD- Tup impact (Weft) - Effect of Layers on Impact Energy	
	Normalized by Composite Areal Density	424

Figure 250.	Tukey HSD- Tup impact (Weft) - Effect of Weave on Impact Energy Normalized by Composite Areal Density	425
Figure 251.	Tukey HSD- Compression (Warp)- Effect of weave on Compression Load	427
Figure 252.	Tukey HSD- Compression (Warp)- Effect of weave on Compression stress	429
Figure 253.	Tukey HSD- Compression (Warp)- Effect of weave on Compression Load Normalized by Preform Areal Density	431
Figure 254.	Tukey HSD- Compression (Warp)- Effect of weave on Compression Load Normalized by Composite Areal Density	433
Figure 255.	Tukey HSD- Compression (Weft)- Effect of weave on Compression Load	435
Figure 256.	Tukey HSD- Compression (Weft)- Effect of Compression on Tensile stress	437
Figure 257.	Tukey HSD- Compression (Weft)- Effect of weave on Compression Load Normalized by Preform Areal Density	439
Figure 258.	Tukey HSD- Compression (Weft)- Effect of weave on Compression Load Normalized by Composite Areal Density	441
Figure 259.	Tukey HSD- Tensile (Weft)- Effect of X-yarn type on Tensile Load	443
Figure 260.	Tukey HSD- Tensile (Weft)- Effect of X-yarn type on peak stress.....	445
Figure 261.	Tukey HSD- Tensile (Weft)- Effect of X-yarn type on Tensile Load Normalized by Preform Areal Density	447
Figure 262.	Tukey HSD- Tensile (Weft)- Effect of X-yarn type on Tensile Load Normalized by Composite Areal Density	449
Figure 263.	Tukey HSD- Tup impact- Effect of X-yarn type on Impact Energy.....	451
Figure 264.	Tukey HSD- Tup impact- Effect of X-yarn type on Impact Energy Normalized by Thickness.....	453

Figure 265.	Tukey HSD- Tup impact- Effect of X-yarn type on Impact Energy Normalized by Preform Areal Density	455
Figure 266.	Tukey HSD- Tup impact- Effect of X-yarn type on Impact Energy Normalized by Composite Areal Density	457
Figure 267.	Tukey HSD- Charpy impact- Effect of X-yarn type on Impact Energy	459
Figure 268.	Tukey HSD- Charpy impact- Effect of X-yarn type on Impact Energy Normalized by Thickness.....	461
Figure 269.	Tukey HSD- Charpy impact- Effect of X-yarn type on Impact Energy Normalized by Preform Areal Density	463
Figure 270.	Tukey HSD- Charpy impact- Effect of X-yarn type on Impact Energy Normalized by Composite Areal Density	465
Figure 271.	Tukey HSD- Compression (Weft)- Effect of X-yarn type on Compression Load.....	467
Figure 272.	Tukey HSD- Compression (Weft)- Effect of X-yarn type on peak stress	469
Figure 273.	Tukey HSD- Compression (Weft)- Effect of X-yarn type on Compression Load Normalized by Preform Areal Density	471
Figure 274.	Tukey HSD- Compression (Weft)- Effect of X-yarn type on Compression Load Normalized by Composite Areal Density	473

1. INTRODUCTION

The environmental concerns have been increased globally during the last centuries. These concerns increased the awareness of using renewable resources as alternative materials in many applications due to their eco-friendly impacts on the environment (1). Recently natural fibers such as flax, hemp, cotton, etc. have been used broadly as composite reinforcements to replace the glass fibers in many industrial products. This is due to their merits as biodegradable materials, energy efficient, the high strength-to-weight ratio (2), good heat, sound and electrical insulators and efficient vibration dampers when compared with other synthetic polymers (3).

The previous advantages of the natural fibers made them proper alternative materials in several applications such as biomedical applications (sutures, bone plates, joint replacements, heart valves, controlled drug-delivery devices, biosensors, and blood tubes) (2), packaging, automobiles, bridges for on-foot passage (1), building constructions (4). Recently, flax fibers have been introduced strongly to replace glass fibers because of their high mechanical properties. Single flax fibers possess acceptable strength and stiffness values in the fiber direction (5).

1.1. Definition of Composites

The composite material is defined as an engineering material made from two or more distinct constituents with significantly different physical and chemical properties that have superior characteristics than that of each individual component (1). Usually, in a composite material, the strongest component is called reinforcement and the other is called matrix as shown in Figure 1.

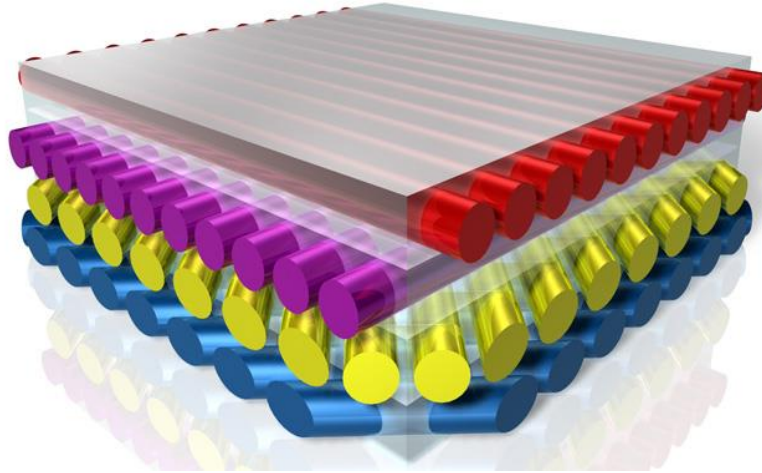


Figure 1. Schematic of composite material (6)

1.2. Classification of Composites

Composite materials can be classified depending on either the type of the reinforcement or the type of the matrix as shown Figure 2. For the reinforcements, composites have two main categories; fibrous and particulate reinforced composites. The fibrous reinforced composites can be continuous fibers reinforced composites and short fibers reinforced composites. Each one can be classified depending on their alignment inside the composite into random or oriented for the short fiber reinforced composites and into unidirectional, bidirectional and multidirectional composites in case of continuous fiber or staple fibers converted into yarns. Other common classifications of fibrous structures (preforms) deals with their method of formation and thickness. Preforms may be produced using nonwoven, weaving, and knitting technologies in form of two-dimensional (2D) for one layer or thin preform or three-dimensional (3D) structures for multilayer and thick preforms. Secondly, depending on the type of the matrix, composite materials can be classified into polymer matrix composites (PMC), metal matrix composites (MMC) and ceramic matrix composites (CMC). The polymer matrices are mostly used in composites because of their low prices and easy processability when compared with the metal or

ceramic matrices (3). In this work, 3D orthogonal woven preforms have been produced from flax yarns then, infused with a Vinylester polymer matrix.

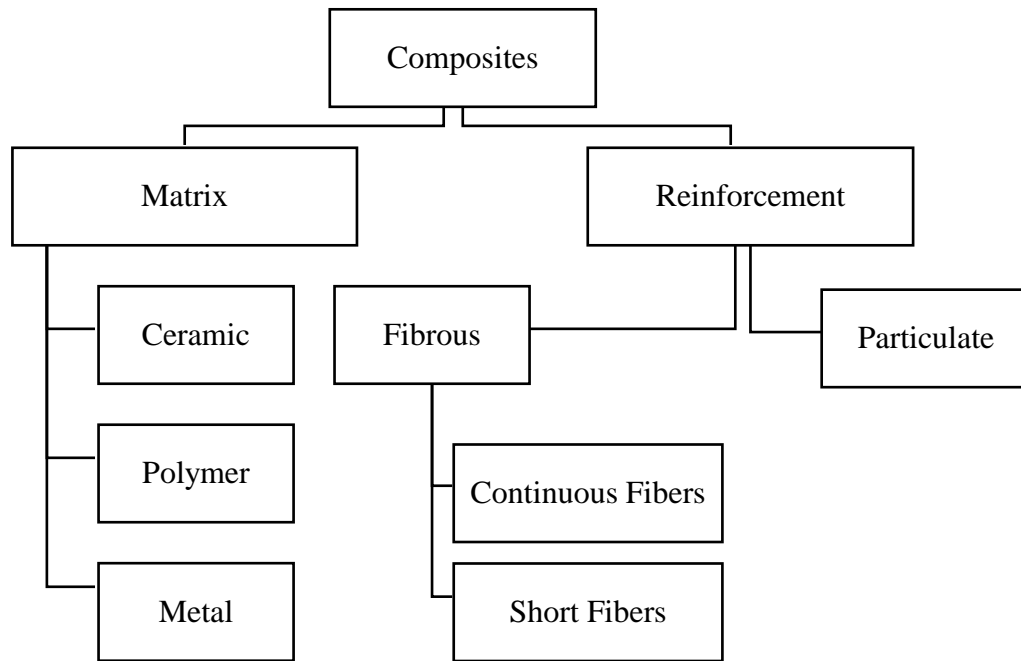


Figure 2. Classification of composite material (3)

1.3. Green Composites

Due to environmental issues and limited petroleum resources, the demand for alternative renewable materials has been increased. This has forced the composite industry to find substitutional ecofriendly “Green” fibers and/or matrices replace the traditional composite constituents. Green composites can be classified into partly renewable composites; if either the reinforcement or the matrix is natural or totally renewable composites; if both components are natural (1).

Besides the merits of the composite materials which include light weight, flexibility, high strength, superior corrosion, impact and chemical resistance, low coefficient of thermal

expansion and superior fatigue resistance, green composites have more advantages (1). For instance, green composites are coming from renewable resources, biodegradable, energy efficient, superior vibration dampers, efficient electrical, heat and sound insulators (1,2,7).

Due to the advantages of green composites, they have been used widely in several applications. Figure 3 shows examples of such applications. Green composites can be used in biomedical, building constructions, automobiles, households, musical instruments, sports equipment and packaging markets (8-10).

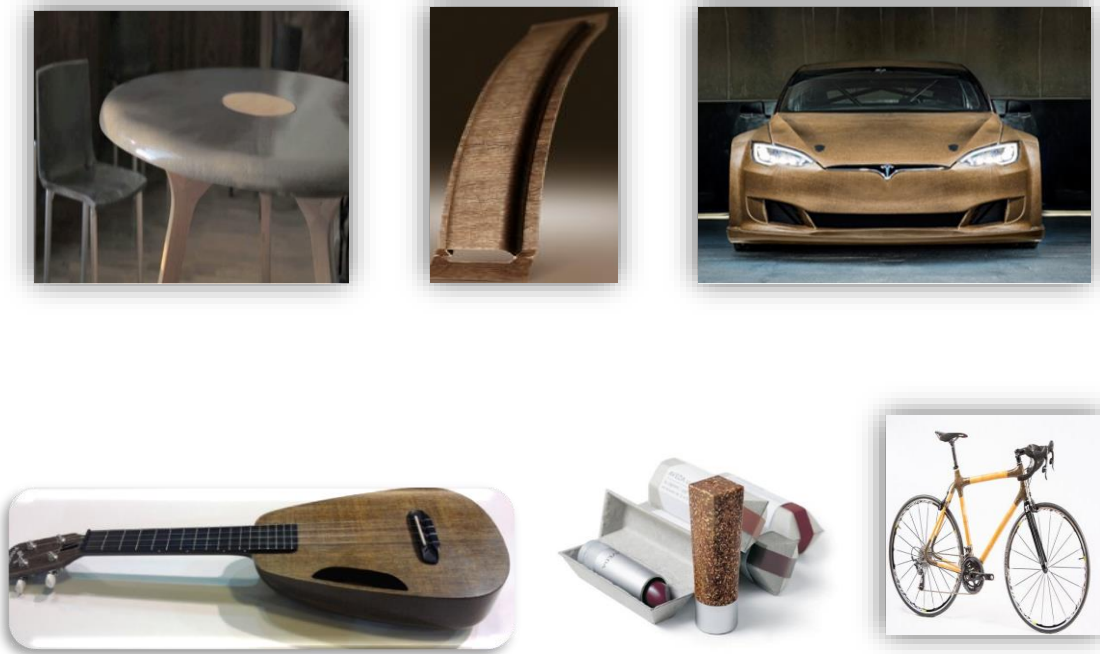


Figure 3. Applications of green composites (8-11)

1.4. Preforms of Green Composites

Fiber preforms used for reinforcing the composites can be fibers, yarns, wovens or nonwovens. Textile structures for composites conducted either 2D or 3D preforms depending on the application. The 2D architectures include woven, braided and nonwoven preforms, however the

3D preforms, the most dominated, include the 3D woven, woven spacer, circular braided, nonwoven, laminated and sandwiches structures. 3D preforms allow the production of fairly thick fabrics (8-10). Figure 4 shows some examples of the textile preforms used in composites.



(a)



(b)

Figure 4. Preforms of green composites; (a) 2D structures, (b) 3D structures (8-10)

1.5. Natural Fibers

Natural fibers are defined as non-uniform structures with irregular cross-sections which contain voids and defects and have more complicated structures than that of the synthetic polymers (12). Natural fibers can be classified into two main categories; inorganic and organic materials. The later can get from plant resources or animal resources (1,12). Figure 5 introduces a simple classification of natural fibers with some examples of each type.

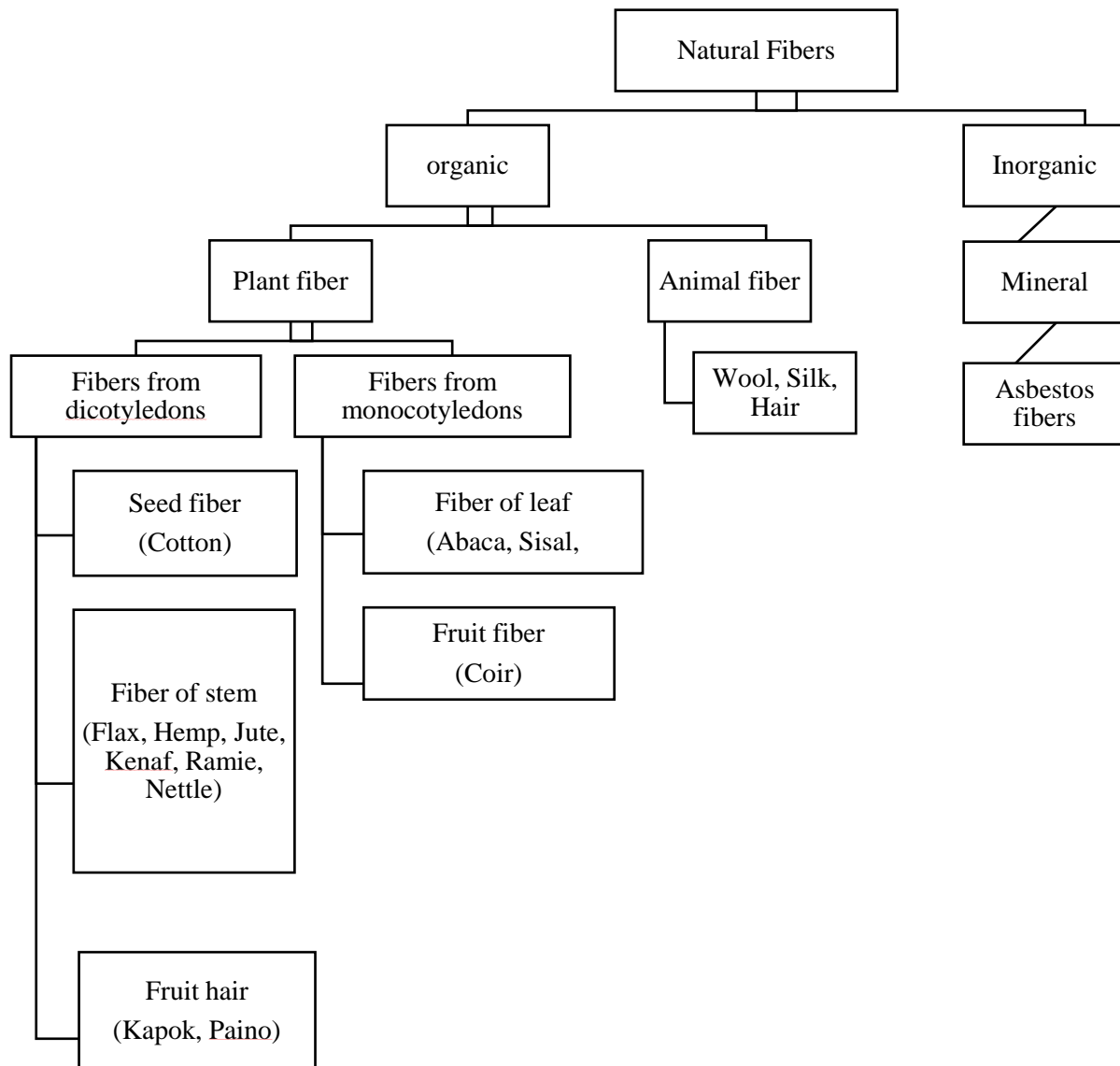


Figure 5. Classification of natural fibers, adapted from (1,13)

1.6. Morphology of Flax Stem

After about 90 days of flax cultivation, the stem turns yellow which indicates the time of harvesting. The stalk should not be cut in this process to keep the sap which affects the quality of the flax fibers. Then, the flax stems go through the rippling process in which the plant is passed through coarse combs in order to remove seeds and leaves from the plant. After that, the woody

bark surrounding the flax fiber is decomposed by water or chemical retting to remove the pectin or gum that attach the fibers to the stem. The retting process is followed by squeezing and breaking processes to crush the decomposed stalks then, go through fluted rollers to break up the stem and separate the fibers. After that, a process known as scutching is conducted to remove the broken stem and release the flax fibers, which then are combed and straightened to be prepared for the spinning process. The very finest flax fibers are called linen or dressed flax. The average length of the fibers is 12-20 inch (30.5-51.0 cm) (14).

Figure 6 (a) presents a cross-section of a flax stem as well as a zoom on the peripheral area where the fibers are arranged into bundles. Bourmaud et al. (15,16) proved that the diameter of the stems has a direct effect on the number of the thickened fibers per section; the number of fibers per section and their diameter increased with the diameter of the stems. In addition, the diameter of the fibers increased significantly with stem height. One flax fiber can be composed of several elementary fibrils (typically 10–40) that are bounded together by the pectin. The elementary flax fiber consists of three distinct layers and the center which is called lumen as shown in Figure 6 (b). The outer layer is called the middle lamella which contains the pectin and lignin, the primary wall contains the hemicelluloses and cellulose and the secondary wall has mainly the cellulose which consists of three other layers (S1, S2, and S3). The spiral angle and S2 layer play a critical role in determining the mechanical properties of the fiber; the smaller the angle the higher is the fiber strength and modulus. The existence of pectin and lignin in these bundles reduces the mechanical properties of the fiber and has a crucial impact on the interfacial properties between the fibers and different matrices when used in composites (16,17).

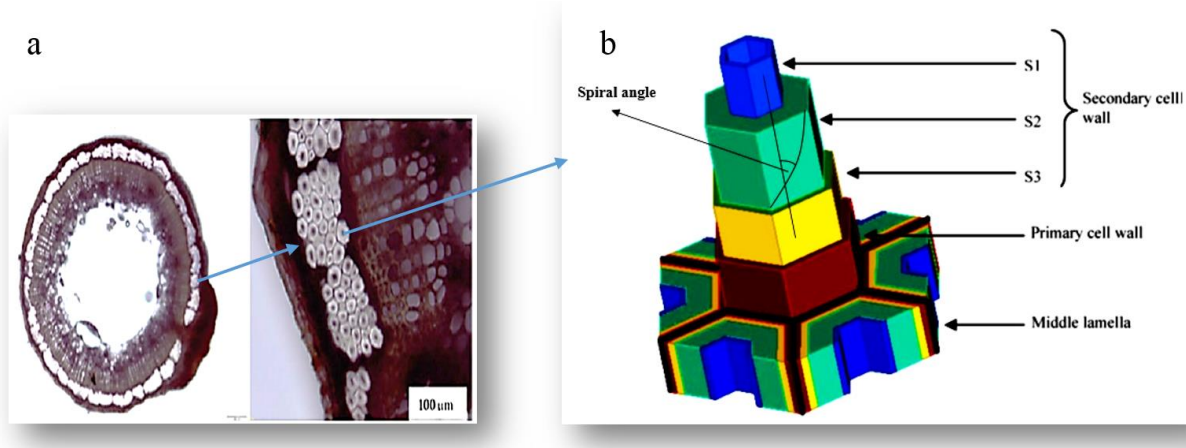


Figure 6. Bundle of flax fibers; (a) Stem cross-section, (b) Elementary flax fiber, adapted from (16,17)

1.7. Lignocellulosic Structures

Plant fibers are called lignocellulosic structures which refer to the three main constituents; cellulose, hemicelluloses, and lignin combined with other minor components such as protein, wax, pectin, tannins, ash, and inorganic salts (13). The percentage of each component varies from plant to plant and even from type to type and within the same fiber as well. These variabilities came from several parameters. For instance, the source of the fibers, the growing conditions, the age of the plant and the digestion processes. Depending on the internal chemical structure and the constituents of the plant fibers, different physical properties can be found. Table 1 shows some of the most widely used natural fibers in green composites and the content of each of the three main components.

Table 1. Natural fiber constituents, adapted from (13)

Fiber Type	Cellulose(%)	Hemicellulose(%)	Lignin(%)
Cotton	82.7-92	5.7-6	0
Flax	71-81	18.6-20.6	2.2-3
Hemp	70.2-74.4	17.9-22.4	3.7-5.7
Bamboo	48.2-60.8	25.1	2.1-32.2
Jute	61-73.2	13.6-20.4	12-16
Kenaf	28-39	21.5-25	15-22.7
Ramie	68.6-76.2	13.1-16.7	0.6-1
Sisal	56.5-78	5.6-16.5	8-14

1.8. Chemical and Mechanical Structure of Cellulose

Cellulose is a linear semicrystalline hydrophilic polymer composed of anhydroglucose units linked by β 1–4 glucosidic bonds. The building unit of the cellulose is the D-glucopyranose unit as shown in Figure 7 which contains many hydroxyl groups leading to a large number of hydrogen bonds. Some of the cellulose molecules align together, highly ordered, and form crystalline regions due to these hydrogen bonds and van der Waals forces, however the rest of the molecules with less packing introduce an amorphous region (3,12,13).

The number of these units in the fiber is called the degree of polymerization (DP) which determines its chemical and physical properties. The DP of the cotton fibers is approximately 7000 however, for flax fibers it is 8000 on average (13).

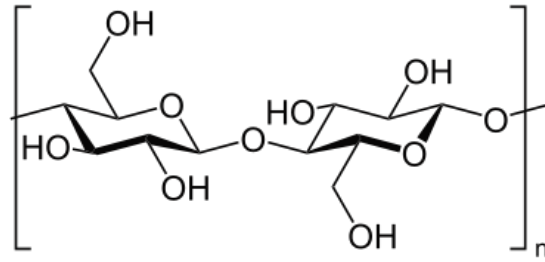


Figure 7. The molecular structure of cellulose (13)

The DP and chemical constituents of natural fibers influence their physical and mechanical properties as it can be seen in table 2.

Table 2. Fiber mechanical properties, adapted from (12)

Fiber Type	Density (g/cm³)	Diameter (μm)	Strength (MPa)	Modulus (Gpa)	Elongation at Break(%)
Cotton	1.5-1.6	15.6-21	287-800	1.1-12.6	6-9.7
Flax	1.5-1.54	-	450-1500	27.6-38	1.5-3.2
Hemp	1.48	53.7	690-873	9.93	1.6-4.7
Bamboo	0.6–1.1	88–125	140–441	11–36	1.3–8
Jute	1.3-1.45	25-200	393-773	2.5-26.5	1-2
Kenaf	0.749	43.3-140	223-624	11-14.5	2.7-5.7
Ramie	1.45	34	400-938	24.5-128	1.2-3.8
Sisal	1.45	50-200	80-640	1.46-15.8	3-15

2. LITERATURE REVIEW

2.1. Geometrical Modeling

Modeling the tensile behavior of industrial materials can be useful in prediction of the performance of the final product to reduce/eliminate unnecessary expensive trials. Due to their homogenous structure, materials such as metals, ceramics and polymers can be easily modeled compared to the heterogeneous fiber reinforced composite materials. Due to its numerous advantages, one class of fiber reinforced composites that drew the attention of researchers during the last three decades is composites from 3D Orthogonal Woven Preforms (3DOW). 3DOW structures offer different directional properties dictated by the yarn spacing, weaving interlacing patterns, yarn count, yarn cross-section and the number of horizontal and vertical yarns. This part of the chapter critically reviews prior relevant work on modeling of tensile behavior of 2D and 3DOW structures.

In 1973 and 1979 Kawabata et al. (18-20) developed a model to predict the entire biaxial load-extension curve of plain weave fabrics, which assumed that warp and weft yarns are perfectly flexible. The measured yarn properties and fabric geometry were used to calculate the forces required to stretch the fabric in the warp and weft directions at the same time. By using finite-deformation theory, where yarns were represented as straight line segments as shown in Figure 8, this model was able to accurately predict the tensile properties of the plain woven fabric. However, this model did not consider the effect of yarn bending stiffness which has been improved after that as a development of the model. Later, the model has been developed to predict the tensile behavior of 2/2 twill fabrics. Using finite deformation theory, this model accounted for the nonlinear nature of woven fabrics tensile properties using the measured yarn

properties to predict the load-extension curve of plain woven fabrics. However, the model was limited to plain and 2x2 twill weaves.

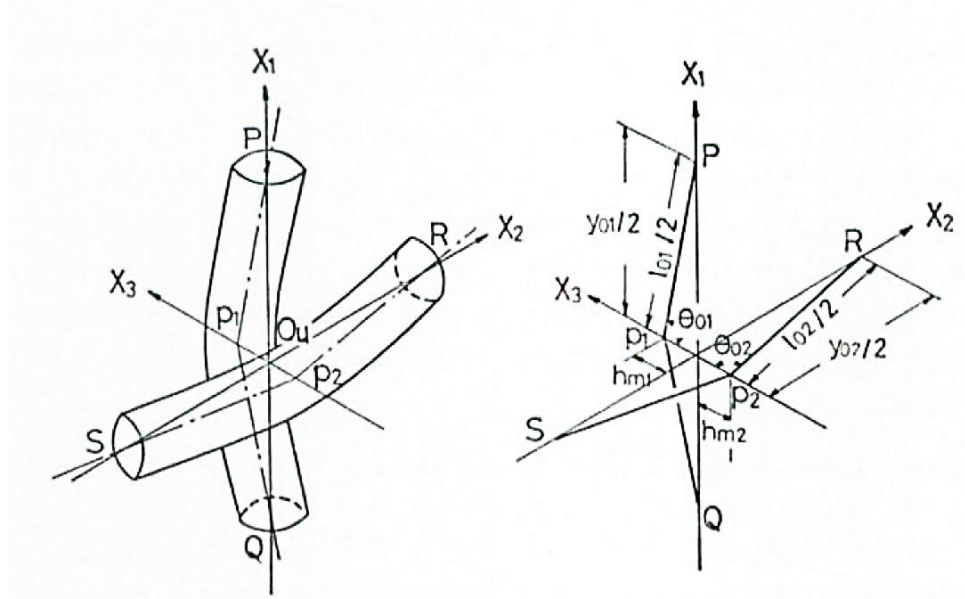


Figure 8. The straight-line segments of a unit structure of plain weave (20)

In 1995, Sun et al. (21) used Kawabata's model to generate a general model that can predict the entire load-extension curve of any weave design. Despite this model used the straight-line geometry of Kawabata, it introduced a parameter that characterizes the interlacing point distribution pattern of the weave. In addition, this model was applicable for hybrid warp and filling yarns and used different thread spacing as shown in Figure 9. Sun et al. divided the woven structure into two portions; portion A which represented the inclined portion at the thread interlacing and portion B which is horizontal portion at the thread float as shown in Figures 9 and 10. This model was successfully verified experimentally with a good agreement between the predicted and the actual results, however, it is still limited to 2D fabrics and cannot be used to predict the stress-strain curve of 3D preforms.

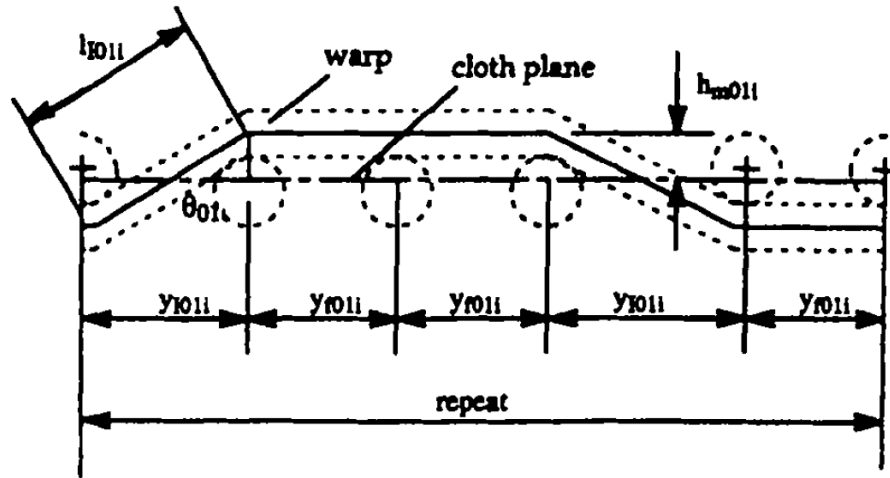


Figure 9. A repeat of one yarn structure in the warp direction (21)

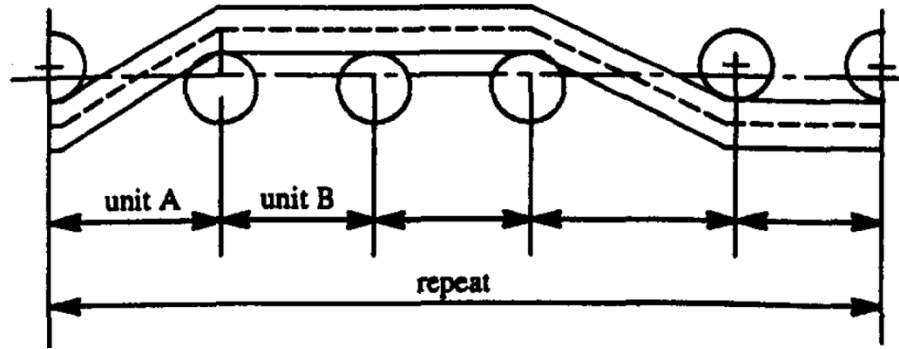


Figure 10. Structure within one repeat along the warp yarn axis (21)

In 1994, Nagai et al. (22) proposed an analytical method to predict the elastic properties of composites made of three-dimensional orthogonal woven (3DOW) preforms using the rule of mixture for composites. Different formulas for Young's modulus, shear stress and Poisson's ratio were derived and verified experimentally and by utilizing these formulas, the failure strain was estimated. In this model, a unit cell of 3D anisotropic space, which is shown in Figure 11, was used with different material properties according to the orientation direction. Then, each unit cell was divided into infinitesimal volume elements, shown in Figure 12, which can represent either a fiber, a matrix or a void. After that, all these infinitesimal volume elements were averaged over

the whole unit cell. Although this model was able to successfully predict the elastic properties of the composite material, it is still limited to the structure introduced in this research and cannot be generalized for any weave design.

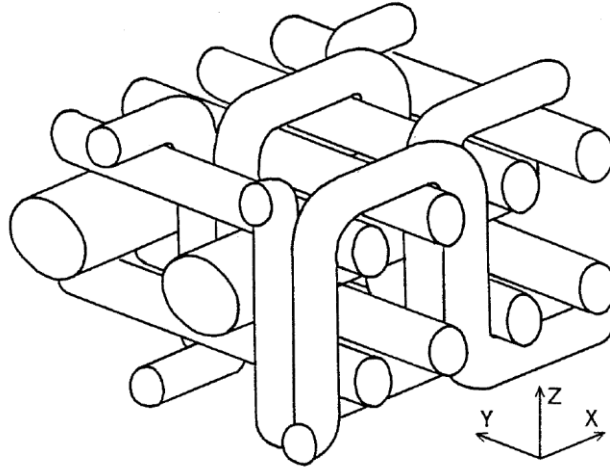


Figure 11. A 3D orthogonal weaving unit cell (22)

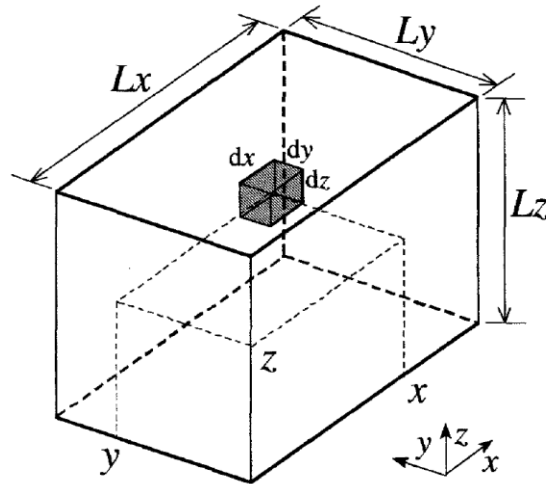


Figure 12. Infinitesimal volume element in the 3D anisotropic space (22)

In 1997, Tan et al. (23) established a unit cell model and a laminate model to predict the elastic properties of 3DOW composites. For the unit cell model, they used a Finite Element Analysis (FEA) and four theoretical analysis. These theoretical models depended on the elastic mechanics

theory and a range of analytical models; the X-model, the Y-model and the Z-model which divided the Representative Volume Element (RVE) into micro blocks (Figure 13). These micro blocks can represent either a fiber (warp, weft or binder yarn) or a matrix. Then the elastic properties of the whole composite were calculated using the micro blocks according to four theoretical models obtained from the X-model, the Y-model and the Z-model which were the XYZ- model, YXZ-model, ZXY- model, or ZYX- model. The models included parameters such as the diameters of warp, weft and binder yarns, the mechanical properties of the constituents of the composite and the fiber volume fraction. The mechanical properties of the matrix were assumed to be homogenous, however, it is assumed to be orthotropic for the preform. This model did not take into account any weaving design structural parameters which make it limited to what was produced for the model. All these models were verified experimentally, and the results showed a good agreement, however, the authors did not recommend one over the other.

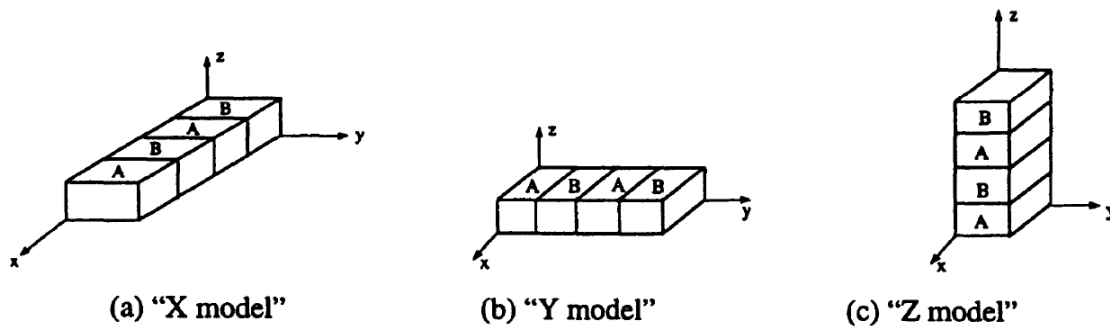


Figure 13. A schematic diagram of (a) X-model, (b) Y-model, and (c) Z-model (23)

In 2002, Zuorong et al. (24) developed a model to predict the thermal elastic properties of 3D orthogonal composites by dividing the composite structure into unit cells and each unit cell again was divided into small segments. Each segment can be consisting of a warp yarn, a filling yarn, a

binder or a matrix as explained in Figure 14. However, this model got good agreements with the experimental data, it is still limited to jammed plain weaves.

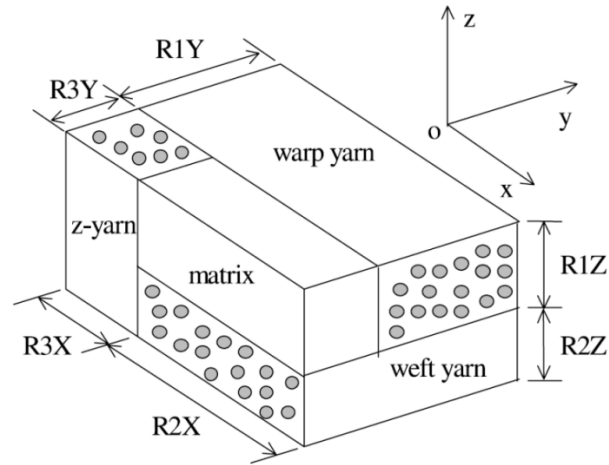


Figure 14. A schematic diagram for a unit cell of 3DOW composite (24)

In 2009, Pankow et al. (25) developed a lamination theory for 3DOW composites to predict the effective linear elastic extensional and bending stiffnesses. A representative unit cell (RUC) of the composite, showed in Figure 15, was used that include the constituents which are warp, filling, and binder yarns and a resin as explained in Figure 16. Each component was assumed to be a transversely isotropic linear elastic solid and the contribution from each to the RUC elastic bending stiffness was calculated by volume averaging using the fiber volume fraction of each component. While the model showed a good correlation with the experimental results, the volume fraction of each constituent layer or ply was determined from micro-computed tomography (micro-CT) scans and a finite element model to convert the slices into a 3D model. The model requires production of the composites and then take CT images to obtain actual geometry, which defeats the purpose of predictive model without actually producing the composite.

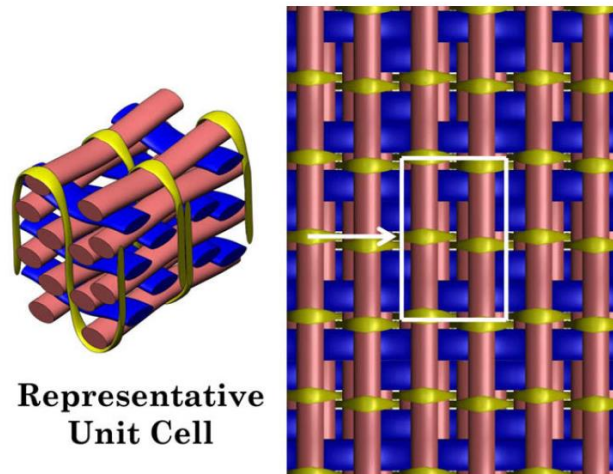


Figure 15. 3DOW composite with its Representative unit cell (RUC) (25)

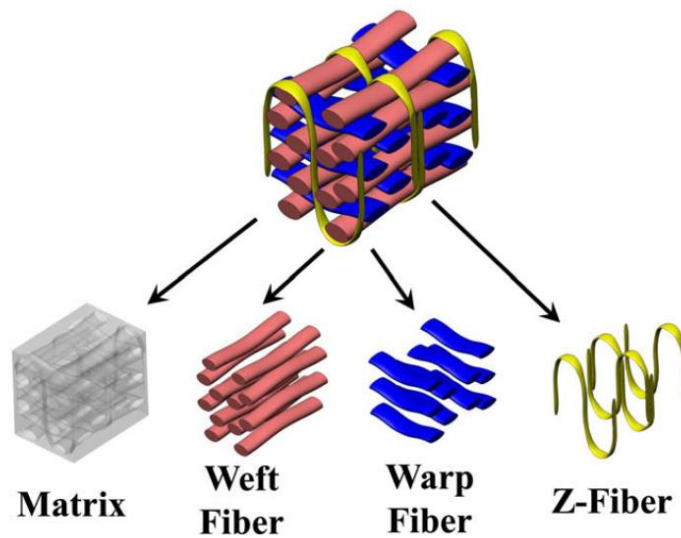


Figure 16. The four constituent layers in the 3D woven composite (25)

In 2013, Seyam and Ince (26) developed a generalized geometrical model of non-jammed and jammed structures of 3DOW preforms from spun yarns, shown in Figure 17, to predict a range of parameters such as fiber volume fraction, preform thickness, preform areal density and maximum thread density to achieve the jammed structure. The model inputs included weave factor, number of layers, Z/Y yarn ratio. The model considered circular cross-sections for

jammed and non-jammed structures in addition to a racetrack cross-section for jammed structure. The model introduced numerical results to reveal the generalized model potential as a design tool to achieve a broad range of preform properties which can be used in simulating the geometry of 3DOW preforms including the shape of the yarn interstices and thus, the resin flow time could be predicted and optimized. The unique advantage of this model is the prediction of the preforms and their composites properties for any weave design and it is specifically for preforms from spun yarns and twisted continuous filament yarns. Therefore, this model can be used to predict tensile properties of composites from any 3DOW in combination with methodology used in previous models such as Sun et al. (21) and Kawabata et al. (18-20).

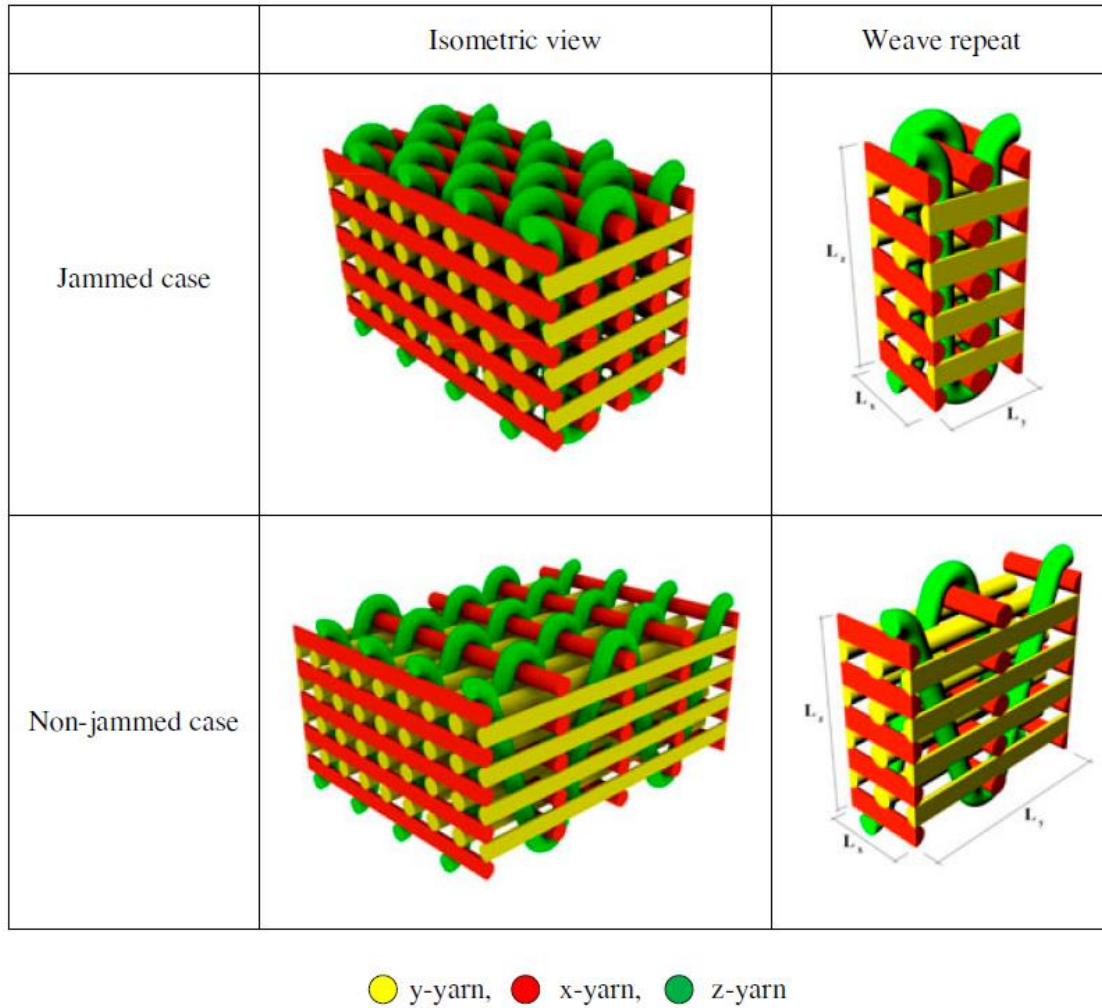


Figure 17. 3DOW preform (jammed and non-jammed structures) (26)

In 2018, Midani et al. (27) developed a generalized model using the finite-deformation approach that depends on Kawabata et al. (18-20), Sun et al. (21), and Seyam and Ince (26) models to predict the entire load-extension curve of 3DOW preforms as well as their composites from flat filament and spun yarns including the non-linear region. The model had two main approaches of the input of the preform which are using the x, y, and z yarns' tensile properties or their fibers' tensile properties. The results showed a better agreement using the fibers' properties than the yarns' properties due to the weak link effect. While the model is general and can be applied for

any 3DOW architecture, including weave and hybrid structures, the model was experimentally verified for composites from flat filament yarns. The flat filament yarns and their fibers are much more uniform compared to natural fibers such as hemp and flax. The latter fibers pose modeling challenges due to their high non-uniformity that need to be accounted for to obtain reasonable prediction of their preforms and composites.

2.2. Fiber Surface Treatments

Despite the advantages of using the natural fibers in composites, there are many disadvantages which created challenges for the application of natural fiber composites. One of the tremendous difficulties is that the natural fibers in composites can absorb moisture by water diffusion through defects in the interface fiber via the microvoids and microcracks, as well as along the crosslinking points. In addition, the variability in the quality of the natural fibers which depends on several parameters including the multitude of different plant varieties, the growing conditions, and the availability of the some types of fibers in some countries than others due to the weather conditions which increases the cost of the fibers due to shipping and handling cost. Besides, natural fibers have low thermal degradation that limits the applications of their composites (1,12).

The mechanical performance of the composite material can be affected by the properties of the reinforcements and matrices, the orientation of the fibers inside the composite and the bonding between the fibers and the matrix. The latter is a crucial parameter because it determines how the matrix is effective in transferring the stresses to the fibers and therefore affect the performance of the final composite material. The non-cellulosic constituents in natural fibers inhibit the bonding between the cellulose and polymer matrices which affects the interfacial bonding between the fibers and the matrix. In order to enhance this bonding, several surface treatments of the natural

fibers have been practiced (12). There are three approaches of the surface treatment; the first depends on removing the non-cellulosic constituents from the surface of the fiber to enhance the relationship between the cellulose and the matrix. The second approach is by separating the large fiber bundle into smaller ones to increase the fiber-matrix interaction by increasing the bonded surface area. The third focuses on the chemical treatments to form covalent bonds between the fiber and the matrix (12,28). Depending on the three approaches applied to the surface treatments, several treatment methods have been utilized. These methods can be classified into four main categories; mechanical treatments, physical treatments, chemical treatments and physicochemical treatments (12,28,29).

2.2.1. Mechanical Treatments

Mechanical treatments are able to change the structural and surface properties of natural fibers and therefore enhance the fiber-matrix relationship. Several mechanical treatments including; fiber stretching, calendaring, rolling or swaging have been investigated, however, using such methods causes fiber damage (29). For this reason, mechanical treatments have not been widely used.

Hearle and Sparrowand (30) studied the effect of suspending cotton fiber into water and applying tension followed by drying without removing the stress. They noticed an increase in its strength and a decrease in the extensibility as a result of removing the convolutions in the cotton fiber as shown in Figure 18. This pretreating had been carried out before mercerizing the cotton fibers to examine the effect on the subsequent process, however their proof about removing the convolutions from the cotton fibers through wetting and drying the fibers under tension still important for any subsequent process including the relationship between natural fibers and the resin.

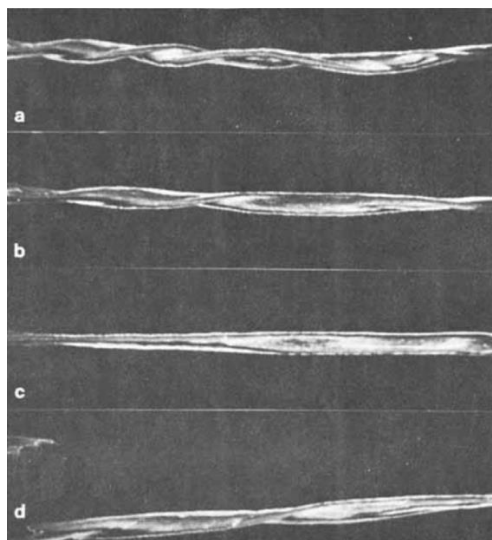


Figure 18. SEM images of cotton fiber (a) before extension; (b) at 3.8% extension; (c) at 6.4% extension; (d) fracture at 7.4% extension (note rupture near left end) (30)

Semsarzadeh (31) used the calendering method for jute laminate woven fabrics to improve the fiber orientation and therefore decrease the micro void content in the composite. However the intensive calendering of jute cloth caused damages in the jute fibers. In addition, a pressure was applied during the curing process to enhance the resin wetting and the bonding between fibers and the polyester resin. The mechanical treatment with the use of poly (vinyl acetate) to treat jute fabric improved the fiber-matrix interaction.

2.2.2. Physical Treatment

Physical treatments including cold plasma, plasma with corona, laser, γ -ray, solvent extraction and steam explosion have been carried out as effective surface treatments of fibers (29). Plasma and laser treatments of lignocellulosic fibers resulted in improving the surface of lignocellulosic fibers, while steam explosion has been reported to reduce stiffness, improve bending properties, and caused narrow fineness (diameter) distribution (17).

2.2.2.1. Plasma Treatment (17)

Plasma treatment is one of the most successful methods that have been carried out by researchers to modify the surface of natural fibers without changing their bulk properties. Two main methods of using plasma have been investigated; discharging plasma by corona and cold plasma. Cold plasma can introduce high-frequency of electric discharge using microwave energy however, corona plasma produces lower frequency by alternating current discharge at atmospheric pressure.

Marais et al. (32) used helium cold plasma to treat a nonwoven sheet made from pure flax fibers and a mixture of flax and polyethylene terephthalate (PET) with a weight ratio 80/20 to reinforce an Unsaturated Polyester Resin (UPR). They compared the plasma treatment with the use of an autoclave to achieve the best improvement in both moisture resistance and stiffness of the composites. The helium plasma introduced some radicals on the surface of the flax fibers that react with the unsaturated polyester chains and reduced the impurities on the surface, as shown in Figure 19, and therefore enhanced the interaction properties between the fibers and the composite as shown in the SEM images in Figure 20. However, the plasma and the autoclave treatments were able to increase the elastic modulus of the composite, the ultimate strength had been decreased as shown in Figure 21 which conflicted with the SEM images that showed enhancement in the relationship between the fibers and matrix after the plasma treatment. On the other hand, autoclave treatment was more efficient in terms of the water resistance of the reinforced composites.

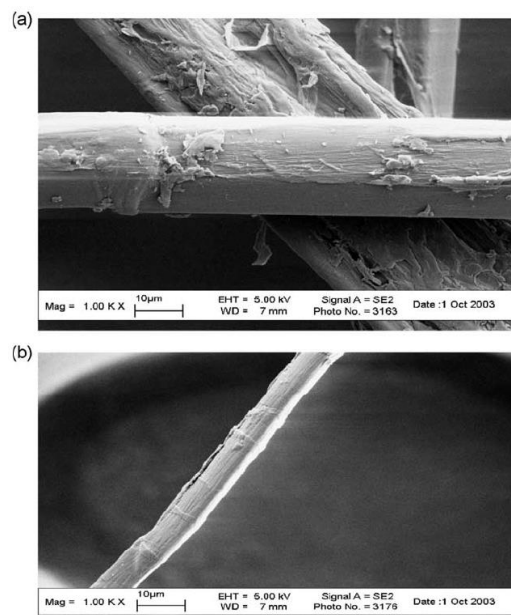


Figure 19. SEM images of flax fibers (a) Untreated, (b) Plasma treated (32)

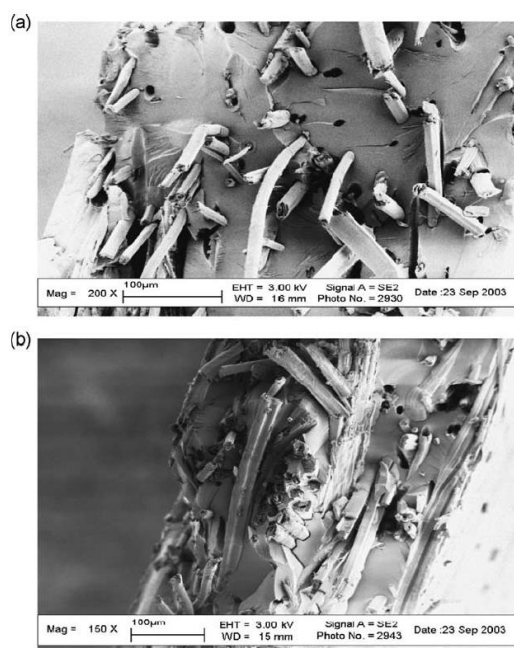


Figure 20. SEM images of fractured flax/PET composite (a) Untreated flax fibers, (b) Plasma treated (32)

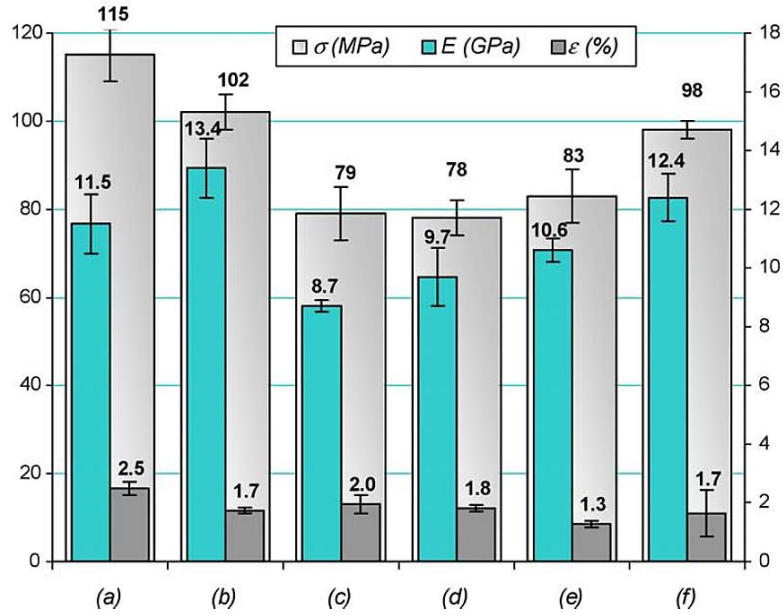


Figure 21. Values of tensile modulus E , breaking strength (σ), and breaking strain (ϵ %) of dry composites: (a) flax/ UPR composite, (b) flax/ UPR composite plasma treated, (c) (flax/PET)/ UPR composite, (d) (flax/PET)/ UPR composite plasma treated, (e) flax/ UPR composite autoclave treated, (f) flax/ UPR composite autoclave plasma treated (32)

Sarikanat et al. (33) studied the effect of flax treatment by argon and air atmospheric pressure plasma to enhance the mechanical properties of flax/ unsaturated polyester composite with the use of three plasma powers; 100, 200 and 300 W. Their experiments of the tensile strength, tensile modulus, flexural strength, flexural modulus, interlaminar shear strength (ILSS), Mode I interlaminar fracture toughness (GIC), and Mode II interlaminar fracture toughness (GIIC) proved that the mechanical properties for flax fiber-reinforced polyester composites have been improved using air plasma treatment much better than that by argon plasma treatment as explained in Figure 22. Changing the plasma power in air plasma improved the tensile properties of the composite, however, this enhancement was up to 200 W in case of argon plasma treated due to the deterioration of the flax fibers. In Figure 23, unlike all other mechanical properties,

the flexural strength of air plasma treated composite at 200 W had been decreased compared to 100 W treatment. No explanation was provided for such deterioration by increasing the plasma power.

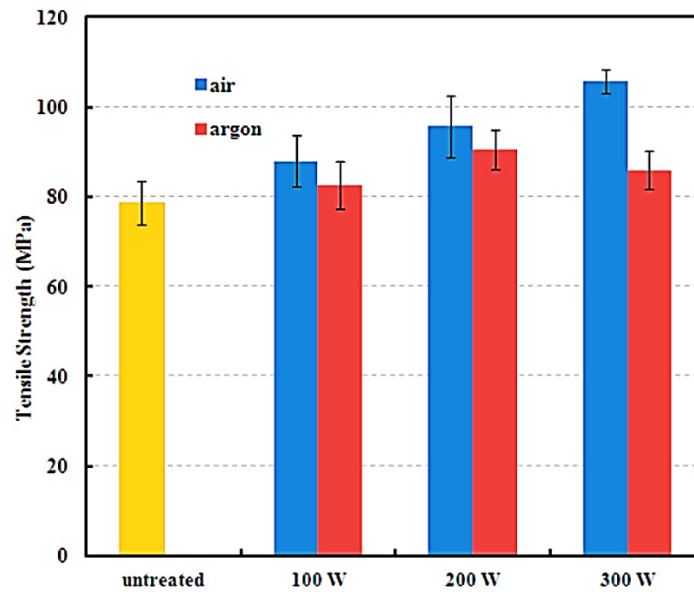


Figure 22. Tensile strength values of flax fiber-reinforced polyester composites (33)

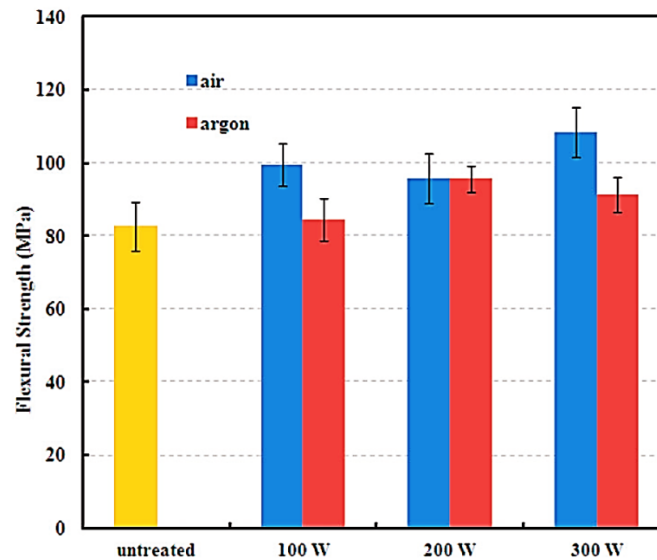


Figure 23. Flexural strength values of flax fiber-reinforced polyester composites (33)

Bozaci et al. (33) treated flax fibers to improve the interfacial adhesion between flax fibers and two matrices; high-density polyethylene (HDPE) and unsaturated polyester by argon and air atmospheric pressure plasma systems under various plasma powers. This treatment changed the surface chemical composition and functional groups and increased the surface roughness. That was obvious in the results of Fourier Transform Infrared Spectroscopy, X-ray Photoelectron Spectroscopy, Scanning Electron Microscopy, and roughness tests. They proved that the interfacial adhesion of argon treated flax fiber for HDPE matrix was superior to those of air treated and untreated flax fiber, however the air plasma treatment was more efficient than argon plasma treatment of flax fiber and polyester matrix and that was the same results showed by Sarikanat et al. Above that, the pull-out tests showed that greater plasma power causes greater interfacial adhesion (34).

2.2.3. Solvent Extraction

The aim of the solvent extraction process is to separate the lignocellulosic components from the fibers with a high content of cellulose by using solvents. These solvents pollute the environment through hazardous substances and vapors produced (12).

Le Digabel and Avérous (35) studied the effect of different extraction conditions on the filler surface and the size distribution which affected the thermal and mechanical properties of the biocomposites. The lignocellulose fillers were a by-product of an industrial fractionation process of wheat straw, however, the used matrix was a biodegradable aromatic copolyester (polybutylene adipate-co-terephthalate). From the raw agro-material, three different filler fractions (TLF1, TLF2, and TLF3) have been obtained by varying the fractionation conditions to extract the lignin according to the liquid media (water or ethanol). Two temperatures had been used; the room temperature and the solvent reflux temperature. Changes in the surface tensions

of the fillers were observed due to the treatments of the fillers. Above that, an increase in the fillers roughness after treatment was noticed. Therefore, variations on the thermal properties were particularly notable on the biocomposites' crystallization temperatures. The elongations at break and at the yield point of the composites with treated fillers had been decreased than that of the untreated fillers, however, there was no clear trend of increasing or decreasing the breaking elongation with different filler fractions.

2.2.4. Thermal Treatment

Thermal treatment depends mainly on depolymerizing or releasing the non-cellulose constituents and chemicals from the fiber bundle. In this process, the lignocellulosic fibers are autoclaved around or below the glass transition temperature of lignin (around 200°C) to separate the single fibers from the bundle. Thermal treatments can increase the crystallinity and dimensional stability of lignocellulosic fibers. The hydrophobicity of the surface of the fibers also can be increased as a result of melting and flowing the non-cellulose chemicals to the surface (12).

2.2.5. Steam Explosion

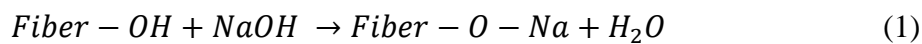
Steam explosion is usually used to separate the lignocellulosic fiber bundles into their elementary fibers and main components. This process is used widely in extracting wood fibers (36), but can also be applied to high cellulose content long fibers to increase the contribution of the cellulose and therefore improve their properties (37). Steam explosion helps in decreasing the amount of minerals, water-extractables, and pectin included in the fibers however, it reduces the length of long fibers. In the steam explosion, the biomass is pressurized with steam for a short time and then exposed to atmospheric pressure for the biomass defibrillation. A steam explosion can significantly increase the crystallinity of the fibers and therefore increase their modulus (38).

Nykter et al. (37) studied the effects of pectinase enzyme treatment followed by thermal treatments which were a steam explosion and dry heating on the chemical composition of hemp fibers. The enzymatic treatment of hemp increased the moulds of the fibers however, the steam explosion reduced the growth of moulds on the hemp fibers. In addition, the steam explosion was found to reduce the number of bacteria. It was noticed that both enzymatic treatment and steam explosion had changed the chemical composition of the hemp fibers. The cellulose content increased by 6% to be 67–70% with the enzymatic treatment, 74% in case of a steam explosion and 78% when steam explosion treatment was used after enzymatic treatment of hemp fibers.

2.2.3. Chemical Treatment

2.2.3.1. Alkaline Treatment

Alkaline treatment or mercerization is one of the most widely used chemical treatments of cellulosic fibers before using them as reinforcements for thermoplastics and thermosets. This process depends mainly on the disruption of hydrogen bonding in the network structure by alkaline treatment and therefore increasing the surface roughness of the fibers. Alkaline treatment removes a certain amount of lignin, wax and oils which cover the external surface of the fiber cell wall as shown in Figure 24, however, it can depolymerize the cellulose and expose the short length crystallites. The addition of aqueous sodium hydroxide (NaOH) to natural fiber results in ionization of the hydroxyl groups to the alkoxide as shown in equation (1) (39). The alkaline treatment changes the orientation of highly packed crystalline cellulose order and forming an amorphous region. Thus, more access to penetrating chemicals can happen (40).



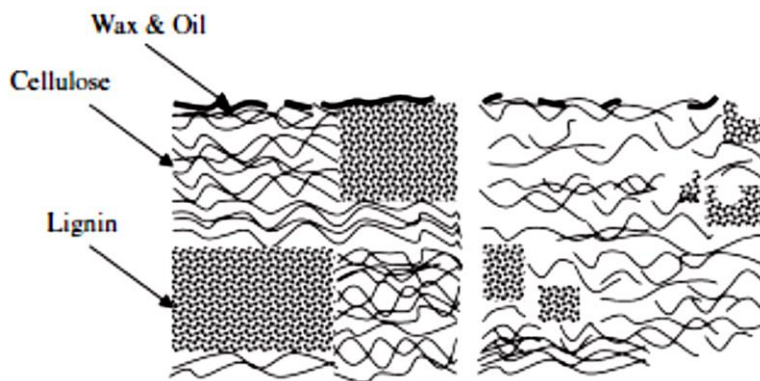


Figure 24. The schematic representation of the fiber contents before and after alkaline treatment

(40)

Mohanty et al. (41) used alkali treatment to enhance the bonding between the chopped kenaf and henequen fibers and polypropylene (PP) matrix. The results showed that the use of alkali was efficient in improving the fiber–matrix adhesion in natural fiber/ PP composites. During alkali treatment, removal of a substantial portion of uronic acid which is a constituent of hemicellulose xylan resulted in changes in the FTIR spectra. The TGA analysis evidenced that the 5% alkali-treatments of natural fibers improved the thermal stability. The alkali treatment of kenaf and henequen fibers resulted in superior mechanical properties of the natural fiber-PP composites.

Balnois et al. (42) chemically modified flax fibers in order to enhance the relationship between flax fibers and unsaturated polyester resins using sodium hydroxide, sodium hydroxide plus acetic anhydride and formic acid-based treatments. The surface structure of treated flax fibers became smoother with a decrease in roughness when compared to the raw flax fibers. Using the AFM results they proved that the chemical modification of the natural fibers contributed to highlight some of the important parameters that are necessary to enhance the mechanical properties of composites.

Huo et al. (43) used three types of cellulosic fiber; long-line European (EU) flax fiber, North American (NA) flax fiber, and North American hemp fiber mats as reinforcements in natural fiber composites. Two alkaline fiber surface treatments had been used with different treatment conditions. The first was alkaline treatment in which the natural fibers were immersed into 1500 mL of 10 g/L sodium hydroxide ethanol solution at a temperature of 78 °C for 2 h and then washed with distilled water with 7 pH. The second was immersing the fibers into 3 wt. % acrylic resin (AR) Tetrahydrofuran (THF) solution for an hour at room temperature after alkaline treatment. In both methods, the treated fibers were dried in an oven for 24 h at 80 °C. Vinyl ester (VE) had been used as a polymer matrix for the treated and untreated fibers. The FTIR spectra were able to show the differences between the treated and the untreated natural fibers. Figure 25 describes the infrared spectra of the treated and untreated hemp fibers. The CH peak stretching around 3000 cm^{-1} to 2800 cm^{-1} was clearer in the spectra of the treated hemp fibers indication of clean surface of the treated fibers. In addition, the peak at 1737 cm^{-1} in the 3% AR treated hemp fibers explained the C=O group that came from the acrylic resin.

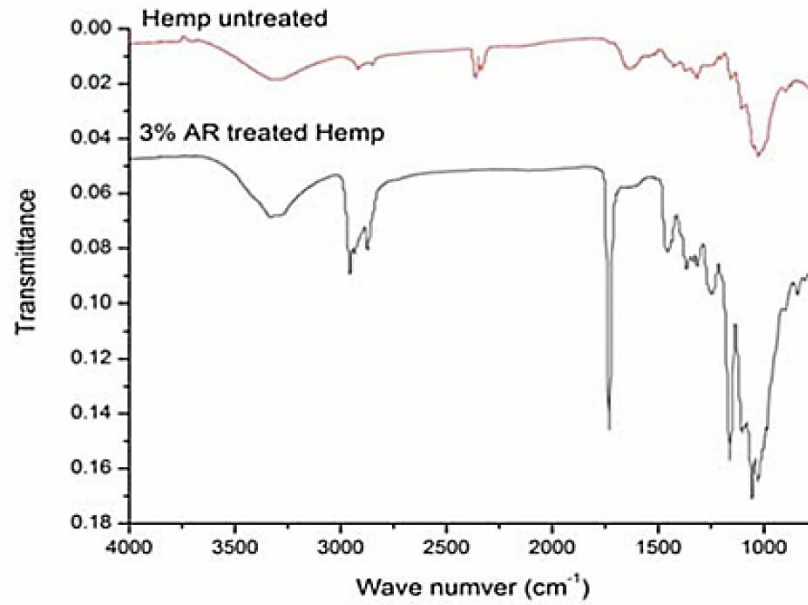


Figure 25. The infrared spectra of untreated and treated hemp fibers

The treatments revealed the high mechanical properties of EU flax fiber reinforced composites, as described in table 3, with minimal voids and fine surface appearance. All surface treatments were able to increase the adhesion between fibers and matrices, however alkaline treatment and 3 % AR THF treatment reduced the fiber modulus. Table 3 shows the tensile properties for the different treatments of the three fibers.

Table 3. Tensile Properties Comparison (43)

<i>Sample</i>	<i>Tensile Strength (MPa)</i>	<i>Tensile Modulus (GPa)</i>	<i>Density (g/cm³)</i>	<i>Fiber Volume Fraction</i>
untreated Hemp	57.65 ± 2.78	5.57 ± 0.27	1.16 ± 0.05	30.90%
untreated Hemp with 1% AR in VE	75.05 ± 2.40	6.18 ± 0.26	1.17 ± 0.01	37.81%
NaOH treated Hemp	70.43 ± 3.19	5.79 ± 0.22	1.26 ± 0.01	32.99%
NaOH treated Hemp with 1% AR in VE	64.05 ± 2.96	5.20 ± 0.62	1.22 ± 0.01	27.12%
NaOH and 3% AR THE treated Hemp	64.14 ± 3.40	5.83 ± 0.48	1.08 ± 0.00	31.21%
untreated NA Flax	17.24 ± 0.30	2.04 ± 0.11	1.09 ± 0.02	25.06%
NaOH treated NA Flax	18.57 ± 1.64	1.84 ± 0.25	1.05 ± 0.03	26.17%
NaOH treated NA Flax with 1% AR in VE	20.10 ± 2.35	2.82 ± 0.22	1.03 ± 0.02	26.24%
NaOH and 3% AR THE treated NA Flax	22.56 ± 1.97	3.36 ± 0.20	1.05 ± 0.01	30.44%
untreated EU Flax	76.32 ± 14.67	13.77 ± 1.07	1.29 ± 0.02	48.38%
untreated EU Flax with 1% AR in VE	101.68 ± 26.69	14.56 ± 2.22	1.23 ± 0.03	43.46%
NaOH treated EU Flax	166.89 ± 43.69	11.64 ± 1.42	1.29 ± 0.03	45.70%
NaOH treated EU Flax with 1% AR in VE	216.13 ± 34.43	14.78 ± 1.09	1.23 ± 0.05	45.35%
NaOH and 3% AR THE treated EU Flax	115.98 ± 26.62	12.96 ± 2.25	1.25 ± 0.03	47.47%

Ishikawa et al. (44) used flax and hemp natural fibers in an epoxy acrylate resin to produce composites. Three different surface treatments had been applied for each type of fibers before producing the composite in order to improve the mechanical properties of the final product by developing the interfacial adhesion between the fibers and the matrix. For flax, the treatments were acetone, laundry detergent, and an aqueous solution of sodium hydroxide (3 wt. % NaOH). For hemp, they used polysilazane, silane coupling agent, and coating by polyvinyl alcohol (PVA). A vacuum assisted resin transfer molding (VARTM) had been used to inject the pressurized resin into the preform as described in Figure 26, however there was no information provided about the used preform. Figure 27 shows that all surface modifications of flax fibers increased the tensile strength of the composite, however the alkali washing was the most

effective that increased the tensile strength of the composite by 19.7%. In contrast, all hemp fiber treatments decreased the tensile strength as described in Figure 28. It was claimed that cracks were partially produced on the polysilazane layer as defects which reduced the tensile strength of the composite. On the other hand, the PVA had filled the gaps between fibers and prevented the epoxy resin from impregnating into the preform. The results of the micro-droplet pull-out test confirmed the weakness of treated hemp fiber composites. However, by looking at the SEM images of fracture surfaces of hemp fiber composites in Figure 29, it is noticed that the treated fiber sample had a cleaner surface without pulled-out fibers. On the other hand, the untreated hemp fiber composite had many pulled fibers which indicated that the adhesion between fibers and matrix was stronger in case of the treated hemp fibers which conflicts with the tensile and the pull-out test results.

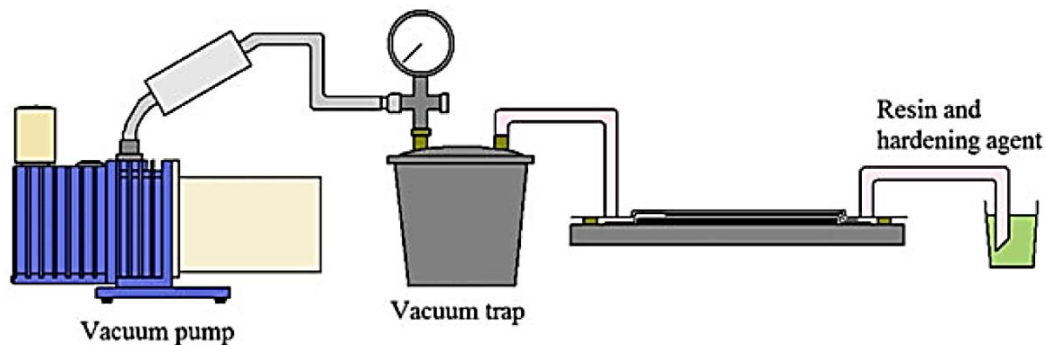


Figure 26. Schematic diagram of VARTM method (44)

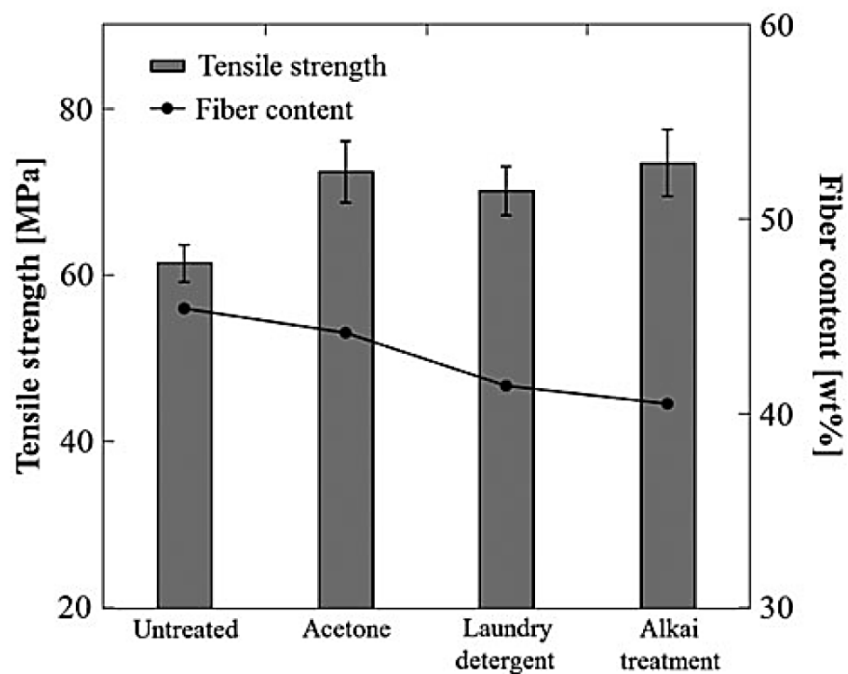


Figure 27. Tensile properties and fiber contents of flax fiber composites (44)

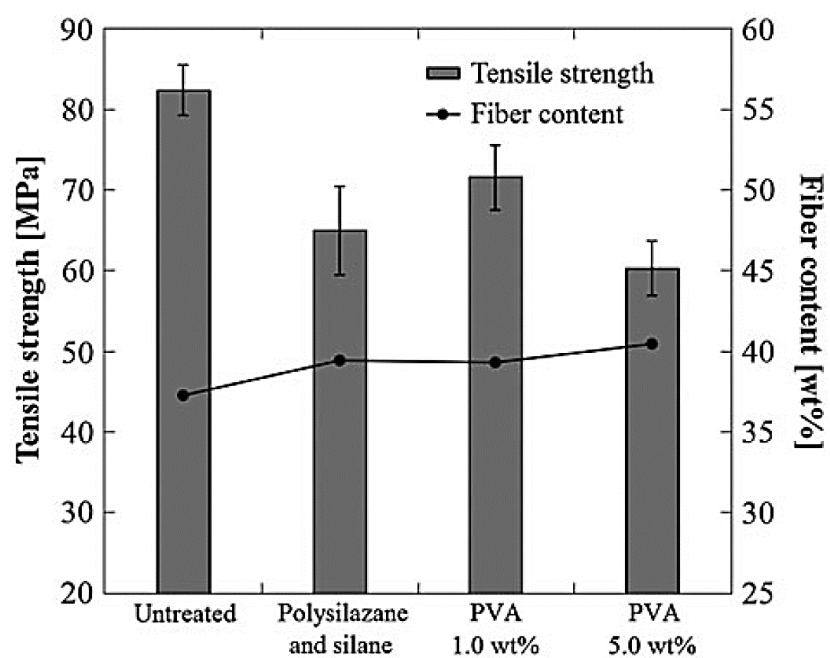


Figure 28. Tensile properties and fiber contents of hemp fiber composites (44)

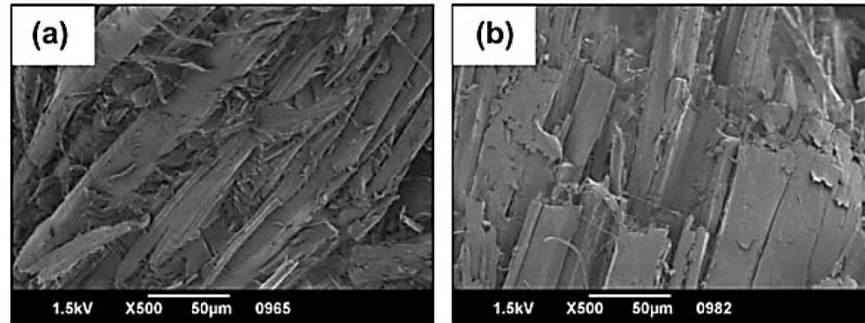


Figure 29. Fracture surfaces of hemp fiber composites; (a) untreated and (b) PVA 5 wt. % (44)

Amiri et al. (45) studied the effect of alkaline treatment of flax fiber and the addition of 1% acrylic resin to vinyl ester matrix on mechanical properties and long-term creep behavior of flax/vinyl ester composites. Flax fibers were immersed into 1500 mL of 10 g/L sodium hydroxide/ethanol solution at a temperature of 78 °C for 2 hours. The alkaline treatment with the use of sodium hydroxide was able to increase the cellulose content by 10% and decrease all other constituents in the flax fibers as shown in table 4. Therefore, it increased the number of reaction sites which resulted in stronger adhesion between the fibers and the matrix. The SEM images of untreated and treated flax fibers in Figure 30, revealed the clean surface of alkali treated flax fibers. This modification resulted in an increase in the interlaminar shear, tensile and flexural strength of the composite, however, the tensile and flexural modulus was decreased by 10%. The addition of 1% acrylic resin to the vinyl ester resin enhanced all the mechanical properties except the flexural modulus that was decreased by 5%. Time-temperature superposition (TTS) had been used to describe the long-term creep behavior. The results of applying the TTS showed that the alkaline fiber treatment and adding 1% acrylic resin to vinyl ester delayed the creep response.

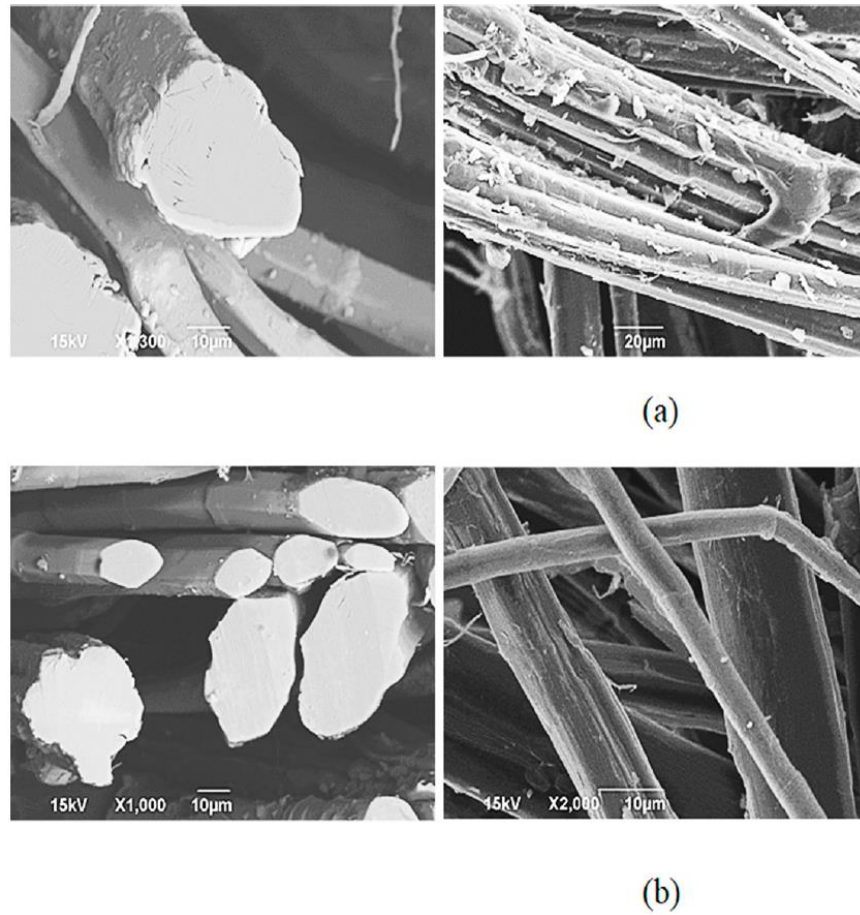


Figure 30. SEM images of flax fiber; (a) untreated; (b) alkaline treated, adapted from (45)

Table 4. Constituent analysis of untreated and alkaline treated flax fibers (45)

Fiber	Cellulose	Hemi cellulose	Moisture	Crude protein	Crude fat	Ash	Other
	%	%	%	%	%	%	%
Untreated	79.56	8.76	2.33	2.44	0.40	1.59	0.73
Alkaline Treated	87.81	7.48	1.62	1.22	0.13	0.89	0.42

2.2.3.2. Coupling Agents

Silane treatments, acylation, benzylation, and graft copolymerization have been used widely for modifying the surface of fibers to enhance the interfacial adhesion between the fibers and the matrix. Coupling agents contain chemical groups that react with fiber and matrix to create

covalent and hydrogen bonds which can improve the interaction between them (12). Many coupling agents have been used in the surface modification of natural fibers depending on the types of the polymer and the matrix. In silane treatments, the composition of silane forms a chemical link between the fiber surface and the matrix through several stages of hydrolysis, condensation and bond formation during the treatment process. The presence of moisture produces silanols and hydrolysable alkoxy groups, one end of silanol reacts with the cellulose hydroxyl group during the condensation process and the other end forms a bond with the functional group of the matrix. These linkages provide molecular continuity across the interface of the composite which can improve the chemical adhesion between the fibers and the matrix and therefore, enhance the properties of the composite. However, in the acylation (known as esterification) method, acetyl groups (CH_3CO) react with the hydrophilic hydroxyl groups (OH) of the fiber and therefore decrease the existence of moisture and decrease the hydrophilicity of natural fibers. This increases the dimensional stability and decreases the void content of the composite. In addition, this treatment provides rough surface topography which leads to better mechanical interlocking with the matrix (46).

Valadez-Gonzalez et al. (47) were able to improve the interfacial shear strength between henequen fibers and a thermoplastic matrix of high-density polyethylene (HDPE) by the presence of a silane-coupling agent after alkali treatment as shown in Figure 31. This treatment increased the surface roughness which resulted in a better mechanical interlocking and it incremented the amount of cellulose exposed on the fiber surface, therefore increasing the number of possible reaction sites. The silane treatment resulted in better interfacial load transfer efficiency in addition to increasing the tensile strength of the composite material from 21 to 27 MPa. In composite materials, the fibers used to have better mechanical properties than the

matrix, however, it was unusual that the tensile strength of the henequen fibers was lower than that of the HDPE matrix.

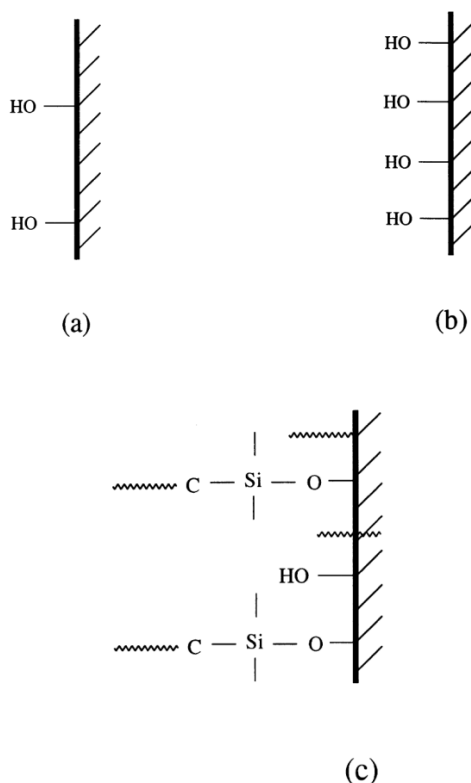


Figure 31. Schematic representation of the interphases formed on the henequen fibers; (a) untreated, (b) alkaline treated, (c) alkaline treated followed by a silane treatment (47)

2.2.3.3. Bleaching

Lignocellulosic fibers usually contain certain amounts of lignin and pectin which can be degraded using bleaching treatments. Bleaching agents can be classified into two types; oxidation bleaching and reduction bleaching. Bleaching treatments are typically used for cotton fibers to deduce the color and increase the whiteness of the fibers. The bleaching agent reacts with the functional groups of the fiber, which cause different colors, to change their structure and therefore, cause the whitening (12).

Cherif et al. (48) produced prepregs with the use of 2/2 twill woven flax fabric and epoxy matrix. They investigated many pre-conventional treatments such as mercerization, bleaching, and leaching of fabrics from long fibers, and yarn leaching for short fibers to study their effect on the water sorption and the mechanical properties and of flax/epoxy composites. The leaching treatment was done with a boiled alkaline, sodium hydroxide was used with the mercerizing treatment, however, a combination of hydrogen peroxide and sodium hypochlorite was used for the bleaching treatment. After these treatments, two composite preparation techniques were implied; hot platen press and autoclave. The fiber volume fractions of all composites prepared by hot platen press were higher than the autoclave as described in Figure 32 which explained the reason behind the higher values of the tensile strength of composites prepared with the hot platen press shown in Figure 33. For the water sorption, table 5 shows that all pretreatments had decreased the water sorption parameters; diffusion coefficient, sorption coefficient, and permeability coefficient. Moreover, the effect of the different chemical treatments on flax yarns had been studied and Figure 34 described their effects on the effective yarn strength. It is obvious that all treatments except leaching for short fibers, improved the mechanical properties of flax yarns. It is noted that the fabric used to produce the composites had different fabric basis weight as described in table 6 and different fiber volume fraction and it is not fair to compare the fabric treatments since other parameters are not equal.

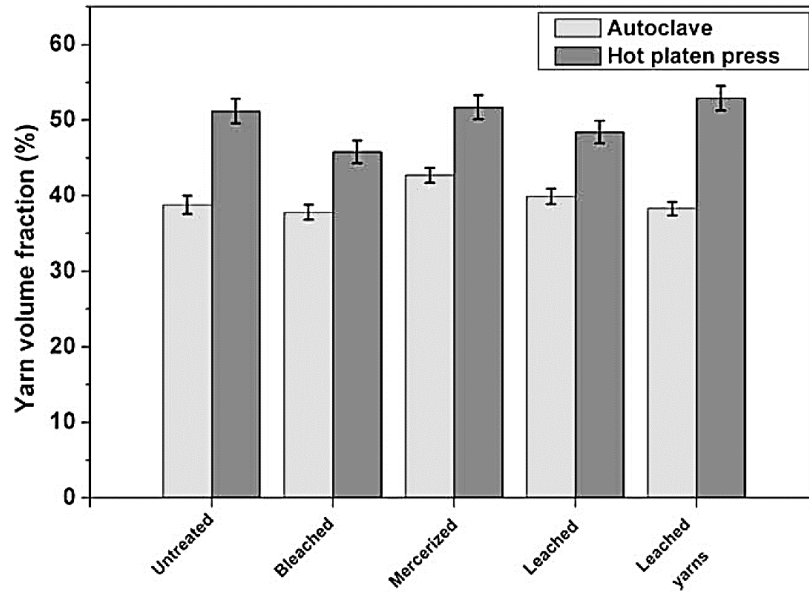


Figure 32. Fiber volume fractions of hot platen press and autoclave prepared composites (48)

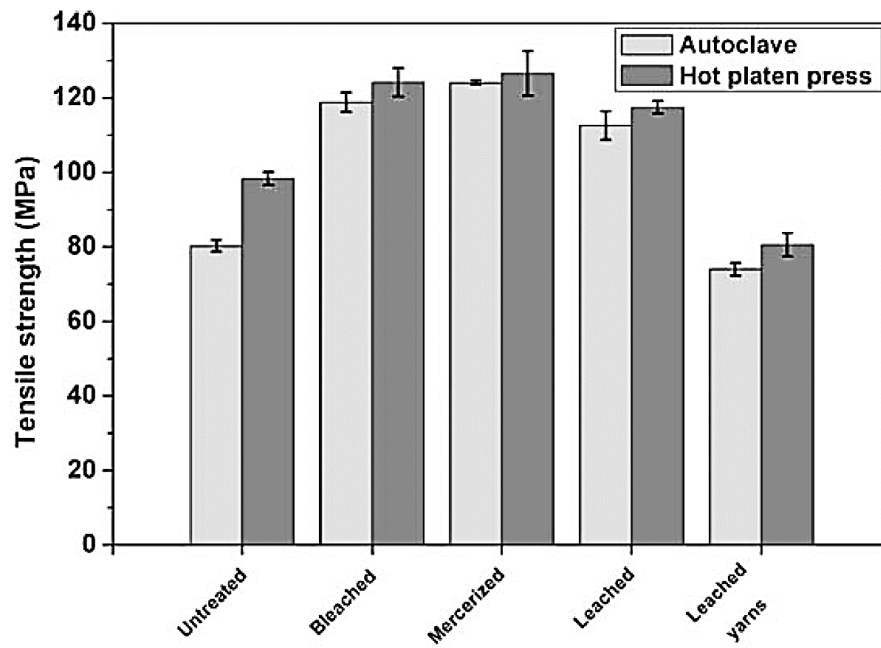


Figure 33. Tensile strength of hot platen press and autoclave prepared composites (48)

Table 5. Diffusion, sorption and permeability coefficients for flax/epoxy composite (48)

	Diffusion coefficient, $D \times 10^7$ (mm ² s ⁻¹)	Sorption coefficient, S (g g ⁻¹)	Permeability coefficient, $P \times 10^7$ (mm ² s ⁻¹)
Untreated	8.46	0.233	1.97
Bleached	3.81	0.167	0.64
Mercerized	3.75	0.157	0.59
Leached	5.56	0.182	1.01
Leached yarns	9.21	0.220	2.02

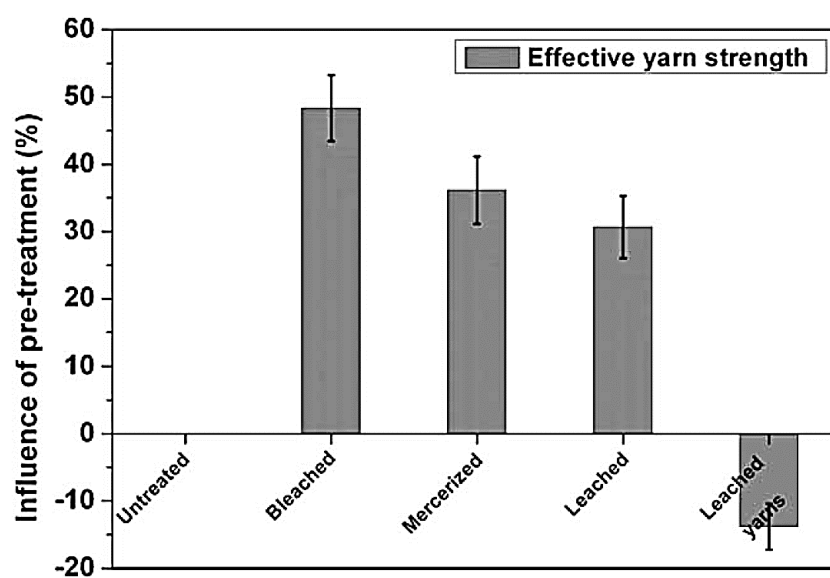


Figure 34. Influence of pretreatments on the effective yarn strength (48)

Table 6. Fabric basis weight of the twill 2/2 fabrics used for the preparation of the composites

(48)

Product name	Basic weight, $g_f (g\ m^{-2})$
Untreated	300
Leached	277
Mercerized	302
Bleached	267
Leached yarns	316

2.2.3.4. Peroxide

Peroxide treatment is an efficient method used to improve the interfacial properties between the natural fibers and the matrix. The initiated peroxide free radicals react with the hydroxyl group of the fiber and the matrix as well. Thus, stronger fiber-matrix adhesion along the interface can be achieved. In addition, this treatment reduces the moisture absorption tendency by the fibers and improves the thermal stability of the composite (46).

Li et al. (49) studied the effect of potassium permanganate surface treatment on ultra-high molecular weight polyethylene (UHMWPE) fibers reinforcement with natural rubber (NR) in composites. The FTIR spectra illustrated in Figure 35 shows an increase in the relative intensity of the $-OH$ peak at $3340\ cm^{-1}$ and the $-C=O$ at $1630\ cm^{-1}$ which indicated that the number of these functional groups on the surface of the fiber had been increased and therefore, enhanced the interfacial bonding between the fiber and the matrix. These changes were obvious in the SEM images of the untreated and treated fiber as described in Figure 36. The better tensile properties of the composites with treated fibers confirmed the enhancement in the interfacial bonding between the fibers and the matrix as shown in Figure 37. Figure 38 shows the fracture of

treated and untreated UHMWPE fibers/NR composites. The untreated fibers had been pulled-out from the natural rubber with clean surfaces which indicated the low interfacial bonding, however, the treated fibers presented less pulled-out fibers accompanied by several micro-fibrillation which can explain the strong interfacial adhesion. It is noted that the type of fracture in the SEM images was not mentioned.

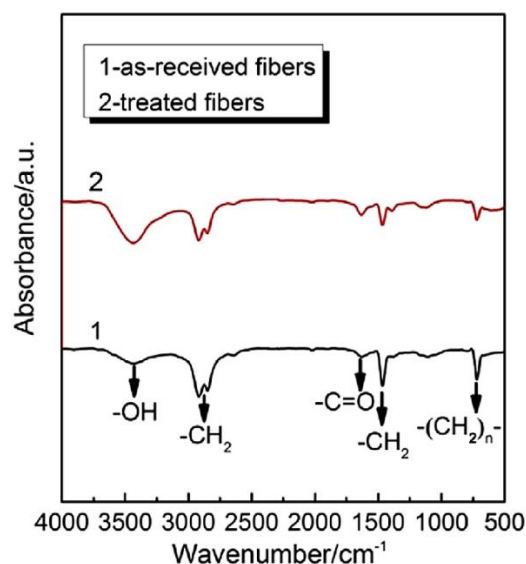


Figure 35. FTIR spectra of UHMWPE fibers (49)

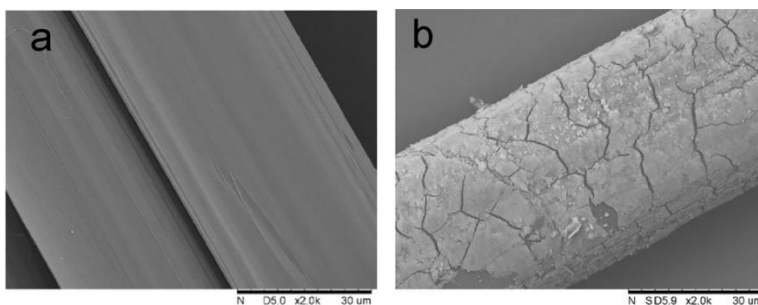


Figure 36. SEM micrographs of (a) untreated fiber, (b) treated fiber (49)

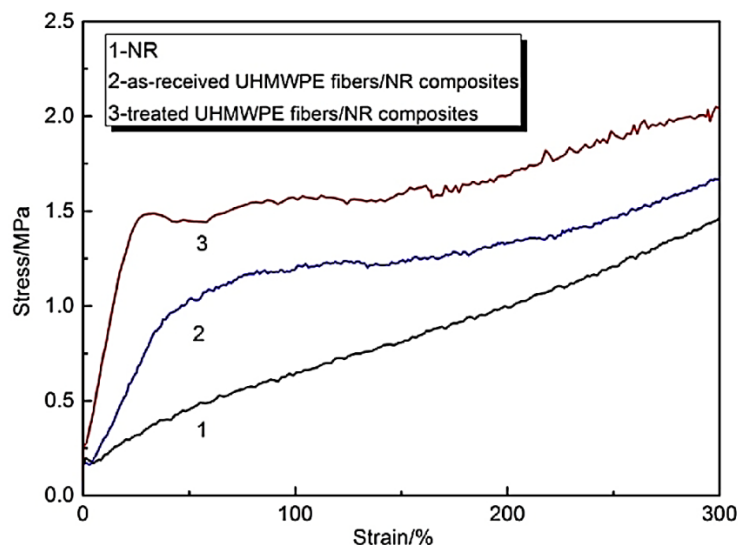


Figure 37. Stress-strain curves of NR and 2 wt. % UHMWPE fibers/NR composites (49)

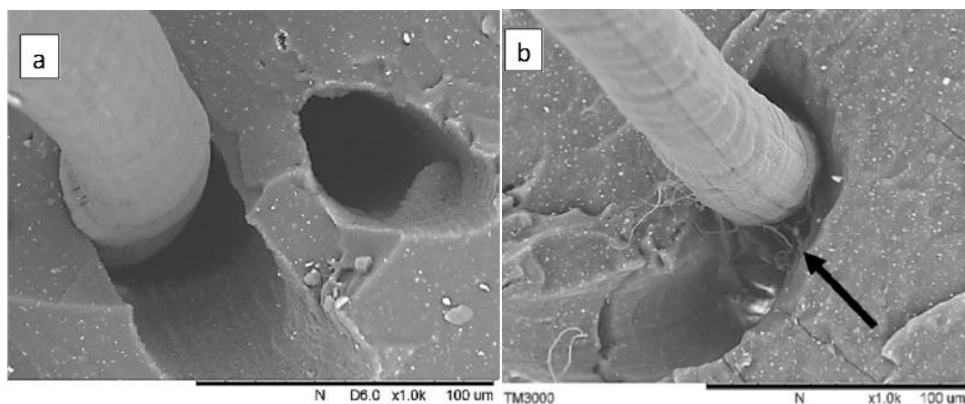
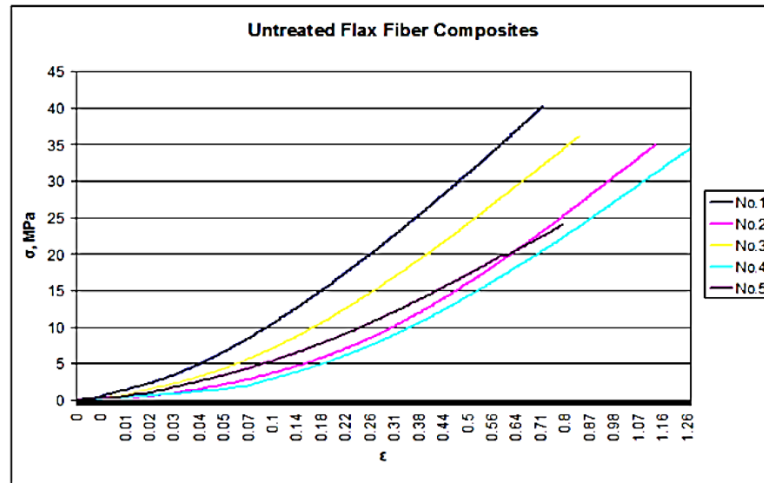


Figure 38. SEM images of fractured surface: (a) UHMWPE fibers/NR composites, (b) treated UHMWPE fibers/NR composites, adapted from (49)

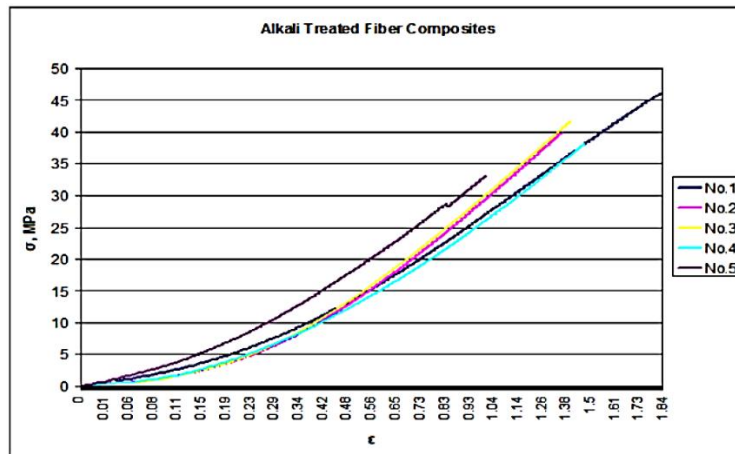
2.2.3.5. Nanoparticles Treatments

Nanotechnology has been considered as one of the most important and newest technologies in this century. Researchers have used the unique properties of nanomaterials to investigate new methods for natural fiber surface treatments (4). Altundal et al. (50) investigated treatment with nano alkali additives of five types of flax fibers, numbered 1-5, in a polymer matrix composites. A

comparison between the effect of the treated and untreated surface fibers on the mechanical behavior of composites was introduced in Figure 39 (a, b). Higher tensile strengths were observed in all treated fiber composite samples than that in untreated fiber composite samples.



(a)



(b)

Figure 39. Stress –deformation curves of (a) untreated, (b) alkali treated fiber reinforced composites, adapted from (50)

Ajith et al. (51) studied the effect of grafting flax fiber yarns by hydrous zirconia nanoparticles on the flax/epoxy interfacial properties. The tensile strength and the interfacial shear strength of the flax fiber to the epoxy resin had been increased after the grafting of the nanoparticles onto the flax fibers. In addition, the glass transition temperature and storage modulus were increased as well which indicated the enhanced bonding strength between the grafted fibers and the epoxy resin. Moreover, the treated flax fiber-based composites showed an antimicrobial performance.

2.2.4. Comparison of Different Surface Treatments

Yu et al. (52) treated ramie fibers, after cutting into 10 mm in average length, with two types of surface treatments; alkali and coupling agents. The used coupling agents were 3-aminopropyltriethoxy silane and γ -glycidoxypolytrimethoxy silane. Rami fibers had been used as a reinforcement with poly lactic acid (PLA) ($M_w = 140,000$) to produce a composite with 30% fiber volume fraction by the two-roll mill. Different characterization techniques were used to study the effect of fiber surface treatment on the tensile, flexural, thermal, and morphological properties of the composite. A neat PLA had been tested to be compared with the produced treated and untreated composites. However, the FTIR spectroscopy confirmed the chemical reaction between the silane and the ramie, it failed to indicate a difference between the alkali treated and untreated fibers. In contrast, the FTIR spectroscopy used by Mohanty et al. (41) was able to differentiate between the untreated and alkali treated kenaf and henequen fibers as shown in Figure 40 which are cellulosic fibers as well. This difference in results maybe because of the settings of the FTIR, since none of the papers mentioned details about the setting of the instrument. The tensile and flexural properties of alkali treated composites showed better results than that treated with silane 2 than that with silane 1(52). This indicated that the interfacial properties of the alkali treated rami and the matrix were the best.

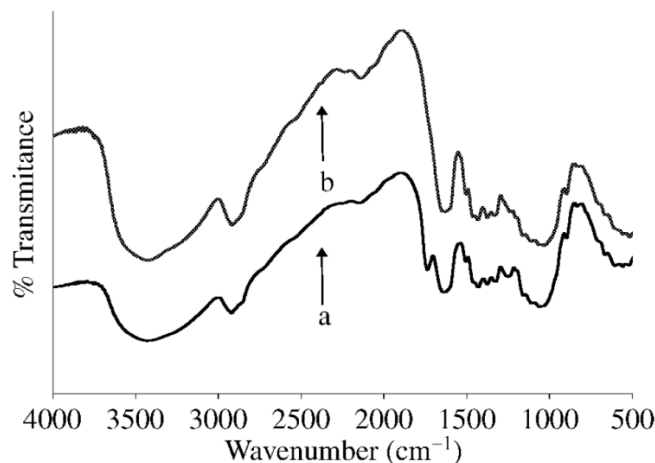


Figure 40. FTIR spectra of (a) raw kenaf, and (b) alkali-treated kenaf fibers (41)

The results of the DMA showed that the storage modulus of the alkali treated composite is higher than that treated with silane 1 than that with silane 2 than that without treatment as shown in Figure 41. Since, the higher the value of storage modulus, the better the interfacial adhesion between the PLA matrix and ramie fibers (52), it was expected that the tensile strength of the composite with silane 1 treated fibers would be higher than the composite with silane 2 treated fibers however, table 7 shows the opposite.

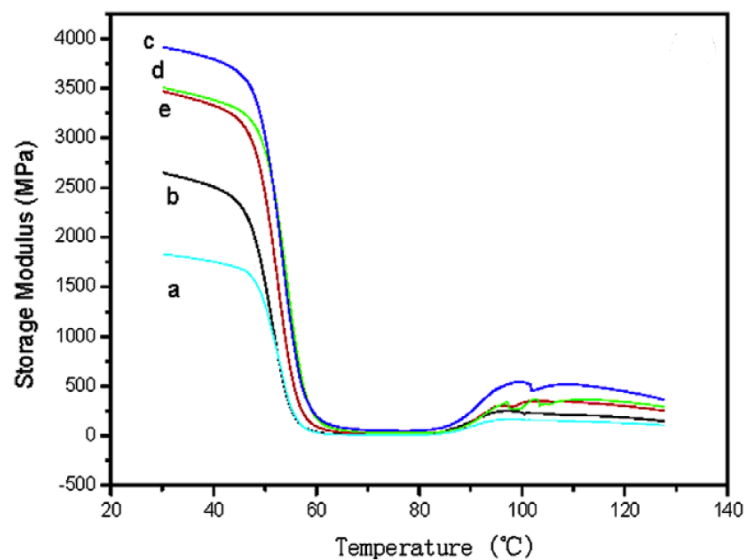


Figure 41. Storage modulus of PLA and PLA-based composites: (a) neat PLA, (b) composite with untreated fiber, (c) composite with fiber treated by alkali, (d) composite with fiber treated by silane 1, and (e) composite with fiber treated by silane 2, adapted from (52)

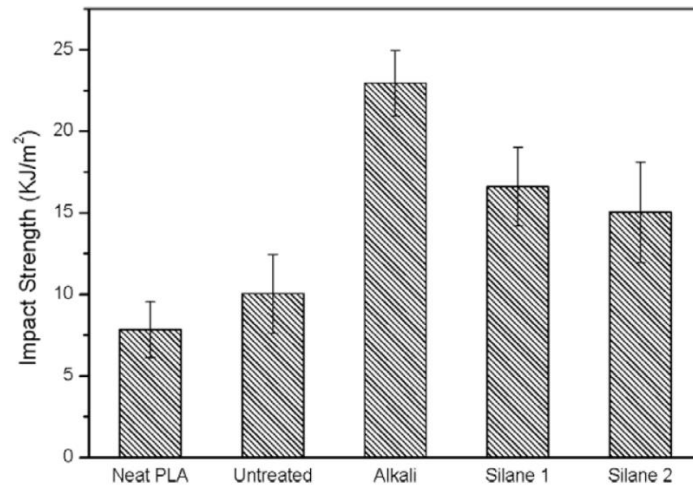


Figure 42. Flexural properties of neat PLA and PLA-based composites, adapted from (52)

Table 7. Mechanical properties of PLA and PLA-based composites, adapted from (52)

Samples	Tensile strength (MPa)	Elongation at break (%)
Neat PLA	45.2 ± 1.5	1.2 ± 0.2
Untreated PLA/ramie composite	52.5 ± 0.8	3.2 ± 0.2
PLA/ramie composite treated by NaOH	66.8 ± 1.7	4.8 ± 0.2
PLA/ramie composite treated by silane 1	59.3 ± 1.2	4.1 ± 0.2
PLA/ramie composite treated by silane 12	64.2 ± 0.7	3.6 ± 0.1

Thermal degradation was tested by the DSC. Despite the strong interfacial adhesion between the PLA matrix and the alkali treated ramie fibers, it showed less thermal degradation compared to the silane treated samples (52). The reasons for such a conflict was not explained by the authors.

The surface morphologies of the fractured specimens of composites with treated and untreated fibers had been tested using SEM. The SEM images differentiated between the untreated and the treated fibers in the composites. For the untreated sample, there were pulled out fibers with a clean surface which clarified the low interfacial adhesion between the untreated fibers and the matrix (52). However, the authors mentioned that the SEM images for the alkali and silane treated specimens were different, they did not list any of these differences between the morphologies.

Sreekumar et al. (53) were able to enhance the interfacial bonding between sisal fibers and polyester resin through different chemical and physical fiber treatments. They used silane, permanganate, benzoylchloride, sodium hydroxide and heating at 100 °C as surface modifications to improve the mechanical properties and decreased the water absorption of the composite. It is noted that the authors mentioned that the FTIR had been used to test the surface modifications of the fibers, however, there was no specific explanation or spectra from the FTIR. The treatments resulted in an improvement in the mechanical properties of the fiber-reinforced

composites such as the tensile and flexural properties as described in table 8, however, all the treatments decreased the impact properties of the composites as shown in Figure 43. The authors claimed that the enhancement in the fiber/matrix adhesion resulted in increasing the tensile properties of the composite while decreasing the impact results due to the crack propagation along the fracture area. This theory can be clear in case of mercerized fibers that had the highest tensile strength and modulus and the lowest impact strength, however, by looking at silane treatment which had the highest tensile strength after mercerization, it had the highest impact strength of all the treatments. Thus, this explanation addressing the comparison between the treatments was not justified. A decrease in the water absorption had been described as a result of the increase of the fiber/matrix bonding.

Table 8. Mechanical properties of treated sisal fiber-reinforced polyester composites, adapted from (53)

Composites	Tensile strength (MPa)	Young's modulus (MPa)	Flexural strength (MPa)
R40	67 ± 2.3	2196 ± 54	84 ± 1.7
RN40	79 ± 1.8	3002 ± 45	102 ± 1.9
RH40	74 ± 2.1	2559 ± 19	101 ± 2.9
RB40	70 ± 1.8	2431 ± 28	93 ± 2.1
RP40	72 ± 1.5	2697 ± 14	105 ± 3.3
RS40	76 ± 2.2	2444 ± 45	102 ± 2.6

Where; (R): resin transfer molding, (N): mercerization, (H): heat treatment, (B): benzoilation, (P): permanganate, (S): silane treatment, and (40): fiber content %.

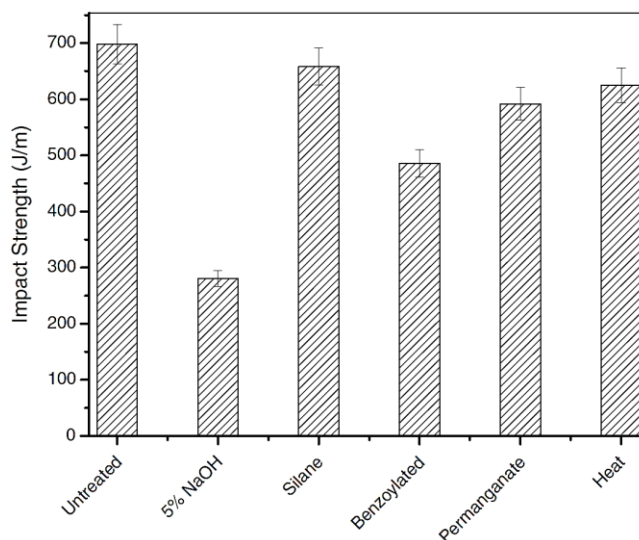


Figure 43. Impact properties of treated and untreated sisal/polyester composites (53)

2.3. Properties of Green Composites

2.3.1. Physical Properties

Usually, natural fibers exhibit dimensional instability due to their nature of hydrophilicity when compared to glass fibers (54). The existing hydrophilic free radicals in natural fibers dictates the response of composite material when exposed to water or relative humidity. This property usually determined by the consequent dimensional changes when the material is immersed in water (4). The hydrophilic nature of plant fibers can cause cracks in the matrix or lack in the adhesion between fibers and matrix due to the water absorption. To reduce the moisture absorption of natural fiber composites, several surface treatments have been suggested by scientists. Pan and Zhong (55) modified the Mori–Tanaka model to measure the mechanical degradation of natural fiber reinforced composites (NFRCs) induced by moisture absorption. They measured the loss in Young's modulus due to the water absorption. The comparison between the theoretically predicted results of the model and the experimental data showed a good

agreement as shown in Figure 44. Above that, their numerical results showed that a stiffer matrix can reduce both the moisture absorption and the mechanical degradation of natural fibers.

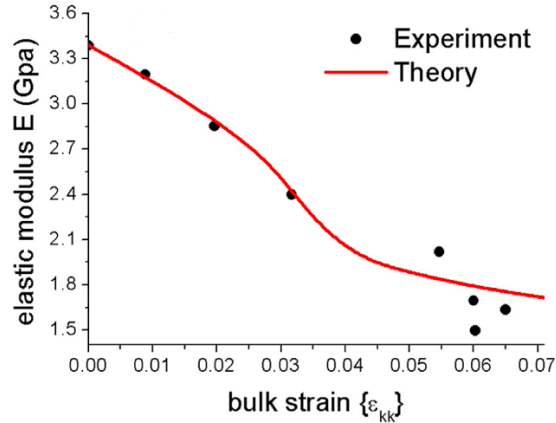


Figure 44. The comparison of Young's modulus E of the composite between theoretical and experimental results (55)

Marais et al. (32) investigated helium cold plasma and/or autoclave treatments by means of water permeation measurements to treat flax fibers in a flax-polyester composite. Water sorption measurements showed a reduction of the water concentration in autoclave-treated fibers compared to untreated fibers, however for the plasma-treated fibers no change has been observed.

Sreekumar et al. (53) were able to decrease the water absorption of the composite by enhancing the interfacial bonding between a nonwoven preform of sisal fibers and polyester resin (R) with 40% fiber content. They used a combination of chemical and physical treatments such as alkali treatment (N), heating at 100 °C (H), permanganate treatment (P), benzylation (B) and silanization (S). Table 9 shows the effects of different surface treatments on the diffusion, sorption, and permeability coefficient of composites. It is noted that all surface treatments were able to decrease the diffusion coefficient of the composite when compared to the untreated fiber-

based composite. Benzoylation had the least diffusion coefficient. Besides, sorption and permeability coefficients had been calculated depending on the diffusion coefficient for a better understanding of water absorption in the composite.

Table 9. Diffusion, sorption and permeability coefficient for treated sisal/polyester composites at different temperatures (53)

Composites	Temperature (°C)	Diffusion coefficient $\times 10^5$ (cm ² /min)	Sorption coefficient (g/g)	Permeability coefficient $\times 10^6$ (cm ² /min)
R40	30	21.5	0.106	23.0
	60	26.9	0.121	33.6
	90	32.5	0.145	47.2
RN40	30	8.8	0.059	4.92
	60	11.1	0.055	6.11
	90	11.3	0.077	8.75
RH40	30	8.8	0.041	8.16
	60	15.0	0.103	15.6
	90	20.1	0.092	19.0
RB40	30	5.11	0.123	2.14
	60	9.64	0.025	2.41
	90	10.60	0.026	2.75
RP40	30	8.91	0.062	5.54
	60	13.1	0.055	7.26
	90	16.9	0.065	11.0
RS40	30	8.35	0.092	6.51
	60	14.3	0.098	14.00
	90	18.1	0.083	15.1

The thermal stability of green composites depends upon the thermal decomposition of fibers and polymers used in the composite and their contribution as well (56). Kabir et al. (40) used peroxide treatment to enhance the thermal stability of natural-fibers composites. However, Araujo et al. used different coupling agents to improve the thermal properties of high-density polyethylene composites with curaua fibers that are usually extracted from the leaves of the *Ananas erectifolius* L. B. Smith plant and is cultivated in the Amazon region (57,58).

2.3.2. Mechanical Properties

Studying the mechanical properties of composites have been carried out using different characterization methods such as tensile, flexural and impact testing. Two approaches for these measurements have been investigated; micro-scale analysis and macro-scale analysis. Most of the characterization testing in natural composited had been done on the micro-scale level for single fibers with droplets of a matrix.

Bax and Mussig (59) compared the mechanical properties of PLA with random fiber webs of Cordenka rayon fibers and flax fibers reinforcements. They used injection molding to produce the samples. Table 10 shows the results of the mechanical properties of the two types of composites depending on the fiber content. Cordenka reinforced PLA at a fiber-mass proportion of 30% showed the highest impact strength (72 kJ/m²) and tensile strength (58 MPa) while the highest Young's modulus (6.31 GPa) was found for the flax/PLA composite.

Table 10. The mechanical properties of flax/PLA and Cordenka/PLA composites (59)

Fibre content in %	Charpy impact in kJ/m ²				Tensile stress in MPa				Young's modulus in GPa			
	Flax		Cordenka		Flax		Cordenka		Flax		Cordenka	
	Average	S.D.	Average	S.D.	Average	S.D.	Average	S.D.	Average	S.D.	Average	S.D.
10	9.97	2.05	43.44	8.11	42.73	1.29	50.40	1.19	3.90	0.18	3.27	0.04
20	10.45	1.53	62.97	6.01	49.23	1.40	50.75	1.90	5.06	0.07	3.97	0.07
30	11.13	1.55	72.24	11.79	54.15	4.57	57.97	5.08	6.31	0.12	4.85	0.03
40			51.34	10.95								

Ramakrishna and Sundararajan (60) compared the impact properties of four natural fibers; coir, sisal, jute and hibiscus cannebinus with of cement mortar slabs with the objective to assess the impact behavior using a simple projectile test. For each fiber, four different fiber contents (0.5%, 1.0%, 1.5% and 2.5% by weight of cement) and three fiber lengths (20mm, 30mm and 40mm)

had been considered. The results showed that coir fiber reinforced mortar slab specimens got the best performance based on the impact resistance (R_u), residual impact strength ratio (I_{rs}), impact crack-resistance ratio (C_r) and the condition of fiber at ultimate failure.

Park (61) utilized the Vacuum Assisted Resin Transfer Molding (VARTM) manufacturing method to produce the flax/vinyl-ester natural fiber composites using a unidirectional and 2D flax nonwovens. He compared the mechanical properties of the produced composite with flax composites data cited from some references. Tables 11 and 12 shows the mechanical properties of a previous work that had been done by other researchers for unidirectional and 2D flax/vinyl-ester composites. The author did not provide explanation about the testing methods or standards that had been used and how that was different or similar to what had been reported in other authors' work he compared his work to. In addition, the author claimed that his method of manufacturing the composite proved that it had better mechanical properties, however, there was no data provided to support his claim.

Table 11. Mechanical properties of UD-flax specimen (61)

Test type	Strength (MPa)	Modulus (GPa)
Tension	157.5	10.4
Compression	102.9	19.4
Flexure	188.0	9.7
In Plane Shear	26.24	3.8

Table 12. Mechanical properties of the 2d-flax specimen (61)

Test type	Strength (MPa)	Modulus (GPa)
Tension	76.7	9.1
Compression	72.8	6.2
Flexure	108.7	6.7
In Plane Shear	36.1	1.6

Zampaloni et al. (62) used a compression molding process utilizing a layered sifting of a microfine polypropylene powder and chopped kenaf fibers to produce a kenaf/PP composite. A thermal treatment was conducted for the fibers in addition to a coupling agent was used for the matrix to enhance the adhesion between the fibers and the matrix. The mechanical properties of the manufactured composites were compared for their tensile strength and flexural strength with hemp/PP, flax/PP, sisal/PP and coir/PP. The results are exhibited in Figures 45 and 46. It is noted that the hemp/PP and flax/PP composites have superior tensile properties, and flax/PP was the best in terms of flexural strength properties. Figure 47 shows a comparison between the specific E-modulus of five natural fibers (flax, hemp, kenaf, sisal, and coir) and E-glass fibers. Kenaf and hemp fibers have higher specific modulus than E-glass fibers, however flax, sisal, and coir got low specific E-modulus.

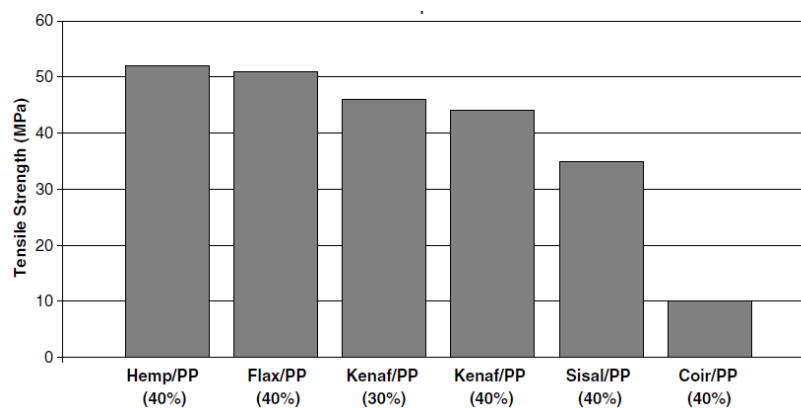


Figure 45. Comparison of the tensile strength of kenaf/PP composites to other natural fiber composites (62)

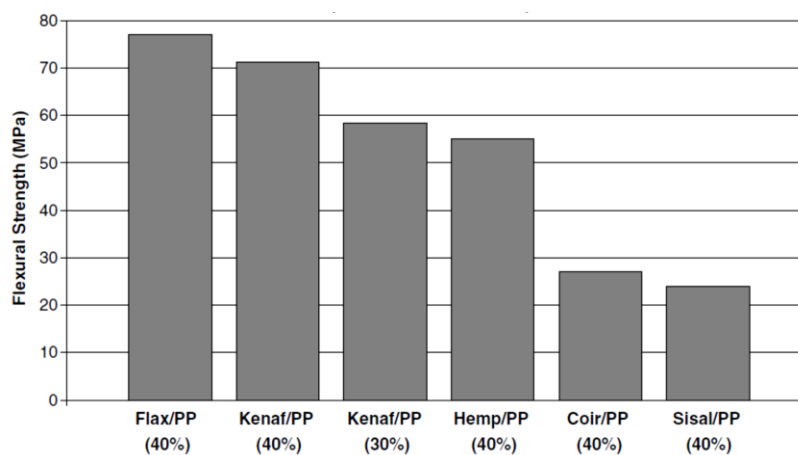


Figure 46. Comparison of flexural strength of kenaf/PP composites to other natural fiber composites (62)

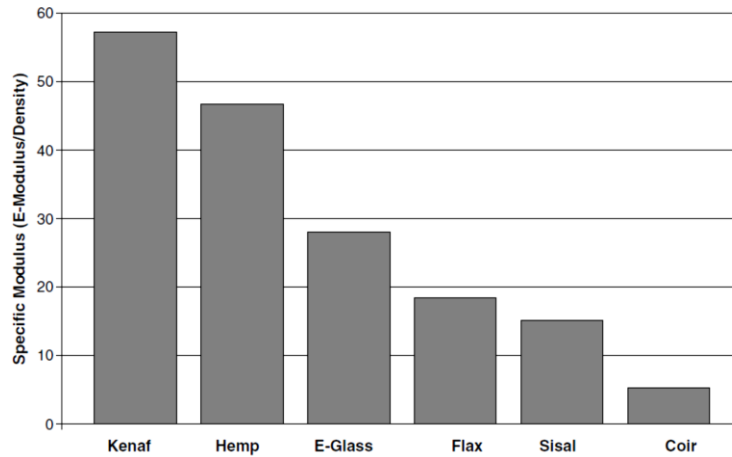


Figure 47. Comparison of the specific modulus of various fibers (62)

Samuel et al. (63) utilized the hand lay-up process to manufacture natural composites with a 30 wt. % fibers using five different natural fibers; ukam, banana, sisal, coconut, and hemp. The mechanical properties of the manufactured composites were compared to that of E-glass fiber reinforced laminates. The natural fibers were treated with alkaline in order to improve the mechanical properties of the resultant laminates. Figures 48-50 show that the e-glass based composites had very high compressive, tensile and bending strength when compared to the values of natural fibers-based composites. On the other hand, natural fibers-based composites proved to be a good competitor with e-glass based composites as described in Figure 51. The authors failed to report the type of matrix used in their work.

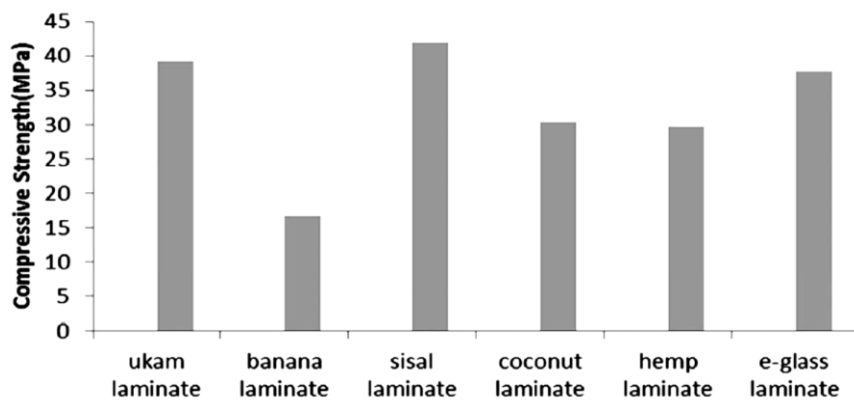


Figure 48. Compressive strength of alkali treatment of natural fiber reinforced laminate samples (63)

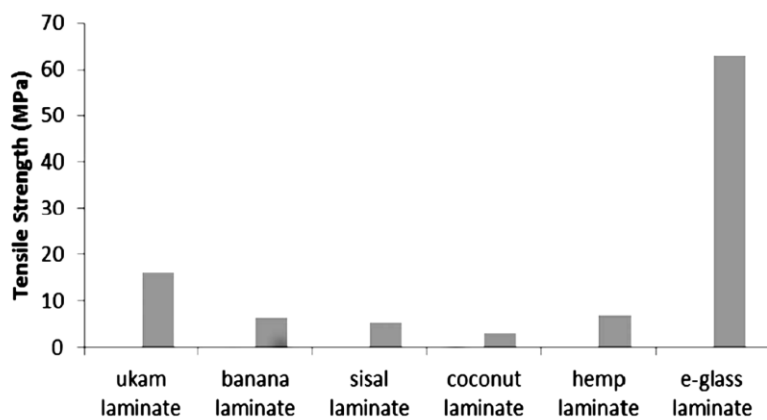


Figure 49. Tensile strength of alkali treatment of natural fiber reinforced laminate samples (63)

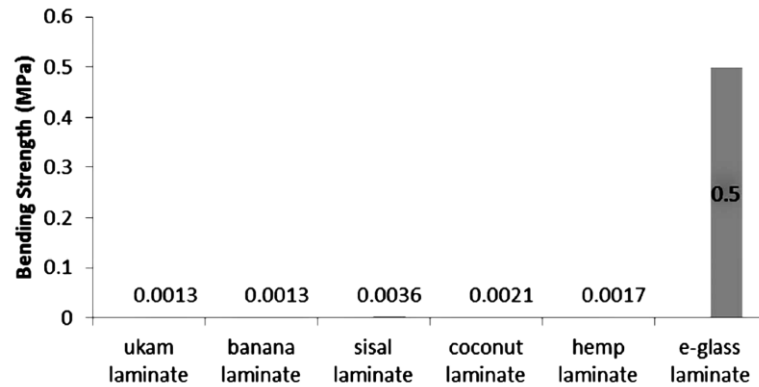


Figure 50. Bending strength of alkalized treatment of natural fiber reinforced laminate samples

(63)

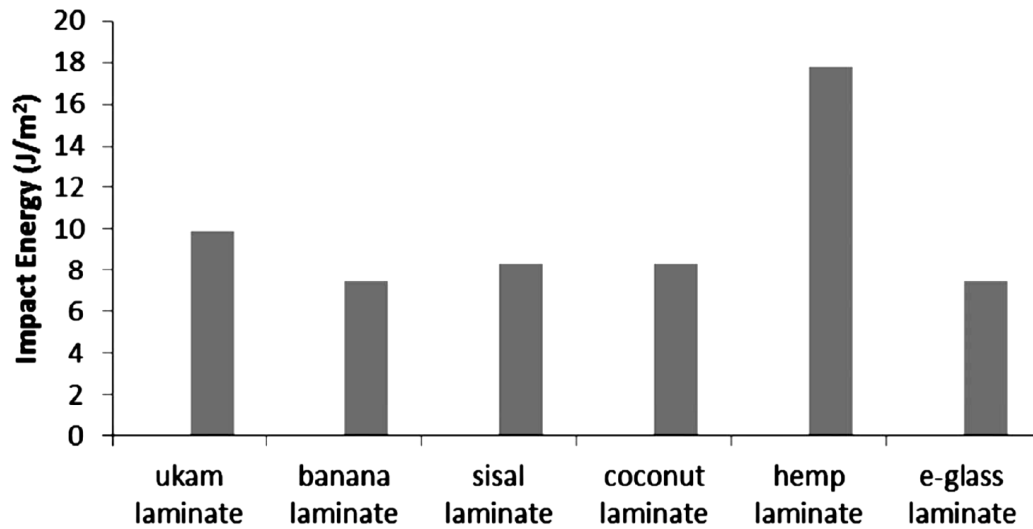


Figure 51. Impact strength of alkalized treatment of natural fiber reinforced laminate samples

(63)

Vuure et al. (64) compared the compressive properties of natural fiber composites from three types of natural fibers; flax, bamboo and coir fibers with epoxy matrix. Flax fibers had been dried for 24 h at 60 °C, however, a wet cleaning was applied to bamboo and coir fibers then dried for 72 h at 60 °C which resulted in aligning the fibers. A Vacuum Assisted Resin Infusion

(VARI) had been utilized for producing the unidirectional fibers composites. Table 13 shows that the compressive properties of bamboo/epoxy were higher than flax/epoxy, higher than coir/epoxy composites, however, the tensile modulus of flax/epoxy composite was higher than bamboo/epoxy composite as shown in table 14.

Table 13. Compressive properties of UD composites with different natural fibers with a fiber volume fraction of 40% (64)

	Compressive strength (MPa)	Compressive modulus (GPa)
Flax-epoxy	136.9 ± 5.5	15.1 ± 2.5
Bamboo-epoxy	149.5 ± 8.9	15.5 ± 2.7
Coir-epoxy	116.2 ± 5.8	3.7 ± 0.3

Table 14. Comparison of tensile and compressive properties for flax and bamboo UD composites with equal fiber volume fractions of 40% (64)

	Flax tensile properties	Flax compressive properties	Bamboo tensile properties	Bamboo compressive properties
Strength (MPa)	222.9 ± 6.1	136.9 ± 5.5	254.7 ± 18.3	149.5 ± 8.9
Modulus (GPa)	23.9 ± 1.9	15.1 ± 2.5	19.5 ± 1.0	15.5 ± 2.7

Le Duigou et al. (65) had used the microbond test, micromechanical analysis and contact angle measurements to examine the interfacial characterization and the mechanical properties of Flax fiber/PLA composite at the micro-scale and compared it with those of Glass/ Polyester, Glass/ Epoxy, Flax/Polyester, and Flax/Epoxy composites. Above that, the matrix mechanical, thermal properties and matrix morphology had been tested. A droplet of the matrix was produced around a fiber to be used for the measurements. A tensile machine with a 2 N load cell and a crosshead

speed of 0.1 mm/min was used in order to measure the maximum force used (F_{max}) to depbond the fiber and the matrix. The mechanical behaviour of PLA was similar to that of standard polyester and epoxy resins so that, the crack appearance from the debonding process for each was not unique after reaching the F_{max} .

F_{max} had been used with the droplet length and the fiber diameter to determine the apparent shear strength (τ_{app}) and the ultimate shear stress (τ_{ult}) by a predeveloped micro-mechanics equation. Slow cooling rates showed better results for τ_{app} and τ_{ult} as the residual stresses were able to be released with the use of longer time. The average τ_{app} of Flax/PLA was the highest of all composites which indicated that their interfacial properties were the best.

The contact angles between the flax fiber and the solid matrix with the microdroplet have been measured by image analysis. Contact angles had been decreased with slower cooling rates because of the difference in shrinkage, viscosity, and the magnitude of residual stress inside the droplet with temperature. Samples had been heated to 190°C to measure the degree of crystallinity. Melting temperature and glass transition temperature were measured using different cooling rates. In order to evaluate the thermal stresses that happened by the cooling process, the difference between the stress-free temperature and the tested temperature had been determined ($\Delta T = T_{free} - T_{test}$). ΔT values referring to the degree of crystallinity were higher with slower cooling rate. Higher values of ΔT produce higher shrinkage of the matrix which increase the difference between thermal expansion coefficients of the fiber and the matrix and thus, affect the stress transfer mechanism between the two. The authors mentioned that they used a suitable cooling rate for the DSC but they did not specify the rate.

DMA in the compression mode was used to estimate the thermal expansion coefficient of the composites with a temperature range of -20°C to 60°C. The slow cooling rate which had a high degree of crystallization showed the best tensile and shear properties. Thermal expansion coefficient did not change with cooling rate because the used temperature range was small. It is noted that the used frequency was missed in the paper. Fracture surfaces were sputter-coated with a thin layer of gold and had been examined via SEM. The fracture of flax/PLA which was interfacial indicated that there were physical interactions such as Van der Waals interactions between flax and PLA however, the interfacial bonding between epoxy and flax was by chemical bonds which is much stronger than Van der Waals interactions. That means the interfacial bonding between epoxy and flax is stronger than PLA and flax which is opposite to what they got from measuring the τ_{app} using the microbond test. An explanation for that conflict should have been provided.

Polymer structure was observed via the polarization microscopy with different cooling rates. The slowest cooling rate showed a crystalline structure with large spherulites unlike the air cooling sample as shown in Figures 52 and 53.

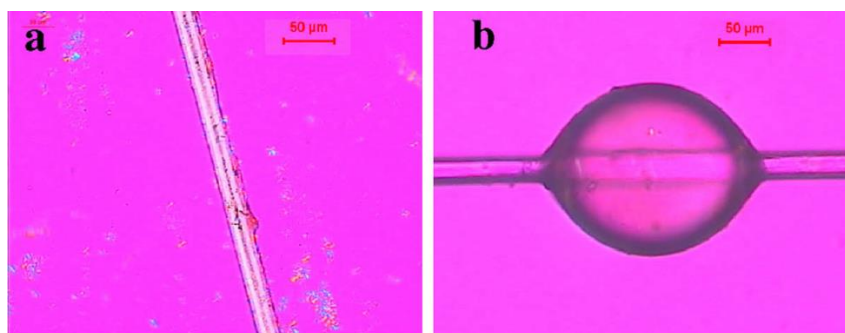


Figure 52. Air cooling: (a) PLA/flax/PLA stack; (b) microdroplet, adapted from (65)

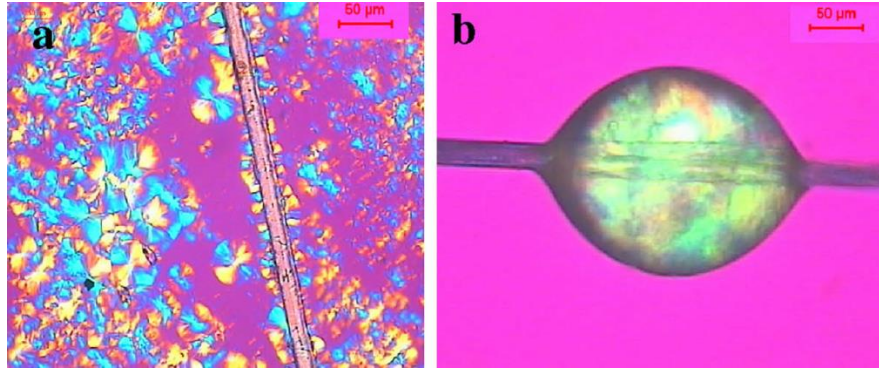


Figure 53. 1°C/min: (a) PLA/flax/PLA stack; (b) microdroplet, adapted from (65)

By reviewing the literature, it is found that most of the researches had been done in natural fiber composites, especially with flax fibers, were in the micro-scale level with single fibers. Only a few papers had been utilized nonwoven fabrics and only one paper used 2x2 twill prepregs laminate. Therefore, there is a gap in the field of green composites with 3D orthogonal woven preforms (3DOW). Thus, this work intended to fill this gap by producing green composites from flax fibers using 3DOW preforms and compare their properties with glass fibers-based composites.

3. OBJECTIVES

In the last decades, the interest in producing composite materials from natural fibers has been increased to reduce environmental impacts of using synthetic fibers, however this is challenging because the significant non-uniformity in the mechanical and the physical properties of natural fibers. To produce a composite material from a 3D preform, there are three main basic technologies to convert sets of yarns into a well oriented and regular structure which are weaving, knitting and braiding. Such structures can effectively carry the internal load in three dimensions without the need for layering to produce laminated composites. A recent technology that has not been fully explored, especially in green products, is 3D orthogonal weaving (3DOW) process. The significance of the 3DOW preforms and their composites have been shown to provide better performance compared to their counter parts using other formation technologies. In this process, structural parameters (such as yarn count, yarn spacing and weave pattern) can be changed to meet the performance requirements to meet products with desired properties. All of these different preform architectures can determine the performance of the preform during the infusion process which will determine the mechanical properties of the produced composite. In addition, the channels resulting from the non-crimp y- and X-yarns in the preform reduce the resin flow time and therefore the cost of the final composite.

From the review in chapter 2, it is found that most of the previous modeling of the mechanical behavior of 3DOW composites focused on linear elastic region however, the plastic region is very important since the stresses are distributed and the damage is accumulated which is different from 3D from 2D laminate composites. In addition, most of the work done was limited to plain jammed structures and few researchers addressed the non-jammed structures. Moreover, few researches addressed different types of weaves which can alter the properties of the preform

and hence the final composite. Additionally, the previous work done on natural fiber surface treatment mostly focused on the small amount of fibers and few researches were found on 2D fabrics. There is a gap in studying the effect of surface treatments on 3DOW preforms and their composites. The lack of research mentioned above directed the objectives of the current proposed work.

The main objective of this work is to develop a generalized model to predict the entire tensile load-extension of 3DOW composites made from natural spun yarns (hemp and flax) and verify the model experimentally. For this purpose, 3D woven preforms with different fabric architectures were produced by changing different structural parameters such as the Z-yarn interlacing (weave) pattern, the number of layers, weft yarn type and the number of Z to Y yarns ratio. The model relies on measured X-, Y-, and Z-yarns and dry resin's tensile properties to predict entire load-extension curve of the composite.

The second objective is to apply the model on 3DOW composites from preforms from as supplied yarns as well as yarns with enhanced surface treatment and find out whether the treatment affects the model prediction. For this objective, different weft yarns with and without fiber surface treatments have been woven as 3DOW preforms.

The third objective of this research is to compare between the properties of composites from natural fibers (hemp and flax) and glass fiber. Hemp and flax have competitive properties to glass fibers which allow them to be a natural substitutional in the future.

4. EXPERIMENTAL

This chapter covers the experimental work used in this research project including the materials, 3DOW preforms and their composites formation, experimental design and the methods and equipment used to determine the physical and mechanical properties of the composites and their constituents.

4.1. Materials

4.1.1. Fibers

The material of warp, weft and binder yarns were made from flax fibers manufactured by ALBANA LINEN, Egypt. Bleached warp yarns were used in the Y and Z direction as warp and binder yarns to produce the 3DOW performs with linear densities 8.5 and 20 metric counts (NM), respectively. In contrast, four different types of flax yarns were used in the X direction with the same linear density of 6 NM. The specifications of all yarns are depicted in table 15. All yarns were produced by wet spinning and the bleached yarns were at ELBANA LINEN with Hydrogen Peroxide (H_2O_2) with a 50% concentration which was applied for 90 minutes.

Table 15. Specifications of warp, weft and binder yarns

Yarn	Linear Density (Nm)	Yarn Type	Doubling	Single Yarn Diameter (mm)
Y-yarn	8.5	Bleached Flax Yarns	3	0.406
X-yarn	6	Grey Flax Yarns	2	0.483
		Bleached Flax Yarns		
		Grey High Strength Flax Yarns		
		Bleached High Strength Flax Yarns		
Z-yarn	20	Bleached Flax Yarns	1	0.264

4.1.2. Resin and Curing Agent

An epoxy-based DERA KANE® 8084 Vinylester resin donated by Ashland Performance Materials, Kentucky was used in this study as a matrix for the 3DOW preforms to produce the composite. The typical properties of the liquid and cured DERA KANE® 8084 Vinylester resin are given in tables 16 and 17. The Vinylester resin can cure in room temperature and less hazardous than polyester resin because of the lower styrene content. The Vinylester during the curing process is forming a gel initially which helps to get a uniform glass transition temperature across the composite. In this research, the Vinylester resin was mixed with curing agents which were an initiator NOROX® MEKP-925H and a promotor Cobalt Naphtenate-6%. The typical

properties of the initiator are shown in table 18. These curing agents can control the gelation time of the Vinylester resin which is an important factor to control the wetting of the preform that affects the performance of the composite. The short gelation time causes unsaturated dry spots because once the gelation happens the flow of the resin stops. On the other hand, the long gelation time decreases the productivity, so it is very critical to be able to control the curing time of the resin. In this research, the following infusion parameters are depicted in table 19.

Table 16. Typical properties of the liquid Derakane® 8084 Vinylester resin

Property	Value
Density, 25°C	1.02 g/mL
Dynamic Viscosity, 25°C	360 mPa·s (cP)
Kinematic Viscosity	350 CST
Styrene Content	40%
Shelf Life, Dark, 25°C	6 months

Table 17. Typical properties of the cured Derakane® 8084 Vinylester resin

Property	Value	Test Method
Tensile Strength	76 MPa	ASTM D-638 / ISO 527
Tensile Modulus	2.9 GPa	ASTM D-638 / ISO 527
Tensile Elongation, Yield	8-10%	ASTM D-638 / ISO 527
Flexural Strength	130 MPa	ASTM D-790 / ISO 178
Flexural Modulus	3.3 GPa	ASTM D-790 / ISO 178
Density	1.14 g/cm ³	ASTM D-792 / ISO 1183
Volume Shrinkage	8.2%	
Heat Distortion Temperature	82°C	ASTM D-648 Method A / ISO 75
Glass Transition Temperature, T _{g2}	115°C	ASTM D-3419 / ISO 11359-2
IZOD Impact (unnotched)	480 J/m	ASTM D-256
Barcol Hardness	30	ASTM D-2583 / EN59

Table 18. Typical properties of the initiator NOROX® MEKP-925H

Property	Value
Active Oxygen	9.0 %, max
Form	Liquid
Color	Water white
Specific Gravity @ 25°C/4°C	1.10

Table 19. The infusion parameters

Temperature	24°C
Time	60±15 Minutes
MEKP (Initiator), wt. %	1.5
CoNap6% (Promoter) , wt. %	0.3

4.2. Experimental Design

Two experimental designs A and B have been structured to: (1) verify the generalized model to predict the entire tensile load-extension of 3DOW composites made from natural spun yarns (hemp and flax) model experimentally, (2) Apply the model on 3DOW composites from preforms with enhanced surface treatment and find out whether the treatment affects the model prediction and (3) Compare between the properties of composites from natural fibers (hemp and flax) and glass and high performance synthetic fibers to identify applications for the green composites.

4.2.1. Design of Experiment A

Design of experiment A aimed to fulfill objectives (1) and (3) in which different levels of three preform architectural parameters have been varied to study their effects on the performance of the 3DOW composites. The preforms were designed to be volume-balanced in the X and Y-directions (the x-fiber volume fraction equals y-fiber volume fraction) to achieve the best interlaminar performance (26). Table 20 shows the variables and levels of experimental design A along with the total number of runs.

Table 20. Variables and their levels of design of experiment A

Variables	Values	Levels
No. of Y layers (X-yarn density Picks/cm for volume-balanced structures)	3 (2.02), 6 (2.31), 9 (2.43)	3
Z/ Y ratio	1:1, 1:3	2
Weaves	Plain, 2x2 warp rib, 3x3 warp rib	3
Total no. of runs	3 x 2 x 3	18

In this design of experiment, the Y-yarns density kept constant and bleached flax X, Y and Z-yarns were used.

4.2.2. Design of Experiment B

The experimental design B was structured to achieve objectives (1) and (2). In this design of experiment, different flax yarns were used in the X-direction to study the effect of the surface

treatment on the model prediction since the treatment affects the fiber surface characteristics and hence the interfacial bonding between the resin and fiber, which in turn impacts the tensile properties of the composites . Two levels of the number of Y-yarn layers are included in this design. The experimental design variables and levels are listed in table 21.

Table 21. Design of experiment B

Variables	Values	Levels
X-Yarn Type	Grey, HS., Bleached HS.	3
No. of layers (X-yarn density Picks/cm for volume-balanced structures)	3 (2.02), 6 (2.31)	2
Total no. of samples	3 x 2	6

The fixed parameters in this experimental design were; plain weave, 1:1 Z/ Y ratio, Y-yarns density, Y, Z-yarns were bleached.

4.3. Preforms Formation

Preforms were woven using the 3D weaving machine, shown in Figure 54, which is housed in the composite core facility at the Wilson College of Textiles, NC State University. This machine was donated by 3TEX Inc. The Y- and Z-yarns are directly supplied from two creels which can hold up to 1088 yarn packages. X-yarn packages are supplied by additional side creel. The weft insertion mechanism in this loom is single rigid rapier/X-yarn. In each insertion cycle, two X-yarns are inserted simultaneously since the yarns are fed continuously without cutting after each

insertion. All yarns were back wound from as supplied large packages to cylindrical packages to fit holders of the two creels utilized.

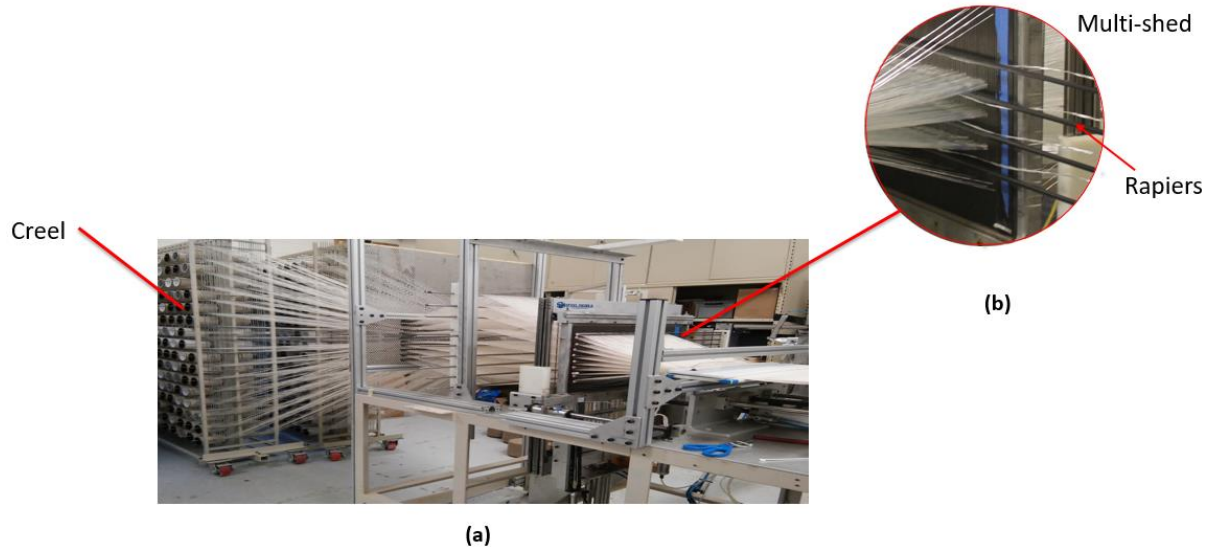


Figure 54. (a) view of the 3D weaving loom, (b) multi-insertion of weft yarns

Each warp yarn layer on the loom has 102 Y-yarns with an even yarn spacing using a reed with a dent density of 2.36 dents/cm (6 dents/inch) with one Y-yarn/layer and one Z-yarn in each dent in case of 1:1 Z to Y-yarn ratio. One Y-yarn/layer in each dent and a Z-yarn every three dents were set in case of 1:3 Z to Y-yarn ratio as shown in figure 55. One meter of each preform (24 preforms in total for design of experiments A and B) was woven with a width of 43 cm excluding the selvages. Two selvage Z-yarns were added at the edges of the preform to prevent the unraveling of X-yarns.

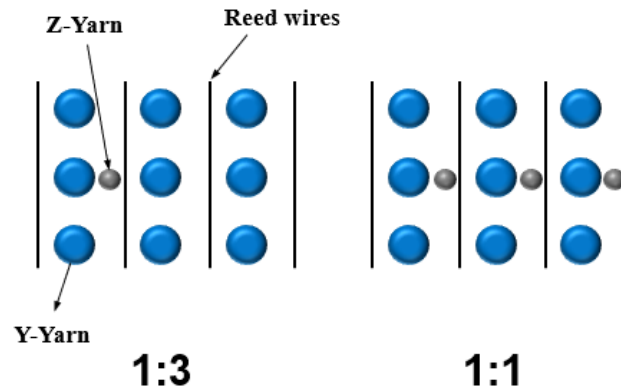


Figure 55. Denting Plan

4.4. Resin Infusion

In order to transform the 3DOW preforms into composites, each sample has been divided into two half-meter each to achieve the best uniform infusion. Each half-sample was consolidated using a vacuum assisted resin transfer molding technique (VARTM) using a VacMobiles® 20/2 equipment shown in Figure 56 (a). The VARTM system is available at the composite core facility, Wilson College of Textiles, NC State University.

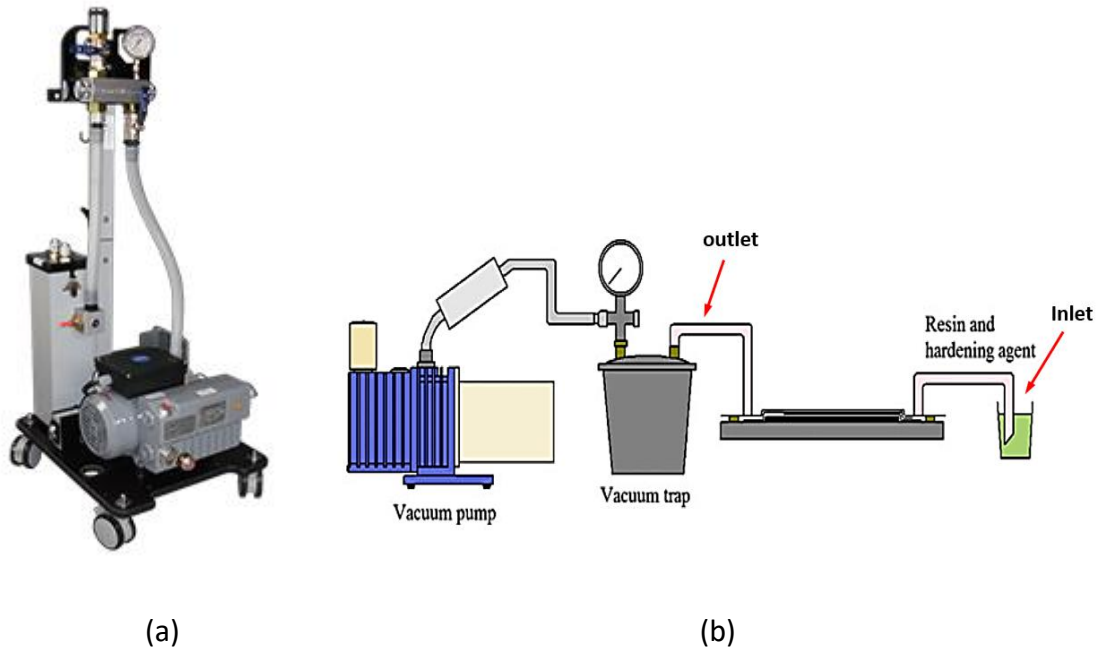


Figure 56. (a) VacMobiles® vacuum pump, (b) A schematic diagram of the VARTM technique

In the VARTM technique, the preform is placed over a release film that is put over a glass top table. After that, another release film of polyester fabric is laid over the preform. Then, a resin distribution (green flow) media was used in order to eliminate the permeability effect in the thickness direction. Resin inlet spiral tubes and resin inlet and outlet port were placed over the preform. In the end, a plastic bagging is placed over all these layers and is sealed using double-sided tape. After vacuum application using the vacuum pump, the system is checked for air leakage using the Amprobe TMULD-300 ultra-sonic leak detector. The resin mixture is prepared and infused through the sample and then a solidified panel of the composite is finalized.

4.5. Testing and Evaluation

4.5.1. Fiber Testing

Fiber density and tensile properties have been measured for the following types of fibers: hemp, grey flax, bleached flax, high strength flax and bleached high strength flax. For each type of

fiber, about 150 single fibers have been extracted carefully and randomly from yarns to be evaluated. Before testing, all the fibers were conditioned for at least 24 hours at 70 ± 2 degree Fahrenheit and $65\% \pm 2$ relative humidity.

The Vibromat testing instrument, shown in Figure 57, was used to measure fiber's linear density (denier) following the ASTM D1577-07. The Vibromat is located at the physical testing lab, Wilson College of Textiles, NC State University. 150 fibers were extracted from yarns for each type of fibers to be tested individually. This method is based on the vibrating string principle in which the linear density of fibers can be measured from the fundamental resonant frequency of transverse vibration of a fiber measured under known conditions of length and tension. A pre-tension of 165 mg was used to straighten the fibers during the measurements.

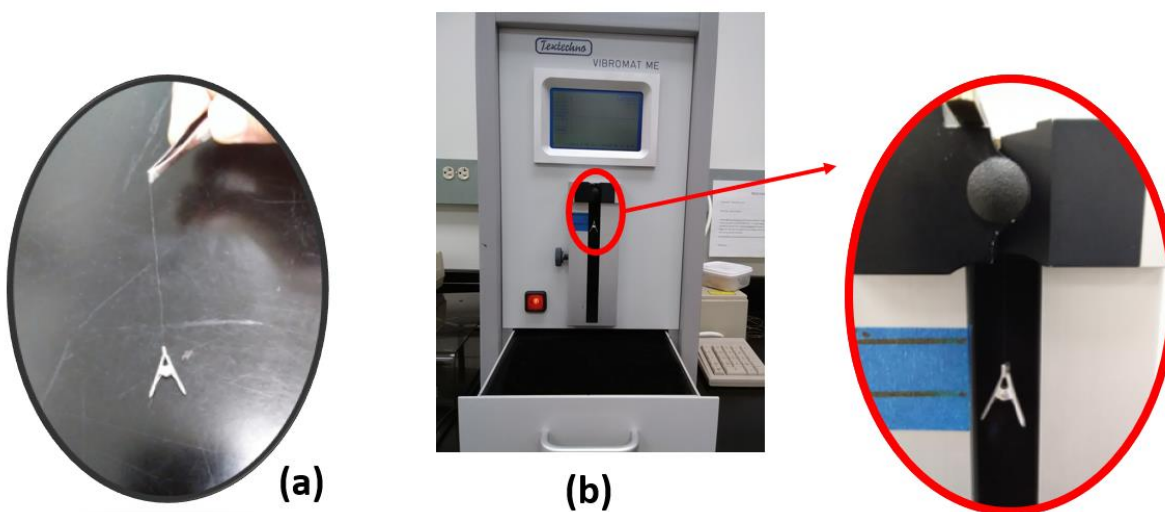


Figure 57. (a) An extracted fiber with a pre-tension at the end, (b) The Vibromat instrument

After measuring the linear density, the tensile properties of about 120 fibers/yarn were measured. Each fiber was mounted on paper frame by using glues and tapes as shown in Figure 58. The gauge length of single fiber specimens was 2.54 cm (1 inch). ASTM D3822 was followed to determine the tensile strength of single fiber using an MTS Q Test machine located at the

physical testing lab, Wilson College of Textiles, NC State University. A 0.2039 Kg (2 N) load cell, 15 mm/min elongation rate and grip pressure of 4.9 kg/cm² (70 psi) were used. The grips were equipped with rubber to reduce the stress concentration and achieve a better pressure distribution, which reduces the possibility of fiber slippage or breakage inside the grips. The paper frame was cut before starting the test as shown in Figure 59. Fibers that broke inside the either grip were not considered in the calculation of the average fiber tensile strength.

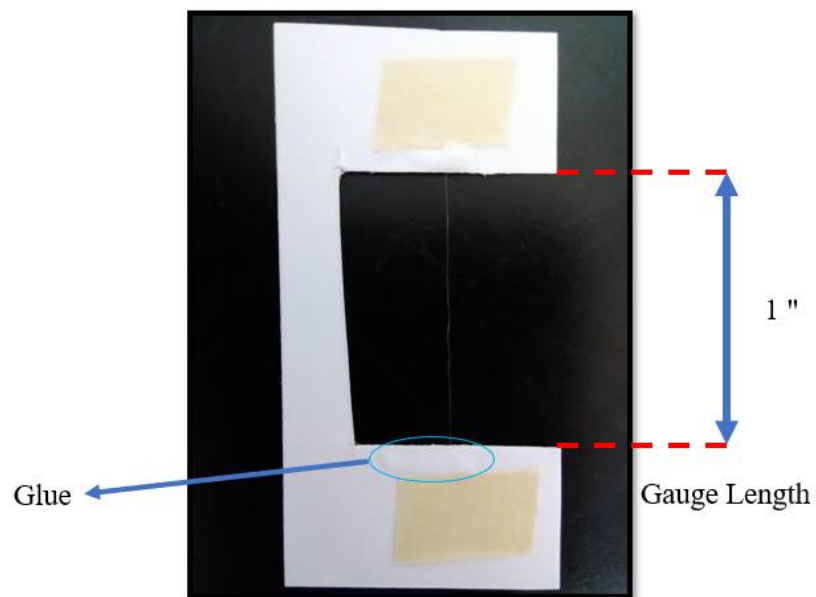


Figure 58. Cardboard frame used in single fiber tensile testing preparation

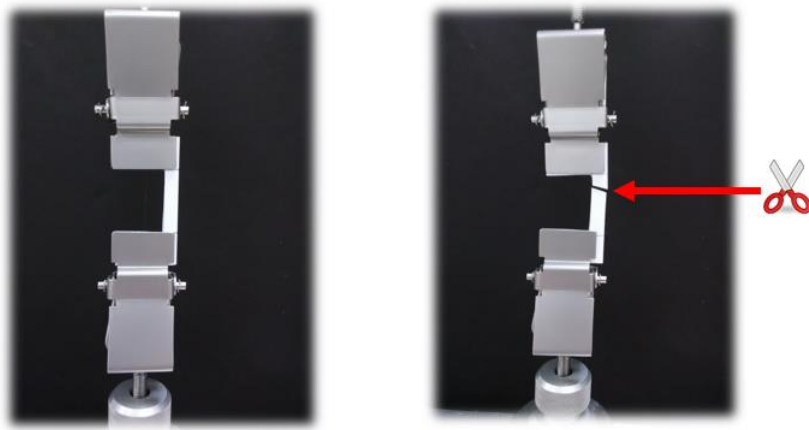


Figure 59. Cardboard frame inside the grips of the MTS Q Test machine

4.5.2. Yarn Testing

The ASTM D1907 was followed to measure the linear density of yarn. A 109.73 m (120 yards) of nine specimens from three different packages (three from each) of each type of yarn were wound on a skein winder and weighed using a four-digit scale (0.0001 milligram accuracy).

Figure 60 pictures the skein winder and the weight scale

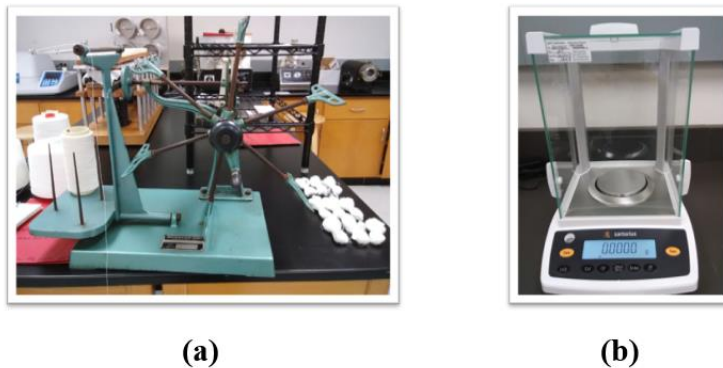


Figure 60. (a) Skein winder, (b) A scale

Hemp and flax yarns' tensile properties were measured according to ASTM D2256/ D2256-10. Different gauge lengths of 25.4 cm (10 inches), 2.45 cm (1 inch), and 1.27 cm (0.5 inch) were

considered using an MTS Q Test machine with different load cells and gripping conditions. The testing parameters of each gauge length are listed in Table 22. The load-extension curves of 2.54 cm gauge length were used as input to the model discussed in chapter 6. For the 25.4 cm gauge length, snipping grips were used, however for the 2.54 cm and the 1.27 cm gauge lengths, each yarn specimen was taped and glued in a paper frame as the one used in the single fiber testing.

Table 22. The testing parameters of yarn tensile properties using the MTS Q Test machine

Gauge length (cm)	Load cell (kg)	Elongation rate (mm/min)	Grip pressure (kg/cm²)	Number of specimens
25.4	453.6	304.8	4.22	10
2.54	113.4	15	5.6	15
1.27	113.4	15	5.6	10

The twist per meter (TPM) for all hemp and flax yarns were measured according to ASTM D1422 using the Twistmeter shown in Figure 61. Twenty-five specimens were measured for each yarn type.



Figure 61. Yarn Twistmeter

In order to predict the composite tensile properties, the load-elongation of the fibers and the number of fibers in yarn cross-section are needed as input parameters to the model. Bleached X-, Y- and Z-yarns from flax fibers were sized using 20% solid sizing solution with the use of PhilBind L-1000 sizing agent from Philchem and a red dye as shown in Figure 62 (a). A sizing winder shown in Figure 62 (b) located at the weaving lab, Wilson College of Textiles, NC State University was used to prepare the sized yarns, which was run at 43 m/min. Sizing the yarn made it stiff enough to cut by a razor to create yarn cross section according to the following procedures. After conditioning, the sized yarns were coated by synthetic fibers and squeezed through a foam using a sewing thread and a sewing needle.

Each sized yarn with accompanied with filament yarn were pulled out from the foam pieces as shown in Figure 63 (b). After that, thin slices of the foam and the sized yarn surrounded by synthetic fibers were cut using sharp razor blades as indicated in Figure 64. Number of fibers in yarn's cross-section was calculated from pictures taken by Confocal microscope. Ten pictures of bleached X-, Y- and Z-flax yarns were captured and the average number of fibers in yarn cross-section of each yarn type was considered in the model in Chapter 6.



(a)



(b)

Figure 62. (a) Sizing winder (b) Size box contains solution with a red dye

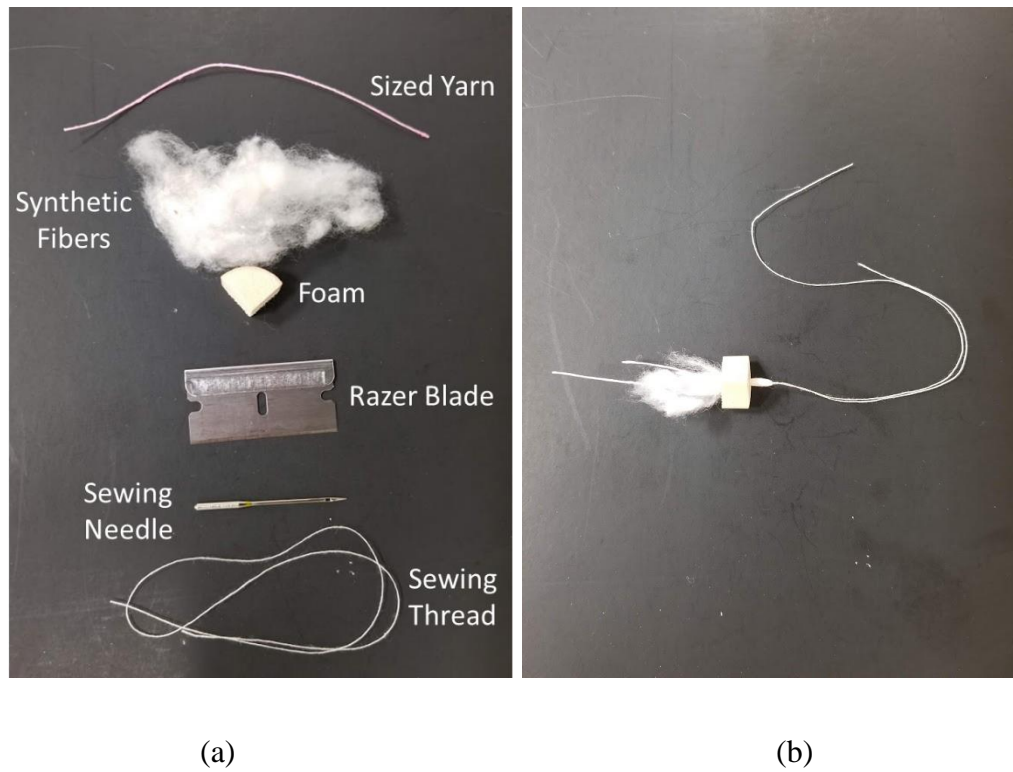


Figure 63. Steps of preparing yarn samples for the confocal: (a) Tools used to prepare the yarn cross-section (b) The sized yarn surrounded by synthetic fibers and squeezed through the foam



Figure 64. Slices of foam with sized yarn surrounded by synthetic fibers



Figure 65. Yarn cross-section captured by the confocal

4.5.3. Composite Testing

4.5.3.1. Sampling

For each sample, two composite panels had been produced with 50 cm length and 45 cm width each in average. The sampling plan was developed to maximize the utilization of each composite panel and to have at least five specimens for each test as required by the ASTM standards followed in this research. Figure 66 shows the cutting plan sufficient representative specimens used in this research. The cutting plan was drawn first using Adobe Illustrator and cut by a computerized waterjet cutting technology available at ADR Hydro-Cut, Inc., Morrisville, NC. Waterjet cutting was chosen due to its preciseness in terms of dimensions with a very low coefficient of variation (less than 0.1%). In addition, it does not cause any thermal induced damages or delamination to the composite which are common with the conventional CNC cutting.

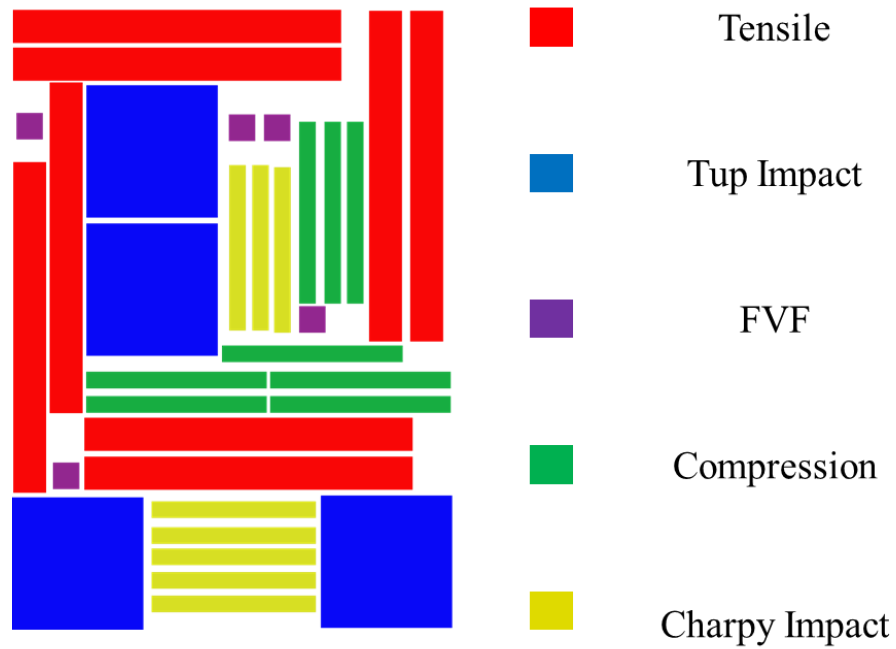
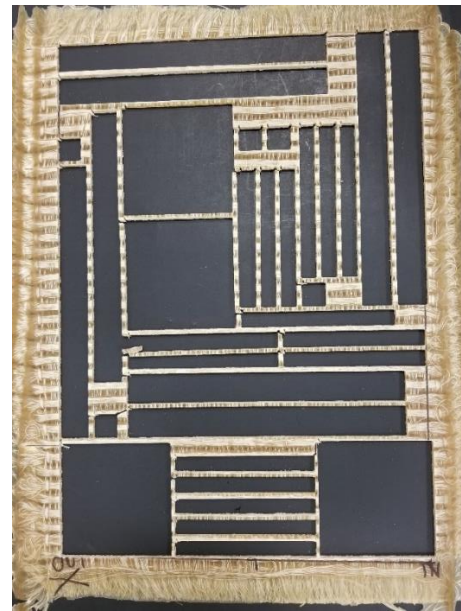


Figure 66. Cutting plan



(a)



(b)

Figure 67. Composite panel (a) after waterjet cutting and (b) after removing specimens

4.5.3.2. Fiber volume fraction

Fiber volume fraction (FVF) plays an important role in the properties of the composite as it represents the fiber percentage within the entire composite. Theoretically, fiber volume fraction can be calculated using a combination of densities, yarns' linear density and the geometrical parameters of the preform. In this research, a theoretical FVF was calculated using equations (17-19) in Chapter 6 and compared to the measured using equation (2). Preform and composite weight was calculated directly from the composite panels before and after infusion. Flax and Hemp fibers' densities were used as 1.43 and 1.48 (g/cm³), respectively (12,66). Composite density was calculated using a density kit. A specimen (8 mm x 8 mm) was placed in a beaker and the weight was measured in air and in water as shown in Figure 68. The average of five specimens from each sample are listed in Tables 23 and 24 which show a comparison between the theoretical and the experimental FVF of the samples of experimental designs A and B, respectively.

$$FVF = \frac{\text{Preform weight (g)}/\text{fiber density } (\frac{\text{g}}{\text{cm}^3})}{\text{composite weight (g)}/\text{composite density } (\frac{\text{g}}{\text{cm}^3})} * 100 \quad (2)$$

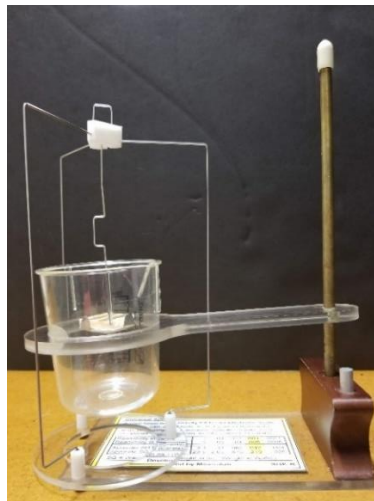


Figure 68. Density Kit

Table 23. Theoretical and experimental FVF of samples- Experimental design A

Sample ID	Y-layers	Z/Y Dent Ratio	Weave	X-yarns density (picks/ inch/ layer)	Measured FVF	Calculated FVF
3L-1	3	1:1	Plain	10.28	22.83	17.75
3L-2	3	1:1	2x2 Warp Rib	10.28	24.42	17.14
3L-3	3	1:1	3x3 Warp Rib	10.28	24.94	16.93
3L-4	3	1:3	Plain	10.28	23.04	16.83
3L-5	3	1:3	2x2 Warp Rib	10.28	22.79	16.63
3L-6	3	1:3	3x3 Warp Rib	10.28	22.84	16.56
6L-1	6	1:1	Plain	11.76	25.81	29.80
6L-2	6	1:1	2x2 Warp Rib	11.76	24.61	27.78
6L-3	6	1:1	3x3 Warp Rib	11.76	24.35	27.10
6L-4	6	1:3	Plain	11.76	25.70	26.98
6L-5	6	1:3	2x2 Warp Rib	11.76	25.53	26.31
6L-6	6	1:3	3x3 Warp Rib	11.76	24.90	26.09
9L-1	9	1:1	Plain	12.34	27.62	30.10
9L-2	9	1:1	2x2 Warp Rib	12.34	27.25	28.04
9L-3	9	1:1	3x3 Warp Rib	12.34	27.36	27.36
9L-4	9	1:3	Plain	12.34	27.29	27.27
9L-5	9	1:3	2x2 Warp Rib	12.34	27.04	26.59
9L-6	9	1:3	3x3 Warp Rib	12.34	27.44	26.36

Table 24. Theoretical and experimental FVF of samples- experimental design B

Sample ID	Y-layers	Filling Yarn	X-yarns density (picks/ inch/ layer)	Measured FVF	Calculated FVF
3L-1	3	Bleached	10.28	22.83	17.75
3L-7	3	BHS	10.28	25.01	17.61
3L-8	3	HS	10.28	24.26	14.69
3L-9	3	Grey	10.28	22.13	15.29
6L-1	6	Bleached	11.76	25.81	29.80
6L-7	6	BHS	11.76	26.05	29.63
6L-8	6	HS	11.76	26.79	26.02
6L-9	6	Grey	11.76	25.71	26.73

4.5.3.3.Tensile

MTS Servo-hydraulic 370 load frame, showed in Figure 69, located at the Composite Core Facility, Wilson College of Textiles, NC State University was used to evaluate the tensile properties of the composite produced in this research. The testing device has 250 KN load capacity. The ASTM D3039 was followed to measure the tensile properties of the composites in the X- and Y-axis directions. A five specimens in each direction (254 mm x 25.4 mm) each were used with a gauge length 154 mm and a 50 mm gripping length. A 1mm/min cross head speed was used with different gripping pressure that was changed accordingly with the number of Y-

yarn layer to obtain optimum gripping and avoid any slippage or crushing in the specimen. A 1000, 1800 and 2000 MPa gripping pressures were used for 3 layers, 6 layers and 9 layers, respectively.



Figure 69. MTS Servo-hydraulic 370 load frame

4.5.3.4. Tup impact

Instron Drop Tower Impact CEAST 9350 showed in Figure 70 (a) and located at the Composite Core Facility, Wilson College of Textiles, NC State University was utilized to measure the impact resistance of the composite in which the specimen was pneumatically clamped and then punched by the hemispherical striker according to ASTM D3763-15 Standard Test Method for High-Speed Puncture Properties of Plastics Using Load and Displacement Sensors. The striker was connected to a piezoelectric transducer to measure the force employed on the specimen in the direction of impact. The specimen size was 101.6 mm x 101.6 mm and the impact velocity

was 4.4 m/s with a maximum 20% change. A 49.7 J force was used for all specimens which was suitable for breaking samples with 9 Y-Yarn layers. No extra dead weight was used because the specimens were sensitive to high impact energy. Five specimens were tested from each sample.

4.5.3.5.Charpy impact

For Testing the Charpy impact properties of the composite, Instron Pendulum Impactor II showed in Figure 70 (b) and located at the Composite Core Facility, Wilson College of Textiles, NC State University was used. The ASTM D6110: Standard Test Method for Determining the Charpy Impact Resistance of Notched Specimens of Plastics was followed to test the Charpy impact resistance of composite specimens in the X- and Y-axis directions. In this research, the specimens were not notched although, this was recommended by the ASTM standard because this would reduce the impact resistance more. Five specimens of 127 mm length and 12.7 mm width in each direction were tested with a striker energy of 10.8 J which was enough to break the specimen while maintaining the absorbed energy level less than 80% of the striker energy.



Figure 70. Instron impact testing equipment, (a) drop tower impact CEAST 9350, and (b) pendulum impactor II

4.5.3.6.Compression

For testing the compression properties of the composites, the MTS Servo-hydraulic 370 load frame in Figure 69 was utilized. The ASTM D-6641 for Compression Properties of Polymer Matrix Composite Materials Using a Combined Loading Compression (CLC) Test Fixture in which the loading is a combination of shear and end loading was followed. The CLC fixture consists of four steel blocks with specimen gripping surfaces coated with tungsten carbide (Figure 71 (a)), each pair are clamped together with four bolts. Five specimens in each direction from each panel were tested with a specimen size of 152.4 mm x 12.7 mm and the gauge length was 12.7 mm. Figure 71 (b) shows a fractured specimen after compression test.

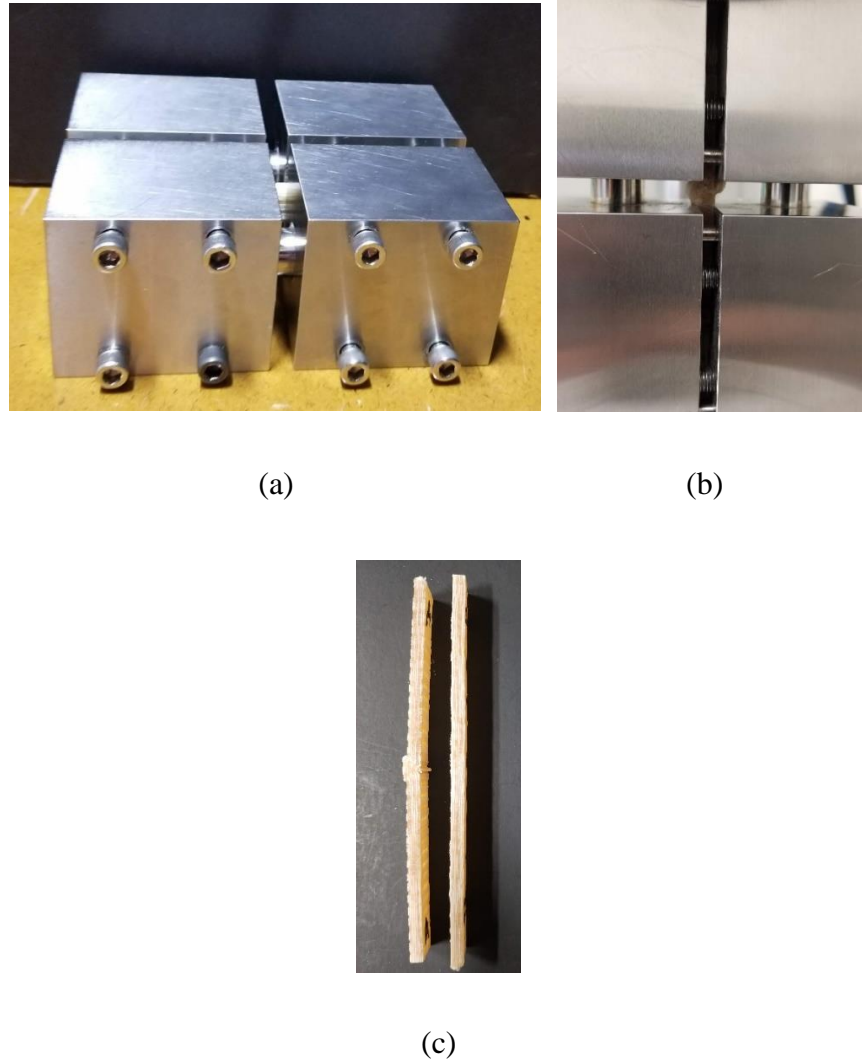


Figure 71. (a) CLC fixture, (b) A compression specimen fixed between CLC fixture (c)

Composite specimens before and after compression

4.5.4. Resin Tensile Properties

Pure resin panels have been produced and cut to obtain the load-extension cure of the resin. A resin mixture was prepared and pored inside a mold then let dry for 24 hours, then the pure resin panel was cut into coupons with sizes 152.4 mm in length, and 35.56 mm in width. MTS Servo-hydraulic 370 load frame (shown in Figure 69), was used to measure the tensile properties of the pure resin coupons following the ASTM D3039.

4.5.5. Statistical Analysis

JMP software was employed to analyze the data. Specifically, ANOVA (Analysis of Variance) and Tukey HSD (Honestly Significant Difference) were used to evaluate the effect of structural parameters of 3DOW composites on their mechanical properties. The independent structural parameters used were number of Y-yarn layers, weave and Z- to Y-yarn ratio. Responses (dependent variables) assessed were composite tensile, impact (Tup and Charpy), and compression properties.

5. RESULTS AND DISCUSSION

This chapter is devoted to present and discuss the results of the fiber, yarn and composites. The effects of structural parameters including weave, number of Y-yarn layers and Z- to Y-yarn ratio in addition to the type of X-yarn on the mechanical properties of the 3DOW composites are discussed in detail. The statistical analysis was used to find out whether a response is significantly influenced by the independent parameters at 95% confidence level.

5.1. Results of Fiber Testing

5.1.1. Fiber Linear Density

Flax and hemp yarns (tables 26) were untwisted to facilitate picking fibers without damage. Single fibers were tested for their denier using the Vibromat testing instrument as discussed in Chapter 4. From each yarn type (list), 150 fibers were tested. Table 25 shows the average denier of each type of fibers. Figure 72 shows the frequency distribution of the denier of bleached flax fibers which revealed the inherent variability in natural fibers in terms of their linear density. The frequency distribution of the other types of fibers are shown in Appendix A.1 (Figures 163- 164).

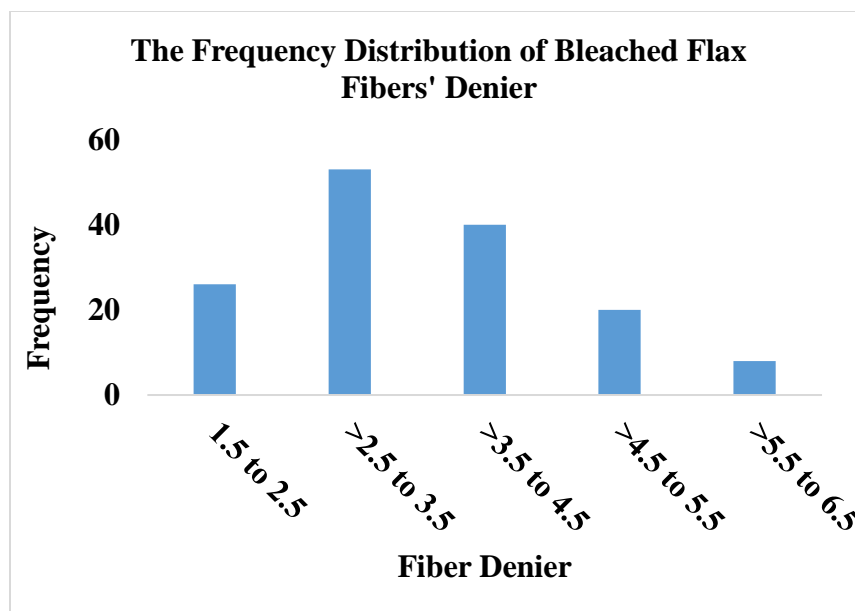


Figure 72. Frequency distribution of denier of bleached flax fibers

5.1.2. Fiber Tensile Properties

After measuring single fiber's linear density, each fiber was mounted on paper frame using glues and tapes and the tensile properties of individual fiber were measured as discussed in Chapter 4. Fibers that broke inside either grips were discarded from the calculation of the average fiber tensile strength. Table 25 shows the average data of fiber strength, elongation and modulus of each fiber type and all the data of glass fibers are averaged from three glass yarn. The glass fiber data obtained from Xie (67). Graphs of fiber tensile properties are in Appendix A.2 (Figures 165-171) and the Load-Elongation curves are in Appendix A.3 (Figure 172). Secant modulus at 10% breaking load was determined for each fiber type since the initial modulus was affected by the manual pretension while fixing the sample in the tensile tester jaws. The specific strength, modulus and secant modulus were calculated by dividing the strength, modulus and secant modulus by fiber linear density. Since the density of flax and hemp fibers are lower than that of glass fibers, the specific strength of all natural fibers used in this research was higher than that of

glass fibers which is a major advantage that supports one of the objectives of this study to produce composites from high strength natural fibers to reduce the environmental impacts of using glass fibers.

It is observed that in general, the CV% of all tensile properties of bleached flax, grey flax and hemp fibers are higher than that of bleached high strength flax and high strength flax fibers. The latter are closer to the CV% of glass fibers' data. This reduction in variability is due to the fiber selection and sorting at the flax yarn supplier (ALBANA LINEN, Tanta, Egypt) manufacturing facility upon our request to obtain high quality, high strength bleached and unbleached flax yarns. This explains the high strength of these two fiber types compared to the other natural fibers.

It is noted that, the bleached flax and the high strength bleached flax fibers has lower strength than grey flax and high strength flax fibers. This was because of the bleaching process that was carried out to clean the surface of the fibers that caused chemical damages to the individual fibers and resulted in reduction in the fiber strength.

Table 25. Average linear density and tensile properties of 150 single fibers of each fiber type

Fiber Type	Fiber Linear Density, Denier (CV%)	Tenacity, gf/ den (CV%)	Specific Strength, gf/ den/g/cm³ (CV%)	Elo., % (CV%)	Modulus, gf/ den (CV%)	Specific Modulus, gf/ den/g/cm³ (CV%)	Specific Secant Modulus at 10% Breaking Load, gf/ den (CV%)
Bl. Flax	3.55 (31)	6.82 (33)	4.48 (33)	2.71 (38)	361.6 (65)	237.6 (65)	281.6 (47)
Grey Flax	3.67 (41)	7.00 (40)	4.60 (40)	2.63 (40)	292.5 (56)	192.5 (56)	247.3 (45)
BHS. Flax	2.87 (31)	8.98 (34)	5.91 (34)	4.79 (30)	115.3 (93)	75.9 (93)	142.2 (50)
HS. Flax	2.85 (32)	9.13 (37)	6.01 (37)	4.37 (26)	235.0 (81)	154.6 (81)	175.1 (67)
Hemp	4.48 (62)	6.02 (65)	3.96 (65)	3.86 (64)	244.1 (71)	160.6 (71)	202.3 (72)
Glass Fiber	5.14 (00)	8.33 (32)	3.28 (32)	3.14 (24)	311.5 (29)	122.7 (29)	122.7 (29)

5.2. Results of Yarn Testing

The linear density of each yarn type was measured according to the procedure explained in chapter 4 using a skein winder and a scale (Appendix A.4 (Figure 173)). For the yarn tensile properties, different gauge lengths of 25.4 cm (10 inches), 2.45 cm (1 inch), and 1.27 cm (0.5 inch) were considered using an MTS Q Test machine with different load cells and gripping conditions. Table 26 summarizes the tensile properties of the yarns of 2.54 cm gauge length. The data of 25.4 cm and 1.27 cm are in Appendix A.4 (Figures 174-183). The Load-Extension curves of yarns from flax and hemp fibers are in Appendix A.5 (Figure 186).

It can be noticed from Tables 25 and 26 that the fiber strength is significantly higher than the yarn strength in all cases. Two main reasons contribute to this effect. The first is the mechanism of yarn breakage during the tensile test where combination of fiber breakage and slippage occur. The slipped fibers do not contribute much to the load sharing. The second reason is the twist, which causes fiber to contribute less in the load direction due to fiber inclination to the yarn axis (test direction).

In general, the CV% of yarn properties are less than that of single fiber because the fibers' properties are averaged in the yarn cross-section. Hemp Z-yarn has the highest yarn tenacity among all the other hemp and flax yarns. The effect of the bleaching process was more significant when comparing bleached high strength flax yarn tenacity (4.9 gf/ den) and that of high strength flax yarn (4.1 gf/ den) even with higher twist level of the high strength flax yarn. The tenacity of grey flax X-yarn (3.3 gf/ den) was lower than that of the bleached flax X-yarn (4.1 gf /den). The high twist level of the grey flax X-yarns than that of the bleached flax X-yarn explains this difference.

Table 26. Average linear density and tensile properties of yarns measured at 2.54 cm gauge
length

Type of Fiber	Linear density, denier (CV%)	Tenacity, gf/ den (CV%)	Specific Strength, gf/ den/g/cm ³ (CV%)	Elongation, % (CV%)	Modulus, gf/ den (CV%)	Specific Modulus, gf/den /g/cm ³ (CV%)	Yarn Twist, TM (CV%)
Bl. Flax- X	1,521 (1.4)	4.1 (20)	2.7 (20)	5.4 (9)	123.3 (11)	81.1 (18)	3.27 (10)
Bl. Flax- Y	1,012 (5.6)	4.0 (13)	2.6 (13)	4.7 (14)	138.5 (13)	91.1 (13)	2.88 (11)
Bl. Flax- Z	446 (2.7)	4.1 (15)	2.7 (15)	3.8 (11)	136.2 (13)	89.6 (13)	2.87 (8)
Grey Flax- X	1,497 (2.8)	3.3 (15)	2.2 (15)	5.0 (11)	98.0 (12)	64.5 (12)	3.71 (6)
BHS Flax- X	1,053 (3.4)	4.1 (18)	2.7 (18)	5.2 (36)	64.9 (43)	42.7 (43)	3.50 (9)
HS Flax - X	1,041 (1.1)	4.9 (12)	3.2 (12)	4.3 (7)	97.0 (26)	63.8 (26)	3.42 (10)
Hemp - X	1,462 (3.2)	2.4 (33)	1.6 (33)	4.9 (22)	72.0 (35)	47.4 (35)	3.55 (14)
Hemp - Y	1,206 (4.1)	2.2 (22)	1.5 (22)	9.5 (17)	37.4 (24)	24.6 (24)	6.59 (3)
Hemp - Z	234 (5.3)	9.7 (21)	6.4 (21)	4.2 (11)	312.3 (42)	205.5 (42)	2.41 (12)
Glass Fiber	10,230 (0)	6.6 (7)	2.6 (7)	2.9 (4)	284.1 (3)	117.9 (3)	0.00

5.3. Results of Composite Testing

5.3.1. Experimental Design A

In design of experiment A, composite thickness (number of Y-yarn layers), Z-yarns interlacing pattern (weave design) and Z- to Y-yarn ratio have been changed to understand their effect on the tensile strength, compression strength and impact resistance of the 3DOW composites. The thicknesses of 3DOW composites are controlled by the number of Y-yarn layers (and X-yarn layers) and the resin saturation. The pick densities were chosen specifically to manufacture a volume balanced preforms in the X- and Y-directions for the different number of Y-yarn layers considering the rapier's double yarn insertion mechanism as two yarns are inserted per shed. In design of experiment A, X-, Y- and Z-yarns were bleached from flax fibers. All samples used in design of experiment A are listed in Table 27 along with their ID and independent variable parameters.

Table 27. Samples ID of experimental design A and their variable parameters

Sample ID	Y-layers	X-layers	Z/Y Dent Ratio	weave	X-yarns density (picks/inch/layer)
3L-1	3	4	1:1	Plain	10.28
3L-2	3	4	1:1	2x2 Warp Rib	10.28
3L-3	3	4	1:1	3x3 Warp Rib	10.28
3L-4	3	4	1:3	Plain	10.28
3L-5	3	4	1:3	2x2 Warp Rib	10.28
3L-6	3	4	1:3	3x3 Warp Rib	10.28
6L-1	6	7	1:1	Plain	11.76
6L-2	6	7	1:1	2x2 Warp Rib	11.76
6L-3	6	7	1:1	3x3 Warp Rib	11.76
6L-4	6	7	1:3	Plain	11.76
6L-5	6	7	1:3	2x2 Warp Rib	11.76
6L-6	6	7	1:3	3x3 Warp Rib	11.76
9L-1	9	10	1:1	Plain	12.34
9L-2	9	10	1:1	2x2 Warp Rib	12.34
9L-3	9	10	1:1	3x3 Warp Rib	12.34
9L-4	9	10	1:3	Plain	12.34
9L-5	9	10	1:3	2x2 Warp Rib	12.34
9L-6	9	10	1:3	3x3 Warp Rib	12.34

5.3.1.1. Tensile properties

The tensile properties of 3DOW composites with different fiber volume fraction and architectural parameters including number of Y-yarn layers (thickness), weave design and Z- to Y-yarns ratio were evaluated. In total, the 18 samples of experimental design A (180 specimens; 90 in the Y-yarn (warp) direction and 90 in the X-yarn (weft) direction) were tested. The results of the tensile test including the peak tensile load, failure strain and peak tensile stress were analyzed. A total of 90 (18x5) specimens from warp (Y-yarn) direction and the same number of specimens from weft (X-yarn) direction were analyzed using ANOVA and Tukey HSD to investigate the effect of the structural parameter on the tensile properties. The results of the tensile test in warp and weft directions are listed in Tables 28 and 29, respectively. Figure 73 shows a sample fixed in the MTS Load Frame with images of specimens after tensile test.

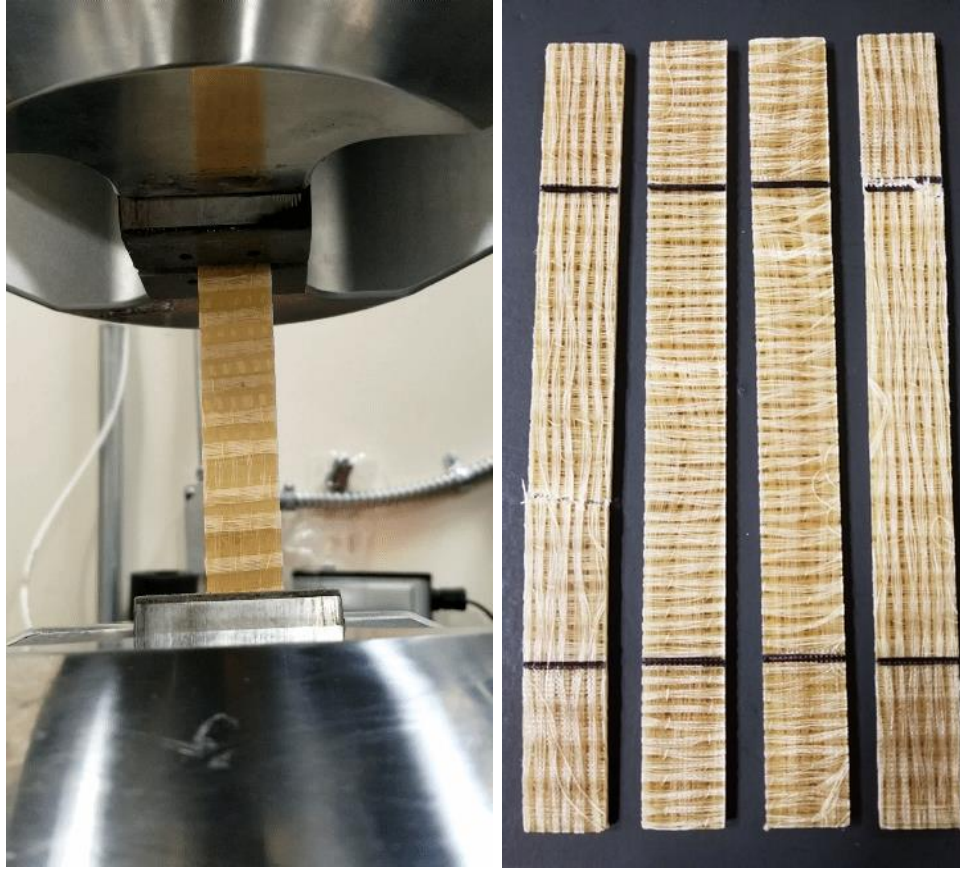


Figure 73. A specimen fixed in the MTS Load Frame along with tested specimens

ANOVA statistical analysis was used to analyze the results for the main effect of different architectural parameters (number of layers, weave design and Z- to Y-yarns ratio) on the tensile properties of the composites in Y- and X-directions as shown in Tables 49 and 53 (Appendix D.1.1). The load-extension curves of the tested specimens in the warp (Y-yarn) and weft (X-yarn) direction as shown in Appendix C.1 (Figures 198-200). In spite of the samples have a balanced structure (total linear density of fibers in the Y-direction/unit width is equal to the total linear density of fibers in the X-direction/unit length), the peak load of all the samples of the X-yarn (weft) direction was steadily higher than that of the Y-yarn (warp) direction because the weft yarns tensile strength is higher than that of the warp yarns (Table 26).

Table 28. Results of tensile test in the warp (Y-yarn) direction- experimental design A

Sample ID	Thickness of Tensile Specimens , mm	Modulus , Gpa (CV%)	Peak Tensile Load, KN (CV%)	Load/ Preform Areal Density, KN/ g/cm²	Load/ Comp. Areal Density, KN/ g/cm²	Peak Tensile Stress, Mpa (CV%)	Failure Strain, % (CV%)
3L-1	2.03	4.83 (0.4)	2.68 (4)	31.53	8.82	88.45 (7)	2.18 (4)
3L-2	1.81	5.23 (5)	2.24 (6)	24.46	7.32	82.76 (10)	1.99 (7)
3L-3	1.81	4.74 (7)	2.12 (10)	24.28	7.42	78.72 (16)	1.95 (7)
3L-4	1.90	5.19 (10)	2.20 (5)	24.12	6.81	77.22 (7)	1.81 (10)
3L-5	1.87	5.86 (10)	2.03 (18)	22.54	6.30	73.40 (22)	1.60 (22)
3L-6	2.02	5.41 (12)	2.26 (7)	24.42	6.92	74.52 (9)	1.70 (11)
6L-1	4.21	3.80 (4)	5.69 (11)	29.75	9.35	53.21 (9)	1.69 (9)
6L-2	3.89	3.91 (3)	5.63 (4)	32.07	9.63	57.04 (5)	1.77 (6)
6L-3	3.95	3.95 (4)	6.05 (5)	34.43	10.07	60.31 (3)	1.83 (6)
6L-4	3.95	3.93 (2)	6.49 (8)	34.69	10.66	64.72 (6)	2.11 (7)
6L-5	3.76	4.16 (2)	6.34 (7)	35.07	10.49	66.35 (5)	1.92 (8)
6L-6	4.00	4.07 (6)	5.73 (16)	31.76	9.45	56.68 (19)	1.66 (21)
9L-1	5.99	3.83 (2)	8.76 (7)	30.23	9.81	57.58 (3)	1.97 (6)
9L-2	5.88	3.66 (3)	8.41 (7)	30.79	9.75	56.34 (7)	1.93 (9)
9L-3	5.76	3.64 (4)	9.07 (10)	33.56	10.68	61.91 (8)	2.10 (10)
9L-4	5.98	3.58 (5)	8.78 (4)	31.68	10.09	57.74 (4)	2.11 (8)
9L-5	5.85	3.59 (6)	8.90 (8)	32.76	10.32	60.15 (12)	2.10 (12)
9L-6	5.86	9.50 (10)	7.90 (14)	28.78	9.27	53.64 (14)	1.79 (17)

Table 29. Results of tensile test in the weft (X-yarn) direction- experimental design A

Sample ID	Thickness of Tensile Specimens, mm	Modulus, Gpa (CV%)	Peak Tensile Load, KN (CV%)	Load/ Preform Areal Density, KN/ g/cm²	Load/ Comp. Areal Density, KN/ g/cm²	Peak Tensile Stress, Mpa (CV%)	Failure Strain, % (CV%)
3L-1	2.06	6.85 (3)	4.77 (3)	56.10	15.70	154.34 (3)	2.41 (2)
3L-2	1.89	7.25 (9)	3.46 (12)	37.84	11.32	123.05 (19)	1.89 (7)
3L-3	1.84	7.33 (22)	4.60 (21)	52.72	16.11	172.67 (32)	2.48 (13)
3L-4	1.92	7.48 (4)	4.71 (9)	51.59	14.57	163.52 (11)	2.34 (8)
3L-5	1.99	7.17 (8)	4.40 (13)	48.76	13.62	147.62 (11)	2.25 (17)
3L-6	1.87	7.74 (9)	4.31 (13)	46.70	13.24	154.68 (18)	2.14 (10)
6L-1	4.27	5.53 (5)	12.26 (5)	64.09	20.15	113.15 (6)	2.32 (7)
6L-2	3.95	5.83 (4)	10.47 (9)	59.59	17.90	104.38 (9)	2.05 (12)
6L-3	3.97	5.88 (4)	10.15 (5)	57.82	16.92	100.76 (6)	1.93 (7)
6L-4	4.04	5.69 (3)	13.04 (3)	69.74	21.42	127.07 (4)	2.52 (5)
6L-5	3.93	5.82 (2)	10.31 (6)	57.04	17.07	103.44 (6)	2.00 (6)
6L-6	3.87	5.91 (6)	9.97 (14)	55.29	16.45	102.11 (17)	1.95 (17)
9L-1	6.07	5.58 (1)	17.65 (6)	60.86	19.76	114.52 (6)	2.48 (6)
9L-2	5.83	5.31 (4)	16.95 (7)	62.07	19.65	114.53 (8)	2.47 (11)
9L-3	5.77	5.29 (3)	14.56 (13)	53.87	17.15	99.50 (15)	2.09 (13)
9L-4	5.86	5.19 (1)	16.72 (1)	60.34	19.22	112.45 (5)	2.53 (2)
9L-5	5.84	5.42 (2)	16.54 (4)	60.86	19.17	111.29 (4)	2.37 (3)
9L-6	5.84	12.27 (6)	14.30 (5)	52.12	16.78	96.61 (7)	2.11 (10)

Main effect of number of layers on tensile properties

Figure 74 shows the effect of number of layers on the tensile peak load in the X- and Y- directions. The graph indicates that there is a significant difference of the tensile load between the samples with different layers or thickness which was confirmed using ANOVA analysis in Appendix D.1.1 (Table 49 & 53 and Figure 211 & 219). As the number of warp layers increased, a gradual rise in the tensile peak load was observed. This was due to the difference in the number of X- and Y-yarns, the higher the number of warp yarn layers, the higher the number of X- and Y-yarns contributed towards the tensile load. The peak load was normalized by several approaches to segregate the effect of dependent parameters from the analysis and to have a rational and fair comparison between the samples regardless of the thickness. The peak load was normalized in the warp and weft directions, by preform areal density and composite areal density as shown in Figures 75 and 76, respectively. The normalized peak load in both warp and weft directions showed a significant difference between composites with different layers (Appendix D.1.1 (Tables 50-52 & 54-56). Tukey multiple mean comparison indicated a significant difference of the normalized tensile load between 3 Y-yarn layers and 6 and 9 Y-yarn layers, however there was no substantial difference between 6 and 9 Y-yarn layers as shown in Appendix D.1.1 (Figures 213, 215, 217, 211, 233 and 225). This was because the low FVF of the 3 Y-yarn layers as indicated in Table 23. In addition, the fabric structure formation in 3D woven composites plays an integral part in determining the tensile properties of the composite. In order to keep the defects as minimum as possible, straight alignment of yarns was very important. However, in case of 3 Y-yarn layers, the probability of missing the straight alignment of yarns within the preform was higher.

The tensile strain and tensile stress in X- and Y-directions are illustrated in Figures 77 and 78, respectively. The graphs indicate no significant effect of number of layers on tensile strain and stress in the warp as it can be seen from the error bars however, the 3 Y-yarn layers showed a higher stress in the weft direction because of the significant difference in specimens' thickness in the 3 warp layers when compared to 6 and 9 warp layers.

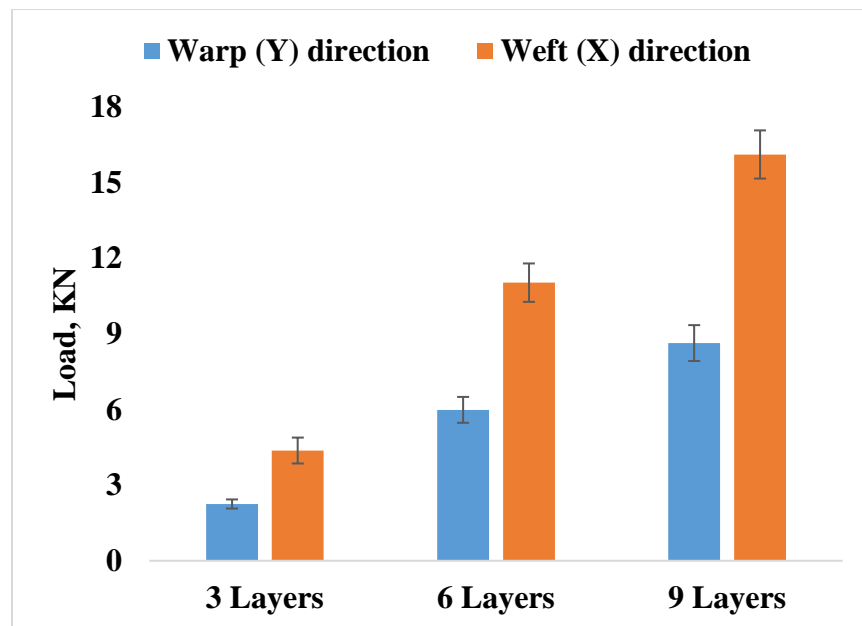


Figure 74. Main effect of layers on tensile load

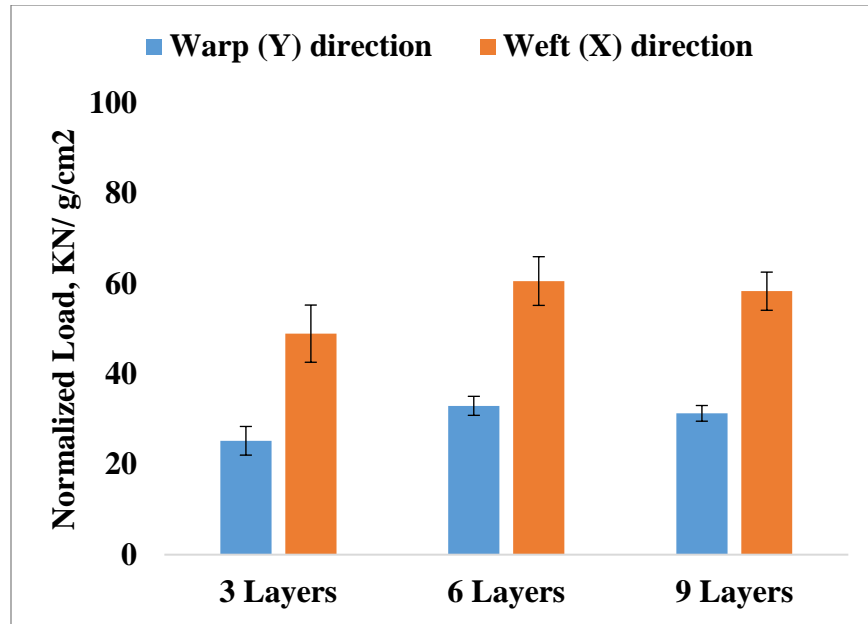


Figure 75. Main effect of layers on tensile load normalized by preform areal density

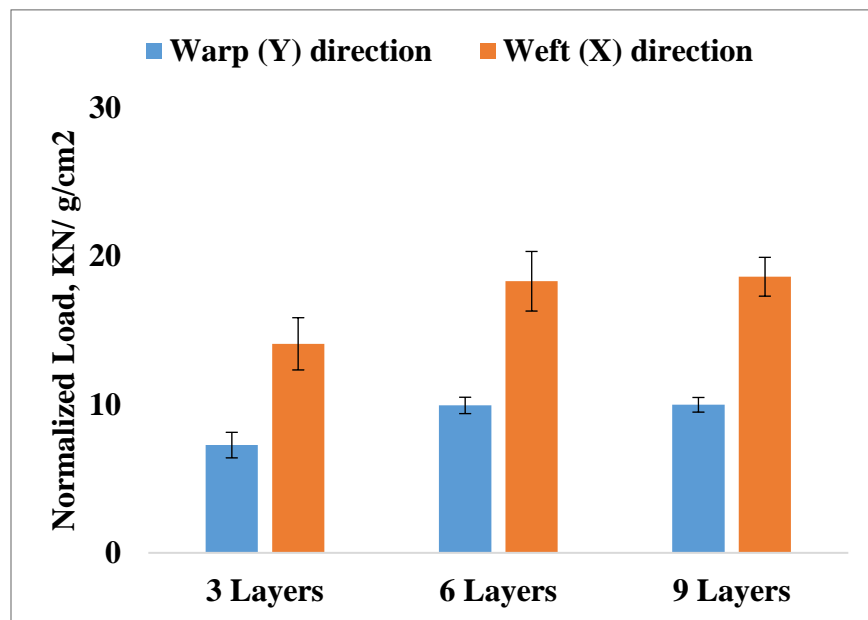


Figure 76. Main effect of layers on tensile load normalized by composite areal density

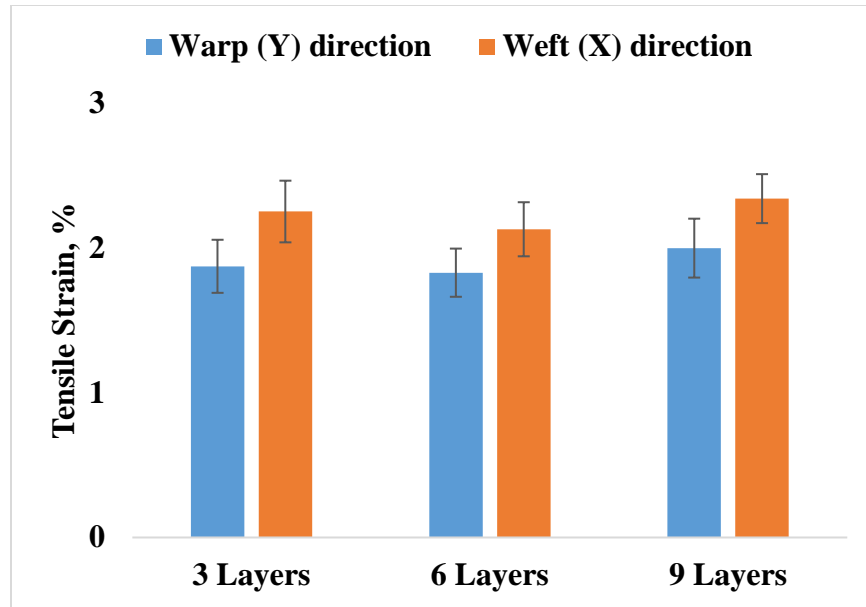


Figure 77. Main effect of layers on tensile strain

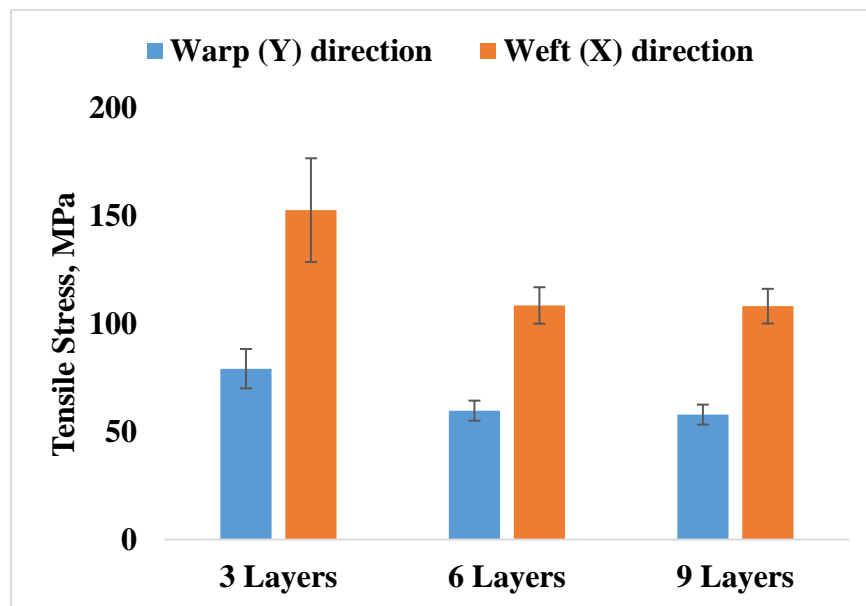


Figure 78. Main effect of layers on tensile stress

Main effect of weave on tensile properties

Figure 79 shows the effect of weave on the tensile peak load in the X- and Y-directions. The graph indicated that there was no significant difference between the samples with different

weave pattern in the Y-direction however, plain weave had a significant high peak load compared to 2x2 warp rib and 3x3 warp rib. This difference happened since plain woven structures provide more reinforcement through the thickness and therefore reduces the formation of resin rich areas compared to the 2x2 warp rib and 3x3 warp rib weaves. The peak load was normalized by the preform areal density and the composite areal density as indicated in Figures 80 and 81, respectively. The figures show the same effect of the weave pattern on the normalized peak tensile load in the X- and Y-direction. Plain weave was significantly different from 2x2 warp rib and 3x3 wrap rib in weft direction however, there was no effect of the weave in the warp direction. Similar trends were seen for the effect of weave on the tensile stress in the warp and weft direction as indicated in Figure 83.

ANOVA and Tukey analyses as indicated in Appendix D.1.1 (Table 49-56 and Figures 212, 214, 216, 218, 220, 222, 224 and 226) illustrate that there was no significant difference between the weave pattern namely plain, 2x2 warp rib and 3x3 warp rib in the warp direction while, plain weave showed a significant difference compared to 2x2 warp rib and 3x3 warp rib in the weft direction.

The tensile strain in X- and Y-directions, as illustrated in Figure 82, indicates that there was no significant difference between the tensile strain of the samples in both warp and weft directions while changing the weave pattern.

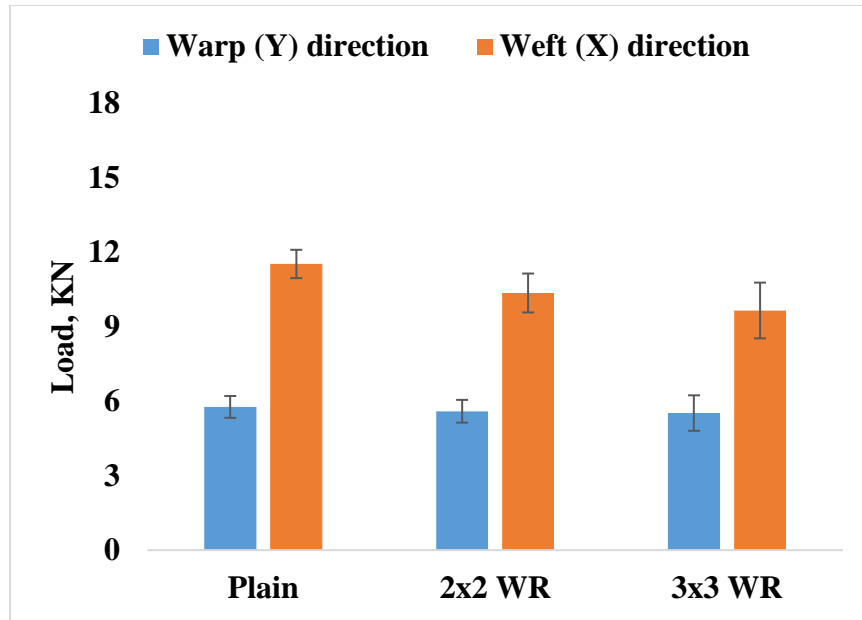


Figure 79. Main effect of weave on tensile load

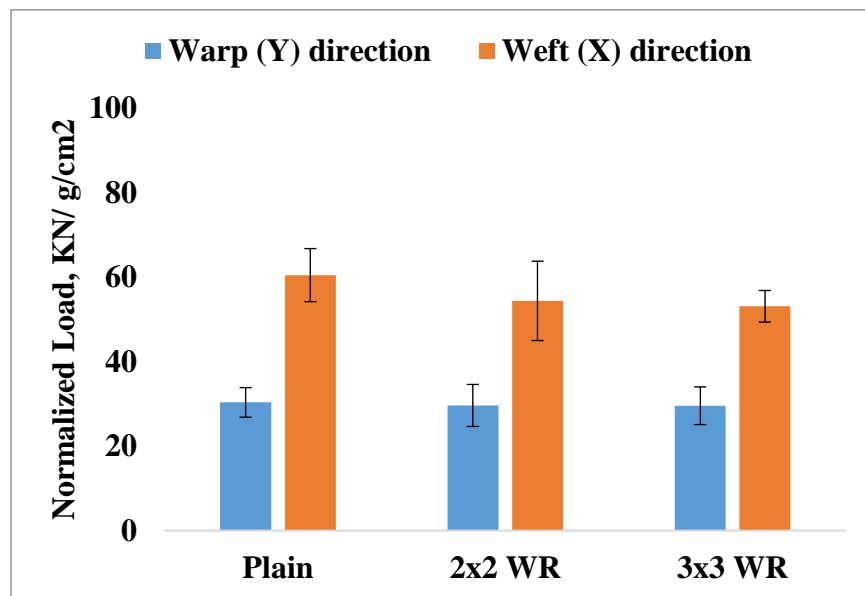


Figure 80. Main effect of weave on tensile load normalized by preform areal density

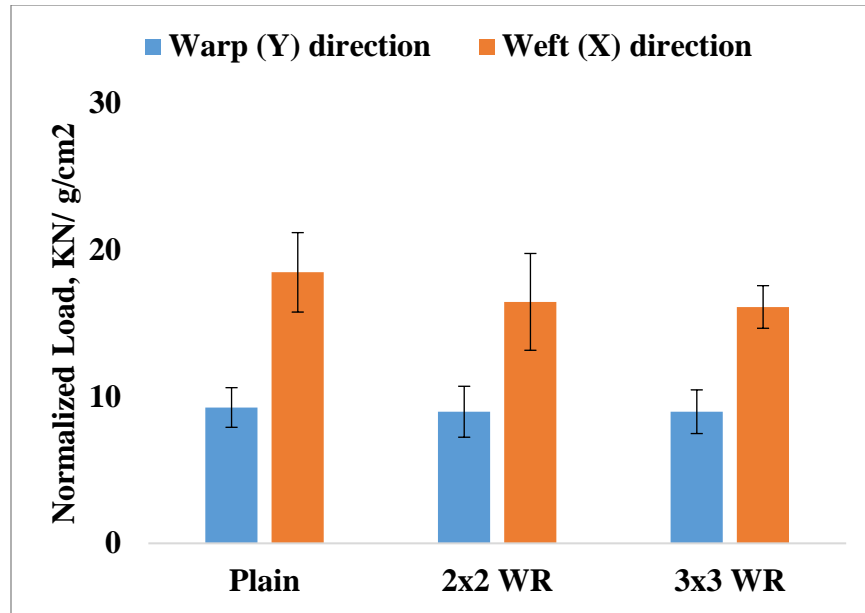


Figure 81. Main effect of weave on tensile load normalized by composite areal density

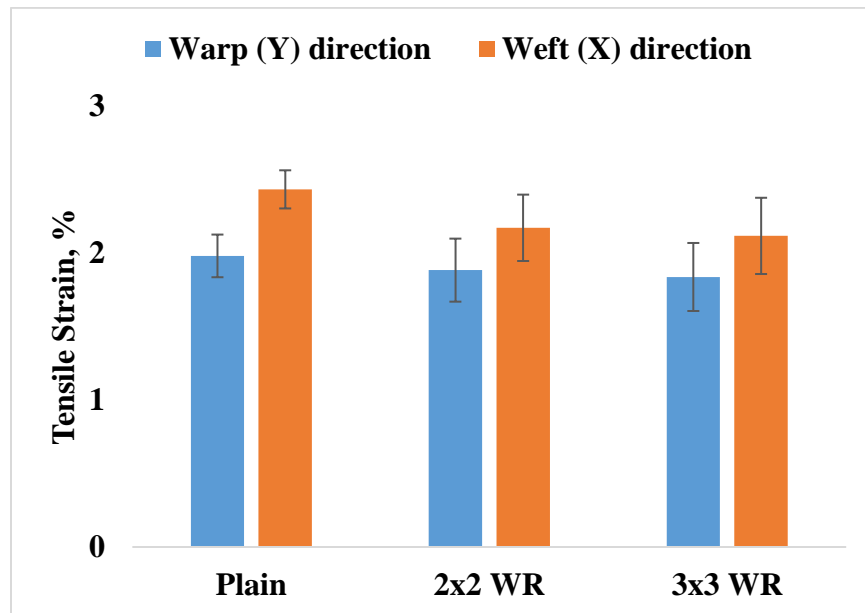


Figure 82. Main effect of weave on tensile strain

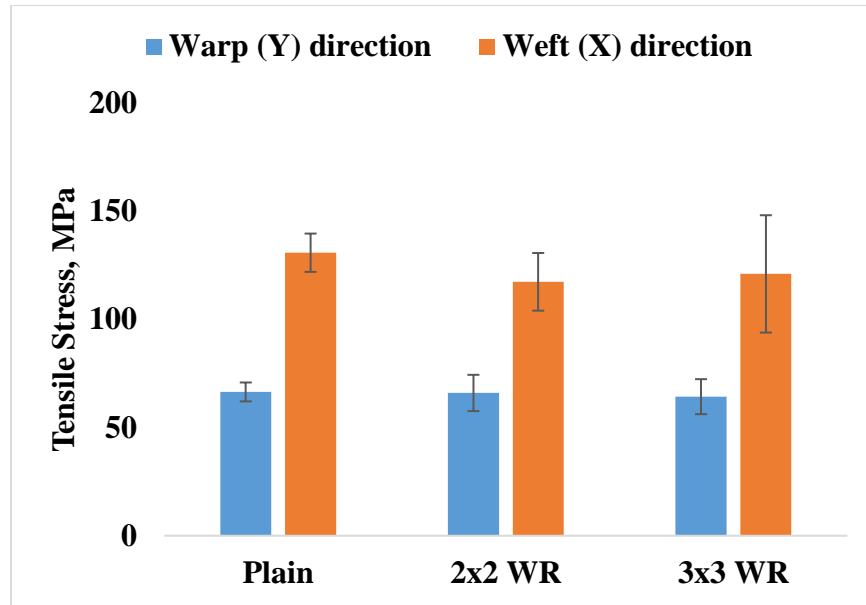


Figure 83. Main effect of weave on tensile stress

Main effect of number of Z- to Y-yarn ratio on tensile properties

Figure 84 shows the effect of number of Z- to Y-yarn ratio on the tensile peak load in the warp and weft direction indicating that there is no significant difference between 1:1 and 1:3 ratio. The Peak load was normalized by the preform areal density and the composite areal density as shown in Figures 85 and 86, respectively. The normalized peak load showed the same trend. Similar trend was experienced by the tensile strain and tensile stress as shown in Figures 87 and 88, respectively. The results were confirmed using ANOVA analysis as indicated in Appendix D.1.1 (Tables 49-56).

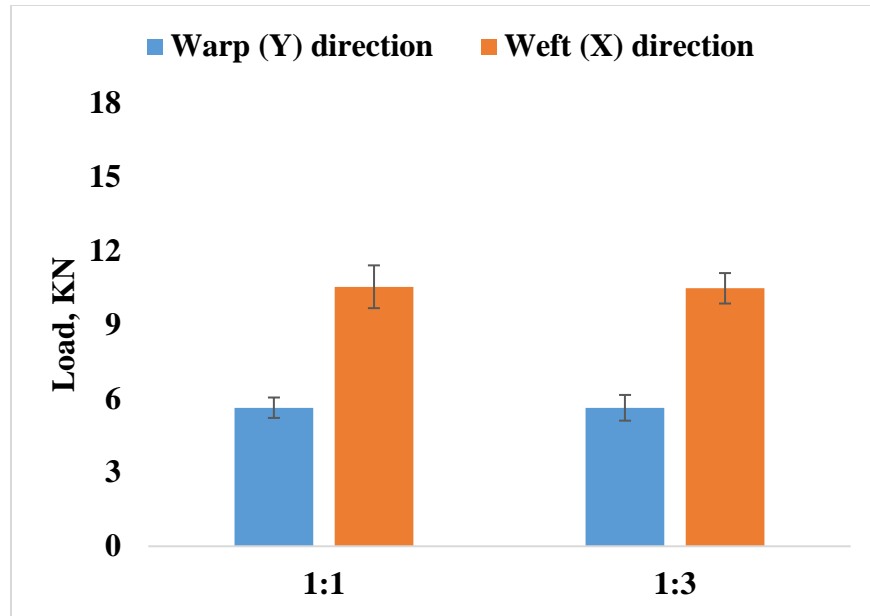


Figure 84. Main effect of Z: Y ratio on tensile load

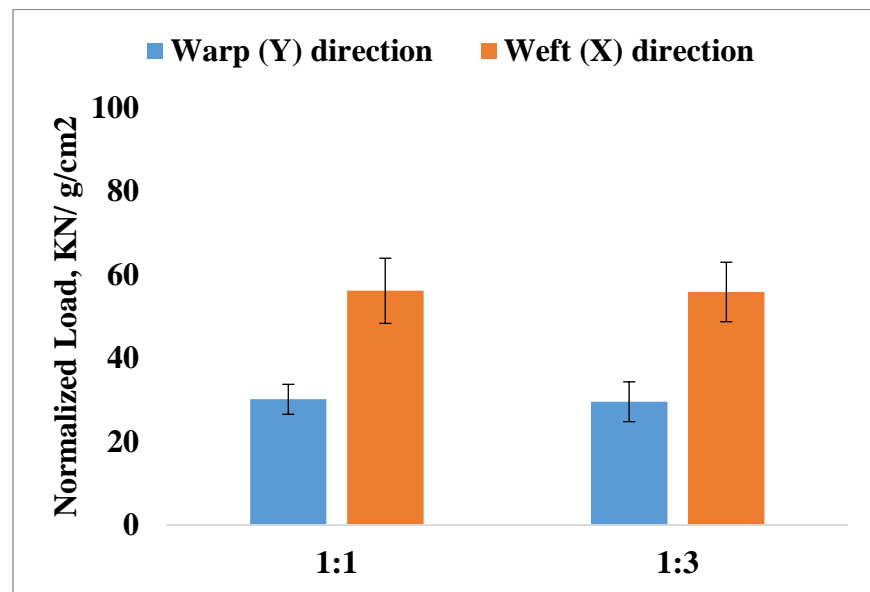


Figure 85. Main effect of Z: Y ratio on tensile load normalized by preform areal density

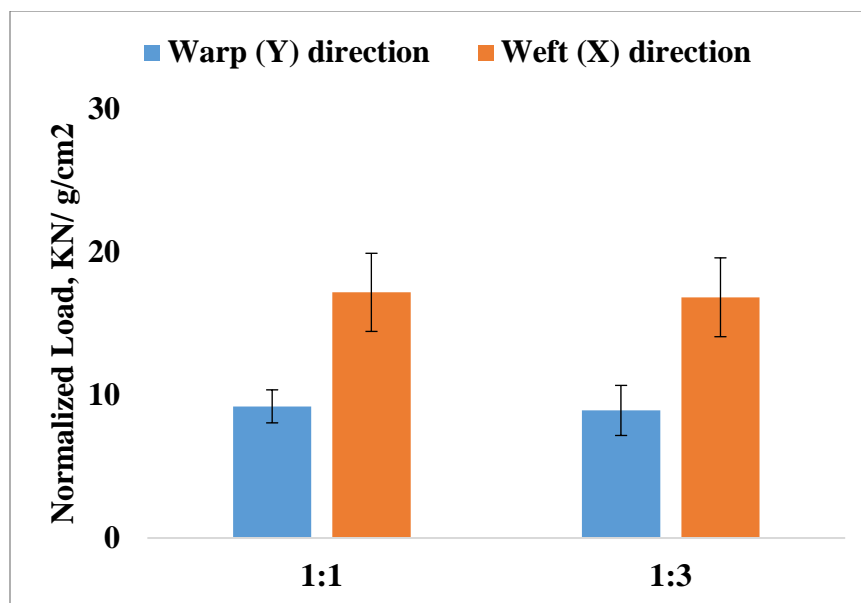


Figure 86. Main effect of Z: Y ratio on tensile load normalized by composite areal density

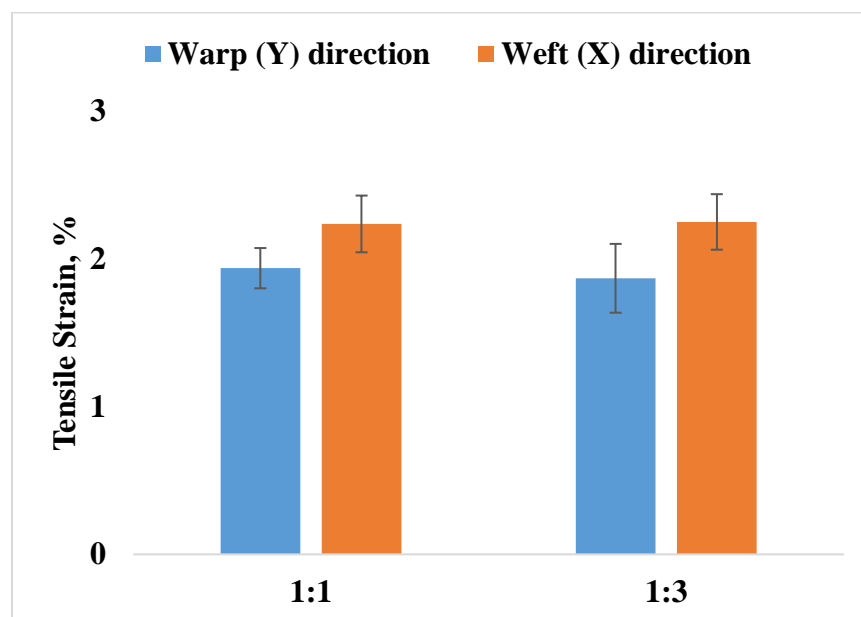


Figure 87. Main effect of Z: Y ratio on tensile strain

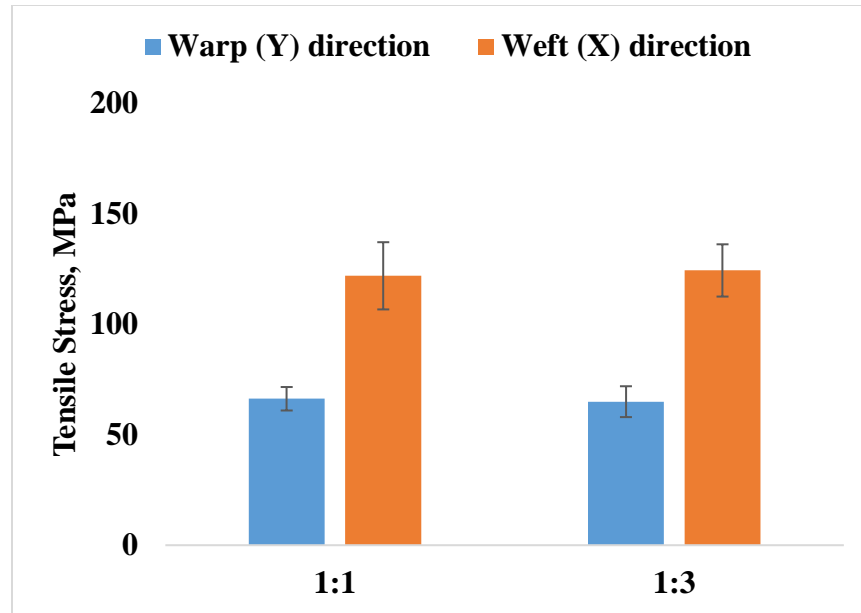


Figure 88. Main effect of Z: Y ratio on tensile stress

Comparison of tensile properties of composites from glass, flax and hemp fibers

As discussed earlier in the literature review, composites from flax and hemp fibers are comparable to composites from glass fibers. The tensile properties of composites from glass, flax and hemp fibers in terms of specific tensile stress and specific modulus are shown in Table 30. The data of composites from glass fibers was obtained from Midani's dissertation (27) and the data of composites from hemp fibers was obtained from Gupta's dissertation (68). Midani and Gupta used 3D orthogonal weaving and vinyl ester resin to produce composites which gave some similar properties for comparison. The number of Y-yarn layers and weave were similar in case of hemp and flax, however they were different for composites from glass fibers. Tensile stress and modulus for composites from flax, hemp and glass were normalized using fiber density. The specific tensile stress of glass composites was found to be significantly higher compared to flax and hemp due to the difference in FVF, however specific modulus was found to be comparable.

It was noted that tensile properties of composites from flax fibers were higher than that from hemp fibers due to the difference in yarns properties (Table 26).

Table 30. Comparison of the tensile properties of composites from glass, flax and hemp fibers

Fiber	Test direction	Fiber Density, g/cm ³	Tensile stress, Mpa	Specific tensile stress, Mpa/ g/cm ³	Modulus, Gpa	Specific modulus, Gpa/ g/cm ³
Glass	Warp	2.54	338- 488	133- 192	13.5- 26.4	5.3- 10.4
Flax		1.47	53- 89	36- 60	3.6- 9.5	2.4- 6.5
Hemp		1.48	13- 40	9- 27.1	1.4- 3.7	1- 2.5
Glass	Weft	2.54	290 - 477	114- 188	13- 30	5.1- 11.8
Flax		1.47	90- 173	61- 118	5.2- 12.3	3.5- 8.4
Hemp		1.48	30- 91	20- 62	2- 6.1	1.4- 4.1

5.3.1.2.Tup impact

Tup impact is a destructive test used to measure the peak force at impact, peak impact energy, as well as the total energy required to penetrate the composite material by a drop weight. In this mode of test, the three yarn systems are contributing to absorbing the impact energy of the sticker. Table 31 shows the results of the Tup impact test for samples of experimental design A

in which different preform architectural parameters such as the number of Y-yarn layers, the weave design and the number of Z- to Y-yarn ratio were changed. A total of 90 (18x5) specimens had been tested and the results were analyzed using ANOVA and Tukey HSD to investigate whether the effect of structural parameters on the impact energy of composite panels are significant. Figure 89 shows a test specimen with a typical puncture from 3 different views.

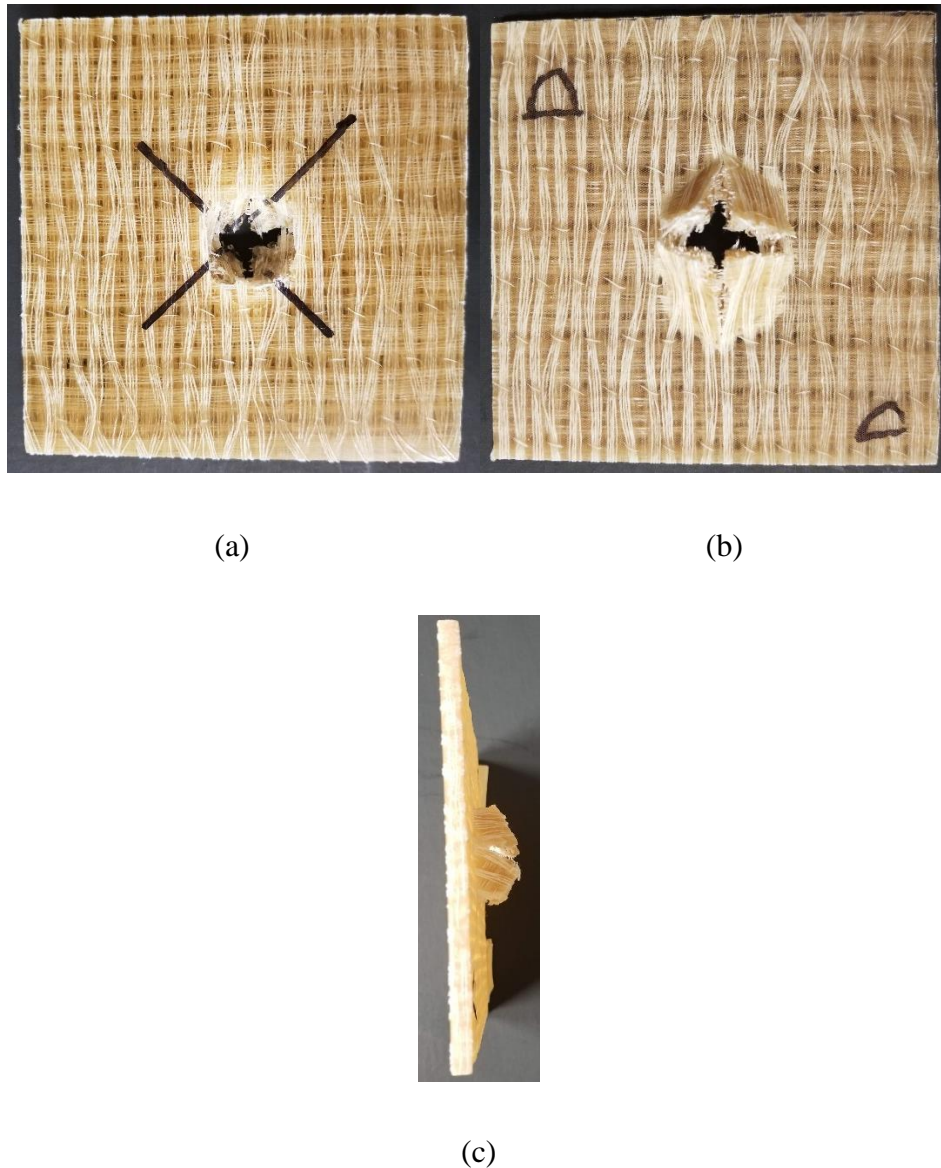


Figure 89. Specimen after Tup impact test (a) Front view, (b) Back view, and (c) Side view

Table 31. Average Tup impact data- experimental design A

Sample ID	Thickness, mm	Peak force, kN	CV, %	Total energy, J	CV, %	Energy/ thickness, J/ mm	Energy/ preform areal density, J/ g/cm²	Energy/ comp. areal density, J/ g/cm²
3L-1	2.03	0.75	15.57	6.17	34.16	3.05	72.57	20.31
3L-2	1.81	0.61	17.69	4.46	35.80	2.46	48.74	14.59
3L-3	1.81	0.59	10.87	4.03	10.21	2.23	46.18	14.12
3L-4	1.90	0.56	9.45	4.19	24.36	2.20	45.90	12.97
3L-5	1.87	0.61	23.15	4.42	63.22	2.37	49.06	13.70
3L-6	2.02	0.52	20.29	3.23	37.36	1.60	34.94	9.90
6L-1	4.21	2.18	5.65	16.32	2.76	3.88	85.34	26.82
6L-2	3.89	2.15	5.51	16.78	12.29	4.31	95.52	28.69
6L-3	3.95	2.15	6.43	16.13	8.56	4.09	91.82	26.86
6L-4	3.95	2.15	5.89	16.25	7.64	4.12	86.86	26.68
6L-5	3.76	2.07	4.71	16.70	7.78	4.44	92.37	27.64
6L-6	4.00	2.01	4.44	15.60	5.70	3.90	86.51	25.74
9L-1	5.99	4.87	2.98	39.38	3.05	6.57	135.80	44.08
9L-2	5.88	4.28	6.42	33.45	5.59	5.69	122.50	38.78
9L-3	5.76	4.38	8.63	34.50	7.32	5.99	127.62	40.63
9L-4	5.98	4.79	5.25	38.85	3.32	6.49	140.23	44.65
9L-5	5.85	4.80	5.24	37.41	6.97	6.39	137.63	43.36
9L-6	5.86	4.49	5.92	35.01	7.45	5.97	127.56	41.07

Main effect of number of layers on impact energy

Figures 90 and 91 show the effect of number of layers on the impact energy. The graphs indicate that there is a significant difference of the impact energy between the samples with different layers (thicknesses) which was confirmed using ANOVA and Tukey analyses in Appendix D.1.2 (Table 57 and Figure 227). As the number of warp layers decreased, a gradual decline in the impact load and energy was observed. This was due to the difference in the number of X- and Y-yarns resisting the impact load/energy. The impact energy was normalized by thickness, preform areal density and composite areal density as shown in figures 92- 94. After normalization, the number of Y-yarn layers showed the same significant difference on the impact energy. ANOVA analysis and Tukey multiple mean comparison showed that there was a significant difference of the normalized impact energy between 3, 6 and 9 Y-yarn layers as shown in Appendix D.1.2 (Tables 58-60 and Figures 229, 231 and 233). This was due to the high component contribution in the impact resistance in 9 Y-yarn layers than 6 than 3 Y-yarn layers. Table 23, showed that the FVF increased with increasing the number of Y-yarn layers since the Z-yarn effect in terms of increasing the resin constituent at the top and the bottom of the composite panel in more significant in 3 Y-yarn layers than 6 than 9 Y-yarn layers.

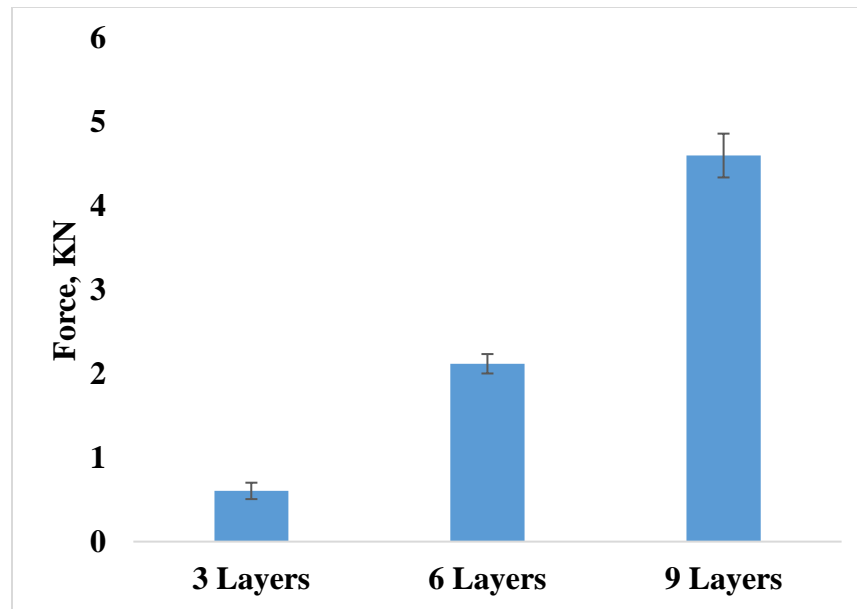


Figure 90. Main effect of layers on peak force

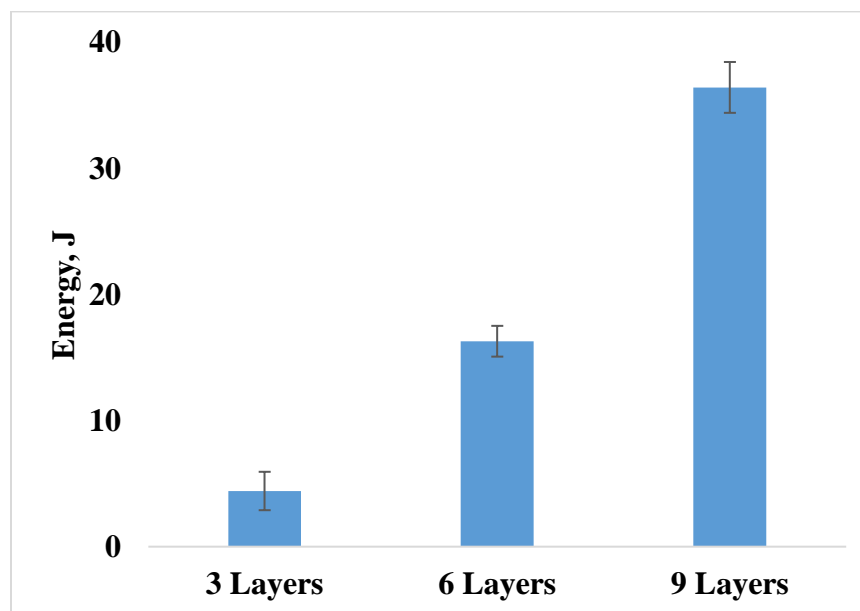


Figure 91. Main effect of layers on impact energy

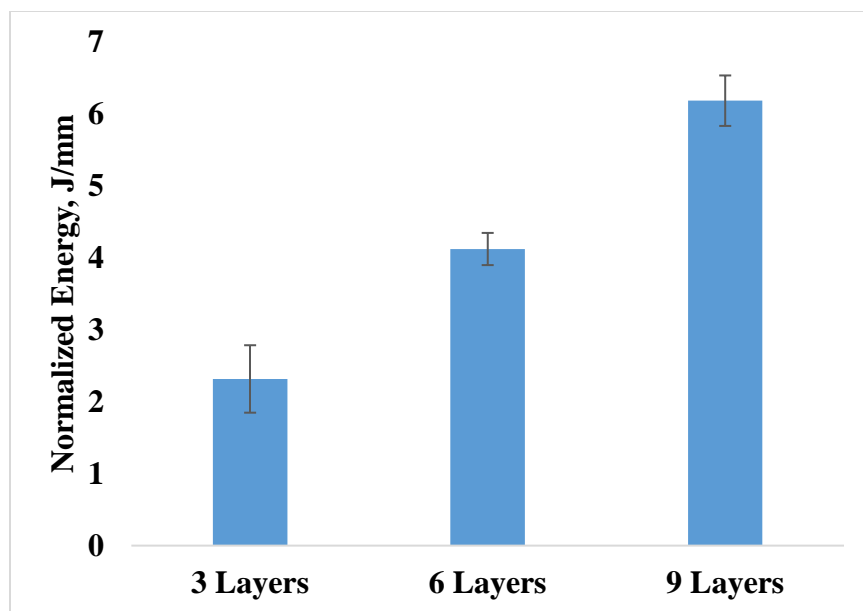


Figure 92. Main effect of layers on impact energy normalized by composite thickness

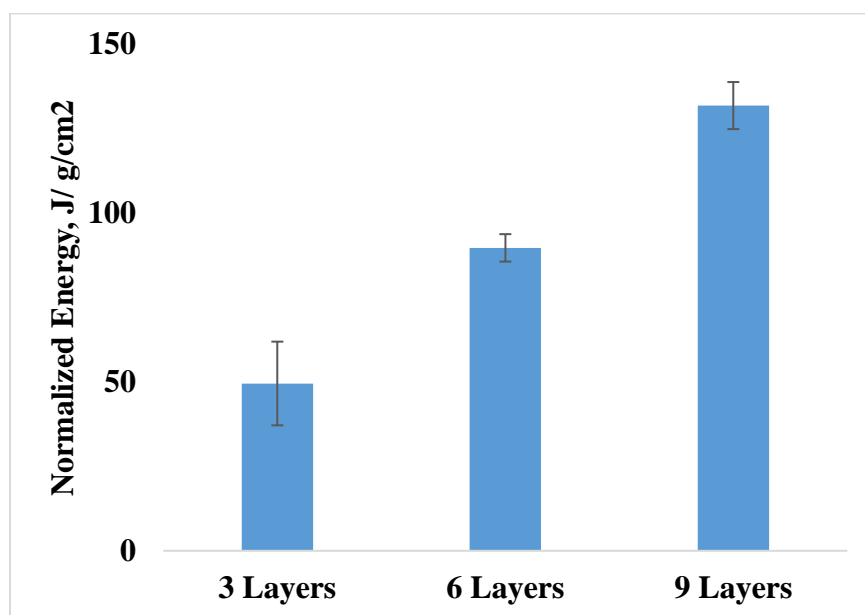


Figure 93. Main effect of layers on impact energy normalized by preform areal density

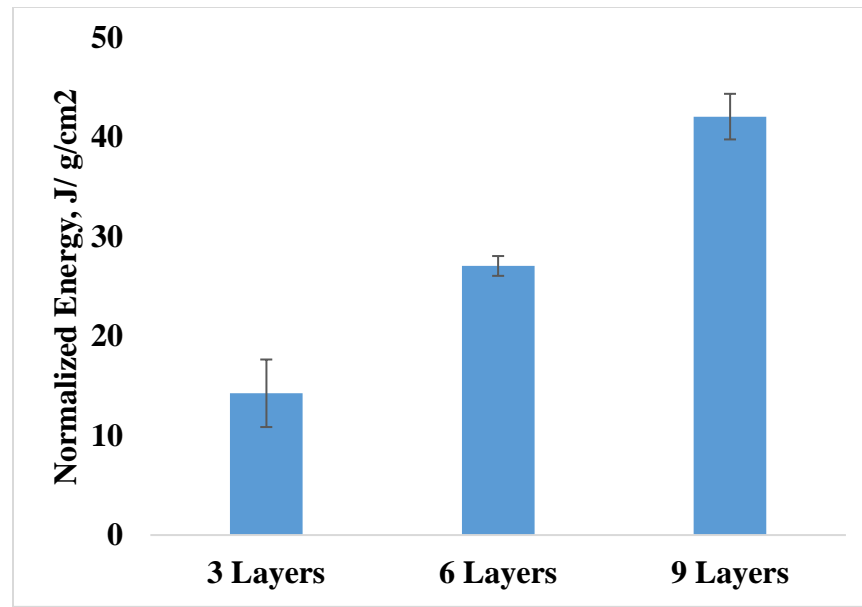


Figure 94. Main effect of layers on impact energy normalized by composite areal density

Main effect of weave on impact energy

Figures 95 and 96 show the effect of weave design on the impact energy. The graphs imply that there is a significant difference of the impact energy between the samples with different weave pattern which was confirmed using ANOVA analysis in Appendix D.1.2 (Table 57). Tukey analysis then used to understand the difference between each level. Tukey analysis indicated that the plain weave was significantly different from 2x2 warp rib and 3x3 warp rib weaves, however there was no difference between 2x2 warp rib and 3x3 warp rip woven composite samples as indicated in Appendix D.1.2 (Figure 228). This was because of the small spaces between yarns in the preform structure which reduces the chance of accumulating resin and producing resin rich areas. The normalized impact energy by thickness and by preform areal density showed the same effect of differentiating between plain weave and the other two weaves, however after normalizing the impact energy by composite areal density, this effect diminished as shown in Appendix D.1.2 (Tables 58-60 and Figures 230, 232 and 234). Figures 97- 99 show the effect of

weave on the normalized impact energy by specimen thickness, preform areal density and composite areal density.

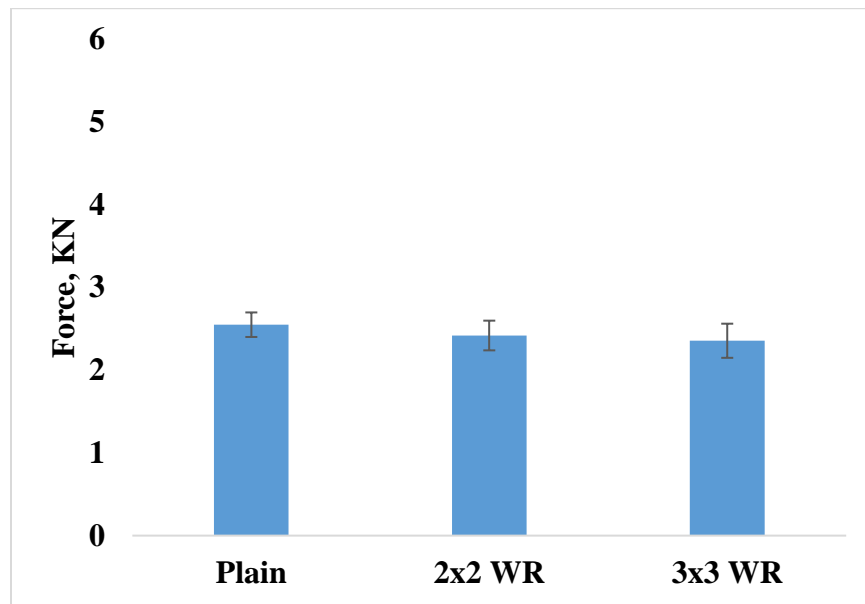


Figure 95. Main effect of weave on peak force

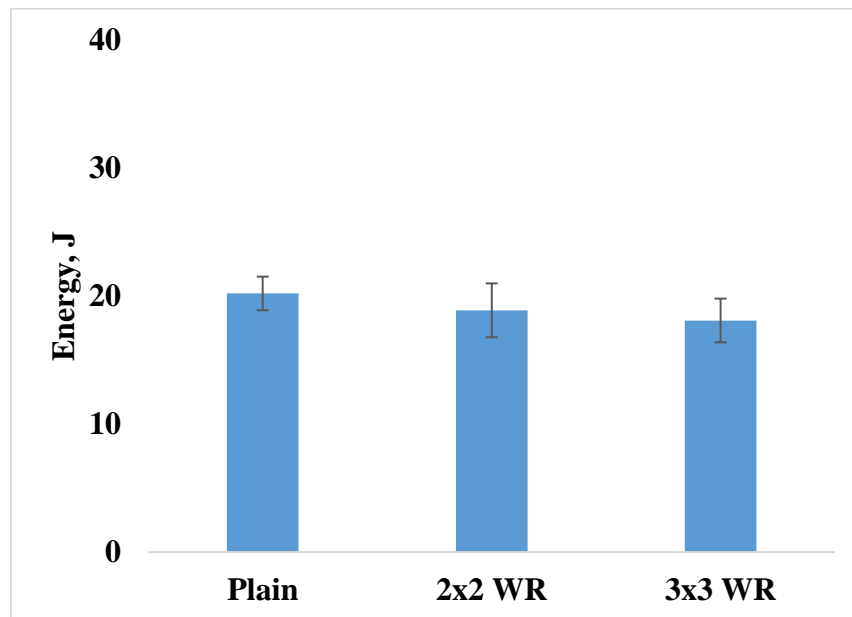


Figure 96. Main effect of weave on impact energy

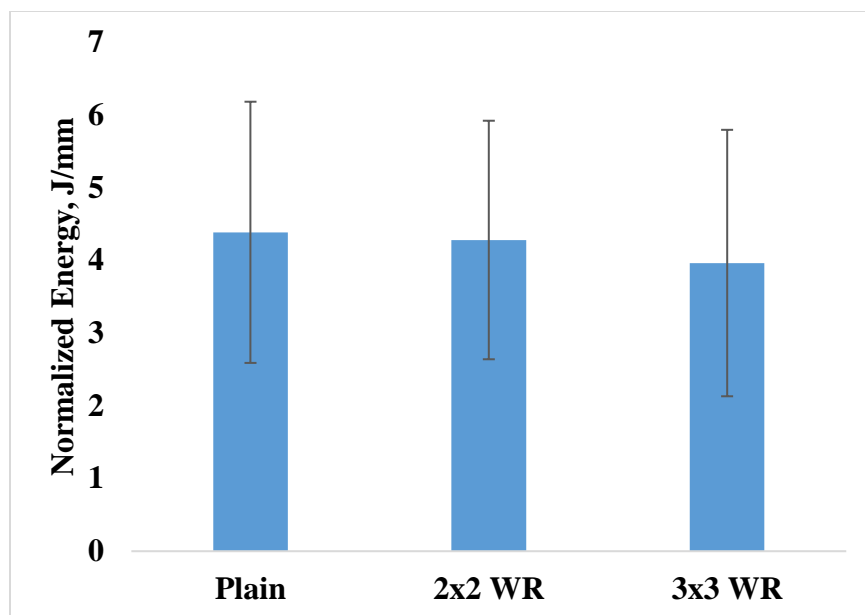


Figure 97. Main effect of weave on impact energy normalized by composite thickness

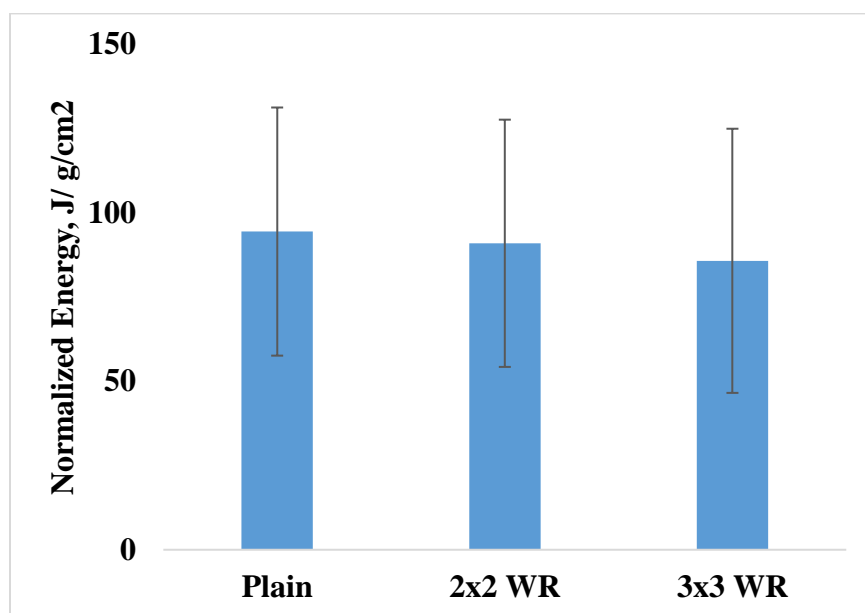


Figure 98. Main effect of weave on impact energy normalized by preform areal density

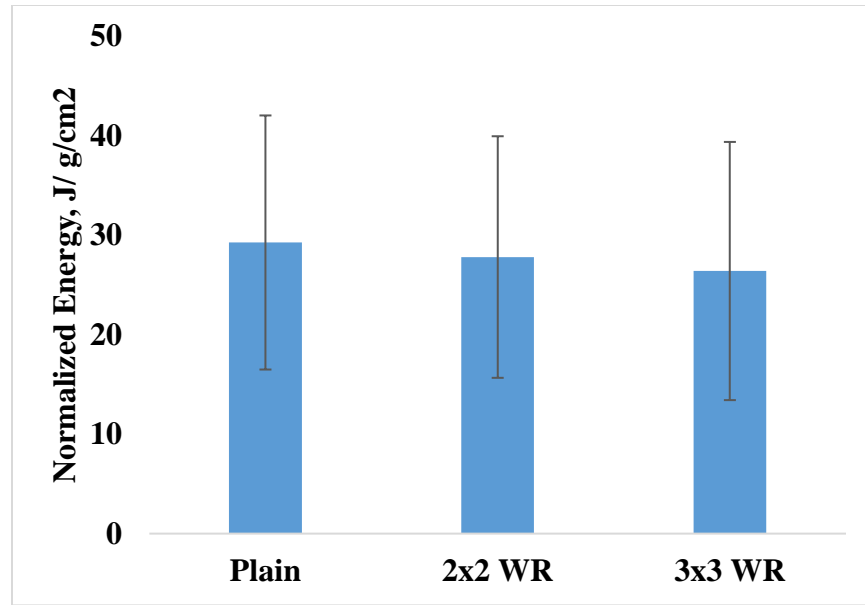


Figure 99. Main effect of weave on impact energy normalized by composite areal density

Main effect of number of Z- to Y-yarn ratio on impact energy

Figures 100 and 101 show the effect of number of Z- to Y-yarn ratio on the peak impact force and the impact energy indicating that there is no significant difference between 1:1 and 1:3 ratio. The normalized peak impact force and the impact energy showed a similar trend. Figures 102- 104 show the effect of number of Z- to Y-yarn ratio on the impact energy after normalizing to thickness, preform areal density and composite areal density, respectively. The results were confirmed using ANOVA analysis as indicated in Appendix D.1.2 (Tables 57-60).

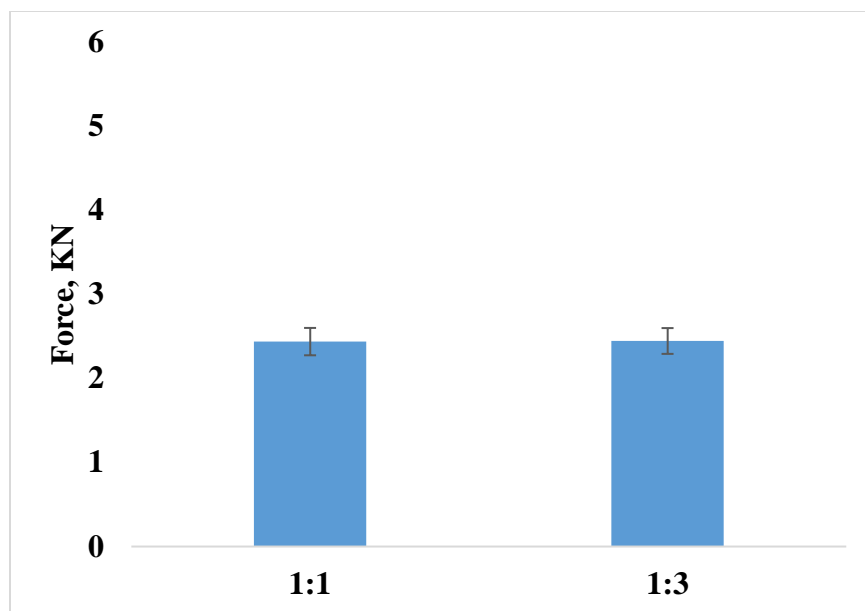


Figure 100. Main effect of Z: Y-yarn ratio on peak force

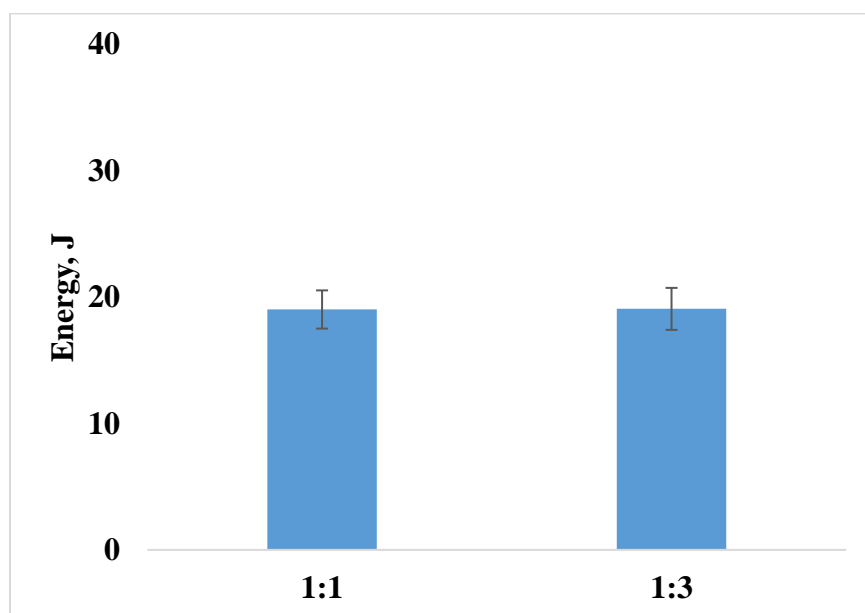


Figure 101. Main effect of Z: Y-yarn ratio on impact energy

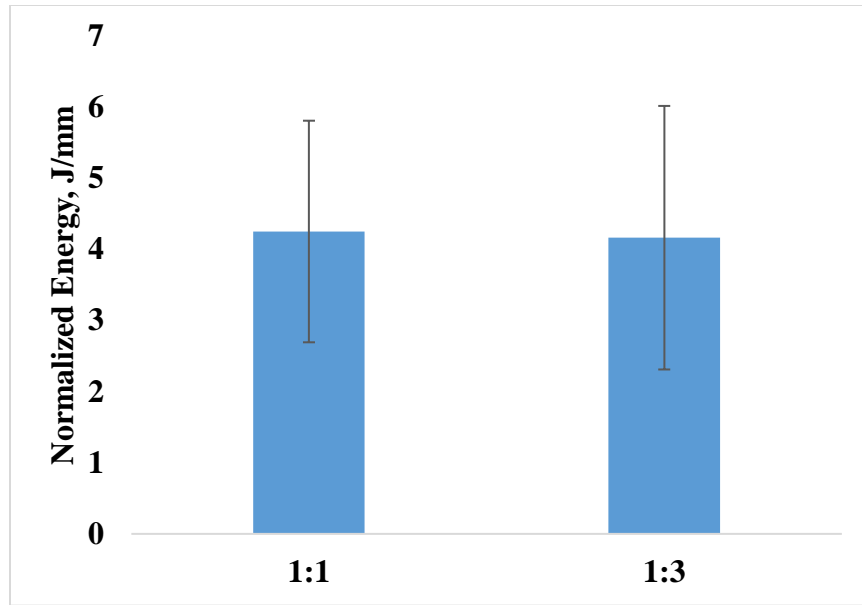


Figure 102. Main effect of Z: Y-yarn ratio on impact energy normalized by composite thickness

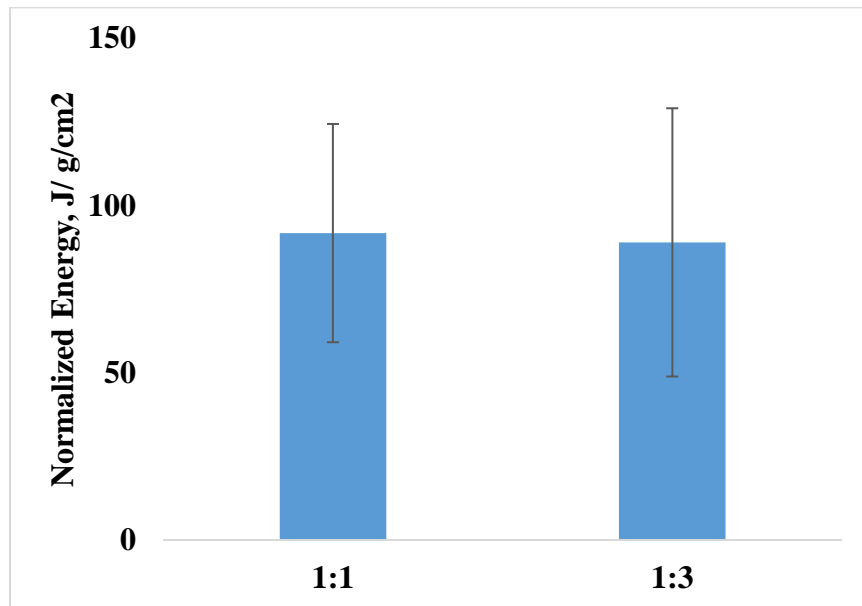


Figure 103. Main effect of Z: Y-yarn ratio on impact energy normalized by preform areal density

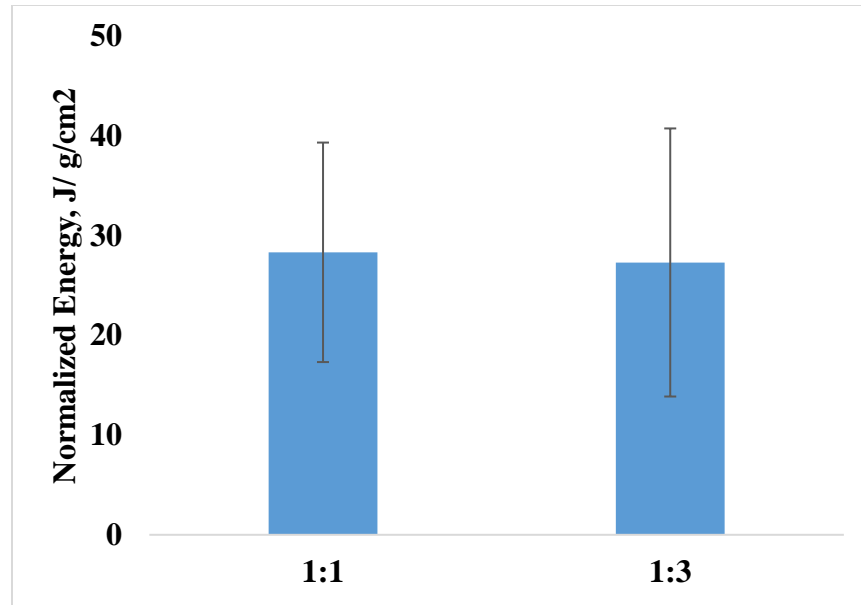


Figure 104. Main effect of Z: Y-yarn ratio on impact energy normalized by composite areal density

Comparison of Tup Impact Properties of Composites from Glass, Flax and Hemp Fibers

Similar to the tensile properties comparison, Tup impact properties of composites from glass, flax and hemp fibers were compared. The total impact energy of flax, hemp and glass composites was used for comparison along with normalized value to thickness, composite areal density as shown in Table 32. The total penetration energy of composites from flax and hemp fibers was found to be comparable to that from glass fibers after normalizing by preform areal density. The thickness of the resultant composites using VARTM process varies. The thickness of the panel is higher at the resin inlet than the thickness at the outlet. The reason behind the thickness variation has been explained before. While the thickness varies, the fiber reinforcement is the same. On other works, the composite thickness variation is due to the increase of the resin at the inlet competed to the outlet. For this reason, normalizing a property using the thickness is questionable and should not be used. Normalization by preform areal density was found to be

the most acceptable way to compare between composites with different construction parameters since it is independent from the thickness variability caused by variation in resin volume fraction.

Table 32. Comparison of Tup impact properties of composites from glass, flax and hemp fibers

Fiber	Total Energy	Energy/ thickness, J/ mm	Energy normalized by preform areal density, kJ/ g/mm ²	Energy normalized by comp. areal density, kJ/ g/mm ²
Glass	26- 70	13.5- 19.8	10.5- 15.2	7.5- 10.6
Flax	3.2- 39	1.6- 6.6	3.5- 14.0	1.0- 4.5
Hemp	3.1- 33	1.1- 5.1	3.5- 13.4	1.1- 4.2

5.3.1.3.Charpy impact

The Charpy impact test is a destructive test in which the energy required to fracture the supported composite specimen as a simple beam until failure with a hammer. The test was conducted to fail X- and Y-composite constituents. The results of the Charpy impact test of 90 (18x5) specimens in each direction including the energy absorbed to fracture the samples and as a percentage in the warp (Y-yarn) direction and the weft (X-yarn) direction are listed in tables 33 and 34, respectively. In general, the energy absorbed to break samples in the X-yarn direction was higher than that in the Y-direction. In Charpy test, the samples can experience complete, hinged, and partial or non-break as shown in Figure 105. However, in this research only

specimens with complete or hinge break were observed for the failure analysis. The data were analyzed using ANOVA and Tukey HSD analyses to investigate the effect of number of Y-yarn layers (thickness), weave design and Z- to Y-yarn ratio.

Table 33. Charpy impact results in the warp direction- experimental design A

Sample ID	Thickness, mm	Energy absorbed, J (CV%)	Energy/ thickness, J/ mm	Energy/ Preform Areal Density, J/ g/cm²	Energy/ Comp. Areal Density, J/ g/cm²	Energy absorbed, % (CV%)
3L-1	2.03	0.42 (24)	0.21	4.99	1.40	3.93 (24)
3L-2	1.81	0.41 (19)	0.22	4.46	1.33	3.77 (19)
3L-3	1.81	0.40 (24)	0.22	4.59	1.40	3.70 (24)
3L-4	1.90	0.57 (25)	0.30	6.24	1.76	5.28 (25)
3L-5	1.87	0.46 (30)	0.24	5.07	1.42	4.23 (30)
3L-6	2.02	0.34 (17)	0.17	3.68	1.04	3.15 (17)
6L-1	4.21	1.97 (13)	0.47	10.29	3.23	18.23 (13)
6L-2	3.89	0.93 (23)	0.24	5.31	1.60	8.65 (23)
6L-3	3.95	1.06 (13)	0.27	6.03	1.76	9.81 (13)
6L-4	3.95	0.83 (18)	0.21	4.46	1.37	7.72 (18)
6L-5	3.76	0.93 (37)	0.25	5.14	1.54	8.60 (37)
6L-6	4.00	0.98 (16)	0.25	5.44	1.62	9.09 (16)
9L-1	5.99	1.40 (17)	0.23	4.84	1.57	13.00 (17)
9L-2	5.88	1.72 (18)	0.29	6.31	2.00	15.97 (18)
9L-3	5.76	1.39 (11)	0.24	5.15	1.64	12.90 (11)
9L-4	5.98	1.64 (23)	0.27	5.91	1.88	15.16 (23)
9L-5	5.85	2.06 (29)	0.35	7.59	2.39	19.11 (29)
9L-6	5.86	1.25 (25)	0.21	4.57	1.47	11.61 (25)

Table 34. Charpy impact results in the weft direction- experimental design A

Sample ID	Thickness, mm	Energy absorbed, J (CV%)	Energy/ thickness, J/ mm	Energy/ Preform Areal Density, J/ g/cm²	Energy/ Comp. Areal Density, J/ g/cm²	Energy absorbed, % (CV%)
3L-1	2.06	0.92 (16)	0.45	10.86	3.04	8.56 (16)
3L-2	1.89	1.34 (47)	0.71	14.70	4.40	12.45 (47)
3L-3	1.84	0.84 (19)	0.46	9.66	2.95	7.80 (19)
3L-4	1.92	0.97 (15)	0.50	10.63	3.00	8.98 (15)
3L-5	1.99	0.73 (11)	0.37	8.07	2.25	6.74 (11)
3L-6	1.87	1.08 (12)	0.58	11.73	3.33	10.04 (12)
6L-1	4.27	2.36 (20)	0.55	12.33	3.88	21.85 (20)
6L-2	3.95	2.77 (20)	0.70	15.79	4.74	25.70 (20)
6L-3	3.97	2.50 (16)	0.63	14.23	4.16	23.16 (16)
6L-4	4.04	2.16 (10)	0.53	11.55	3.55	20.01 (10)
6L-5	3.93	2.94 (19)	0.75	16.29	4.87	27.28 (19)
6L-6	3.87	2.22 (37)	0.58	12.33	3.67	20.60 (37)
9L-1	6.07	3.46 (14)	0.57	11.93	3.87	32.03 (14)
9L-2	5.83	3.36 (28)	0.58	12.31	3.90	31.13 (28)
9L-3	5.77	4.13 (15)	0.72	15.28	4.86	38.27 (15)
9L-4	5.86	3.36 (13)	0.57	12.11	3.86	31.08 (13)
9L-5	5.84	3.65 (24)	0.63	13.44	4.23	33.84 (24)
9L-6	5.84	3.30 (6)	0.57	12.02	3.87	30.57 (6)

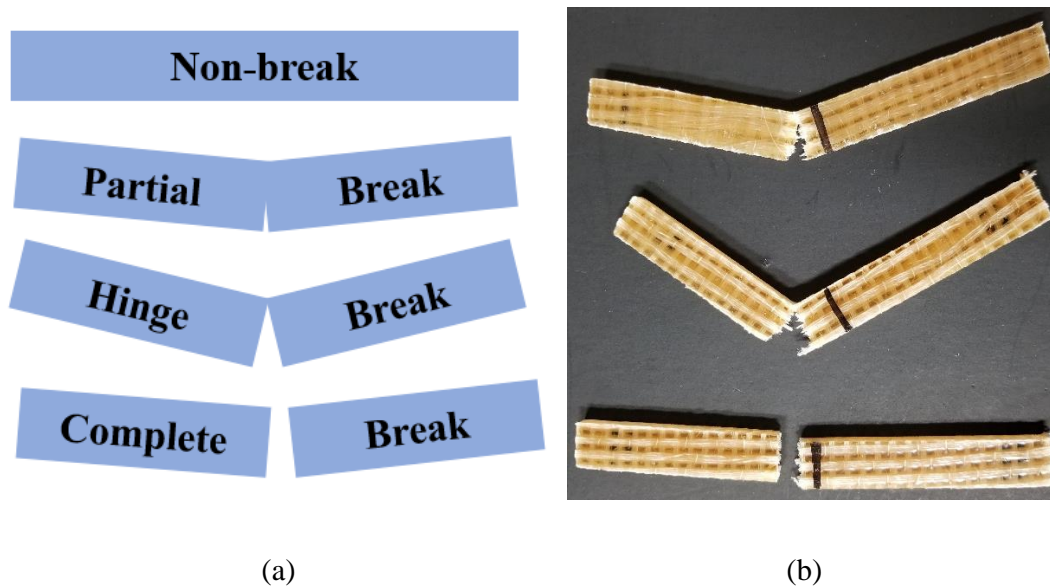


Figure 105. (a) Type of breaks in Charpy (b) Specimens showing complete and hinge break

Main effect of number of layers on impact energy

Figure 106 shows the effect of increasing the number of Y-yarn layers on the energy absorbed by the samples to break in the warp and weft directions. It was observed that increasing the number of Y-yarn layers caused a significant increase in the total impact energy used to fracture the 3DOW composite samples. The impact energy was normalized by thickness, preform areal density and composite areal density as shown in Figures 107- 109. The ANOVA analysis in Appendix D.1.3 (Tables 61-68) indicated that the rise in the impact energy due to the increase of the warp layers was significant however, it was observed from Figures 107- 109 that the normalized impact energy of the samples with 6 Y-yarn layers was higher than that of the 9 Y-yarn layers. Therefore, the Tukey HSD was performed to understand the effect of layers and it indicated that the samples with 3 Y-yarn layers was significantly different than the 6 and 9, however there was no substantial difference between the 6 and 9 Y-yarn layers as shown in Appendix D.3.1 (Figures 235, 237, 239, 241, 243, 245, 247 and 249).

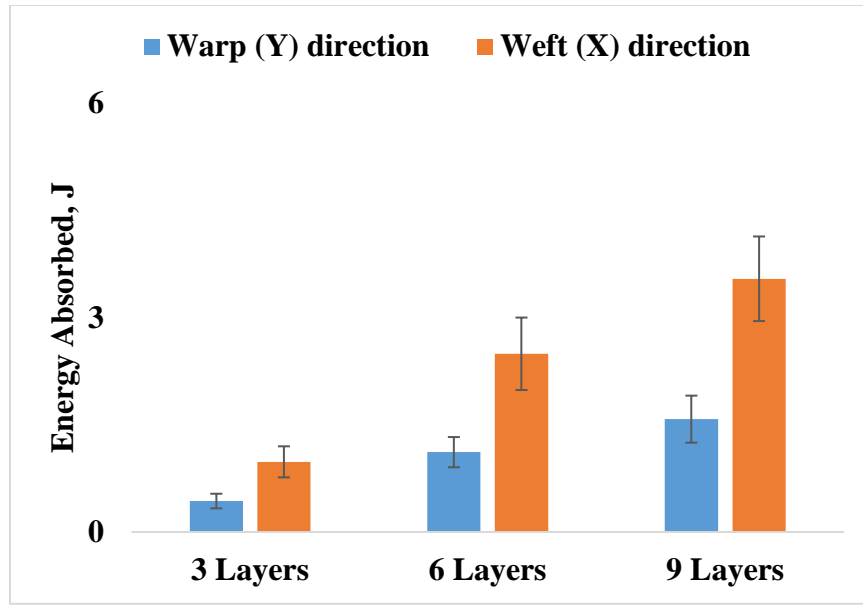


Figure 106. Main effect of layers on energy absorbed

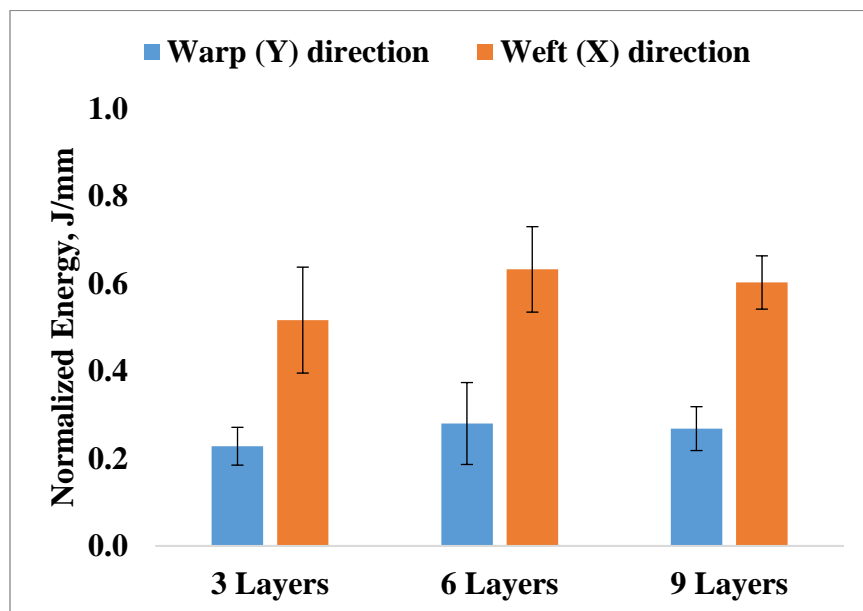


Figure 107. Main effect of layers on energy absorbed normalized by composite thickness

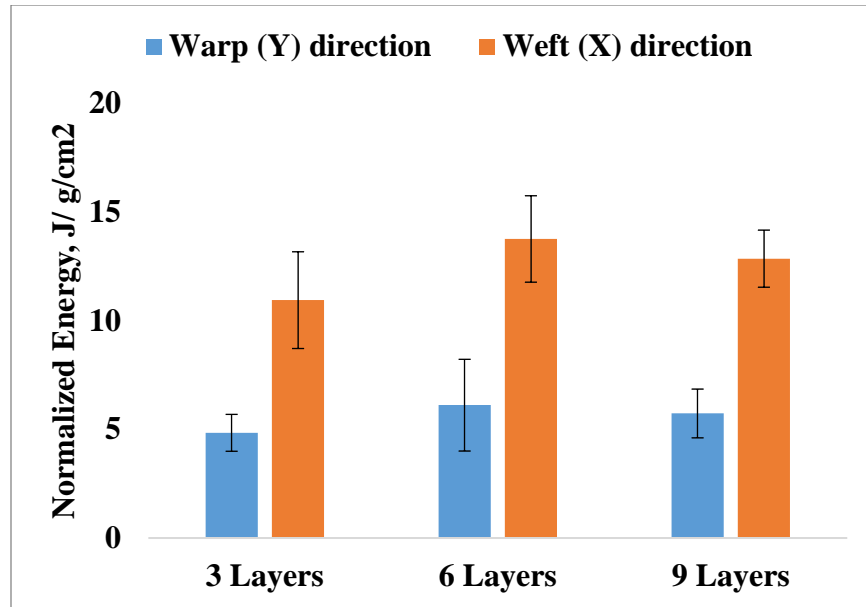


Figure 108. Main effect of layers on energy absorbed normalized by preform areal density

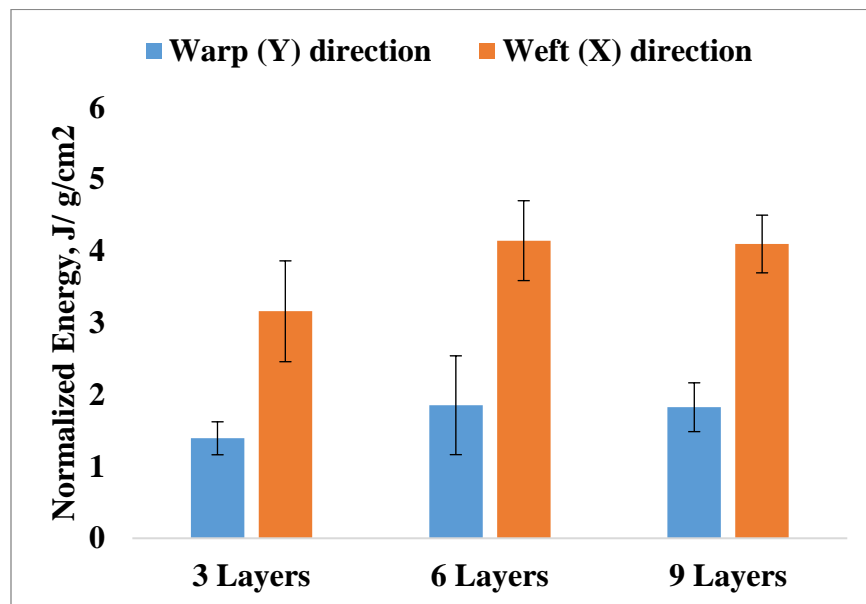


Figure 109. Main effect of layers on energy absorbed normalized by composite areal density

Main effect of weave on impact energy

Figure 110 explains the effect of changing the weave pattern on the Charpy impact energy in the warp and weft directions. It was noticed that the plain woven samples had a slightly higher

impact energy than that of 2x2 warp rib and 3x3 warp rib and this was confirmed by ANOVA and Tukey analyses as indicated in Appendix D.1.3 (Tables 61 and 65 and Figures 236 and 244). The impact energy was normalized by thickness, preform areal density and composite areal density as shown in Figures 111- 113, respectively. The normalized impact energy showed similar results in terms of Y-yarn direction which was confirmed by ANOVA and Tukey HSD analyses as shown in Appendix D.1.3 (Tables 62-64 and 65-67 & Figures 238, 240, 242, 246, 248 and 250). The reason behind this is that plain weave is more uniform with less resin rich areas than 3x3 warp rib. In terms of X-yarn direction, the weave pattern did not affect the impact energy significantly.

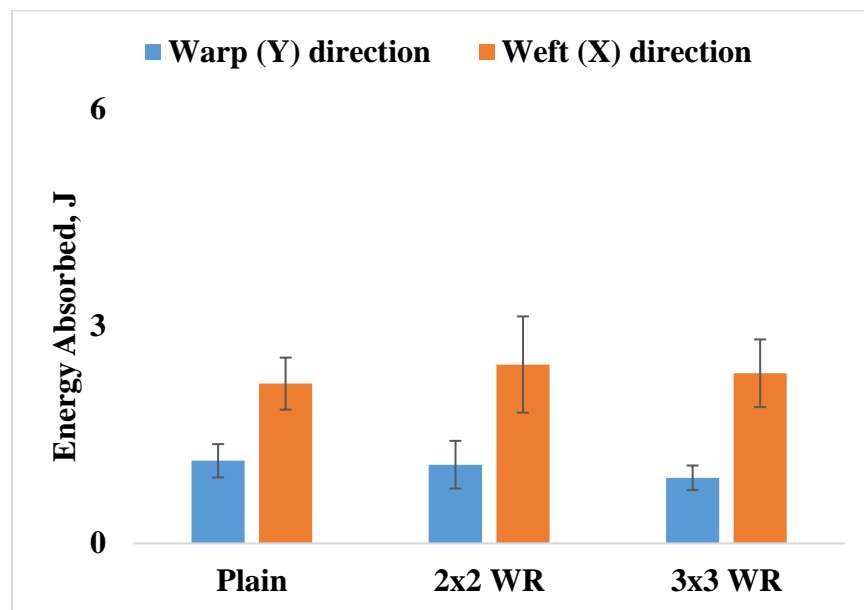


Figure 110. Main effect of weave on energy absorbed

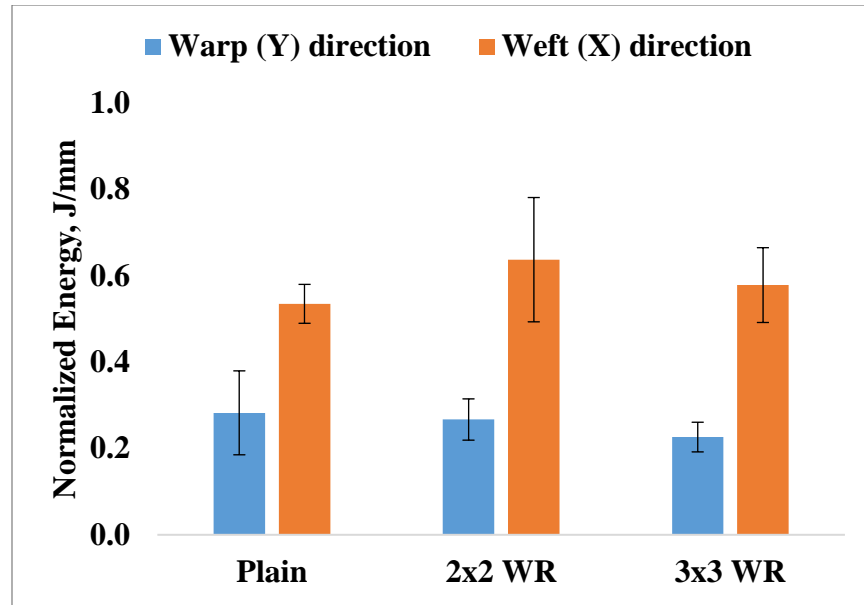


Figure 111. Main effect of weave on energy absorbed normalized by composite thickness

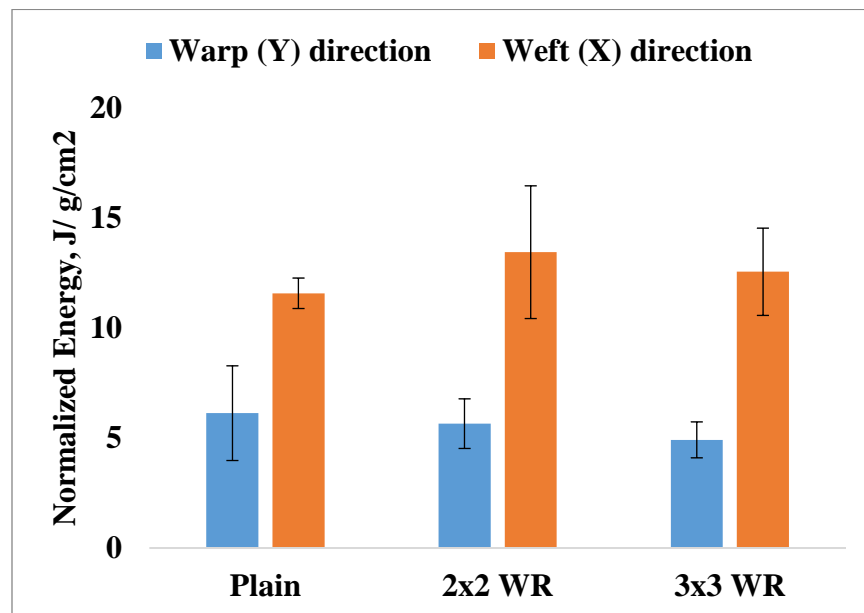


Figure 112. Main effect of weave on energy absorbed normalized by preform areal density

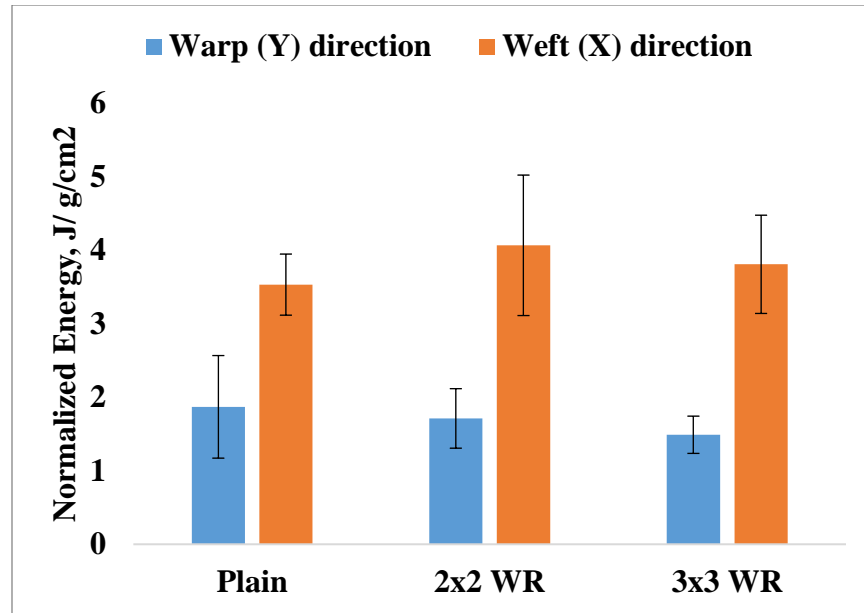


Figure 113. Main effect of weave on energy absorbed normalized by composite areal density

Main effect of number of Z- to Y-yarn ratio on impact energy

Figure 114 shows the effect of number of Z- to Y-yarn ratio on the Charpy impact energy indicating that there is no significant difference between 1:1 and 1:3 ratio in both the warp and the filling directions. The impact energy was normalized by the thickness, the preform areal density and the composite areal density. The normalized impact energy by all three normalizing approached showed that the samples with 1:1 Z- to Y-yarn ratio was significantly higher than that with 1:3 Z- to Y-yarn ratio in terms of the Y-yarn (warp) direction. For the X-yarn (weft) direction, the effect of the Z- to Y-yarn ratio showed a significant difference using ANOVA analysis when the impact energy was normalized by the composite areal density. It was clear that the number of Z-yarns had more effect on the warp direction because this was the direction where they were woven earlier. The results were confirmed using ANOVA analysis as indicated in Appendix D.1.3 (Tables 61-68).

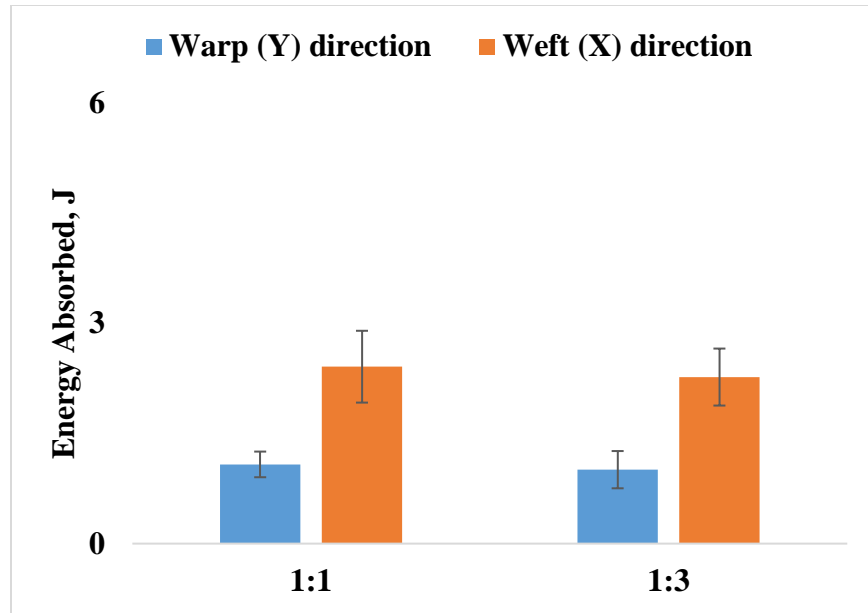


Figure 114. Main effect of Z: Y-yarn ratio on absorbed energy

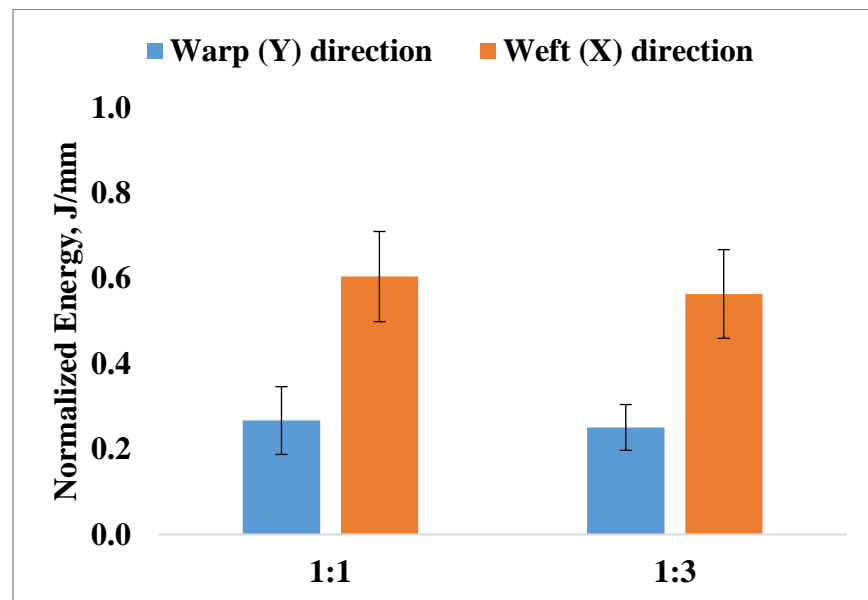


Figure 115. Main effect of Z: Y-yarn ratio on absorbed energy normalized by composite thickness

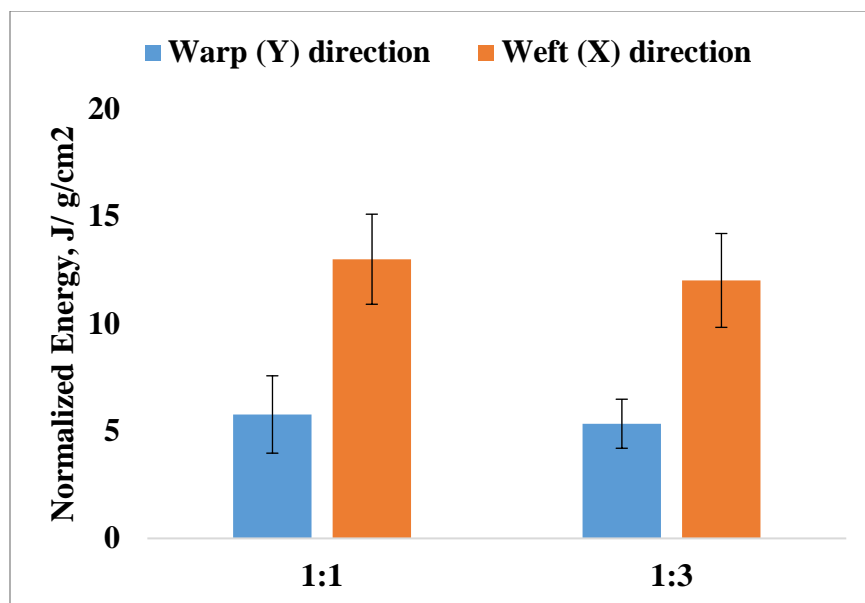


Figure 116. Main effect of Z: Y-yarn ratio on absorbed energy normalized by preform areal

Density

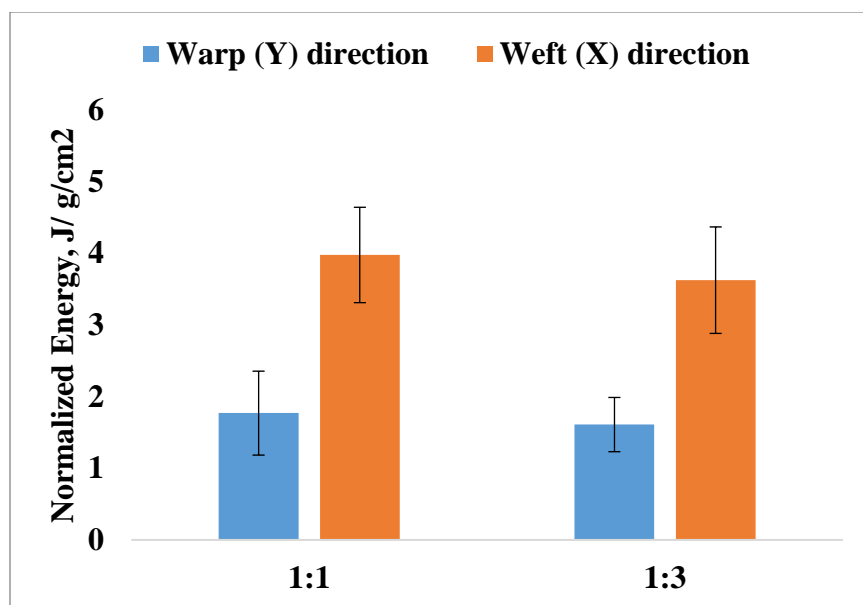


Figure 117. Main effect of Z: Y ratio on absorbed energy normalized by composite areal density

Comparison of Charpy Impact Properties of Composites from Glass, Flax and Hemp Fibers

Charpy impact properties of composites from glass, flax and hemp fibers were compared. The total impact energy of flax, hemp and glass composites was used for comparison along with normalized value to thickness, composite areal density as shown in Table 35. The total energy of composites from flax and hemp fibers was found to be comparable to that from glass fibers after normalizing by preform areal density.

Table 35. Comparison of Charpy impact properties of composites from glass, flax and hemp fibers

Fiber	Test direction	Total Energy	Energy/ thickness, J/mm	Energy normalized by preform areal density, kJ/ g/mm ²	Energy normalized by comp. areal density, kJ/ g/mm ²
Glass	Warp	2.2- 11.5	1.2- 3.6	0.9- 2.6	0.7- 1.9
Flax		0.7- 4.1	0.4- 0.8	0.8- 1.6	0.2- 0.5
Hemp		0.2- 1.1	0.1- 0.2	0.3- 0.5	0.1- 0.2
Glass	Weft	2.6- 13	1.3- 3.7	1.2- 2.9	0.8- 2.1
Flax		0.8- 3.0	0.4- 0.8	1.0- 1.7	0.3- 0.5
Hemp		0.7- 2.3	0.2- 0.5	0.6- 1.6	0.2- 0.5

5.3.1.4.Compression Test

The combines loading compression (CLC) governs compression and stiffness properties of the 3DOW composites. This test was performed to 6 and 9 Y-yarn layers with three different weaves; plain, 2x2 warp rib and 3x3 warp rib and two Z- to Y-yarn ratios 1:1 and 1:3. 60 specimens in each direction were accomplished to investigate the compression properties of 3DOW composites. In general, the weave design showed a significant difference in the compression peak load only in the filling direction while changing either the number of Y-yarn layers or the Z- to Y-yarn ratio did not show a significant effect. Tables 36 and 37 shows the results of the compression test including the peak load, the normalized peak load by the preform and the composite areal densities and the compression stress. Figure 118 shows a typical specimen before and after compression test. The results have been statistically analyzed using ANOVA and Tukey HSD analyses.



Figure 118. Compression specimens before and after testing

Table 36. Compression test results – Warp direction

Sample ID	Thickness, mm	Peak Load, KN (CV%)	Load/ Preform Areal Density, KN/ g/cm ²	Load/ Comp. Areal Density, KN/ g/cm ²	Compression Stress, Mpa (CV%)
6L-1	4.09	5.37 (2)	28.09	10.68	45.28 (3)
6L-2	3.88	5.52 (37)	31.43	11.06	112.60 (39)
6L-3	3.95	4.51 (3)	25.66	8.90	39.32 (3)
6L-4	3.98	5.27 (8)	28.17	10.60	45.64 (9)
6L-5	3.98	4.80 (2)	26.54	9.73	41.62 (2)
6L-6	3.85	4.53 (1)	25.10	9.28	40.23 (3)
9L-1	6.03	7.58 (5)	26.16	10.24	104.80 (5)
9L-2	5.87	7.72 (15)	28.27	10.57	103.40 (14)
9L-3	5.99	8.39 (12)	31.02	11.51	48.30 (12)
9L-4	5.95	7.45 (1)	26.88	10.06	43.17 (1)
9L-5	5.96	7.36 (6)	27.07	10.02	42.54 (4)
9L-6	5.71	6.60 (4)	24.04	9.42	39.81 (3)

Table 37. Compression test results – Weft direction

Sample ID	Thickness, mm	Peak Load, KN (CV%)	Load/ Preform Areal Density, KN/ g/cm ²	Load/ Comp. Areal Density, KN/ g/cm ²	Compression Stress, Mpa
6L-1	4.11	5.38 (2)	28.13	8.84	45.17 (2)
6L-2	3.94	5.32 (16)	30.26	9.09	106.09 (15)
6L-3	3.88	5.00 (3)	28.47	8.33	44.51 (6)
6L-4	4.02	4.98 (4)	26.64	8.18	43.30 (6)
6L-5	3.93	4.98 (3)	27.53	8.24	43.72 (4)
6L-6	3.90	4.80 (3)	26.59	7.91	42.47 (5)
9L-1	6.04	7.12 (2)	24.57	7.97	98.22 (2)
9L-2	5.79	6.87 (2)	25.15	7.96	93.37 (2)
9L-3	5.81	7.00 (6)	25.90	8.25	41.54 (5)
9L-4	6.02	7.06 (0)	25.48	8.11	40.67 (11)
9L-5	5.98	7.61 (5)	27.99	8.82	43.86 (5)
9L-6	5.78	6.63 (3)	24.16	7.78	39.54 (3)

Main effect of number of layers on compression properties

Figure 119 shows the effect of number of Y-yarn layers on the compression peak load in the X- and Y-directions. The graph indicates that there is a significant difference between the samples with different layers which was confirmed by ANOVA analysis in Appendix D.1.4 (Tables 69-71). The 9 layers samples in the warp and weft directions have a higher peak load compared to 6 layers of composite samples. This is due to the presence of higher number of yarns in the 9 layers compared to 6 layers. This indicates that in 9 layers, more yarns contribute towards the compression strength. The compression stress in Y- and X-directions is illustrated in Figure 120,

indicated that 9 layers has a slightly better compression results than that of 6 Y-yarn layers, however the ANOVA analysis exhibited that the number of layers does not affect the compression behaviors of the samples in both warp and weft direction. The compression peak load was normalized by the preform areal density and the composite areal density. The 9 Y-yarn layers had a slightly lower compression load after normalization by preform areal density however, the different between 6 and 9 Y-yarn layers was not significant when the compression peak load was normalized by composite areal density.

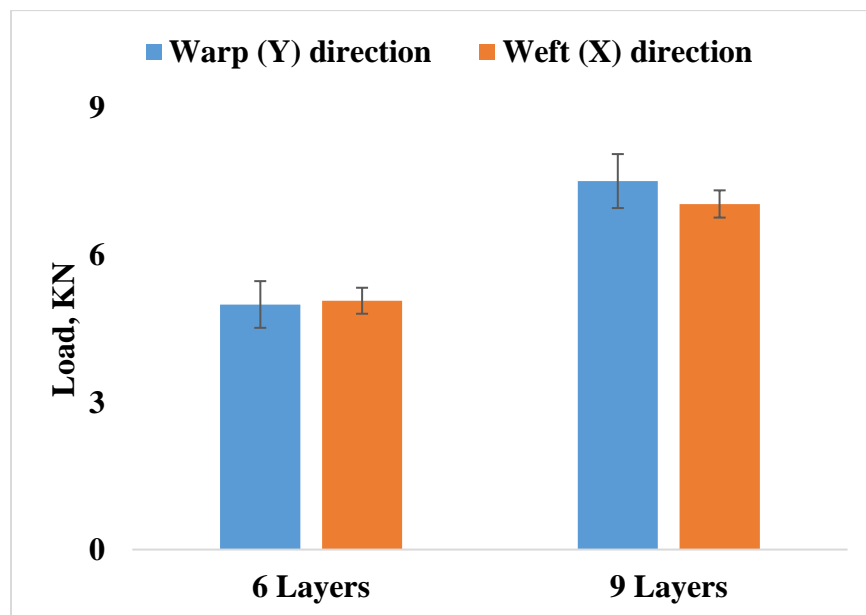


Figure 119. Main effect of layers on the compression peak load

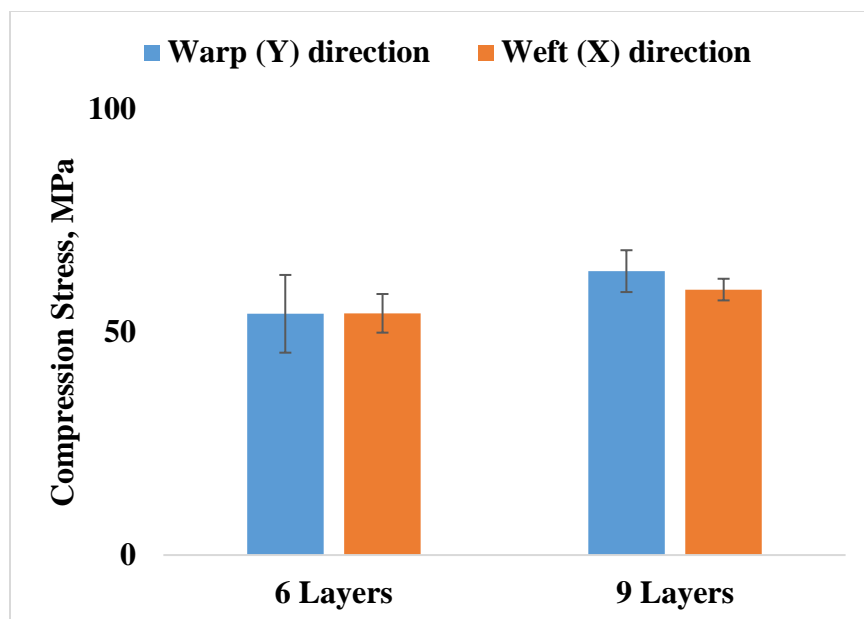


Figure 120. Main effect of layers on the compression stress

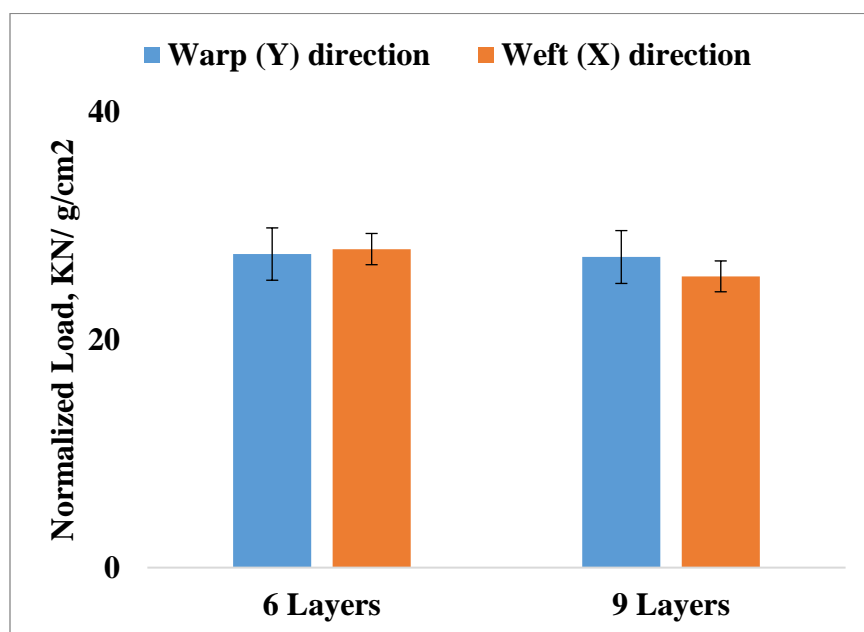


Figure 121. Main effect of layers on the normalized compression peak load by preform areal density

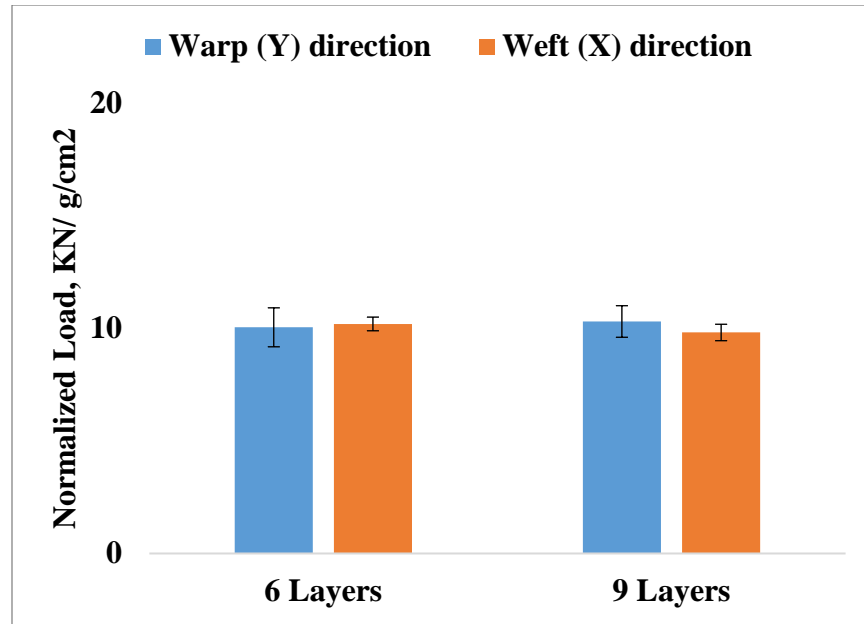


Figure 122. Main effect of layers on the normalized compression peak load by composite areal density

Main effect of weave on compression properties

Figure 123 shows the effect of the weave on the compression peak load in the X- and Y-directions indicating that 2x2 warp rib specimens have the highest compression peak load followed by plain weave and 3x3 warp rib specimens. ANOVA and Tukey analyses indicated that there was no significant difference between the samples with different weaves in the Y-direction, however in case of X-direction, the weave design affected the compression peak load significantly as shown in Appendix D.1.4 (Tables 69 and 73 & Figures 251 and 255). This is due to the resin rich areas in 2x2 warp rib and 3x3 warp rib when compared to plain weave. After normalizing the compression peak load was normalized by thickness, 2x2 warp rib showed higher values than plain weave and 3x3 warp rib. This is due to the difference in specimens' thickness from composite panel to another which depend namely on the pressure induced during the VARTM process. Therefore, normalizing the peak load to thickness did not indicate a fair

comparison. In contrast, the normalized compression peak load by preform and composite areal densities (Figures 125 and 126) showed no significant difference between different weaves. The results were confirmed using ANOVA and Tukey analyses as shown in Appendix D.1.4 (Tables 70-72 and 74-76 & Figures 252-254 and 256-258).

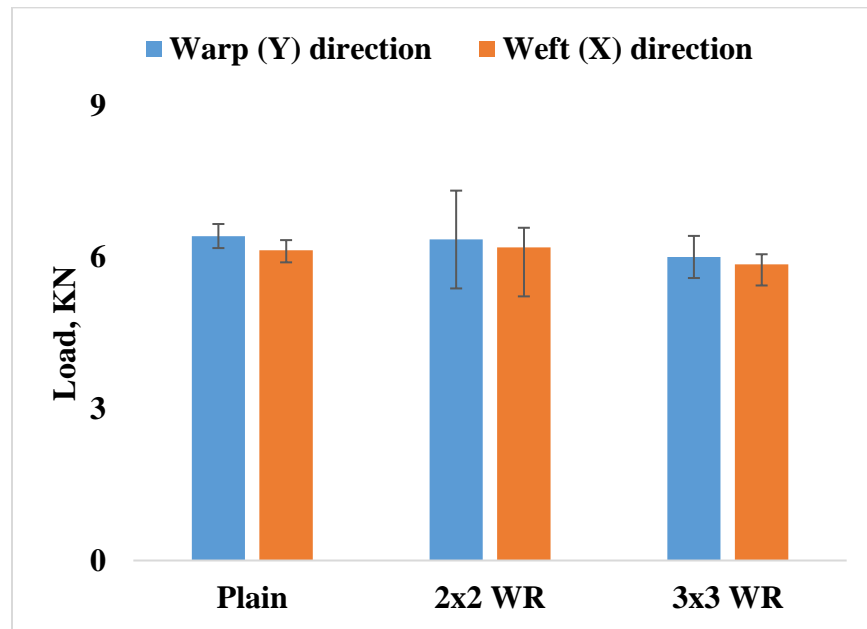


Figure 123. Main effect of weave on the compression peak load

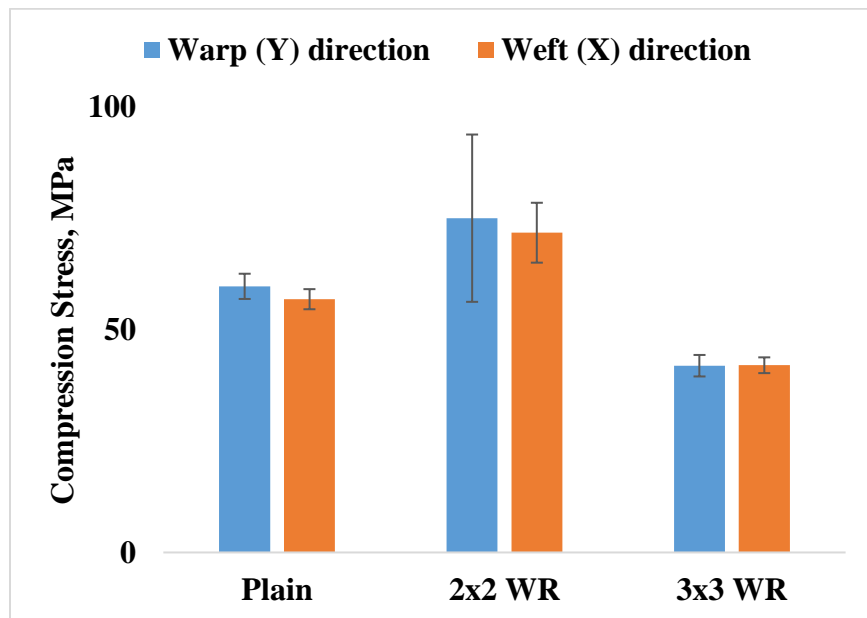


Figure 124. Main effect of weave on the compression stress

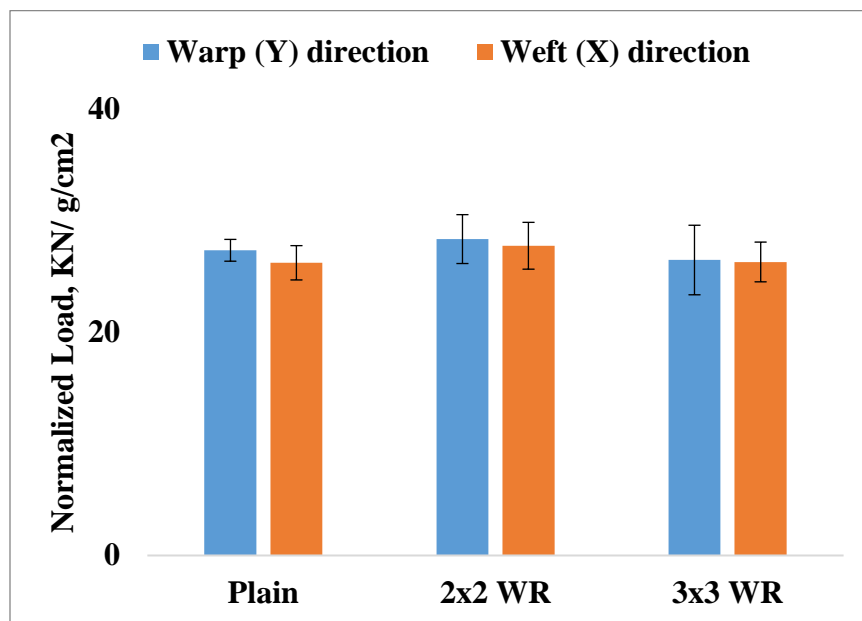


Figure 125. Main effect of weave on the normalized compression peak load by preform areal density

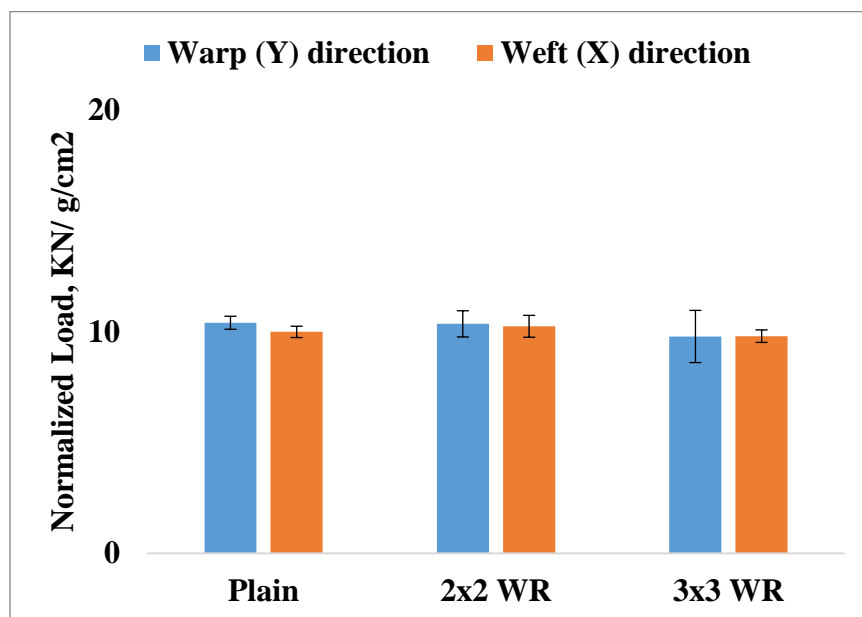


Figure 126. Main effect of weave on the normalized compression peak load by composite areal density

Main effect of number of Z- to Y-yarn ratio on compression properties

Figure 127 shows the effect of Z- to Y-yarn ratio on the compression peak load in the X- and Y-directions which indicates that 1:1 ratio samples has higher compression peak load than that of 1:3 ratio. ANOVA test showed that the effect of changing the Z- to Y-yarn ratio was significant only in the Y-direction as indicated in Appendix D.1.4 (Tables 69 and 73). The compression stress and the normalized compression load by composite areal density showed similar trend however, the normalized load by preform areal density indicated that the effect was not significant in both directions as shown in Figures 128-130. The results was confirmed by ANOVA test in Appendix D.1.4 (Tables 70-72 and 73-75). Although the normalized Peak compression load by preform areal density showed no significant difference between 1:1 and 1:3 Z:Y yarns ratio, the interaction between the weave and Z:Y ratio showed a significant effect in the Y-direction as shown in Appendix D.1.4 (Table 71).

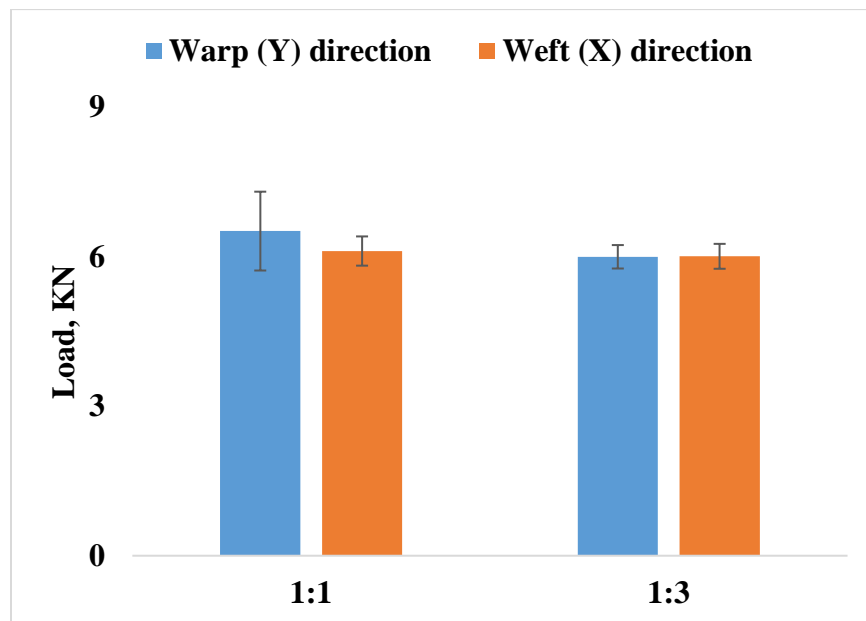


Figure 127. Main effect of Z: Y-yarn ratio on the compression peak load

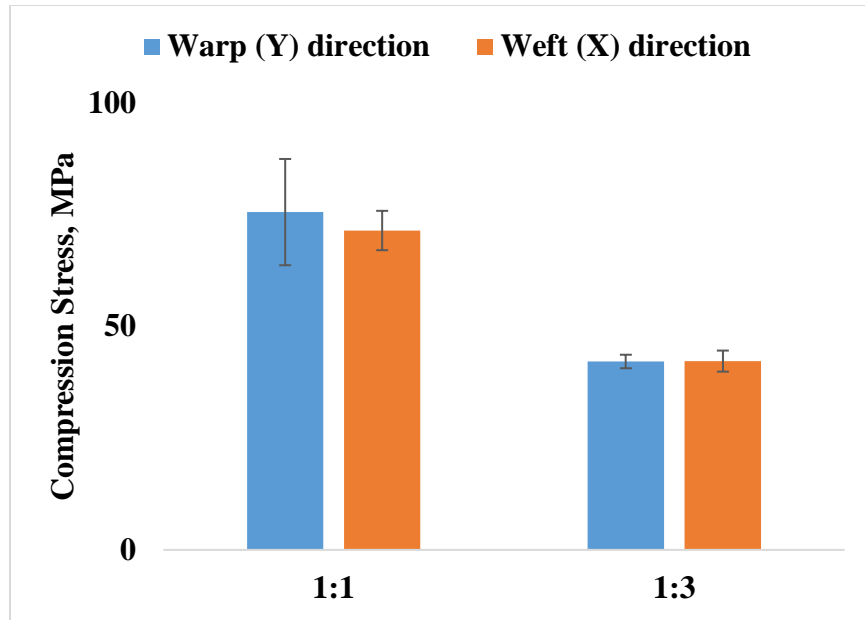


Figure 128. Main effect of Z: Y-yarn ratio on the compression stress

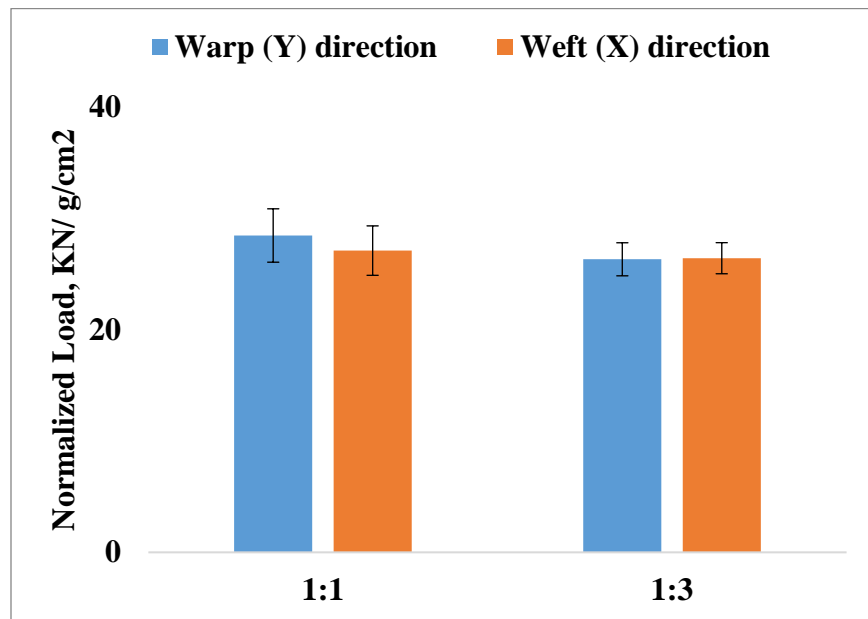


Figure 129. Main effect of Z: Y-yarn ratio on the normalized compression peak load by preform areal density

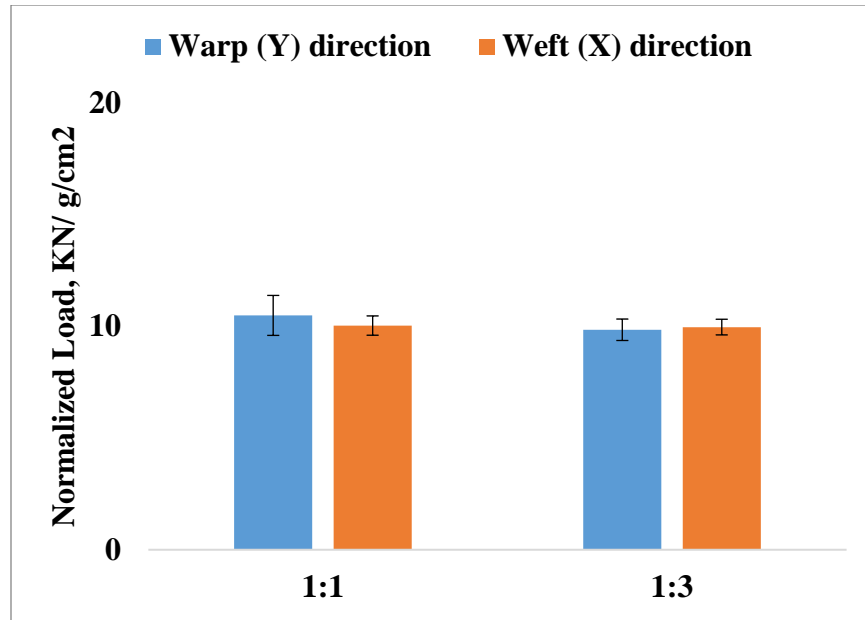


Figure 130. Main effect of Z: Y-yarn ratio on the normalized compression peak load by composite areal density

5.3.2. Experimental Design B

In design of experiment B, the type of X-yarn had been changed to study the effect of the surface treatment on the model prediction. Two levels of the number of Y-yarn layers (3 and 6) were considered in this design. Plain weave and 1:1 Z:Y yarns ratio were used for all the samples in experimental design B. The experimental design variables and levels are listed in table 38.

Table 38. Variable used in experimental design B

Sample ID	Y-layers	Filling Yarn	X-yarns density (picks/ inch/ layer)
3L-1	3	Bleached	10.28
3L-7	3	BHS	10.28
3L-8	3	HS	10.28
3L-9	3	Grey	10.28
6L-1	6	Bleached	11.76
6L-7	6	BHS	11.76
6L-8	6	HS	11.76
6L-9	6	Grey	11.76

The fixed parameters in this experimental design were; plain weave, 1:1 Z- to Y-yarn ratio, Y-yarns density, Y- and Z-yarns were bleached.

5.3.2.1. Tensile properties

The tensile properties of 3DOW composites with different X-yarns and two different thicknesses were tested. The results of the tensile test including the peak tensile load, failure strain and peak tensile stress were analyzed. A total of 40 (8x5) specimens from weft (X-yarn) direction were analyzed using ANOVA to investigate the effect of surface treatment on the tensile properties.

The results of the tensile test in weft direction are listed in Tables 39

Table 39. Results of tensile test in the weft (X-yarn) direction- experimental design B

Sample ID	Thickness of Tensile Specimens, mm	Modulus, Gpa (CV%)	Peak Tensile Load, KN (CV%)	Load/ Preform Areal Density, KN/ g/cm²	Load/ Comp. Areal Density, KN/ g/cm²	Peak Tensile Stress, Mpa (CV%)	Failure Strain, % (CV%)
3L-1	2.06	6.85 (3)	4.77 (3)	56.10	15.70	154.34 (3)	2.41 (2)
3L-2	1.95	7.42 (2)	4.93 (8)	55.39	16.24	169.23 (10)	2.55 (10)
3L-3	1.93	7.08 (4)	4.31 (4)	48.29	14.36	149.27 (4)	2.33 (4)
3L-4	2.08	5.81 (4)	3.98 (8)	47.56	12.59	127.34 (5)	2.48 (10)
3L-5	4.27	5.53 (5)	12.26 (5)	64.09	20.15	113.15 (6)	2.32 (7)
3L-6	4.00	5.62 (3)	11.97 (3)	64.61	20.23	117.97 (5)	2.50 (5)
6L-1	3.91	5.78 (4)	11.78 (6)	62.74	19.52	118.74 (7)	2.46 (7)
6L-2	4.03	4.15 (8)	9.23 (4)	49.89	15.16	90.18 (5)	2.81 (13)

Figure 131 shows the peak tensile load of 3DOW composites in the X-direction of different X-yarns. The ANOVA and Tukey HSD analyses indicated that there was no significant difference between the tensile peak loads of different types of yarns as shown in Appendix D.2.1 (Table 77 and Figure 259). After normalizing the peak load by the specimens' thickness, preform areal density and the composite areal density, the ANOVA analysis in Appendix D.2.1 (Tables 78-80) induced that there was a significant difference in the tensile peak load between specimens with

different types of X-yarn. Tukey HSD in Appendix D.2.1 (Figures 260-262) confirmed that there was a substantial difference between specimens with bleached flax and grey flax, however the difference was not significant between the samples of BHS flax and the HS flax. While the difference was not statistically significant, samples with BHS flax showed a higher average peak load compared to the samples with HS flax. In general, the samples with bleached yarns (bleached flax and BHS flax) showed higher tensile loads than their corresponding unbleached yarns (grey flax and HS flax). This was because of the effect of the surface treatment that increased the (OH) groups on the surface of the fibers and therefore enhanced the interaction between the fiber and the matrix. Although, as indicated before in Table 25 that the bleaching surface treatment caused damages to the surface of the fibers, it helped to improve the interfacial bonding between the flax fibers and the Vinylester resin which is a very crucial aspect in determining the tensile properties of the composite. Another reason was that grey flax yarns had higher variability in yarn tenacity than bleached flax yarns as indicated in Table 26. This variability caused a higher probability for the yarns to break at the weakest points (weak-link effect).

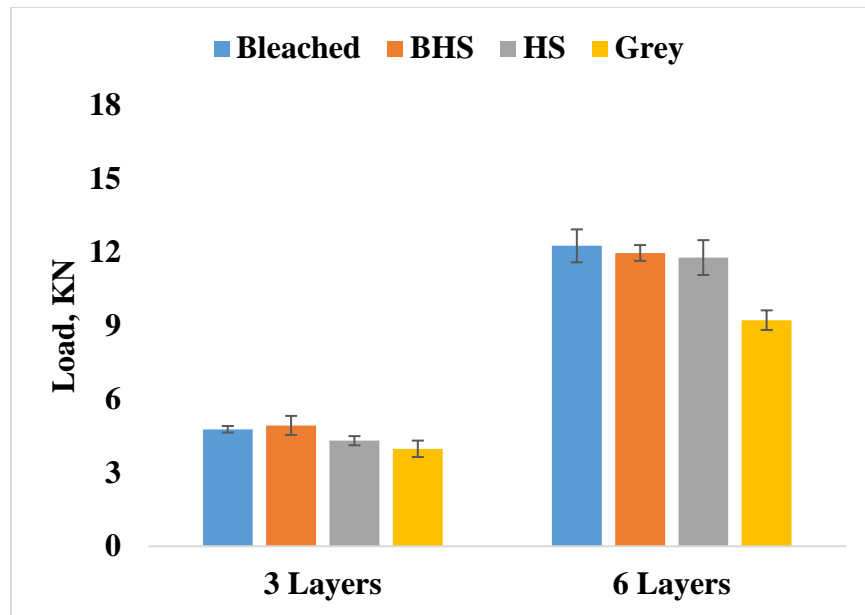


Figure 131. Effect of filling yarn type on tensile load

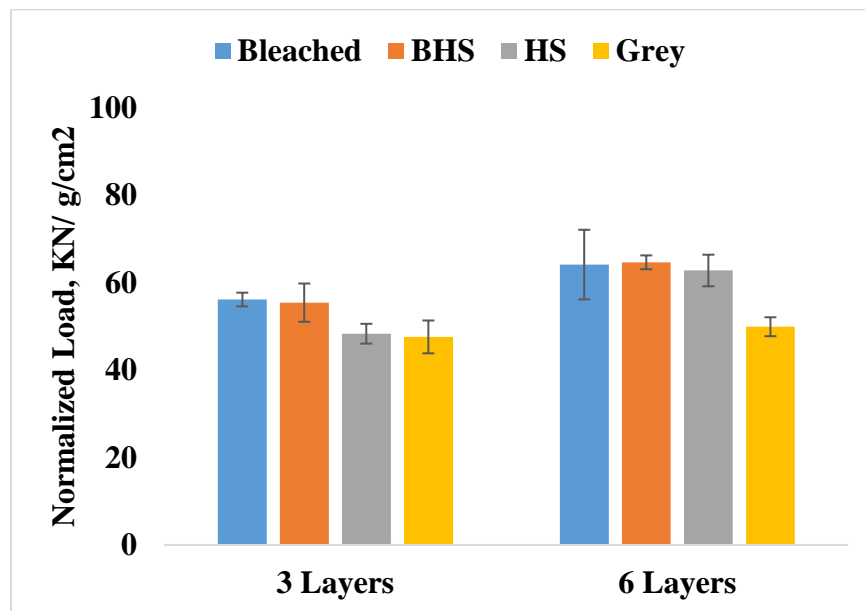


Figure 132. Effect of filling yarn type on tensile load normalized by preform areal density

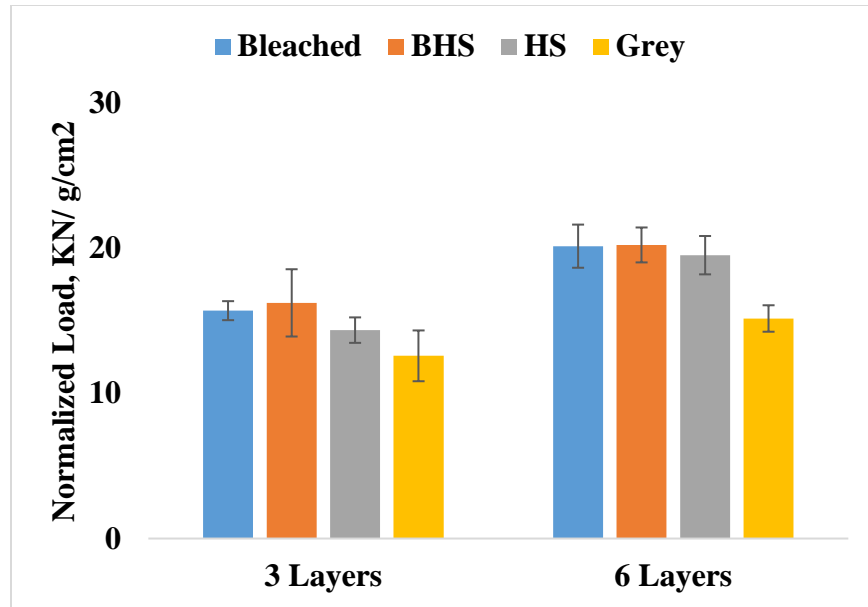


Figure 133. Effect of filling yarn type on tensile load normalized by composite areal density

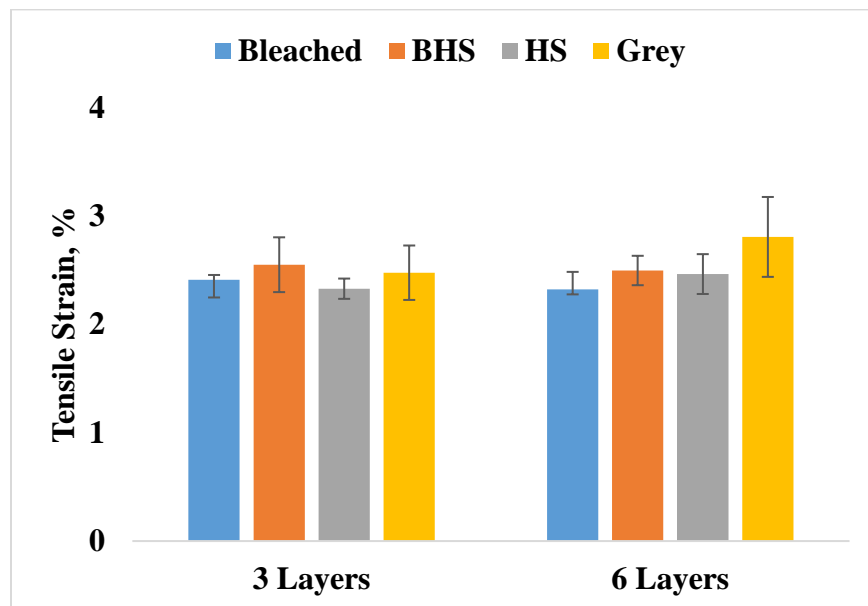


Figure 134. Effect of filling yarn type on tensile strain

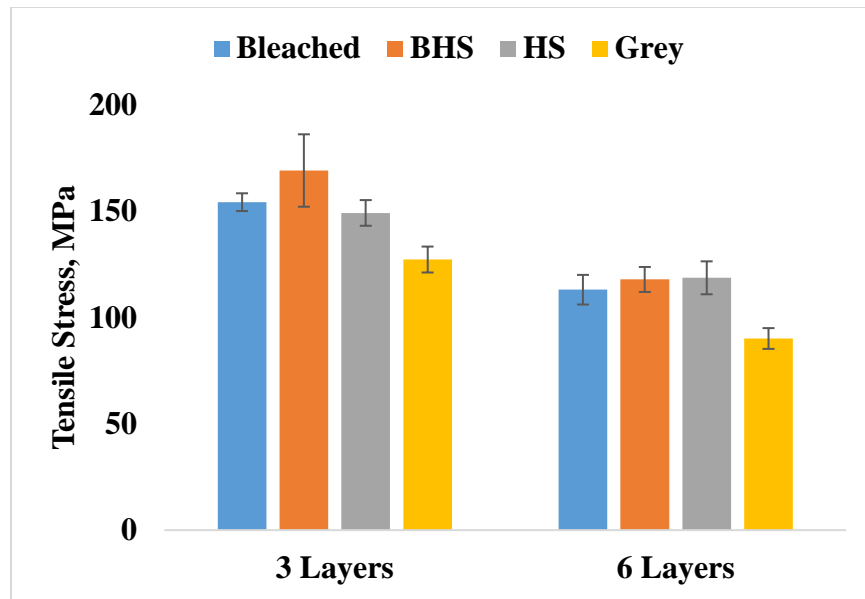


Figure 135. effect of filling yarn type on tensile stress

5.3.2.2. Tup impact

The Tup impact test was performed using 3DOW composites with different X-yarns and two different thicknesses. The results of Tup impact test including the peak impact force and the impact energy were analyzed. A total of 40 (8x5) specimens were analyzed using ANOVA and Tukey HSD analyses to investigate the effect of surface treatment on the impact results. The results of the Tup impact test are listed in Table 40.

Table 40. The Tup impact test results- experimental design B

Sample ID	Thickness, mm	Peak force, kN	CV, %	Total energy, J	CV, %	Energy/ thickness, J/ mm	Energy/ preform areal density, J/ g/cm²	Energy/ comp. areal density, J/ g/cm²
3L-1	2.03	0.75	15.57	6.17	34.16	3.05	72.57	20.31
3L-7	1.95	0.60	6.37	4.23	20.83	2.18	47.57	13.95
3L-8	1.93	0.57	12.19	4.19	9.57	2.18	46.96	13.97
3L-9	2.08	0.69	12.48	4.99	21.54	2.40	59.69	15.80
6L-1	4.21	2.18	5.65	16.32	2.76	3.88	85.34	26.82
6L-7	4.00	2.17	6.74	19.15	17.04	4.79	103.36	32.36
6L-8	3.91	2.00	2.91	14.40	4.06	3.68	76.69	23.86
6L-9	4.03	2.11	2.64	19.62	12.72	4.87	106.07	32.24

Figures 136 and 138 show the peak impact force and impact energy of 3DOW composites of different filling yarns in the X-direction. The ANOVA and Tukey HSD analyses in Appendix D.2.2 (Table 81 and Figure 263) indicated that there was no significant difference between impact results of different types of yarns. After normalizing the peak impact force and the impact energy by specimens' thickness, preform areal density and composite areal density, ANOVA and Tukey HSD analyses induced a similar trend as indicated in Appendix D.2.2 (Tables 82-84 and Figures 264-266). Figures 138- 140 show the effect of X-yarn type on the normalized impact energy by thickness, preform areal density and composite areal density, respectively.

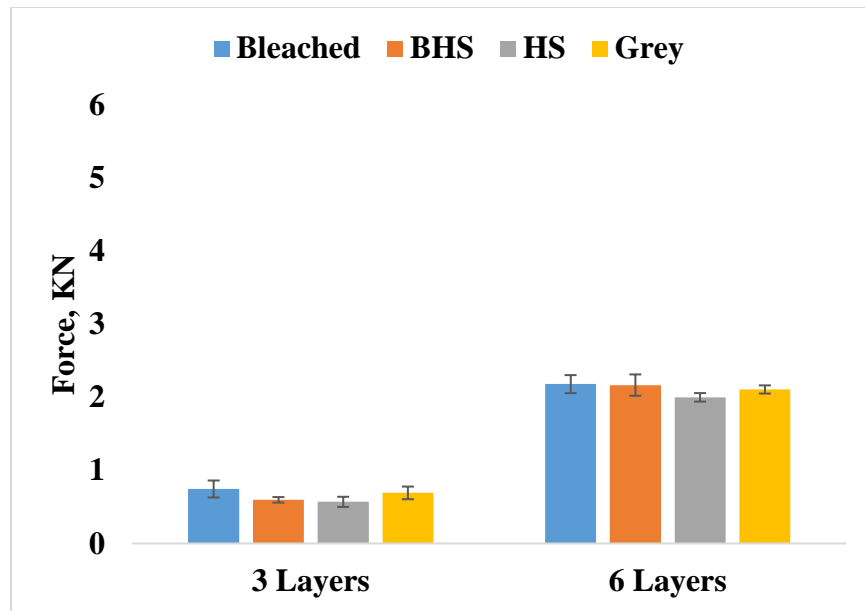


Figure 136. Effect of filling yarn type on peak force

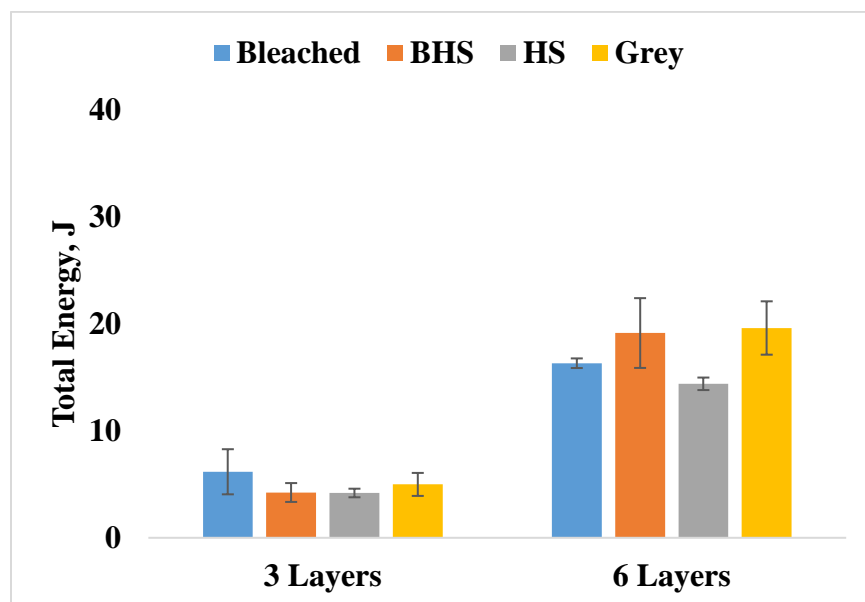


Figure 137. Effect of filling yarn type on impact energy

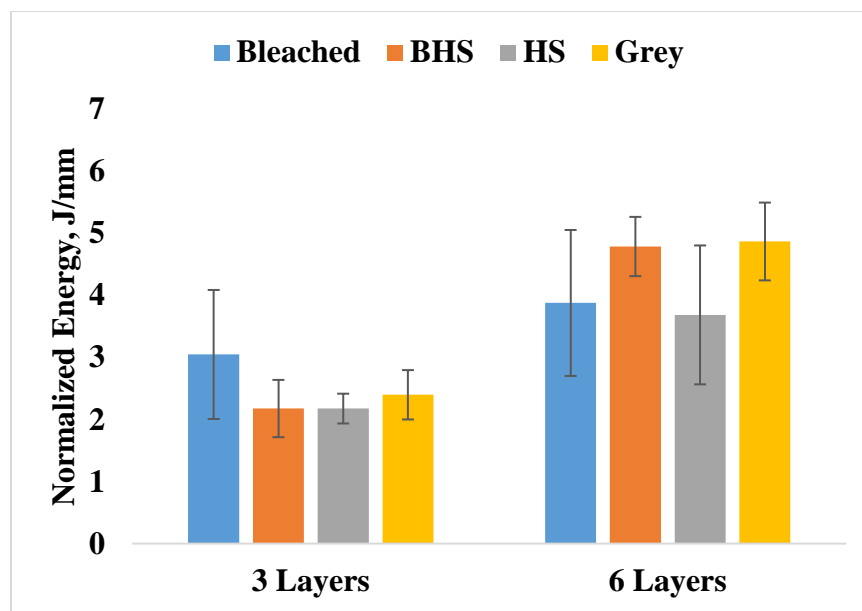


Figure 138. Effect of filling yarn type on impact energy normalized by composite thickness

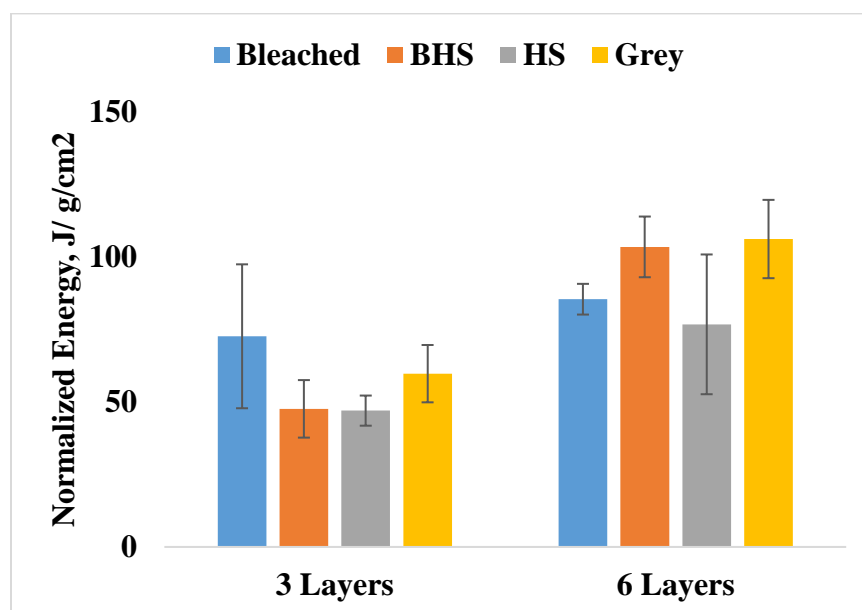


Figure 139. Effect of filling yarn type on impact energy normalized by preform areal density

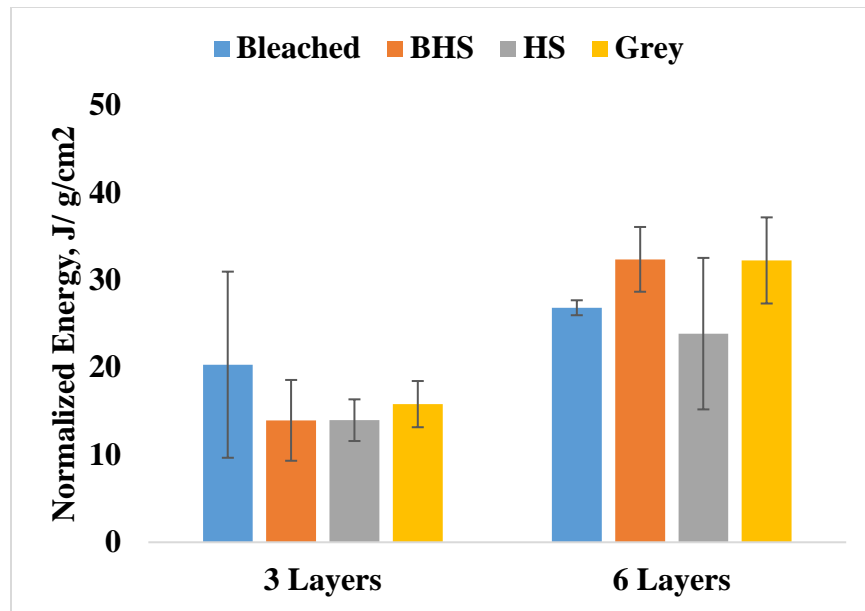


Figure 140. Effect of filling yarn type on impact energy normalized by composite areal density

5.3.2.3. Charpy impact

Samples of 3DOW composites with different types of X-yarns and two different thicknesses were tested using the Charpy impact instrument. The results of Charpy impact test are listed at Table 41. The data of 40 (8x5) specimens were analyzed using ANOVA and Tukey HSD analyses to investigate the effect of surface treatment on the impact results. The impact energy was normalized by thickness, preform areal density and composite areal density.

Table 41. Charpy impact results in the weft direction- experimental design B

Sample ID	Thickness, mm	Energy absorbed, J (CV%)	CV, %	Energy/ thickness, J/ mm	Energy/ Preform Areal Density, J/ g/cm²	Energy/ Comp. Areal Density, J/ g/cm²	Energy absorbed, % (CV%)
3L-1	2.06	0.92 (16)	15.55	0.45	10.86	3.04	8.56 (16)
3L-7	1.95	0.92 (20)	9.57	0.47	10.31	3.02	8.51 (20)
3L-8	1.93	1.23 (52)	51.61	0.64	13.80	4.10	11.41 (52)
3L-9	2.08	0.84 (24)	24.33	0.40	10.04	2.66	7.78 (24)
6L-1	4.27	2.36 (21)	20.77	0.55	12.33	3.88	21.85 (21)
6L-7	4.00	2.61 (13)	12.49	0.65	14.08	4.41	24.17 (13)
6L-8	3.91	2.06 (11)	10.47	0.53	10.99	3.42	19.12 (11)
6L-9	4.03	3.04 (7)	7.02	0.76	16.46	5.00	28.19 (7)

Figures 141 show the impact energy of 3DOW composites of different X-yarns in the weft direction. The ANOVA analysis and Tukey HSD analyses indicated that there was no significant difference between impact results of different types of yarns as shown in Appendix D.2.3 (Table 89 and Figure 272). After normalizing the impact energy by specimens' thickness, preform areal density and composite areal density, ANOVA and Tukey HSD analyses showed a similar trend as indicated in Appendix D.2.3 (Tables 90-92 and Figures 272-274). Figures 142- 144 show the effect of X-yarn type on the normalized impact energy by thickness, preform areal density and composite areal density, respectively.

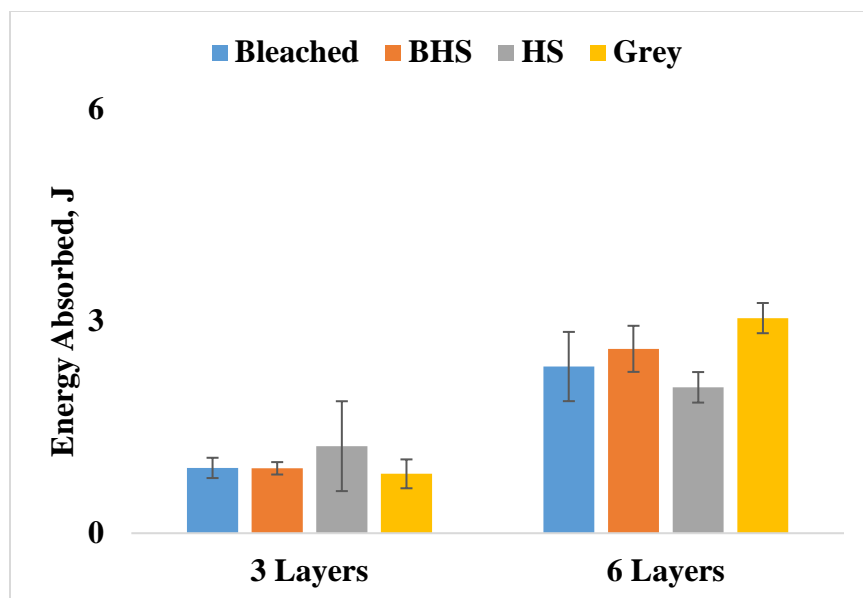


Figure 141. Effect of filling yarn type on energy absorbed

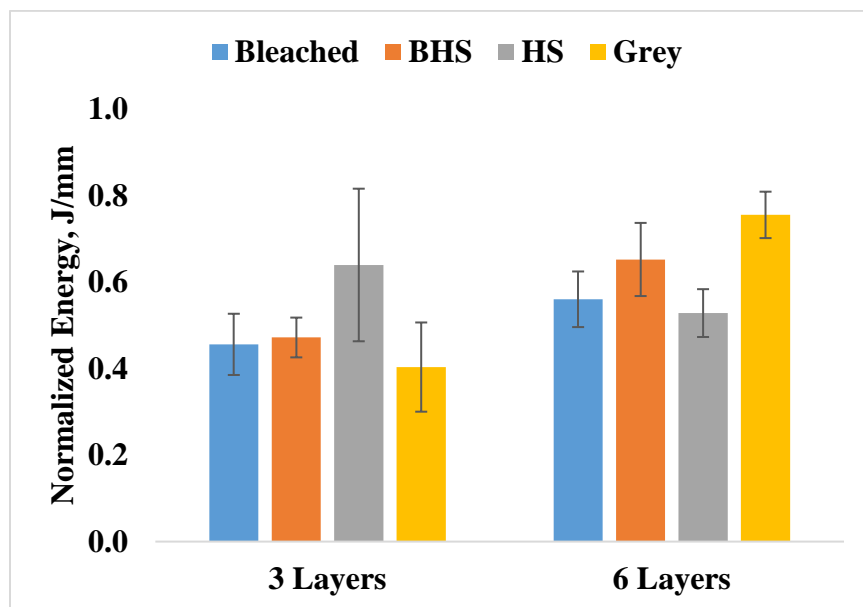


Figure 142. Effect of filling yarn type on absorbed energy normalized by composite thickness

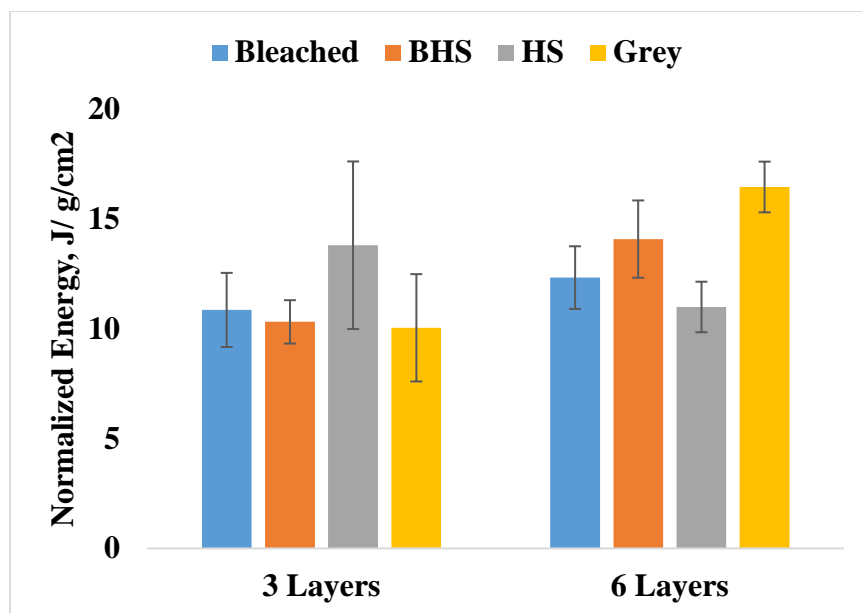


Figure 143. Effect of filling yarn type on absorbed energy normalized by preform areal density

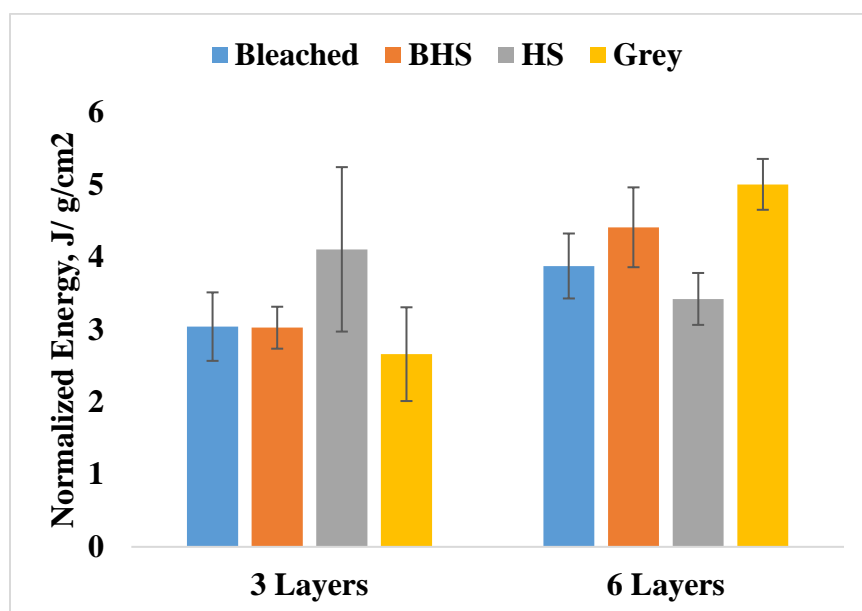


Figure 144. Effect of filling yarn type on absorbed energy normalized by composite areal density

5.3.2.4. Compression test

The compression test was performed for samples of 6 Y-yarn layers of 3DOW composites with different types of X-yarns. The results of the compression test are listed at Table 42. The data of

20 (4x5) specimens were analyzed using ANOVA and Tukey HSD analyses to investigate the effect of surface treatment on the impact results. The compression peak load was normalized by preform areal density and composite areal density.

Table 42. Compression test results in the weft direction – experimental design B

Sample ID	Thickness, mm	Peak Load, KN (CV%)	Load/ Preform Areal Density, KN/g/cm ²	Load/ Comp. Areal Density, KN/g/cm ²	Compression Stress, Mpa
6L-1	4.09	5.38 (2)	28.13	10.70	45.17 (2)
6L-7	3.79	4.32 (14)	23.33	8.88	39.40 (15)
6L-8	3.75	4.66 (3)	24.82	9.60	42.91 (4)
6L-9	4.05	4.92 (13)	26.58	9.95	41.89 (13)

Figure 145 shows the peak tensile load of 3DOW composites in the X-direction of different X-yarns. The ANOVA and Tukey HSD analyses induced that there was a significant difference between the compression peak loads of different types of yarns as shown in Appendix D.2.4 (Table 93 and Figure 275). Similar trend was experienced by compression stress and normalized compression load by preform areal density and composite areal density as shown in Figures 146-148. The results of ANOVA and Tukey HSD analyses are in Appendix D.2.4 (Tables 94-96 and Figures 276-278). Tukey HSD, indicated that there was a considerable difference between the samples with bleached flax and with grey flax, however the difference was not significant between the samples of BHS flax and the HS flax. Samples with bleached flax yarns showed higher compression load than that of grey flax yarns while, the BHS flax yarn samples got lower results than that of HS flax yarn.

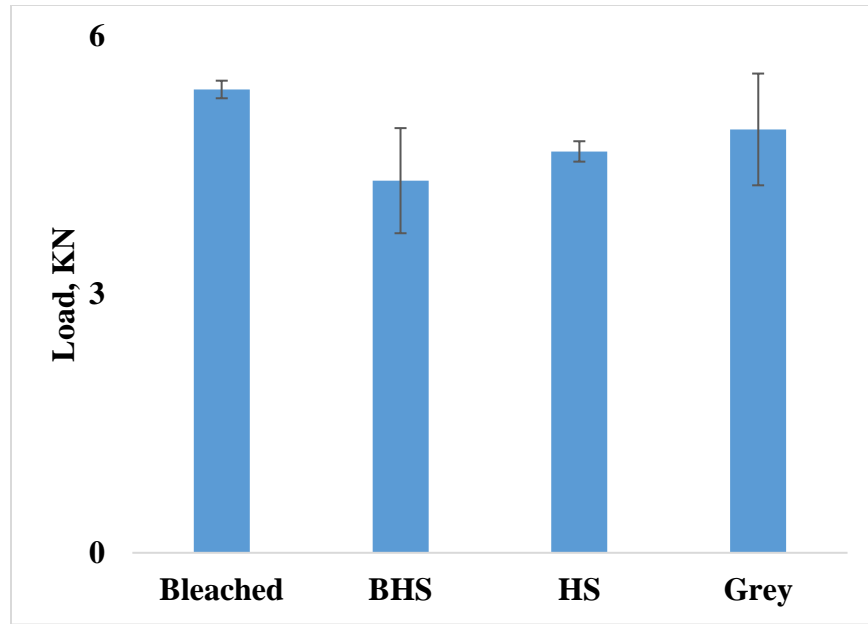


Figure 145. Effect of filling yarn type on the compression peak load

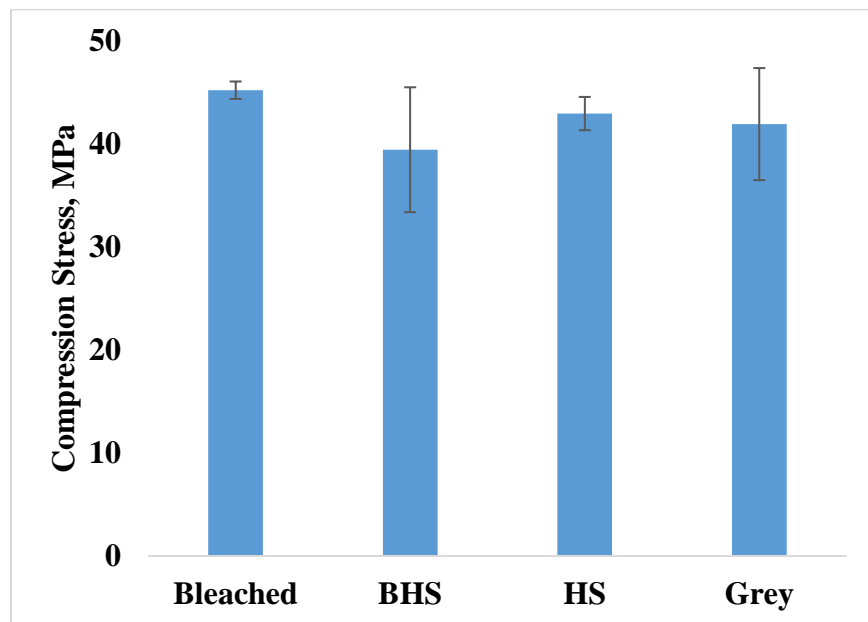


Figure 146. Effect of filling yarn type on the compression stress

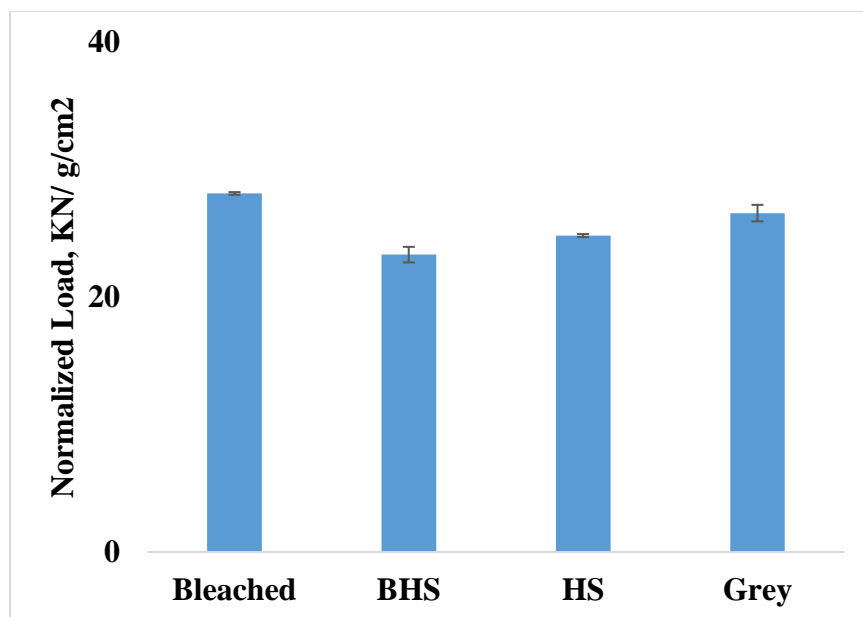


Figure 147. Effect of filling yarn type on the compression peak load normalized by preform areal density

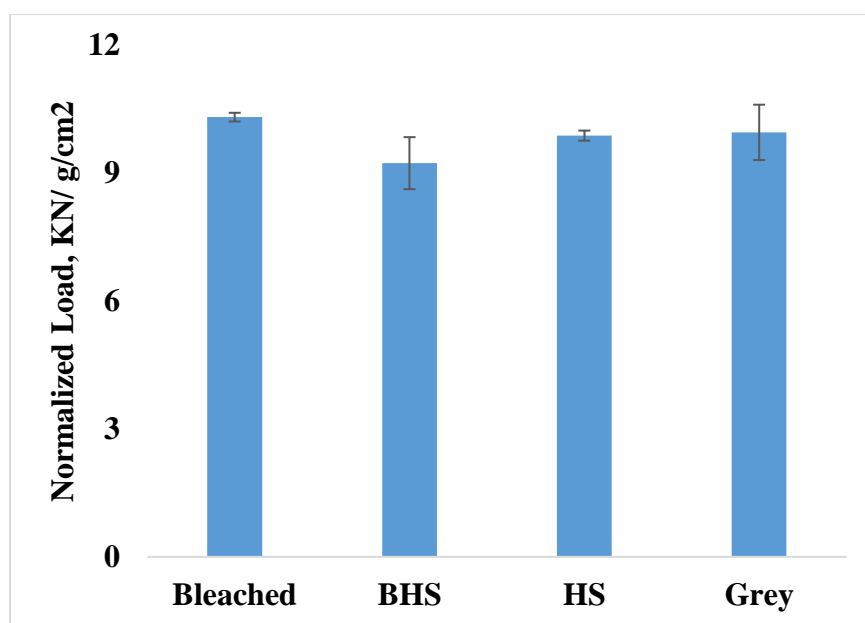


Figure 148. Effect of filling yarn type on the compression peak load normalized by composite areal density

6. GENERALIZED MODEL AND EXPERIMENTAL VERIFICATION FOR THE LOAD-EXTENSION BEHAVIOR OF 3DOW COMPOSITES

This chapter is dedicated to developing the theory for a generalized model for the load-extension behavior of 3D orthogonal woven composites from spun yarns and verifying the model with the experimental tensile results of 3DOW composite in Chapter 5.

6.1. Generalized Load-Extension Model of 3DOW Preforms

Green composites are the promising solution to reduce the environmental impacts of most advanced composites made from epoxy resin and tows of continuous flat filaments that are manufactured from petroleum precursors. Green composites can have the reinforcement or the matrix from natural components and it will be named as partial green composites, or both the components can be bio-based and then be totally green composite. Natural fiber usually spun and twisted to bind the fibers together by friction, which causes the cross-section of the yarn tends to be circular. Thus, this model will only deal with circular cross-sections of yarns.

There is a lack in developing a generalized model that can adapt the huge variabilities of natural fibers properties, as discussed in chapter 2, therefore, this research will fill the gap in this area. The objective here is to develop a generalized model for 3DOW preforms from natural spun yarns, to be able to predict its entire load-extension curve under biaxial loading. The benefits of predicting the entire load-extension include estimating the initial modulus, secant modulus at a desired elongation, peak load and stress, and toughness that are useful in characterizing the materials' performance. This model will be depending on three basic approaches: (1) Kawabata's finite deformation approach that for prediction of entire load-extension curve of plain and 2x2 twill weaves (20), (2) Sun et al. generalized model, which introduced the weave factor and can

be used for any weave design (21), and (3) use of the geometry of 3DOW preforms from spun yarns defined by Ince (26) as shown in Figure 149.

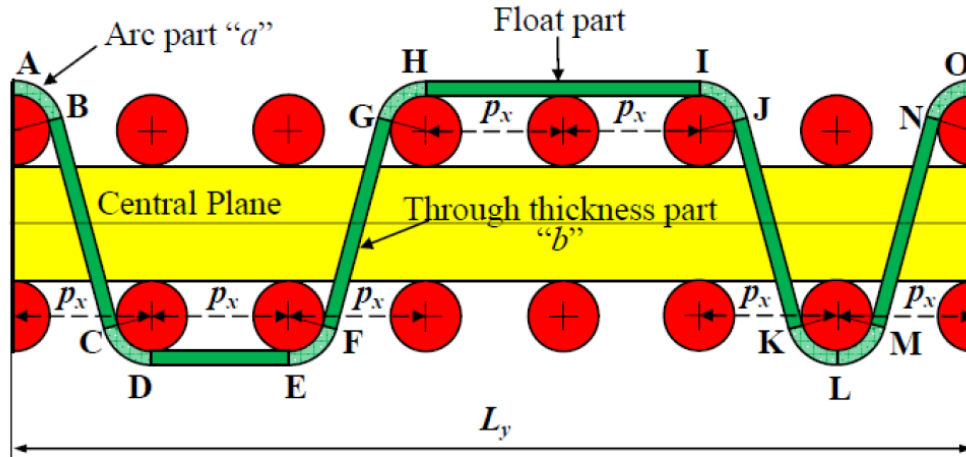


Figure 149. Ince's generalized 3D woven preform geometry of non-jammed structure for circular yarns cross-section (26)

The nonlinear actual yarn properties will be utilized as input to this model, which employs yarn segments geometry to simplify the analytical modeling of the structure. The predicted entire load-extension curve will be representative of small strains to strains near breaking values. This model can predict the performance of 3D preforms of any weave architecture including hybrid, under biaxial loading, which represents the loading in composites since the transvers (and hence Poisson's ratio) sample dimension is negligible. In any weave, the Z-yarn geometry is divided into two straight-line segments; one is parallel to the preform plane at yarn floats, and the other is inclined to the preform plane at yarns intersection. Figure 150 shows the geometry of an identical unit cell of the 2D plain weave of warp yarn at the intersection with filling yarn, which was used by Kawabata (20).

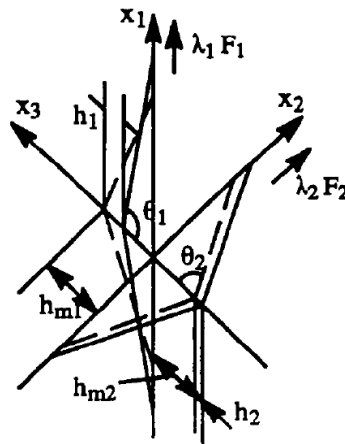


Figure 150. A unit at weave intersection in the deformed state used by Kawabata (20)

6.1.1. Nomenclature

A consistent system of nomenclature representing the 3D orthogonal preform structural parameters is listed here.

P = average yarn spacing

T = thread density

N = number of threads in the weave repeat

I = number of intersections in the weave repeat

M = weave factor = N/I

X = X-yarns direction

Y = Y-yarns direction

Z = Z-yarns direction

Θ = angle between the Z-yarn axis and the normal to the cloth plane.

L_I = Z-yarn length at intersection (slanted part)

h_m = distance between fabric neutral plane and yarn at the crossover point

n = number of layers

c = Z-yarn crimp

λ_y = stretch ratio of yarn

λ = stretch ratio of fabric along the coordinate axis, which is defined by;

$$\lambda = \frac{\text{length in the stretched state}}{\text{length in the unstretched state}} = 1 + \text{strain}$$

F_T = yarn tension

F = tensile force per single yarn end on fabric along the coordinate axis X and Y

f = tensile force per unit fabric length along the coordinate axis X and Y

g_x, g_y, g_z = tensile behavior of X-, Y-, and Z-yarns

d = yarn diameter

ϕ = yarn packing factor

ρ_1 = linear density of yarn (g/km or tex)

ρ_v = volumetric density of yarn material (g/cm³)

F_f = fiber volume fraction of a yarn

t = preform thickness

Suffix x denotes the value of X-yarn

Suffix y denotes the value of Y-yarn

Suffix z denotes the value of Z-yarn

Suffix i denotes the value of the i^{th} X-yarn

Suffix j denotes the value of the j^{th} Y-yarn

Suffix k denotes the value of the k^{th} Z-yarn

Suffix t denotes total

6.1.2. Assumptions and a Generalized Model of Any Weave

Unlike engineering materials, textile structures are not uniform in terms of their geometry and properties. Therefore, assumptions have to be made to simplify the derivation of geometrical relationships from which the model to predict the tensile properties can be achieved. The following assumptions relevant to the 3DOW structures and their constituents are made:

1. X, Y and Z-yarns are uniform cylinders
2. The bending rigidities of X, Y and Z-yarns are neglected
3. X, Y and Z-yarns are incompressible during tensile testing
4. X-yarn and Y-yarn spacing are constant
5. Z-yarn is formed of straight segments (Figure 152)

It is assumed that X, Y and Z-yarns have uniform circular cross-sections, assumption 1, with a diameter that can be calculated from yarn linear density, packing factor, and fiber density. This assumption was firstly used by Peirce in 1937 (69) for spun yarns from cotton and many researches followed this assumption (26,27,70). Yarns from staple fibers are twisted during spinning process to increase the coherent between fibers. This twist creates lateral forces, which cause the yarn be round and the circular cross-section is a good approximation.

Since X and Y-yarns are straight in the 3DOW preform with approximately zero crimp (crimp was measured Mehmet (71) and found to be insignificant), the contribution of the yarn bending rigidity to tensile property in Y- and X-directions is negligible and thus yarn bending rigidity is ignored in this research. For the Z-yarn which has crimp (Figure 152), the forces in Y-direction required to straighten the Z-yarns is negligible. The 3DOW structures are designed to maximize the in-plane properties and this is achieved by reducing the Z-yarn linear density and count. Thus the fiber volume fraction of Z-yarn is extremely low compared to Y-yarn.

Assumption 3 is valid for Y-yarns since these are not interlaced with the Z-yarn. Since Z- and X-yarns are interlaced and in contact with each other at the top and bottom layers they may be compressed during tensile loading of their composites. While this has been the case on testing woven fabrics/preforms (18-20,72), the situation is expected to be different in composites. To check the validity of this assumption specimens' dimension and images of Y-cross section before and after tensile testing were taken. It was found that the Y-yarns' remained unchanged in geometry and dimensions (Figure 151). Additionally, the thickness and width of the tested specimens did not change significantly from the specimens before testing.

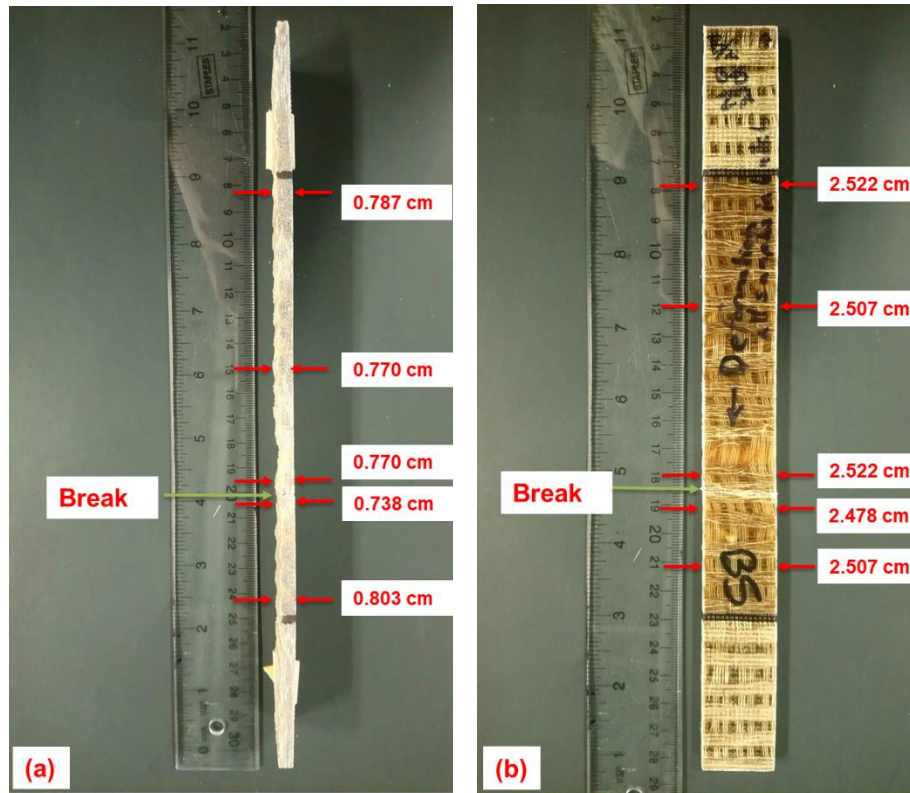


Figure 151. The dimensions of the thickness (a) and width (b) of a specimen after tensile testing

Since Y-yarns do not interlace, Y-yarns' spacing is uniform. For X-yarns, the spacing under the float is smaller than that at the intersection (21). X-yarns' spacing under the float varies depends on the preform degree of tightness. While the X-yarn spacing can be easily determined for jammed structures, it is extremely difficult to model the spacing under the float for non-jammed preforms. Additionally, it is time consuming to establish the relationship between the X-yarn spacing and degree of tightness experimentally. For this reason the X-yarn spacing is assumed to be uniform in this research to decrease the complexity.

Z-yarns follow a straight path parallel to the cloth plane at weave floats and follow inclined path to the cloth plane at weave intersections. In the case of 3D orthogonal weaving looms, the filling yarn is fed continuously without cutting after each insertion and as such, each filling yarn is doubled per insertion cycle. The filling yarn geometry is then treated as parallel double (side-by-

side) yarns. A schematic diagram of one repeat of a 3DOW fabric structure is shown in Figure 152. Figure 153 shows a hypothetical general repeat of j^{th} Y-yarn in a 3DOW structure.

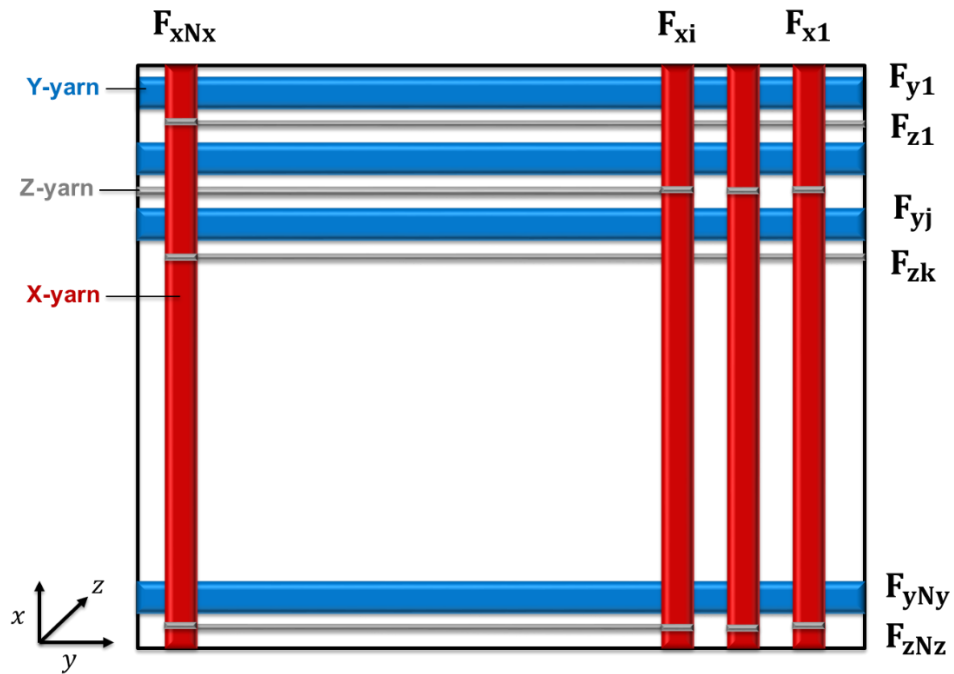


Figure 152. A schematic diagram of a generalized repeat of the 3DOW preform, including hybrid yarns

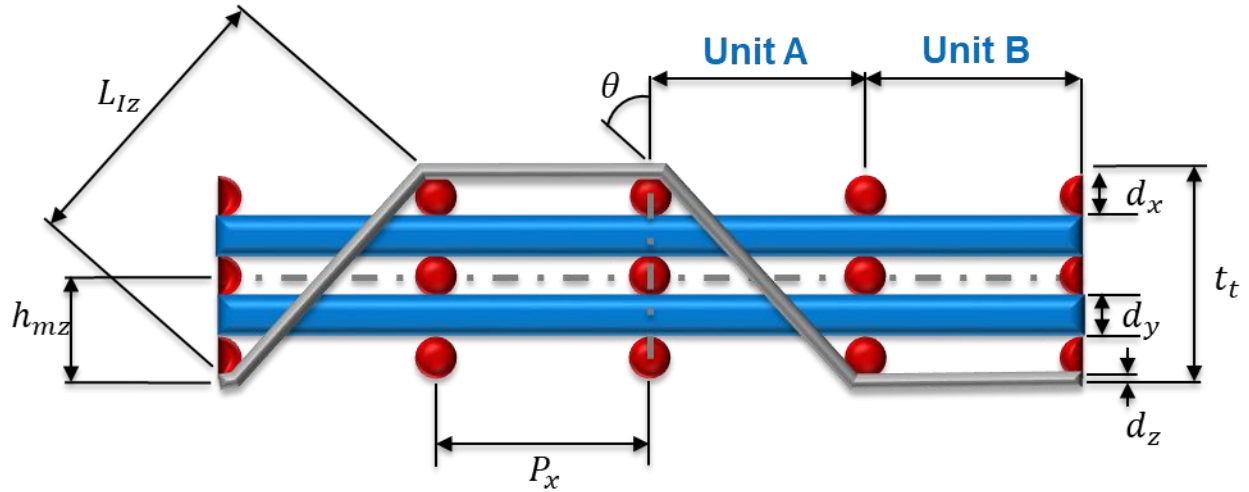


Figure 153. X-yarn cross section of a general weave repeat, X-yarns are in red, Y-yarns are in blue, and Z-yarns are in gray

The yarn diameter d (cm), can be calculated using the generalized formula (70) described in equation (3)

$$d = \frac{1}{280.2} * \sqrt{\frac{\rho_1}{\varphi * \rho_V}} \quad (3)$$

Figure 153 shows the geometry of the 3DOW structure of a general weave. The following equations can be derived from the geometry;

$$P_x = \frac{1}{T_x} \quad (4)$$

$$\sin\theta = \frac{P_x}{L_{Iz}} \quad (5)$$

$$t_t = 2d_z + d_y n_y + d_x n_x \quad (6)$$

$$\left(\frac{L_{Iz}}{2}\right)^2 = \left(\frac{P_x}{2}\right)^2 + (h_{mz})^2 \quad (7)$$

$$L_{Iz} = 2\sqrt{\left(\frac{P_x}{2}\right)^2 + (h_{mz})^2} \quad (8)$$

$$h_{mz} = (2d_z + d_y n_y + d_x n_x)/2 \quad (9)$$

6.1.3. Load-Extension Properties of X, Y and Z-yarns

Unlike engineering materials, textile structures are not uniform in terms of their geometry and properties. Therefore, the tensile properties of X and Y-yarns are represented by the following functions, which is derived from experimental measurements;

$$F_{TX} = g_x(\lambda_{yX}) \quad (10)$$

$$F_{TY} = g_y(\lambda_{yY}) \quad (11)$$

The total load acting on the X- and Y-yarns in the repeat unit can be calculated using the schematic shown in Figure 152 in which N_x is the number of X-yarns in the weave repeat in one layer, and N_y is the number of Y-yarns in the weave repeat in one layer. Therefore, the total load on the X and Y-yarns is calculated by multiplying the load on the i^{th} X-yarn, and j^{th} Y-yarn by the number of yarns per weave repeat per layer and then by the number of layers as shown in equations (12) and (13). This approach can also be used in case of using different types of X and Y-yarns.

$$F_X = n_x \sum_{i=1}^{N_x} F_{xi} \quad (12)$$

$$F_Y = n_y \sum_{j=1}^{N_y} F_{yi} \quad (13)$$

For the Z-yarn, it is divided into two-unit structures A (inclined portion) and B (straight line segment). Figure 153 shows that the total number of unit structures A and B equals the number of X-yarns in the weave repeat. The tensile properties of the straight part (B) is calculated using equation (14) which was determined from the experimental measurements.

$$F_{TZ} = g_z(\lambda_{yz}) \quad (14)$$

However, the value of the tensile force on the inclined portion of Z-yarn along the Y-axes F_z is calculated as shown in equation (15).

$$\text{Since, } F_z = F_{Tz} \sin\theta \quad (15)$$

The total load acting on the Z-yarn ends in the repeat unit is calculated by multiplying the load on the k^{th} Z-yarn by the number of yarns per weave repeat as shown in equation (16)

$$F_z = \sum_{k=1}^{N_z} F_{zk} \quad (16)$$

6.1.4. Volume Fraction of Yarns and Matrix Components

The volume fraction of each yarn component is calculated using equations (17-19) (26). By assuming that there are no voids in the composite, the matrix component volume fraction in a specific direction is calculated by subtracting the sum of the yarns volume fractions in this direction from unity.

$$F_{fx} = \frac{\frac{n_x \rho_{1x}}{\rho_{vx} 10^3}}{p_x(n_y d_y + n_x d_x + 2d_z)} \quad (17)$$

$$F_{fy} = \frac{\frac{n_y \rho_{1y}}{\rho_{vy} 10^3}}{p_y(n_y d_y + n_x d_x + 2d_z)} \quad (18)$$

$$F_{fz} = \frac{\left[\frac{L_{Iz}}{M_z} + \left(1 - \frac{1}{M_z}\right) p_x \right] N_z \rho_{1z}}{\rho_{vz} 10^3} \quad (19)$$

6.1.5. The Load-Extension Properties of General 3DOW Preform Under Biaxial Loading

To determine the load-extension behavior of any 3DOW preform, the repeat unit approach used in the model with target to predict the entire load-extension behavior by considering the preform constituents within the repeat, which represents the entire preform. Each repeat has a certain number of X-, Y-, and Z-yarns where the X- and Y-yarns are straight line segments (non-

crimped), however, the Z-yarn is divided into two unit structures A and B. Unit structure A is the inclined portion of the Z-yarn at the intersection as a result of interlacing with X-yarns, while unit structure B is the straight portion (parallel to the preform plane) at the float. The sum of numbers of unit structures A and B equals the number of X-yarns in the weave repeat as described in Figure 152. This approach is generalized for any interlacing pattern of the Z-yarn, and for hybrid structures which contain different X- and/or Y-yarns.

As mentioned, the repeat unit consists of different numbers of A and B unit structures. Thus, it is important to calculate the load-extension curve for each segment then, the entire load-extension behavior of the woven preform is computed from the behavior of individual units according to the weave pattern. For unit structure A which is the inclined segment, the load-extension behavior at a given local fabric stretch ratio λ_{zk}^A will be calculated and obtain the fabric tensile force of the Z-yarn end F_{zk} . While the load-extension behavior of unit structure B which is the straight segment is identical to X- and Y-yarns' load-extension.

For the X-axis direction, the 3DOW preform load-extension properties are decided by the properties of the X-yarns. On the other hand, it is obvious that Y and Z-yarns that have different geometry in the 3DOW contribute differently to the tensile properties in the Y-direction. Hamburger's theory (66) of blended yarns is considered since the 3DOW preform and its composite is formed from constituents of different tensile properties. The theory of blend (known also as law of mixture) predicts the tensile properties of a structure with its constituents they bear the load together until the component with the lower extension is ruptured, and then the other components continue to stand the load until the structure is ruptured. Figure 154 shows a structure with two components with component 1 ruptured first then component 2. The some of the load at a given extension is used to construct the entire load-extension of the structure. A

numerical example showing how the model handles the input parameter to derive the entire load-extension curve of 3DOW composites is indicated in Appendix B.4.

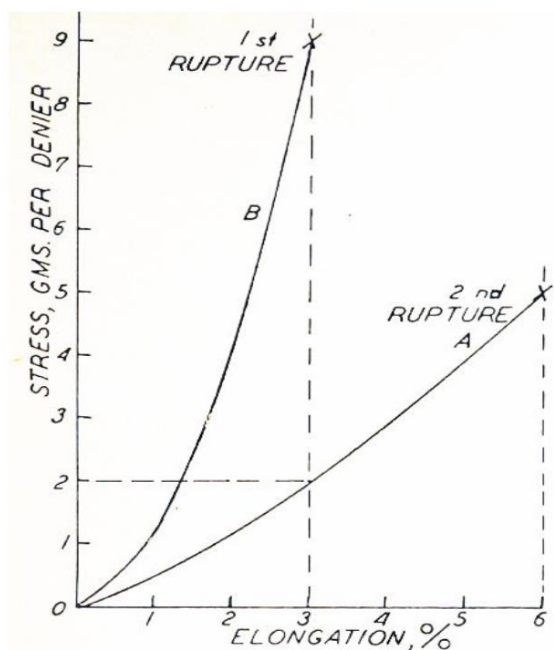


Figure 154. Effect of stress-elongation characteristics on blend strength (73)

Since the composite consists of two main components; reinforcement and matrix, Hamburger theory of blended yarns is used to obtain the entire load-extension curve of the composite from its two components. In order to apply this theory of blended yarns, it is required to know the volume fraction in addition to the load-extension properties of each component. Ince's generalized geometrical model equations for calculating the volume fraction have been used (26), and the equations are included in equations (17-19). However, the load-extension properties of fibers, yarns and resin were experimentally measured as discussed in chapter 4.

6.2. Experimental Data

In order to verify the model experimentally, the load-extension curves of the reinforcement (3DOW) and the matrix are required as inputs for the model as indicated in Figure 155. Spun

yarns from hemp and flax fibers were acquired and converted to 3DOW preforms of different architectures, then resin treated to obtain final composite panels in order to verify the model. The tensile properties of composites from hemp fibers are taken from Gupta (68).

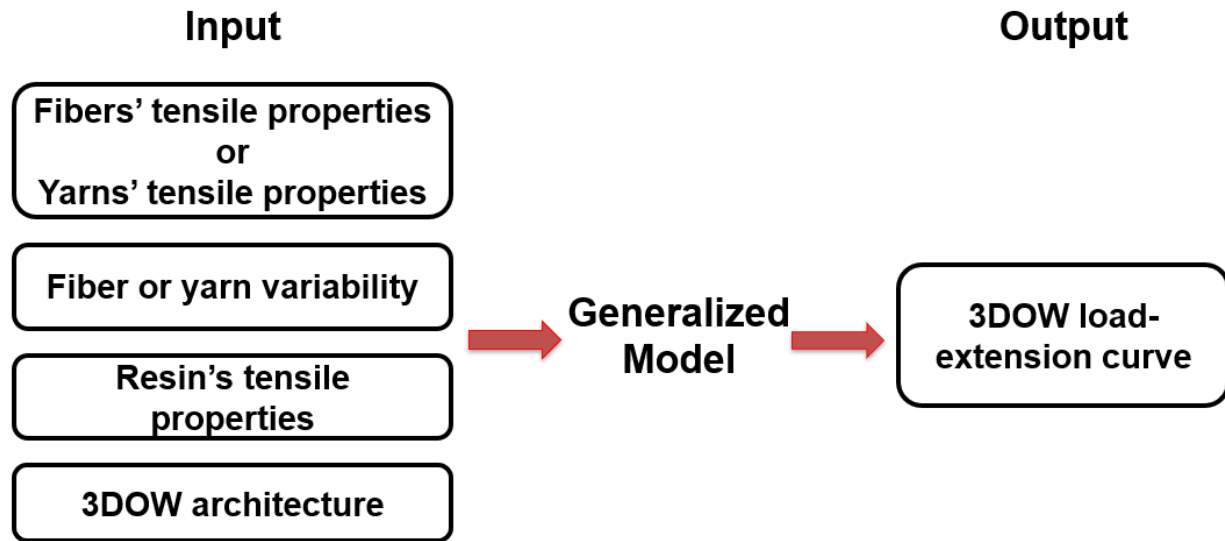
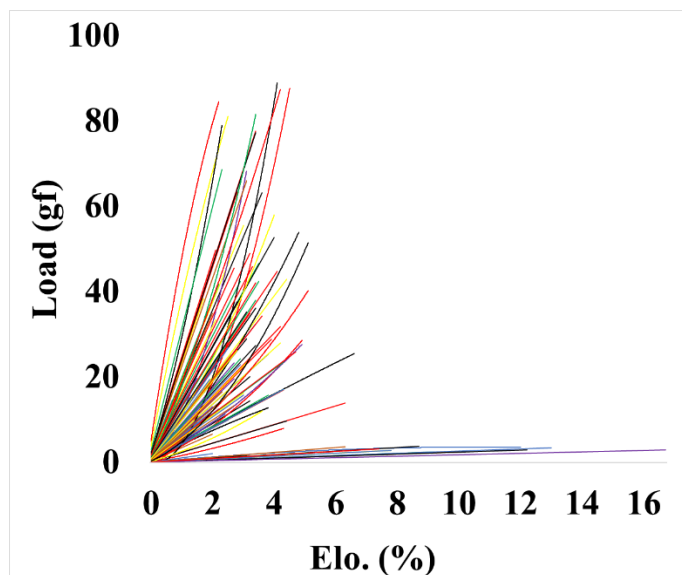


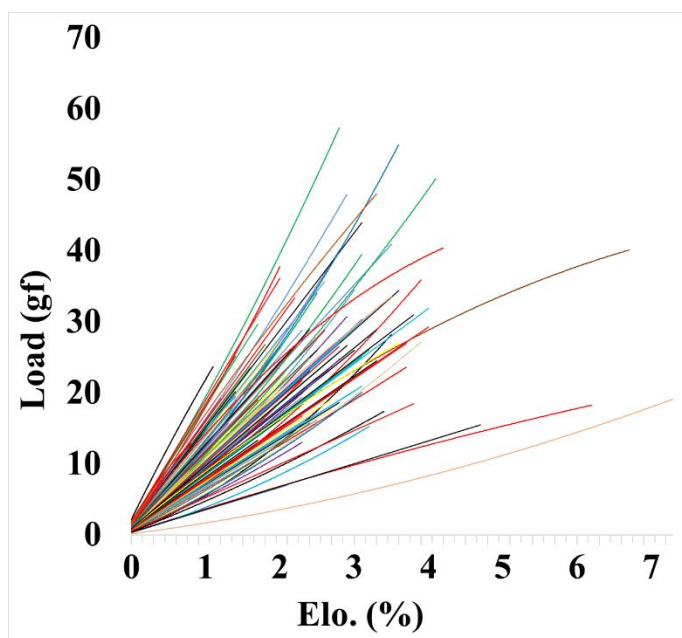
Figure 155. Summary of the input and output parameters of the generalized model

6.2.1. Load-Extension Curves of Natural Fibers and Yarns

The load-extension curves of hemp and flax fibers were determined experimentally. The ASTM D3822 was followed to determine the tensile strength of single fibers using an MTS Q Test machine, more details about the testing parameters and conditions are discussed in chapter 4. In Figure 156, the load-extension curves of hemp and bleached flax fibers are shown. Load-extension of other types of flax fibers are included in Appendix A.1. All fibers were taken out randomly from as supplied yarns by untwisting the yarns to ease the fibers removal. The figures indicate the high non-uniformity of fiber tensile properties that poses challenge in predicting their 3DOW preforms and their composites.



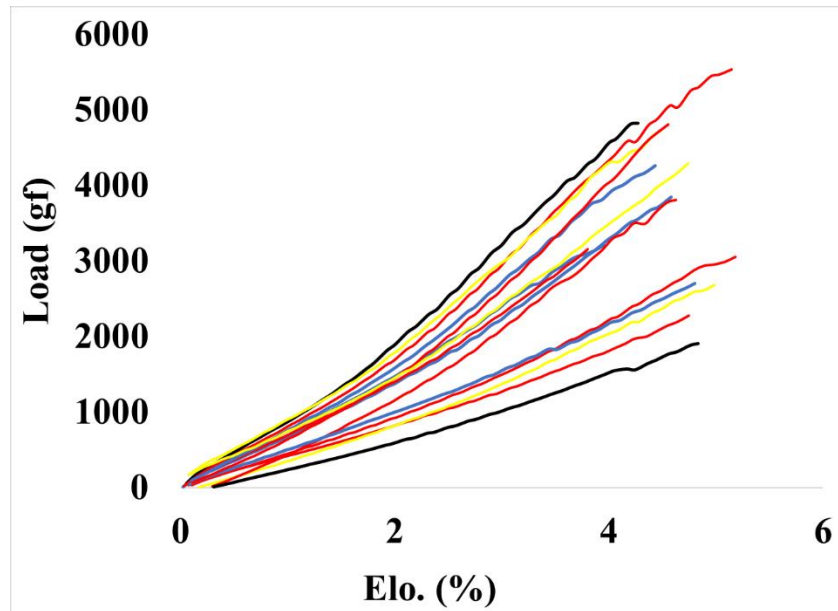
(a)



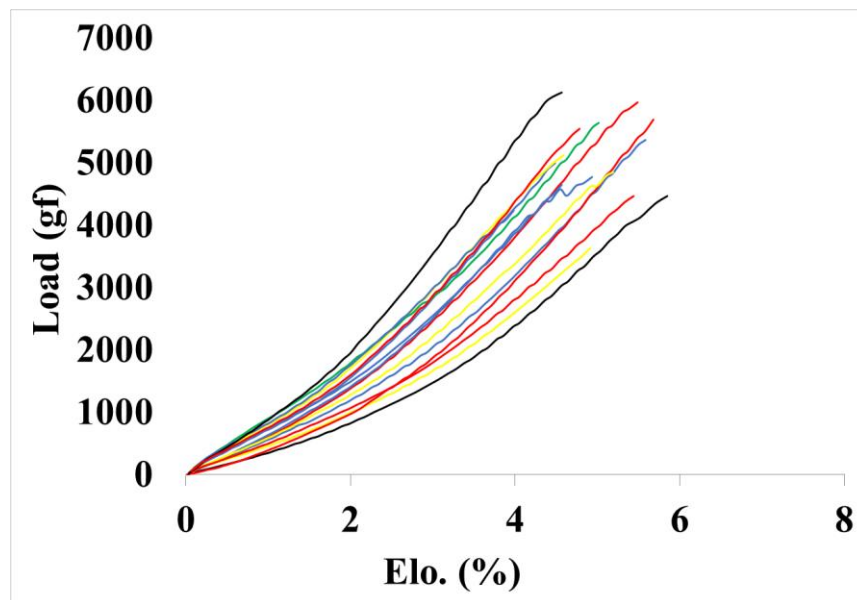
(b)

Figure 156. Load-extension curves of (a) 119 hemp fibers taken from yarns, (b) 121 bleached flax fibers taken from yarns

To get the load-extension curves of hemp and flax yarns, the ASTM D2256/ D2256-10 was followed using an MTS Q Test machine, and the procedure of measurements and testing parameters are discussed in chapter 4. The load-extension curves of hemp X-yarns and bleached flax X-yarns are shown in Figure 157. The reminder tensile data of yarns are provided in Appendix A.2. While the variability of tensile properties of the yarns are less than the fibers, it is still broad compared to yarns made from synthetic fibers.



(a)



(b)

Figure 157. Load-extension curves of (a) 17 samples of hemp X-yarn, (b) 30 samples of bleached flax X-yarn

6.2.2. Load-Extension Curve of Vinylester Resin

MTS Servo-hydraulic 370 load frame was used to measure the tensile properties of the pure Vinylester resin coupons produced for this research. It was noticed that the resin broke with different manners; single break, double break and shattered as described in the pictures in Figure 158. The load-extension curves of all specimens are shown in Figure 159. The typical load-extension curve of the pure resin was used in the model calculations.

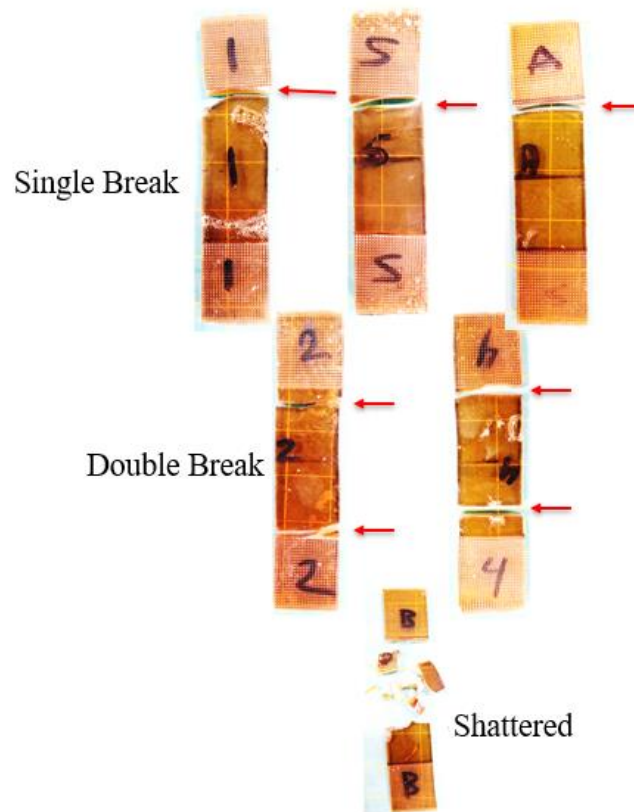


Figure 158. Breaking modes of pure resin tensile test

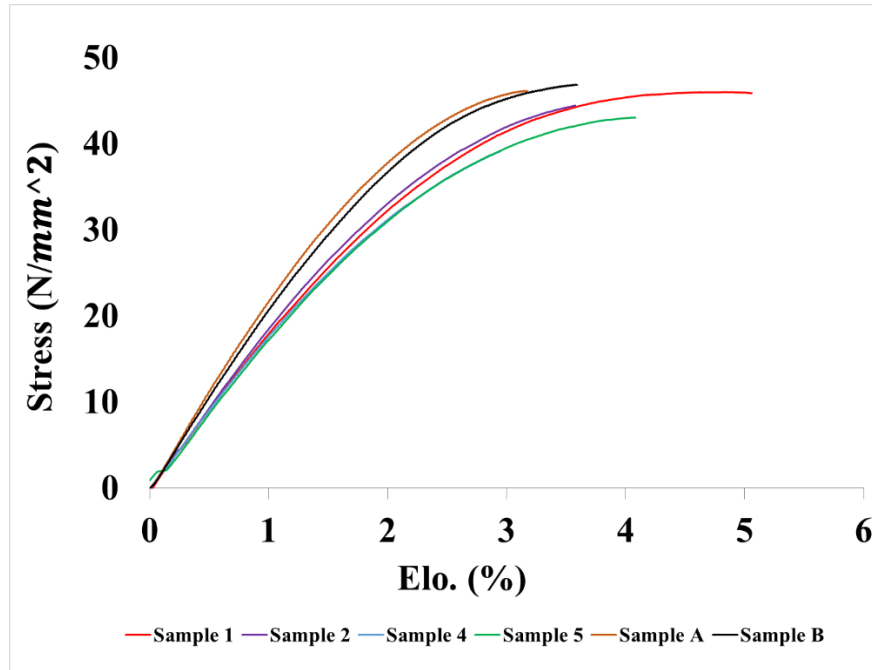


Figure 159. Load-extension curves of 5 pure resin specimens

As noticed earlier, there is significant variability in both fibers and yarns tensile properties. Using single average or typical fiber or yarn tensile curve as input to predict the tensile properties of final composites would not consider the variability. Additionally, the use of such prediction may lead to erroneous decision and deviation from the real value. To overcome this serious issue, it was decided to derive upper and lower limits load-extension curves for each yarn and use them as input to the model to predict upper and lower limits of composite tensile properties based on equation (2) in which μ is the mean value calculated from the entire experimental data points collected by the tensile tester during testing load-elongation of fibers/yarns specimens, α is critical value equals 1.96 at 95% Confidence level, σ is the standard deviation and n is the sample size. A MATLAB code was created to derive the upper and lower limits tensile curves at 95% confidence level and regression equation of each yarn and fiber used in this research. An example of flax yarn with the regression line and the upper and lower limits

is exhibited in Figure 160. All yarns' tensile and regression curves are exhibited in Appendix A.3.

$$\mu \pm \alpha \frac{\sigma}{\sqrt{n}} \quad (2)$$

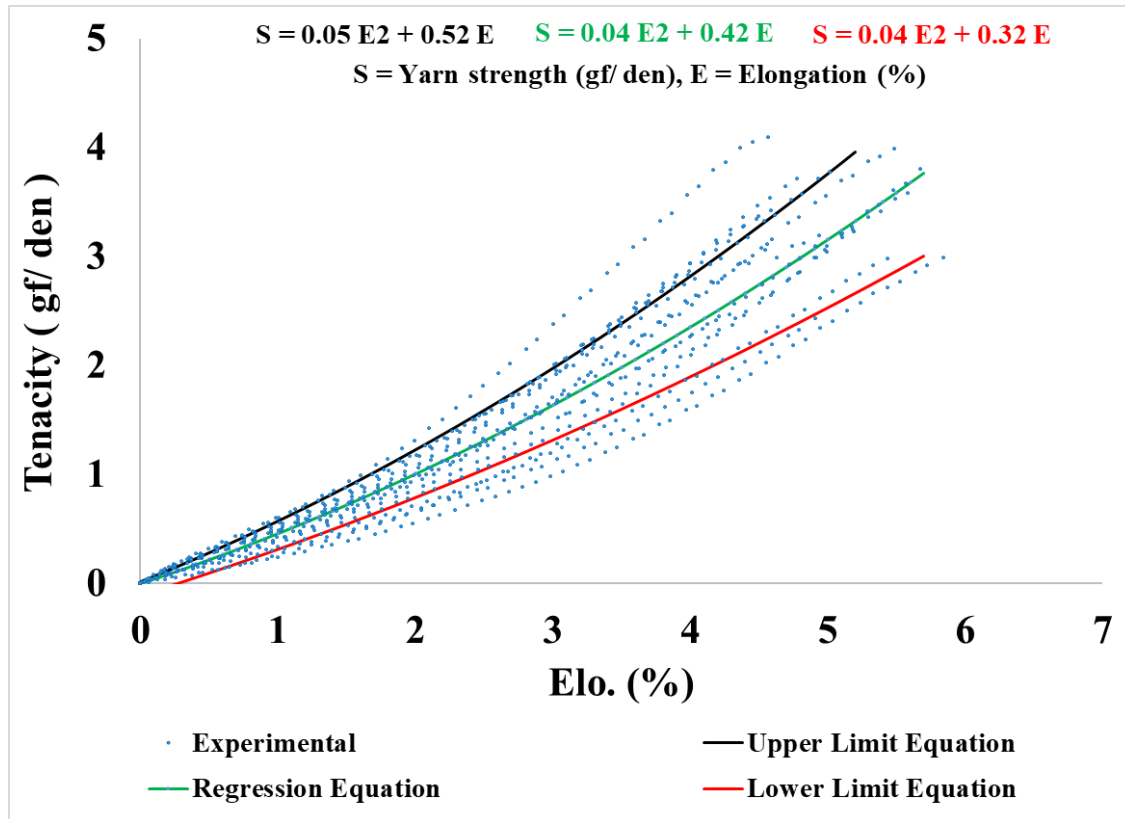


Figure 160. The experimental data, regression equation and the upper and lower limits of a flax

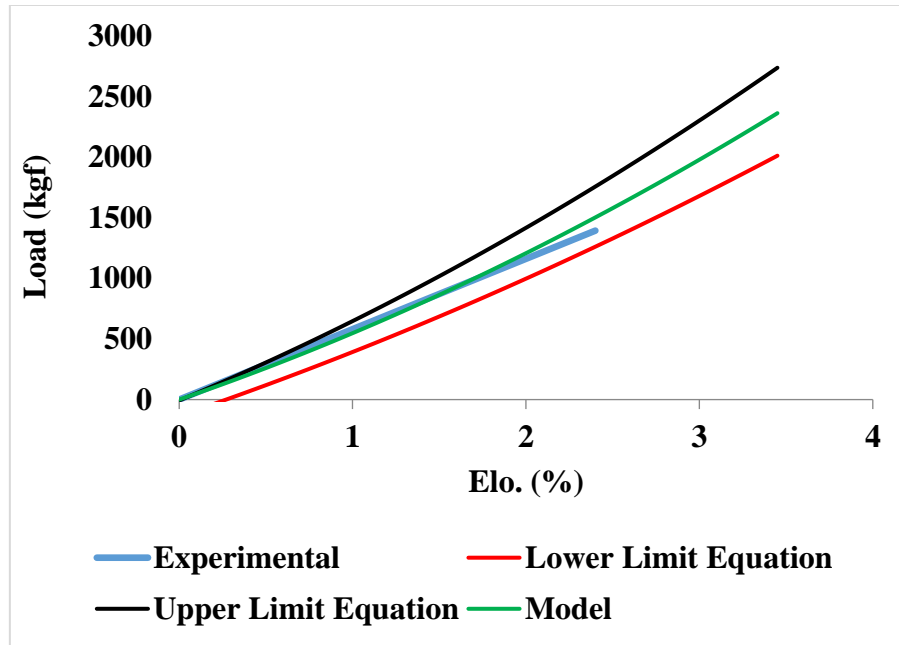
X-yarn

6.3. Model Verification

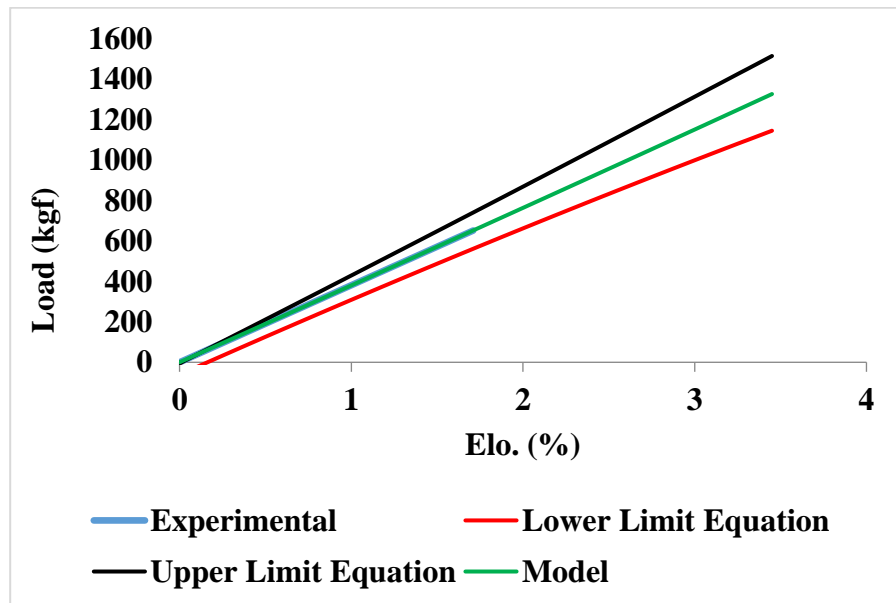
To verify the model experimentally, preforms of hemp and flax yarns were woven into 3D orthogonal structures with different architectures and Z-yarn weave patterns, then they were infused to produce composite panels. These panels were cut into specimens and tested using the MTS Servo-hydraulic 370 load frame located at the Composite Core Facility, Wilson College of

Textiles, NC State University according to the ASTM D3039. The tensile results of hemp reinforced composites were generated by Gupta (68).

Figure 160 illustrates one example of the model verification of bleached flax/ vinyl ester composite while the rest of figures which indicate the model verification of 96 composite specimens in the X- and Y-directions are in appendix B.1 and B.2 for composites from flax and hemp fibers, respectively. In general, the figures show a good agreement between the experimental and predicted composite tensile properties. The experimental curves are within the upper and lower limits in both X and Y-directions tensile results. The samples in Figure 161 are for composite from bleached flax spun yarns with 6 Y-yarn layers (7 X-yarn layers), 2.31 picks/cm, plain weave, 1:1 Z- to Y-yarns ratio and linear densities of X, Y and Z-yarns of 1462, 1207 and 234 denier, respectively.



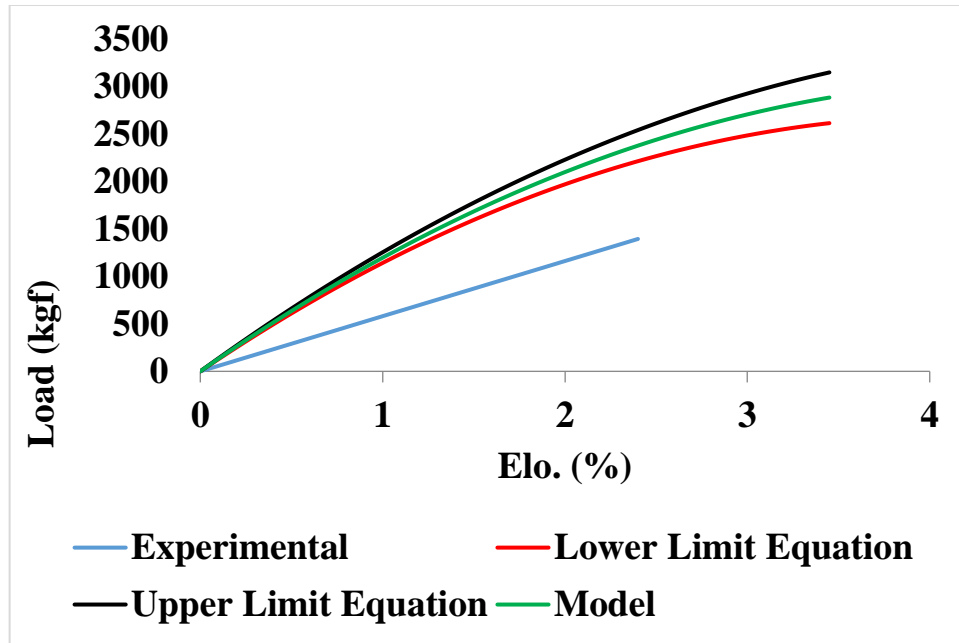
(a)



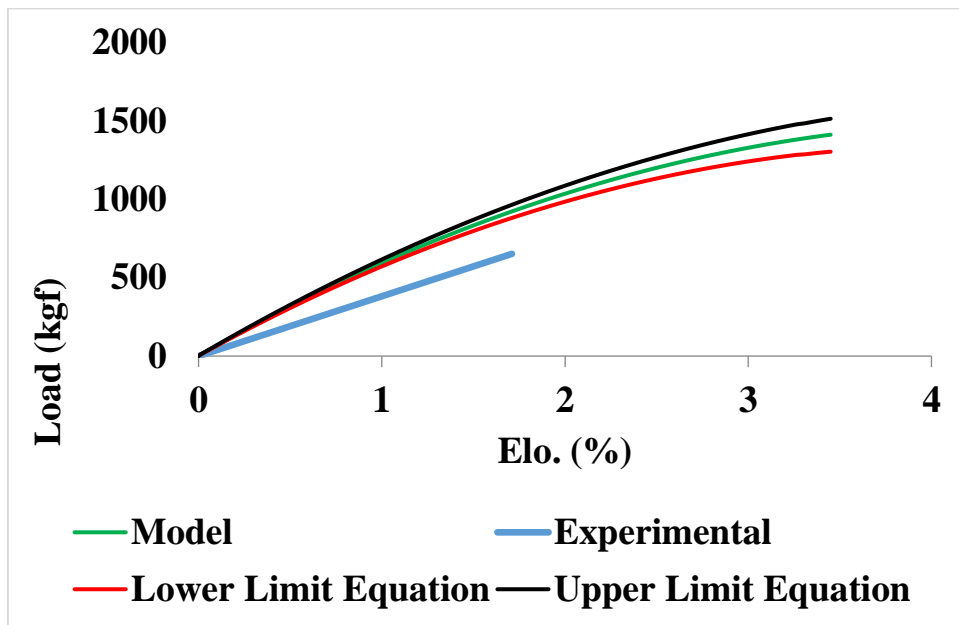
(b)

Figure 161. Experimental vs. model tensile load-elongation for 6 Y-yarn layers 3DOW plain weave and 1:1 Z to Y-yarn ratio from bleached flax fibers (a) X-direction, (b) Y-direction

The results show that there is a general good agreement between the experimental and the theoretical curves derived from the load-elongation properties of the yarns used to produce the composite however, some deviations were noted. One source of the deviation could be the weak-link effect which is a phenomenon explains the effect of sample length on breaking strength and it is commonly associated with textile materials. The weak-link effect indicates that the measured strength of a specimen decreases as the sample length is increased due to the presence of local defects which have higher probability to be there with increasing the sample length which makes the theoretical strength of any material can never be achieved in practice. Thus, the strength of a specific fiber material decreases with moving to a bundle of fibers. This weak-link effect decreases when the preform transferred into composites because the fibers are interlocked inside the matrix however, the twist inserted to the bundle of fibers to produce the yarns earlier moves the fibers; center line form the yarn's center line which prevents the fiber from sharing with its whole strength into the yarn's strength and then the preform. Therefore, the yarn strength cannot be calculated from multiplying the fibers strength by the number of fibers in the yarn cross-section. This explains why the theoretically predicted load-strain curves that were based on the tensile properties of the yarn had better agreement with the experimental curves, than the ones based on the tensile properties of the single fiber as shown in Figure 162. The samples in Figure 162 are for composite from bleached flax spun yarns with 6 Y-yarn layers, 2.31 picks/cm, plain-weave, 1:1 Z- to Y-yarns ratio.



(a)



(b)

Figure 162. Experimental vs. model tensile load-elongation for 6 Y-yarn layers 3DOW plain weave and 1:1 Z to Y-yarn ratio from bleached flax fibers (a) X-direction, (b) Y-direction

Another source of deviation as well as the low failure strain levels of the composite that are even lower than its constituents is the manufactured induced defects. The first cause of the manufactured induced defects is the weaving process. During the weaving process, the X- Y and Z-yarns are forced to slide against many machine elements such as the warp creel, tensioning devices, heddles, reed and rapiers which results in abrasion and breakage due to the friction. This abrasion causes broken fibers and creates more defects in the yarns and therefore degrades the tensile properties. Another phenomenon that affects the tensile properties of the woven preform is the strain hardening of the yarns during weaving. This is since the yarns undergo consecutive cycles of loading and unloading during weaving which cause a strain hardening of the yarns and therefore reducing its extensibility and failure strain. The second cause of the manufactured induced defects is the VARTM process in which the preform is induced to high level of vacuum (100 kPa) which compresses the preform creating local stress concentrations at the cross over points between the Z- and X-yarns. In addition, these local stresses deform the outermost X-yarns and increases the waviness of the X-yarns. During the resin infusion process, air bubbles can enter the system and got trapped results in voids after hardening which might be another form of local defects in the composite system. These defects are considered nuclei for cracks initiation which then propagate across the resin during loading and cause an early failure at a lower strain level. Finally, the interfacial adhesion between the fibers and the matrix is a significant factor that strongly affects the load transfer in the composite system. In this model, it is assumed that there is a perfect adhesion between the fibers and the matrix, which is not always true.

7. OVERALL CONCLUSION AND SUGGESTION FOR FUTURE WORK

A generalized model considering jammed and non-jammed structures to predict the load-extension properties of the 3DOW composites made of natural spun yarns (hemp and flax) was developed. The model introduced a reasonable prediction that considers the inherent variability of natural fibers. The model relies on the preform architecture, and the measured tensile properties of the constituent yarns and resin as input parameters, and the output of this model is the entire load-extension diagram of the composite, including the nonlinear region. The model is generalized to predict the load-extension properties of 3DOW composite with any weave architecture, including hybrid composites which can be used as a design tool to predict the tensile properties of the 3DOW composites from flax and hemp fibers without the need to form the preforms and the composites.

The model was verified experimentally for a broad range of experimental composites. The main independent parameters were number of Y-yarn layers, weave (Z-yarn interlacing pattern), Z- to Y-yarn ratio and X-yarn type. The results show that there is a general good agreement between the experimental and the theoretical load-extension curves. The theoretical curves generated using the yarn properties had better agreement with the experimental curves than the ones created using the fiber properties, due to the inherent variability in the properties of natural fiber. The model overestimated the failure point of 3DOW composites by $30 \pm 3\%$ due to the induced defects by weaving, VARTM and material defects. The model can assist in designing composites from natural fibers with targeted performance.

The model was applied to 3DOW composites from preforms from as supplied yarns as well as yarns with enhanced surface treatment. Different X-yarns from flax fibers with surface treatment (bleached and BHS) and without surface treatment (grey and HS) were woven as 3DOW

preforms. The results showed that the model prediction improved when using bleached flax yarns than that of grey flax yarns which was due to enhancing the interaction between the fibers and the matrix to meet the model assumption of having a strong adhesion between the composite constituents. In contrast, the difference between the theoretical and the experimental curves of composites from HS and BHS yarns was insignificant compared to the difference between that from grey and bleached.

In design of experiment A, a full numerical parametric study was conducted to reveal the architecture potential of 3DOW composites. The study included the effect of changing the number of Y-yarn layers, the weave design and the amount of Z- to Y-yarns ratio. A wide range of 3DOW preforms were woven, transformed into composites and tested using different mechanical tests including tensile, impact (Tup & Charpy) and compressing tests to study their responses.

Changing the number of Y-yarn layers affected the tensile strength of the composite samples significantly in both warp and weft direction. Plain weave was significantly different from 2x2 warp rib and 3x3 wrap rib in weft direction, however, there was no effect of the weave in the warp direction. The difference in weft direction came from the fact that plain woven structures are more compact and therefore reduces the formation of resin rich areas compared to the 2x2 warp rib and 3x3 warp rib weaves. There was no significant effect on the tensile properties with changing number of Z- to Y-yarns ratio. While comparing composites from natural fibers (flax and hemp) with glass composites, it was found that the specific tensile stress of glass was significantly higher compared to flax and hemp. Unlike tensile stress, specific modulus of flax and hemp and glass composite was found to be comparable.

In case of impact test (Tup and Charpy), it was noted that changing the number of Y-yarn layers increased the total impact energy significantly. The statistical analysis indicated that there was a significant difference between samples of different weaves. While plain weave was significantly different from 2x2 warp rib and 3x3 warp rib, there was no difference between 2x2 warp rib and 3x3 warp rib. The effect of a change in Z- to Y-yarns ratio was not substantial. The comparison of the normalized total penetration energy between composites from flax and hemp fibers to the ones from glass fibers was found to be comparable.

In the compression test, the increase in the number of Y-yarn layers or thickness increased the compression peak load in both warp and weft directions. 2x2 warp rib showed a significant higher compression peak load than that of plain and 3x3 warp rib in the weft direction, however the weave design had no effect in the warp direction. The effect of Z- to Y-yarns ratio was significant in the warp direction while had no effect in the filling direction. 1:1 Z- to Y-yarn ratio showed higher compression load than 1:3 ratio.

In design of experiment B, the type of X-yarn was changed to compare the mechanical properties of composites from bleached and BHS flax yarns to composites from grey and HS flax yarns. In general, the samples with bleached yarns (bleached flax and BHS flax) showed higher tensile loads than their corresponding unbleached yarns (grey flax and HS flax). The X-yarns from as supplied yarns to bleached yarns showed no significant effect on the impact tests (Tup and Charpy). In case of compression test, Tukey analysis induced that while composites from bleached flax yarns had higher compression load than that of grey flax yarns, BHS flax yarns samples showed lower results than that of HS flax yarns.

For future investigations, processing defects (material, weaving, infusion) should be factored in the model to overcome the limitations in predicting the composite failure. Fiber surface

characteristics are crucial in determining the interfacial properties, therefore more chemical and physical surface treatments are required. Totally renewable composites should be considered using plant-based resins from natural resources such as soybean and starch.

REFERENCES

- (1) Thakur VK. Green composites from natural resources. : CRC Press; 2013.
- (2) Ramakrishna S, Mayer J, Wintermantel E, Leong KW. Biomedical applications of polymer-composite materials: a review. *Composites Sci Technol* 2001;61(9):1189-1224.
- (3) Rana S, Figueiro R. *Fibrous and Textile Materials for Composite Applications*. : Springer; 2016.
- (4) Fan M, Fu F. *Advanced High Strength Natural Fibre Composites in Construction*. 1st ed.: Woodhead, Elsevier; 2016.
- (5) Joffe R, Andersons J, Wallström L. Strength and adhesion characteristics of elementary flax fibres with different surface treatments. *Composites Part A: Applied Science and Manufacturing* 2003;34(7):603-612.
- (6) Composite Material. Available at:
https://en.wikipedia.org/wiki/Composite_material#/media/File:Composite_3d.png.
 Accessed 10/15, 2016.
- (7) Zafeiropoulos N, Baillie C, Matthews F. A study of transcrystallinity and its effect on the interface in flax fibre reinforced composite materials. *Composites Part A: Applied Science and Manufacturing* 2001;32(3):525-543.
- (8) Composites world. Available at: <http://www.compositesworld.com/>. Accessed 10/20, 2016.
- (9) Flax Composites. Available at: <http://flaxcomposites.com/>. Accessed 10/20, 2016.

- (10) Procotex. Available at: <http://en.procotex.com/products/flax/composites.php>. Accessed 10/20, 2016.
- (11) Composites Manufacturing Magazine. Available at: <http://compositesmanufacturingmagazine.com/2018/10/bcomps-powerribs-improves-cost-efficiency-without-sacrificing-performance/>. Accessed 03/07, 2019.
- (12) Fuqua MA, Huo S, Ulven CA. Natural fiber reinforced composites. *Polymer Reviews* 2012;52(3):259-320.
- (13) Ichhaporia PK. Composites from natural fibers. : ProQuest; 2008.
- (14) How Linen Is Made. Available at: <http://www.madehow.com/Volume-4/Linen.html>. Accessed 10/14, 2016.
- (15) Fangueiro R, Rana S. Natural Fibres: Advances in Science and Technology Towards Industrial Applications: From Science to Market. : Springer; 2016.
- (16) Bourmaud A, Gibaud M, Lefeuvre A, Morvan C, Baley C. Influence of Stem Morphology and Fibers Stiffness on the Loading Stability of Flax. *Natural Fibres: Advances in Science and Technology Towards Industrial Applications*: Springer; 2016. p. 49-59.
- (17) Baley C, Busnel F, Grohens Y, Sire O. Influence of chemical treatments on surface properties and adhesion of flax fibre–polyester resin. *Composites Part A: Applied Science and Manufacturing* 2006;37(10):1626-1637.
- (18) Kawabata S, Niwa M, Kawai H. 4—the finite-deformation theory of plain-weave fabrics. Part II: the uniaxial-deformation theory. *Journal of the textile institute*

- 1973;64(2):47-61.
- (19) Kawabata S, Niwa M, Kawai H. 5—The finite-deformation theory of plain-weave fabrics. Part III: The shear-deformation theory. *Journal of the textile institute* 1973;64(2):62-85.
 - (20) Kawabata S, Niwa M, Kawai H. 3—The finite-deformation theory of plain-weave fabrics part I: the biaxial-deformation theory. *Journal of the textile institute* 1973;64(1):21-46.
 - (21) Sun F, Seyam AM, Gupta B. A generalized model for predicting load-extension properties of woven fabrics. *Text Res J* 1997;67(12):866-874.
 - (22) Nagai K, Yokoyama A, Maekawa Z, Hamada H. The stress analysis method for three-dimensional composite materials. *Applied Composite Materials* 1994;1(3):197-216.
 - (23) Tan P, Tong L, Steven G. Modeling approaches for 3D orthogonal woven composites. *J Reinf Plast Compos* 1998;17(6):545-577.
 - (24) Zuorong C, Shouwen Y, Xiqiao F, Lu M, Ye L. Evaluation of thermo-elastic properties of three-dimensional orthogonal woven composites. *Composites Part B: Engineering* 2002;33(3):241-251.
 - (25) Pankow M, Waas AM, Yen C, Ghiorse S. A new lamination theory for layered textile composites that account for manufacturing induced effects. *Composites Part A: Applied Science and Manufacturing* 2009;40(12):1991-2003.
 - (26) Seyam AM, Ince ME. Generalized geometric modeling of three-dimensional orthogonal woven preforms from spun yarns. *Journal of The Textile Institute* 2013;104(9):914-928.

- (27) Midani M, Seyam A, Pankow M. A generalized analytical model for predicting the tensile behavior of 3D orthogonal woven composites using finite deformation approach. *The Journal of The Textile Institute* 2018:1-12.
- (28) Kalia S, Kaith B, Kaur I. Pretreatments of natural fibers and their application as reinforcing material in polymer composites—A review. *Polymer Engineering & Science* 2009;49(7):1253-1272.
- (29) Satyanarayana KG, Arizaga GG, Wypych F. Biodegradable composites based on lignocellulosic fibers—An overview. *Progress in polymer science* 2009;34(9):982-1021.
- (30) Hearle J, Sparrow J. Mechanics of the extension of cotton fibers. I. Experimental studies of the effect of convolutions. *J Appl Polym Sci* 1979;24(6):1465-1477.
- (31) Semsarzadeh MA. Fiber matrix interactions in jute reinforced polyester resin. *Polymer composites* 1986;7(1):23-25.
- (32) Marais S, Gouanvé F, Bonnesoeur A, Grenet J, Poncin-Epaillard F, Morvan C, et al. Unsaturated polyester composites reinforced with flax fibers: effect of cold plasma and autoclave treatments on mechanical and permeation properties. *Composites Part A: Applied Science and Manufacturing* 2005;36(7):975-986.
- (33) Sarikanat M, Seki Y, Sever K, Bozaci E, Demir A, Ozdogan E. The effect of argon and air plasma treatment of flax fiber on mechanical properties of reinforced polyester composite. *Journal of Industrial Textiles* 2014:1528083714557057.
- (34) Bozaci E, Sever K, Sarikanat M, Seki Y, Demir A, Ozdogan E, et al. Effects of the atmospheric plasma treatments on surface and mechanical properties of flax fiber and

- adhesion between fiber–matrix for composite materials. *Composites Part B: Engineering* 2013;45(1):565-572.
- (35) Le Digabel F, Avérous L. Effects of lignin content on the properties of lignocellulose-based biocomposites. *Carbohydr Polym* 2006;66(4):537-545.
- (36) Ayrlmis N, Jarusombuti S, Fueangvivat V, Bauchongkol P. Effect of thermal-treatment of wood fibres on properties of flat-pressed wood plastic composites. *Polym Degrad Stab* 2011;96(5):818-822.
- (37) Nykter M, Kymäläinen H, Thomsen AB, Lilholt H, Koponen H, Sjöberg A, et al. Effects of thermal and enzymatic treatments and harvesting time on the microbial quality and chemical composition of fibre hemp (*Cannabis sativa* L.). *Biomass Bioenergy* 2008;32(5):392-399.
- (38) Ibrahim MM, Dufresne A, El-Zawawy WK, Agblevor FA. Banana fibers and microfibrils as lignocellulosic reinforcements in polymer composites. *Carbohydr Polym* 2010;81(4):811-819.
- (39) Li X, Tabil LG, Panigrahi S. Chemical treatments of natural fiber for use in natural fiber-reinforced composites: a review. *Journal of Polymers and the Environment* 2007;15(1):25-33.
- (40) Kabir M, Wang H, Lau K, Cardona F. Chemical treatments on plant-based natural fibre reinforced polymer composites: An overview. *Composites Part B: Engineering* 2012;43(7):2883-2892.
- (41) Mohanty A, Drzal L, Misra M. Engineered natural fiber reinforced polypropylene

- composites: influence of surface modifications and novel powder impregnation processing. *J Adhes Sci Technol* 2002;16(8):999-1015.
- (42) Baiardo M, Zini E, Scandola M. Flax fibre–polyester composites. *Composites Part A: Applied Science and Manufacturing* 2004;35(6):703-710.
- (43) Huo S, Fuqua M, Chevali VS, Ulven CA. Effects of natural fiber surface treatments and matrix modification on mechanical properties of their composites. 2010.
- (44) Ishikawa H, Takagi H, Nakagaito AN, Yasuzawa M, Genta H, Saito H. Effect of surface treatments on the mechanical properties of natural fiber textile composites made by VaRTM method. *Composite Interfaces* 2014;21(4):329-336.
- (45) Amiri A, Ulven CA, Huo S. Effect of chemical treatment of flax fiber and resin manipulation on service life of their composites using time-temperature superposition. *Polymers* 2015;7(10):1965-1978.
- (46) Kabir M, Wang H, Lau K, Cardona F. Chemical treatments on plant-based natural fibre reinforced polymer composites: An overview. *Composites Part B: Engineering* 2012;43(7):2883-2892.
- (47) Valadez-Gonzalez A, Cervantes-Uc J, Olayo R, Herrera-Franco P. Effect of fiber surface treatment on the fiber–matrix bond strength of natural fiber reinforced composites. *Composites Part B: Engineering* 1999;30(3):309-320.
- (48) Cherif ZE, Poilâne C, Falher T, Vivet A, Ouail N, Doudou BB, et al. Influence of textile treatment on mechanical and sorption properties of flax/epoxy composites. *Polymer Composites* 2013;34(10):1761-1773.

- (49) Li W, Meng L, Ma R. Effect of surface treatment with potassium permanganate on ultra-high molecular weight polyethylene fiber reinforced natural rubber composites. *Polym Test* 2016;55:10-16.
- (50) Altundal S, Krasnikovs A, Linins O, Telnova I. Mechanical Properties of Flax Fiber Based Polymer (with Nano Additives) Matrix Composites. *Rigas Tehniskas Universitates Zinatniskie Raksti* 2014;35:26.
- (51) Ajith A, Xian G, Li H, Sherief Z, Thomas S. Surface grafting of flax fibres with hydrous zirconia nanoparticles and the effects on the tensile and bonding properties. *J Composite Mater* 2015:0021998315580450.
- (52) Yu T, Ren J, Li S, Yuan H, Li Y. Effect of fiber surface-treatments on the properties of poly (lactic acid)/ramie composites. *Composites Part A: Applied Science and Manufacturing* 2010;41(4):499-505.
- (53) Sreekumar P, Thomas SP, marc Saiter J, Joseph K, Unnikrishnan G, Thomas S. Effect of fiber surface modification on the mechanical and water absorption characteristics of sisal/polyester composites fabricated by resin transfer molding. *Composites Part A: Applied Science and Manufacturing* 2009;40(11):1777-1784.
- (54) Sgriecia N, Hawley M, Misra M. Characterization of natural fiber surfaces and natural fiber composites. *Composites Part A: Applied Science and Manufacturing* 2008;39(10):1632-1637.
- (55) Pan Y, Zhong Z. A micromechanical model for the mechanical degradation of natural fiber reinforced composites induced by moisture absorption. *Mech Mater* 2015;85:7-15.

- (56) Borysiak S. The thermo-oxidative stability and flammability of wood/polypropylene composites. *Journal of Thermal Analysis and Calorimetry* 2015;119(3):1955-1962.
- (57) Araujo J, Waldman W, De Paoli M. Thermal properties of high density polyethylene composites with natural fibres: Coupling agent effect. *Polym Degrad Stab* 2008;93(10):1770-1775.
- (58) Spinacé MAS, Lambert CS, Fermoselli KKG, De Paoli M. Characterization of lignocellulosic curaua fibres. *Carbohydrate Polymers* 2009 22 May 2009;77(1):47-53.
- (59) Bax B, Müssig J. Impact and tensile properties of PLA/Cordenka and PLA/flax composites. *Composites Sci Technol* 2008;68(7):1601-1607.
- (60) Ramakrishna G, Sundararajan T. Impact strength of a few natural fibre reinforced cement mortar slabs: a comparative study. *Cement and concrete composites* 2005;27(5):547-553.
- (61) Investigation on Mechanical Properties of Natural Fiber Composite Using RTM Manufacturing Method. *Applied Mechanics and Materials: Trans Tech Publ*; 2015.
- (62) Zampaloni M, Pourboghraat F, Yankovich S, Rodgers B, Moore J, Drzal L, et al. Kenaf natural fiber reinforced polypropylene composites: a discussion on manufacturing problems and solutions. *Composites Part A: Applied Science and Manufacturing* 2007;38(6):1569-1580.
- (63) Samuel OD, Agbo S, Adekanye TA. Assessing mechanical properties of natural fibre reinforced composites for engineering applications. *Journal of Minerals and Materials Characterization and Engineering* 2012;11(08):780.

- (64) Van Vuure A, Baets J, Wouters K, Hendrickx K. Compressive properties of natural fibre composites. *Mater Lett* 2015;149:138-140.
- (65) Le Duigou A, Davies P, Baley C. Interfacial bonding of flax fibre/poly (l-lactide) bio-composites. *Composites Sci Technol* 2010;70(2):231-239.
- (66) Amiri A, Triplett Z, Moreira A, Brezinka N, Alcock M, Ulven CA. Standard density measurement method development for flax fiber. *Industrial crops and products* 2017;96:196-202.
- (67) Xie H. The Role of Fiber Type in Performance of their Composites from 3D Orthogonal Woven Preforms. 2016.
- (68) Anuradha Gupta. Composites from Natural Fibers: Hemp Fiber Reinforced Composites from 3D Orthogonal Woven Preforms and their Potential Applications in the USNorth Carolina State University; 2019.
- (69) Peirce FT. 5—the geometry of cloth structure. *Journal of the Textile Institute Transactions* 1937;28(3):T45-T96.
- (70) Seyam A, Harrison P. The Structural Design of Woven Fabrics: Theory and Practice-A critical appreciation of recent developments. *Textile Progress* 2002;31(3).
- (71) Ince ME. Performance of composites from 3D orthogonal woven preforms in terms of architecture and sample location during resin infusion. ; 2013.
- (72) Clulow EE, Taylor H. 30—AN EXPERIMENTAL AND THEORETICAL INVESTIGATION OF BIAXIAL STRESS–STRAIN RELATIONS IN A PLAIN-WEAVE CLOTH. *Journal of the Textile Institute Transactions* 1963;54(8):T323-T347.

- (73) Hamburger WJ. The industrial application of the stress-strain relationship. Journal of the Textile Institute Proceedings 1949;40(7):P700-P720.

APPENDICES

Appendix A

A.1. Results of Fiber Denier Measurements

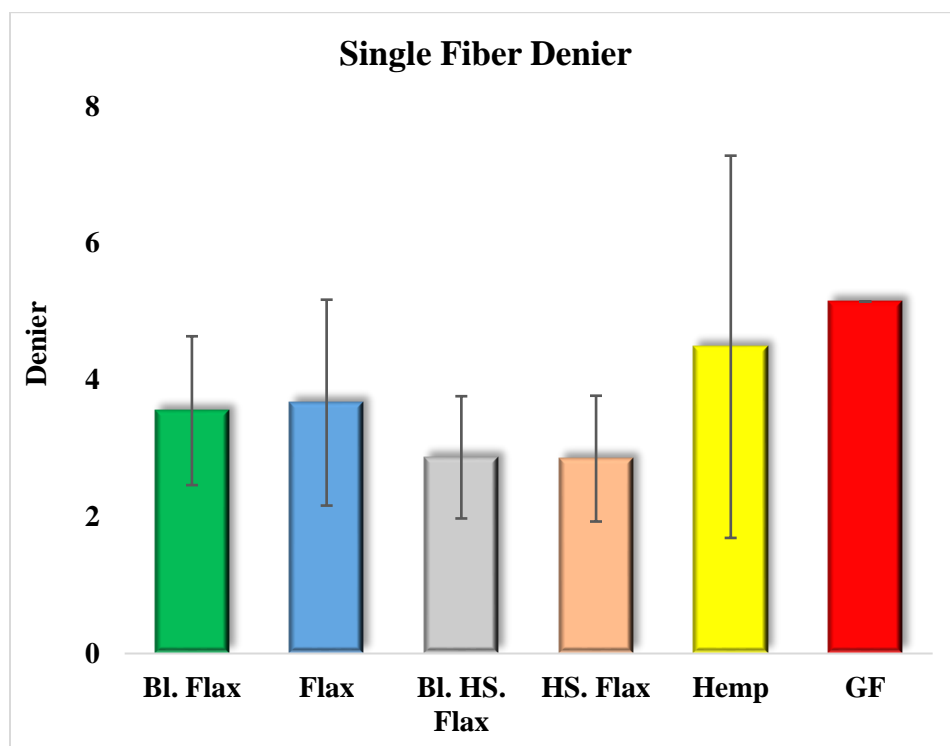
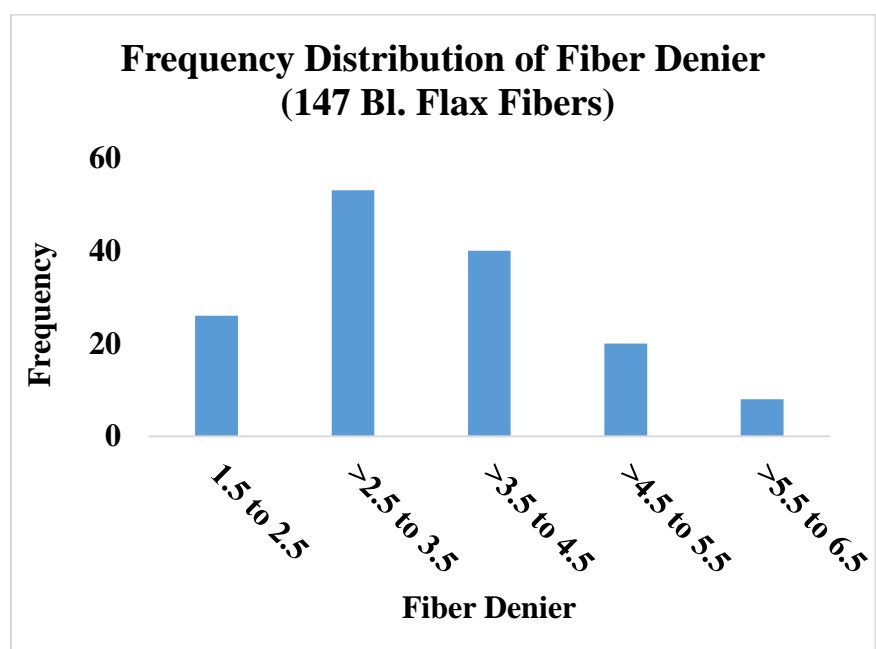
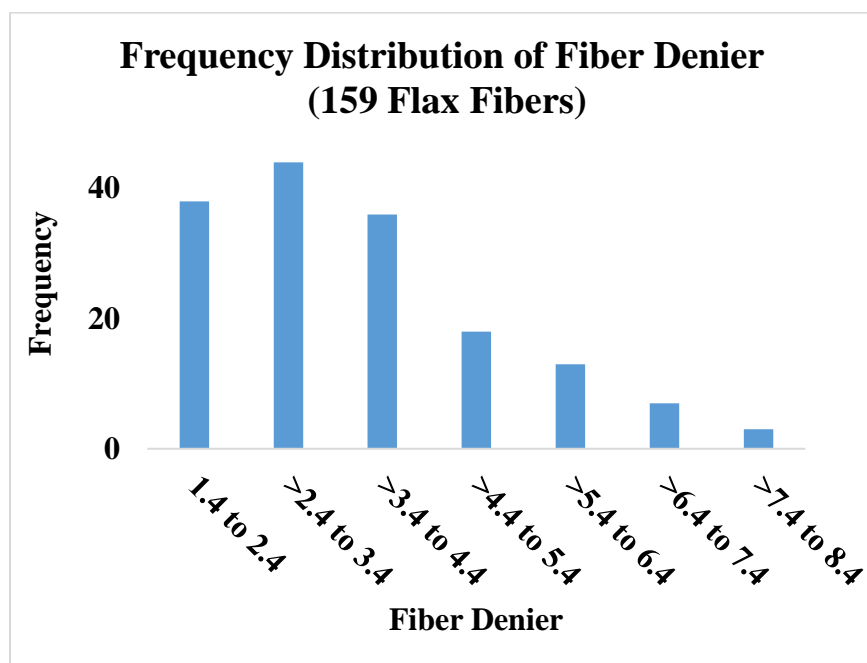


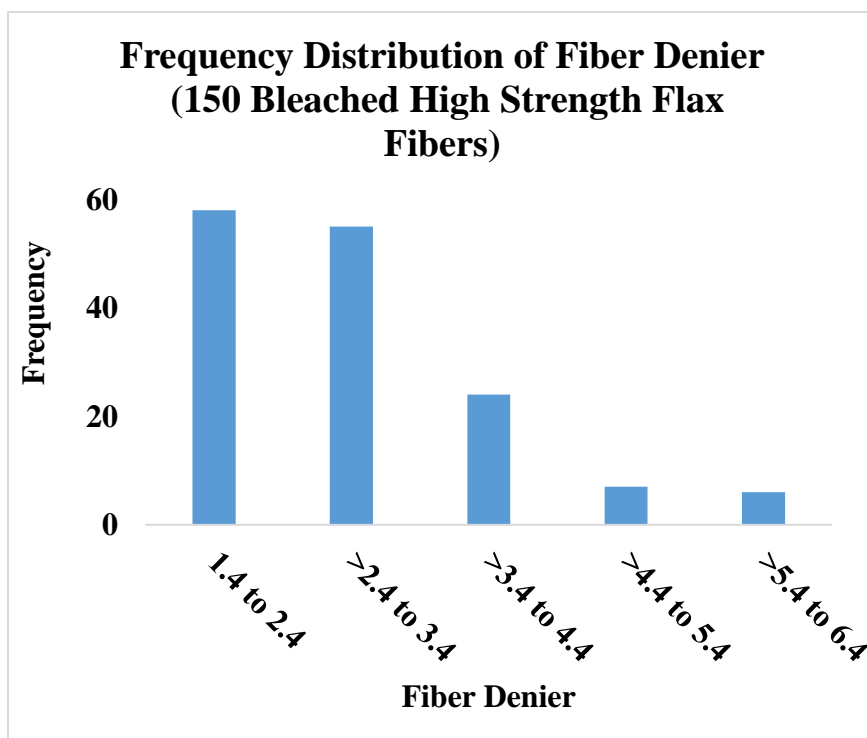
Figure 163. Average denier of 150 single fibers of each fiber type



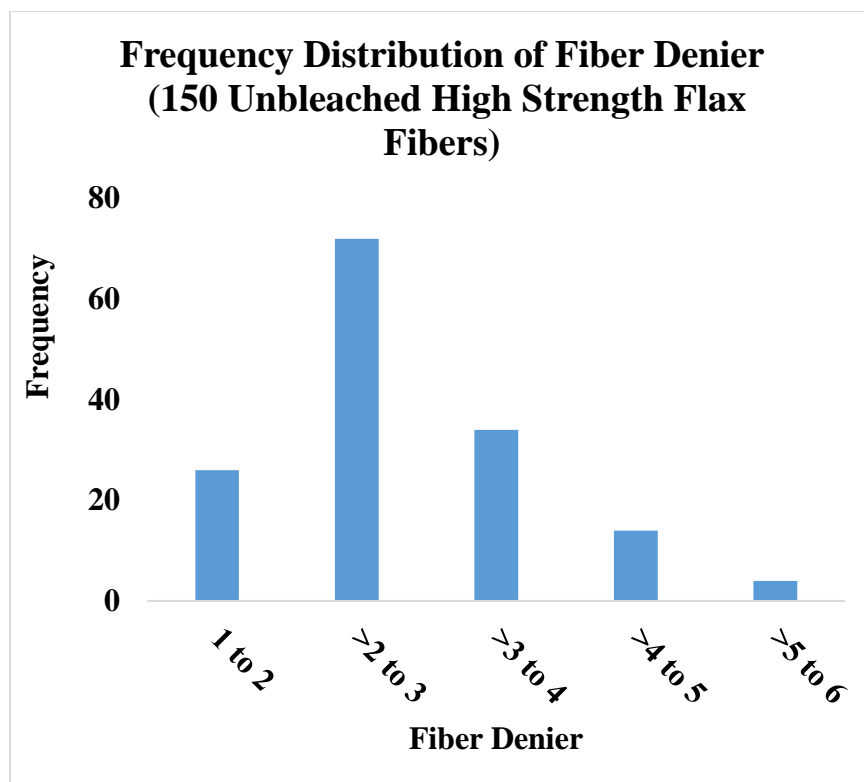
(a)



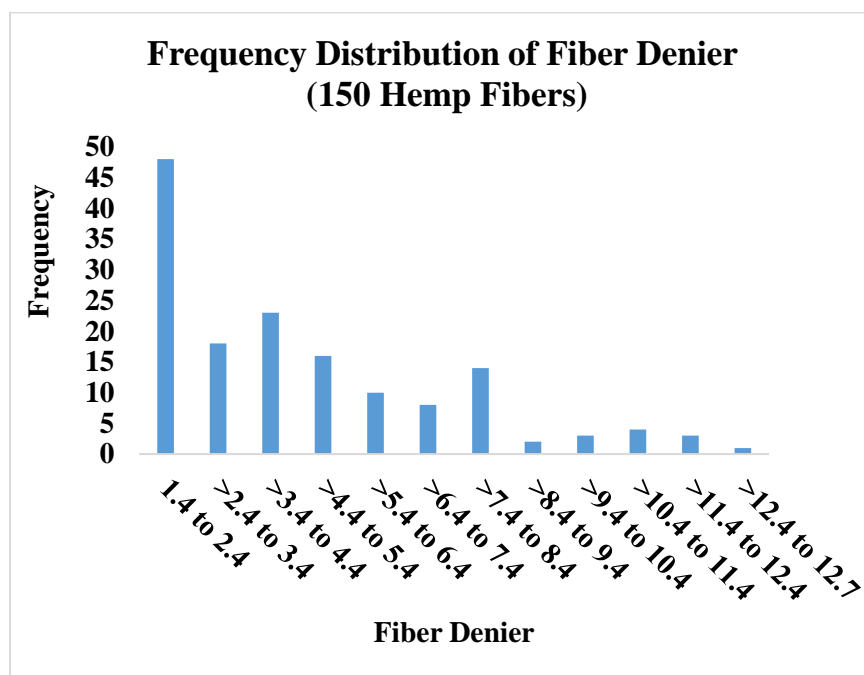
(b)



(c)



(d)



(e)

Figure 164. Frequency distribution of fiber denier (a) Bleached flax, (b) Grey flax, (c) BHS (Bleached High Strength) flax, (d) HS (High Strength) flax and (e) Hemp

Table 43. Minimum number of samples of fiber denier

Fiber Type	Confidence Level		
	90%	95%	99%
Flax	613	870	1503
Bl. Flax	320	455	785
HS. Flax	229	325	561
Bl. HS. Flax	216	307	530
Hemp	2112	2999	5180

A.2. Results of Fiber Tensile Properties

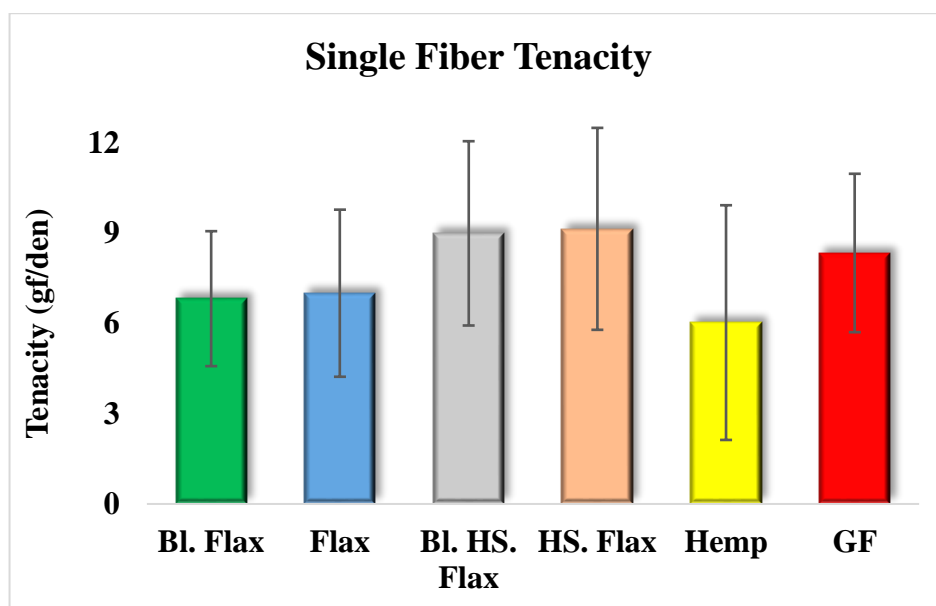


Figure 165. Single fiber tenacity

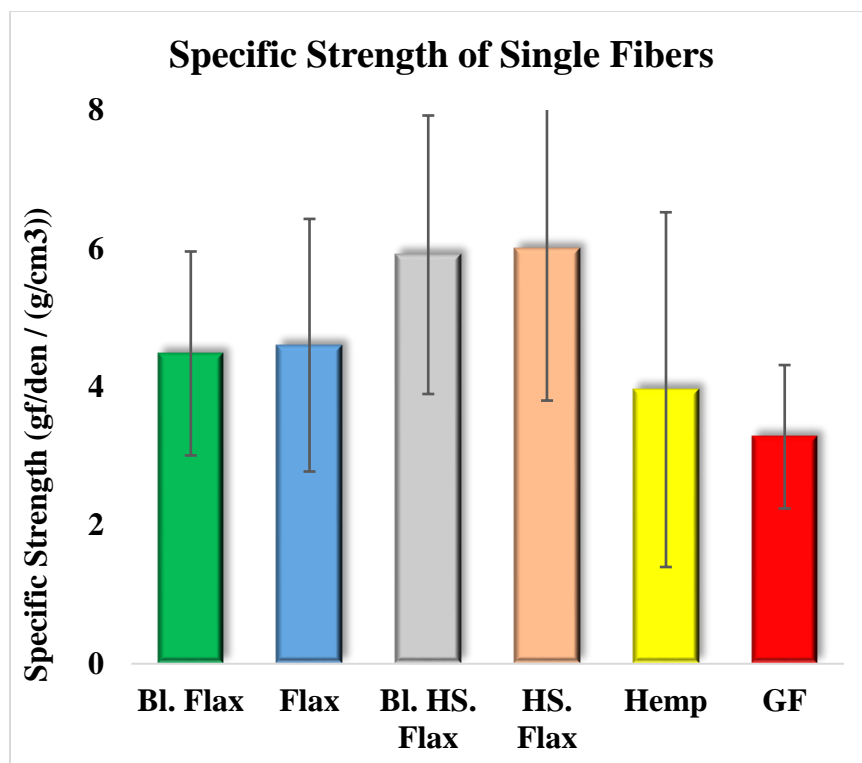


Figure 166. Specific strength of single fibers

Table 44. Minimum number of samples of fiber tenacity

Fiber Type	Confidence Level		
	90%	95%	99%
Flax	2083	2957	5107
Bl. Flax	1358	1928	3331
HS. Flax	3042	4318	7459
Bl. HS. Flax	2532	3595	6210
Hemp	4109	5833	10075

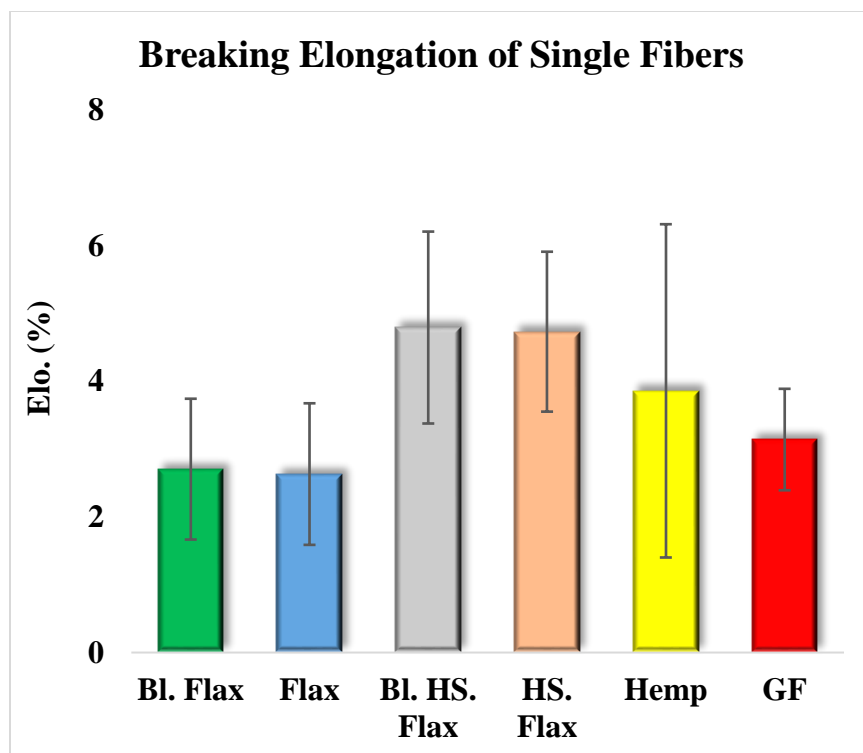


Figure 167. Breaking elongation of single fibers

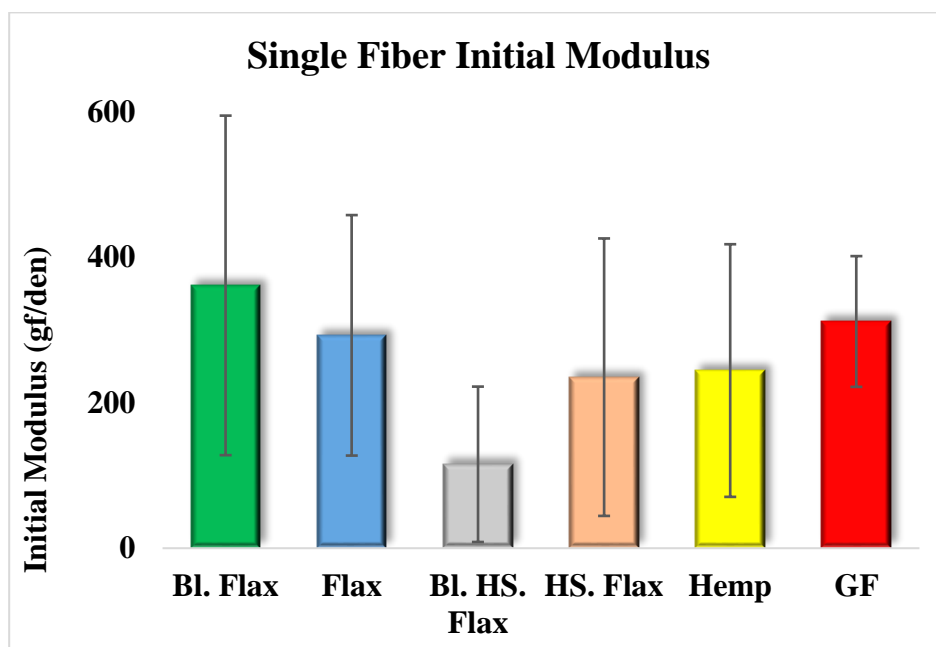


Figure 168. Single fiber initial modulus

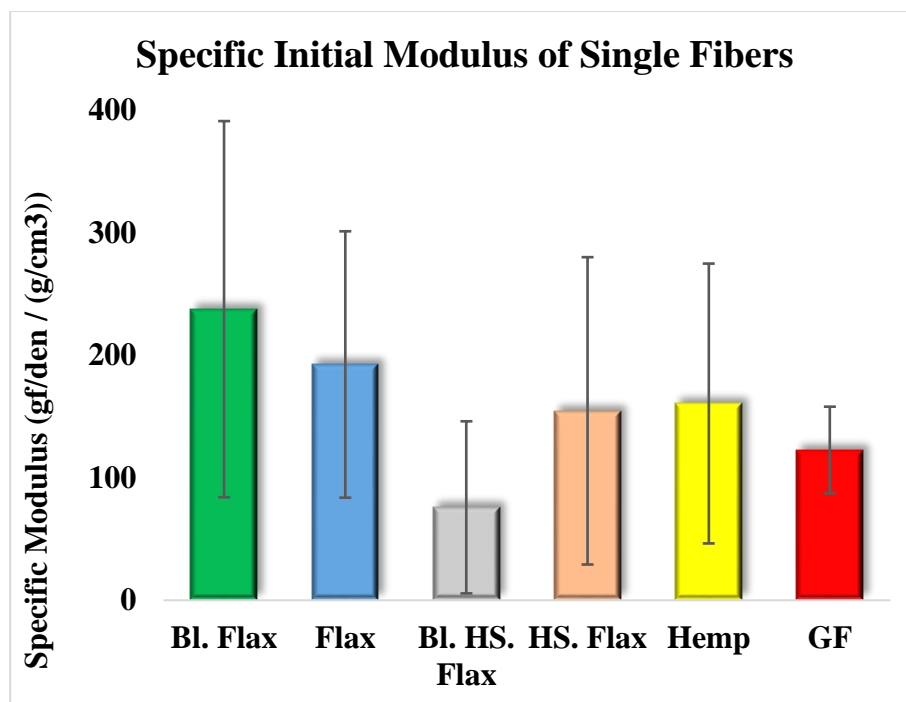


Figure 169. Specific initial modulus of single fibers

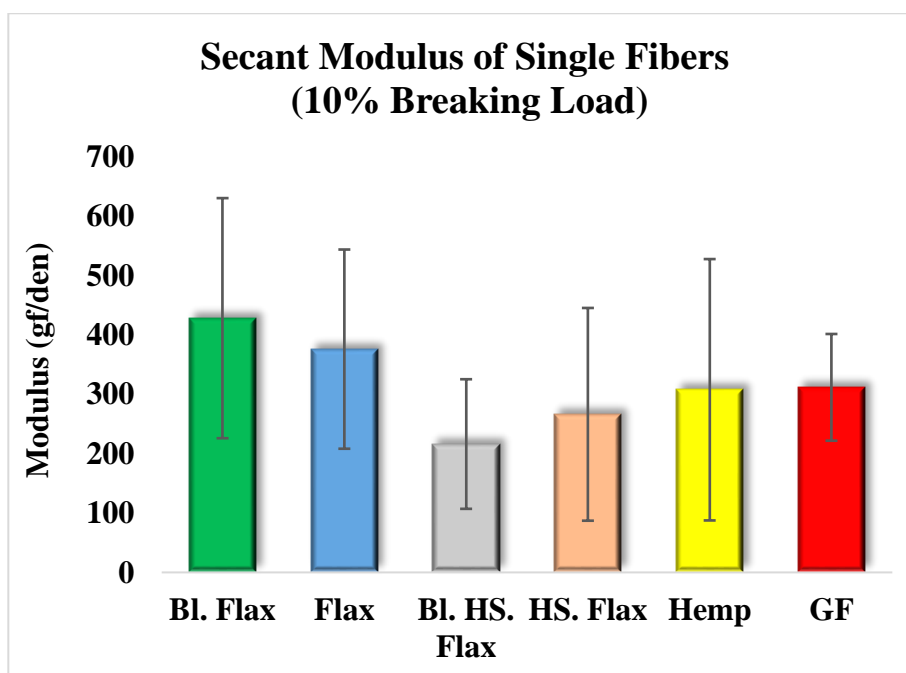


Figure 170. Secant modulus at 10% breaking load of single fibers

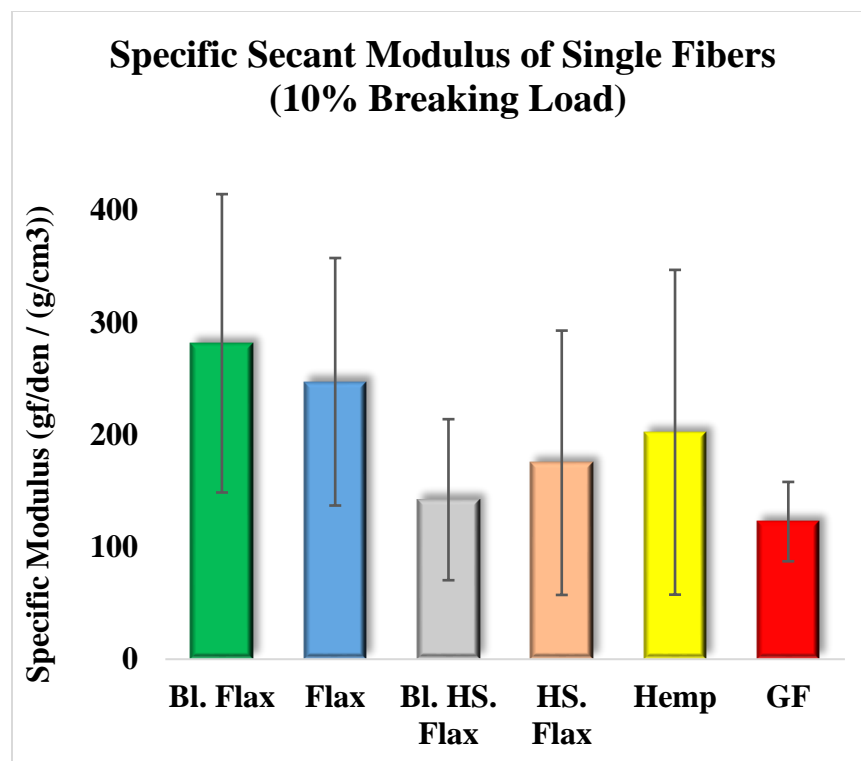
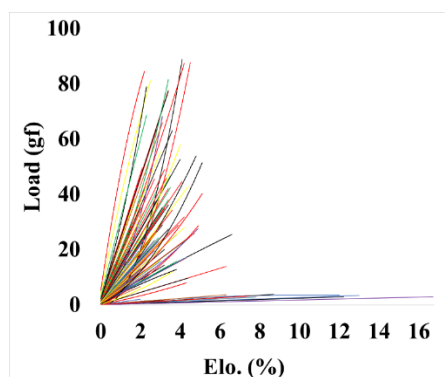
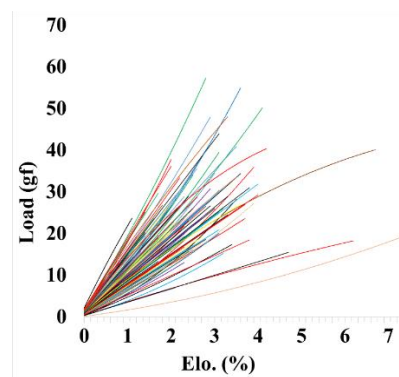


Figure 171. Specific secant modulus at 10% breaking load of single fibers

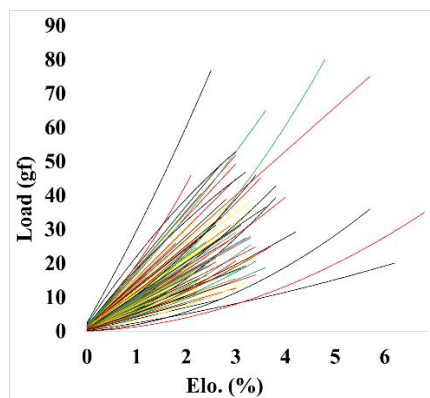
A.3. Load-Extension Curves of Hemp and Flax Fibers



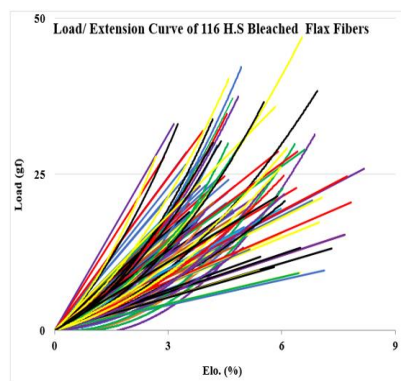
(a)



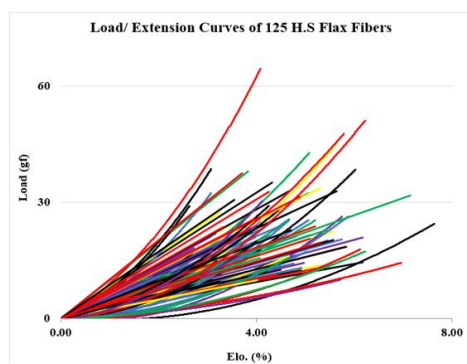
(b)



(c)



(d)



(e)

Figure 172. Load-Extension curves of (a) 119 hemp fibers, (b) 121 bleached flax fiber, (c) 124 flax fibers, (d) 116 high strength bleached flax fibers, and (e) 125 high strength flax fibers

A.4. Linear Density and Tensile Properties of Hemp and Flax Yarns

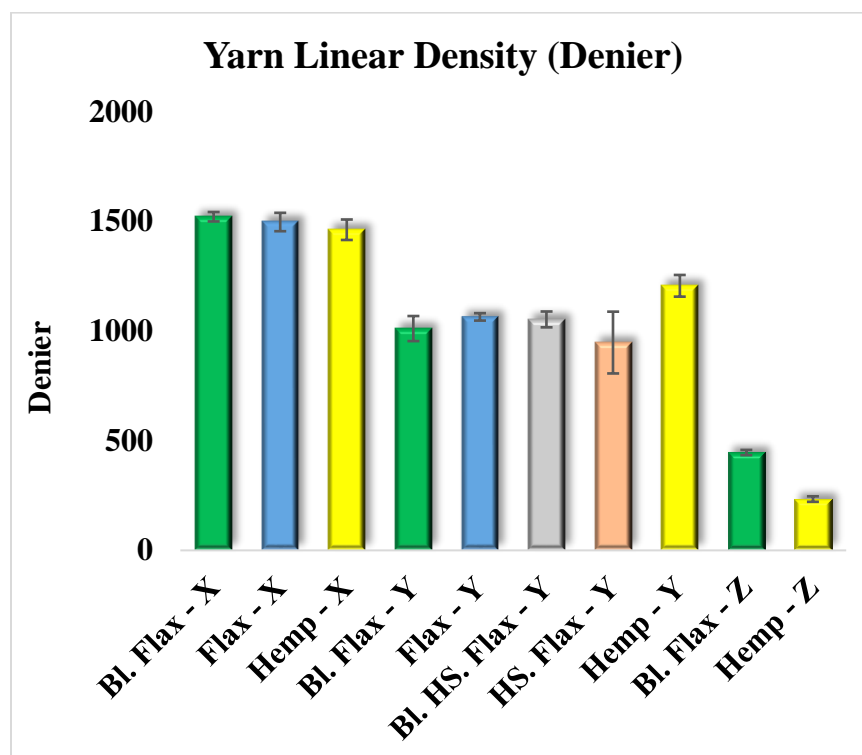


Figure 173. Linear density of flax and hemp yarns

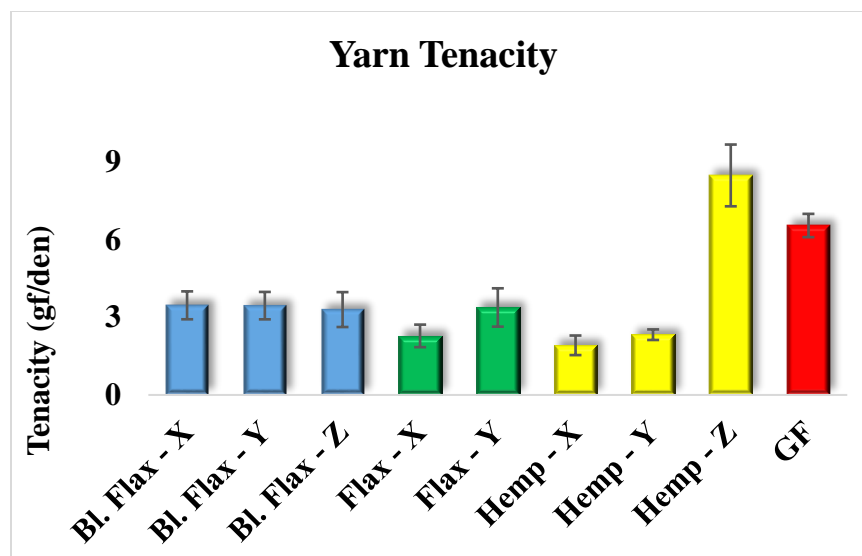


Figure 174. Yarn tenacity of 25.4 cm gauge length

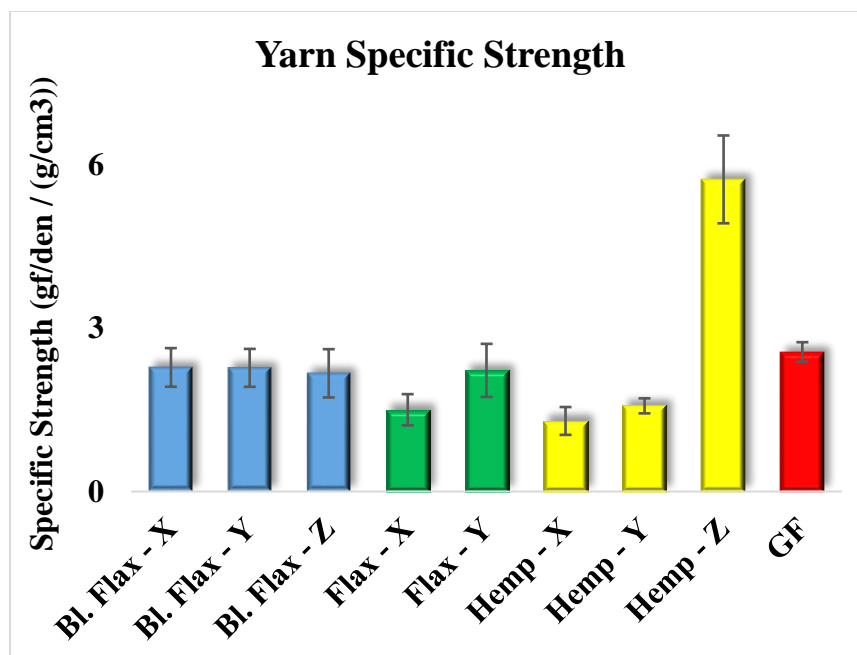


Figure 175. Yarn specific strength of 25.4 cm gauge length

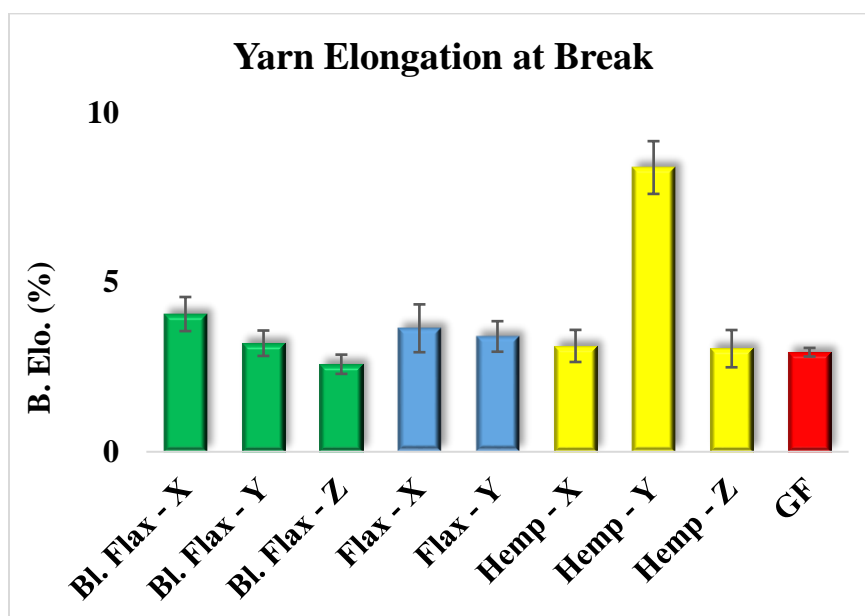


Figure 176. Yarn elongation of 25.4 cm gauge length

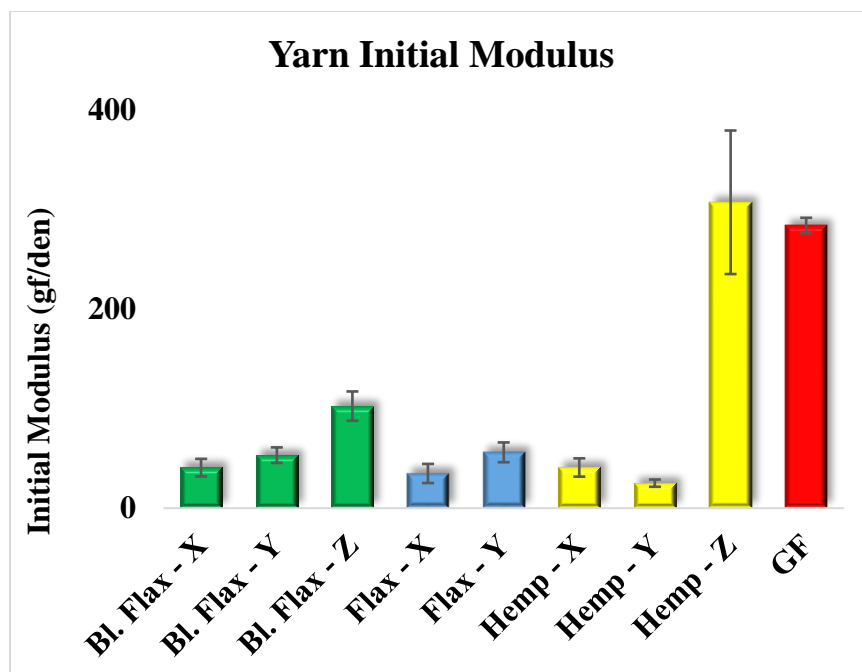


Figure 177. Yarn initial modulus of 25.4 cm gauge length

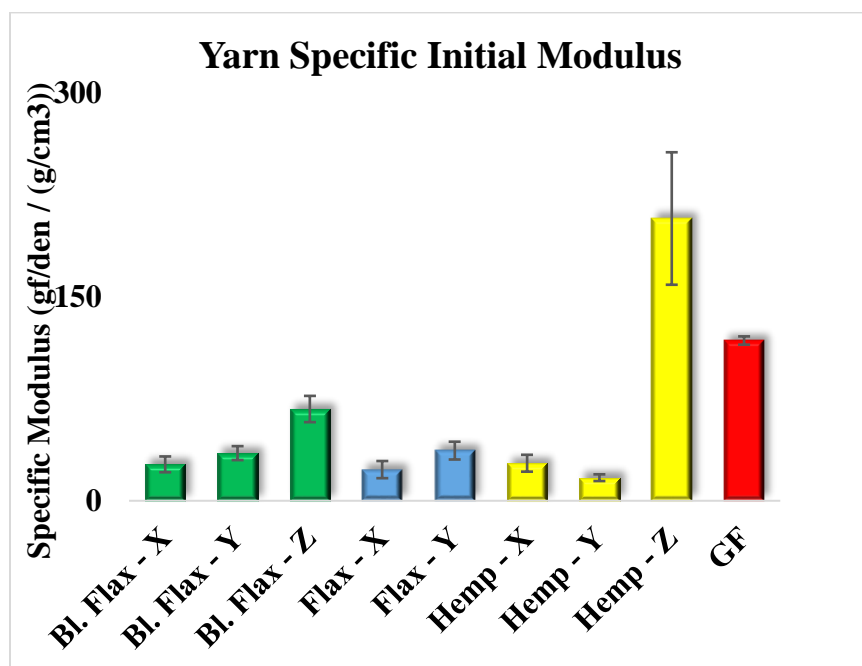


Figure 178. Yarn specific initial modulus of 25.4 cm gauge length

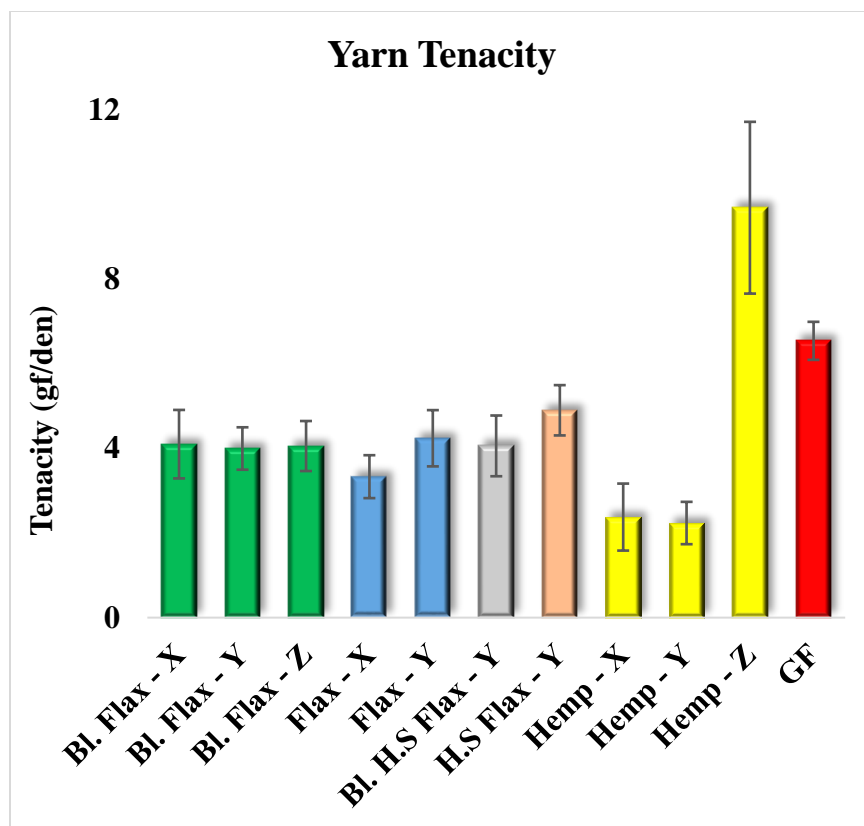


Figure 179. Yarn tenacity of 2.54 cm gauge length

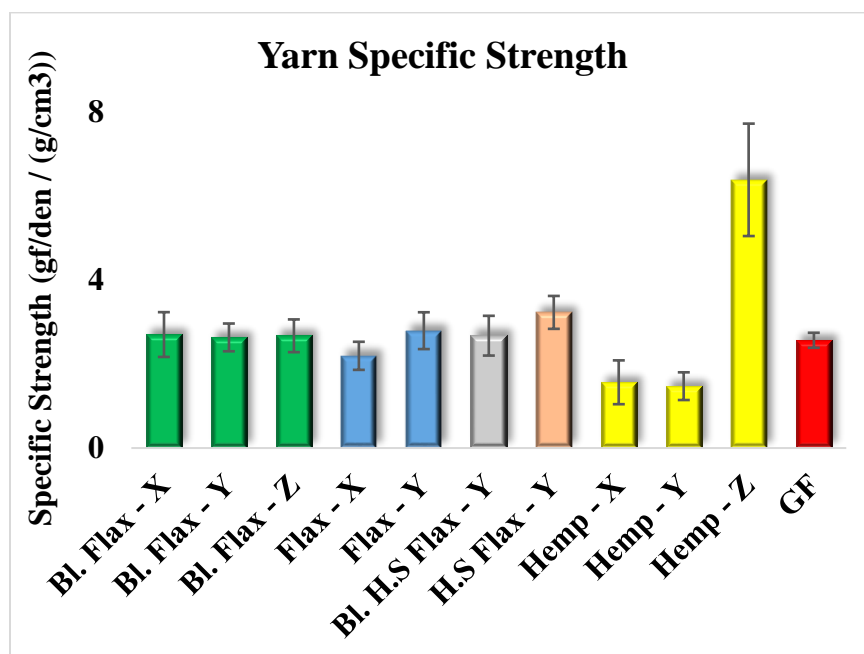


Figure 180. Yarn specific strength of 2.54 cm gauge length

Table 45. Minimum number of samples of yarns' tensile properties of 2.54 cm gauge length

Fiber Type	Confidence Level		
	90%	95%	99%
Bl. Flax - X	177	252	435
Bl. Flax - Y	68	97	167
Bl. Flax - Z	95	134	232
Flax - X	70	99	171
Flax - Y	120	170	294
Bl. H.S Flax - Y	140	198	342
H.S Flax - Y	96	136	235
Hemp - X	170	241	417
Hemp - Y	68	96	167
Hemp - Z	1117	1585	2738

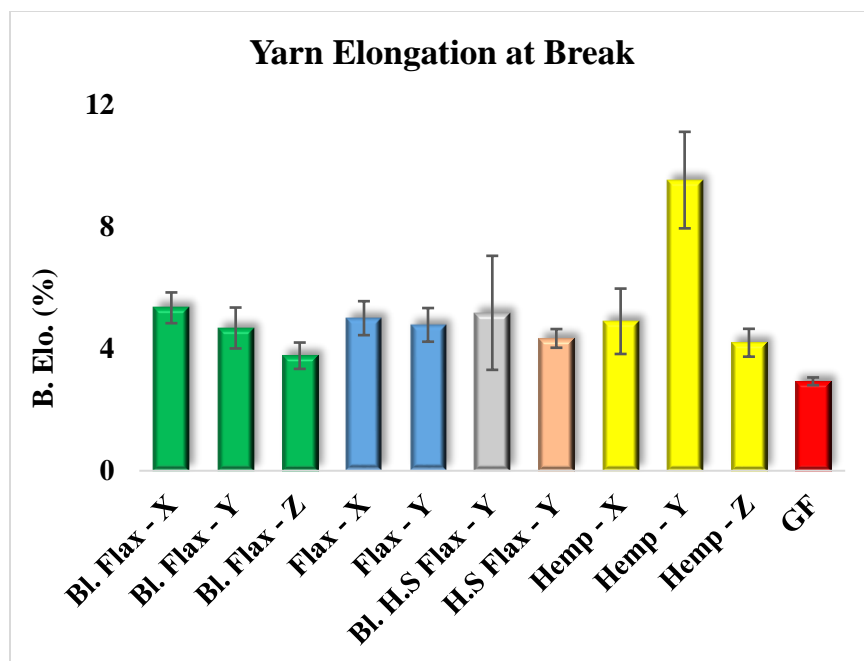


Figure 181. Yarn elongation of 2.54 cm gauge length

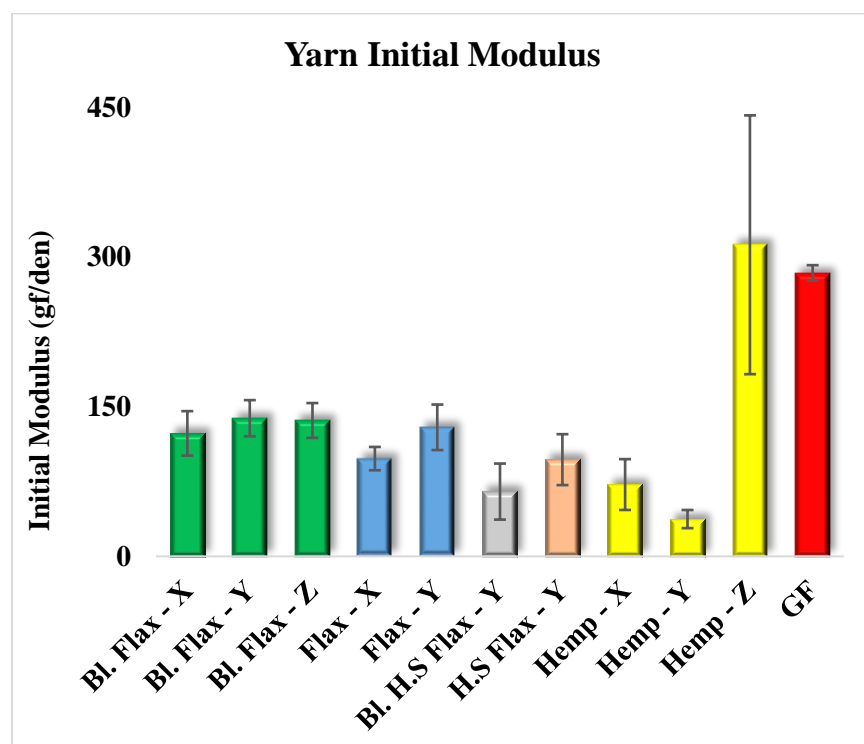


Figure 182. Yarn initial modulus of 2.54 cm gauge length

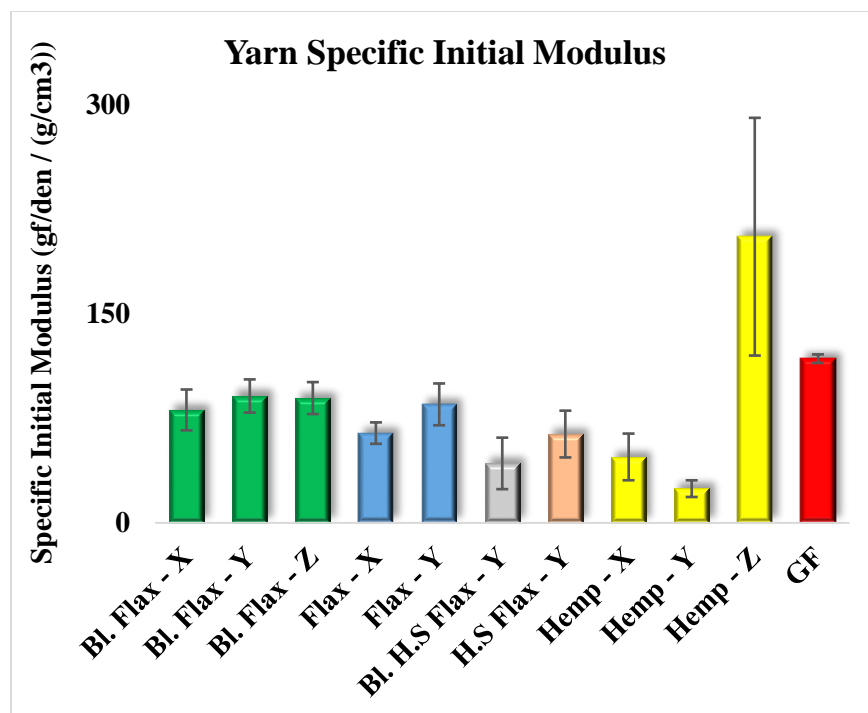


Figure 183. Yarn specific initial modulus of 2.54 cm gauge length

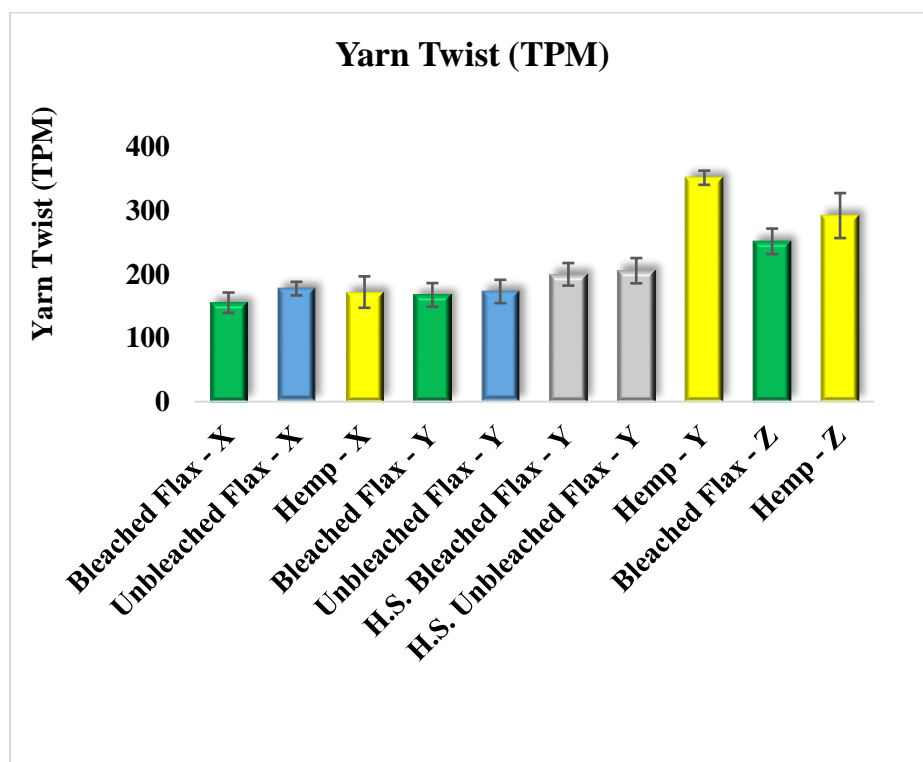


Figure 184. Yarn twist (twist/ m)

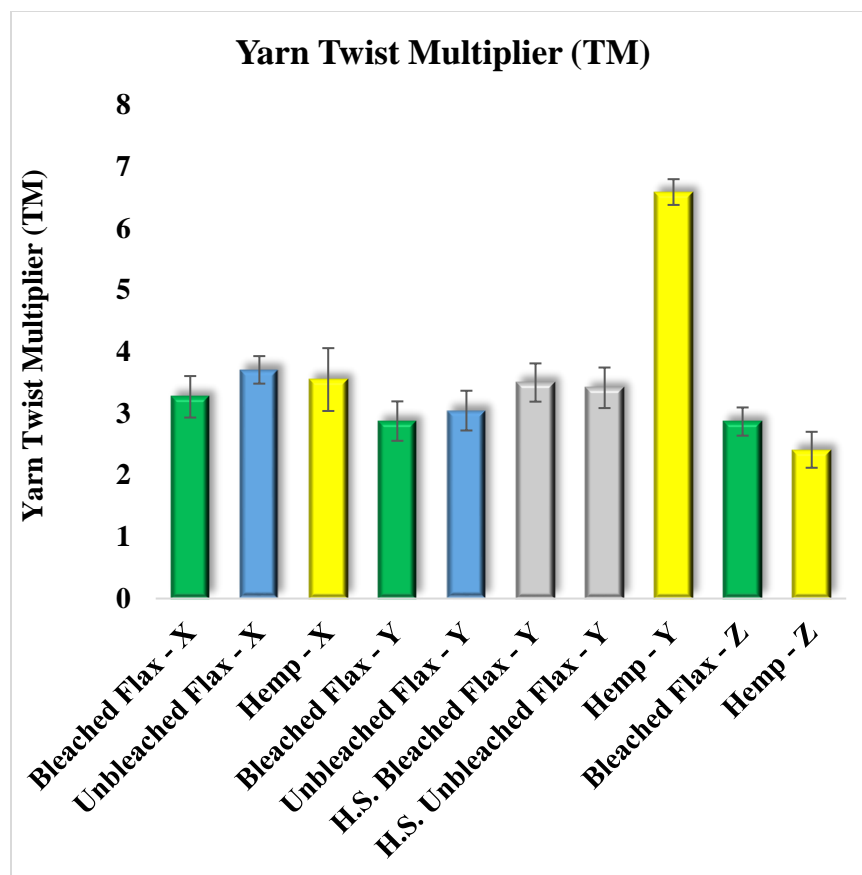
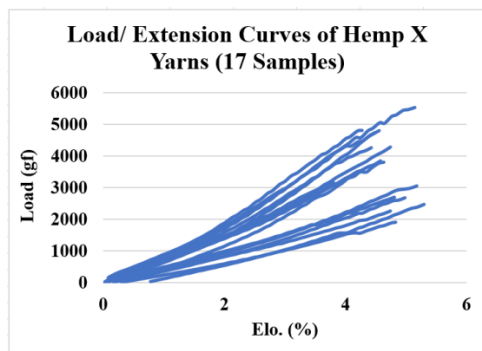
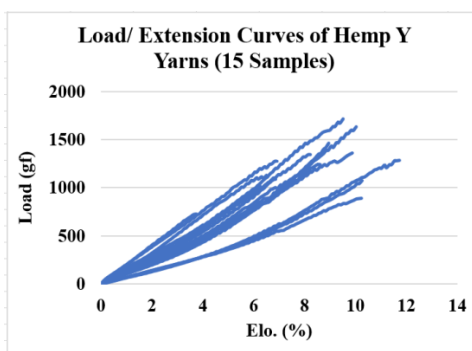


Figure 185. Yarn twist multiplier

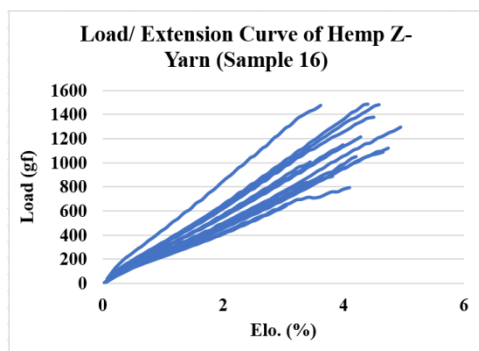
A.5. Load-Extension Curves of Hemp and Flax Yarns



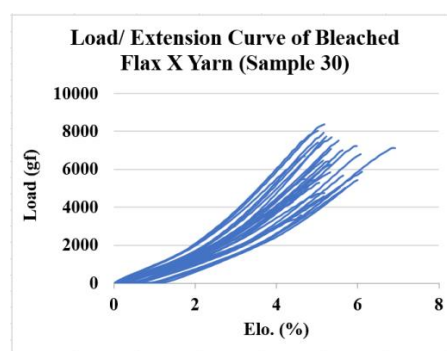
(a)



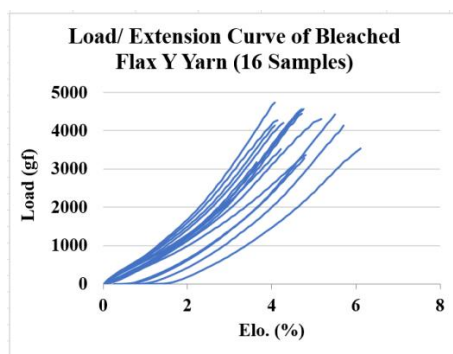
(b)



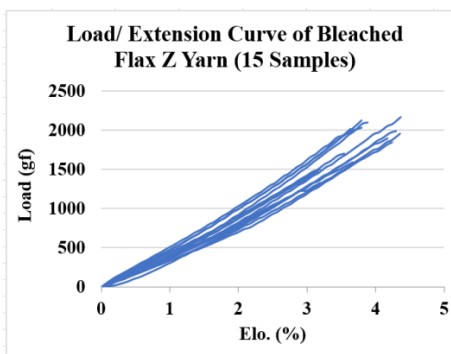
(c)



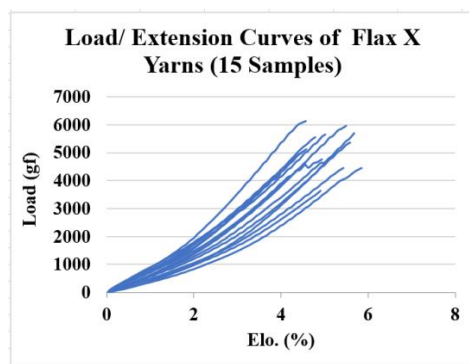
(d)



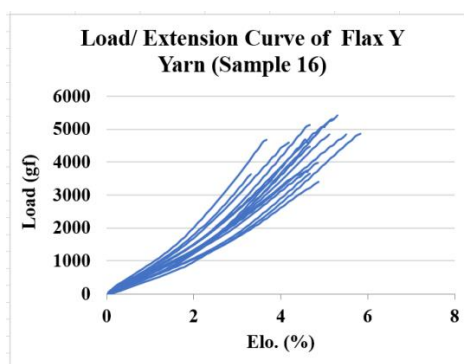
(e)



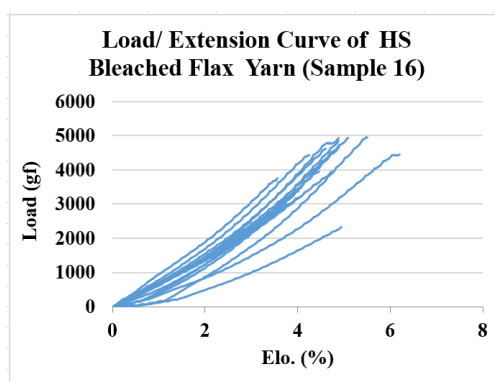
(f)



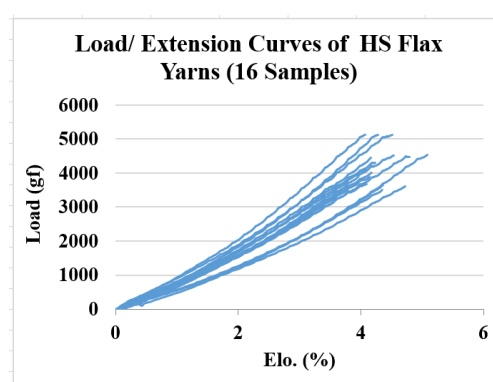
(g)



(h)



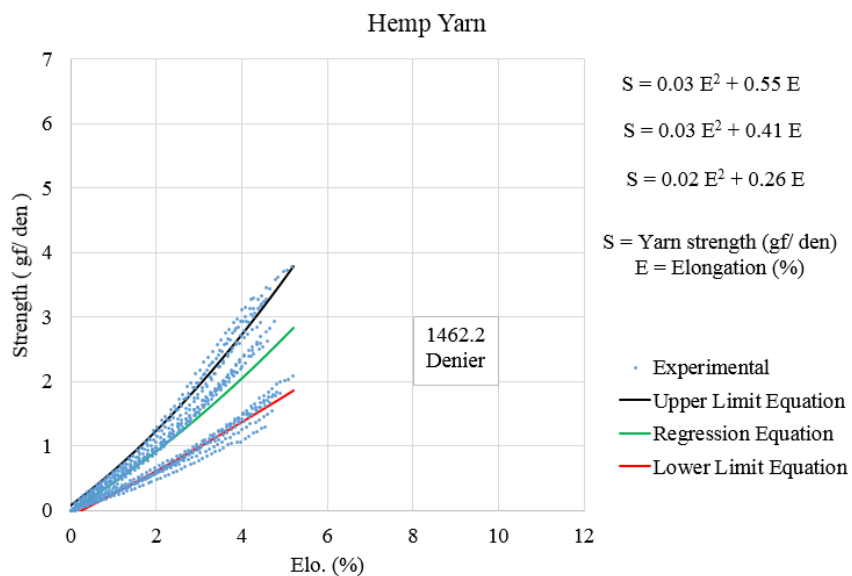
(i)



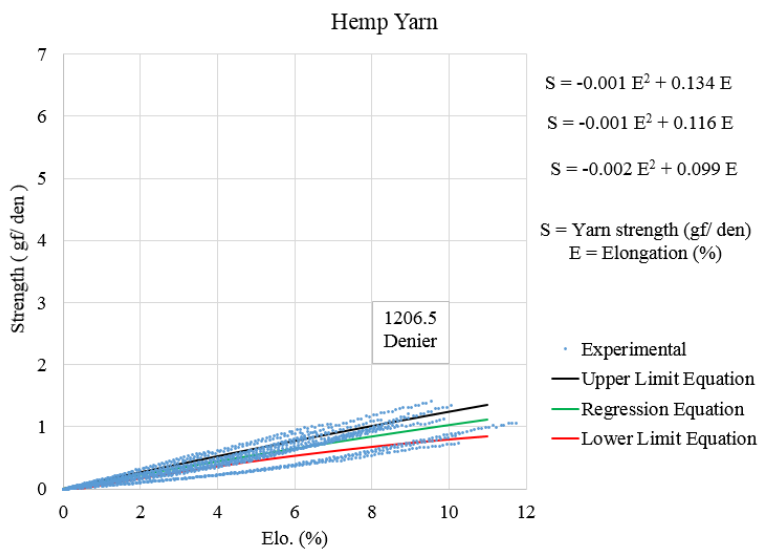
(j)

Figure 186. Load-extension curves of (a) hemp X-yarns, (b) hemp Y-yarns, (c) hemp Z-yarns, (d) bleached flax X-yarns, (e) bleached flax Y-yarns, (f) bleached flax Z-yarns, (g) flax X-yarns, (h) flax Y-yarns, (i) bleached high strength flax X-yarns, (j) high strength flax X-yarns

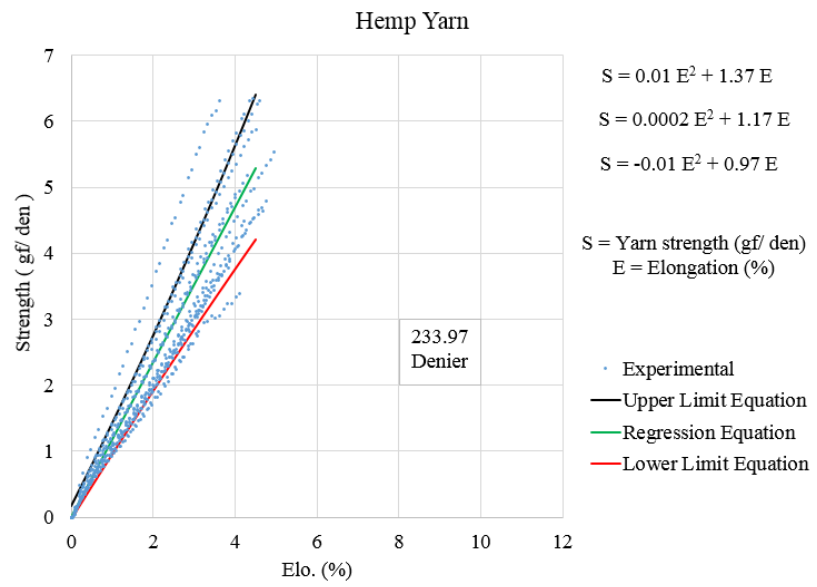
A.6. Regression Equation, Upper and Lower Limits of Load-Extension Curves of Hemp and Flax Yarns



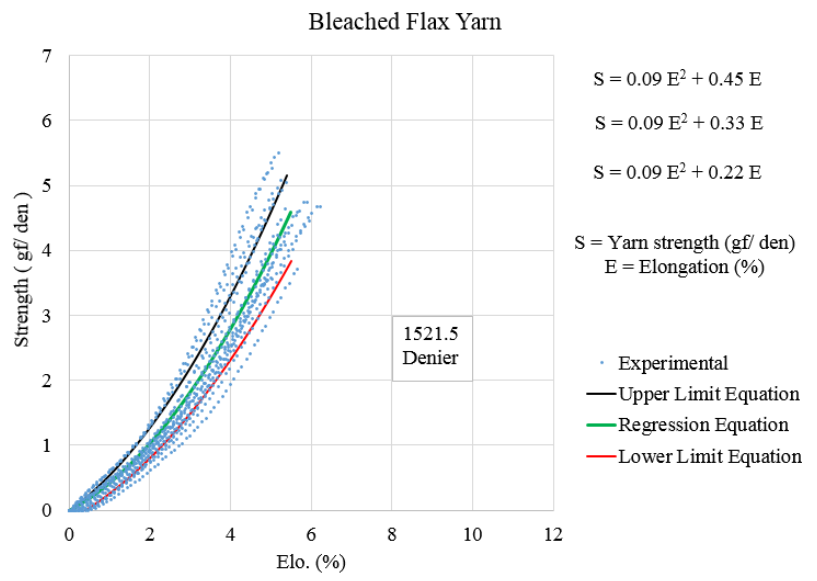
(a)



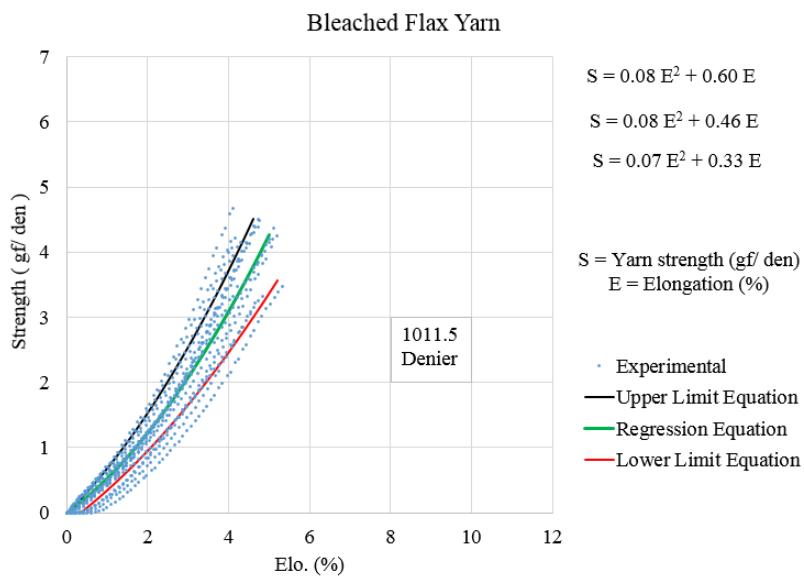
(b)



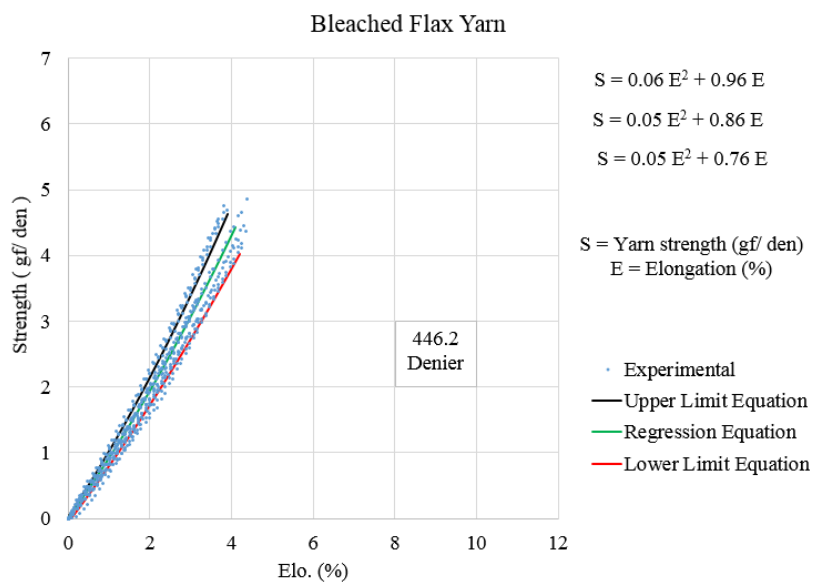
(c)



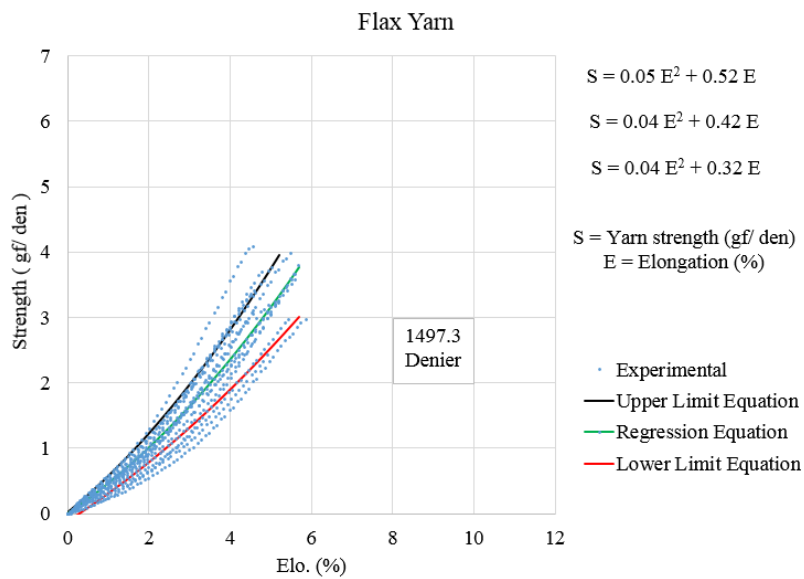
(d)



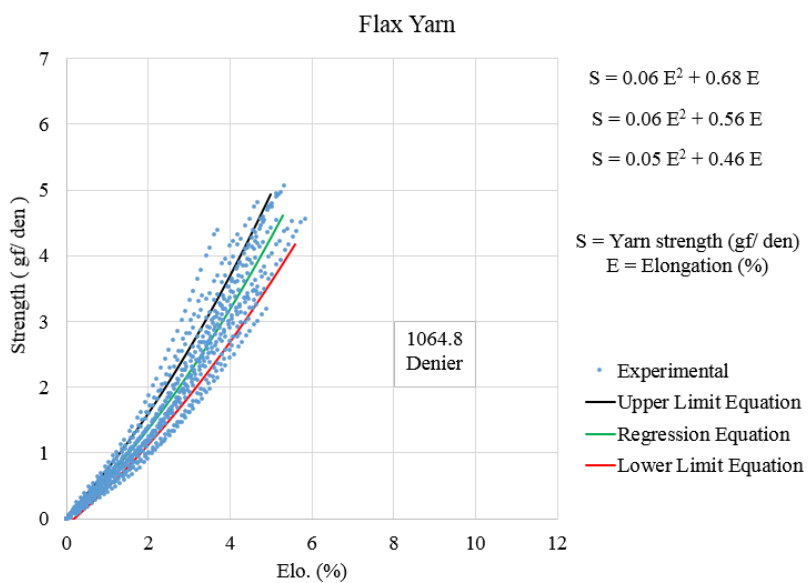
(e)



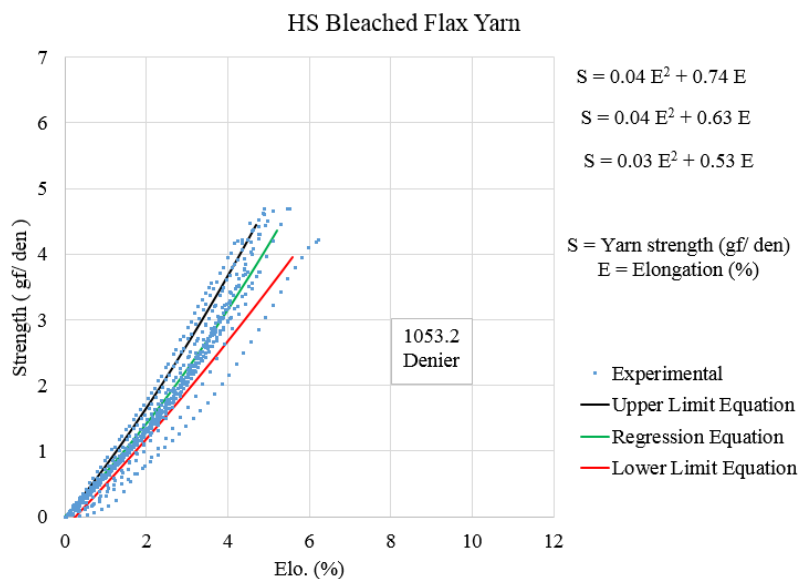
(f)



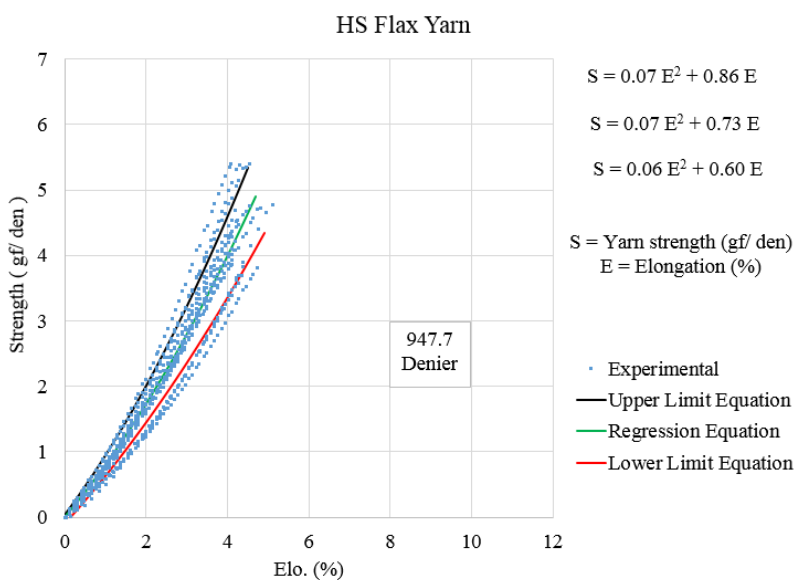
(g)



(h)



(i)

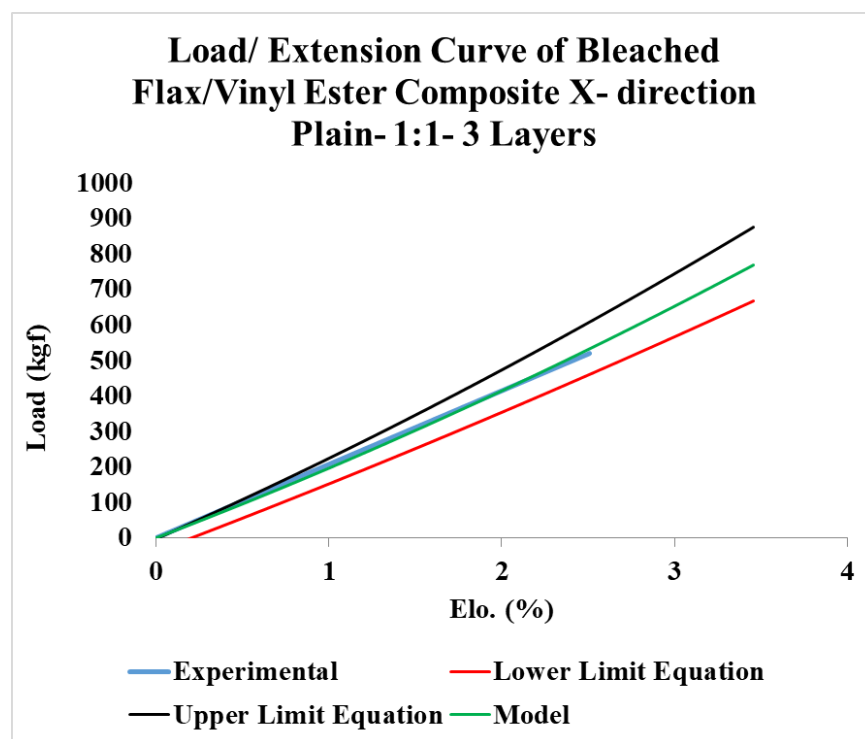


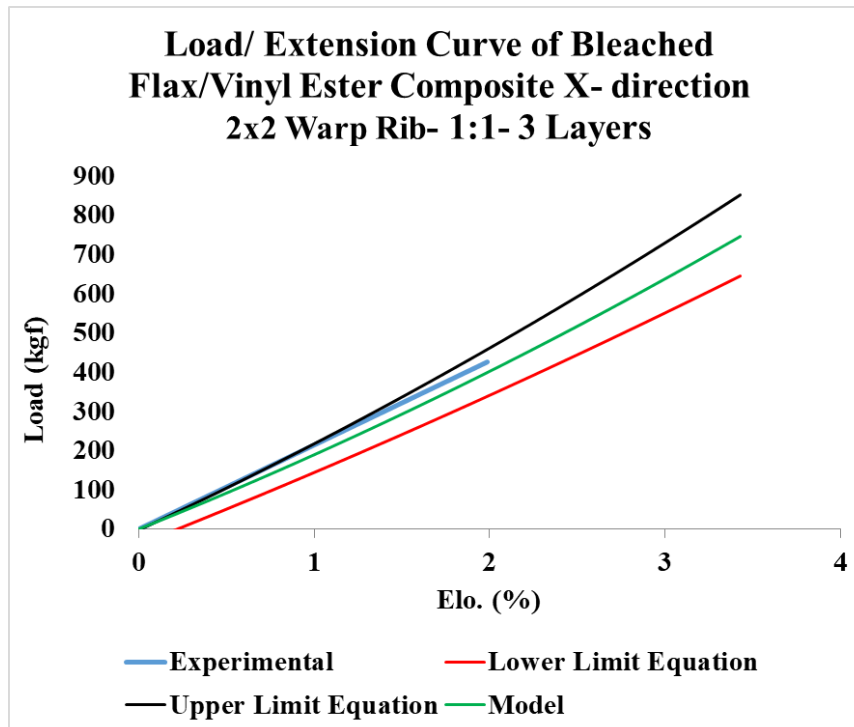
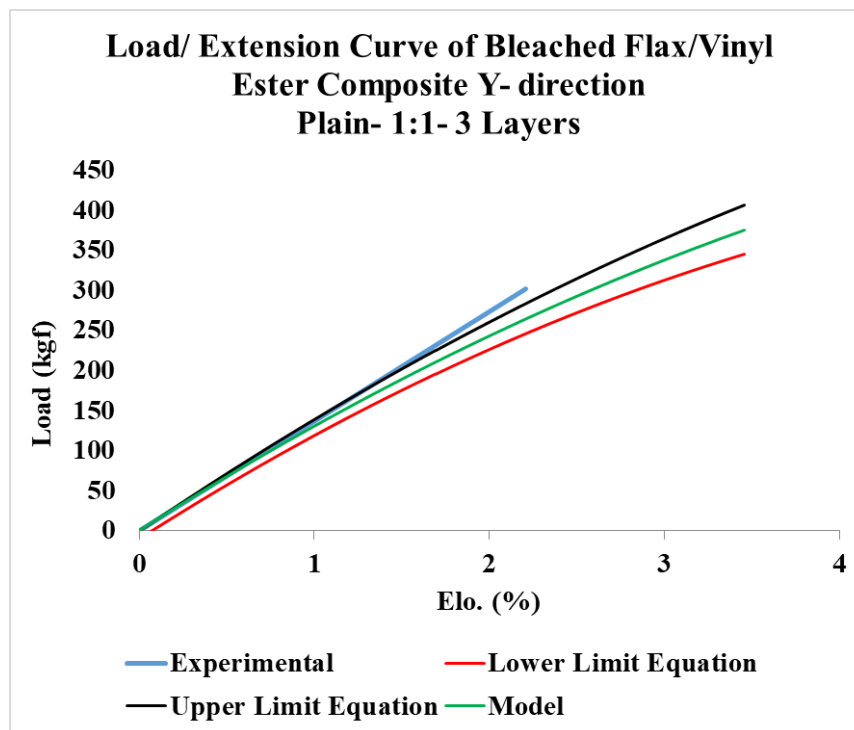
(j)

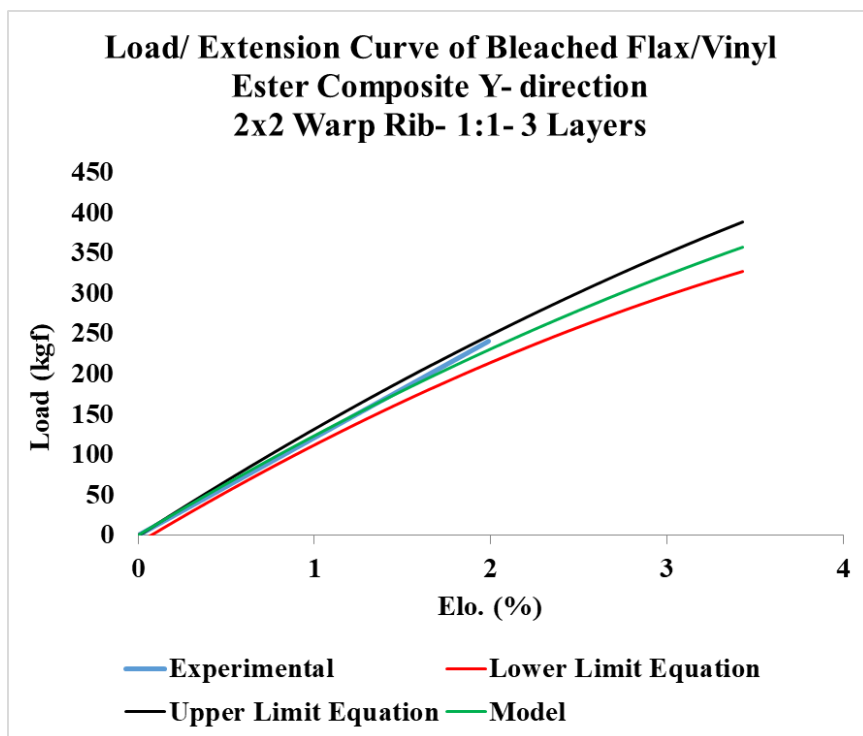
Figure 187. Regression equation, upper and lower limits of load-extension curves of (a) hemp X-yarns, (b) hemp Y-yarns, (c) hemp Z-yarns, (d) bleached flax X-yarns, (e) bleached flax Y-yarns, (f) bleached flax Z-yarns, (g) flax X-yarns, (h) flax-Y-yarns, (i) bleached high strength flax yarns, (j) high strength flax yarns

Appendix B

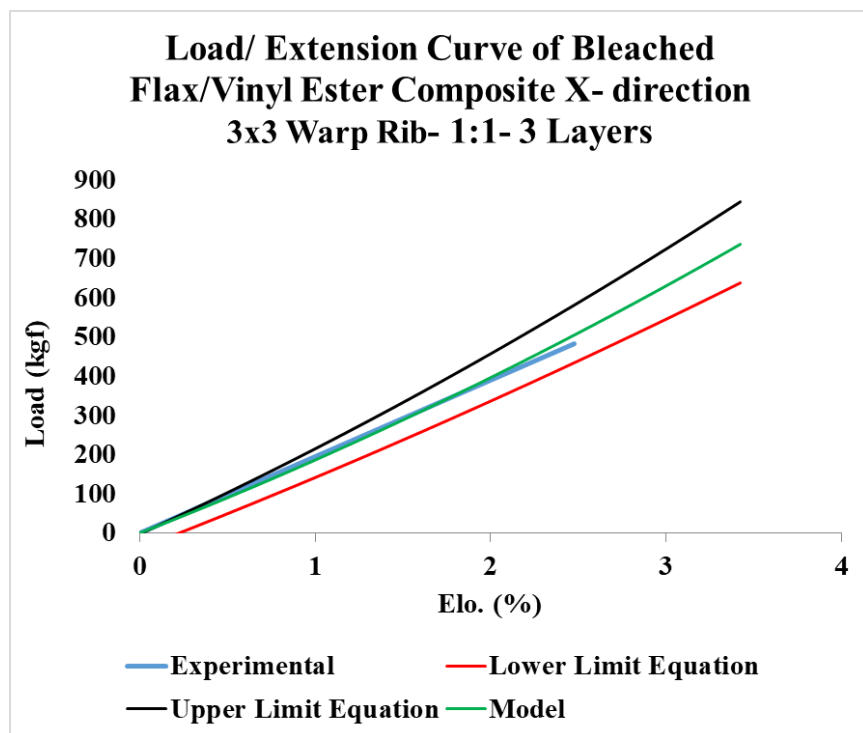
B.1. Experimental vs. Model Tensile Load-Elongation Curves of 3DOW Composites from Flax Fibers Based on the Tensile Properties of the Yarn

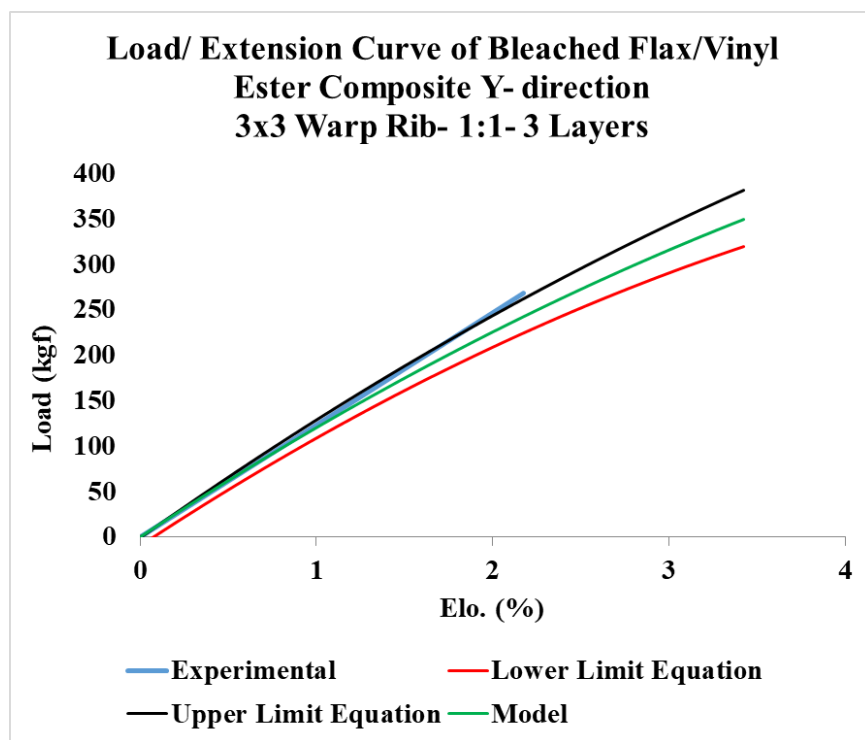




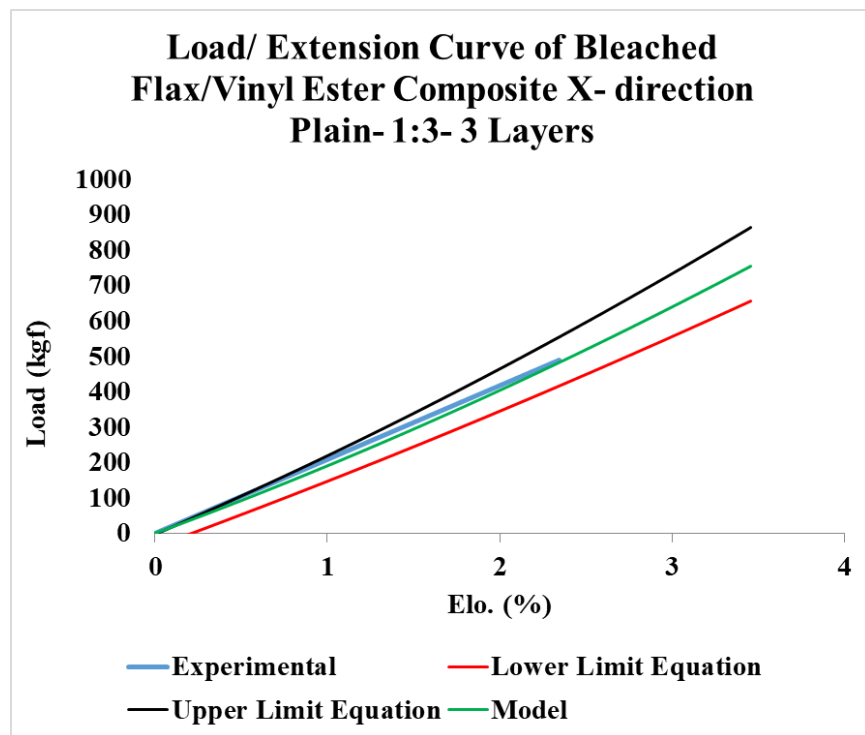


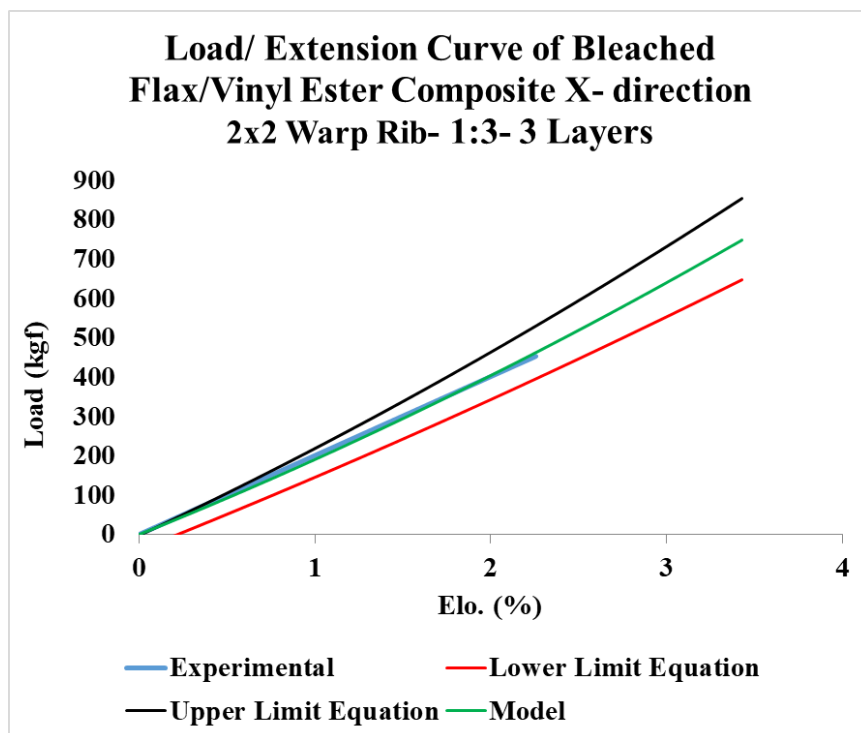
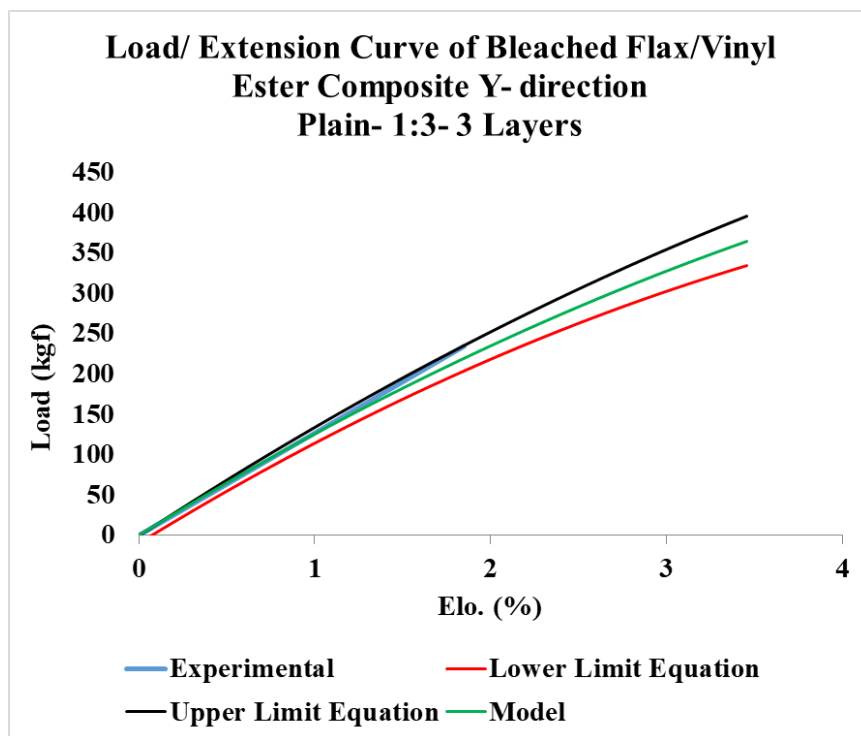
(b)

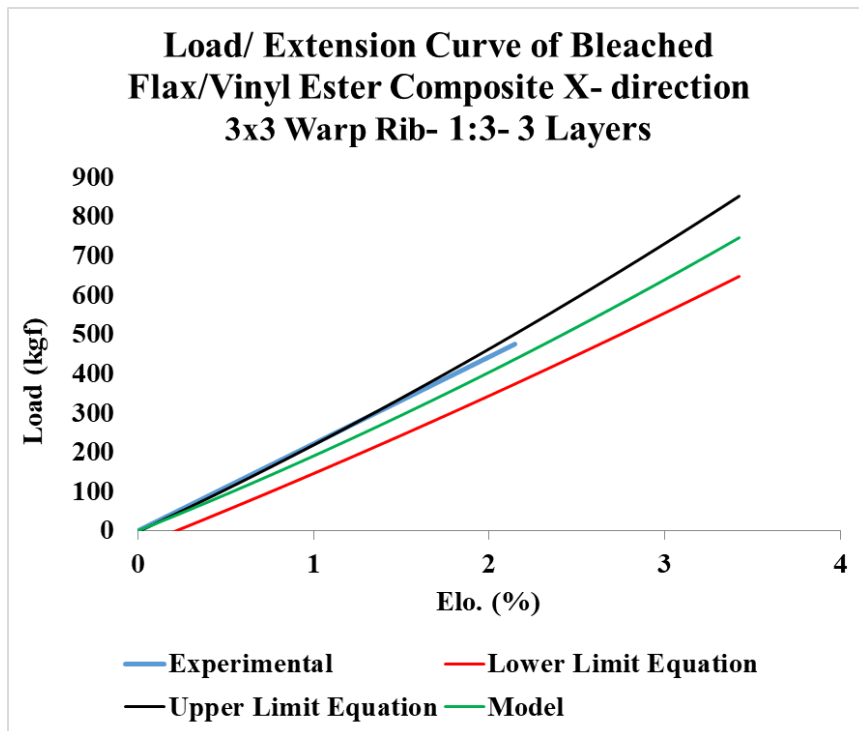
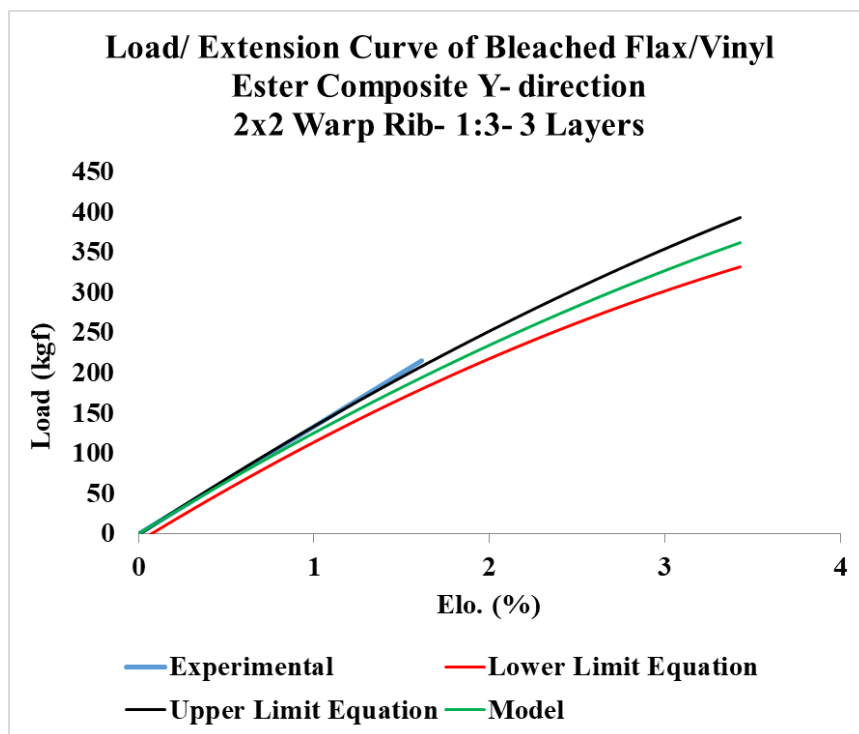


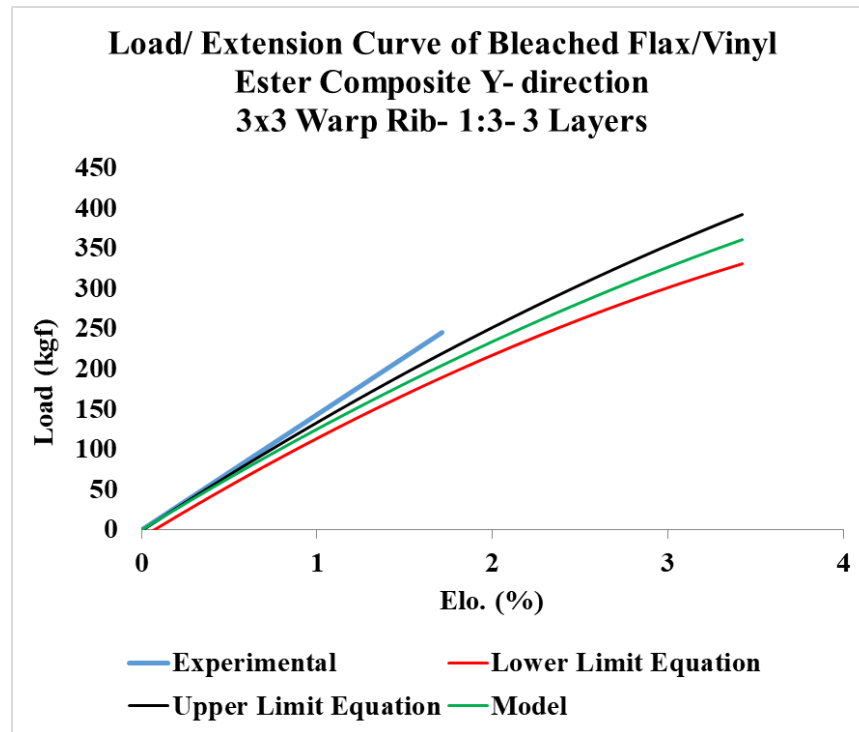


(c)



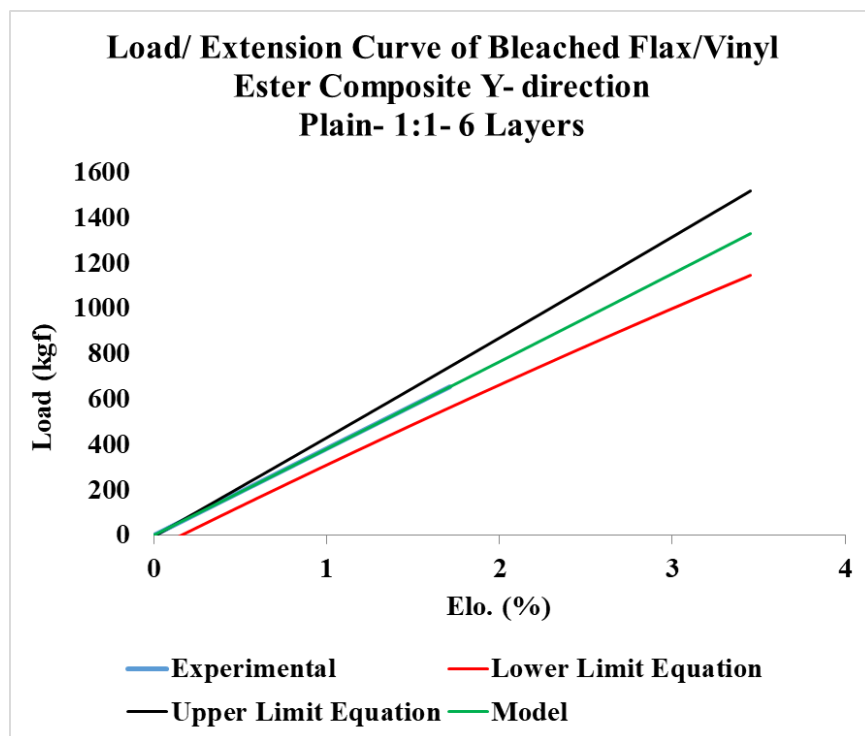
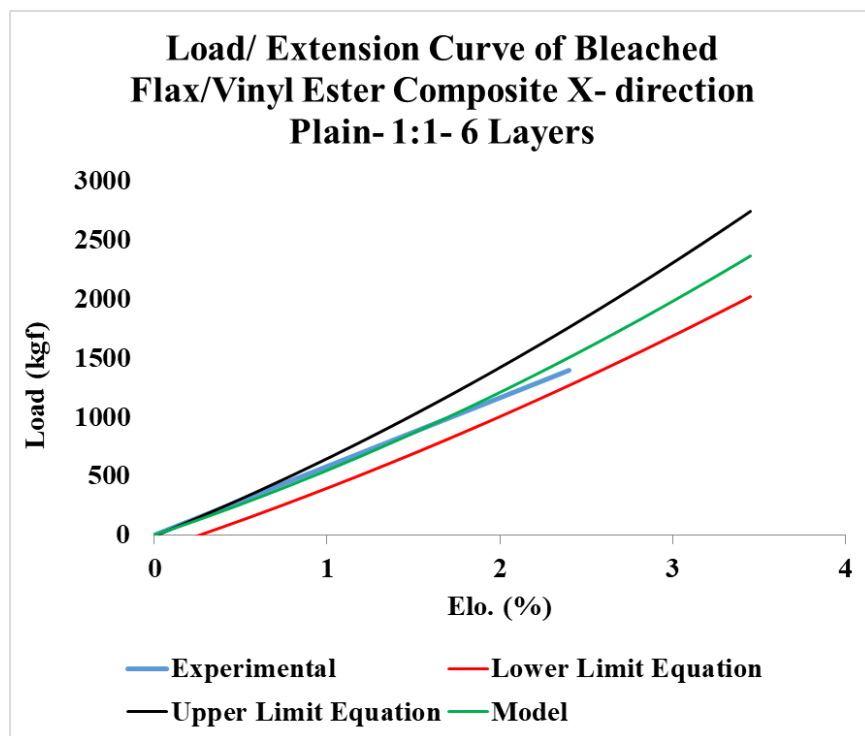




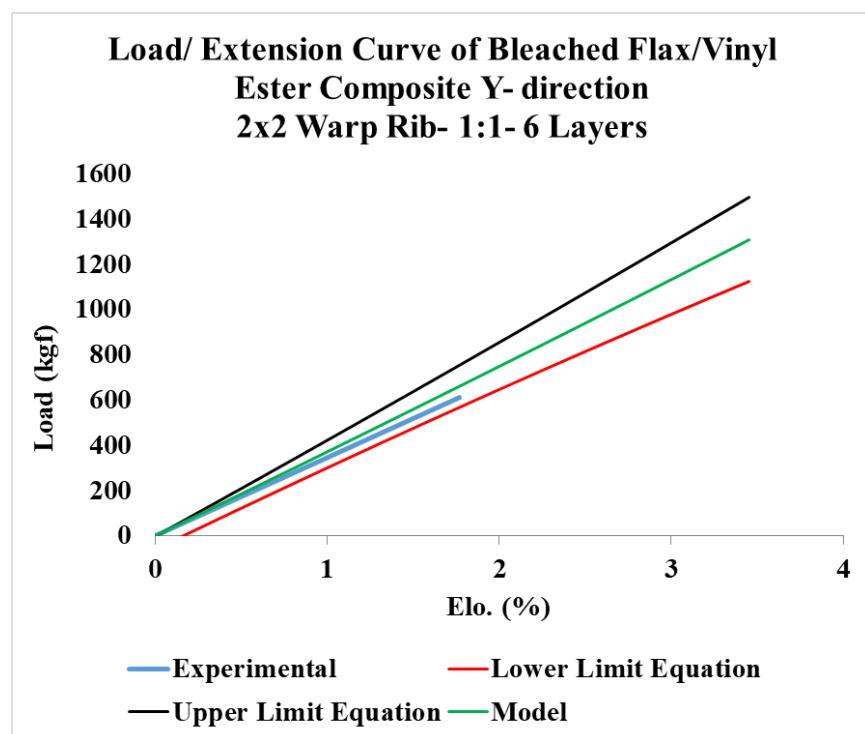
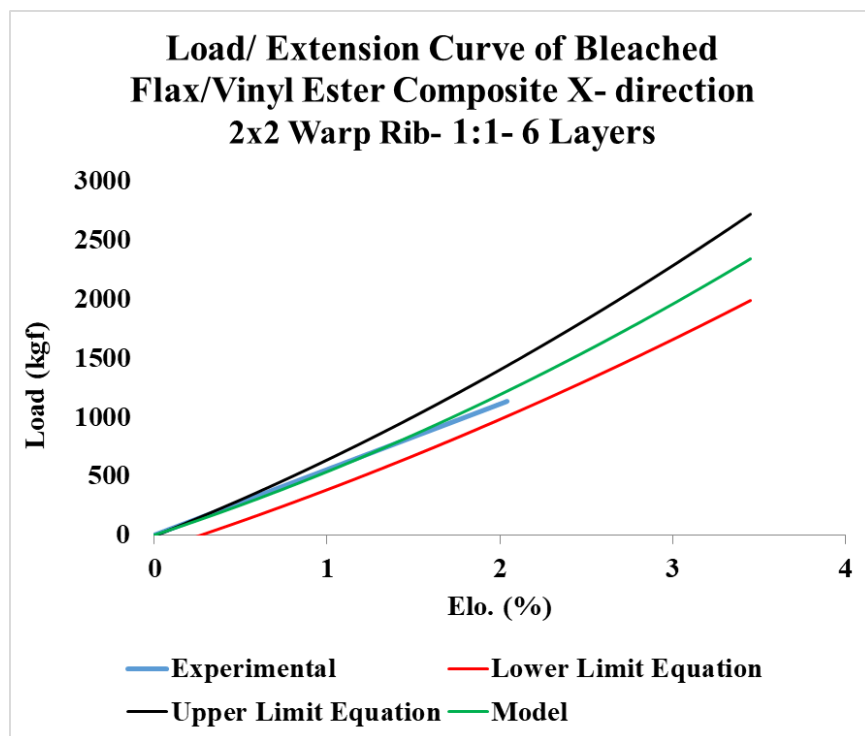


(f)

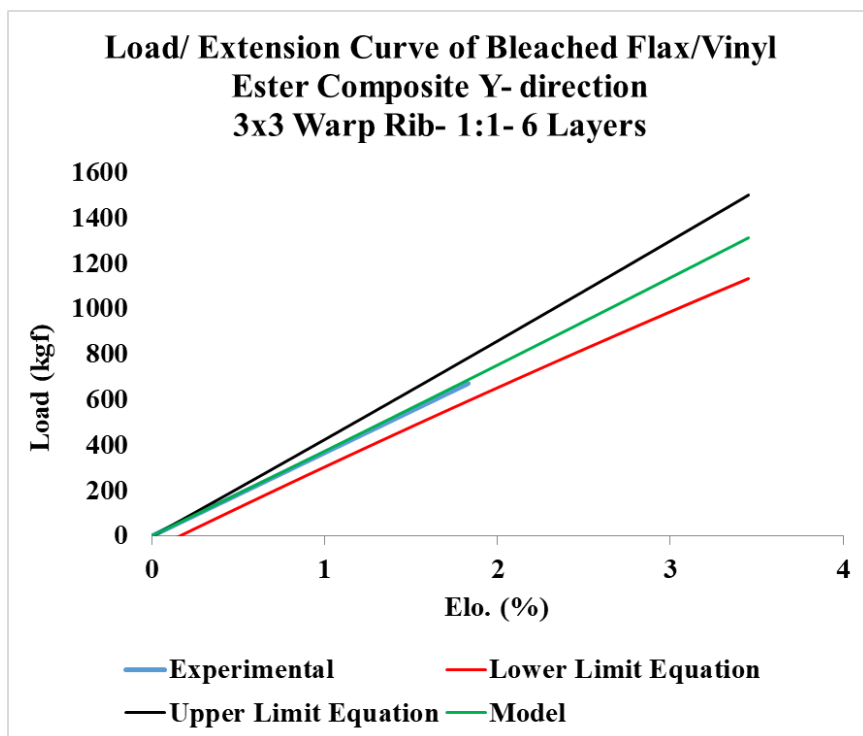
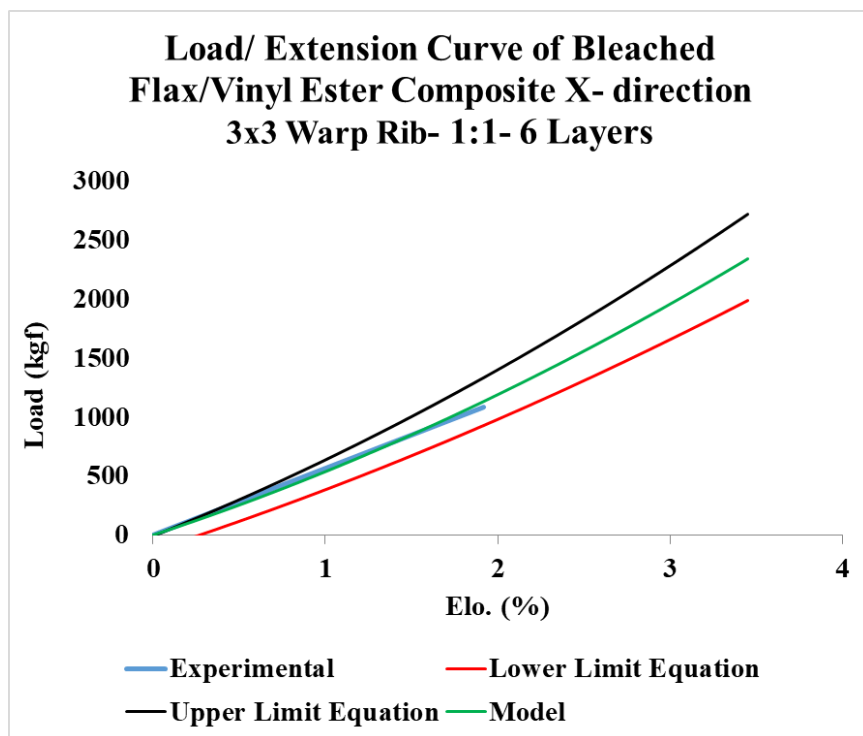
Figure 188. Experimental vs. model tensile load-elongation curves of 3 Y-yarn layers 3DOW composites from bleached flax in the X- and Y-directions (a) plain and 1:1 Z to Y-yarn ratio, (b) 2x2 warp rib and 1:1 Z to Y-yarn ratio, (c) 3x3 warp rib and 1:1 Z to Y-yarn ratio, (d) plain and 1:3 Z to Y-yarn ratio, (e) 2x2 warp rib and 1:3 Z to Y-yarn ratio, (f) 3x3 warp rib and 1:3 Z to Y-yarn ratio



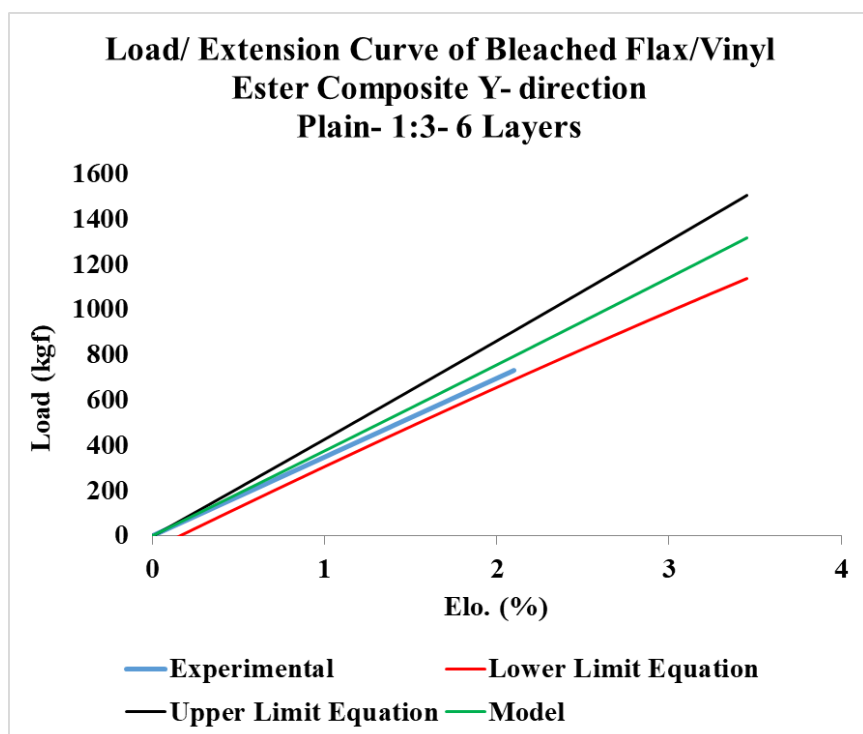
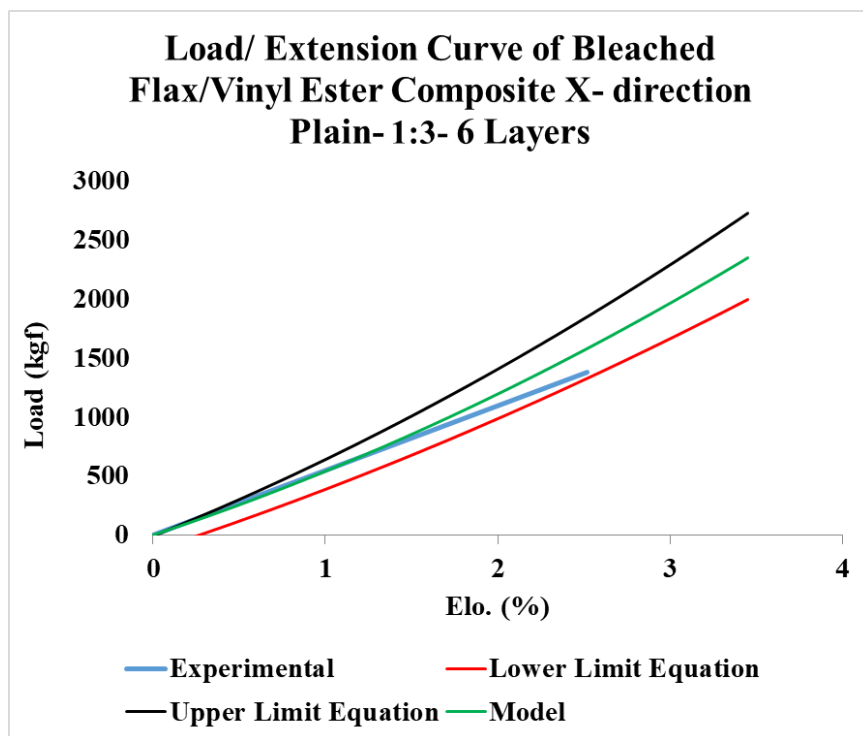
(a)



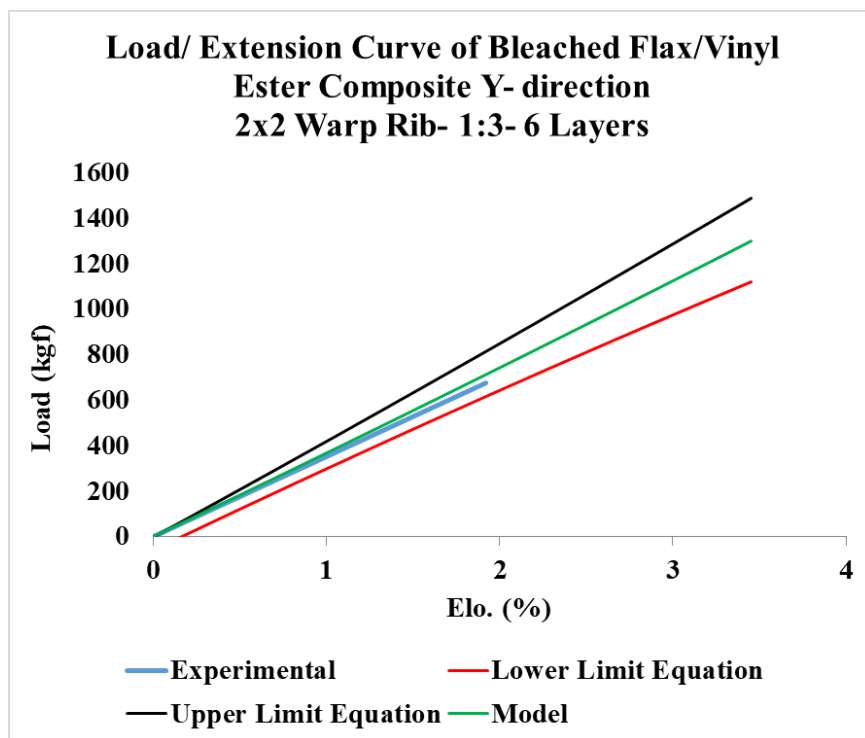
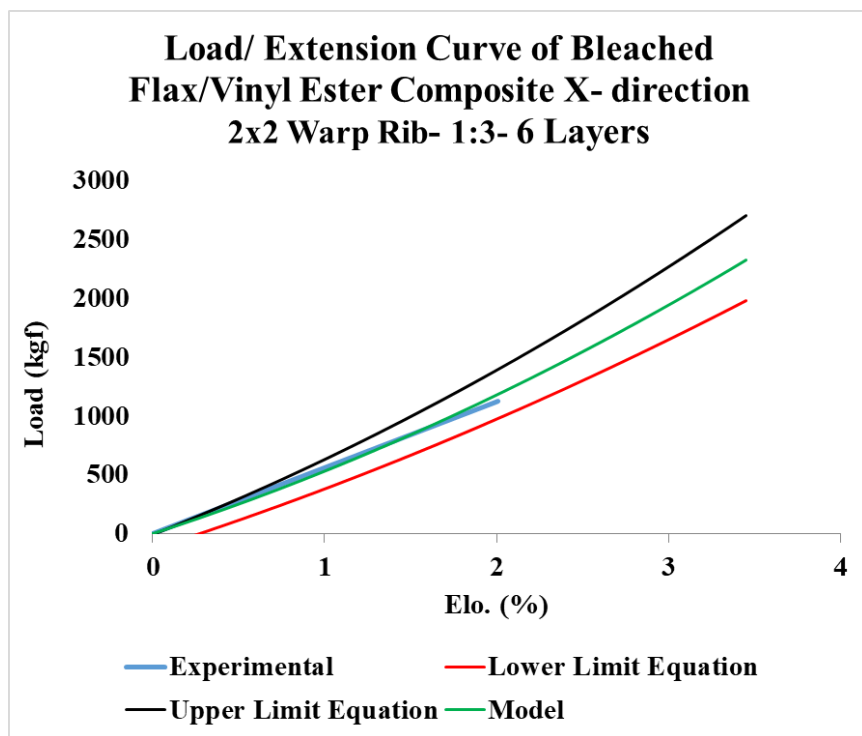
(b)



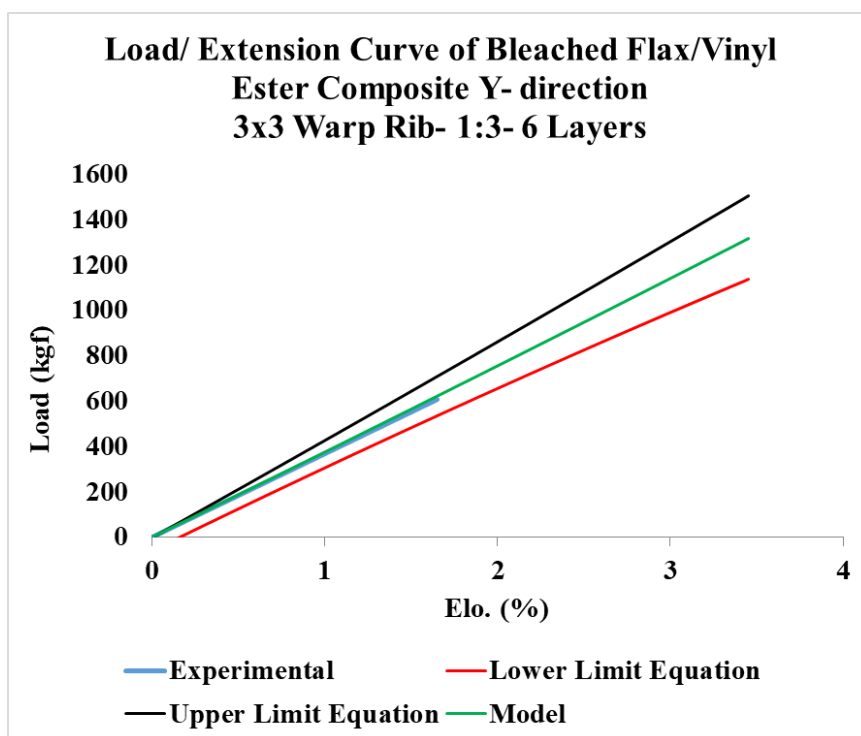
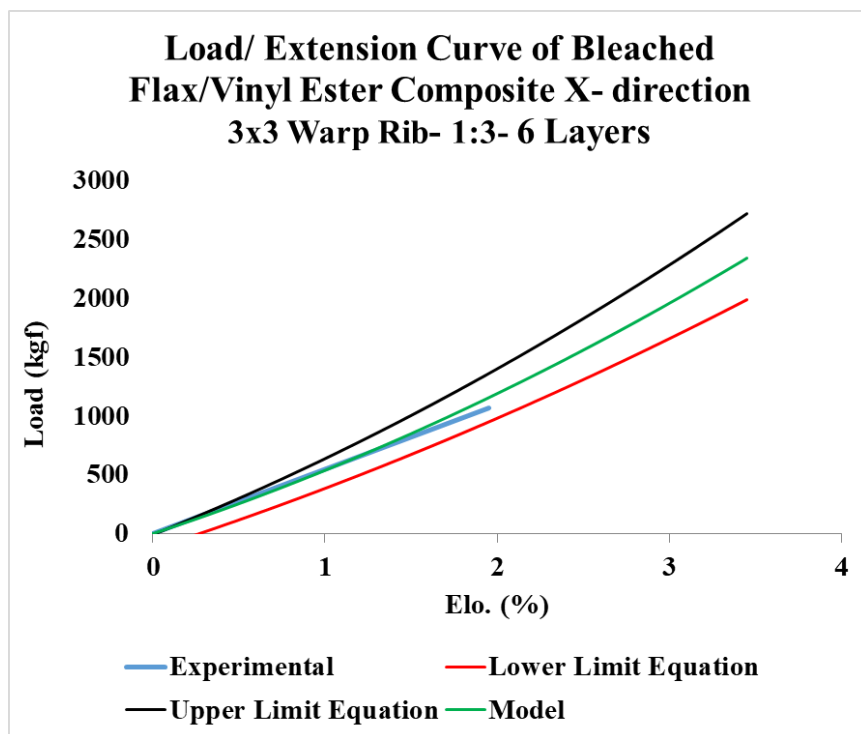
(c)



(d)

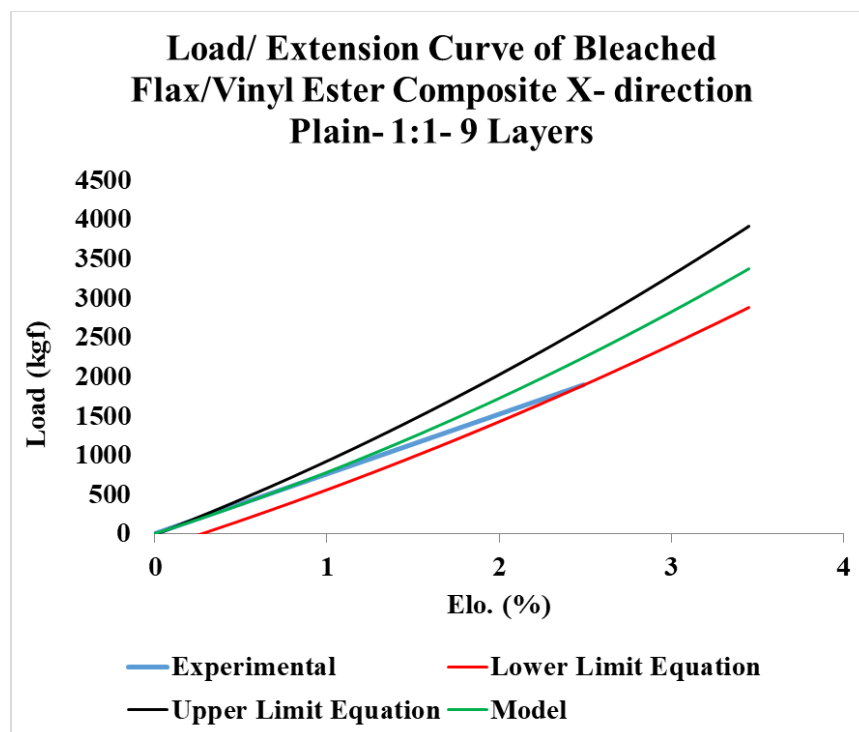


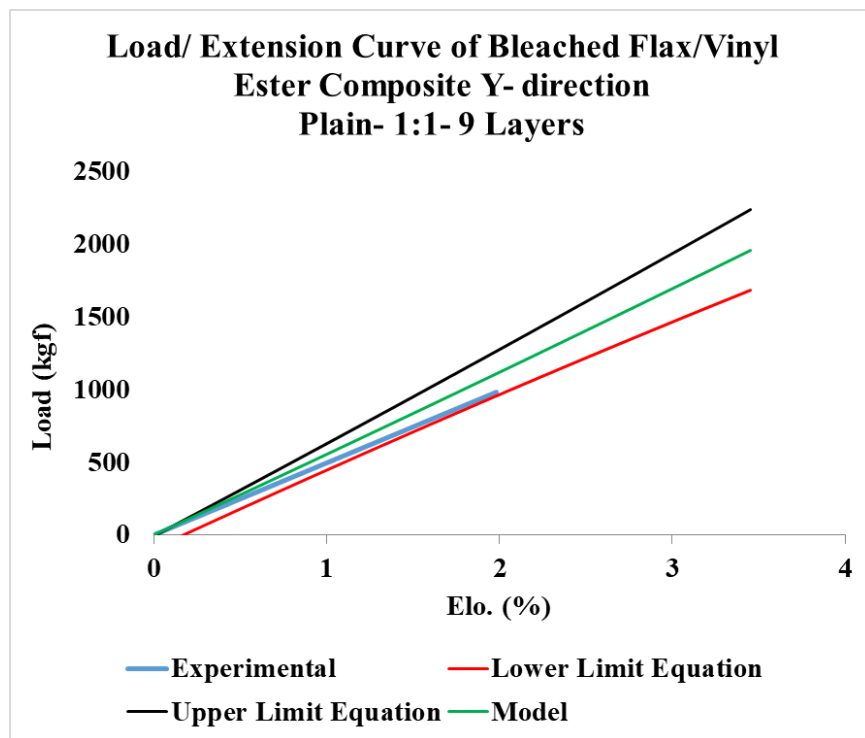
(e)



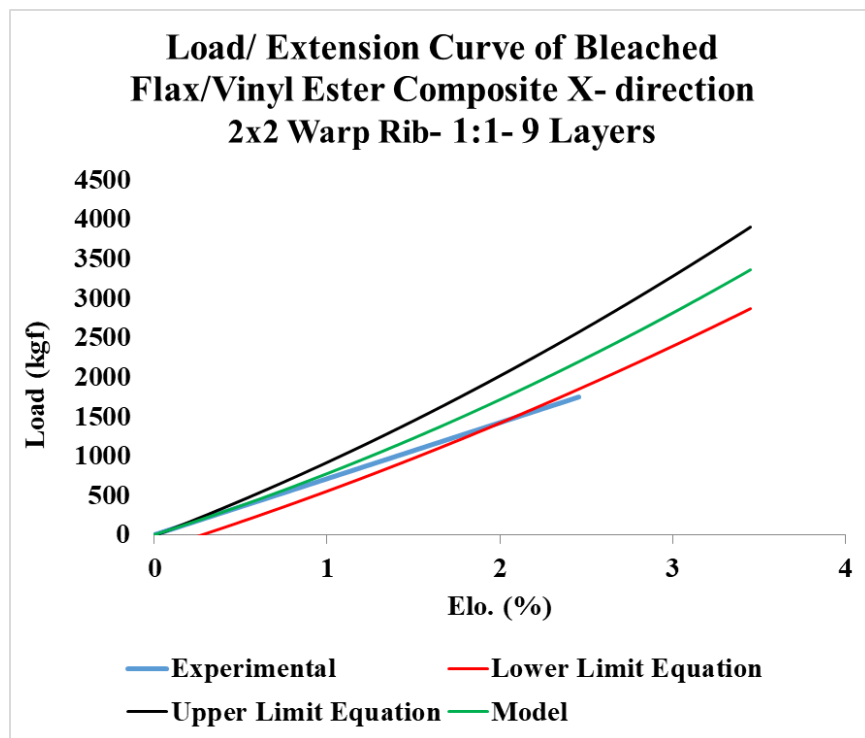
(f)

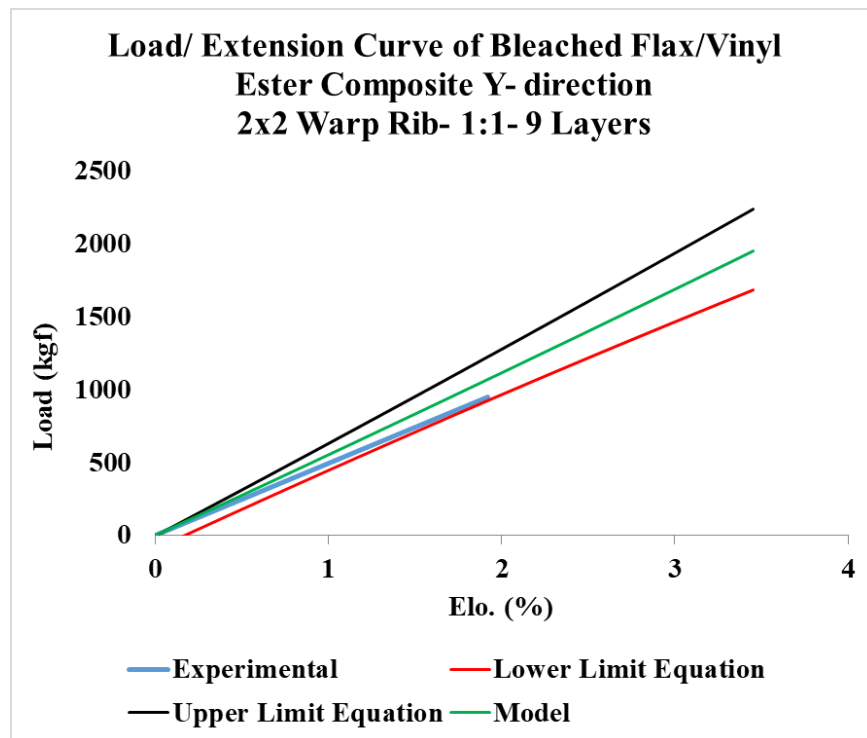
Figure 189. Experimental vs. model tensile load-elongation curves of 6 Y-yarn layers 3DOW composites from bleached flax in the X- and Y-directions (a) plain and 1:1 Z to Y-yarn ratio, (b) 2x2 warp rib and 1:1 Z to Y-yarn ratio, (c) 3x3 warp rib and 1:1 Z to Y-yarn ratio, (d) plain and 1:3 Z to Y-yarn ratio, (e) 2x2 warp rib and 1:3 Z to Y-yarn ratio, (f) 3x3 warp rib and 1:3 Z to Y-yarn ratio



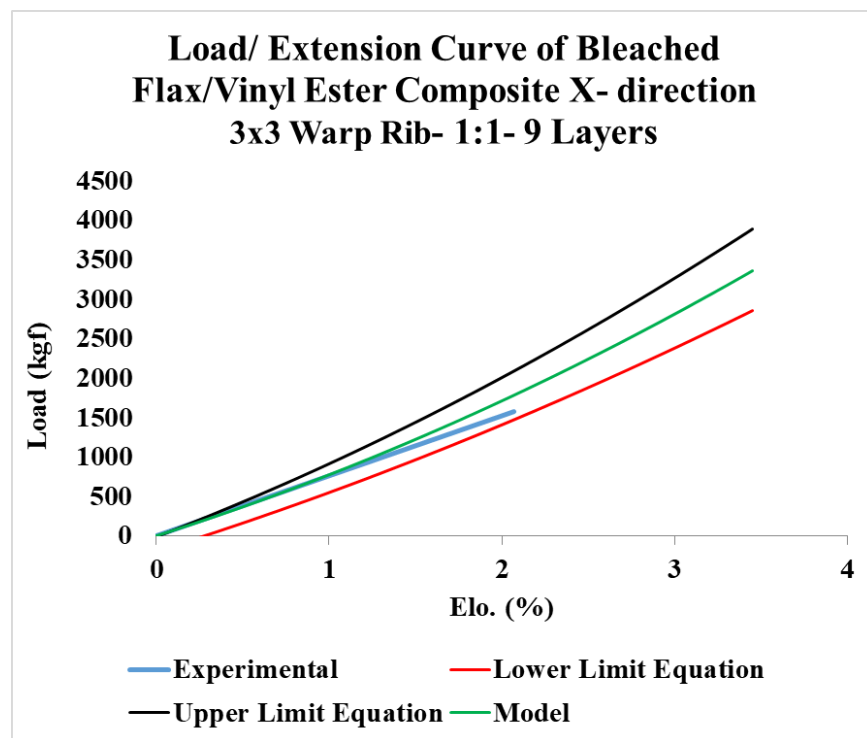


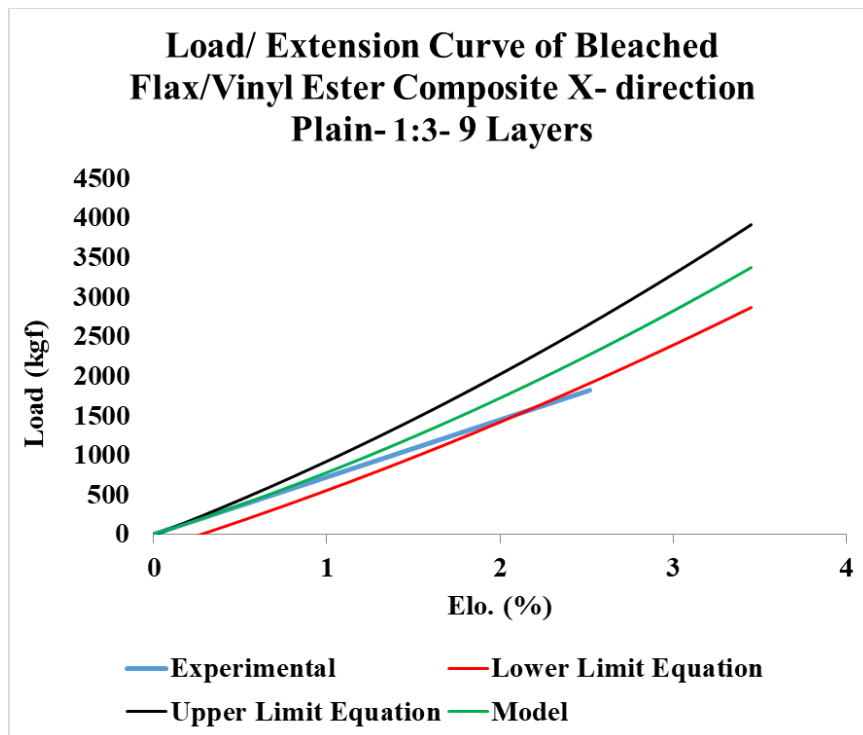
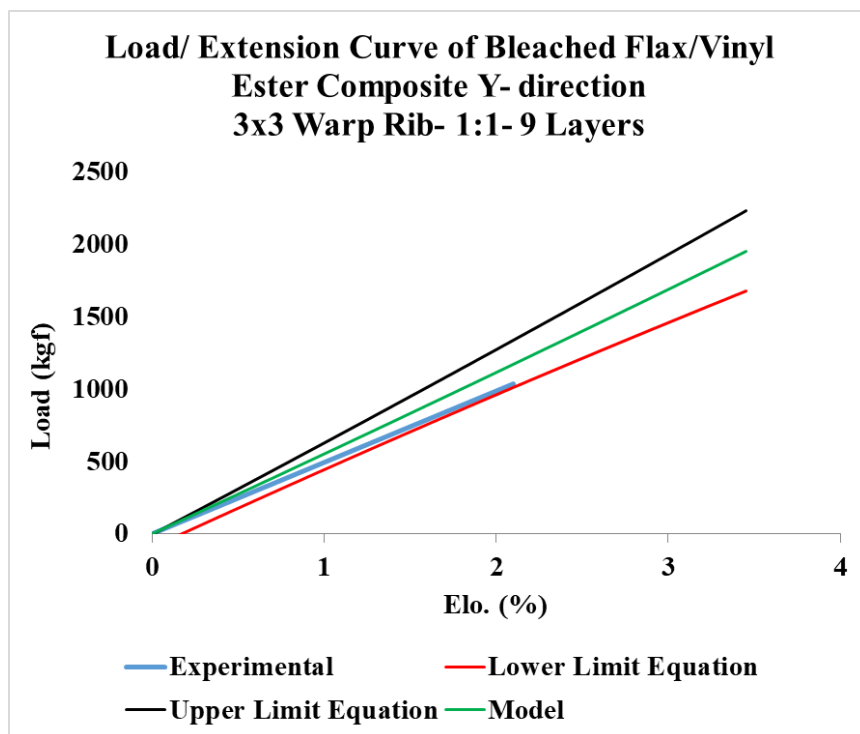
(a)

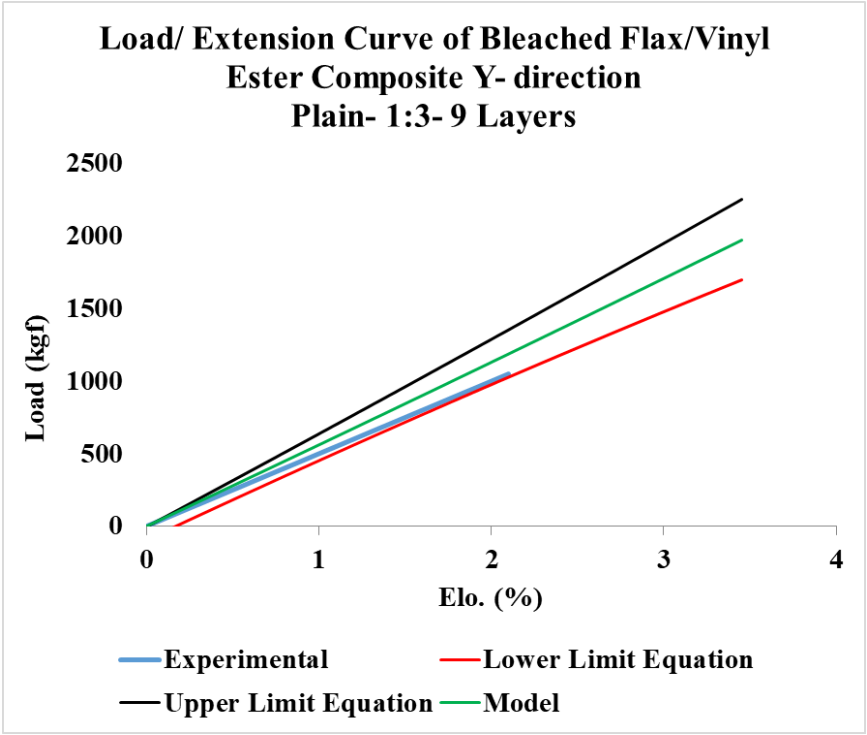




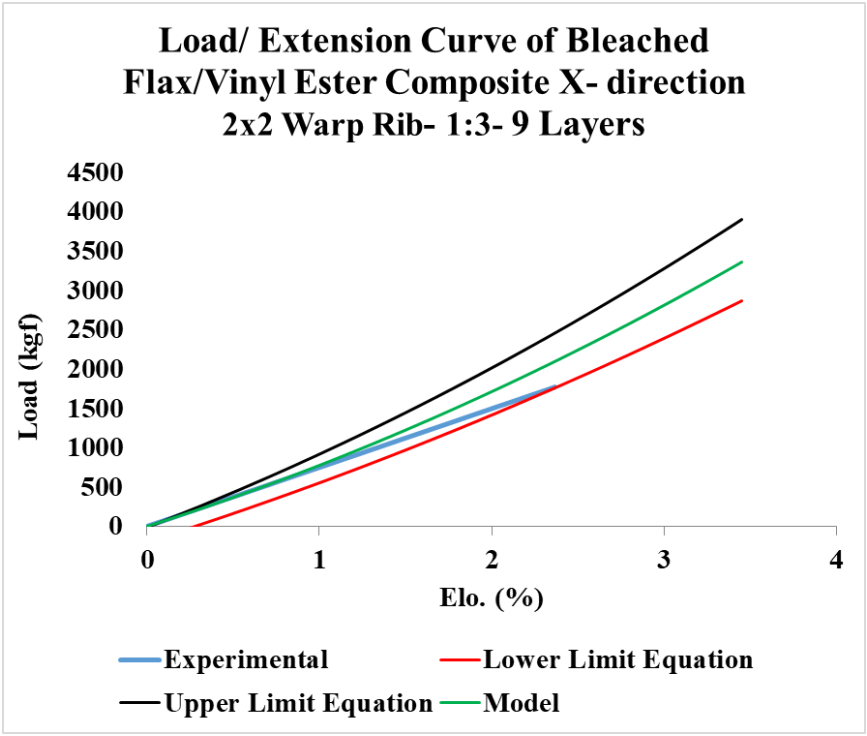
(b)

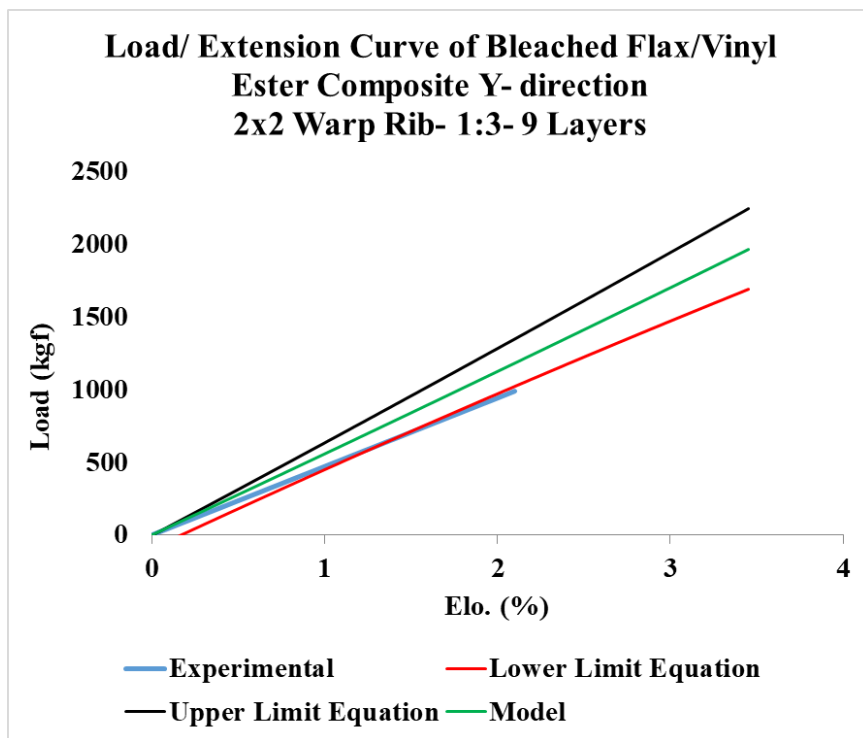




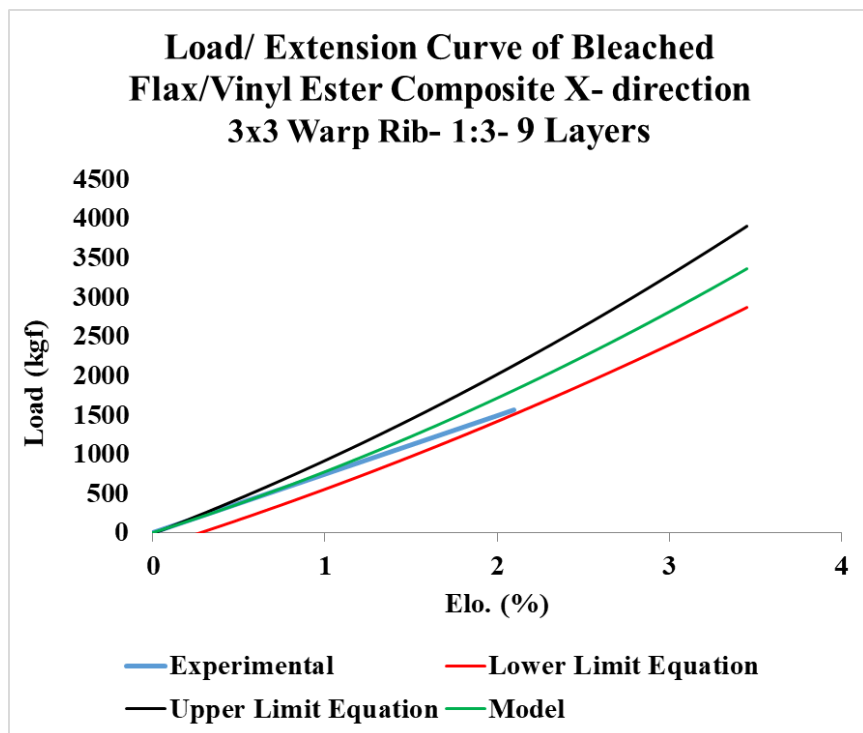


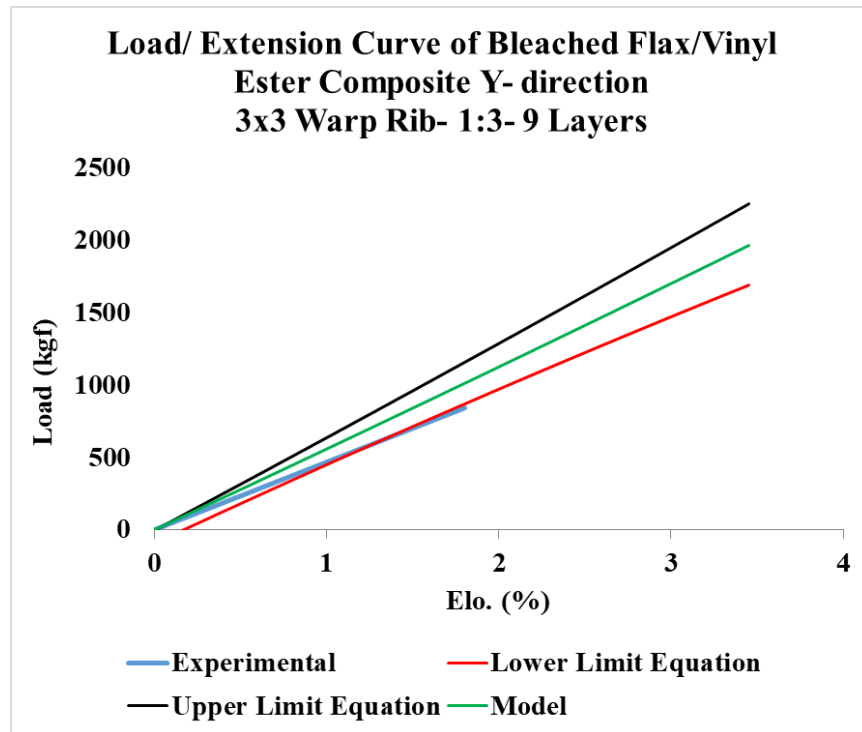
(d)





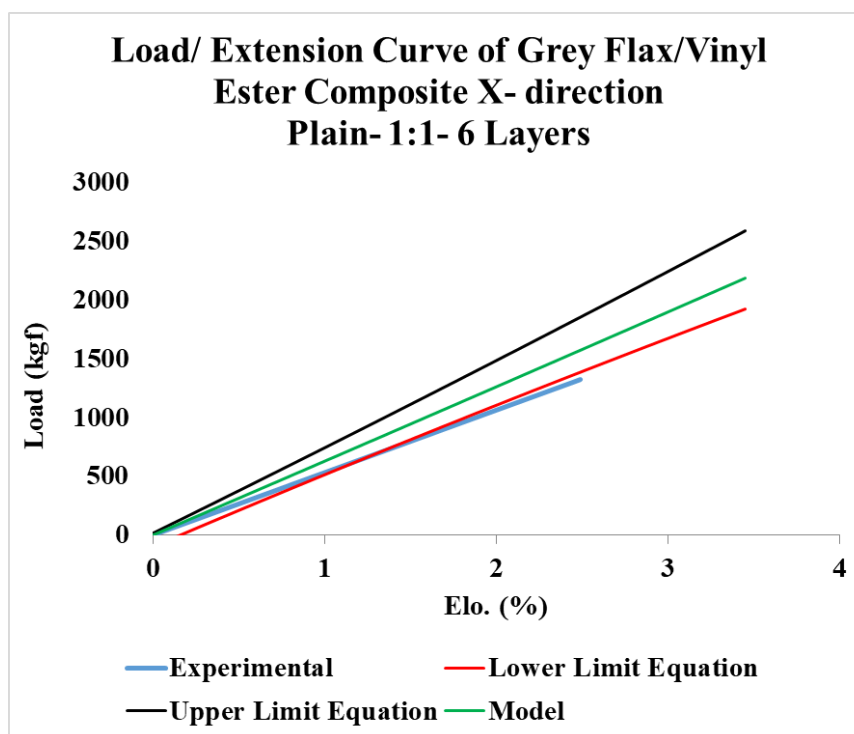
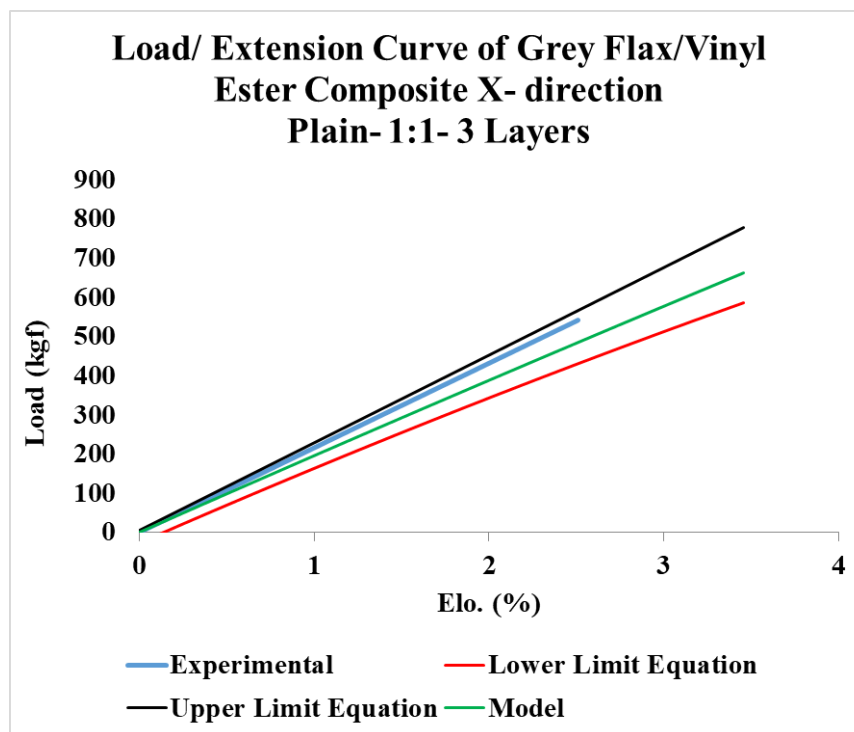
(e)



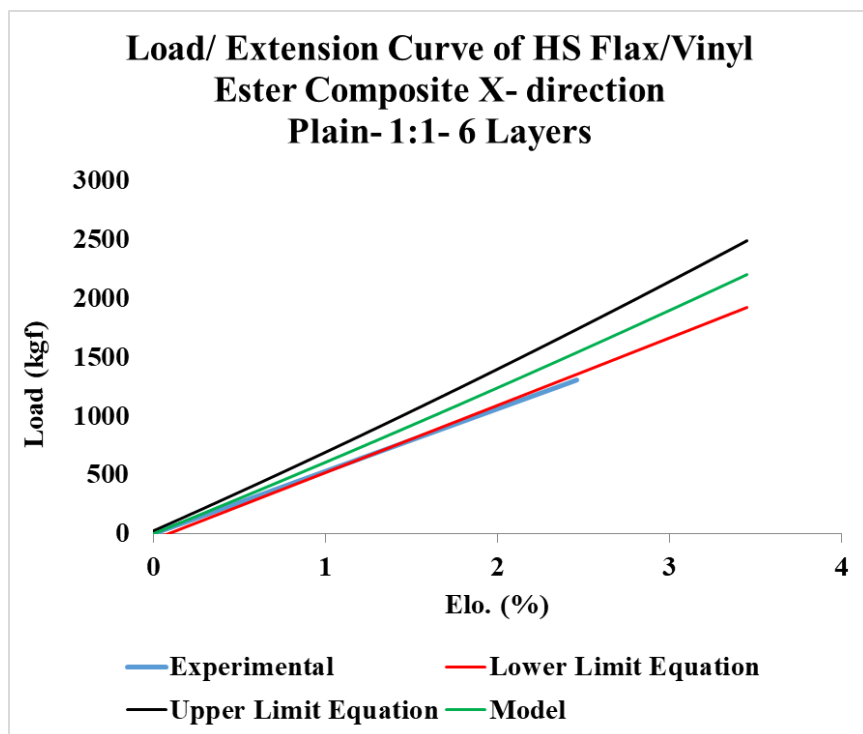
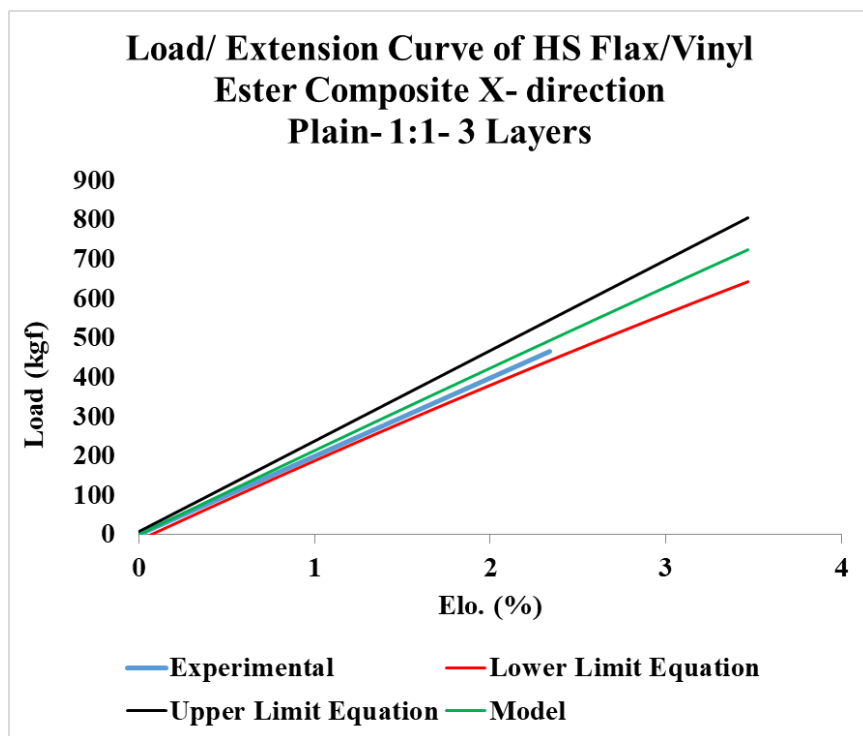


(f)

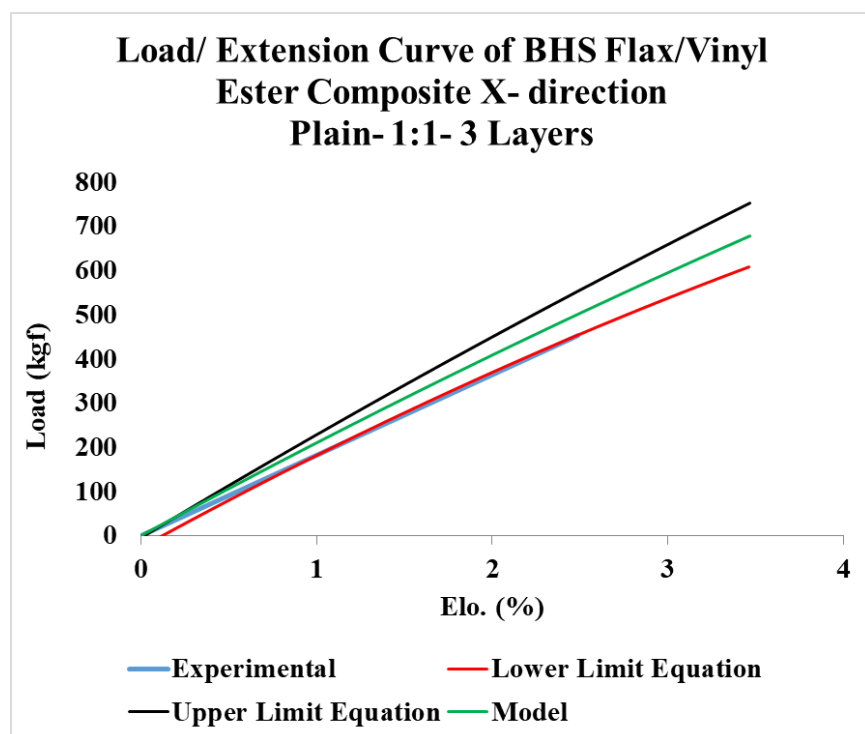
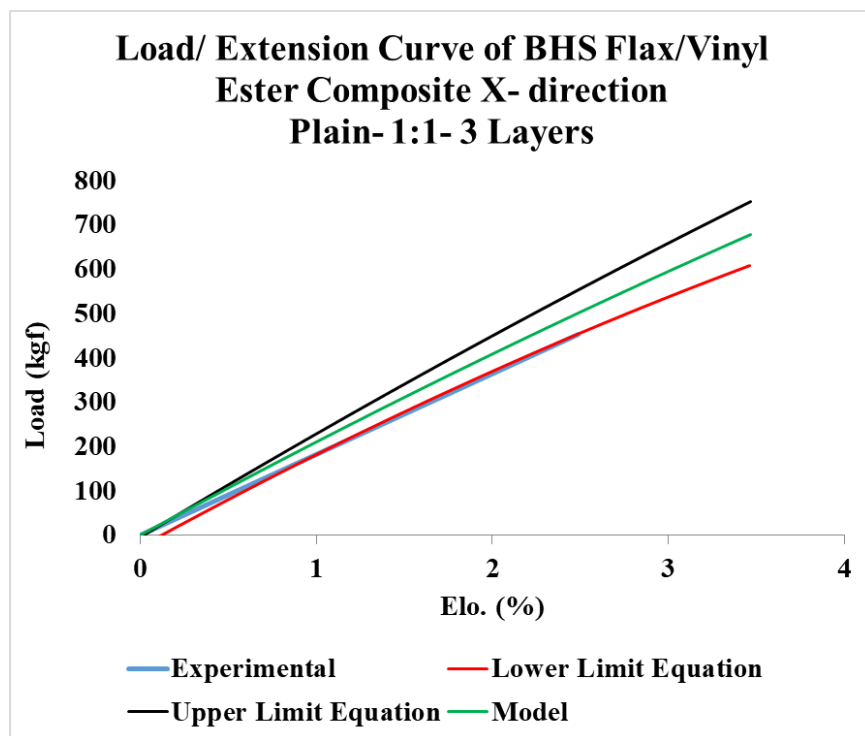
Figure 190. Experimental vs. model tensile load-elongation curves of 9 Y-yarn layers 3DOW composites from bleached flax in the X- and Y-directions (a) plain and 1:1 Z to Y-yarn ratio, (b) 2x2 warp rib and 1:1 Z to Y-yarn ratio, (c) 3x3 warp rib and 1:1 Z to Y-yarn ratio, (d) plain and 1:3 Z to Y-yarn ratio, (e) 2x2 warp rib and 1:3 Z to Y-yarn ratio, (f) 3x3 warp rib and 1:3 Z to Y-yarn ratio



(a)



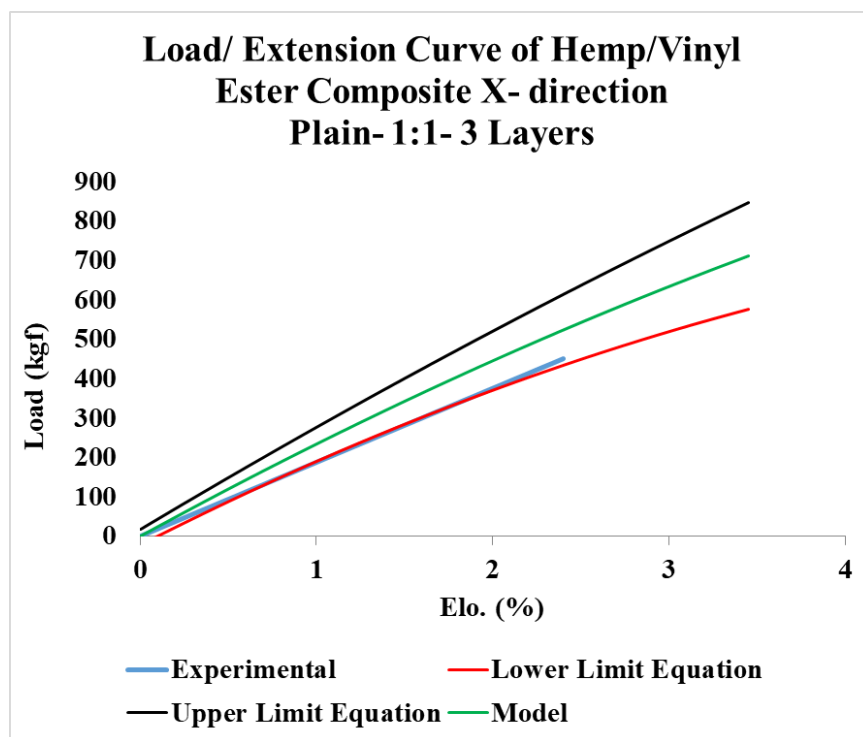
(b)

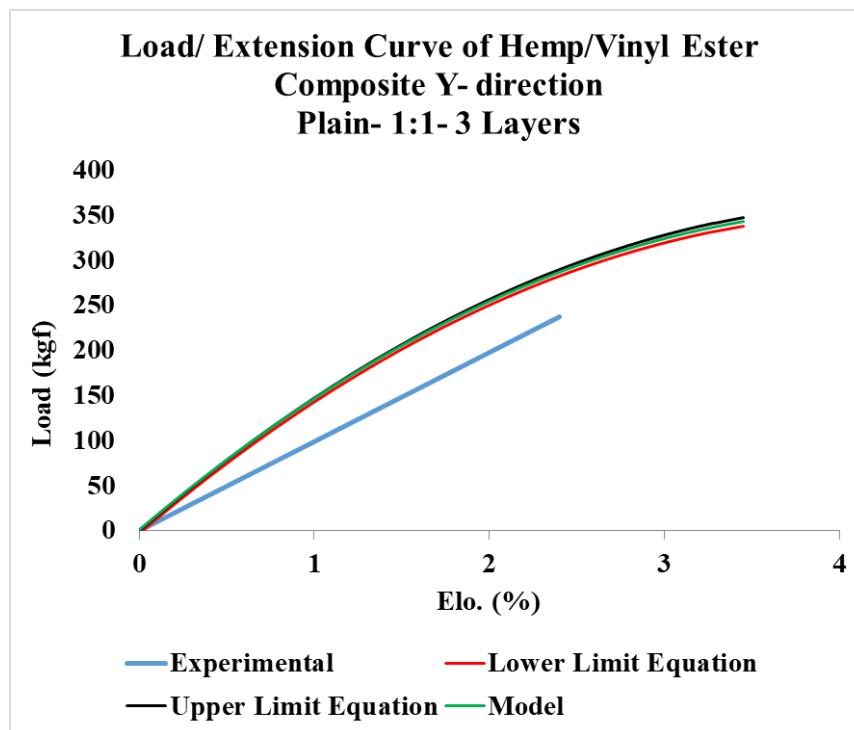


(c)

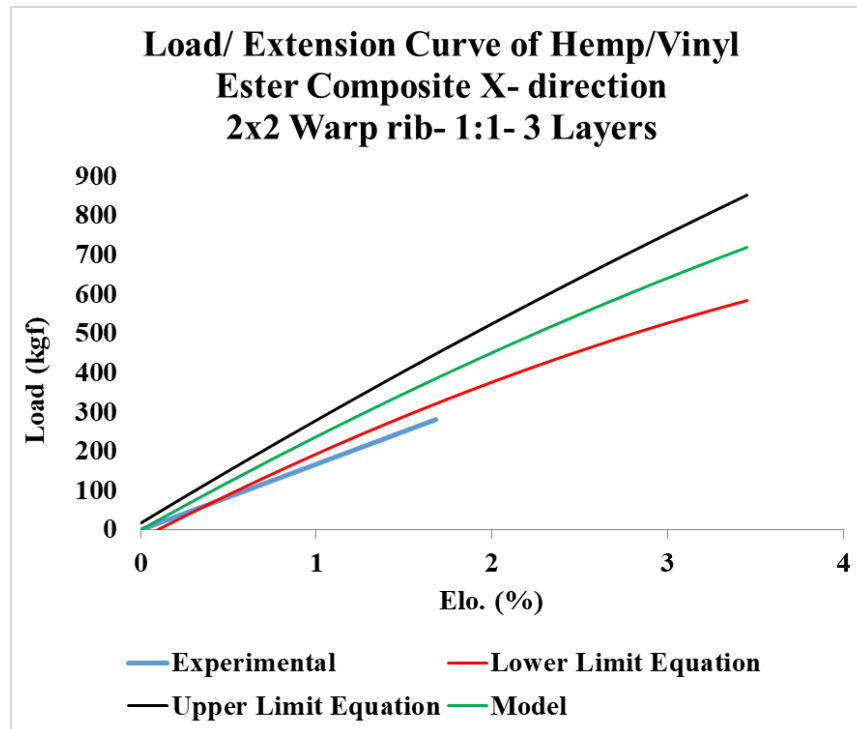
Figure 191. Experimental vs. model tensile load-elongation curves of 3 and 6 Y-yarn layers 3DOW composites of plain weave and 1:1 Z to Y-yarn ratio (a) grey flax X-yarns, (b) HS flax X-yarns and (c) BHS flax X-yarns in the X-direction

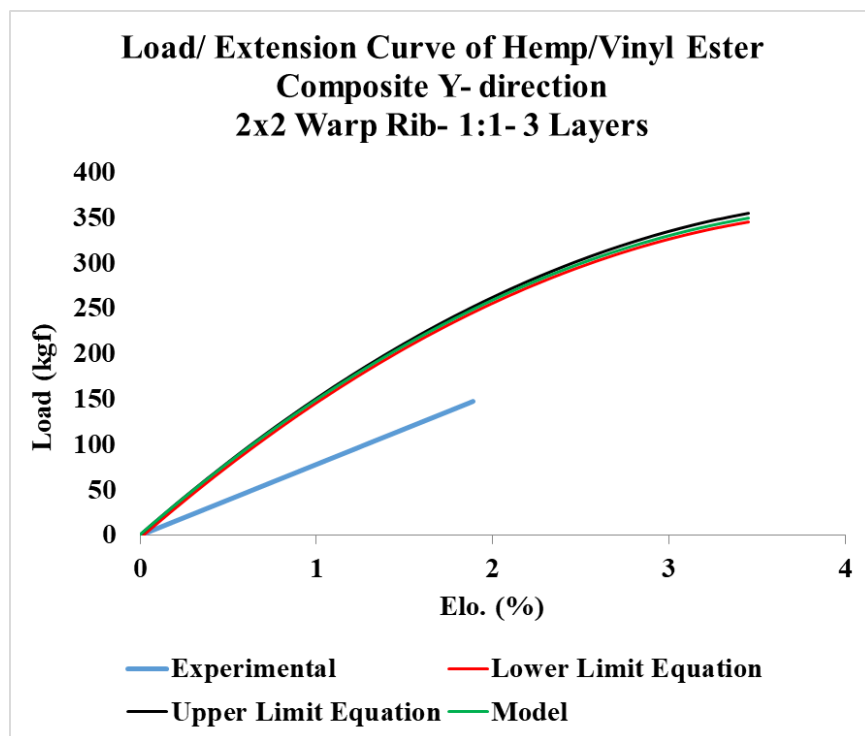
B.2. Experimental vs. Model Tensile Load-Elongation Curves of 3DOW Composites from Hemp Fibers Based on the Tensile Properties of the Yarn



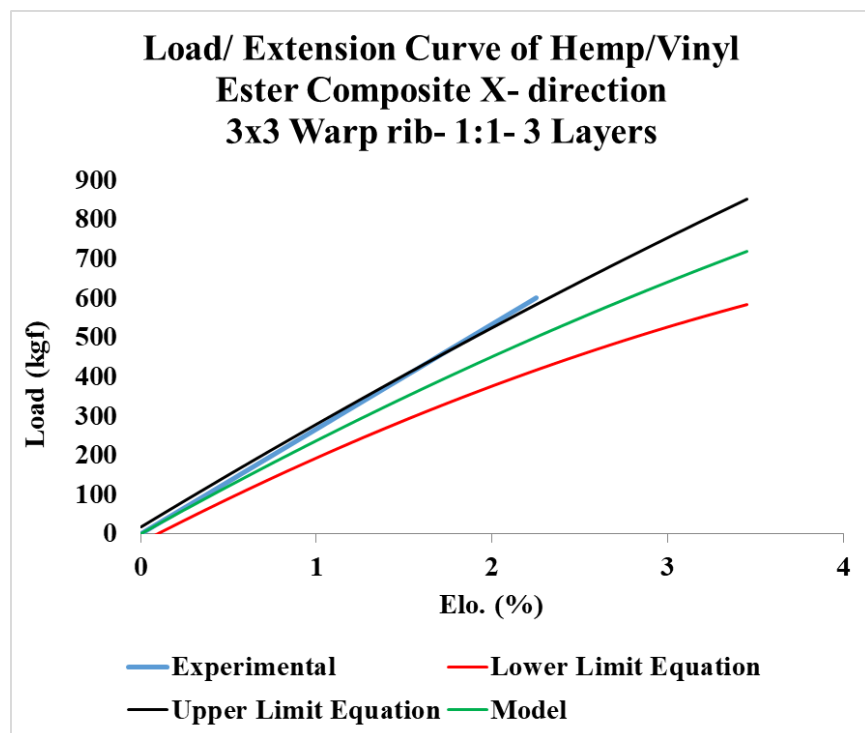


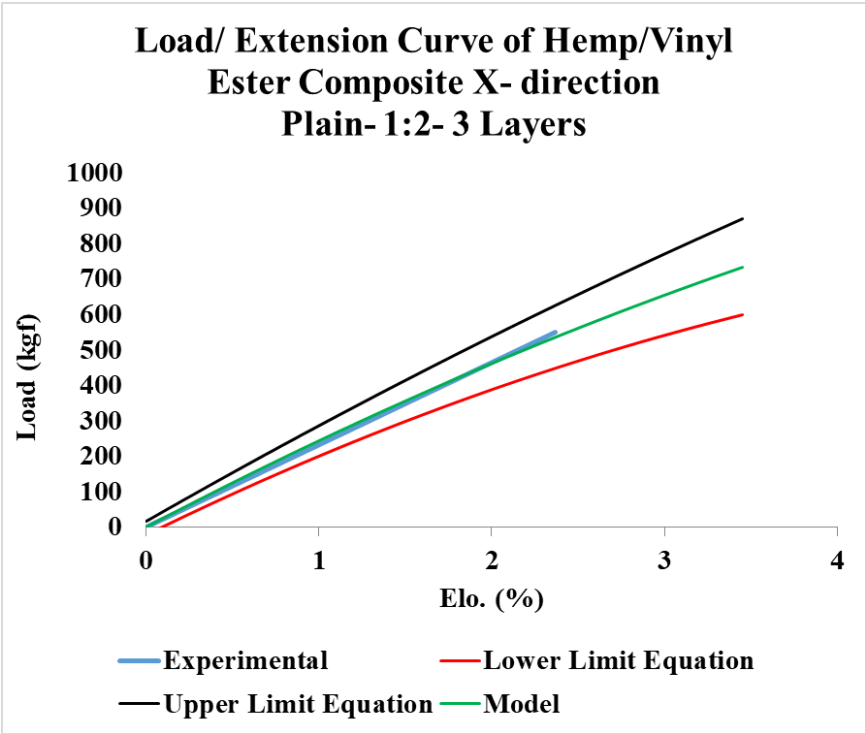
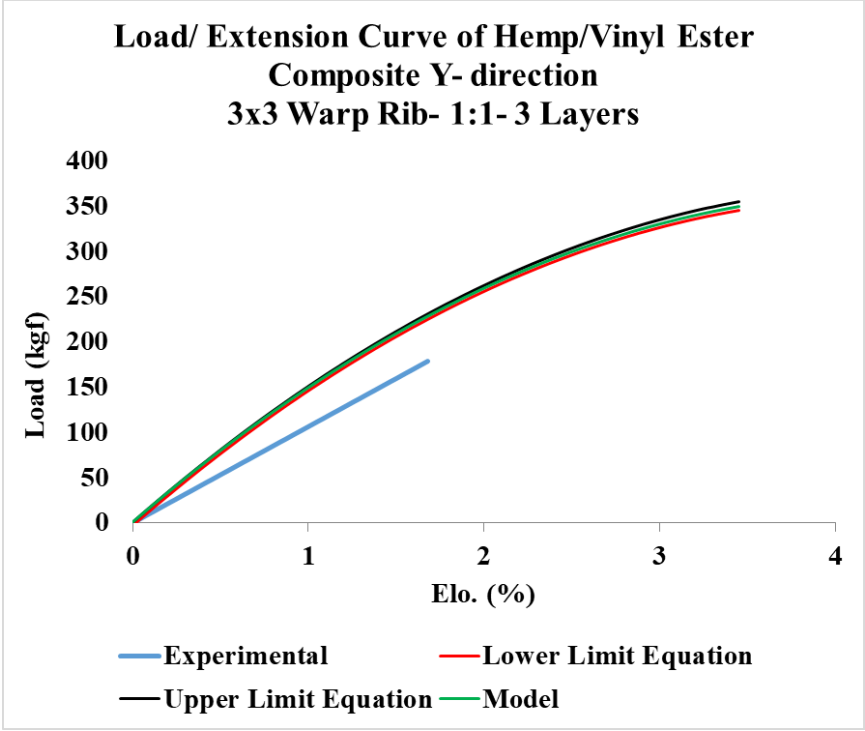
(a)

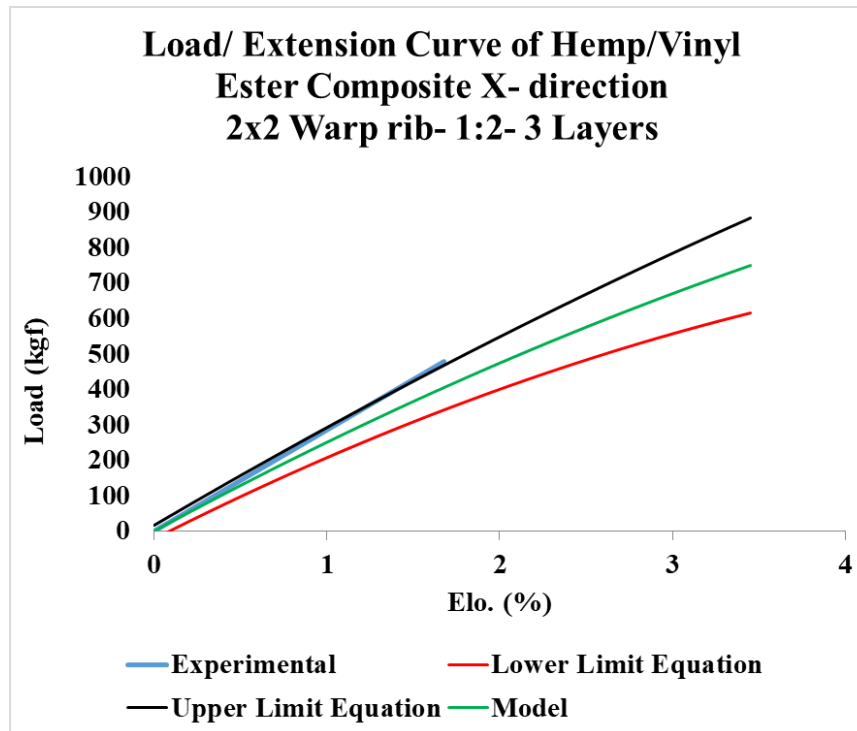
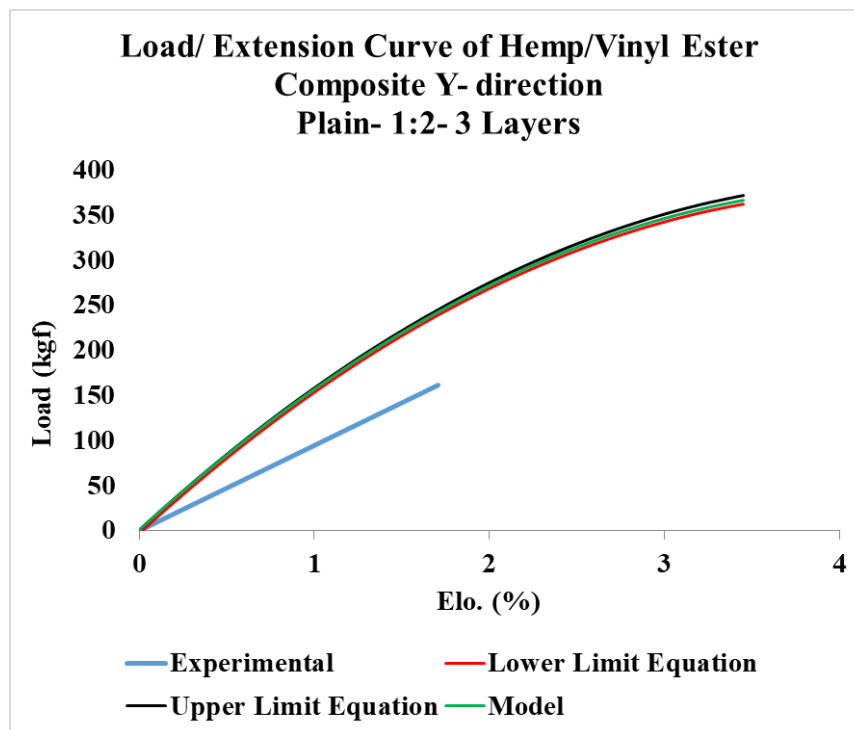


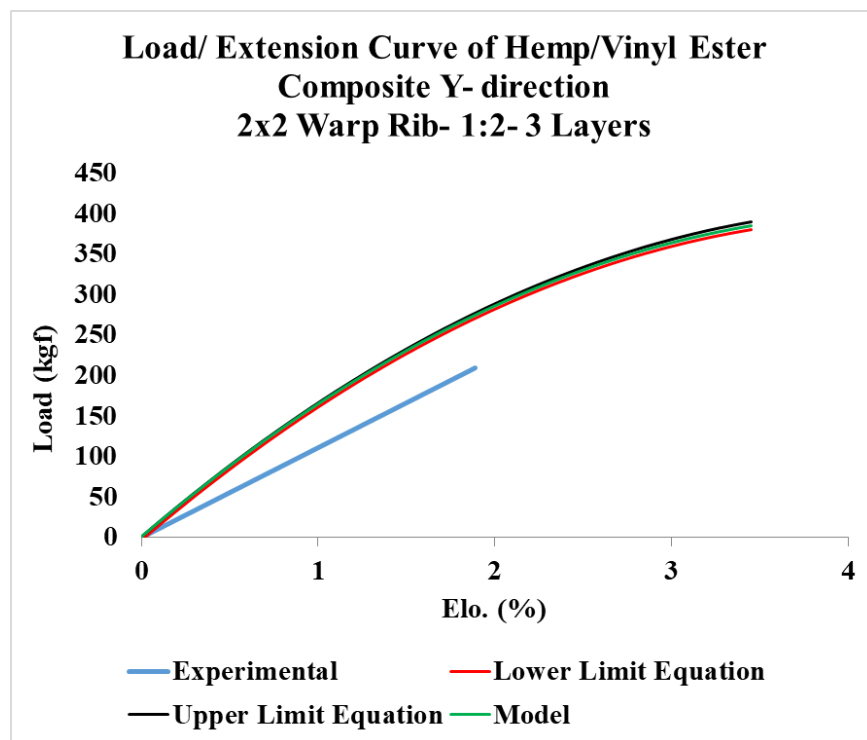


(b)

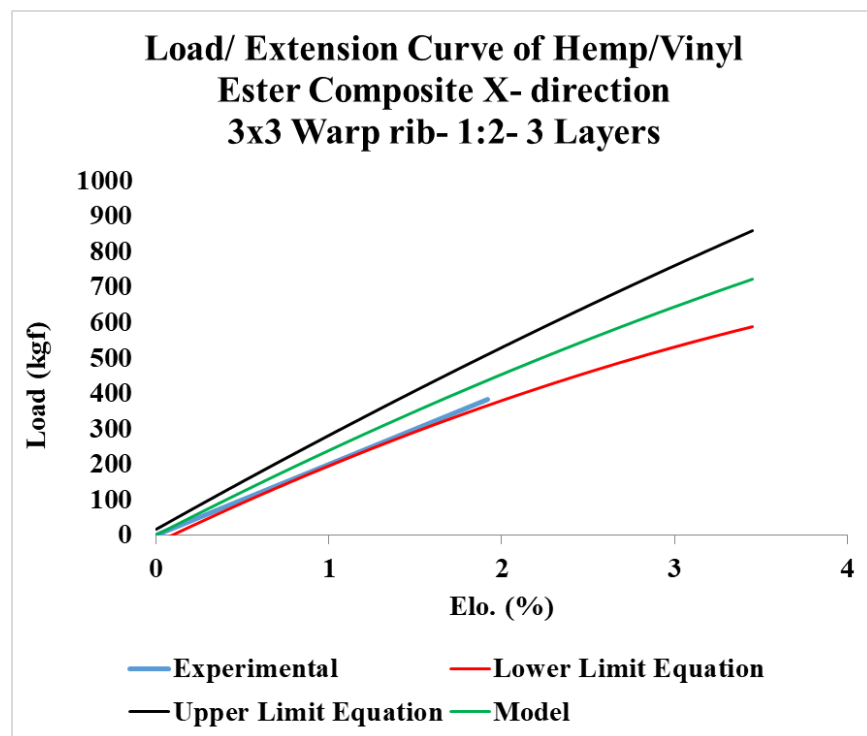


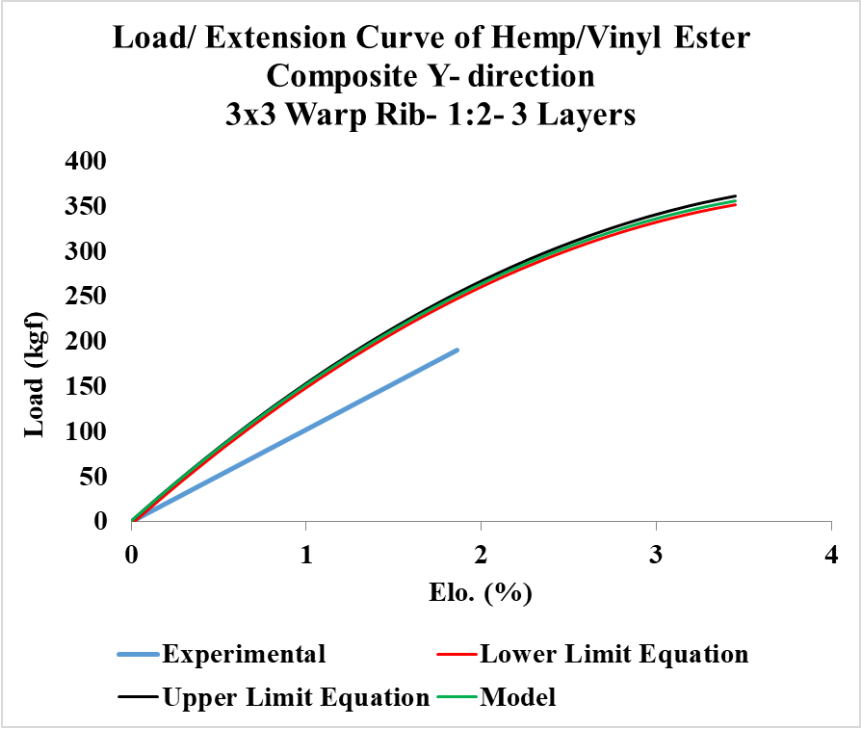




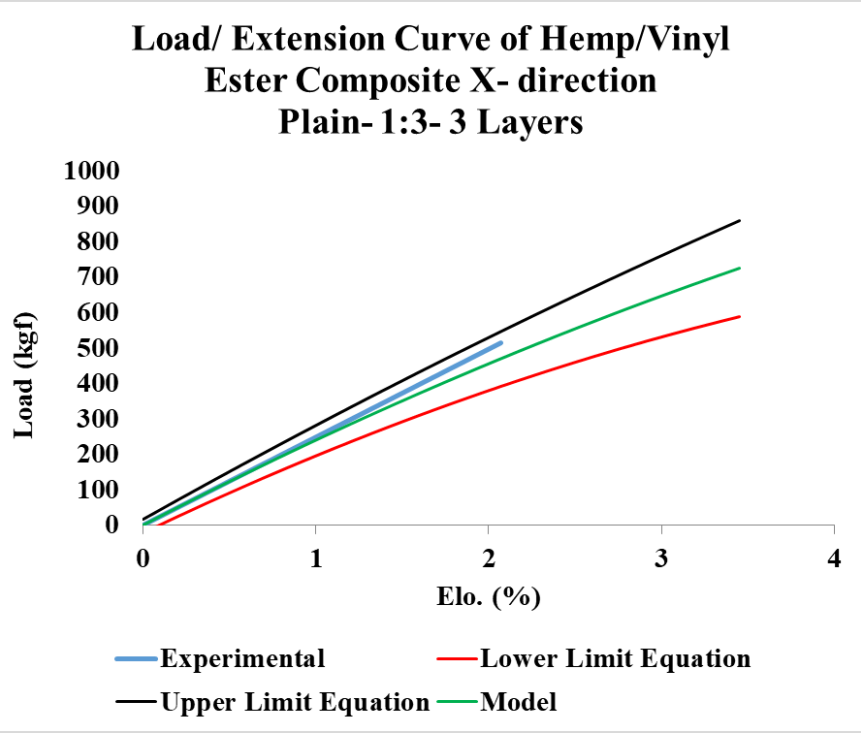


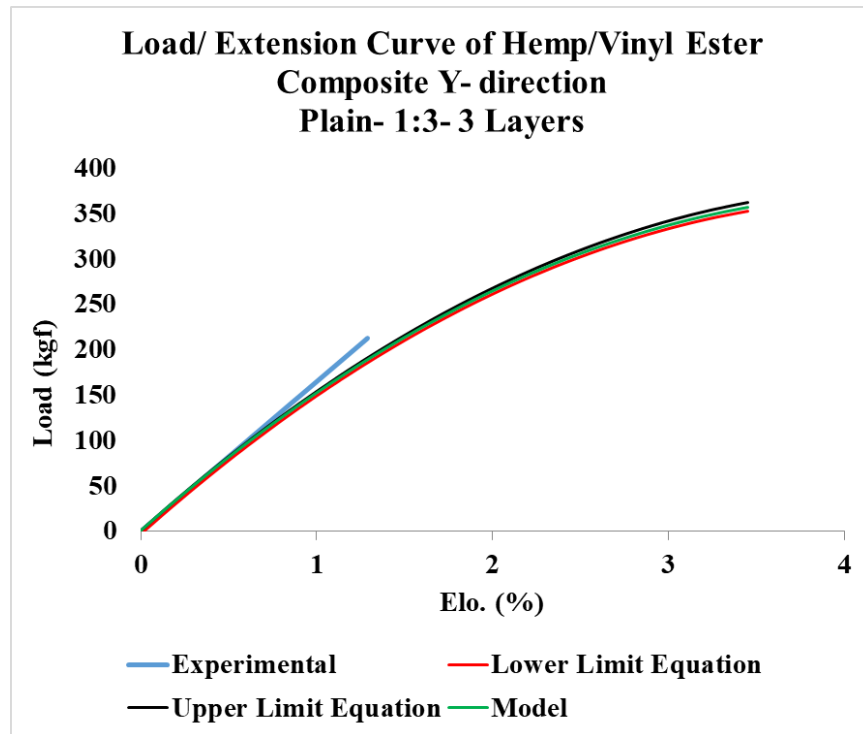
(e)



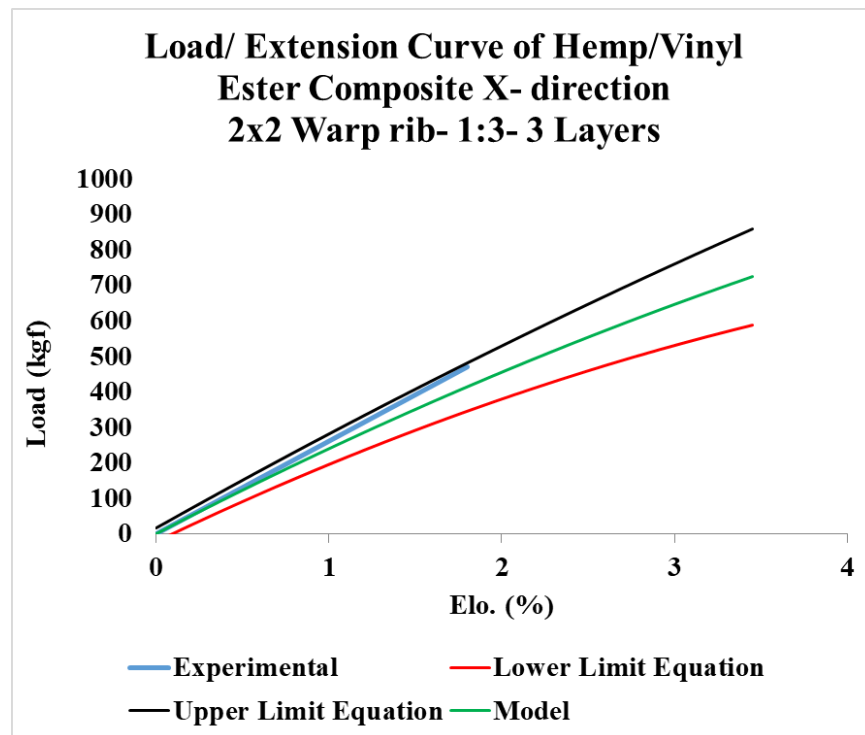


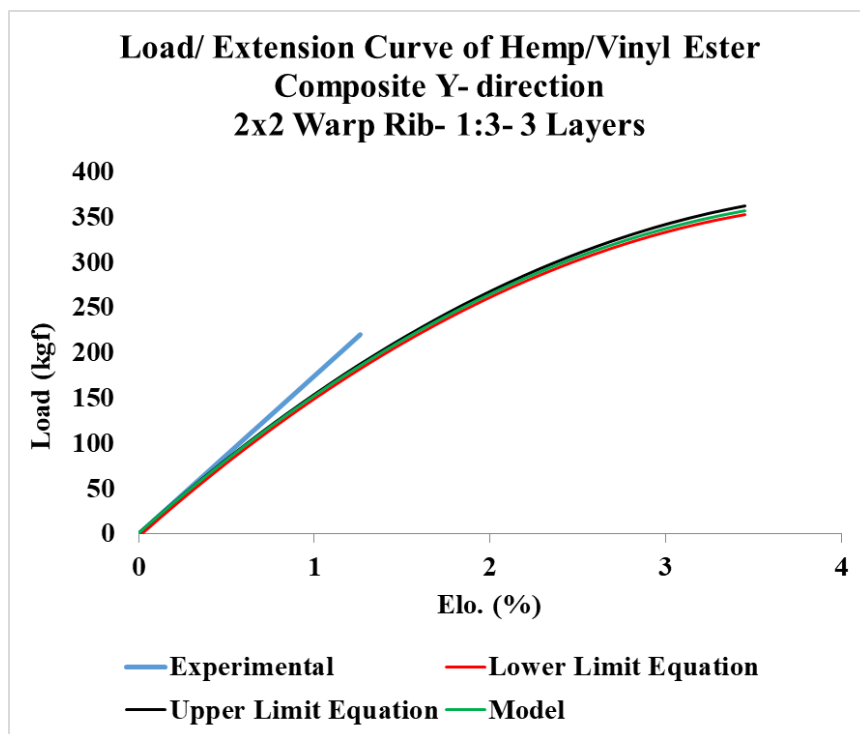
(f)



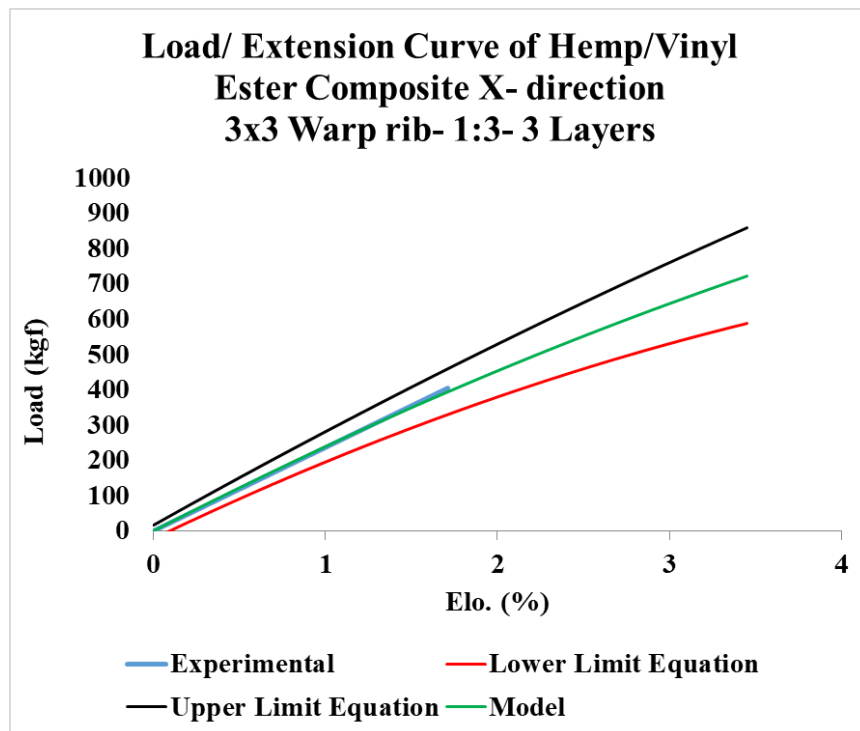


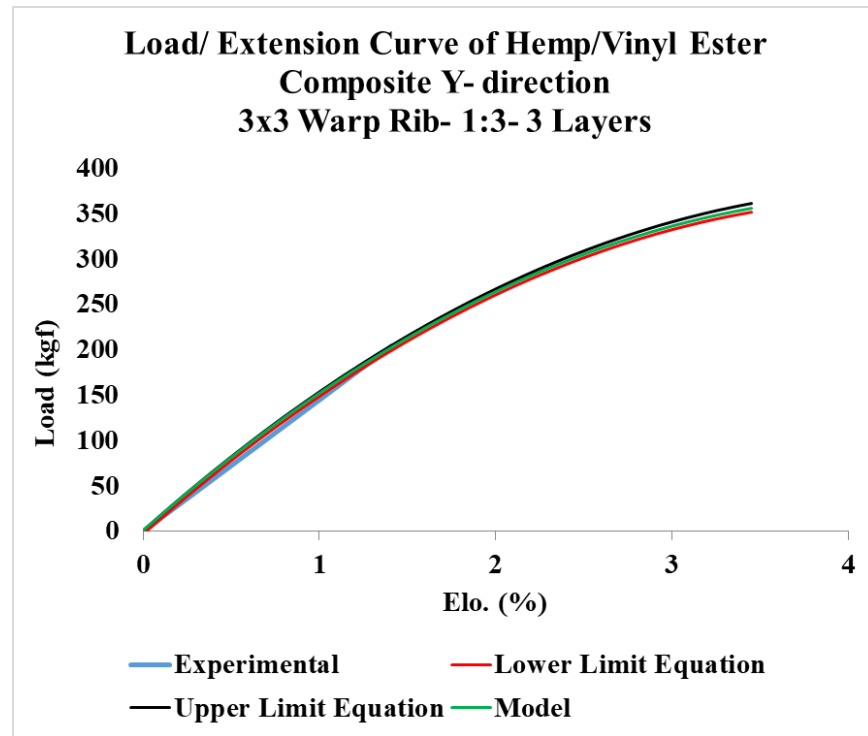
(g)





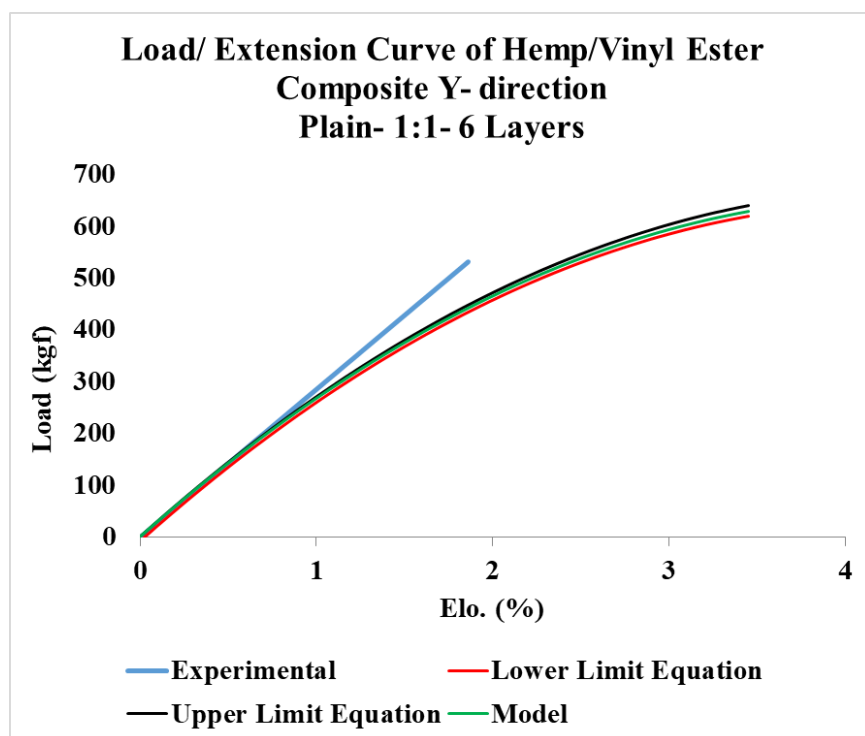
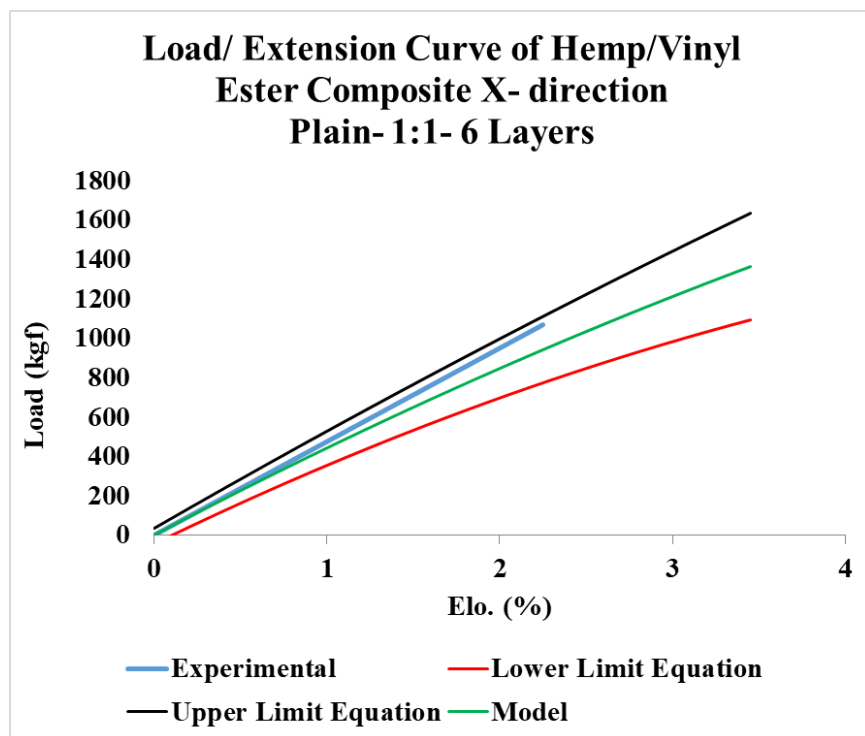
(h)



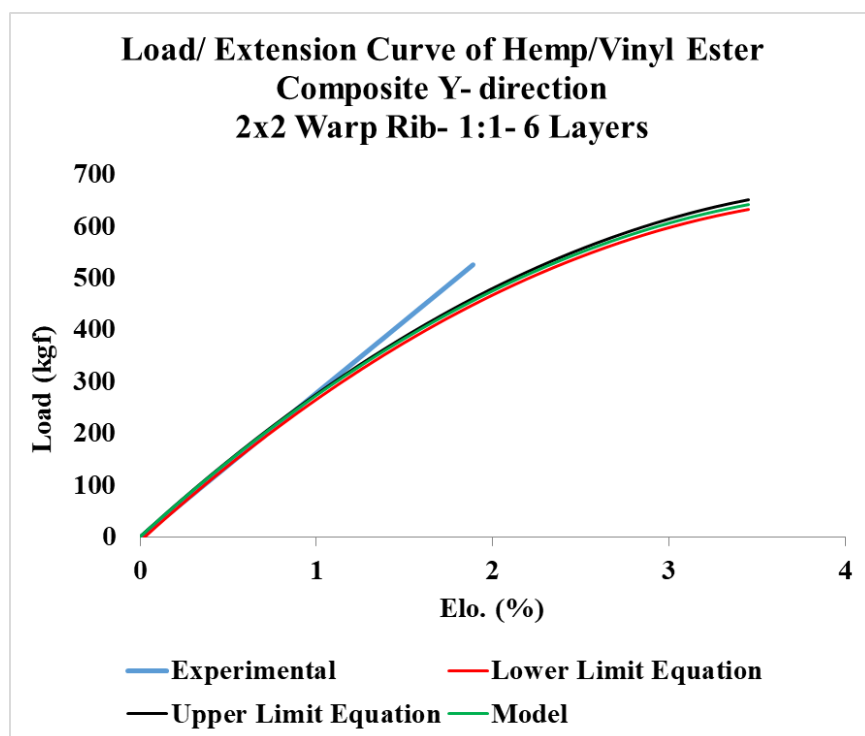
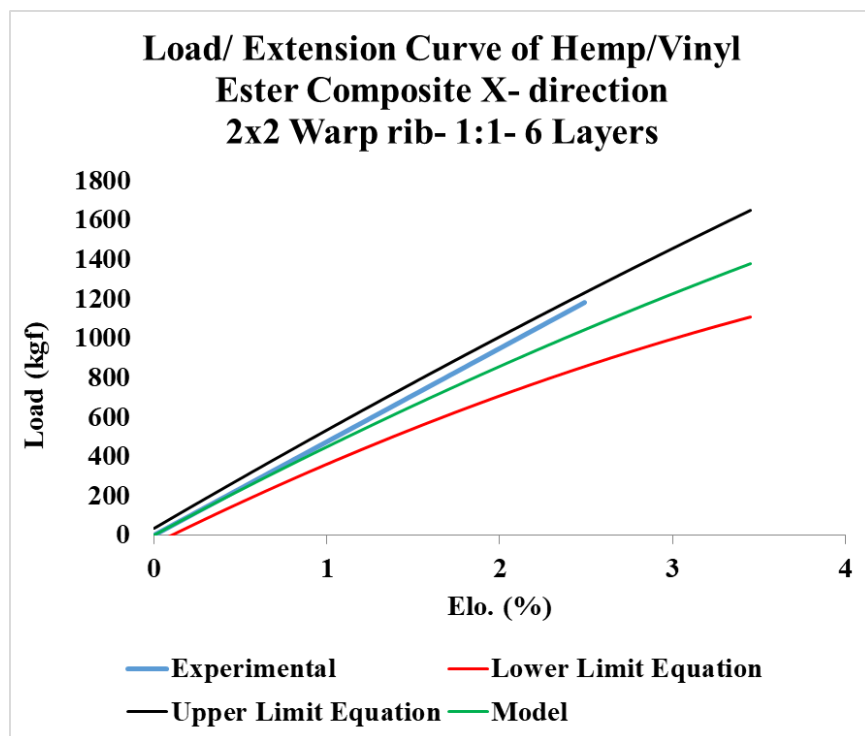


(i)

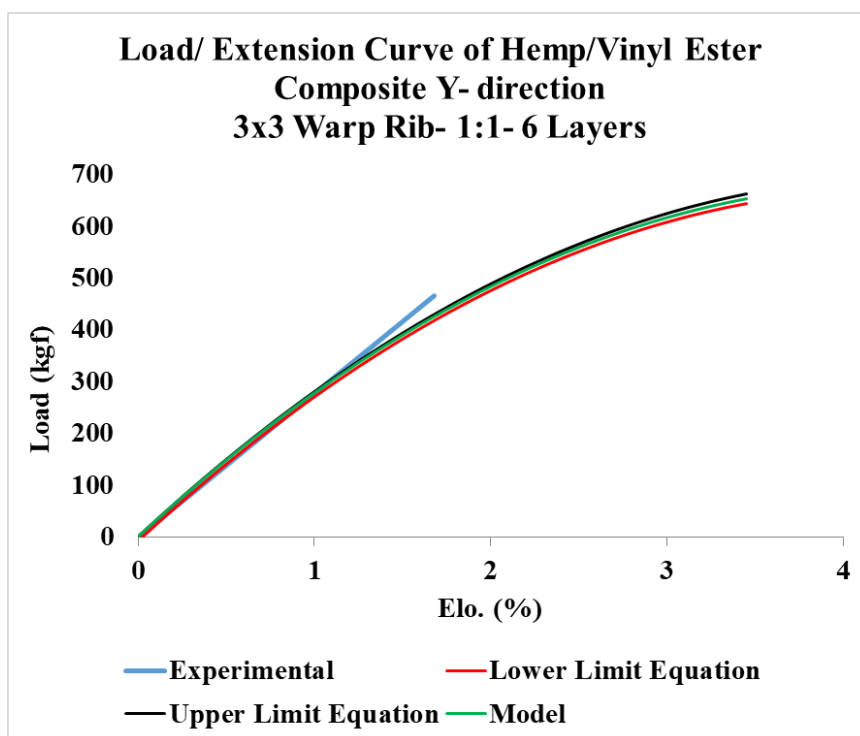
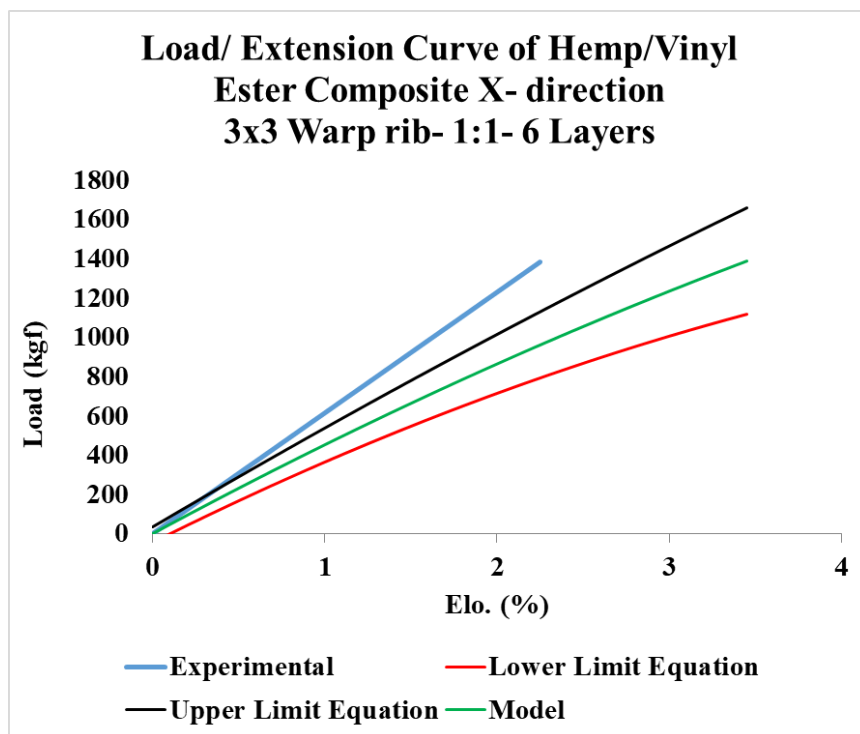
Figure 192. Experimental vs. model tensile load-elongation curves of 3 Y-yarn layers 3DOW composites from Hemp in the X- and Y-directions (a) plain and 1:1 Z to Y-yarn ratio, (b) 2x2 warp rib and 1:1 Z to Y-yarn ratio, (c) 3x3 warp rib and 1:1 Z to Y-yarn ratio, (d) plain and 1:2 Z to Y-yarn ratio, (e) 2x2 warp rib and 1:2 Z to Y-yarn ratio, (f) 3x3 warp rib and 1:2 Z to Y-yarn ratio (g) plain and 1:3 Z to Y-yarn ratio, (h) 2x2 warp rib and 1:3 Z to Y-yarn ratio, (i) 3x3 warp rib and 1:3 Z to Y-yarn ratio



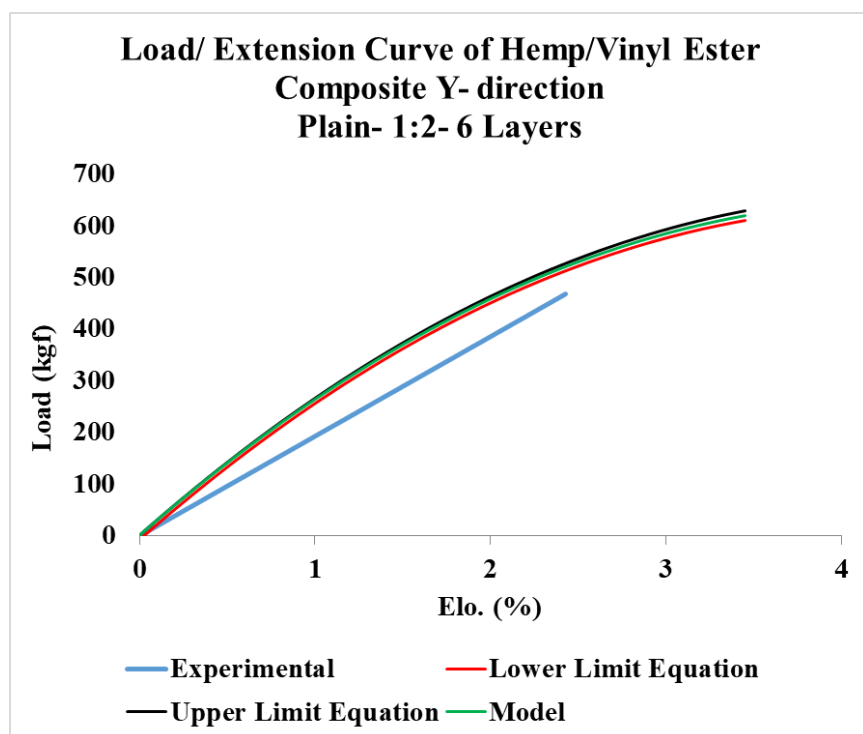
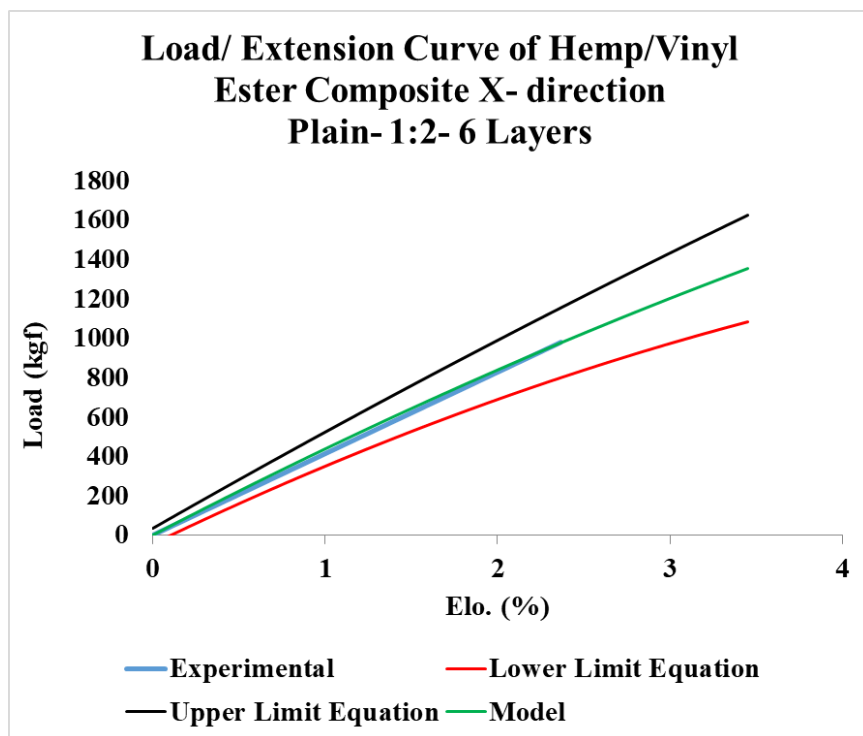
(a)



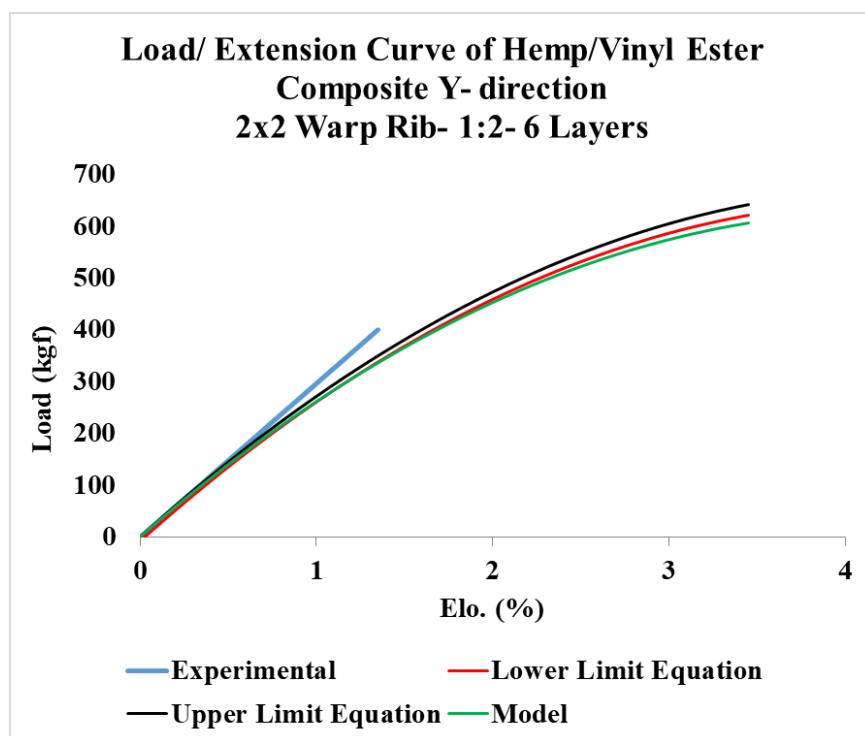
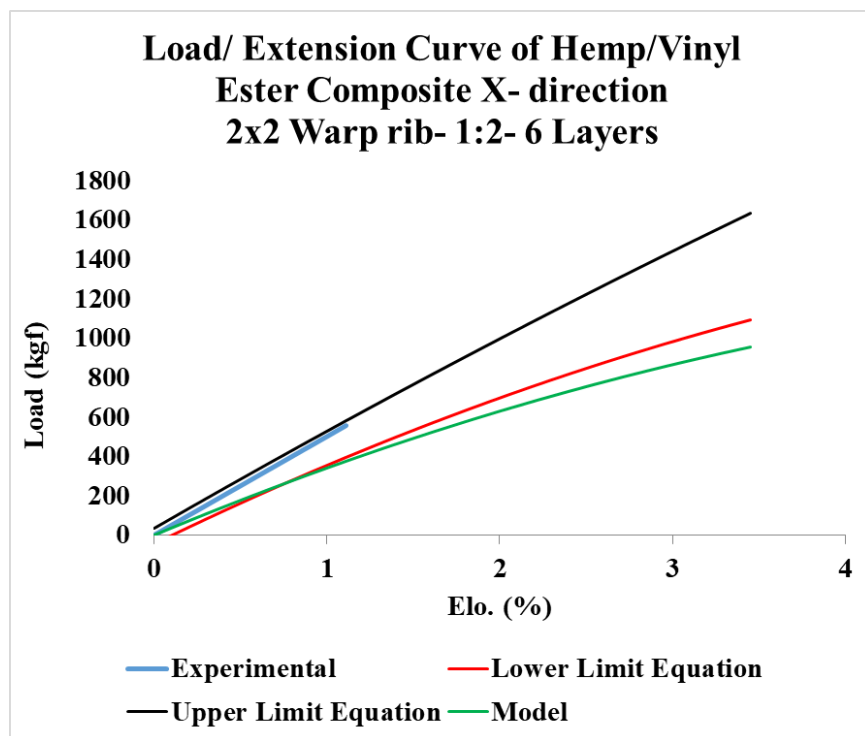
(b)



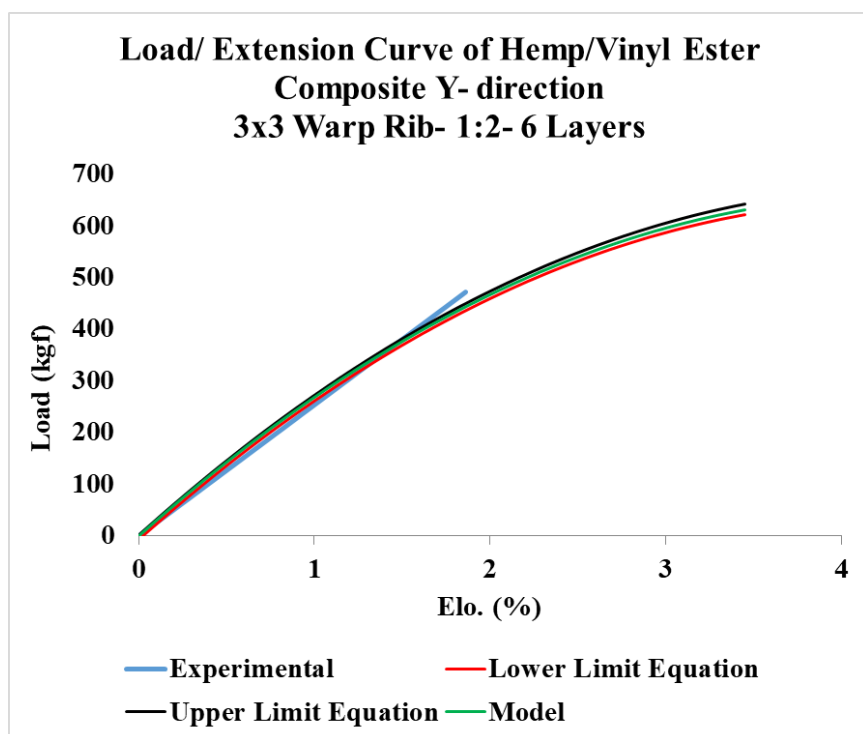
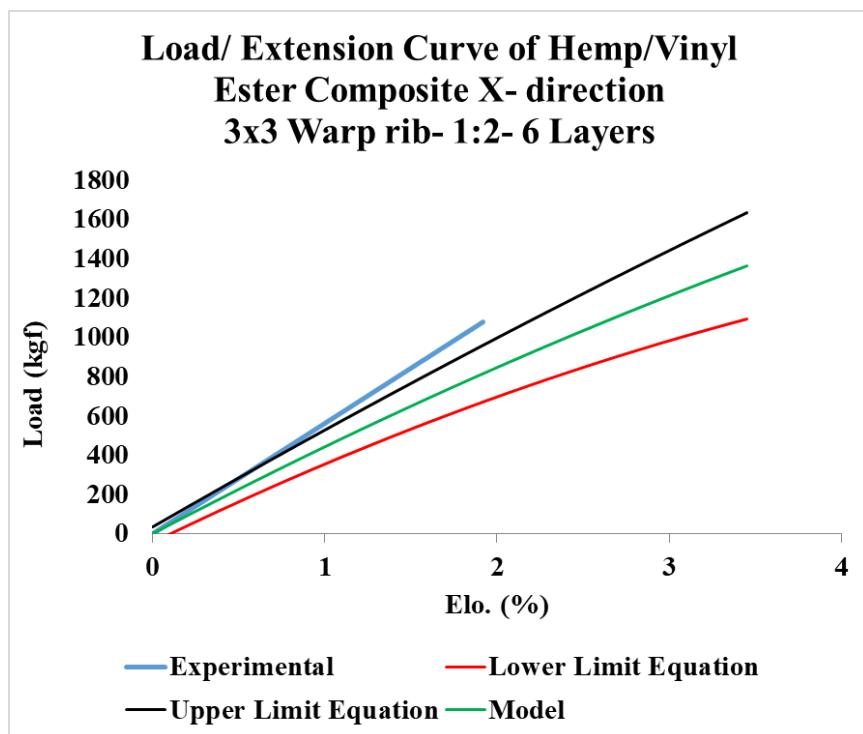
(c)



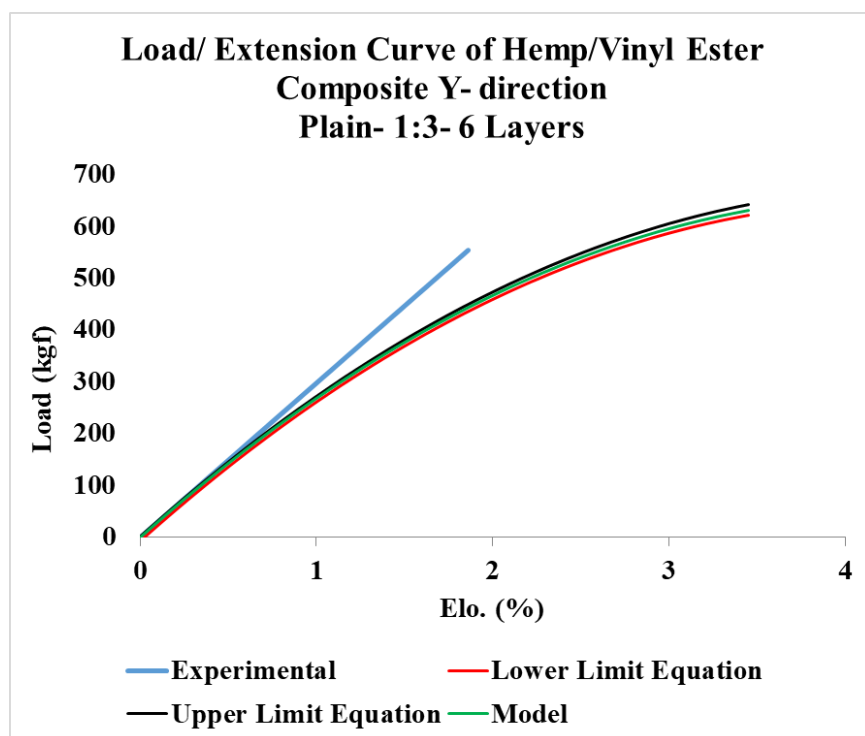
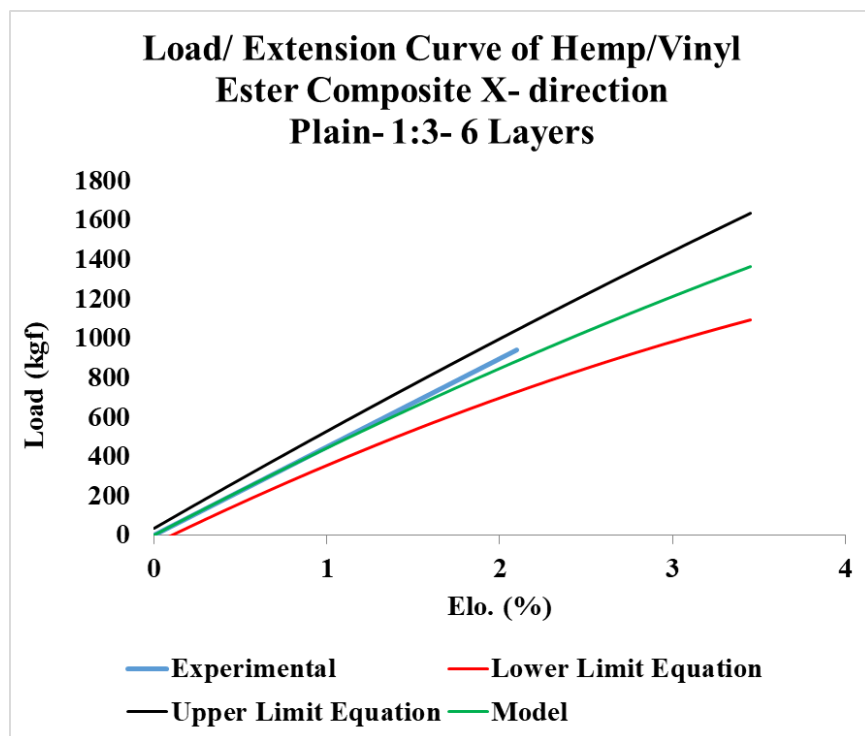
(d)



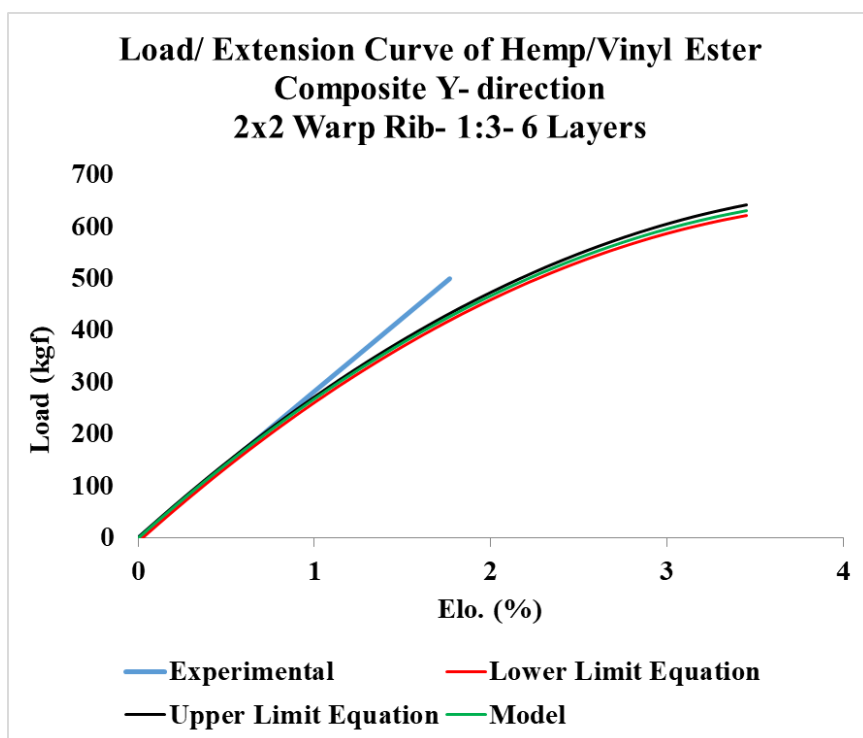
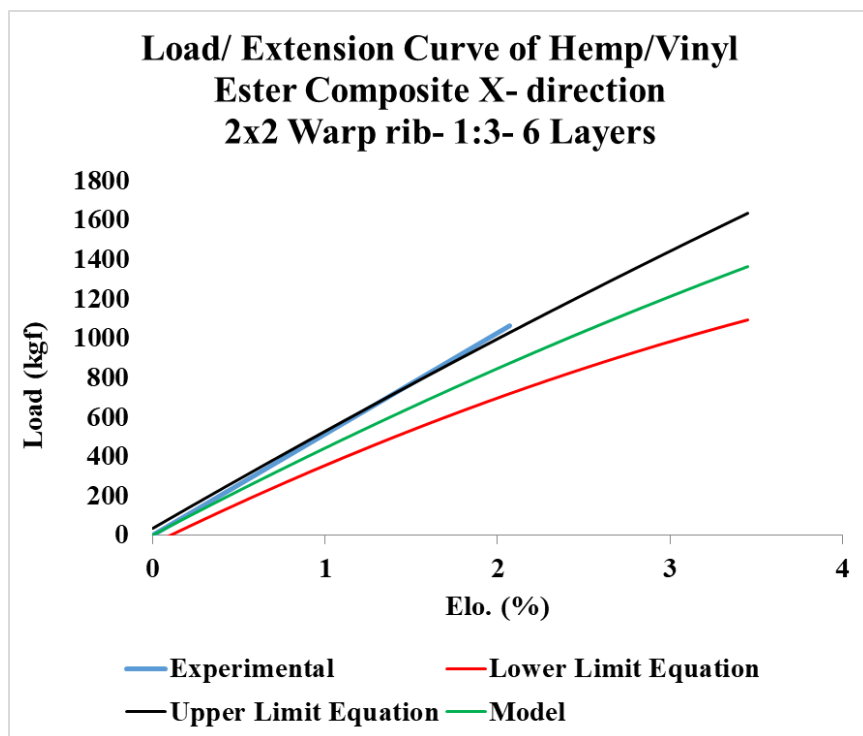
(e)



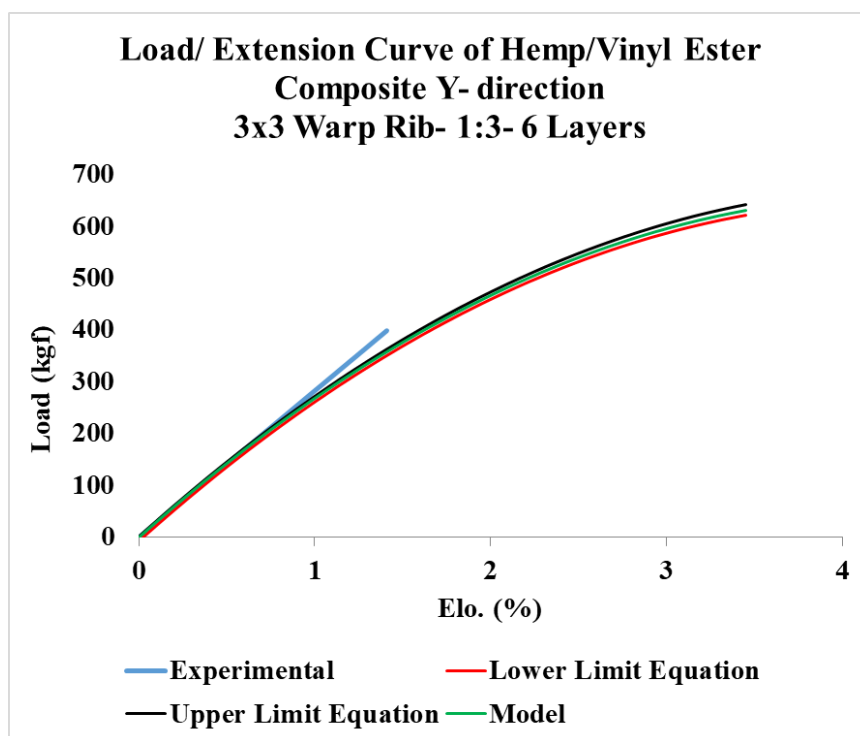
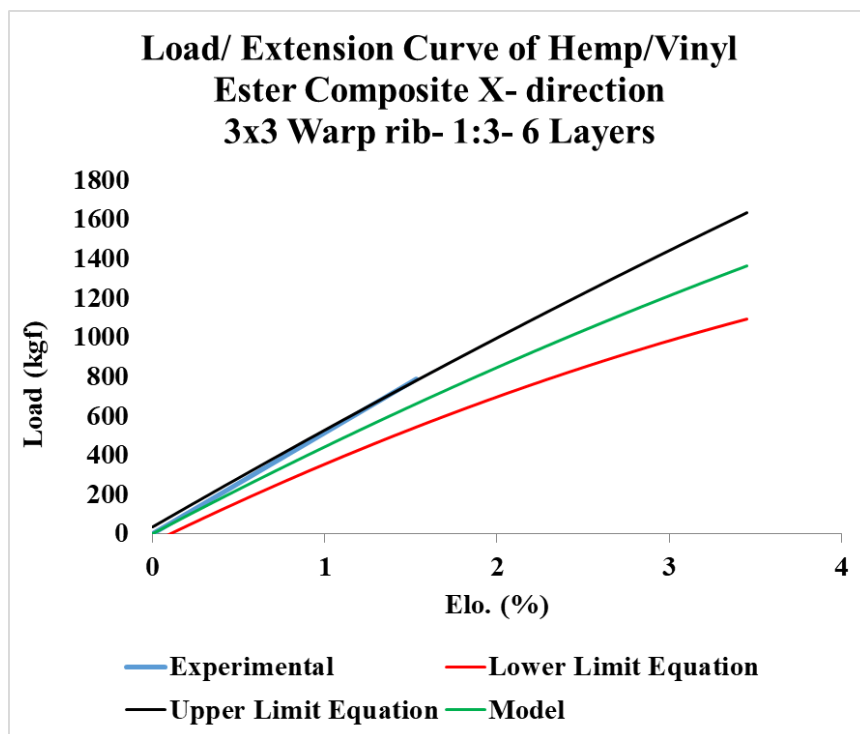
(f)



(g)

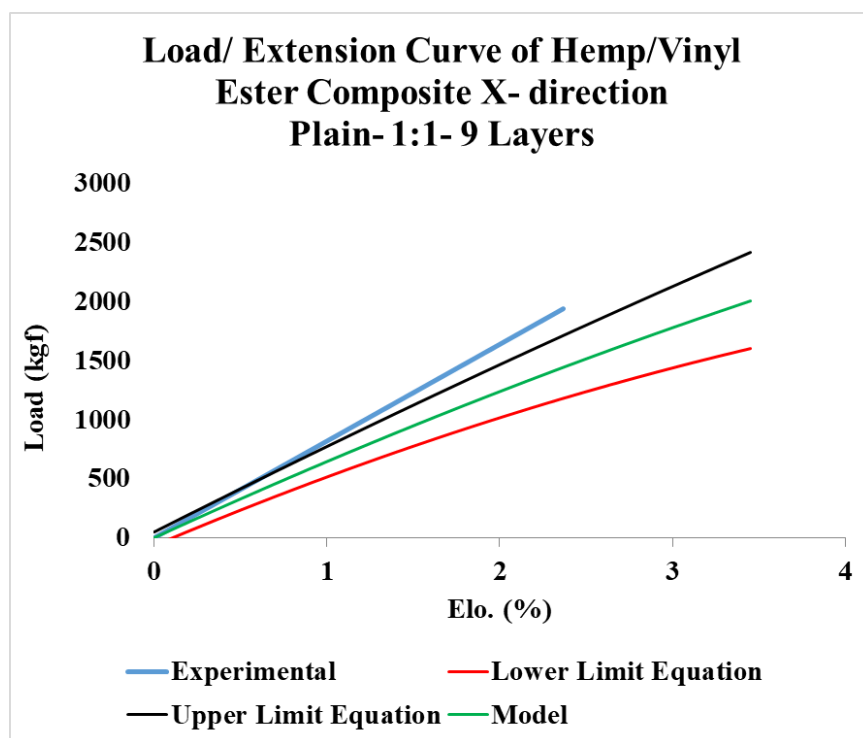


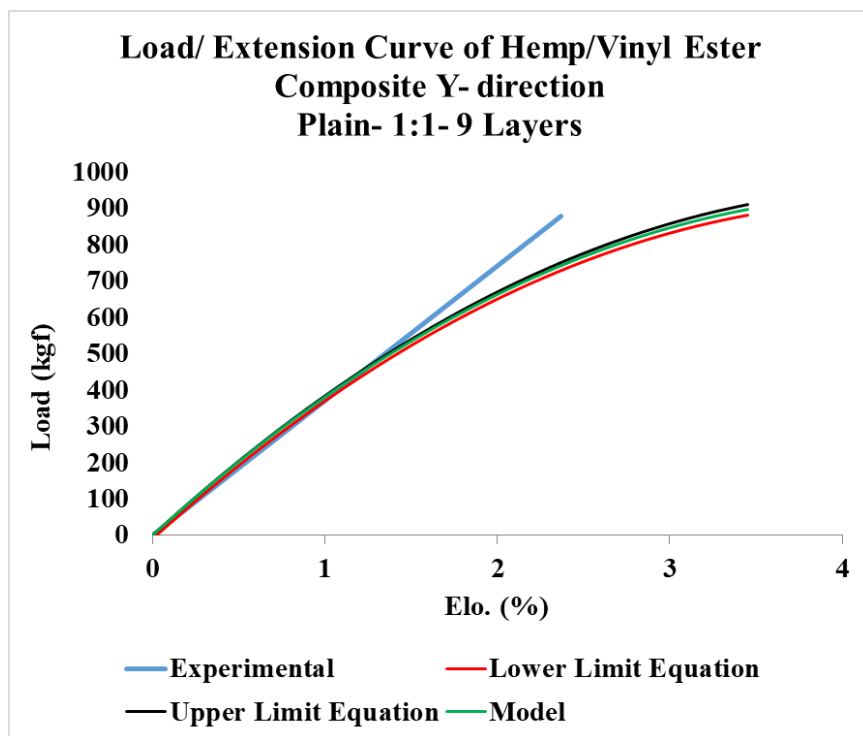
(h)



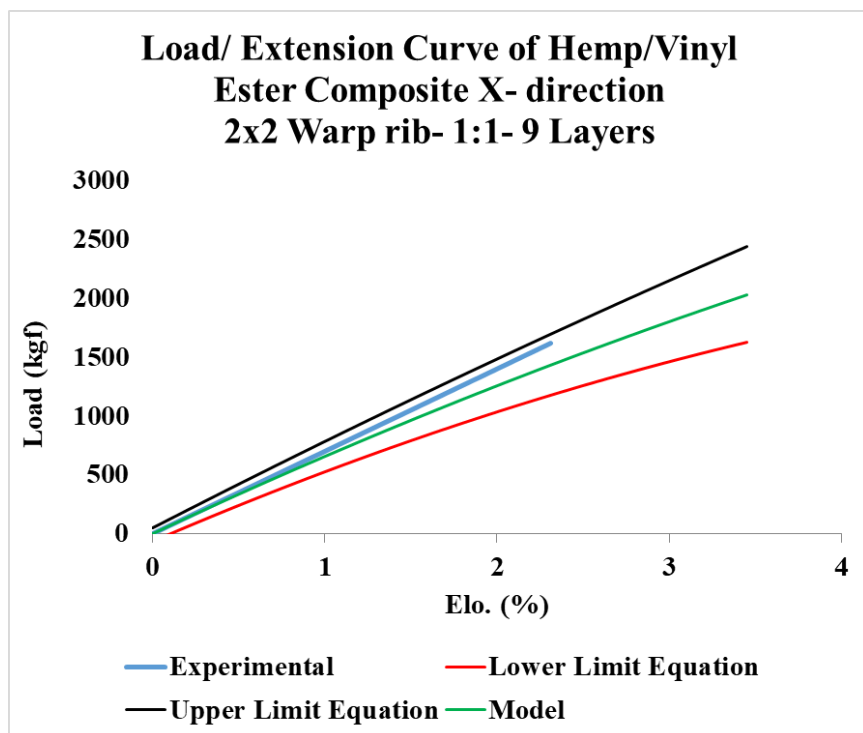
(i)

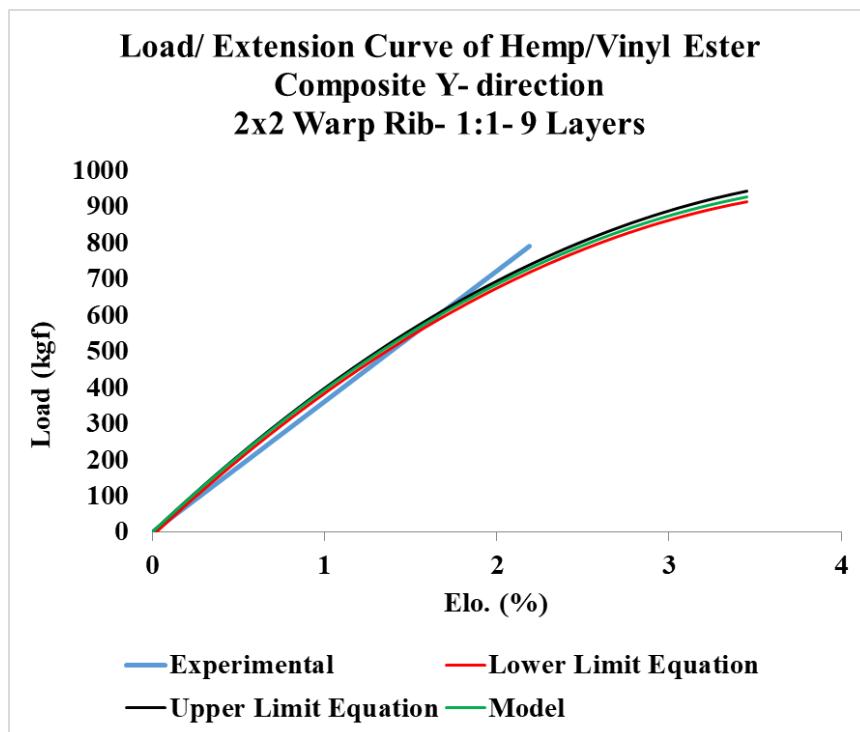
Figure 193. Experimental vs. model tensile load-elongation curves of 6 Y-yarn layers 3DOW composites from Hemp in the X- and Y-directions (a) plain and 1:1 Z to Y-yarn ratio, (b) 2x2 warp rib and 1:1 Z to Y-yarn ratio, (c) 3x3 warp rib and 1:1 Z to Y-yarn ratio, (d) plain and 1:2 Z to Y-yarn ratio, (e) 2x2 warp rib and 1:2 Z to Y-yarn ratio, (f) 3x3 warp rib and 1:2 Z to Y-yarn ratio (g) plain and 1:3 Z to Y-yarn ratio, (h) 2x2 warp rib and 1:3 Z to Y-yarn ratio, (i) 3x3 warp rib and 1:3 Z to Y-yarn ratio



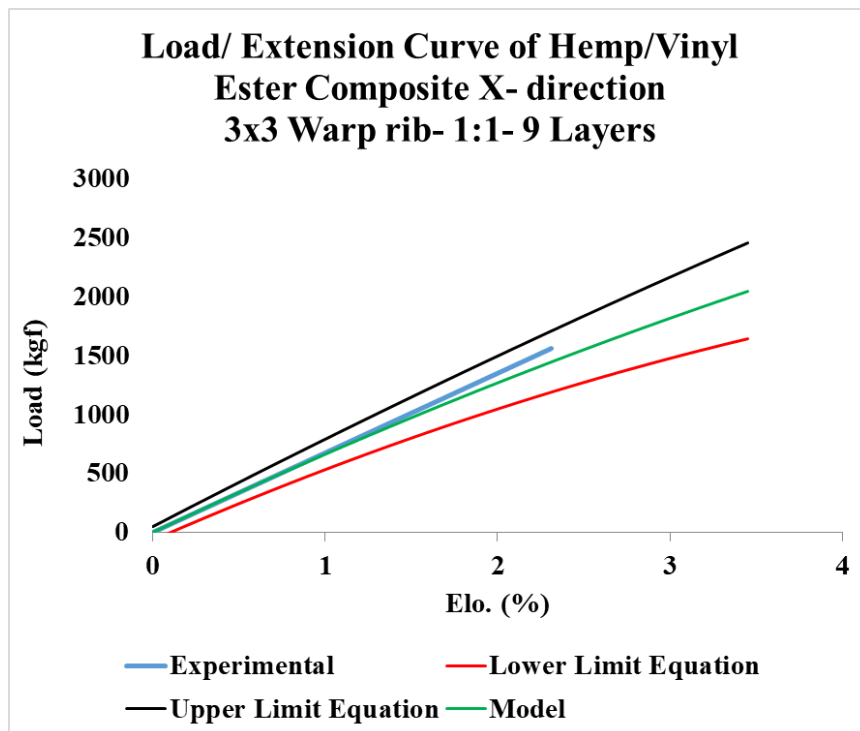


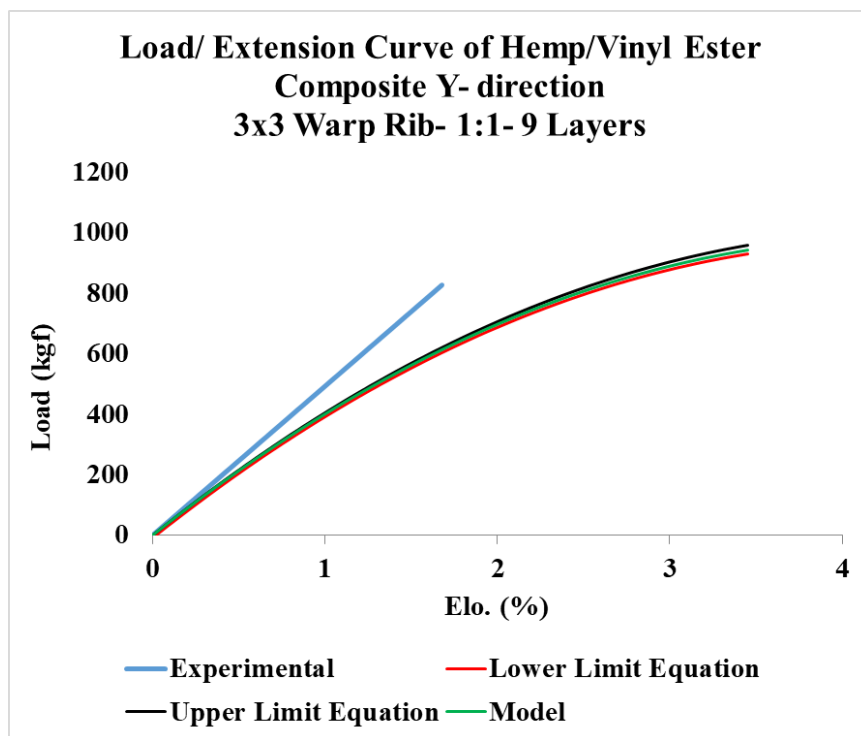
(a)



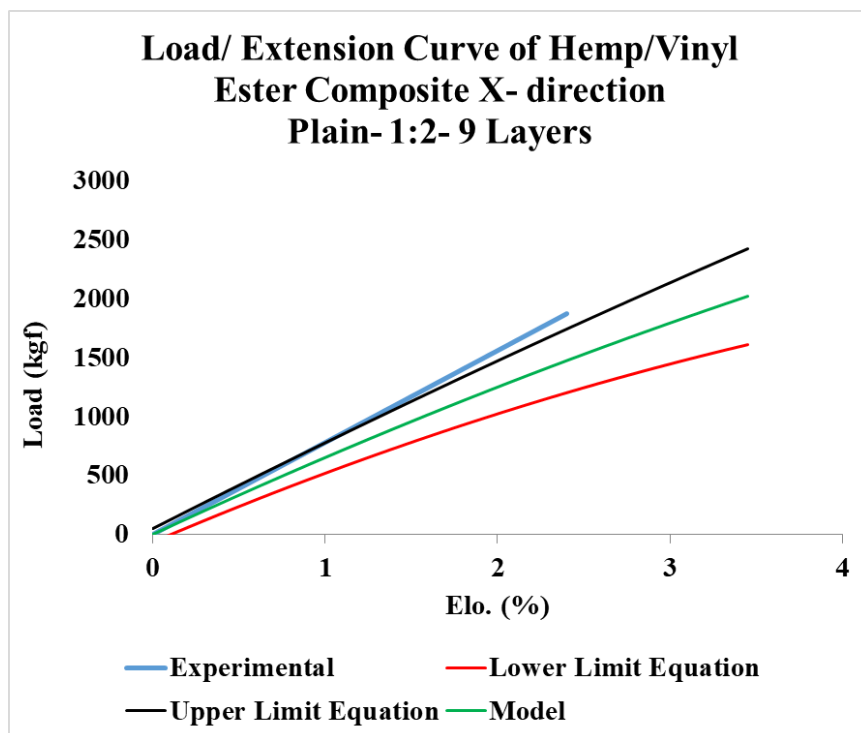


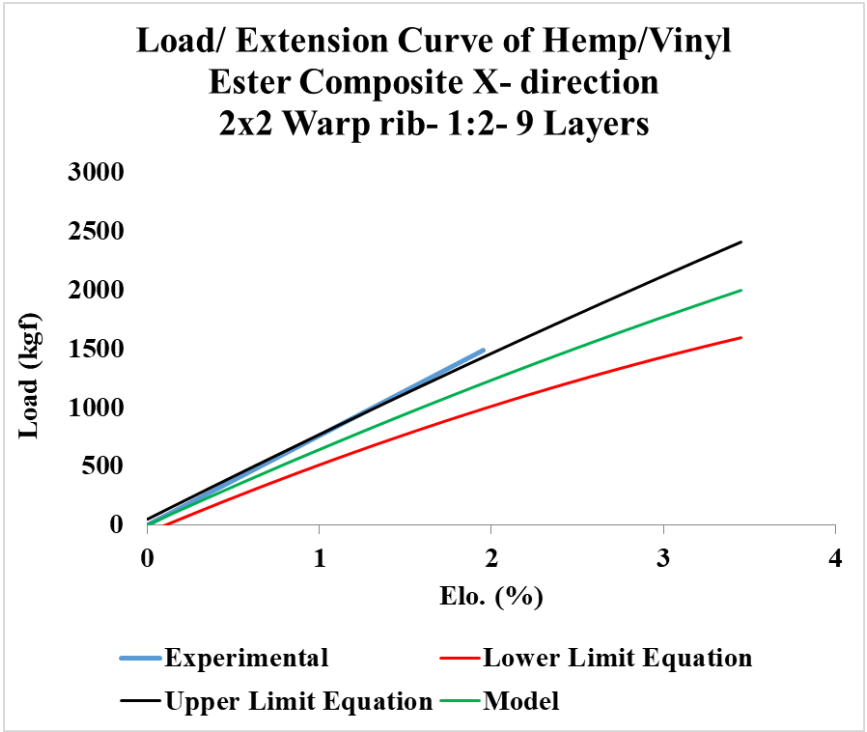
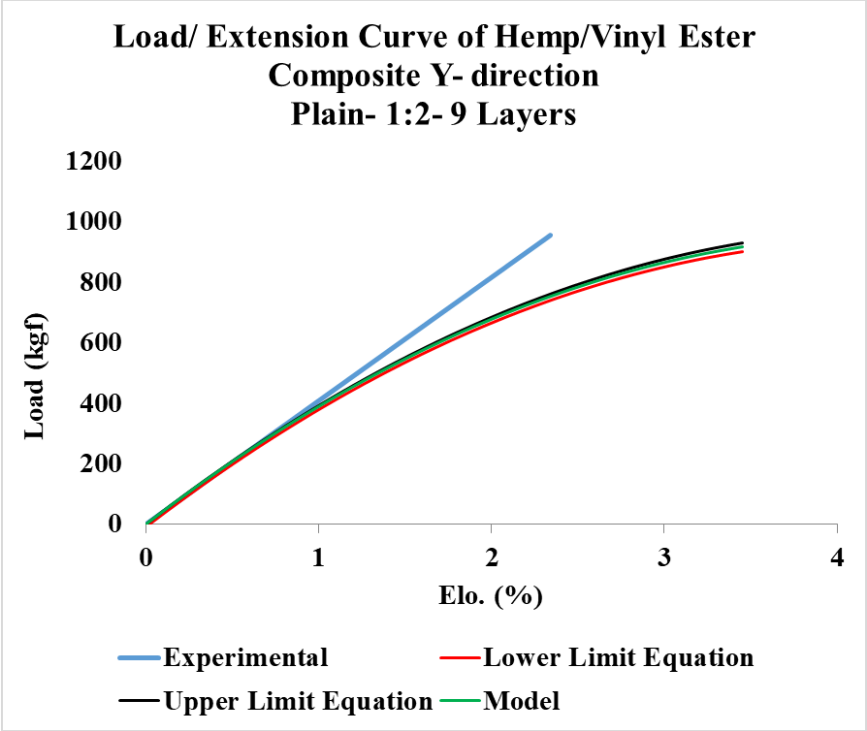
(b)

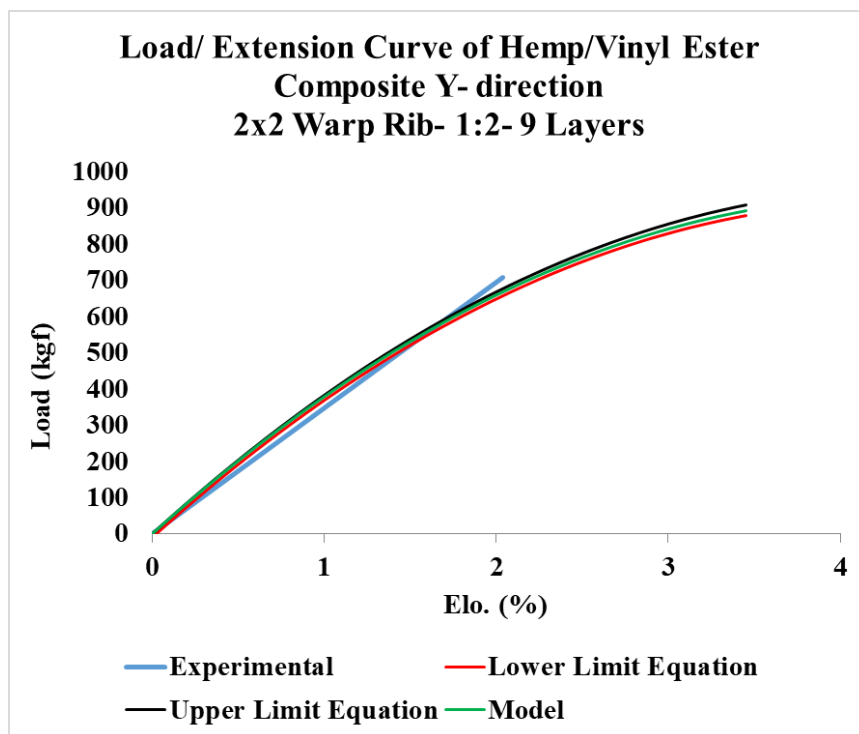




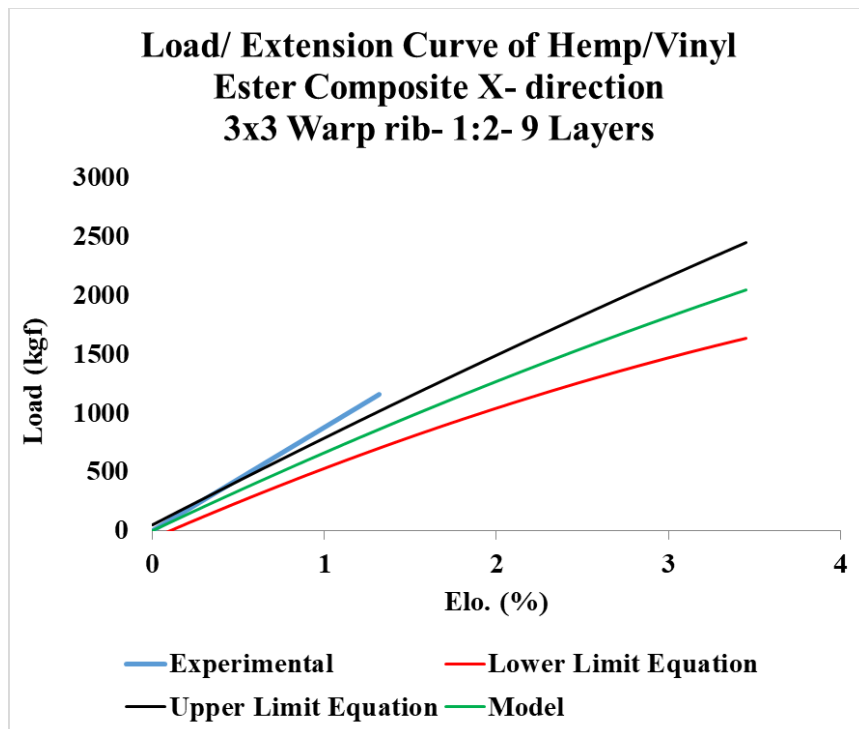
(c)

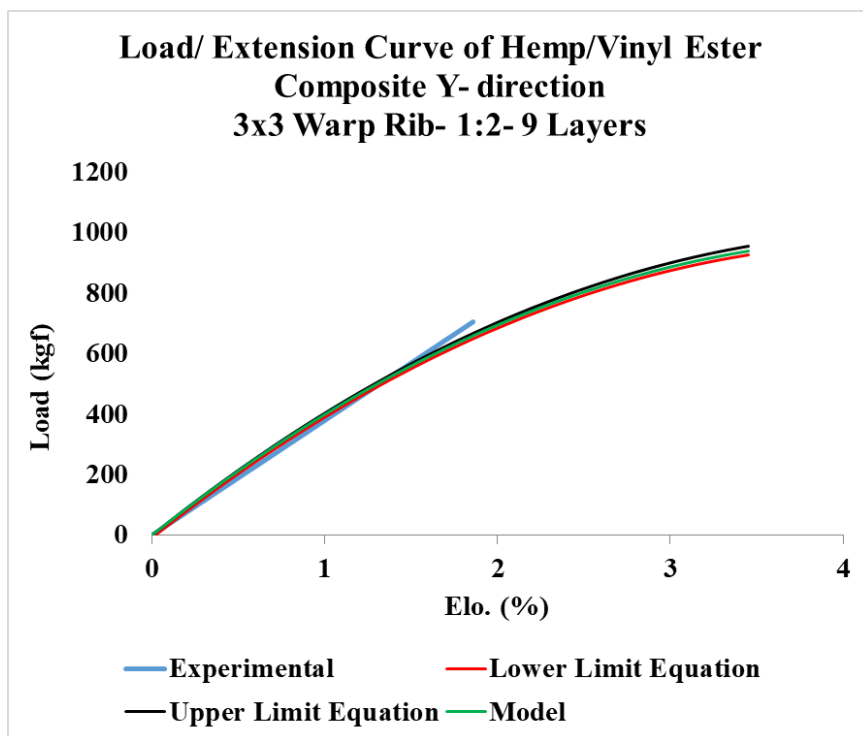




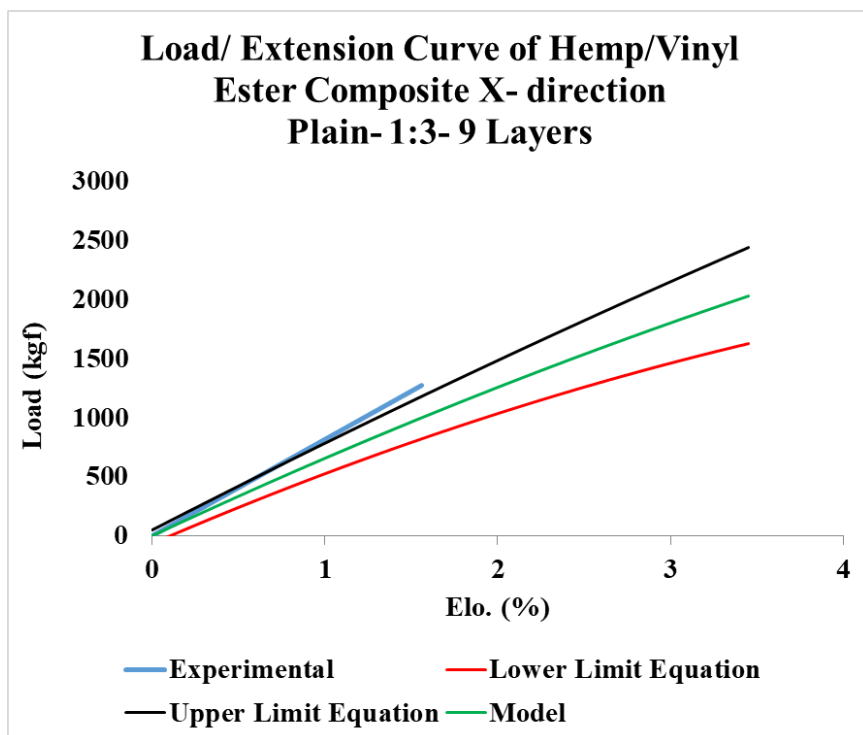


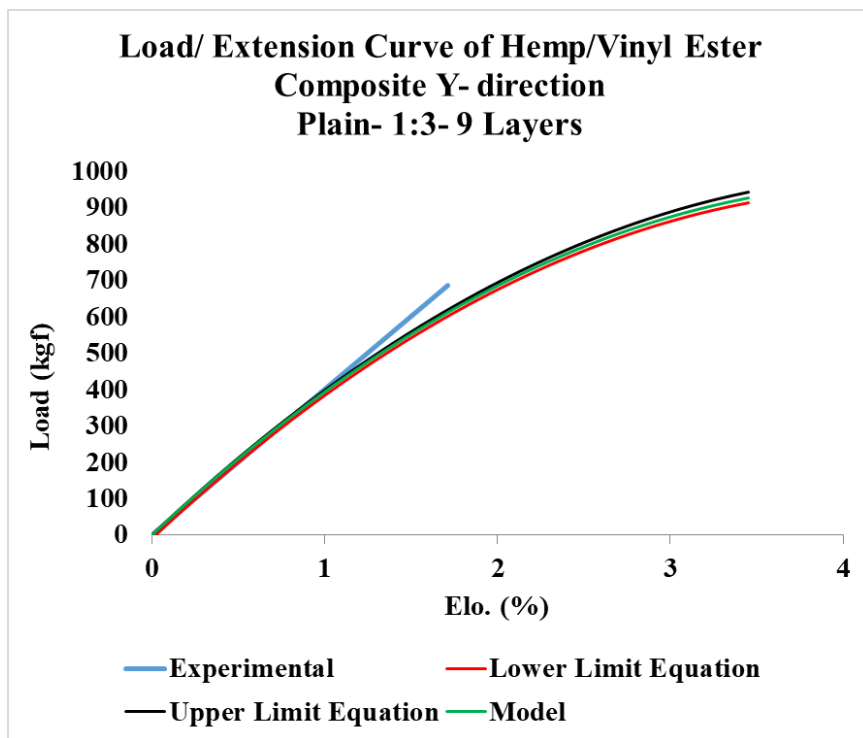
(e)



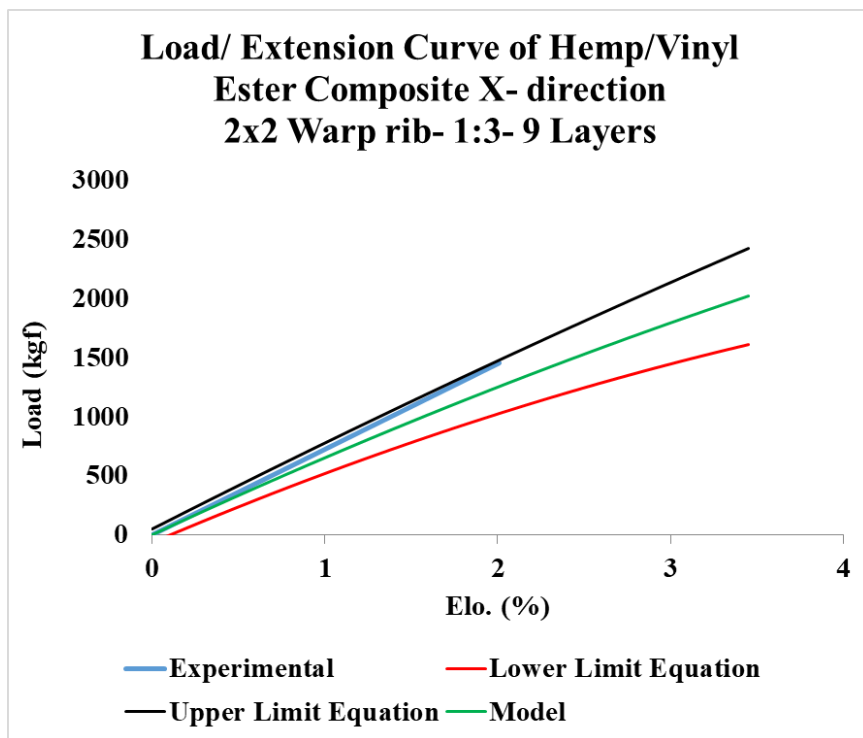


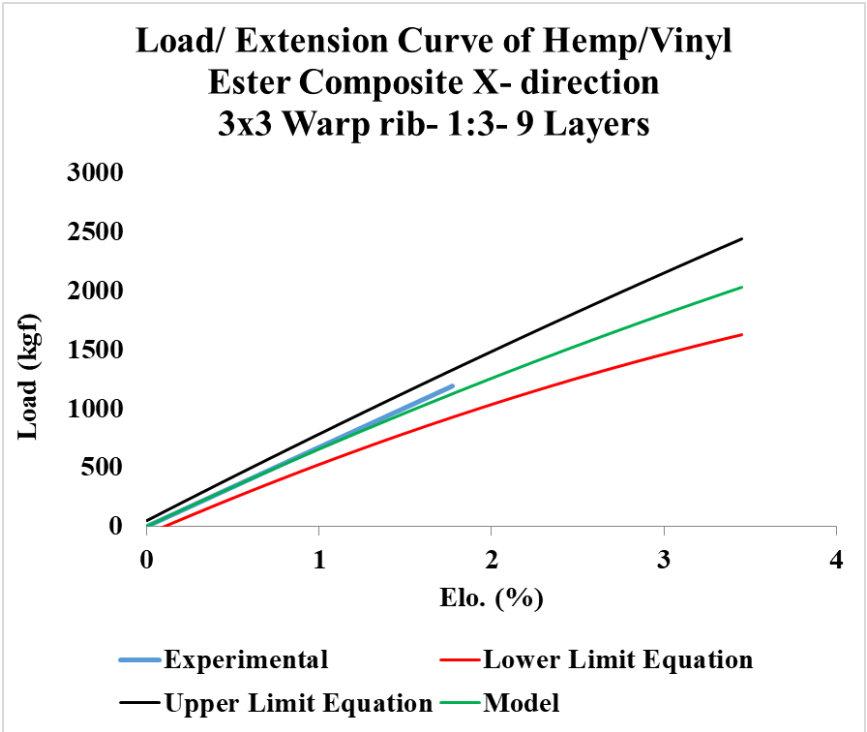
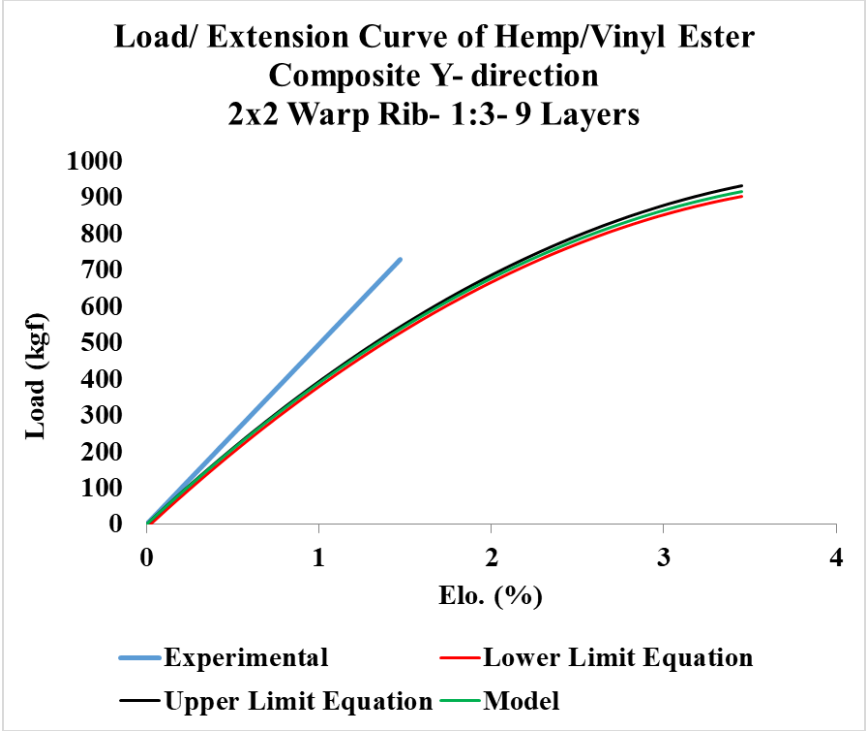
(f)

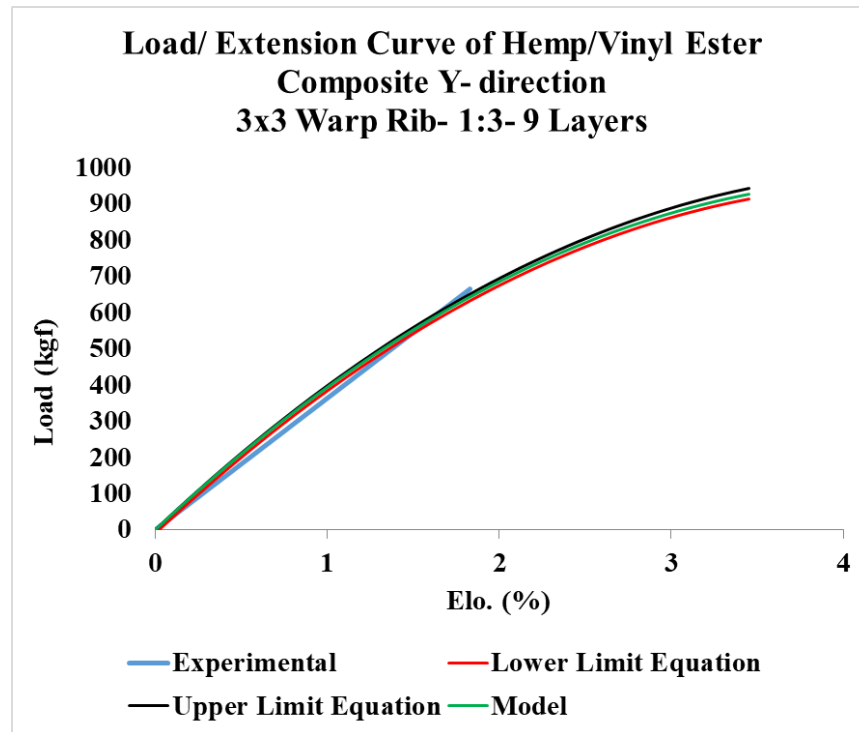




(g)



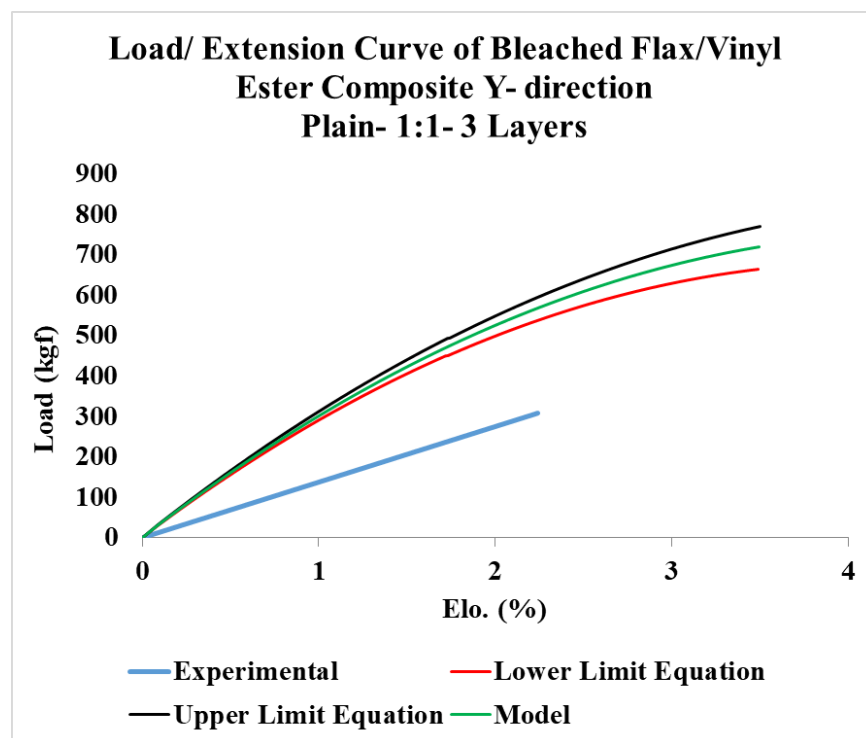
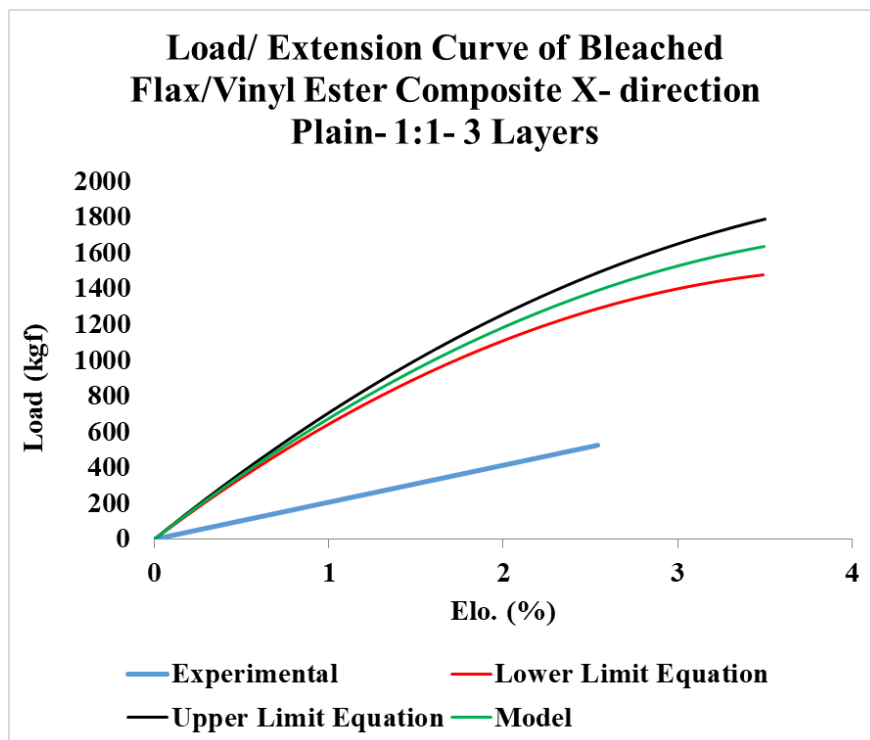




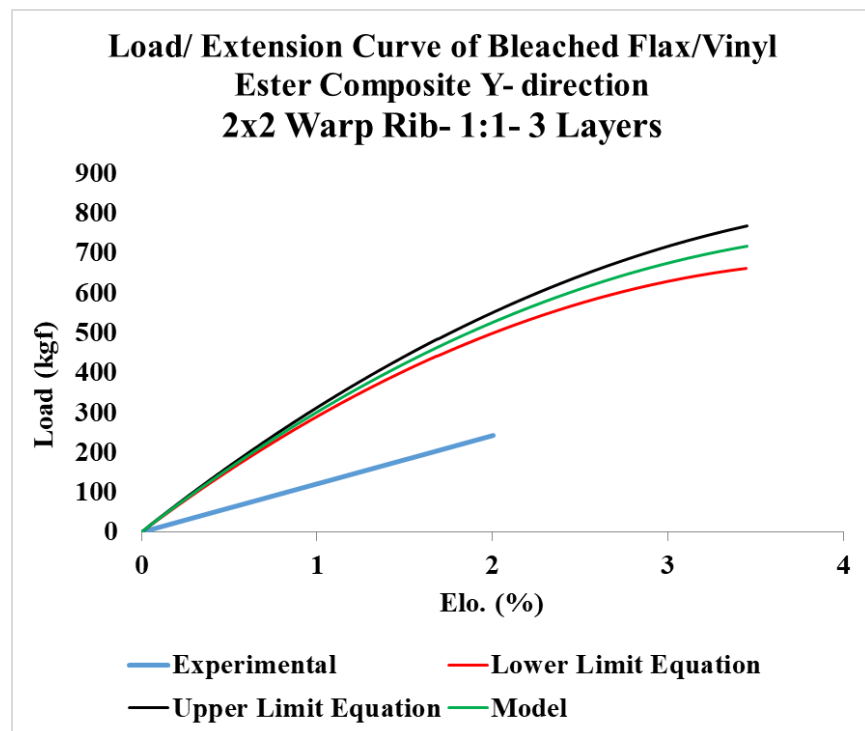
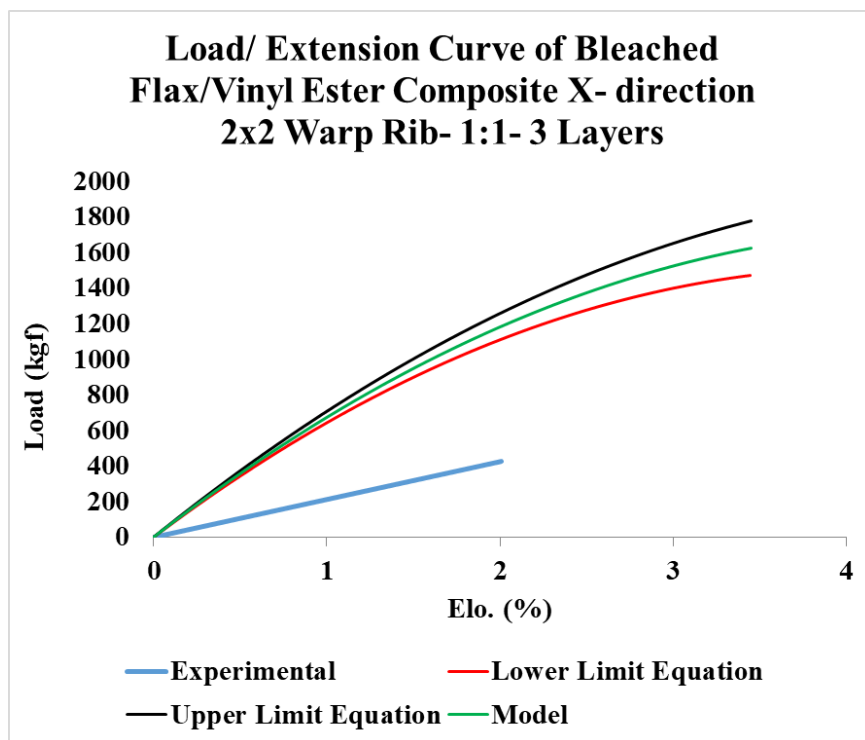
(i)

Figure 194. Experimental vs. model tensile load-elongation curves of 9 Y-yarn layers 3DOW composites from Hemp in the X- and Y-directions (a) plain and 1:1 Z to Y-yarn ratio, (b) 2x2 warp rib and 1:1 Z to Y-yarn ratio, (c) 3x3 warp rib and 1:1 Z to Y-yarn ratio, (d) plain and 1:2 Z to Y-yarn ratio, (e) 2x2 warp rib and 1:2 Z to Y-yarn ratio, (f) 3x3 warp rib and 1:2 Z to Y-yarn ratio (g) plain and 1:3 Z to Y-yarn ratio, (h) 2x2 warp rib and 1:3 Z to Y-yarn ratio, (i) 3x3 warp rib and 1:3 Z to Y-yarn ratio

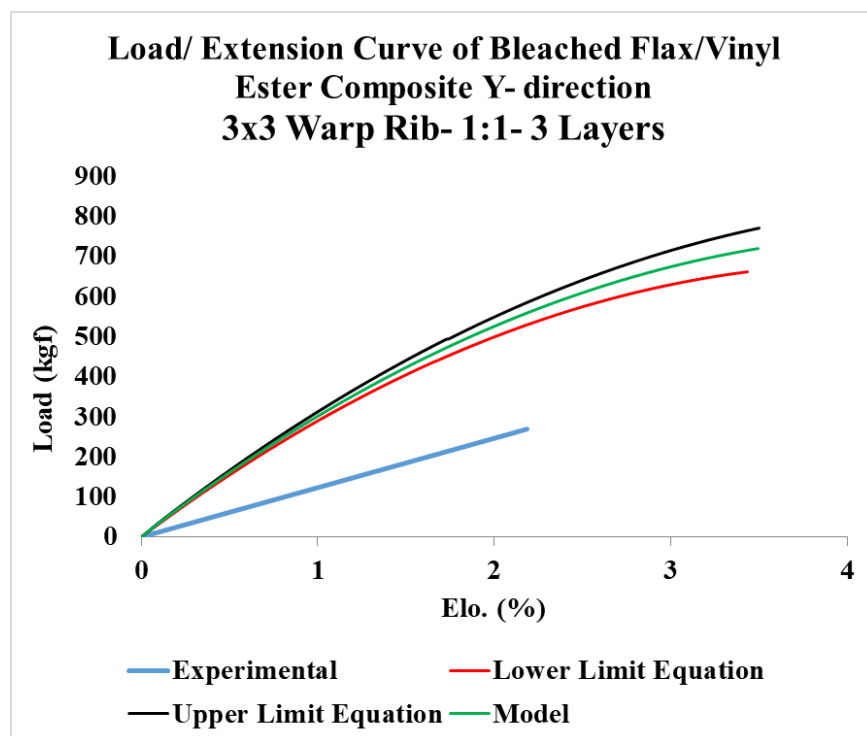
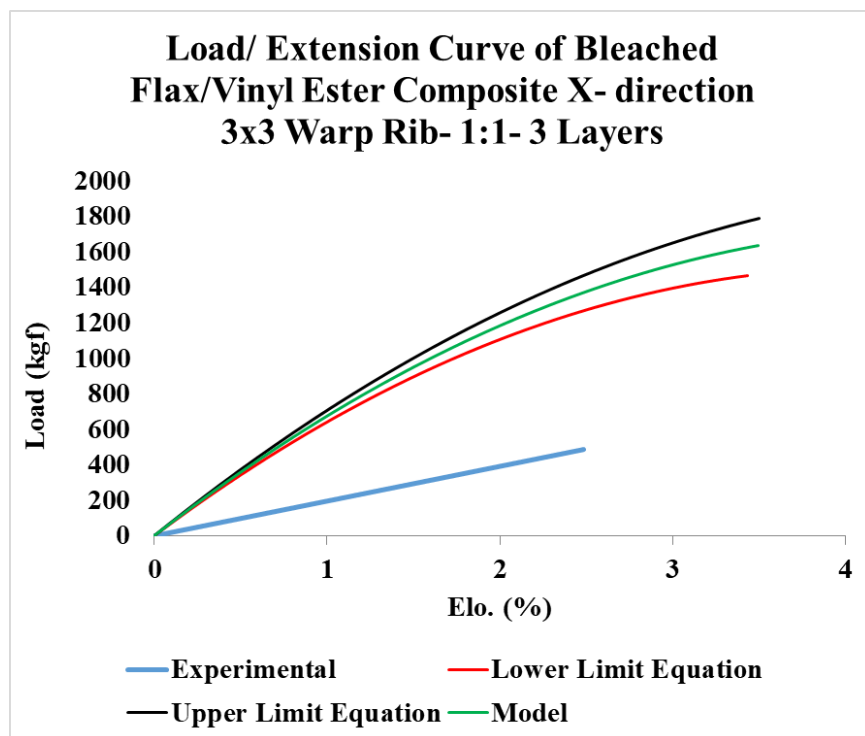
B.3. Experimental vs. Model Tensile Load-Elongation Curves of 3DOW Composites from Flax Fibers Based on the Tensile Properties of the Single Fiber



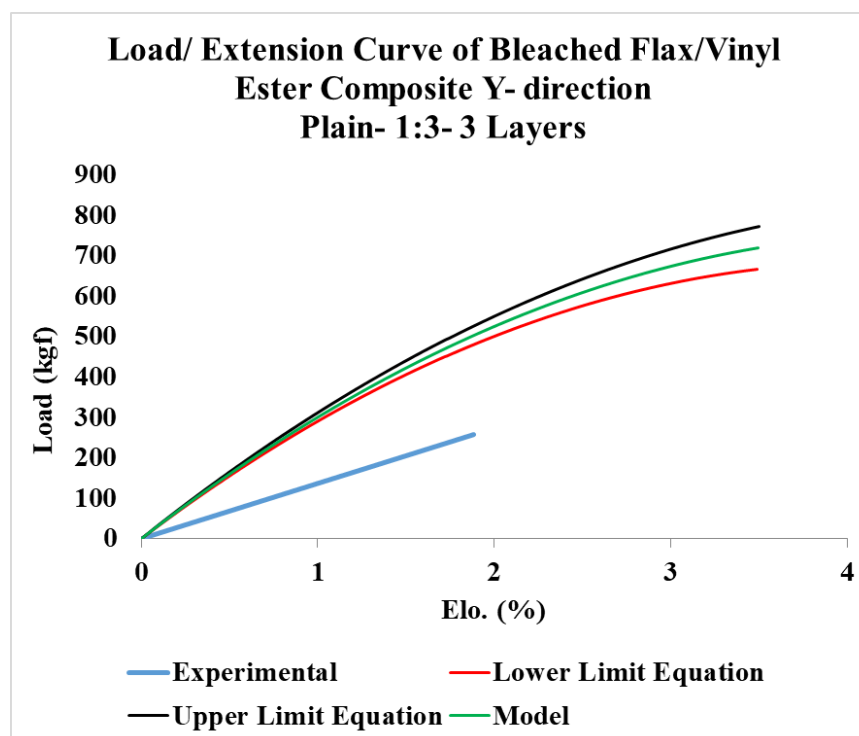
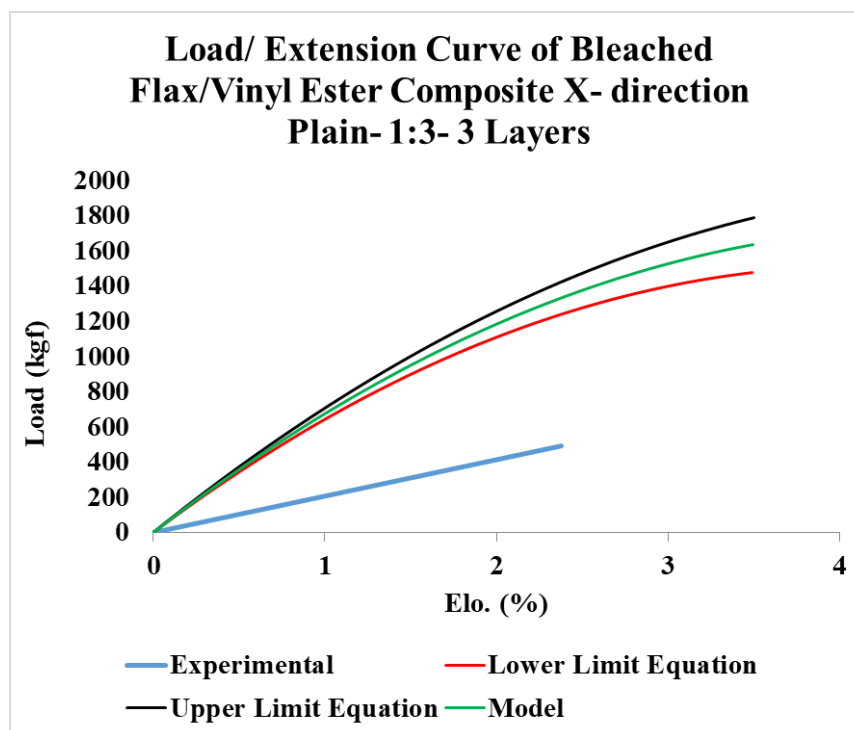
(a)



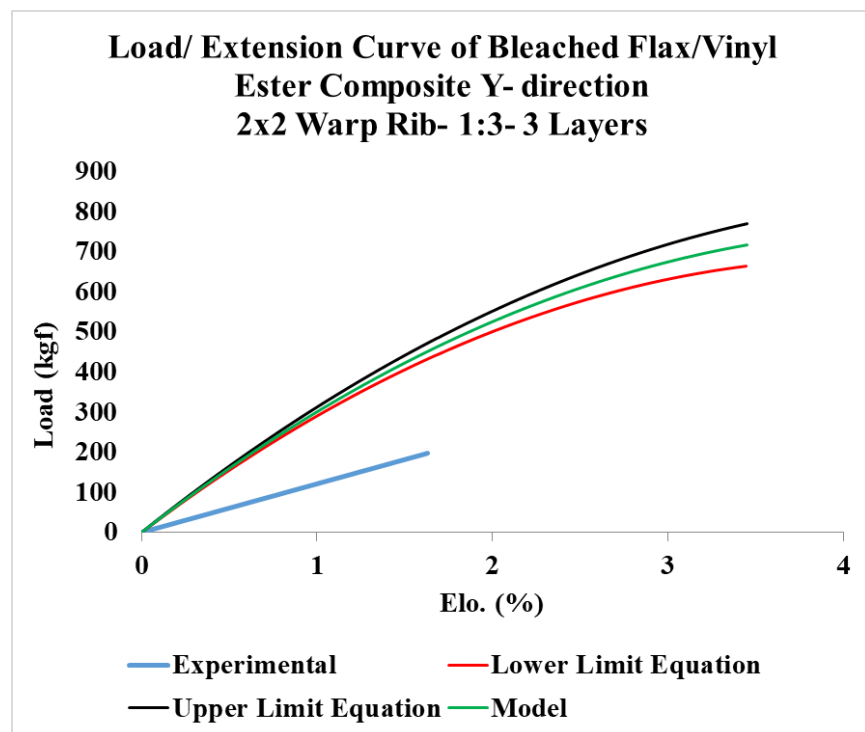
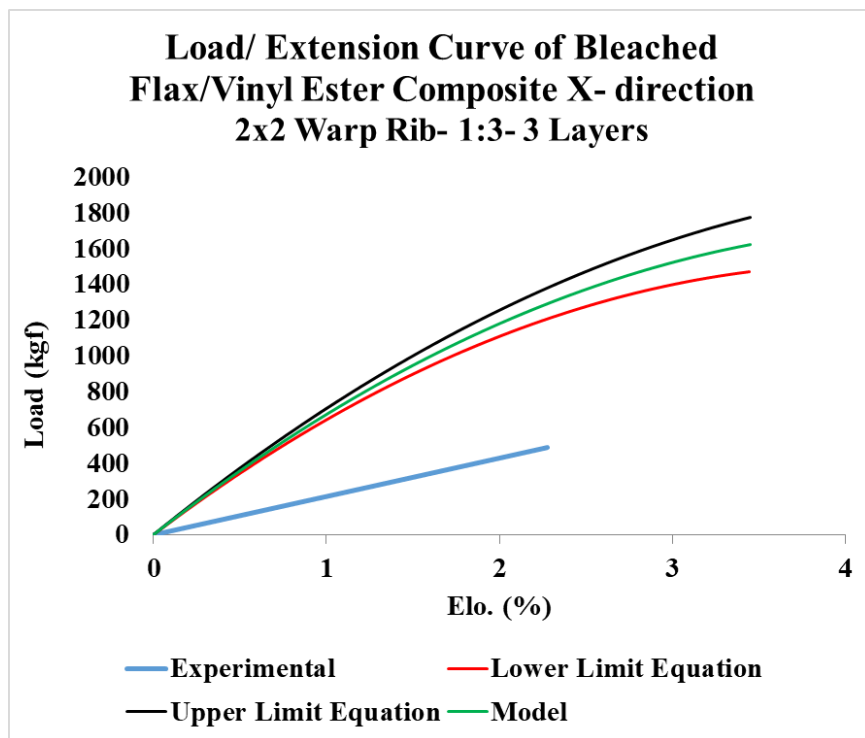
(b)



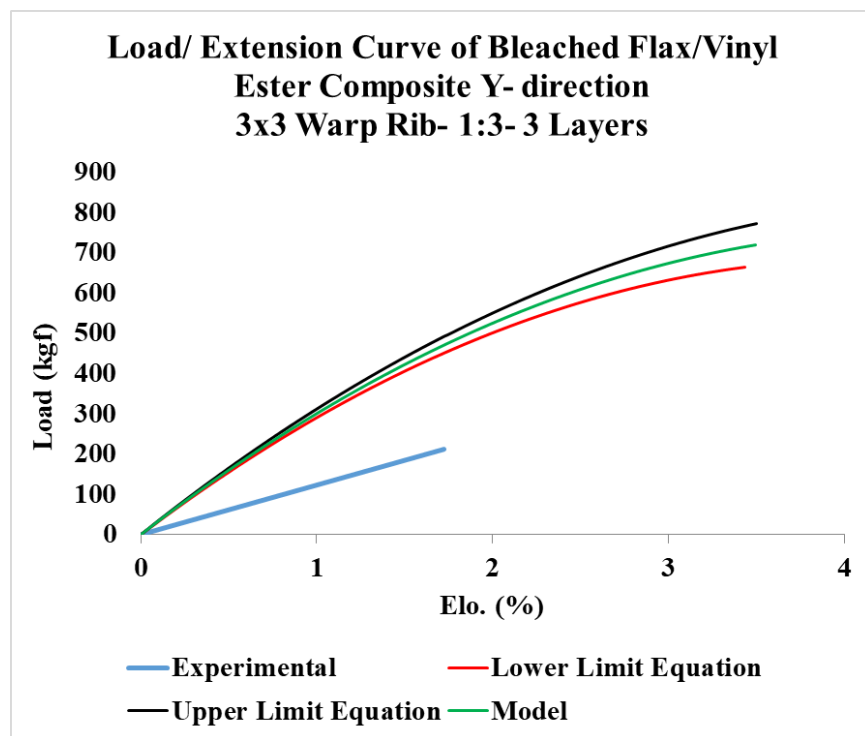
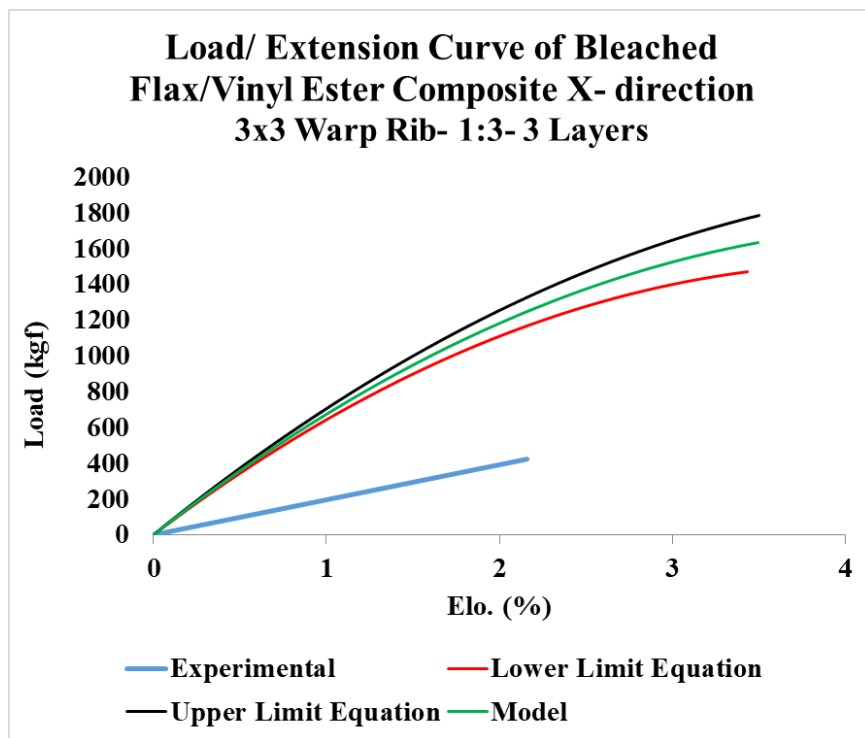
(c)



(d)

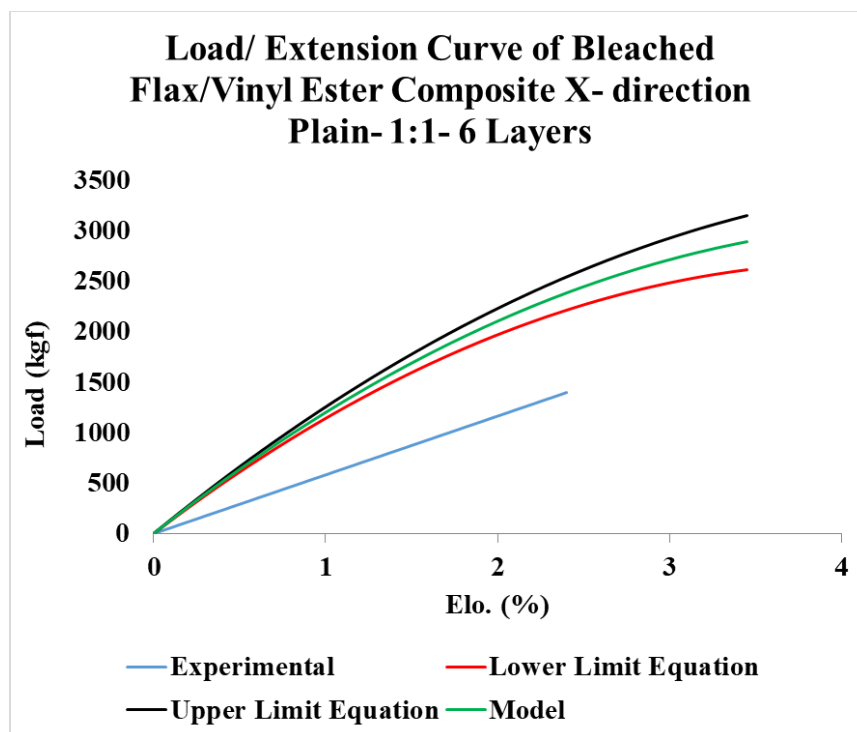


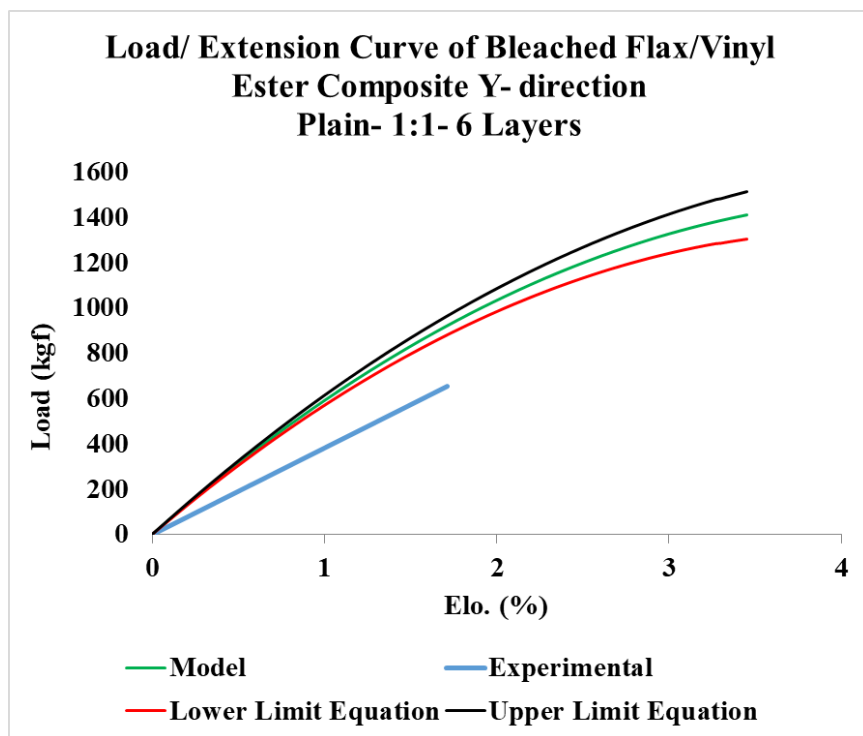
(e)



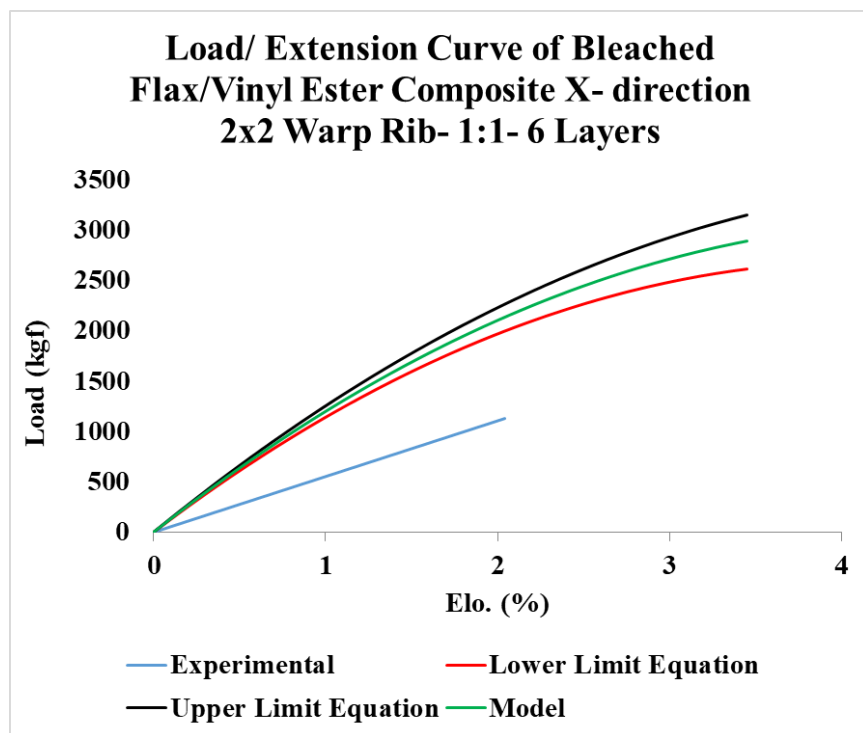
(f)

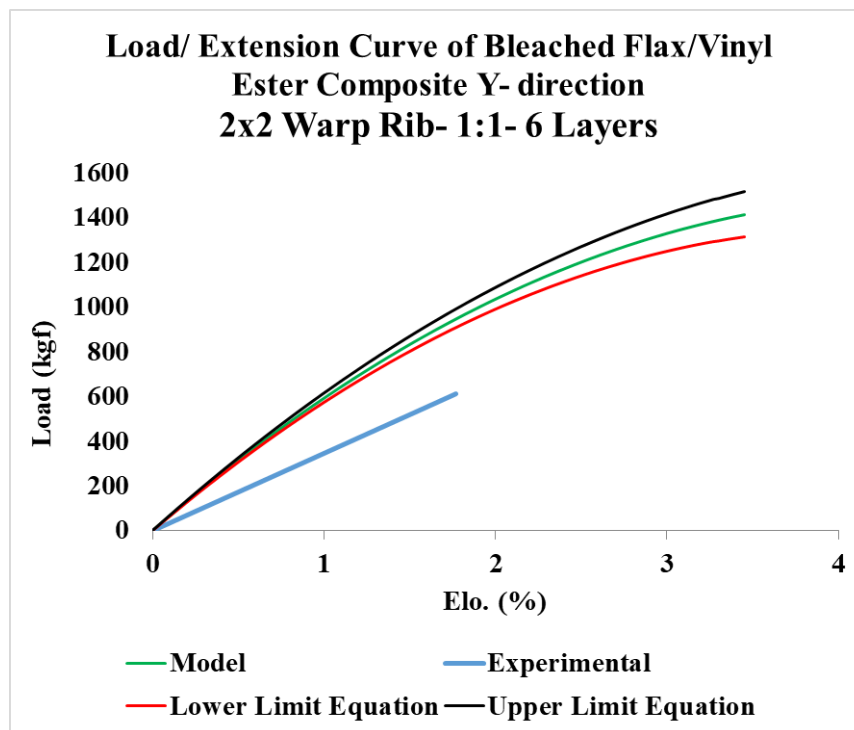
Figure 195. Experimental vs. model tensile load-elongation curves of 3 Y-yarn layers 3DOW composites from Flax in the X- and Y-directions (a) plain and 1:1 Z to Y-yarn ratio, (b) 2x2 warp rib and 1:1 Z to Y-yarn ratio, (c) 3x3 warp rib and 1:1 Z to Y-yarn ratio, (d) plain and 1:3 Z to Y-yarn ratio, (e) 2x2 warp rib and 1:3 Z to Y-yarn ratio, (f) 3x3 warp rib and 1:3 Z to Y-yarn ratio



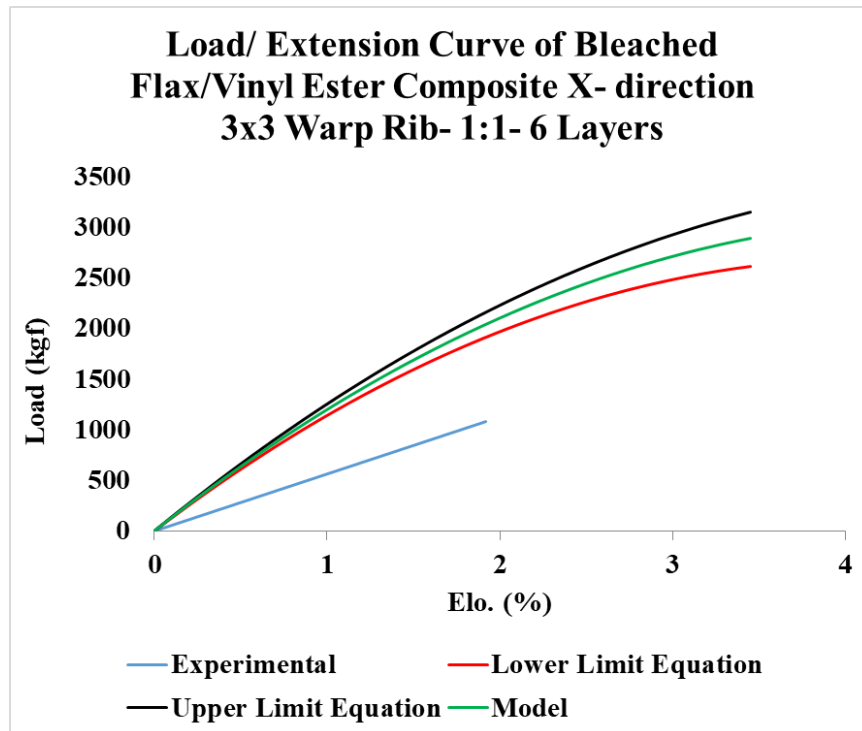


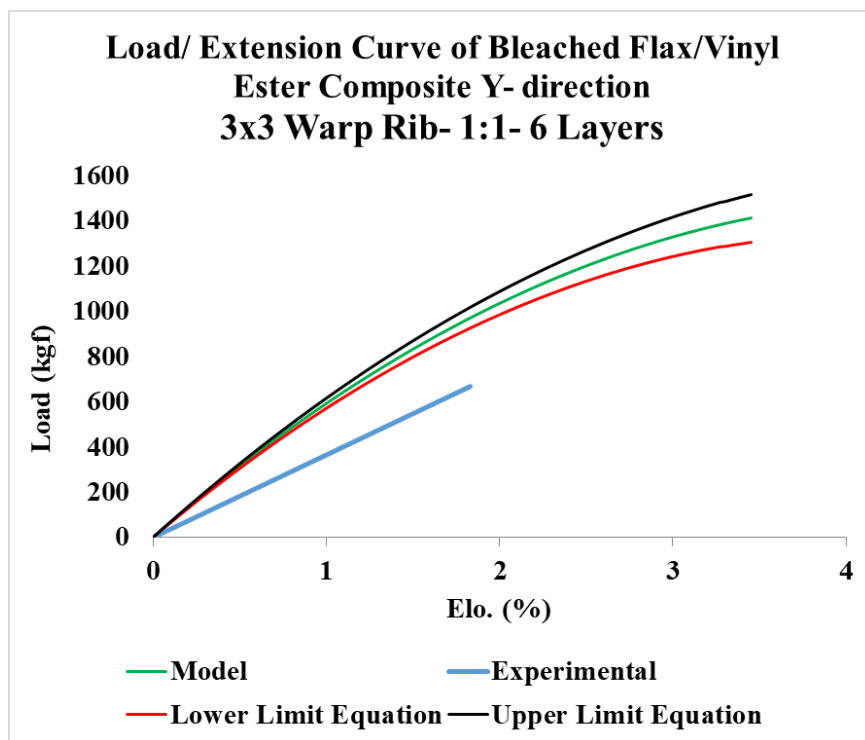
(a)



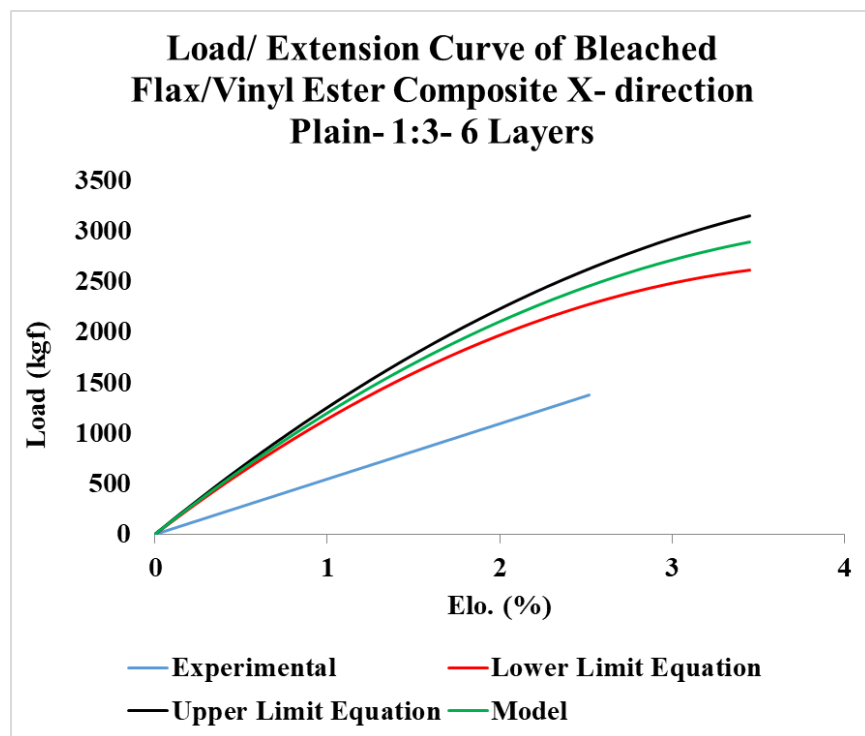


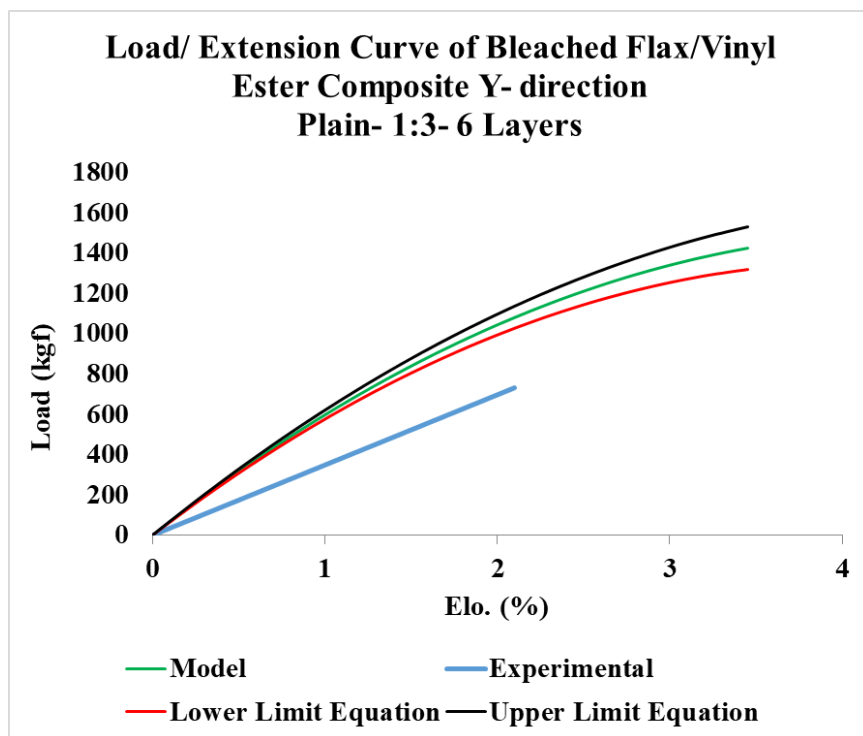
(b)



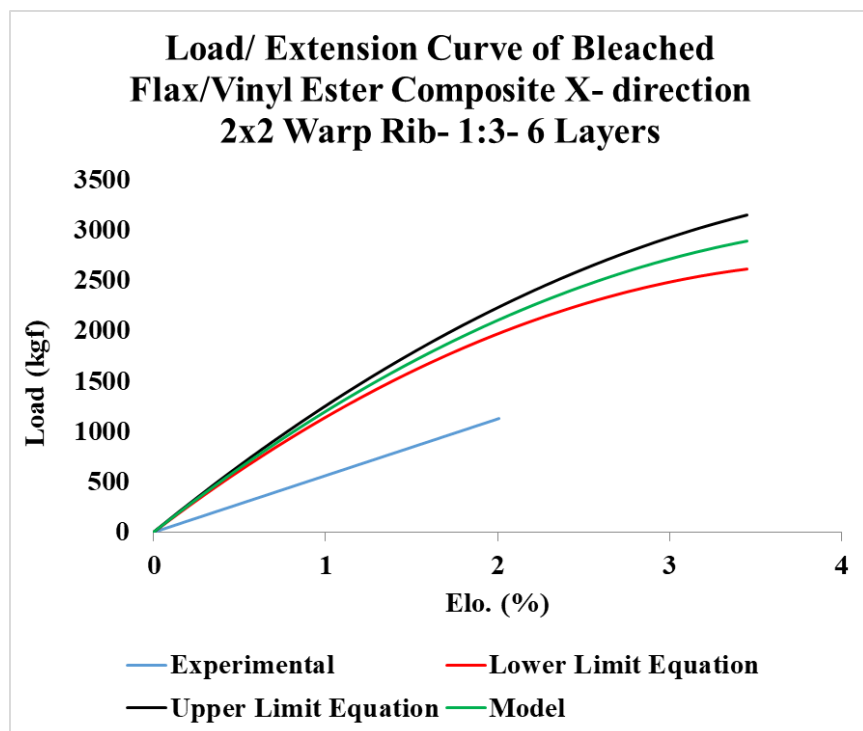


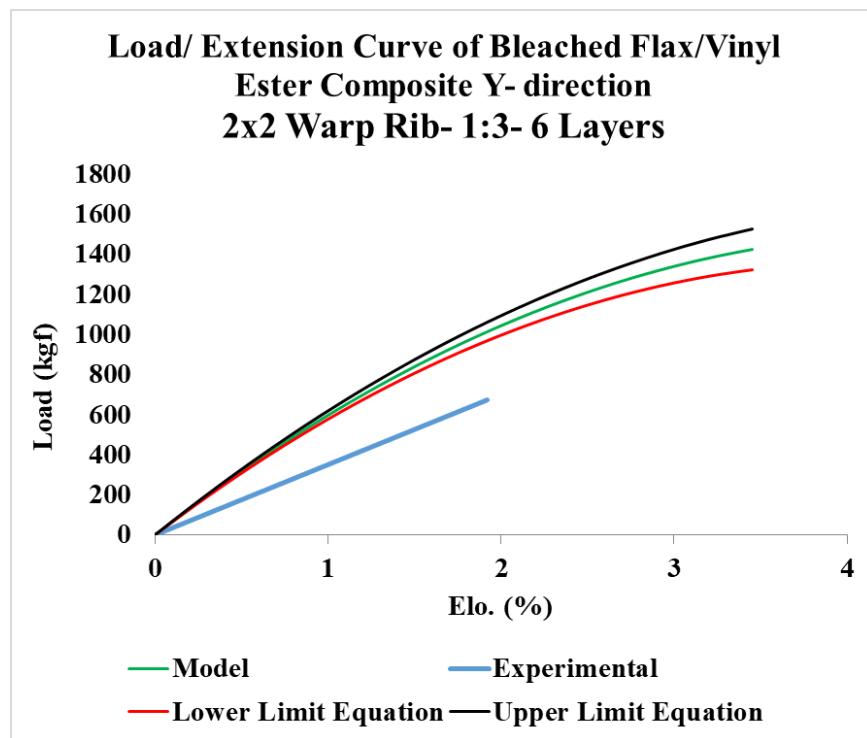
(c)



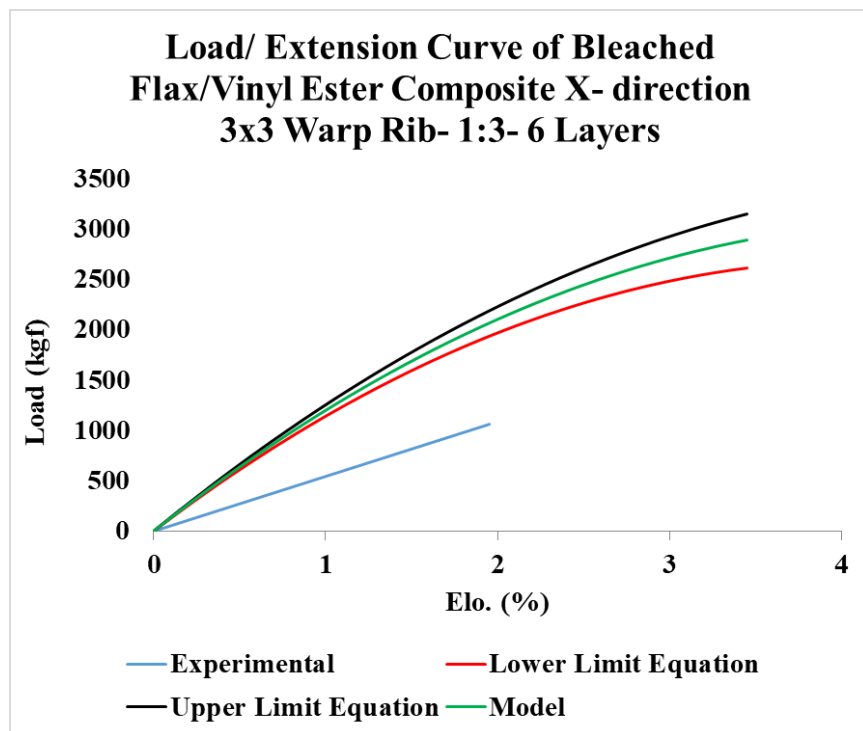


(d)





(e)



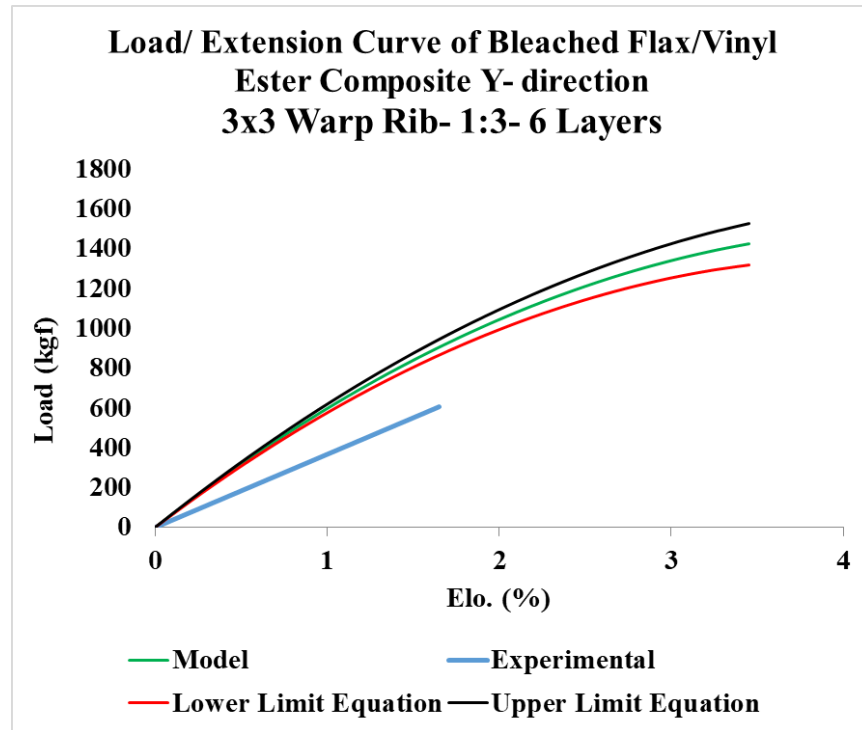
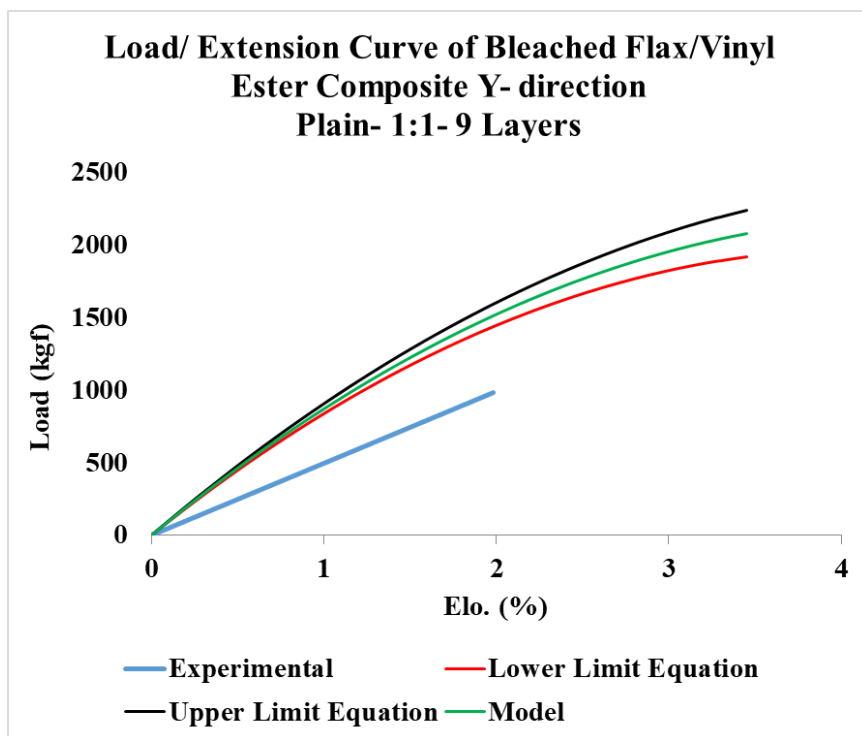
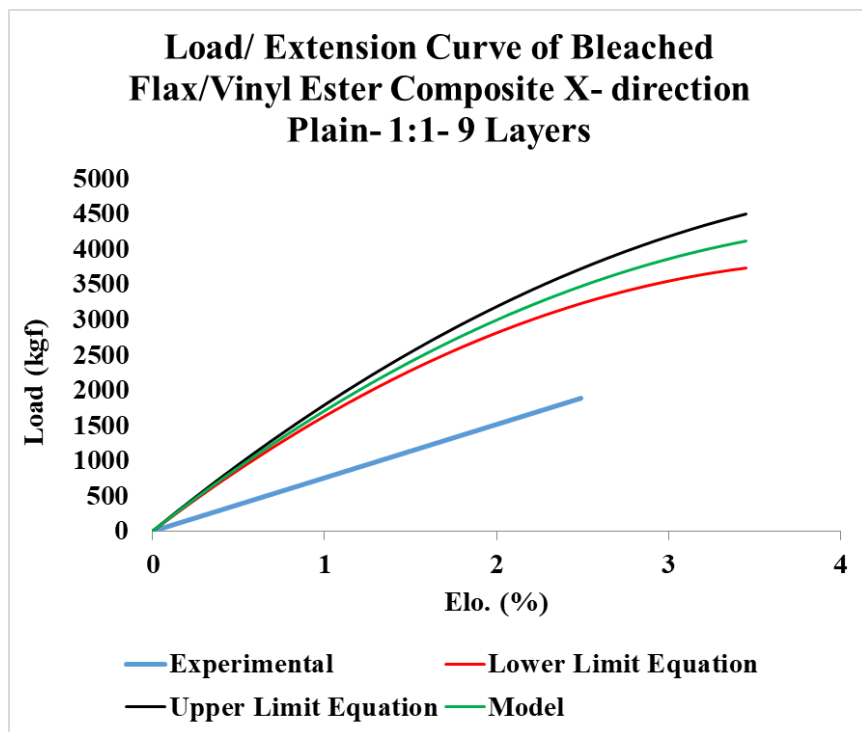
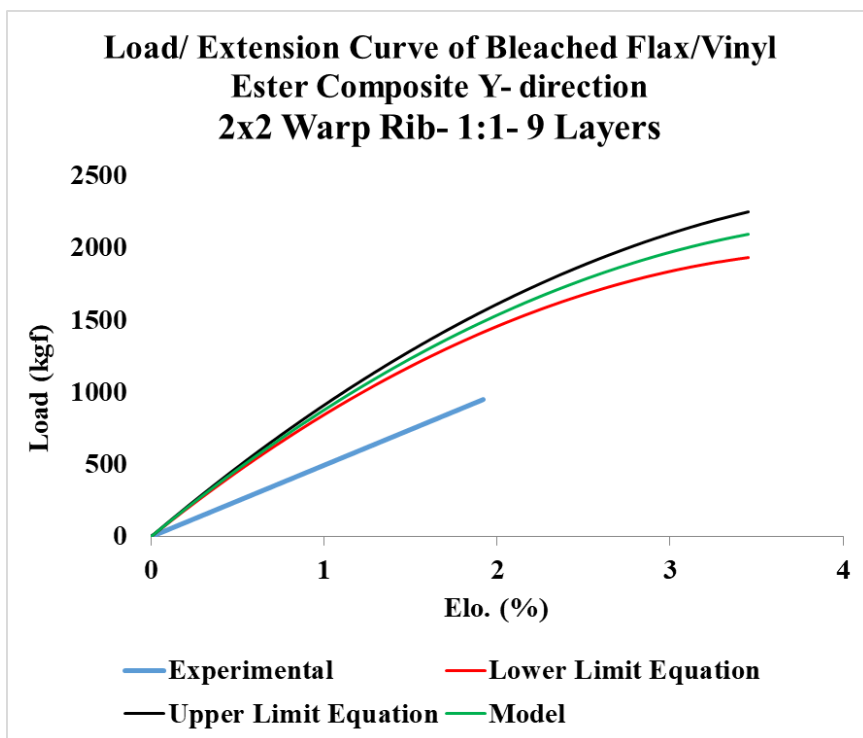
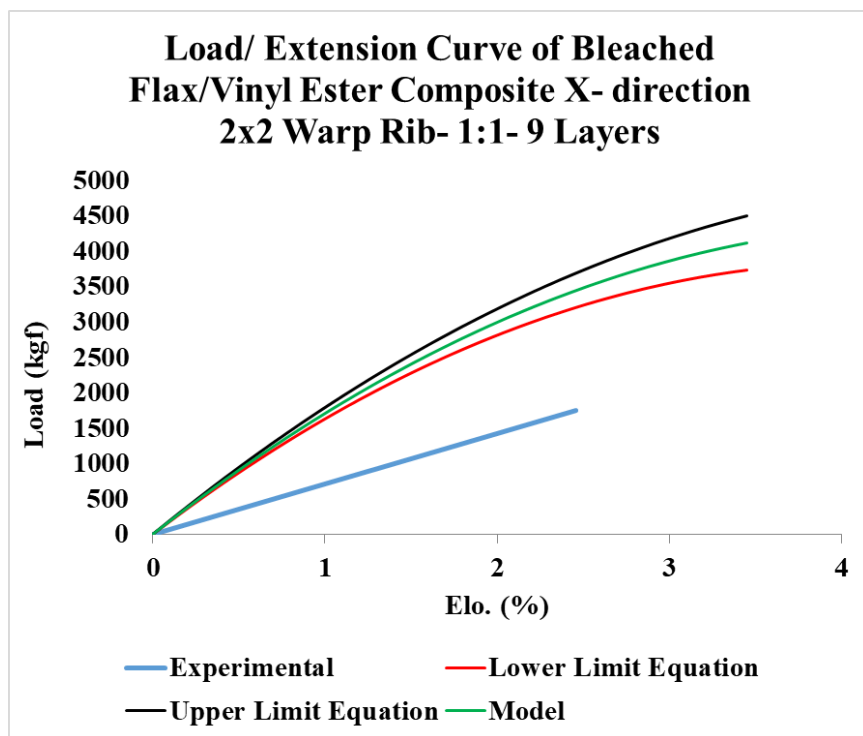


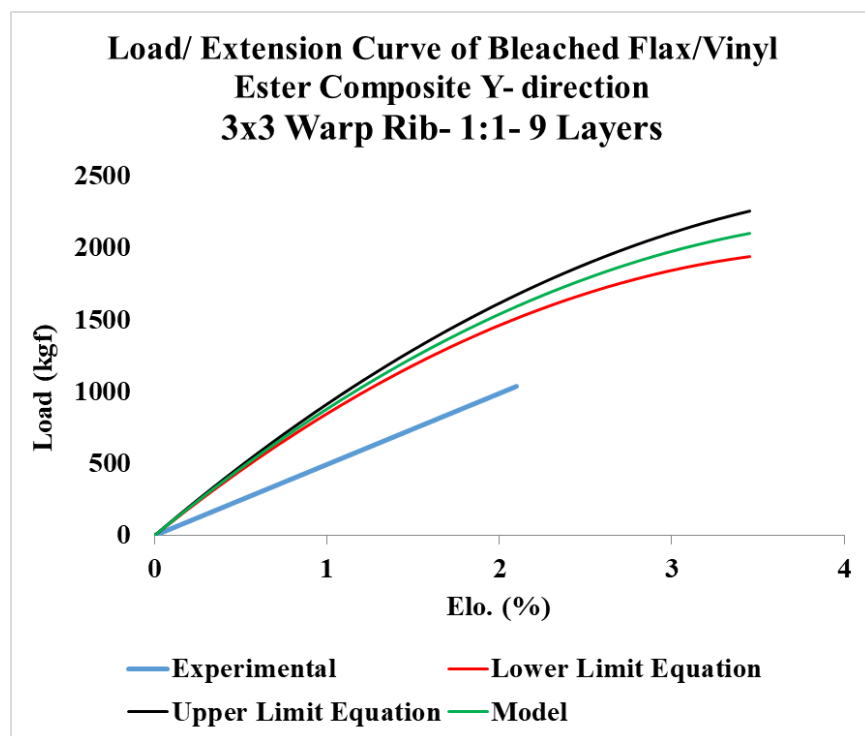
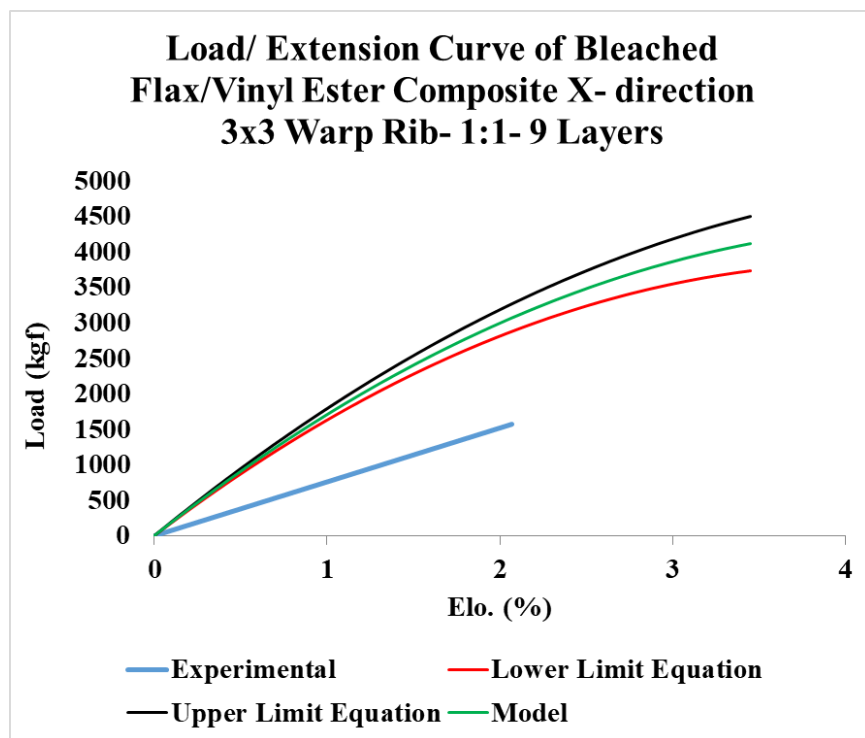
Figure 196. Experimental vs. model tensile load-elongation curves of 6 Y-yarn layers 3DOW composites from Flax in the X- and Y-directions (a) plain and 1:1 Z to Y-yarn ratio, (b) 2x2 warp rib and 1:1 Z to Y-yarn ratio, (c) 3x3 warp rib and 1:1 Z to Y-yarn ratio, (d) plain and 1:3 Z to Y-yarn ratio, (e) 2x2 warp rib and 1:3 Z to Y-yarn ratio, (f) 3x3 warp rib and 1:3 Z to Y-yarn



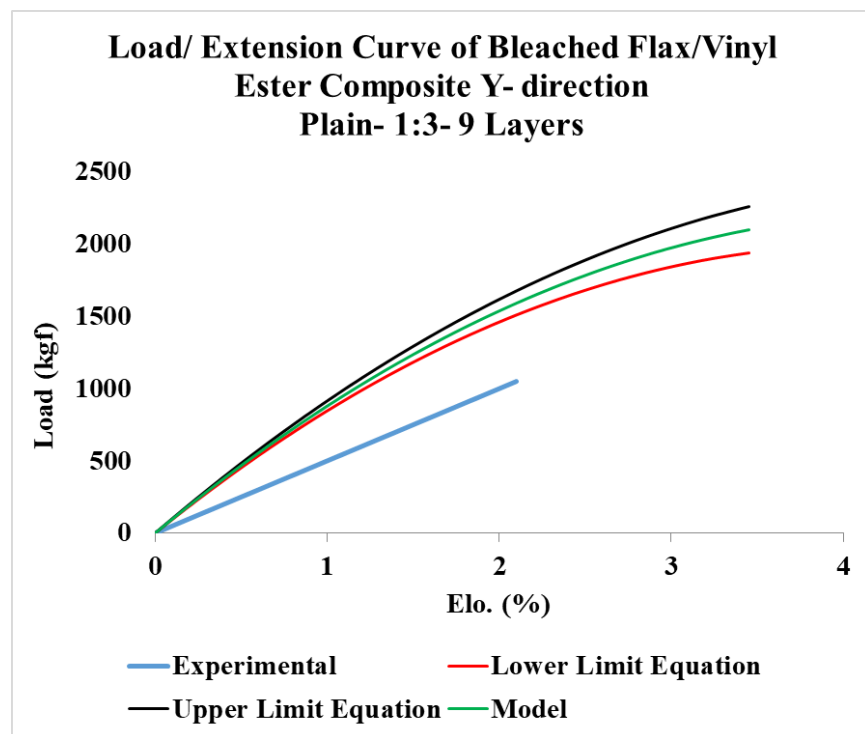
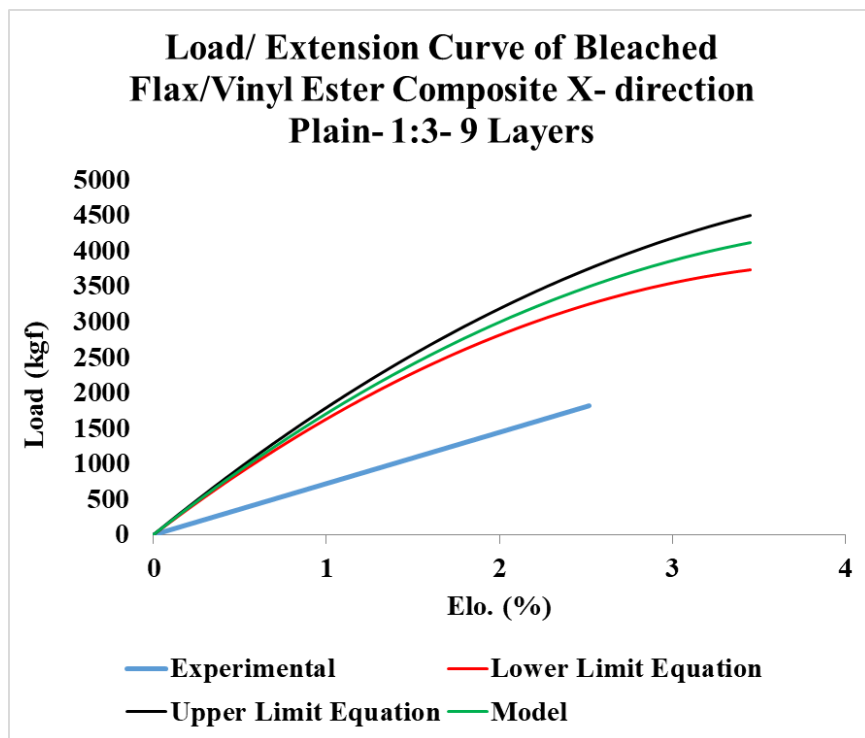
(a)



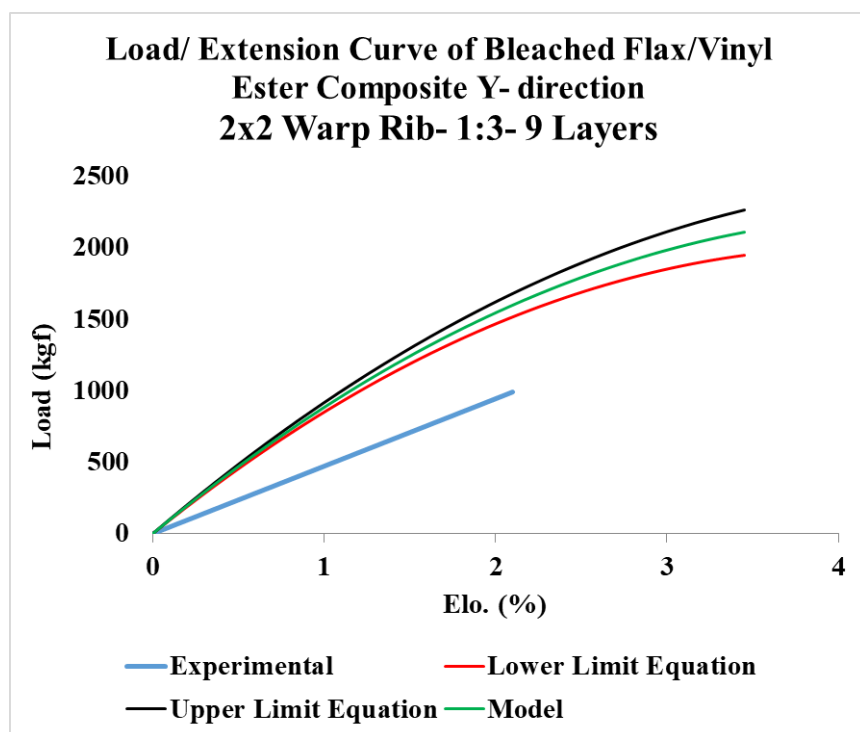
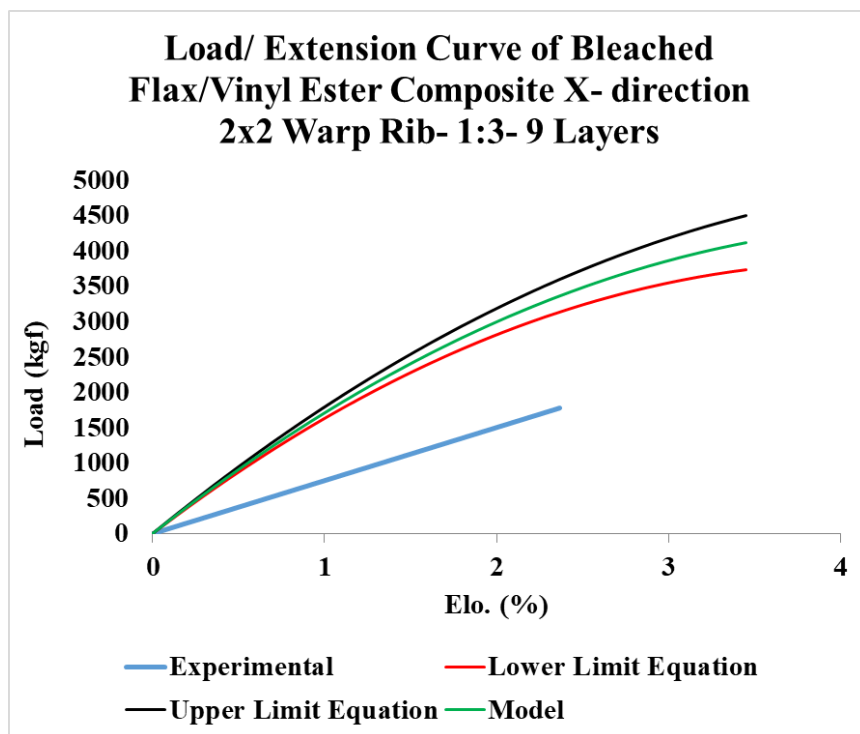
(b)



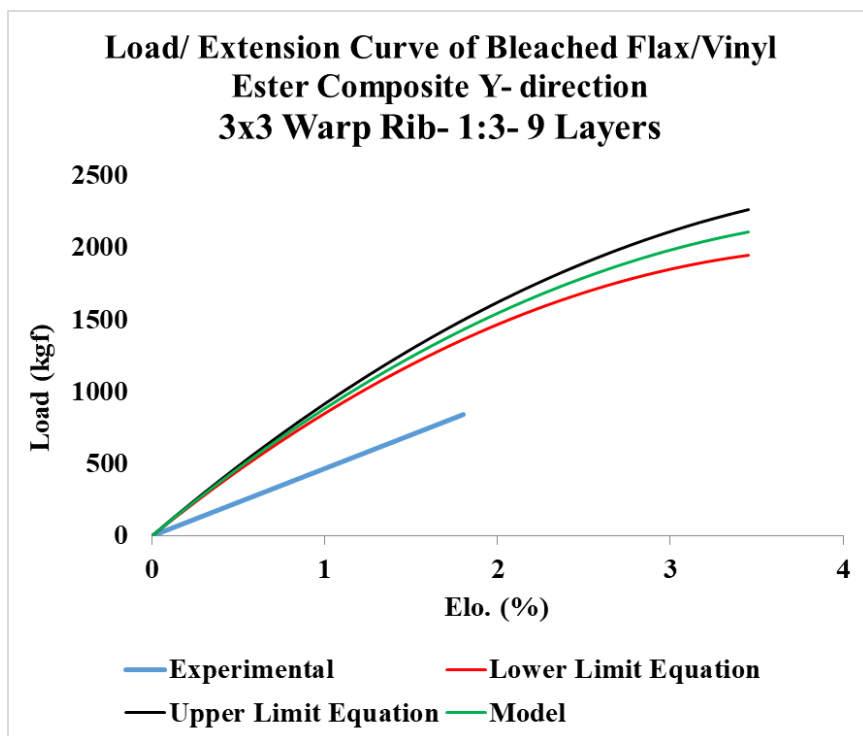
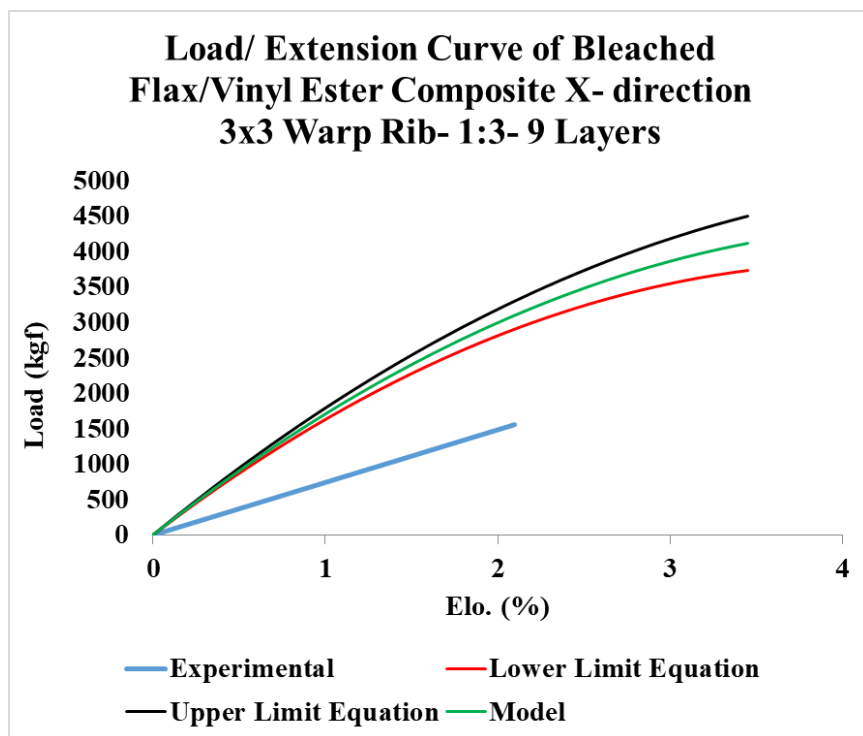
(c)



(d)



(e)



(f)

Figure 197. Experimental vs. model tensile load-elongation curves of 9 Y-yarn layers 3DOW composites from Flax in the X- and Y-directions (a) plain and 1:1 Z to Y-yarn ratio, (b) 2x2 warp rib and 1:1 Z to Y-yarn ratio, (c) 3x3 warp rib and 1:1 Z to Y-yarn ratio, (d) plain and 1:3 Z to Y-yarn ratio, (e) 2x2 warp rib and 1:3 Z to Y-yarn ratio, (f) 3x3 warp rib and 1:3 Z to Y-yarn ratio

B.4. Numerical Example of Calculating Load-Extension Curve of 3DOW Composites

An example is given below to demonstrate the theoretical calculations of obtaining the load-extension curve of 3DOW composites. The structural parameters of the used 3DOW preform are in Table 46.

Table 46. Structure of Sample Preform

Constituent	ρ_1 , Tex	ρ_v , g/cm ³	T, cm ⁻¹	d, mm	n	N	M
X-yarn	338	1.43	4.04	1.4167	7	2	-
Y-yarn	337.2	1.43	7.63	0.7075	6	2	-
Z-yarn	49.6	1.43	2.55	0.2713	-	2	1

X-, Y- and Z-yarns and resin tensile properties are derived directly from their experimental measurements. Fiber Volume Fraction (FVF) of each yarn is calculated using equations (20-22). To calculate the contribution of the preform in the X- and Y-direction at a certain value of strain, the load of each yarn at this strain is multiplied by the number of yarns per weave repeat and the number of layers as indicated in equations (23 & 24). The load of coupon of pure resin is calculated from equation (25) then multiplied by resin volume fraction to calculate its

contribution in the X- and Y- direction as indicated in equations (26 & 27), respectively. After that, the load of the 3DOW composites is obtained using Hamburger's theory of blended yarns by adding the corresponding load of the preform and the resin in the X- and Y-directions as shown in equations (28 & 29), respectively. These calculations are repeated for all strain points to obtain the entire Load-Extension curve of 3DOW composites in the X- and Y-direction.

From the data in Table 46,

$$h_{mz} = \frac{(2d_z + d_y n_y + d_x n_x)}{2}$$

$$h_{mz} = \frac{2*0.27 + 0.71*6 + 1.42*7}{2} = 7.37 \text{ mm}$$

$$L_{Iz} = 2 \sqrt{\left(\frac{P_x}{2}\right)^2 + (h_{mz})^2}$$

$$L_{Iz} = 2 \sqrt{\left(\frac{0.62}{2}\right)^2 + (7.37)^2} = 14.75 \text{ mm}$$

$$\sin \theta = \frac{P_x}{L_{Iz}}$$

$$\Theta = 2.4$$

$$F_{fx} = \frac{\frac{n_x \rho_{1x}}{\rho_{vx} 10^3}}{p_x(n_y d_y + n_x d_x + 2d_z)} \quad (20)$$

$$F_{fx} = \frac{\frac{7*338}{1.43*10^3}}{0.62(6*0.71 + 7*1.42 + 2*0.27)} = 0.18$$

$$F_{fy} = \frac{\frac{n_y \rho_{1y}}{\rho_{vy} 10^3}}{p_y(n_y d_y + n_x d_x + 2d_z)} \quad (21)$$

$$F_{fy} = \frac{\frac{6*337.2}{1.43*10^3}}{1.31(6*0.71 + 7*1.42 + 2*0.27)} = 0.07$$

$$F_{fz} = \frac{\left[\frac{L_{fz}}{M_z} + \left(1 - \frac{1}{M_z}\right) p_x \right] N_z \rho_{fz}}{\rho_{fz} 10^3} \quad (22)$$

$$F_{fz} = \frac{\left[\frac{14.45}{1} + \left(1 - \frac{1}{1}\right) * 0.62 \right] * 2 * 49.6}{1.43 * 10^3} = 0.04$$

$$F_X = 2 \left(139 \lambda_{yX}^2 + 508 \lambda_{yX} \right) * n_x * N_x * \frac{W}{P_x * N_x} \quad (23)$$

At 0.01 stain,

$$F_X = 2 \left(139 * 1.01^2 + 508 * 1.01 \right) * 7 * 2 * \frac{25.4}{0.62 * 2} = 377000 \text{ gf}$$

$$F_{TY} = 80 \lambda_{yY}^2 + 463 \lambda_{yY}$$

The straight part (B) of Z-yarn,

$$F_{TZ} = 24 \lambda_{yZ}^2 + 383 \lambda_{yZ}$$

The inclined portion (A) of Z-yarn,

$$F_Z = F_{TZ} \sin 15.66$$

$$F_Y = \left(80 \lambda_{yY}^2 + 463 \lambda_{yY} \right) * n_Y * N_Y * \frac{W}{P_Y * N_Y} + \left(24 \lambda_{yZ}^2 + 383 \lambda_{yZ} \right) * \sin \theta \quad (24)$$

At 0.01 stain,

$$F_Y = 3 \left(80 * 1.01^2 + 463 * 1.01 \right) * 6 * 2 * \frac{25.4}{1.31 * 2} + \left(24 * 1.01^2 + 383 * 1.01 \right) * \sin 2.4$$

$$= 191966 \text{ gf}$$

For Resin,

$$F_{resin} = \left(-2.7 \lambda_{yZ}^2 + 22.35 \lambda_{yZ} \right) * W * t * 101.97 \left(\frac{gf}{N} \right) \quad (25)$$

At 0.01 stain,

$$F_{resin} = (-2.7 * 1.01^2 + 22.35 * 1.01) * 25.4 * 4.22 * 101.97 = 216623 \text{ gf}$$

Load of resin in the X-direction,

$$F_{X \text{ resin}} = F_{resin} * (1 - F_{fx}) \quad (26)$$

At 0.01 stain,

$$F_{X \text{ resin}} = 216623 * (1 - 0.18) = 177631 \text{ gf}$$

Load of resin in the Y-direction,

$$F_{Y \text{ resin}} = F_{resin} * (1 - (F_{fy} + F_{fz})) \quad (27)$$

At 0.01 stain,

$$F_{Y \text{ resin}} = 216623 * (1 - (0.07 + 0.04)) = 192795 \text{ gf}$$

Load of 3DOW composite in the X-direction,

$$F_{X \text{ composite}} = F_X + F_{X \text{ resin}} \quad (28)$$

At 0.01 stain,

$$F_{X \text{ composite}} = 377000 + 177631 = 554631 \text{ gf}$$

Load of 3DOW composite in the Y-direction,

$$F_{Y \text{ composite}} = F_Y + F_{Y \text{ resin}} \quad (29)$$

At 0.01 stain,

$$F_{Y \text{ composite}} = 191966 + 192795 = 384761 \text{ gf}$$

By following the same procedure for all the strain points, the entire load-extension curves of 3DOW composite are predicted in the X- and Y-directions as shown in Figure 196 (a). Table 47 shows the force of 3DOW composite at different strain point in the X- and Y-directions.

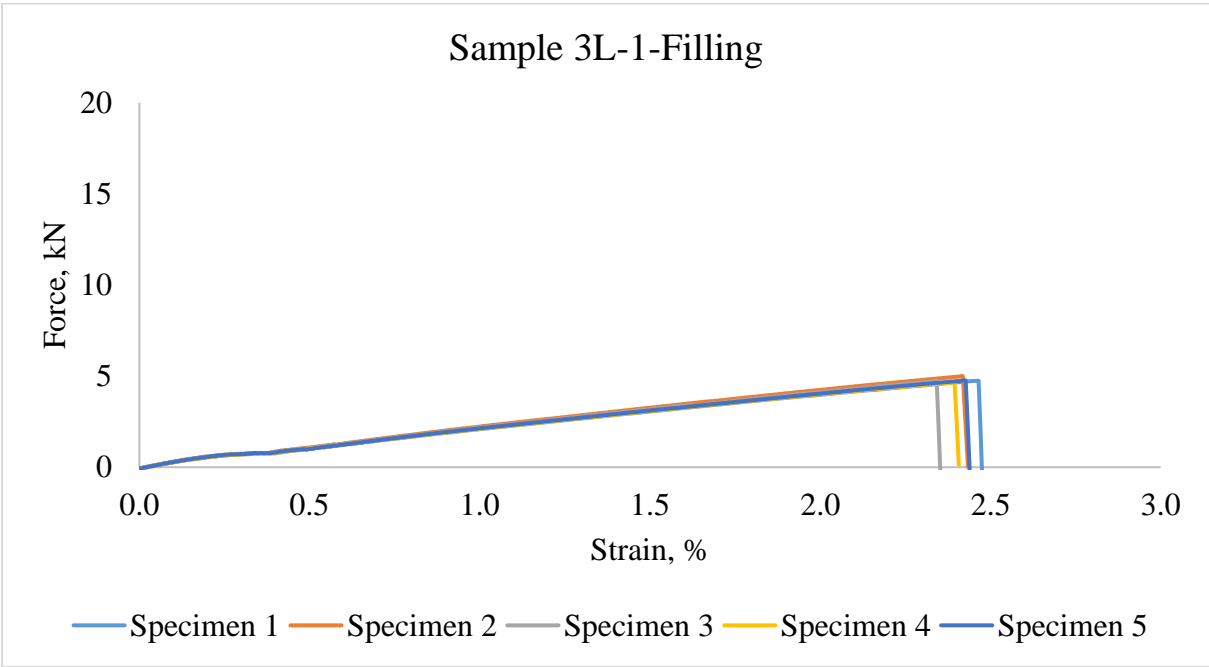
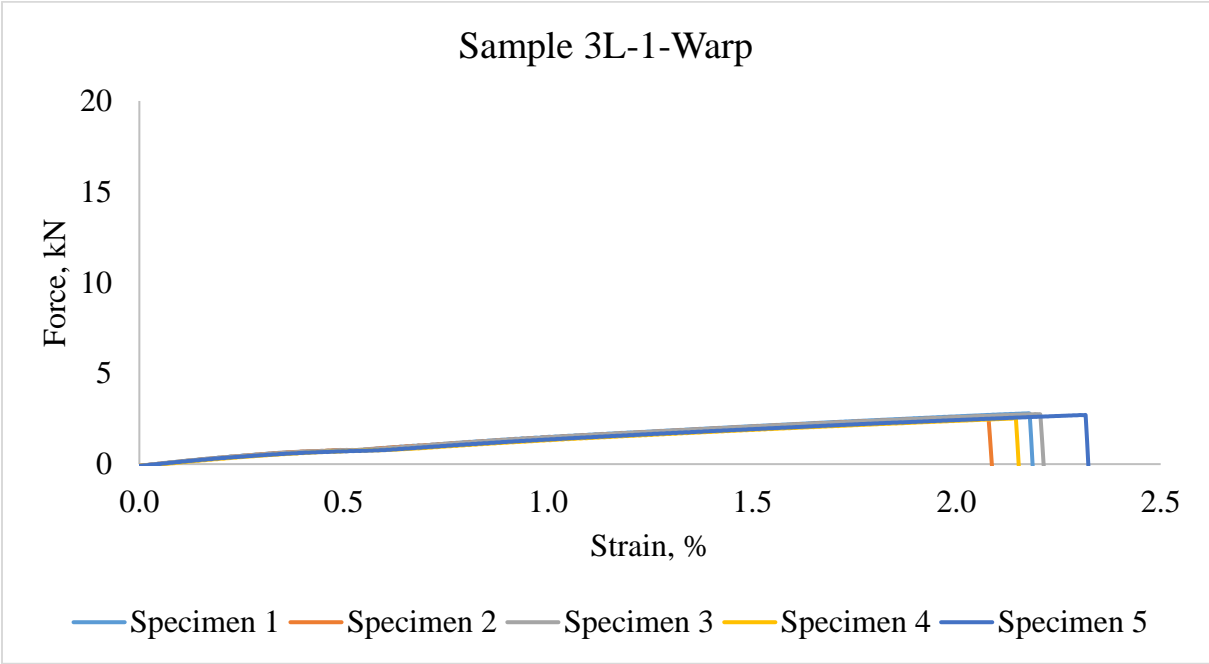
Table 47. Predicted force of 3DOW composites in the X- and Y-directions

Direction	Strain Ratio	F _{preform} , gf	F _{resin} , gf	F _{composite} , gf
X	0.0050	374732	176873	551605
	0.0150	377000	177631	554632
	0.0200	379273	178388	557661
	0.0250	381549	179143	560692
	0.0300	383830	179897	563727
	0.0345	386114	180650	566764
Y	0.0050	190875	191972	382848
	0.0150	191966	192795	384761
	0.0200	193058	193616	386674
	0.0250	194152	194436	388587
	0.0300	195247	195254	390501
	0.0345	196343	196071	392414

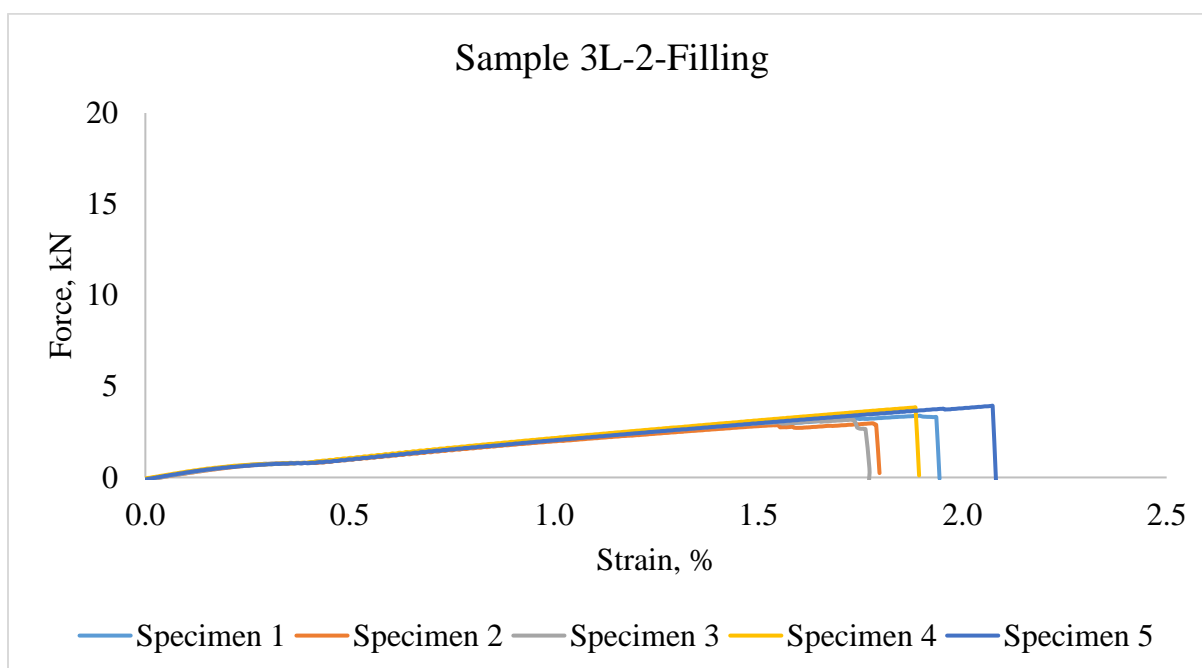
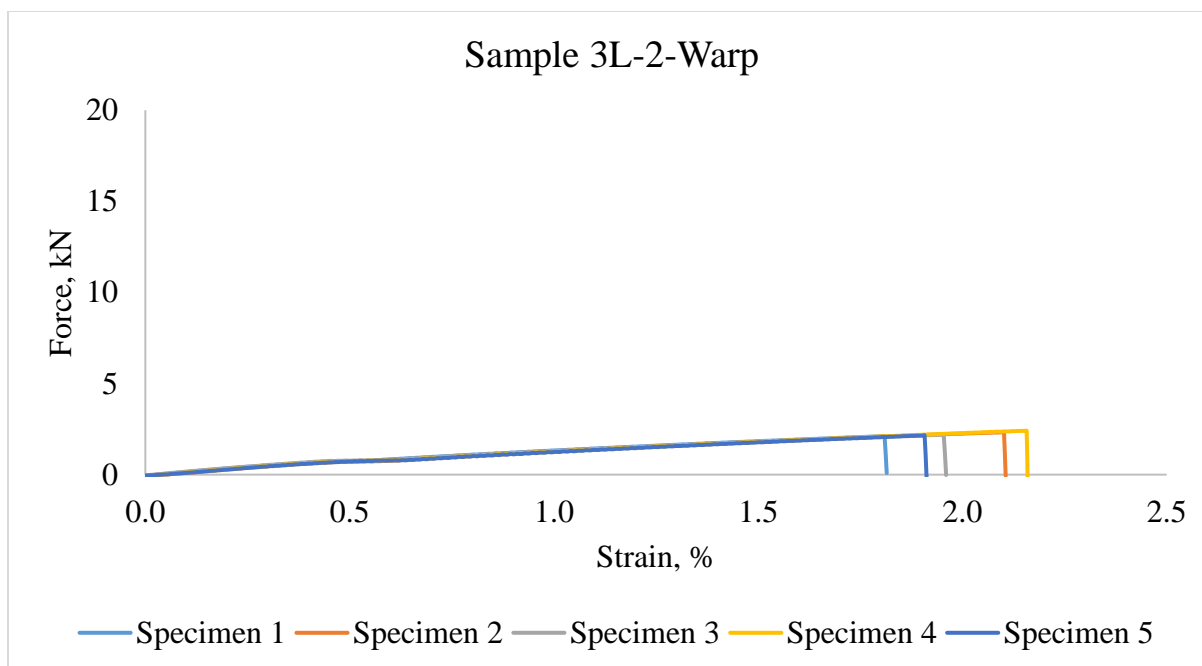
Appendix C

C.1. Load-Elongation Curves of 3DOW Composites of Tensile Test- Experimental

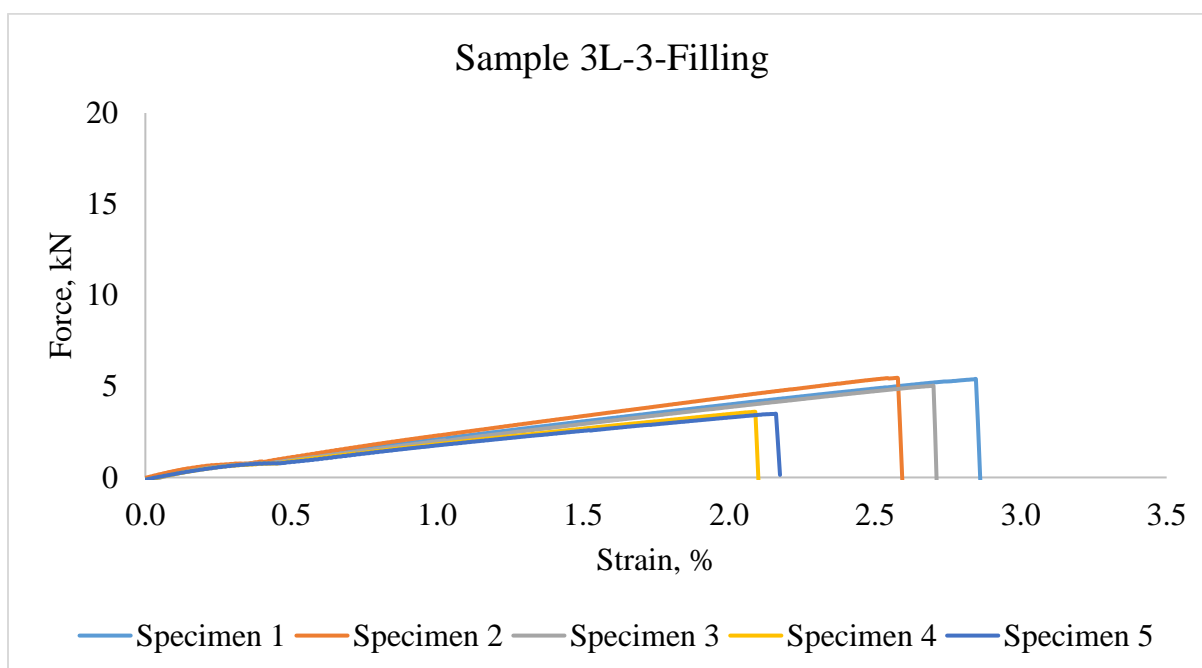
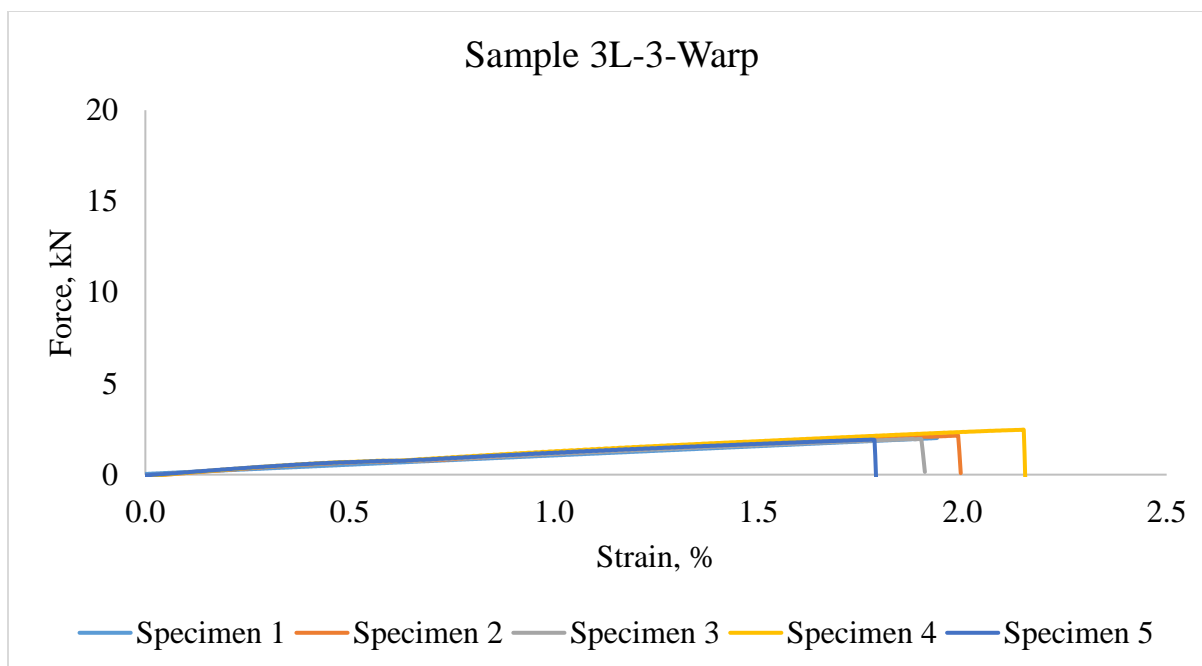
Design A



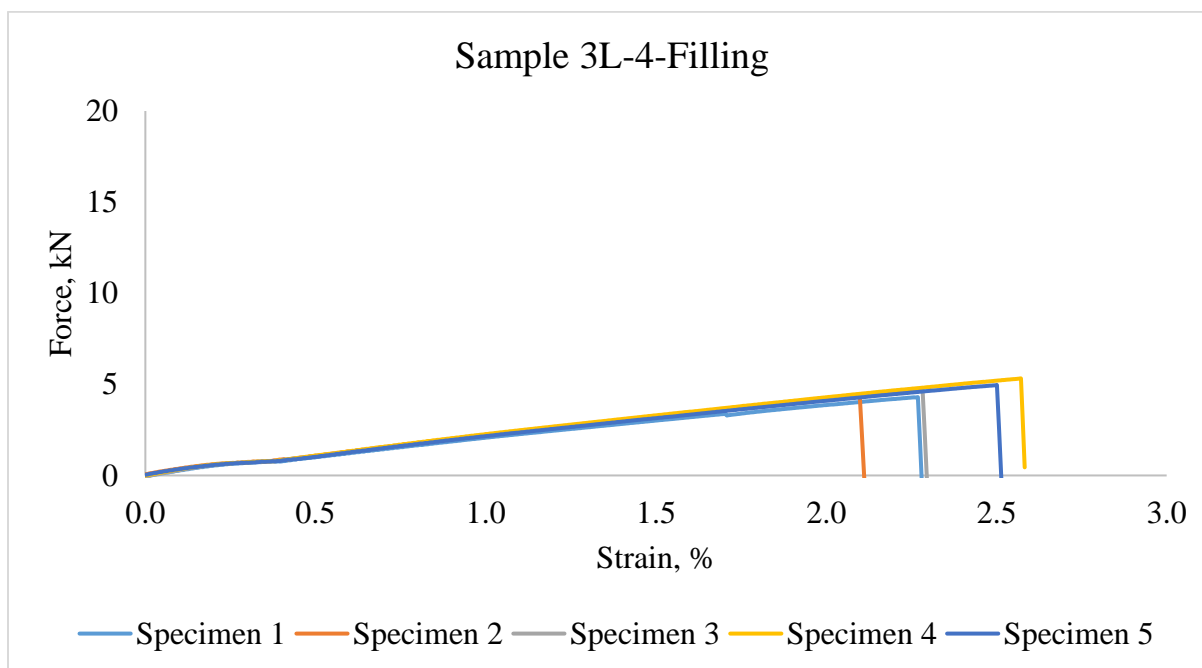
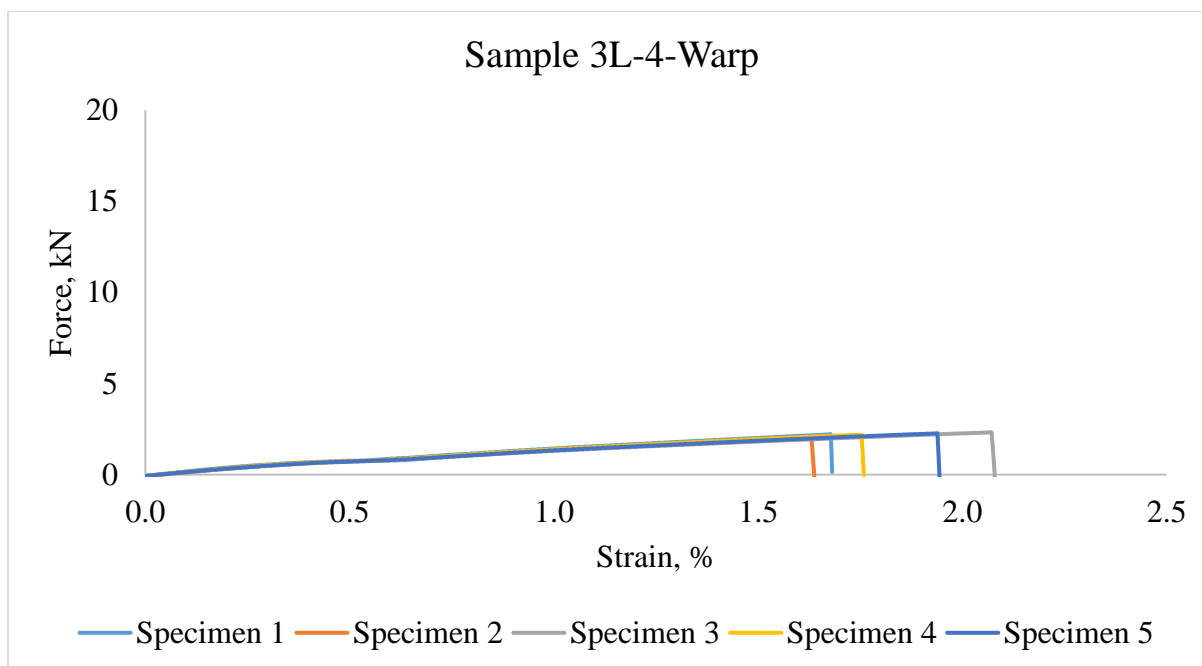
(a)



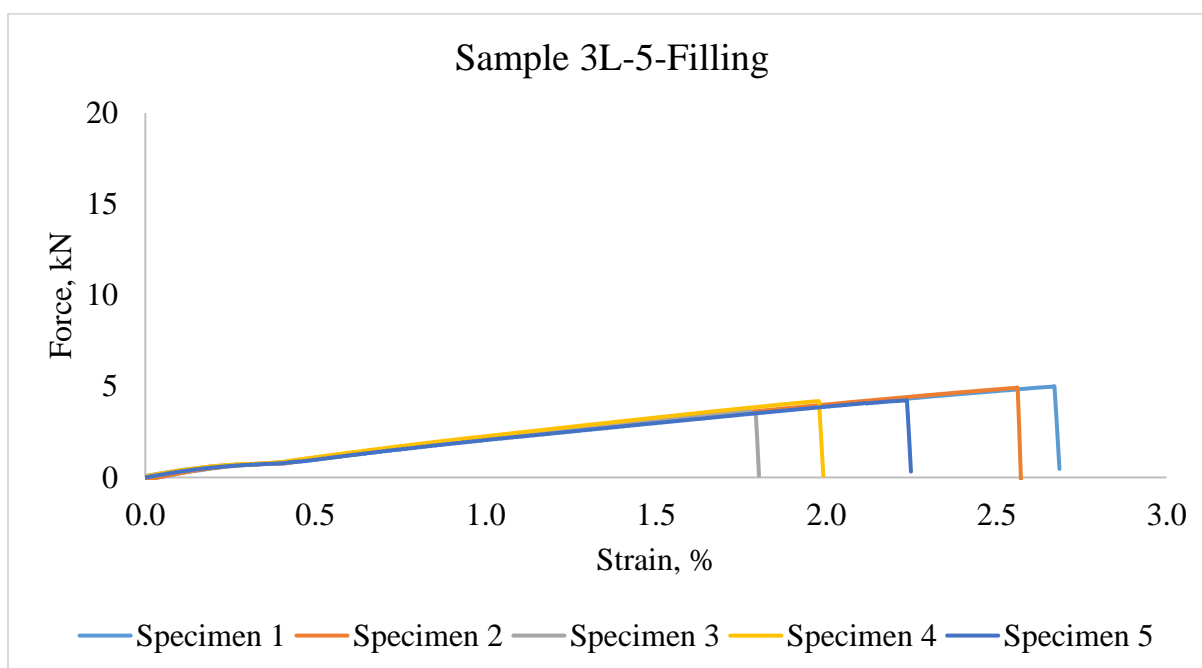
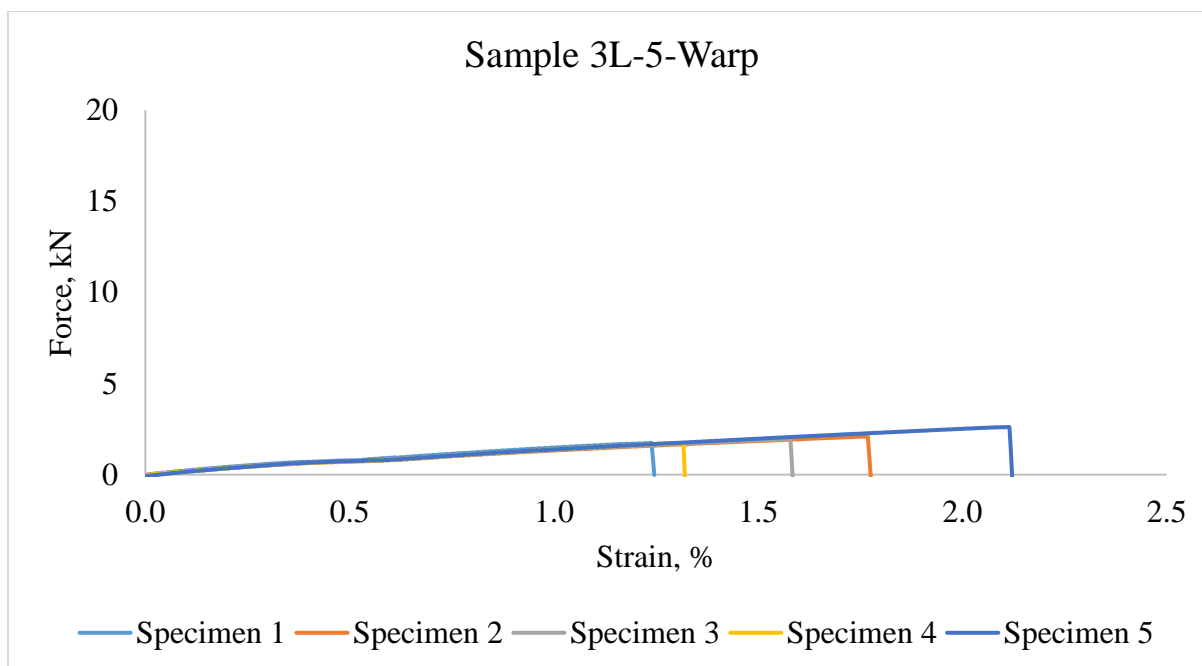
(b)



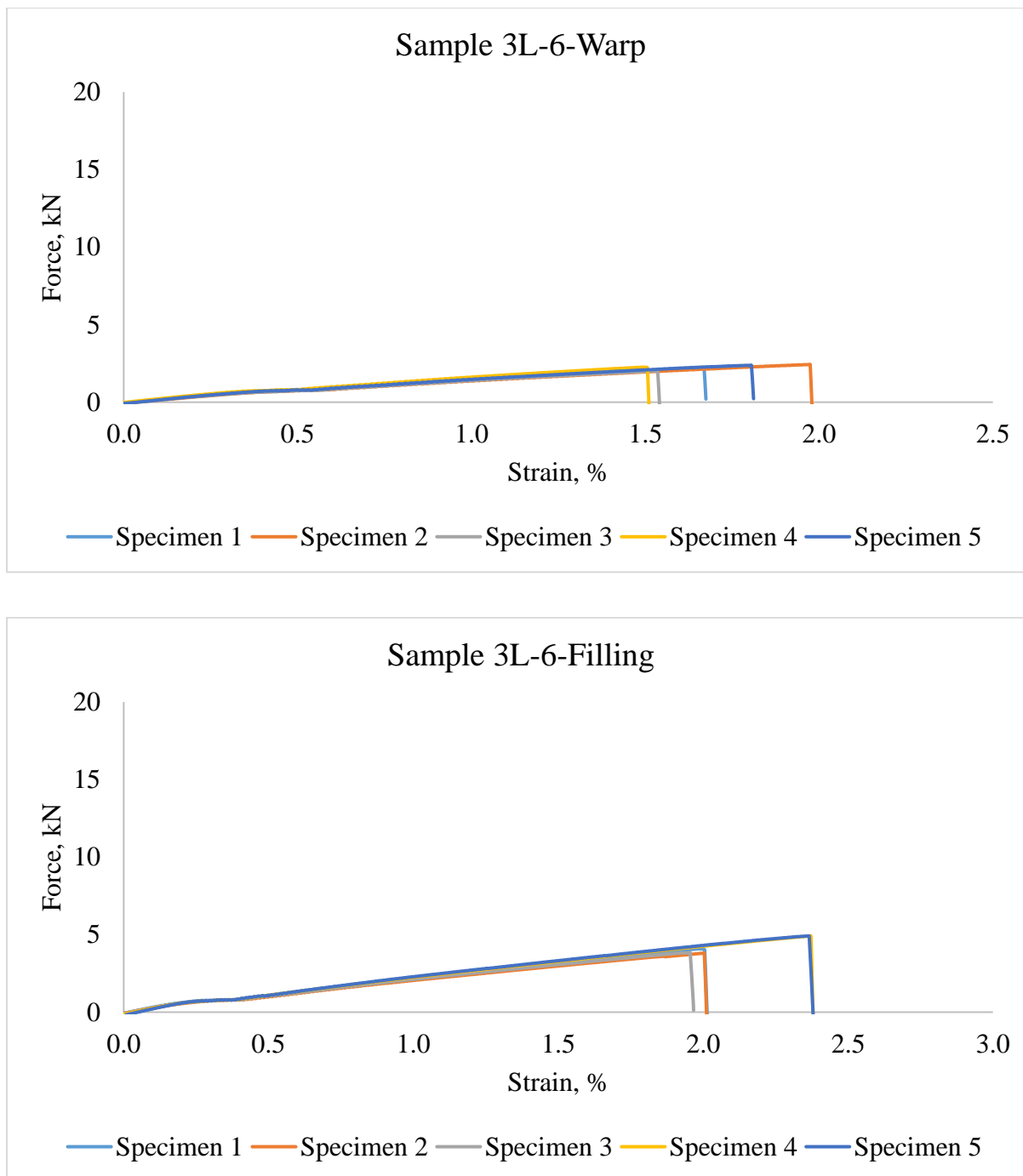
(c)



(d)



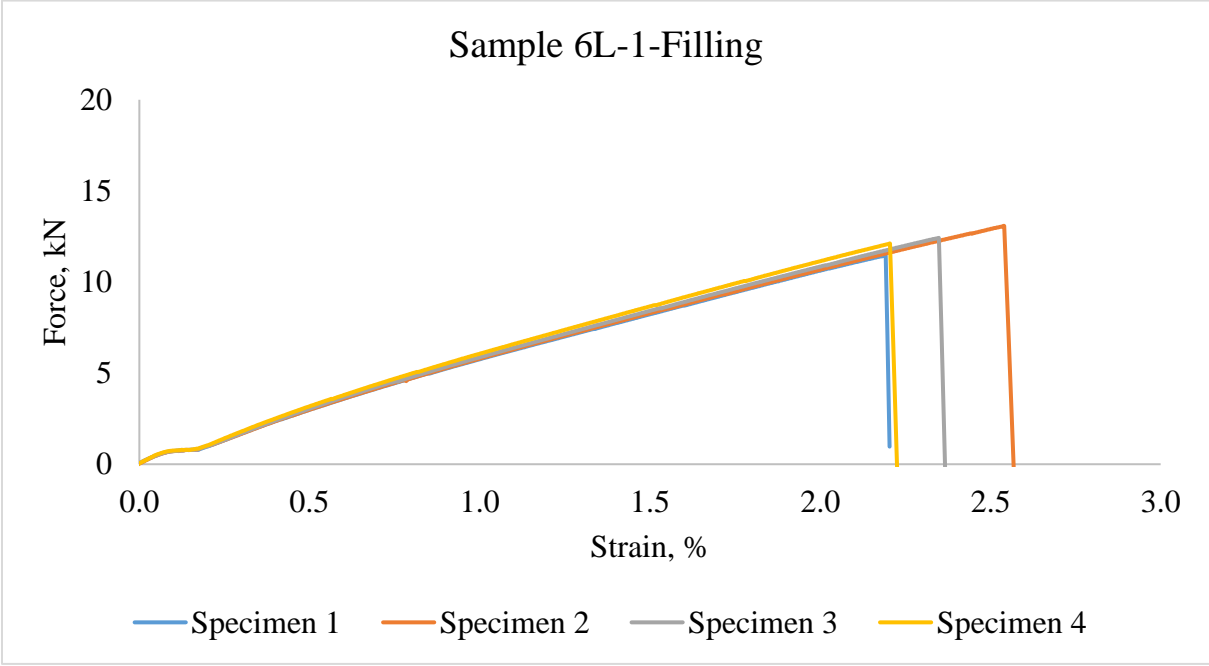
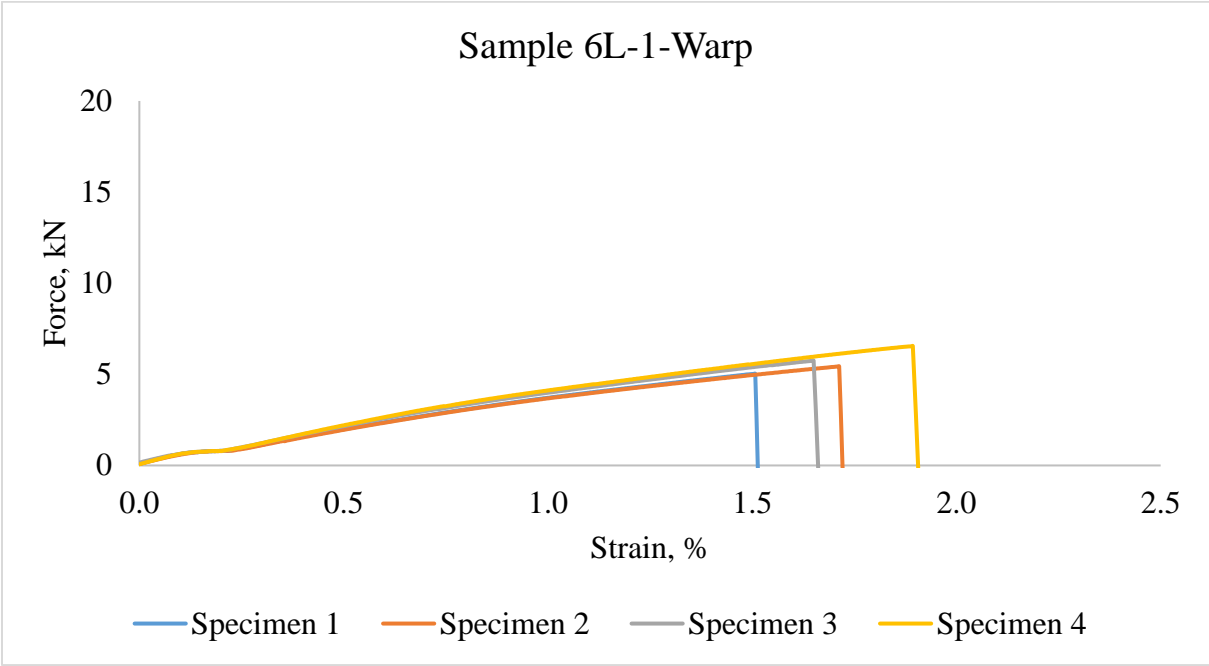
(e)



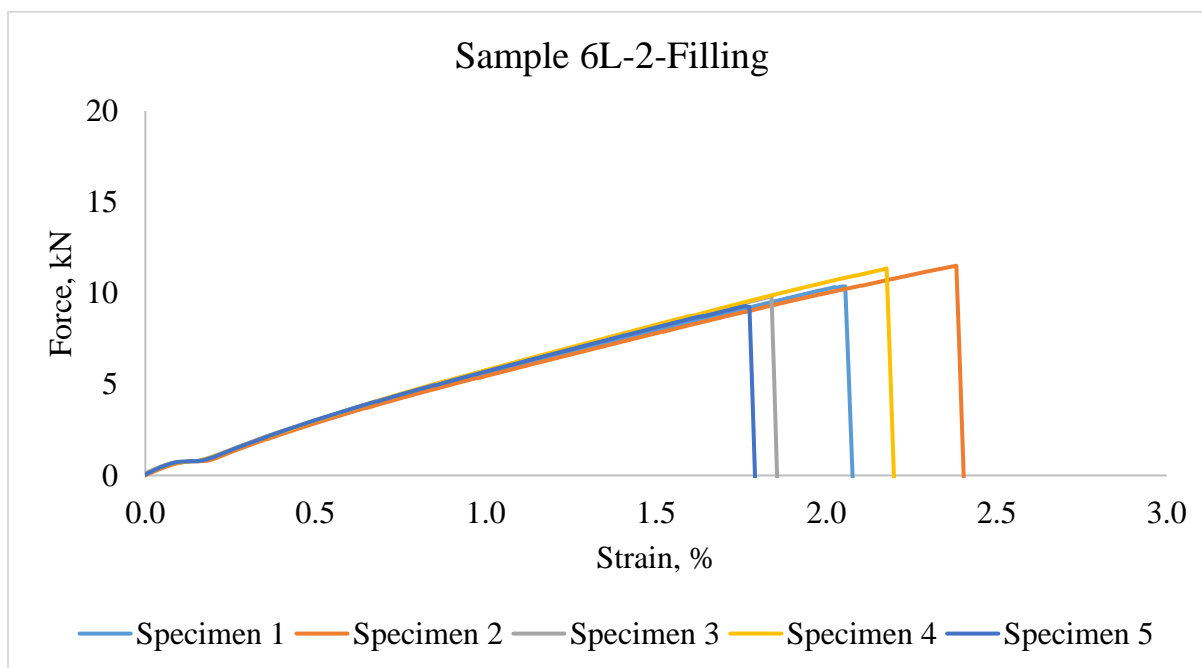
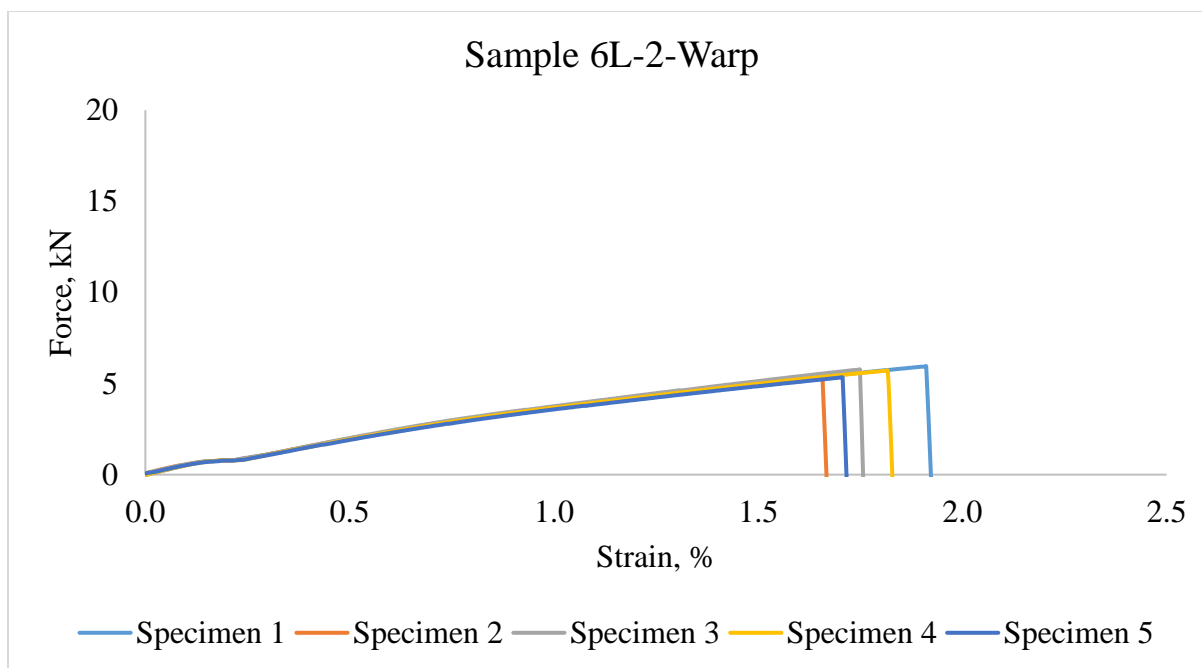
(f)

Figure 198. Load- extension curves of 3 Y-yarn layers 3DOW composites in the Y-yarn (warp) and X-yarn (filling) (a) plain and 1:1 Z to Y-yarn ratio, (b) 2x2 warp rib and 1:1 Z to Y-yarn

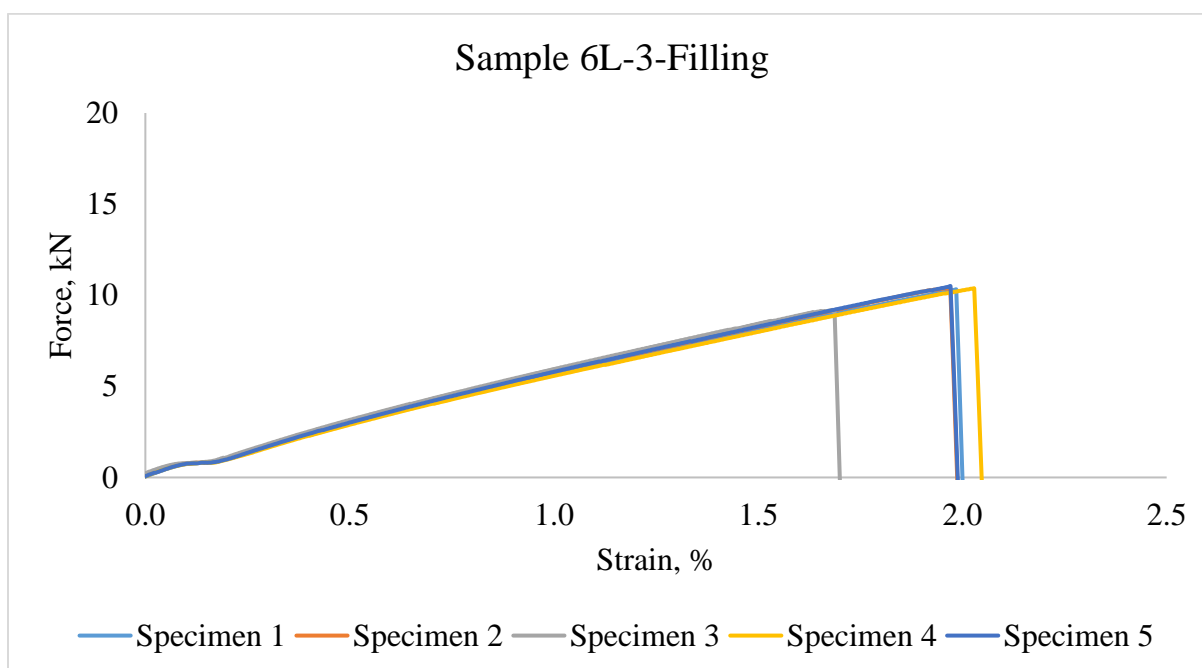
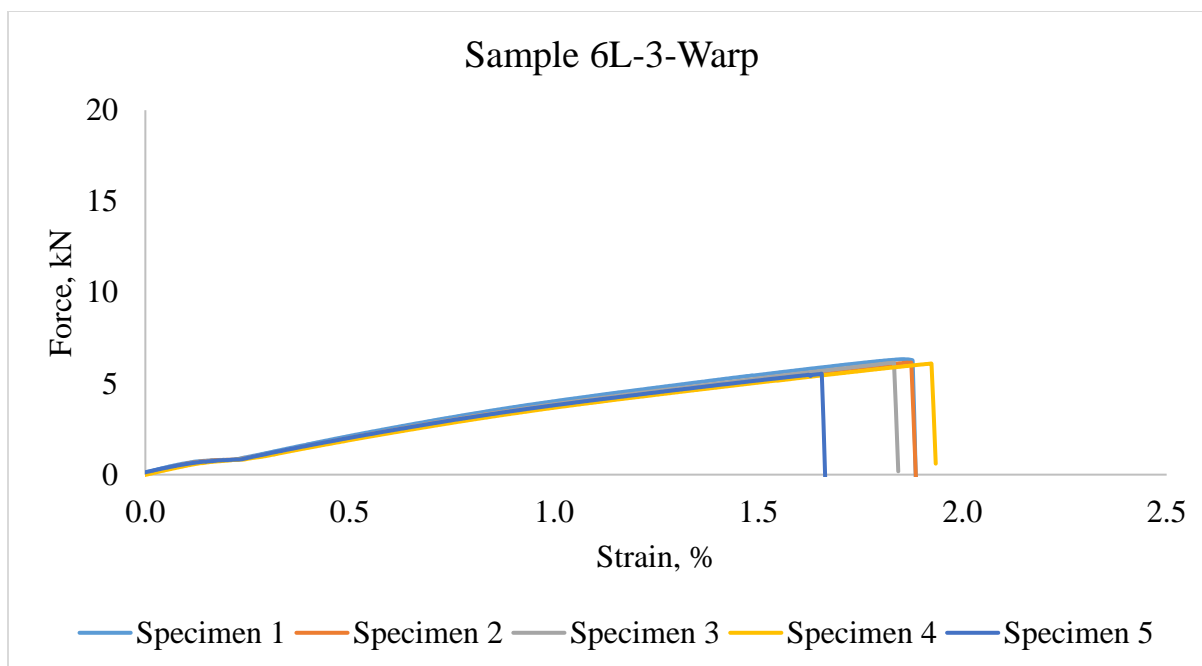
ratio, (c) 3x3 warp rib and 1:1 Z to Y-yarn ratio, (d) plain and 1:3 Z to Y-yarn ratio, (e) 2x2 warp rib and 1:3 Z to Y-yarn ratio, (f) 3x3 warp rib and 1:3 Z to Y-yarn ratio



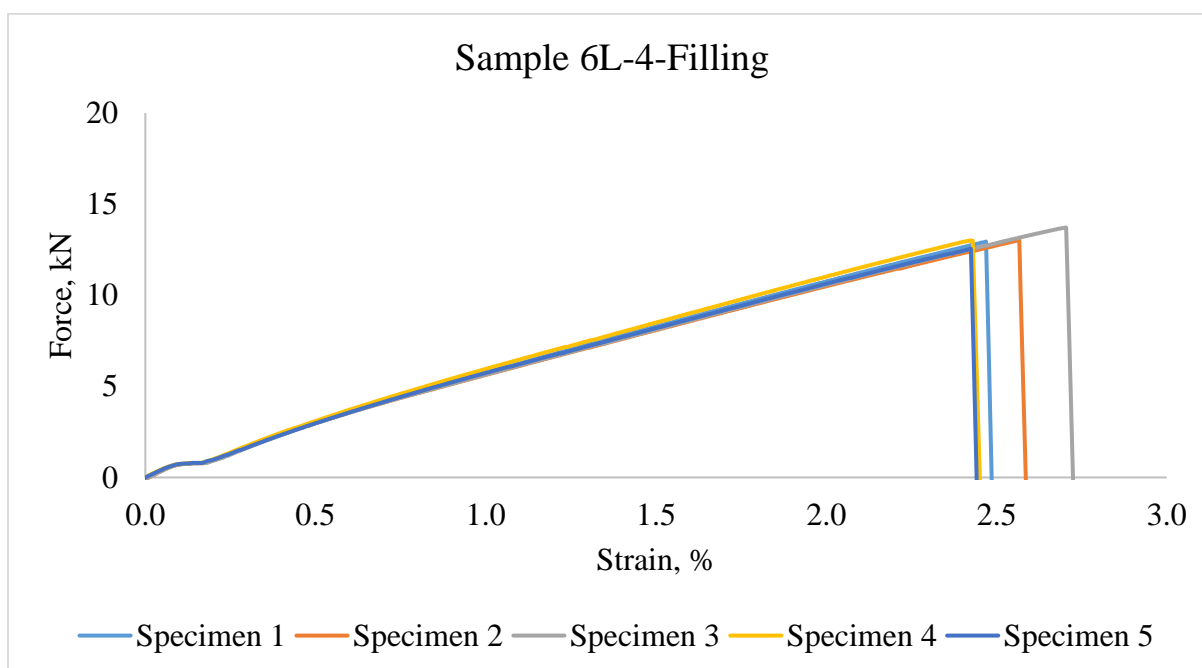
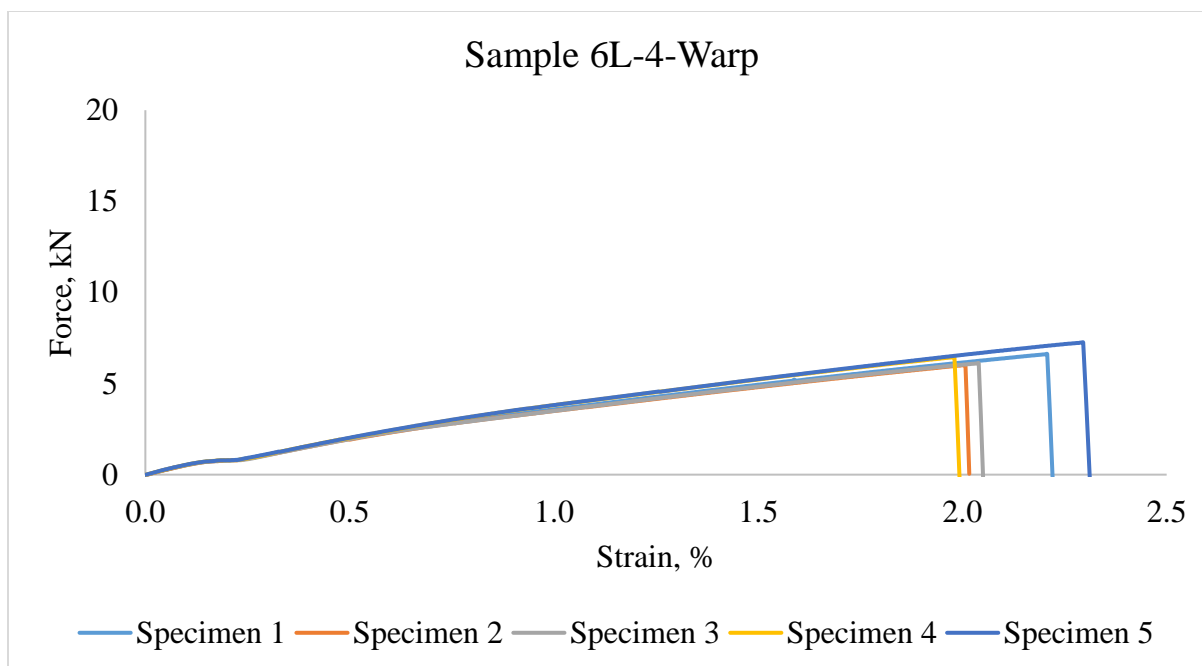
(a)



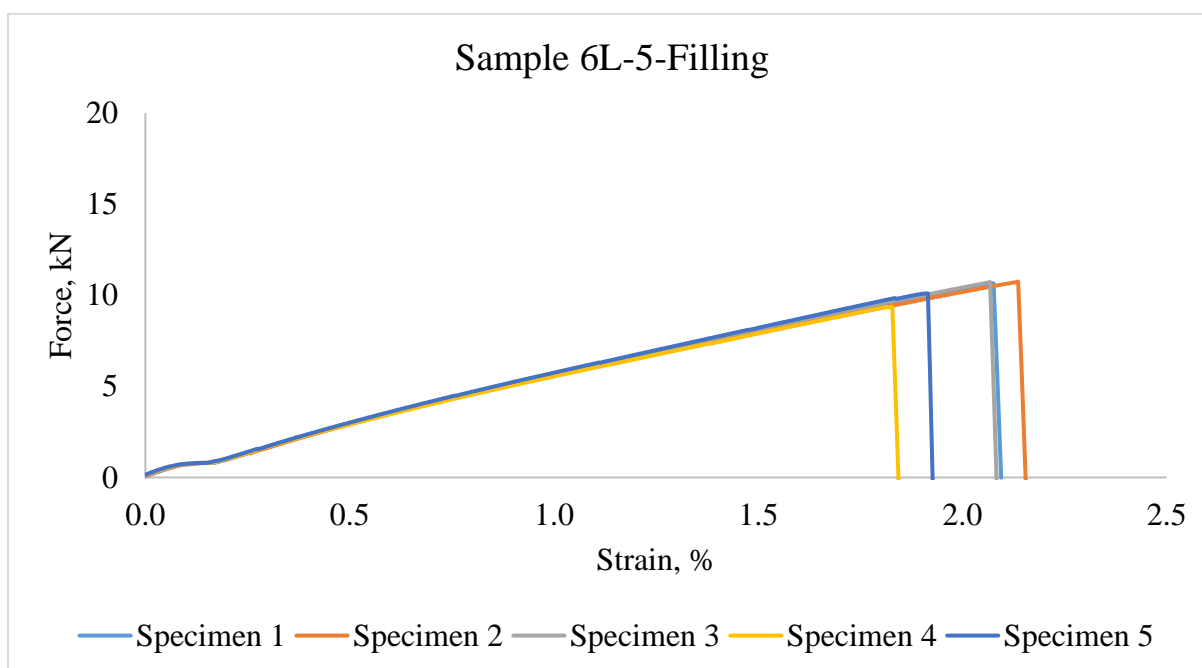
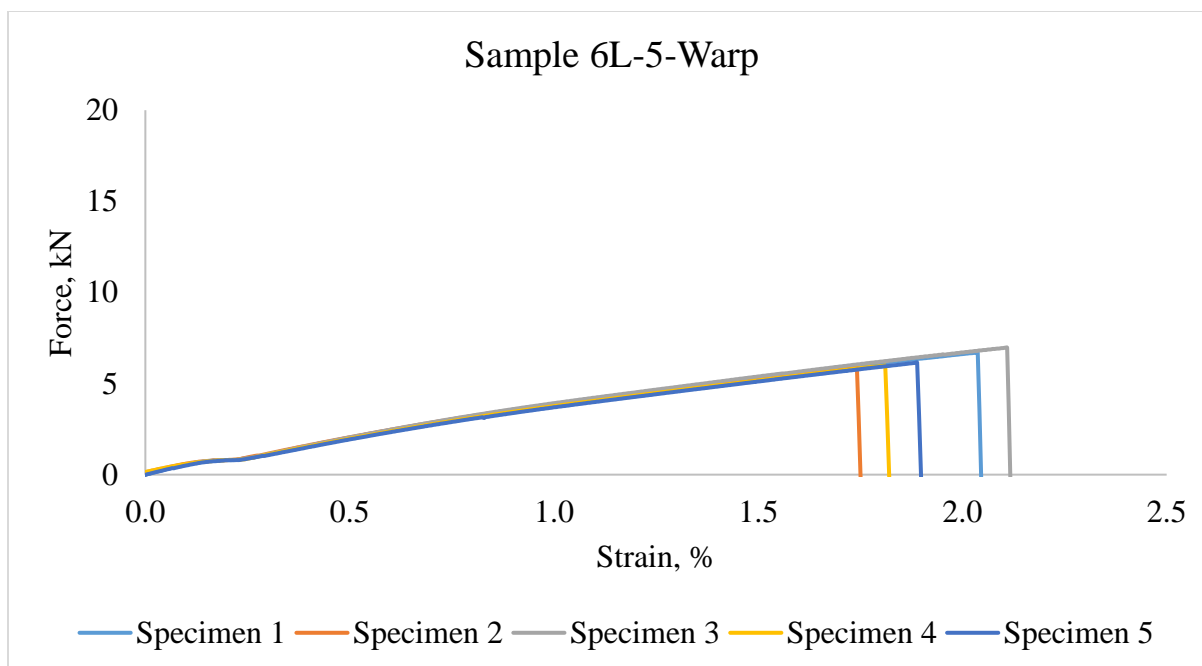
(b)



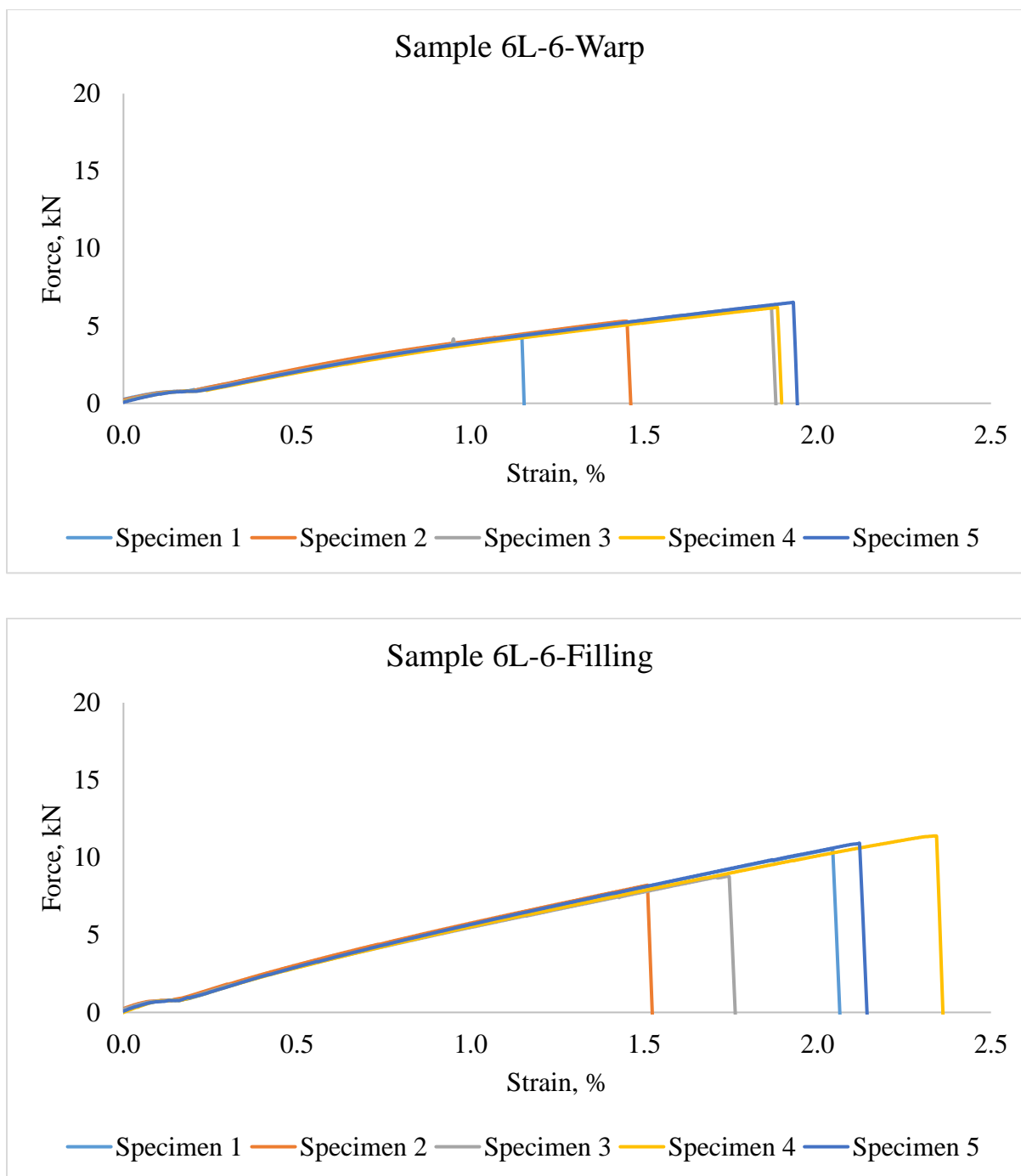
(c)



(d)



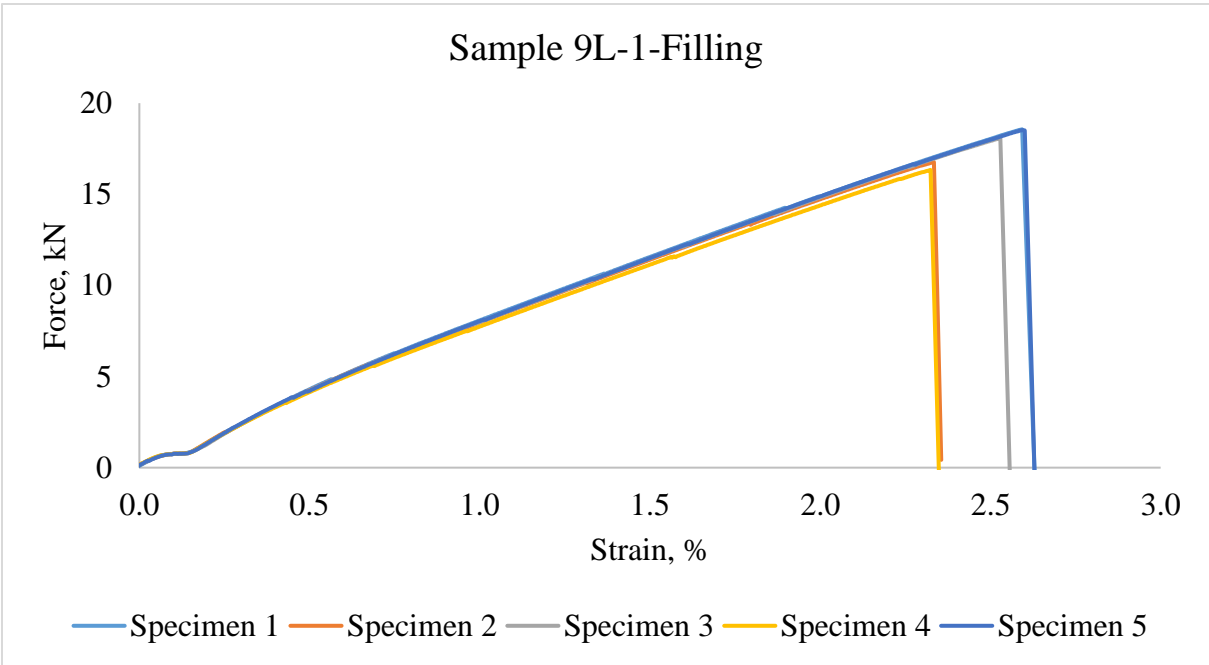
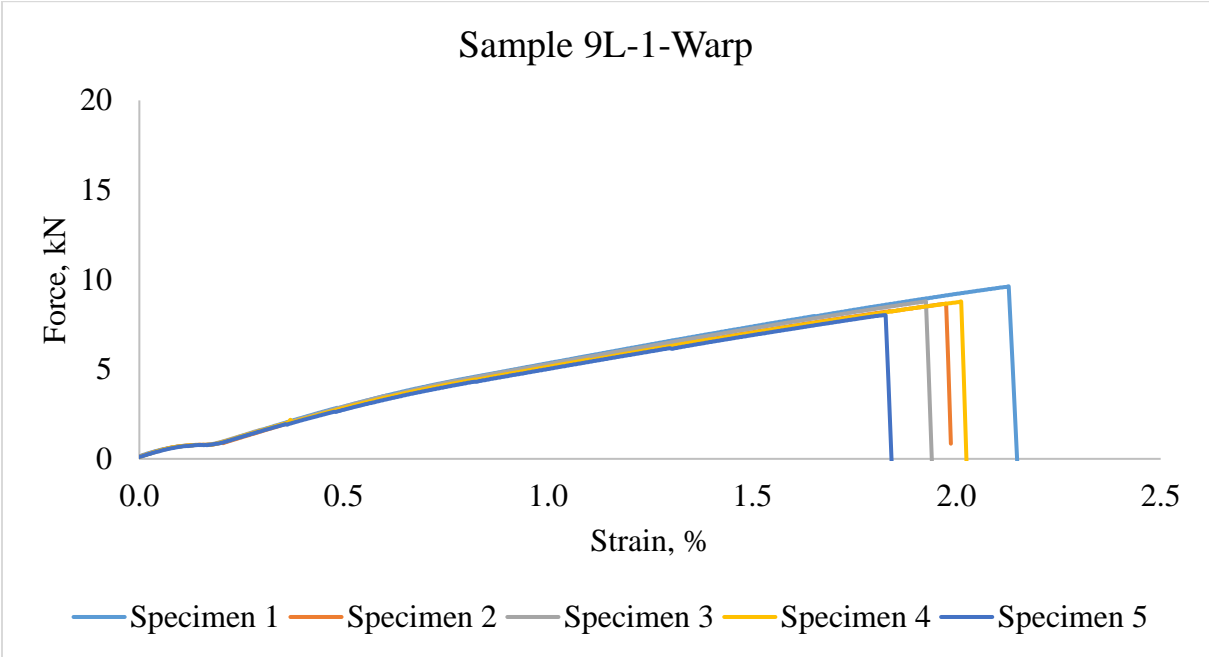
(e)



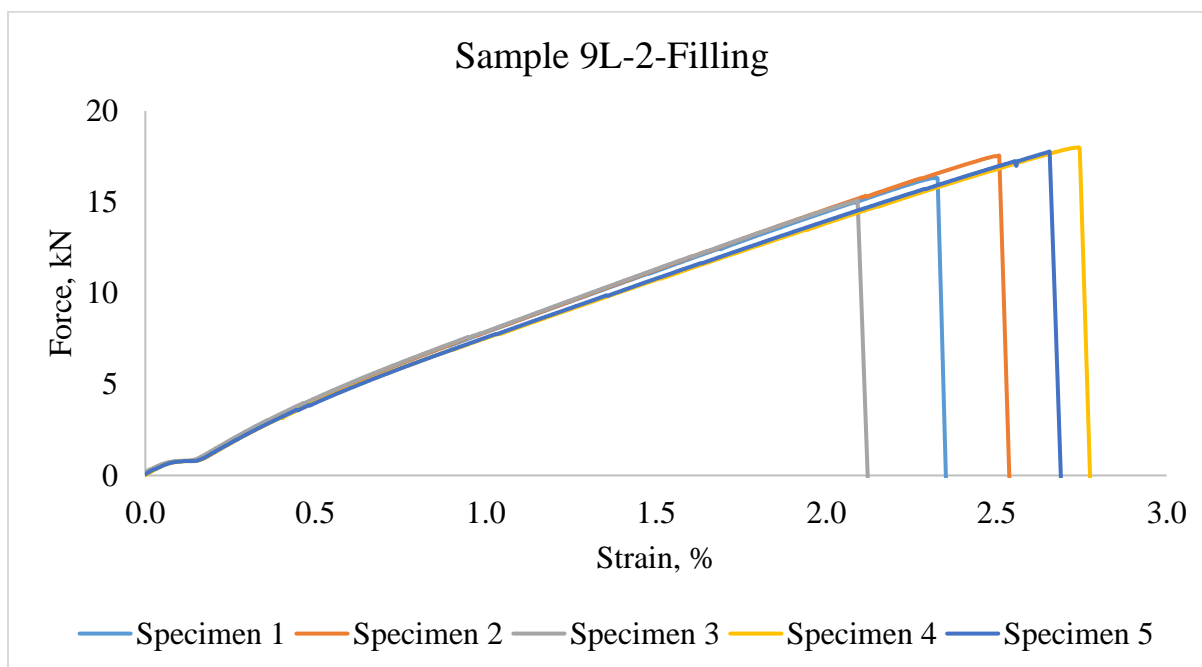
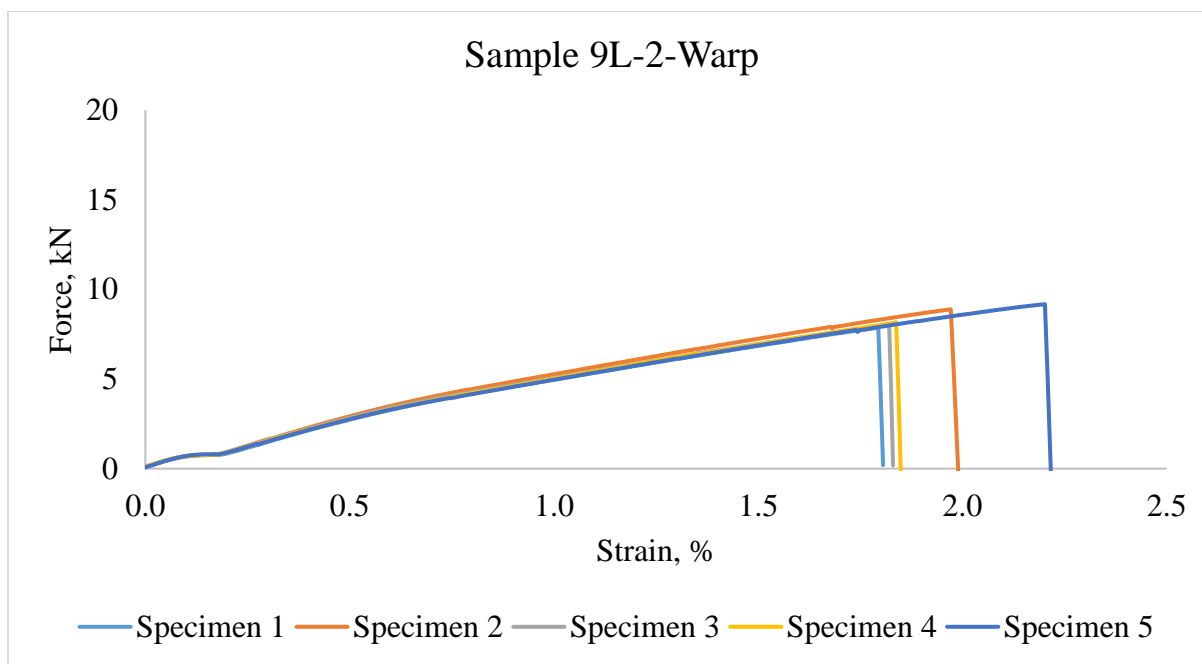
(f)

Figure 199. Load- extension curves of 6 Y-yarn layers 3DOW composites in the Y-yarn (warp) and X-yarn (filling) (a) plain and 1:1 Z to Y-yarn ratio, (b) 2x2 warp rib and 1:1 Z to Y-yarn

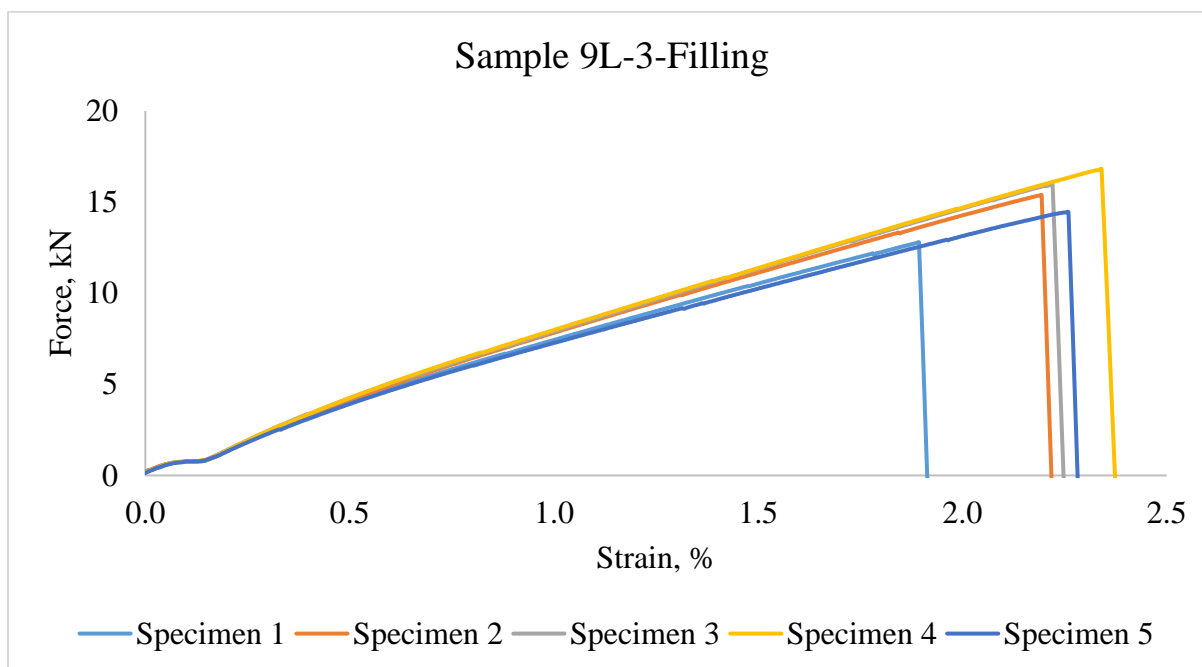
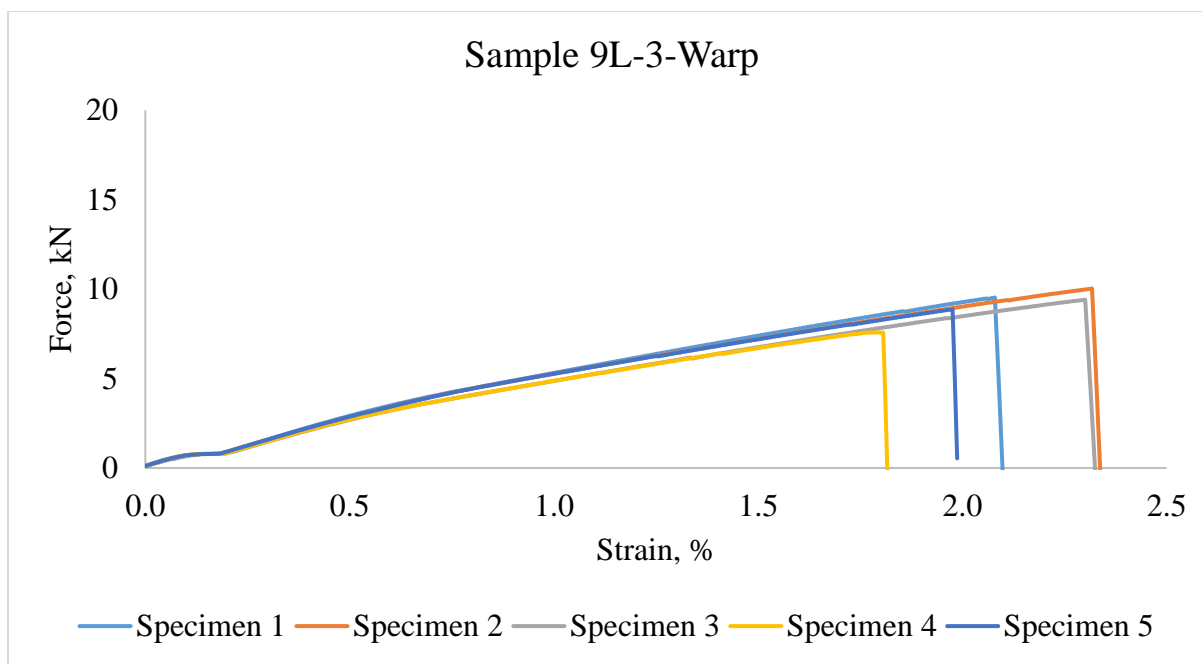
ratio, (c) 3x3 warp rib and 1:1 Z to Y-yarn ratio, (d) plain and 1:3 Z to Y-yarn ratio, (e) 2x2 warp rib and 1:3 Z to Y-yarn ratio, (f) 3x3 warp rib and 1:3 Z to Y-yarn ratio



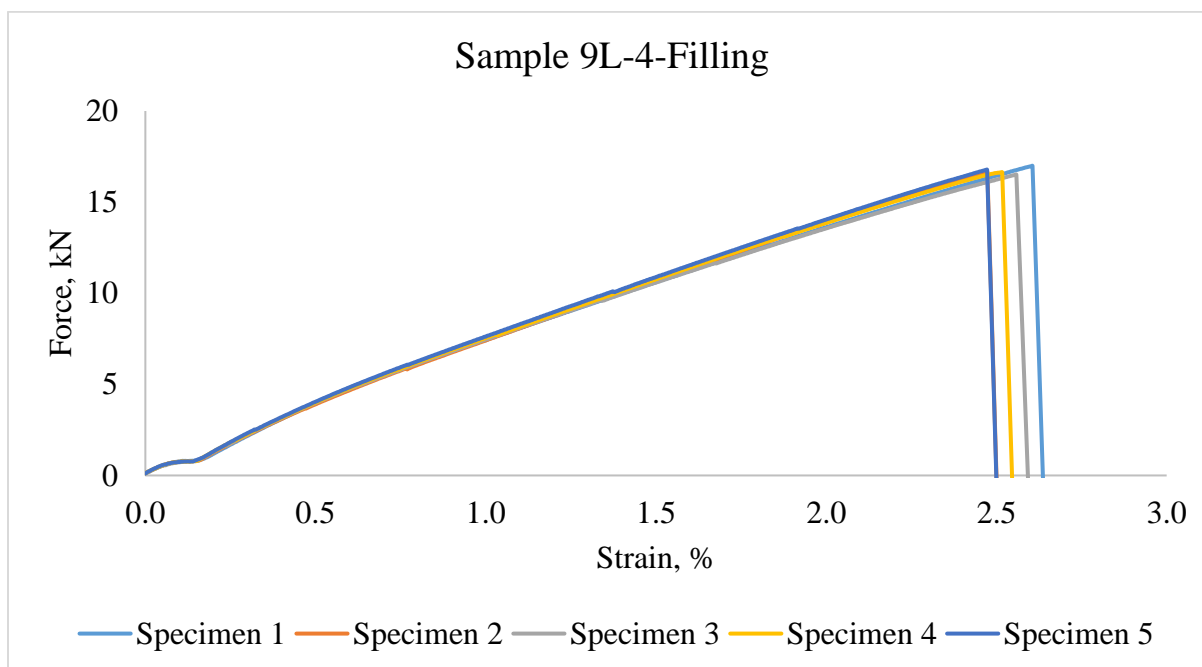
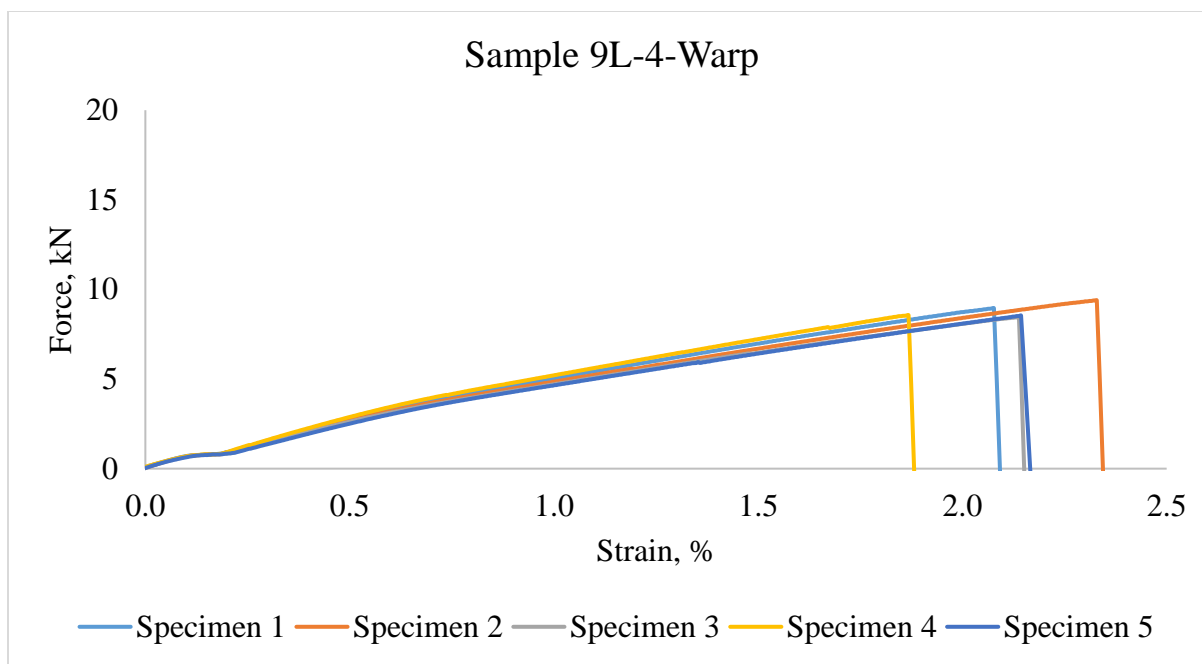
(a)



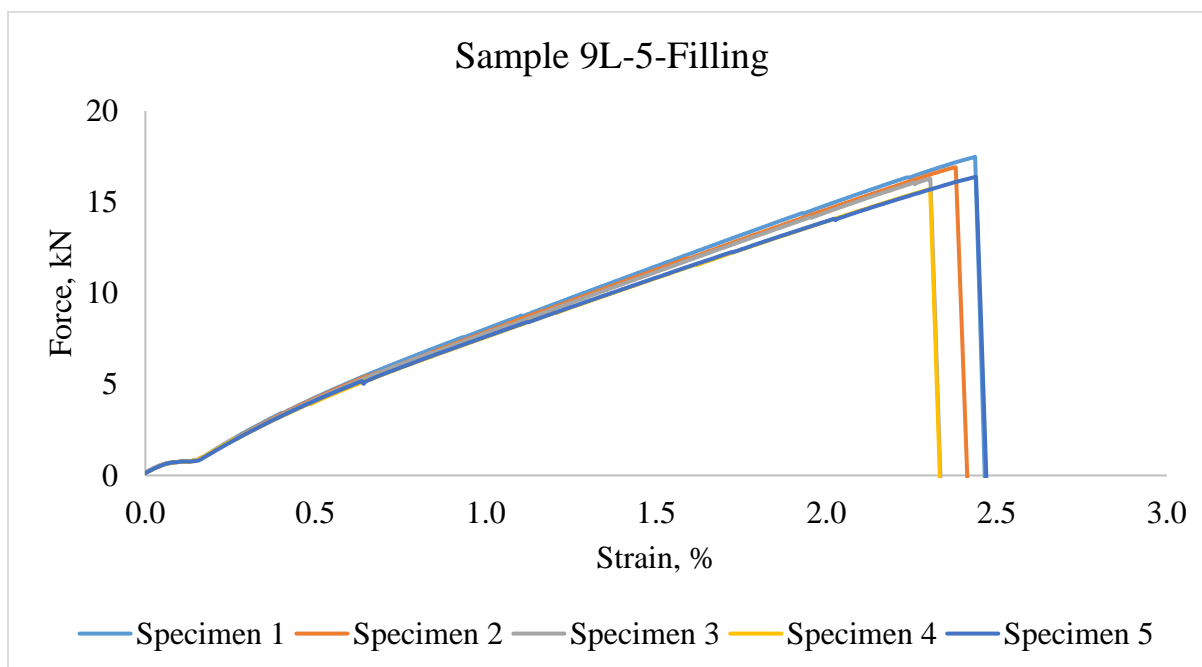
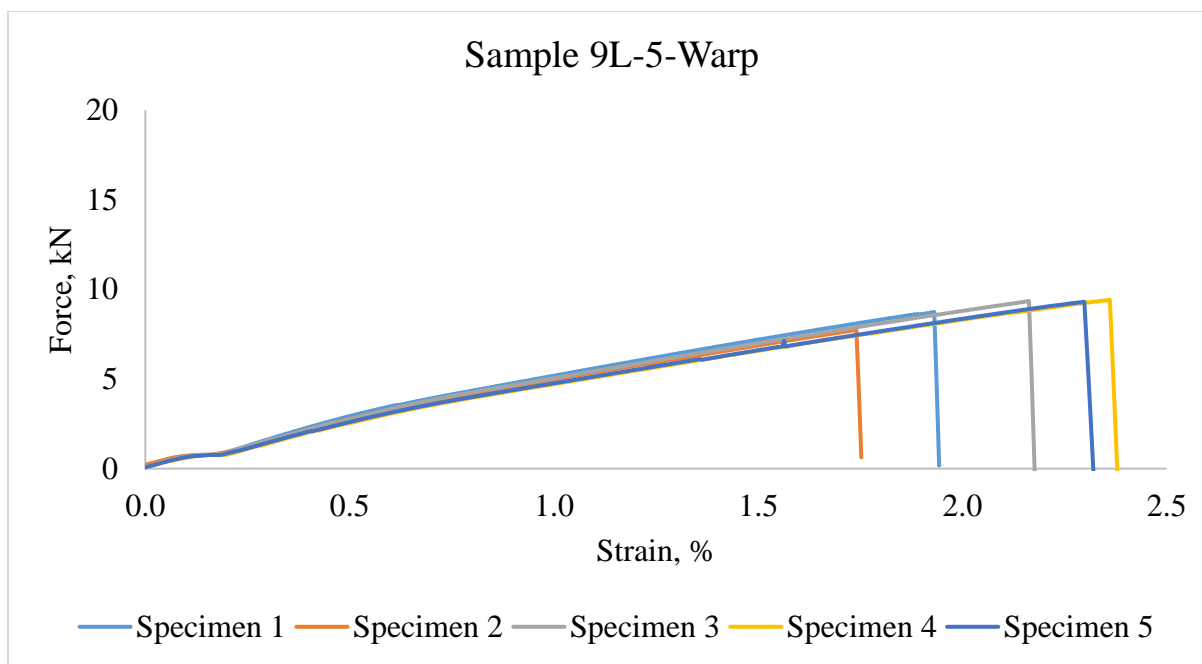
(b)



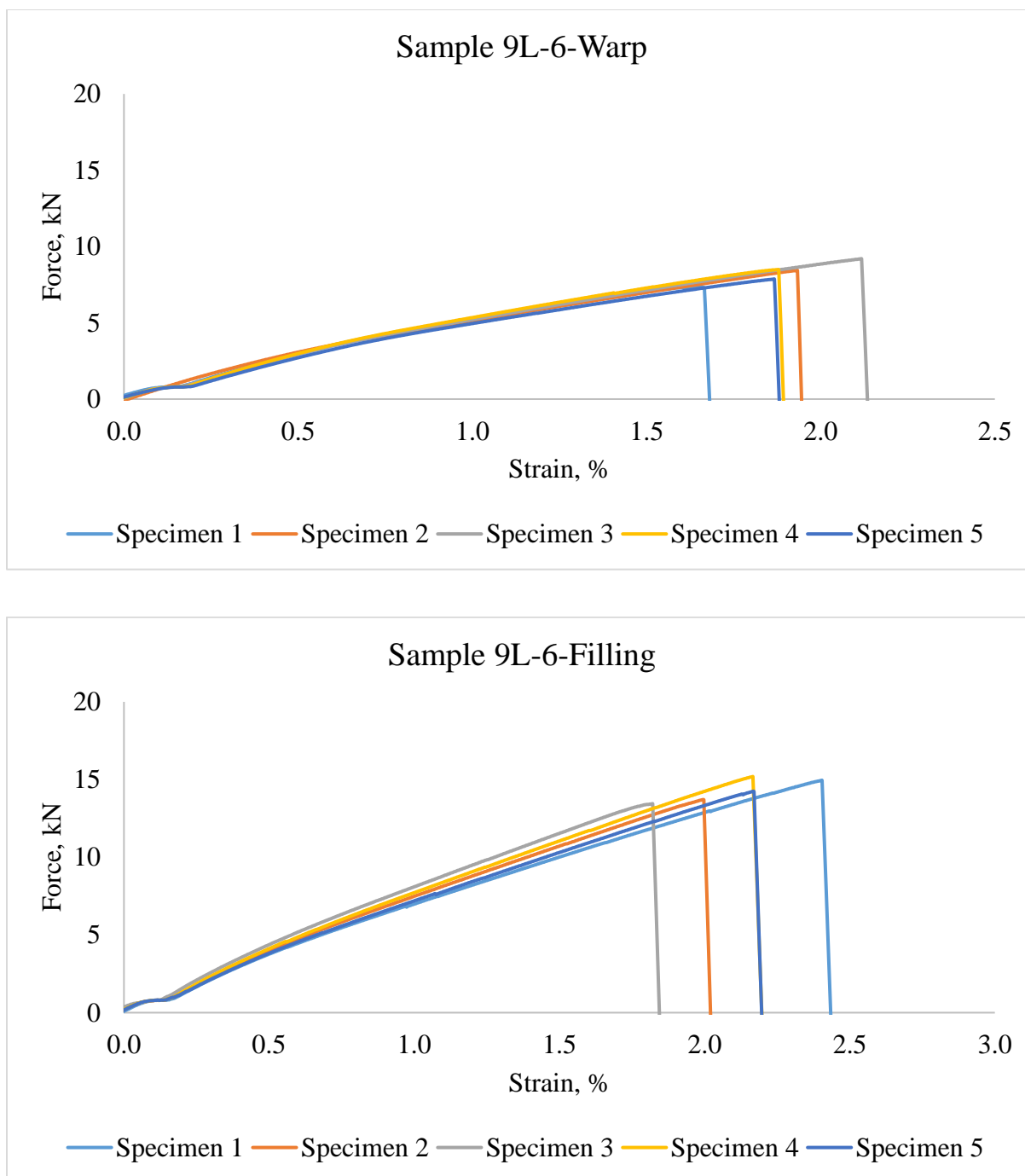
(c)



(d)



(e)



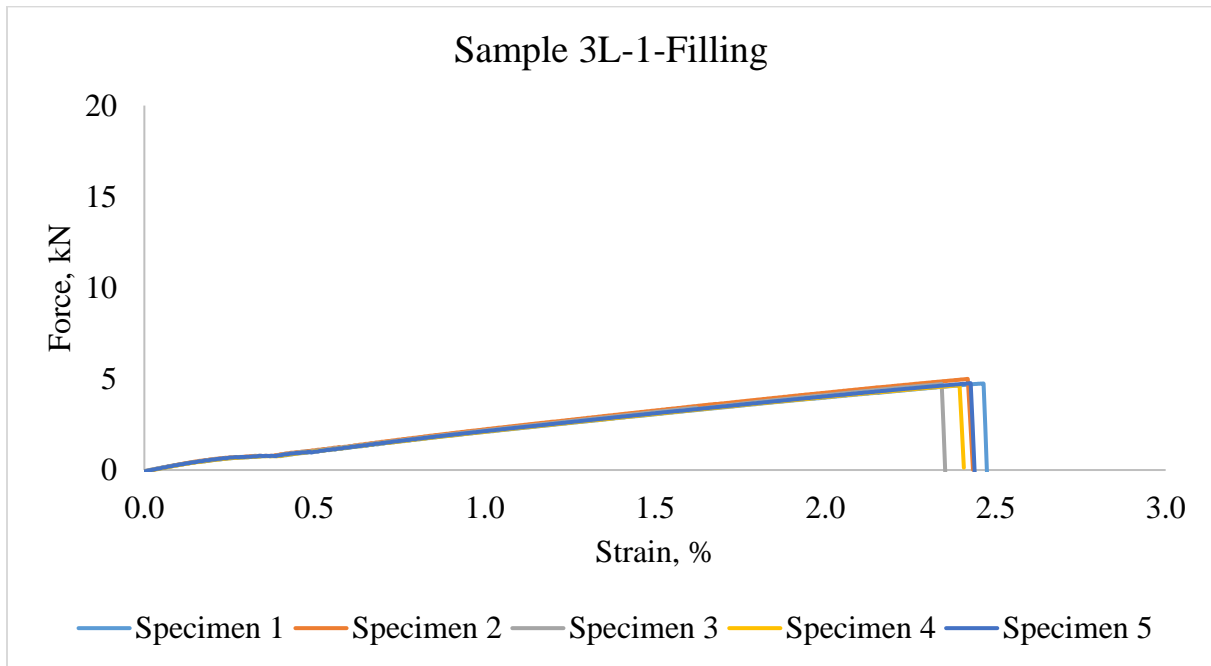
(f)

Figure 200. Load- extension curves of 9 Y-yarn layers 3DOW composites in the Y-yarn (warp) and X-yarn (filling) (a) plain and 1:1 Z to Y-yarn ratio, (b) 2x2 warp rib and 1:1 Z to Y-yarn

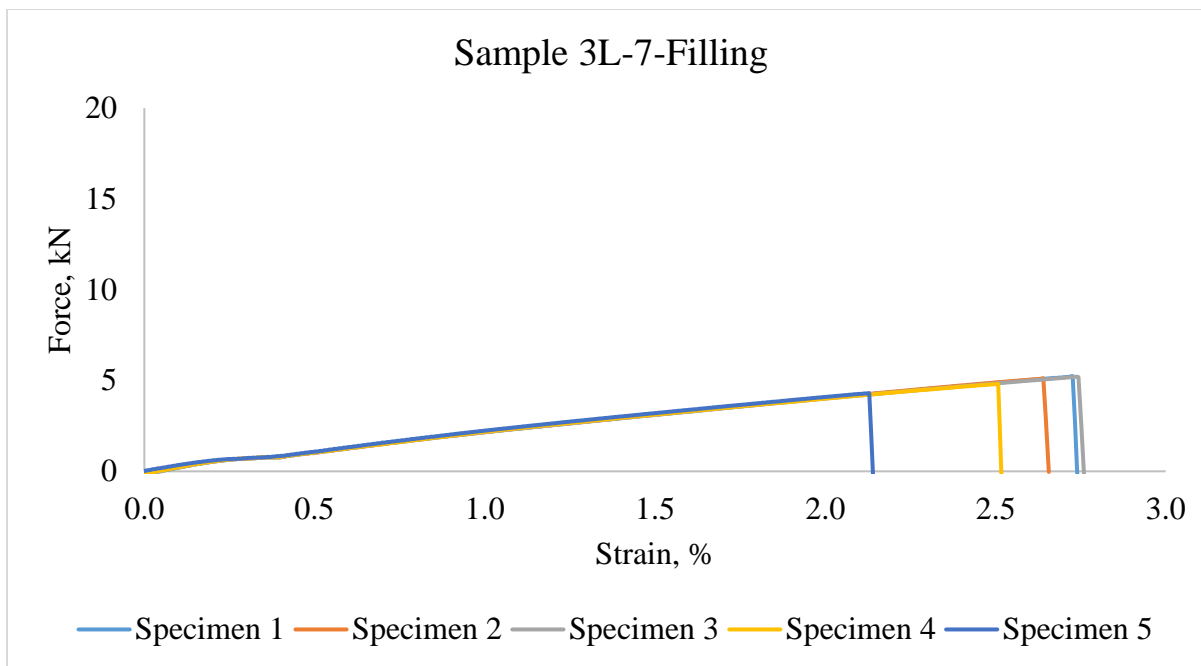
ratio, (c) 3x3 warp rib and 1:1 Z to Y-yarn ratio, (d) plain and 1:3 Z to Y-yarn ratio, (e) 2x2 warp rib and 1:3 Z to Y-yarn ratio, (f) 3x3 warp rib and 1:3 Z to Y-yarn ratio

C.2. Load-Elongation Curves of 3DOW Composites of Tensile Test- Experimental

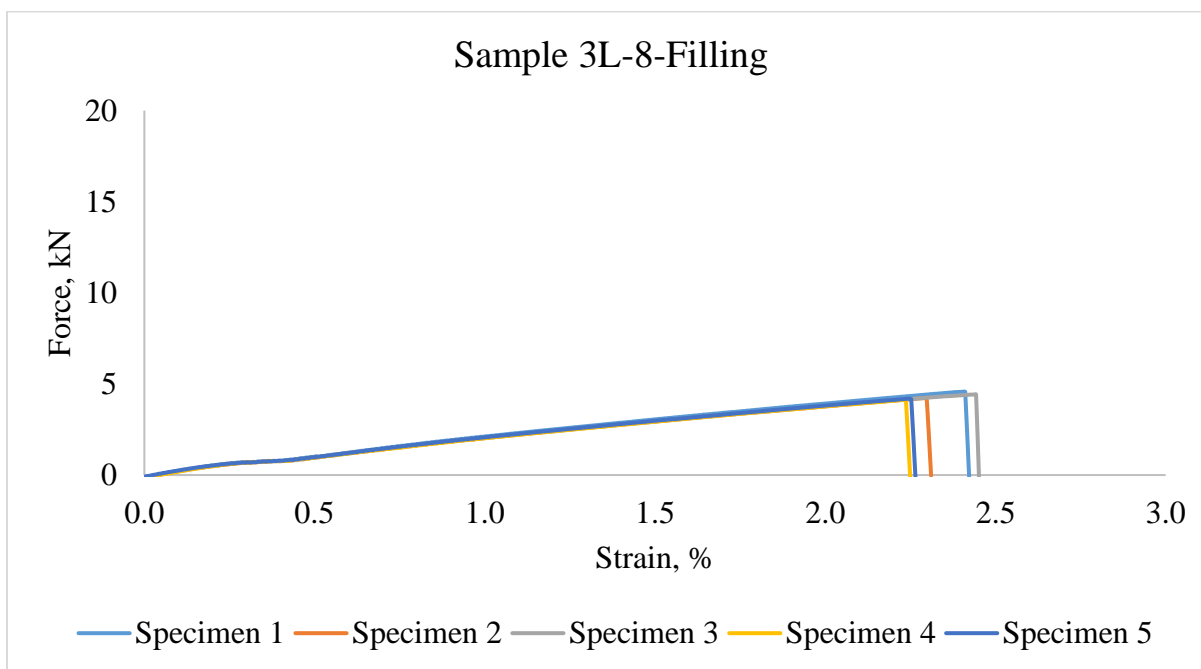
Design B



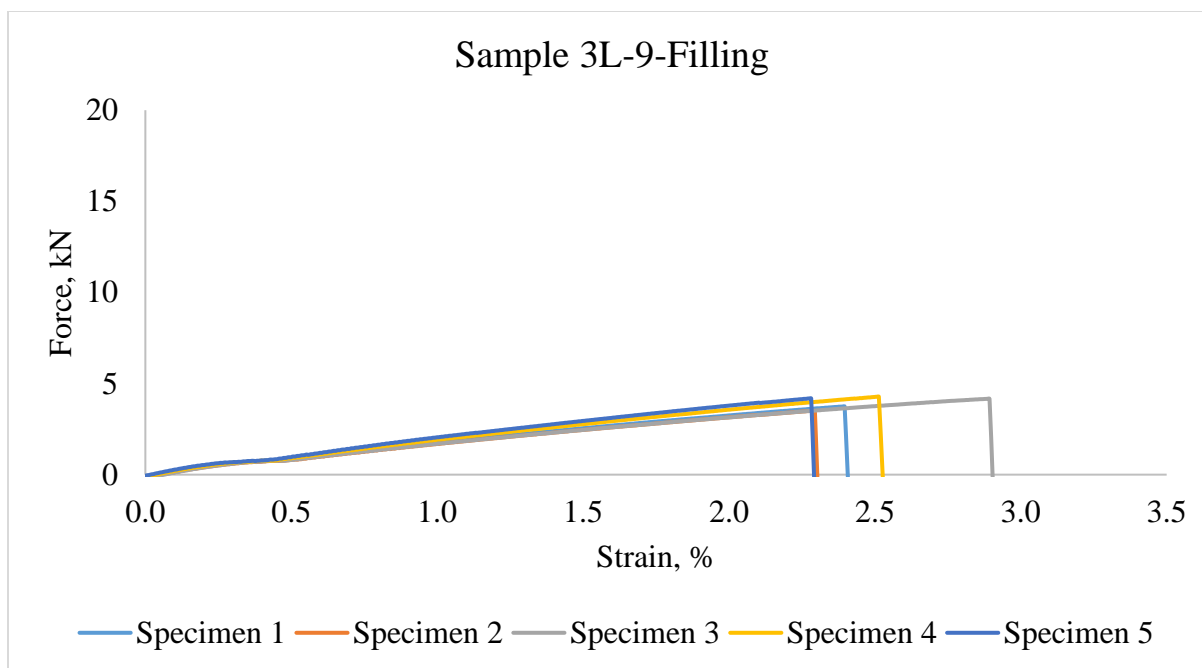
(a)



(b)



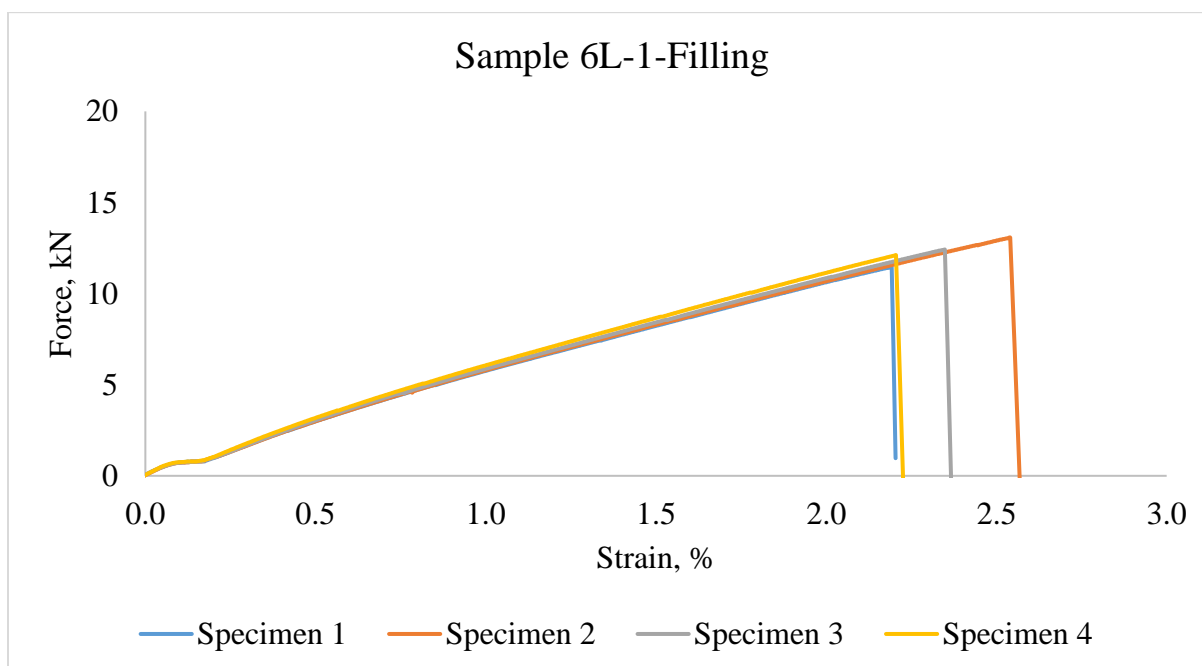
(c)



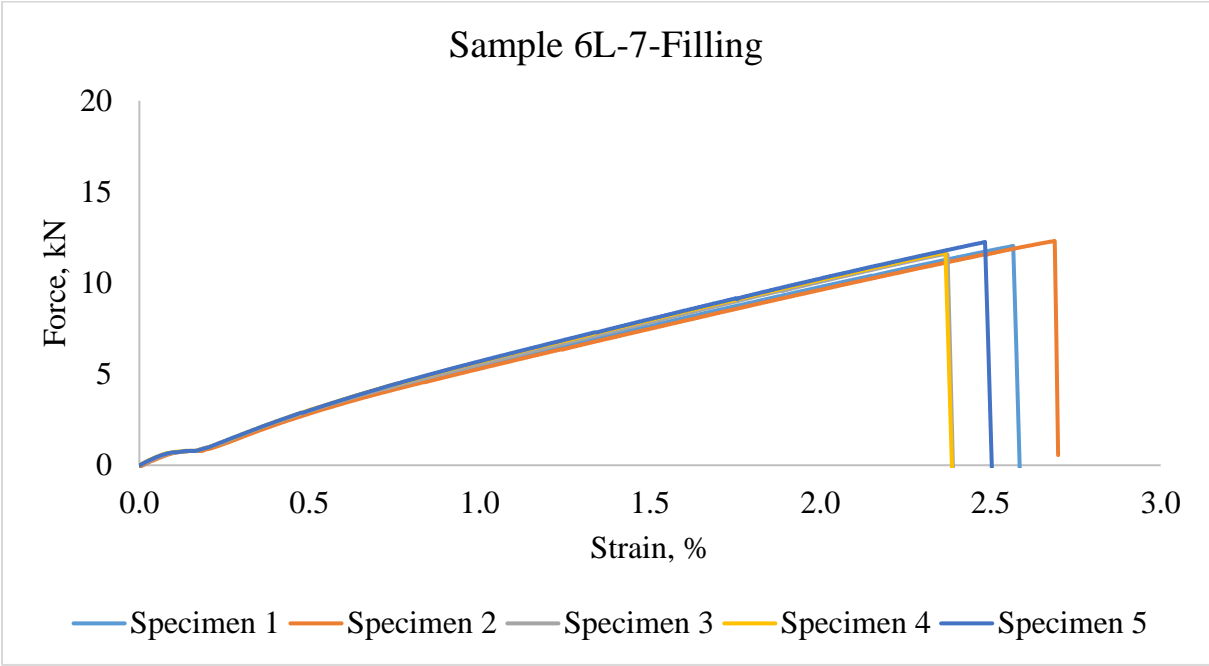
(d)

Figure 201. Load- extension curves of 3 Y-yarn layers 3DOW composites in the X-yarn (filling)

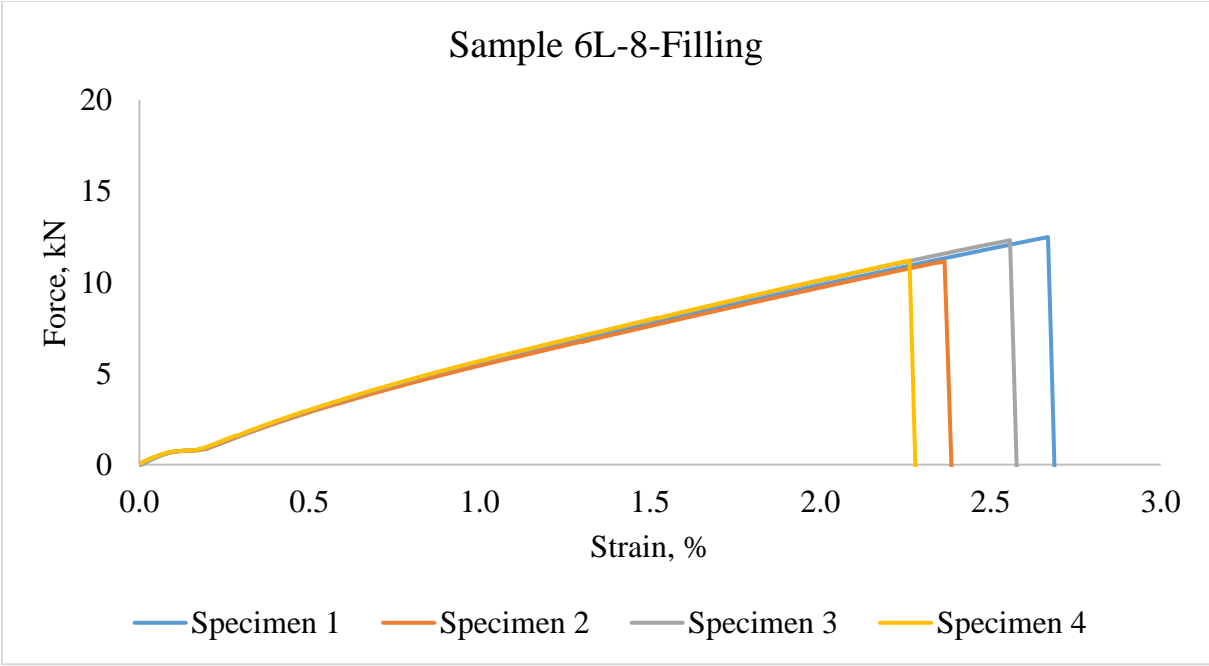
(a) bleached flax yarns, (b) BHS flax yarns, (c) HS flax yarns and (d) grey flax yarns



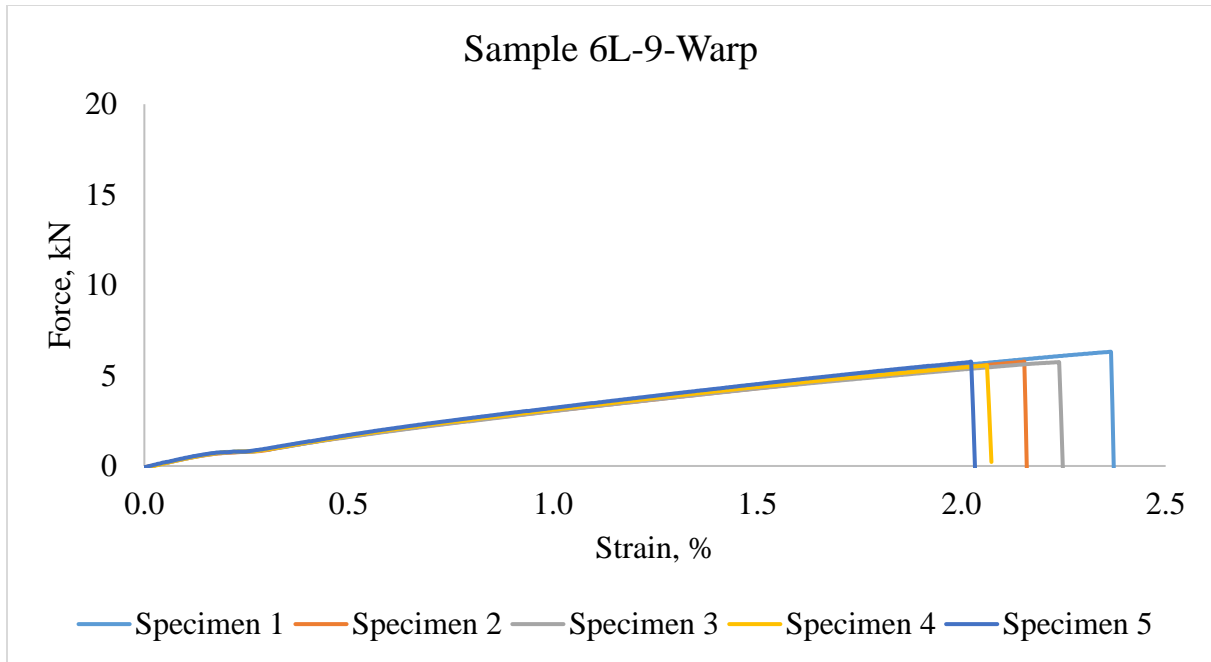
(a)



(b)



(c)



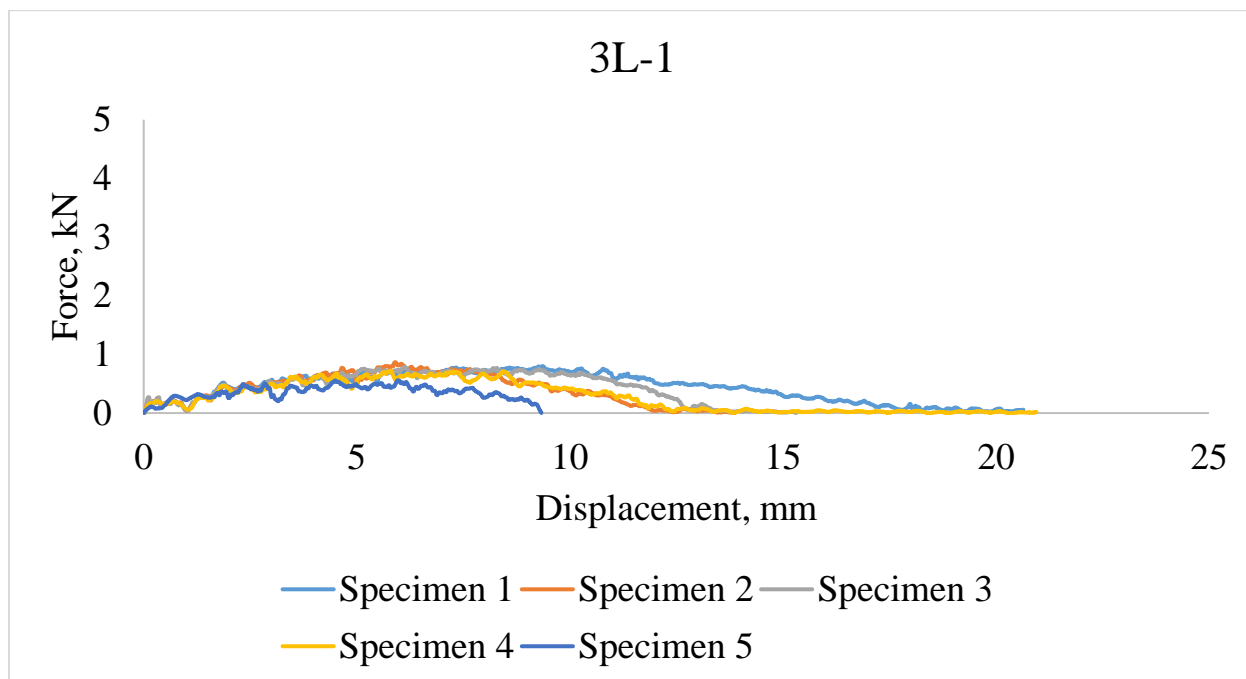
(d)

Figure 202. Load- extension curves of 6 Y-yarn layers 3DOW composites in the X-yarn (filling)

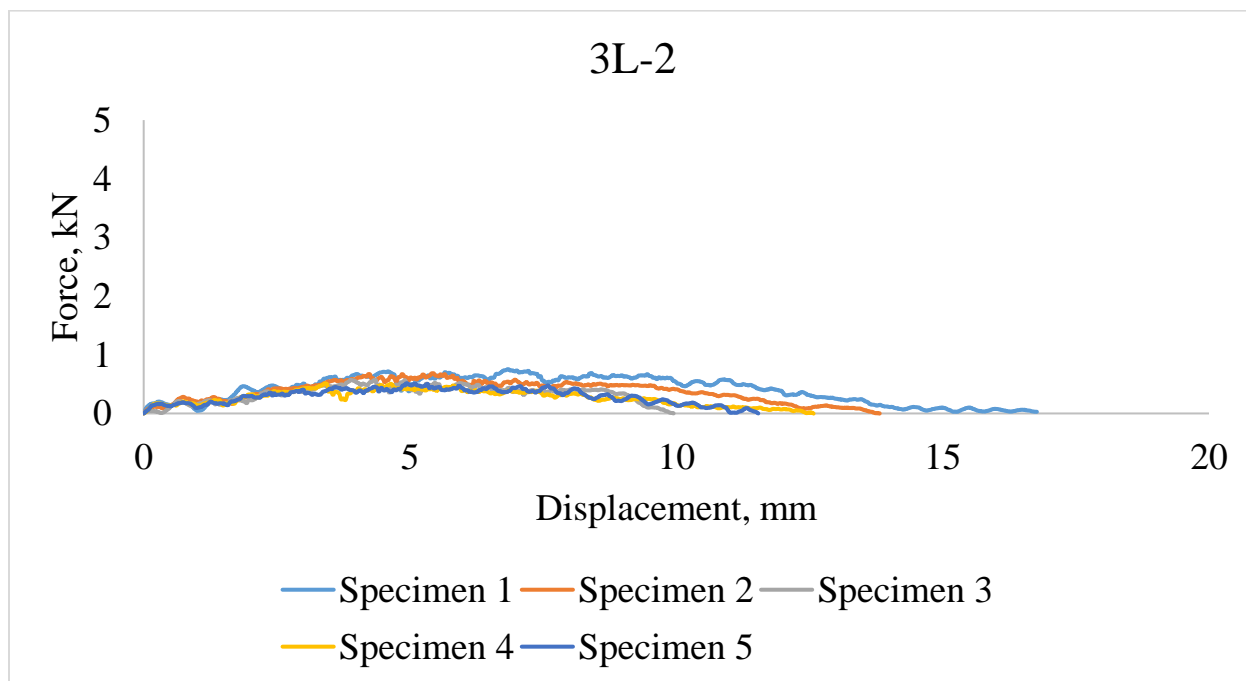
(a) bleached flax yarns, (b) BHS flax yarns, (c) HS flax yarns and (d) grey flax yarns

C.3. Force-Displacement Curves of 3DOW Composites of Tup Impact Test-

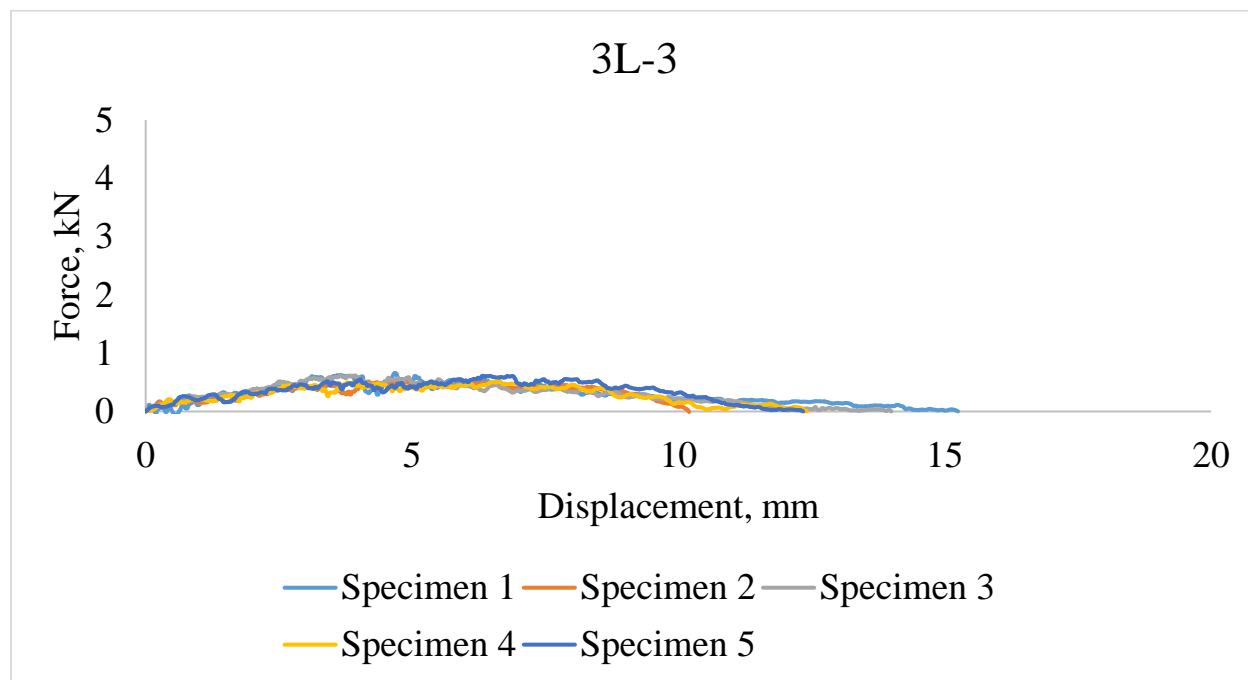
Experimental Design A



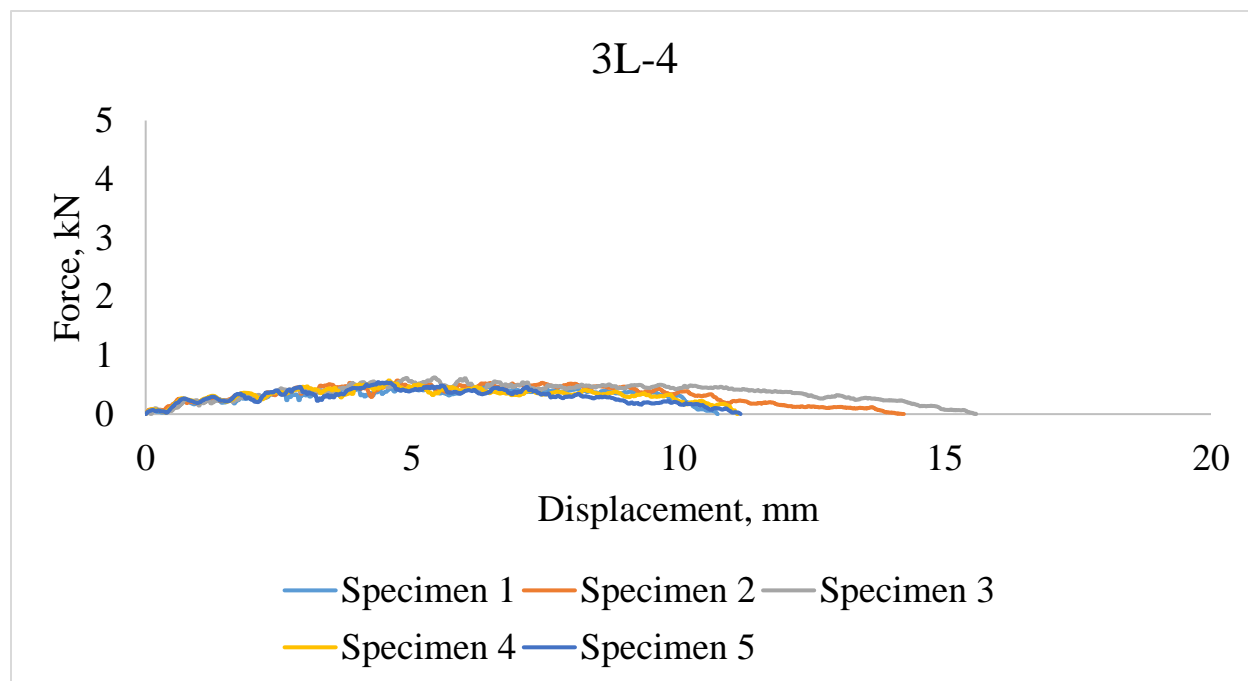
(a)



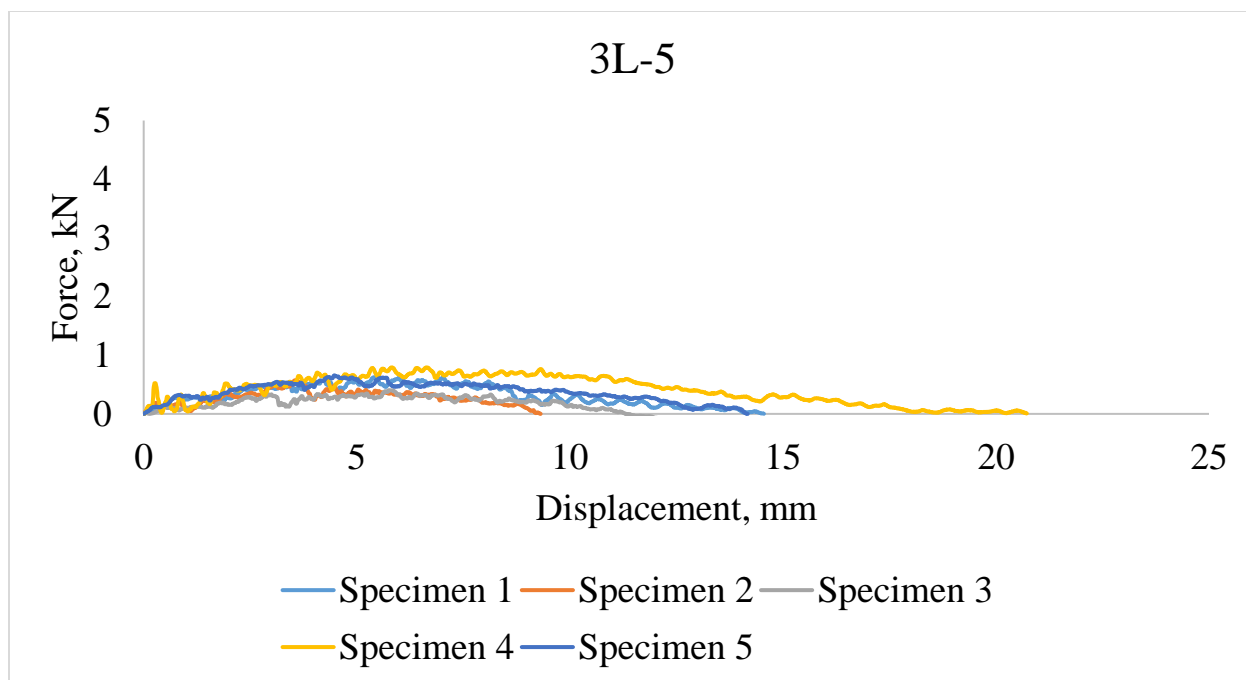
(b)



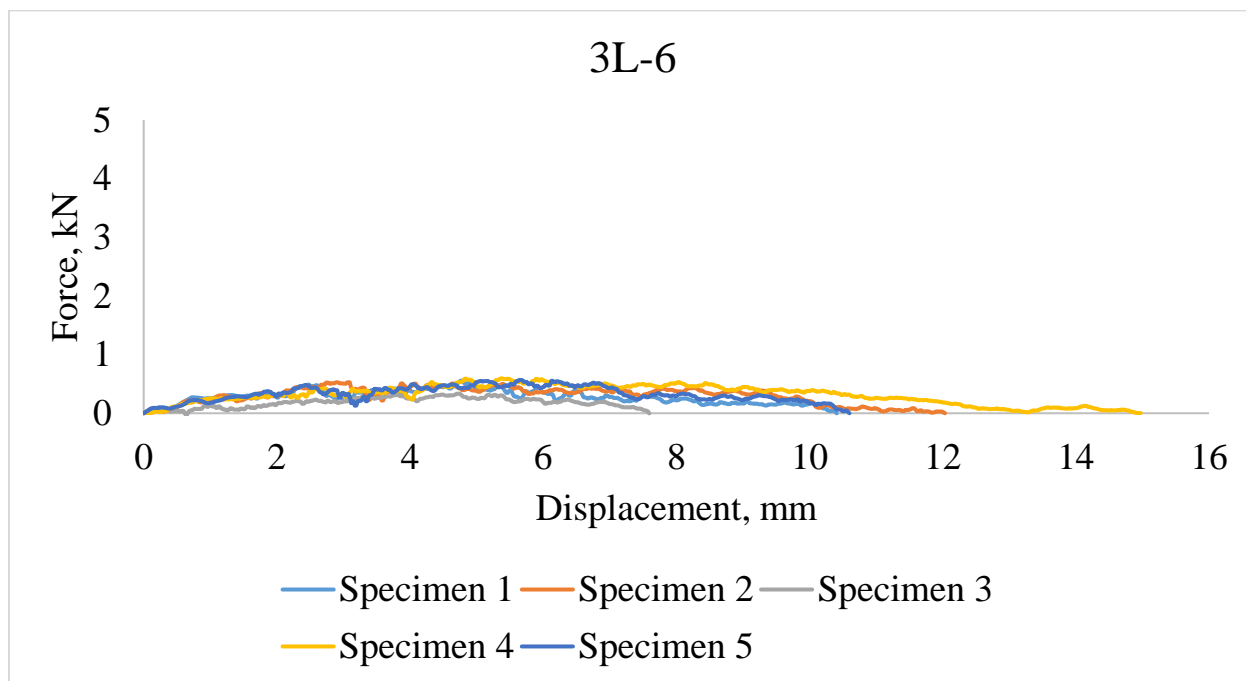
(c)



(d)

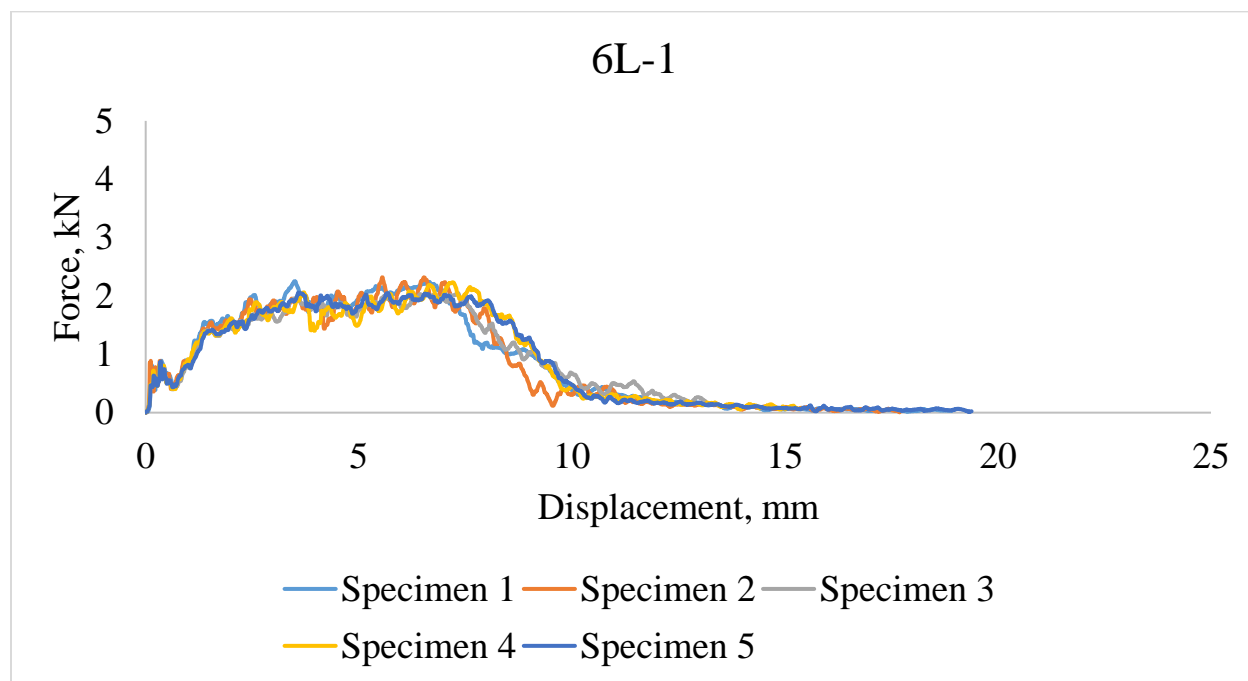


(e)

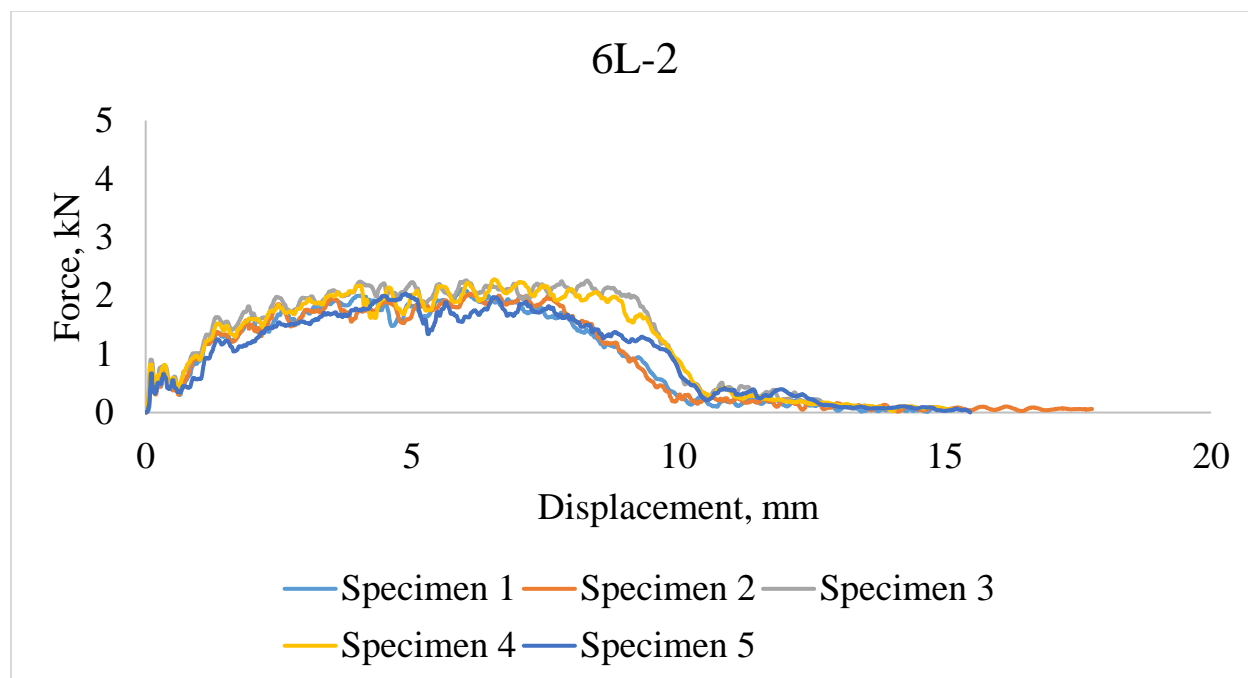


(f)

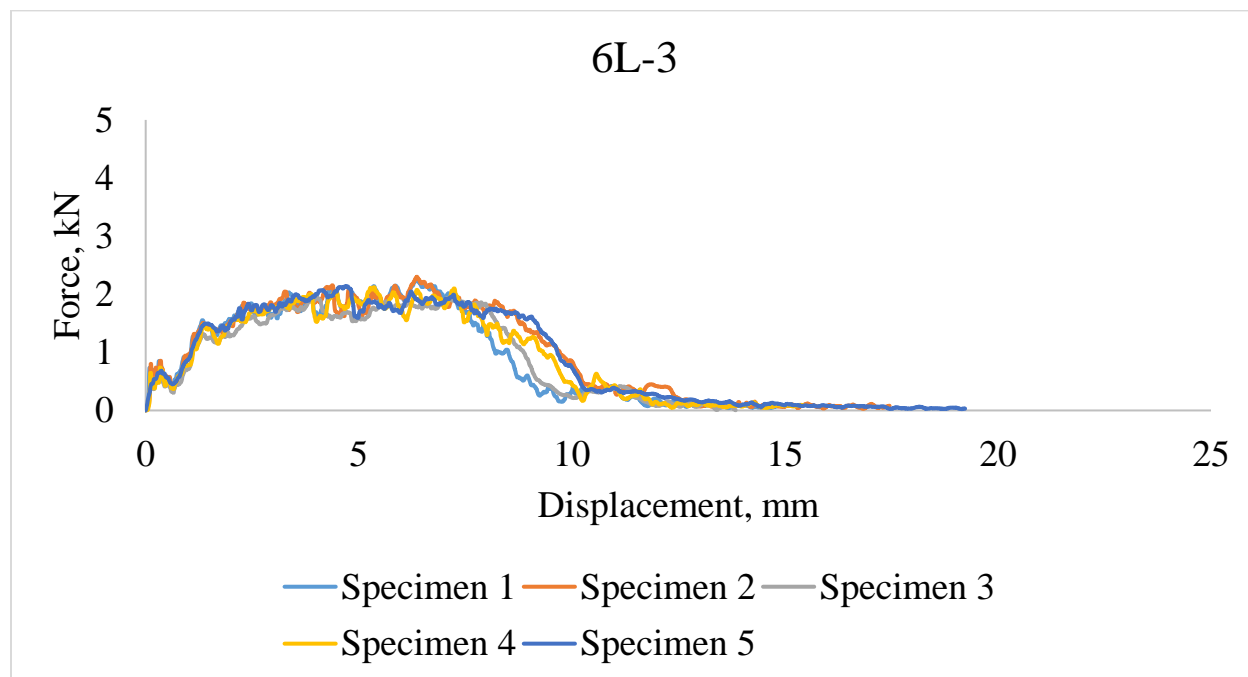
Figure 203. Force- displacement curves of 3 Y-yarn layers 3DOW composites (a) plain and 1:1 Z to Y-yarn ratio, (b) 2x2 warp rib and 1:1 Z to Y-yarn ratio, (c) 3x3 warp rib and 1:1 Z to Y-yarn ratio, (d) plain and 1:3 Z to Y-yarn ratio, (e) 2x2 warp rib and 1:3 Z to Y-yarn ratio, (f) 3x3 warp rib and 1:3 Z to Y-yarn ratio



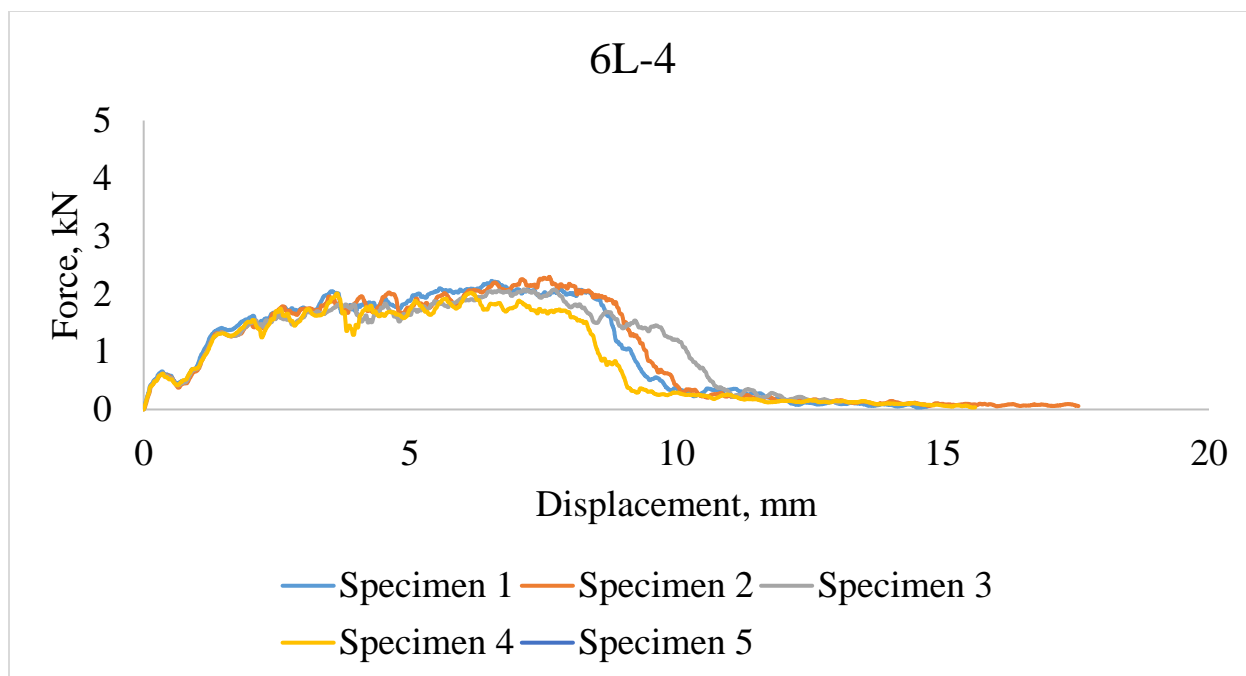
(a)



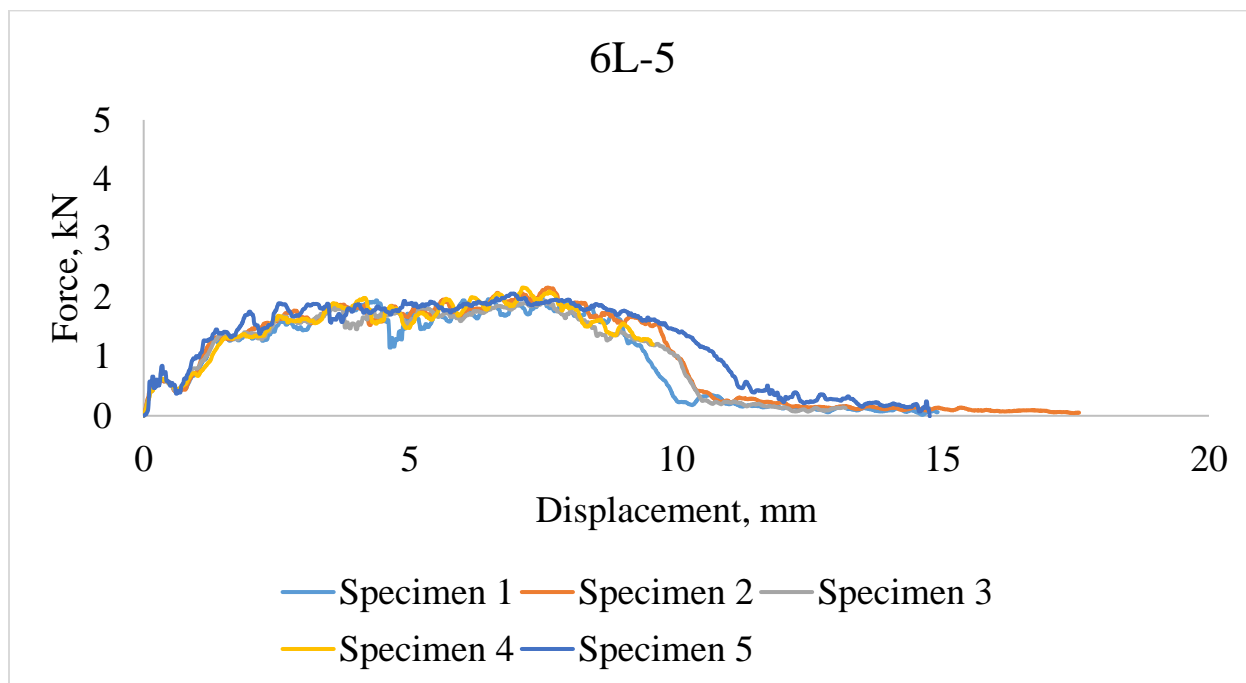
(b)



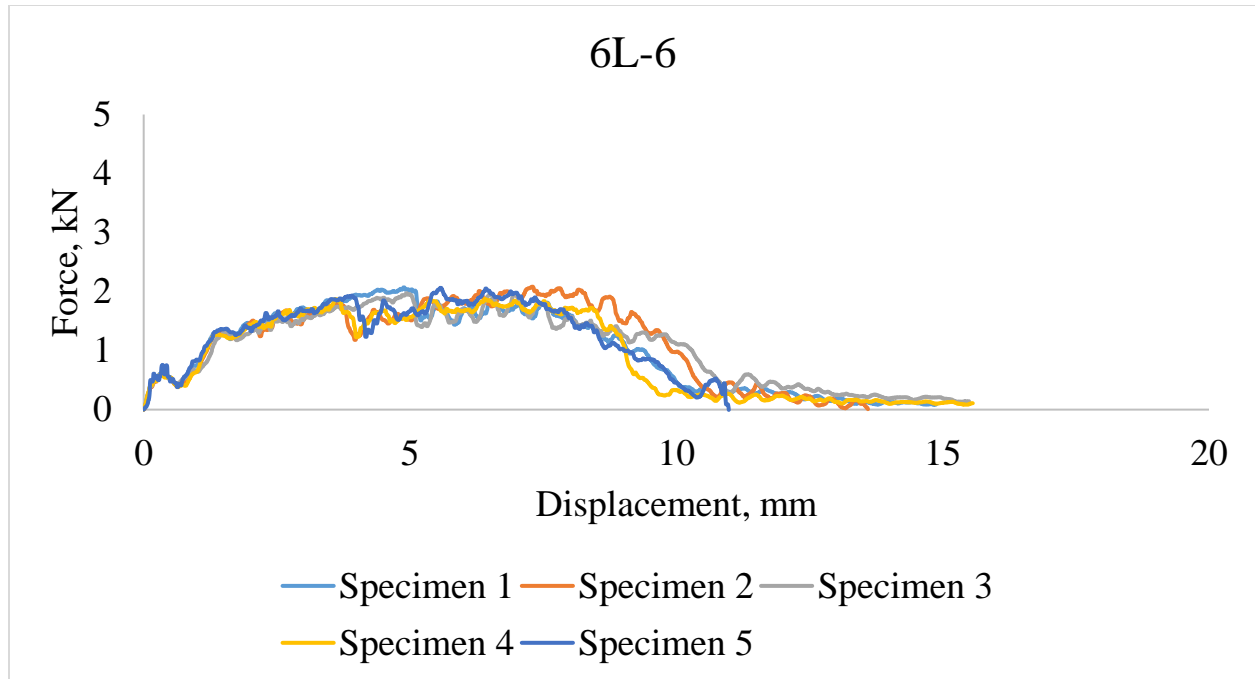
(c)



(d)

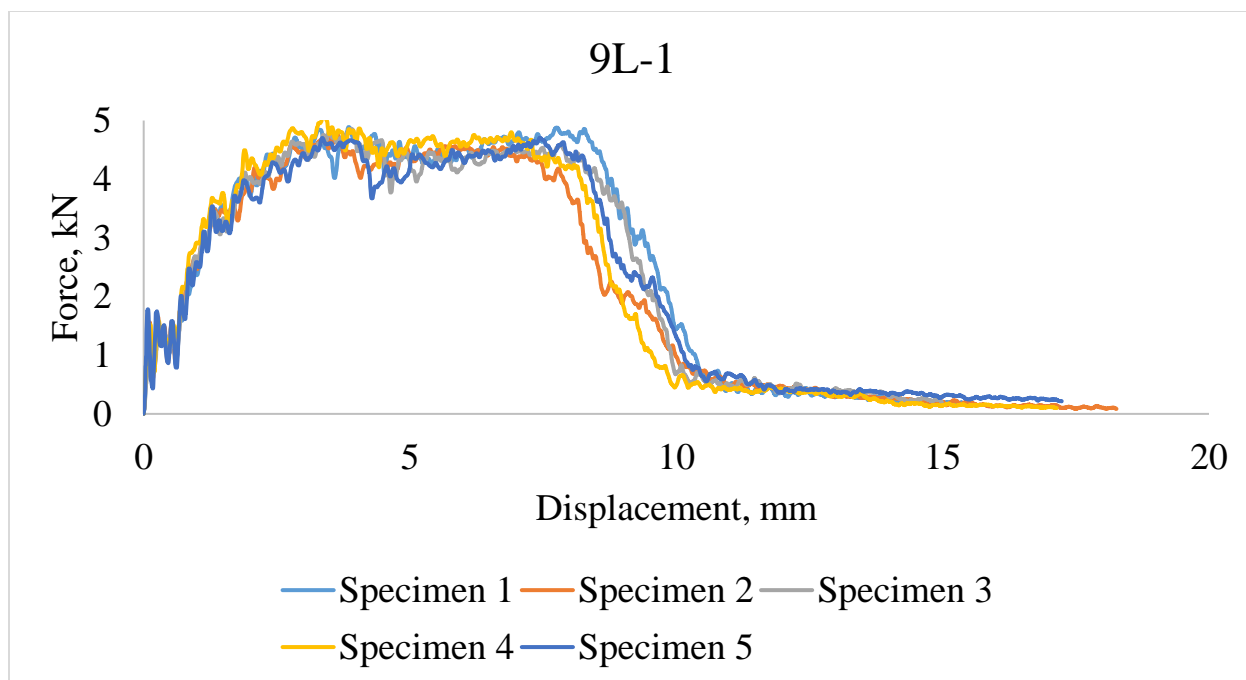


(e)

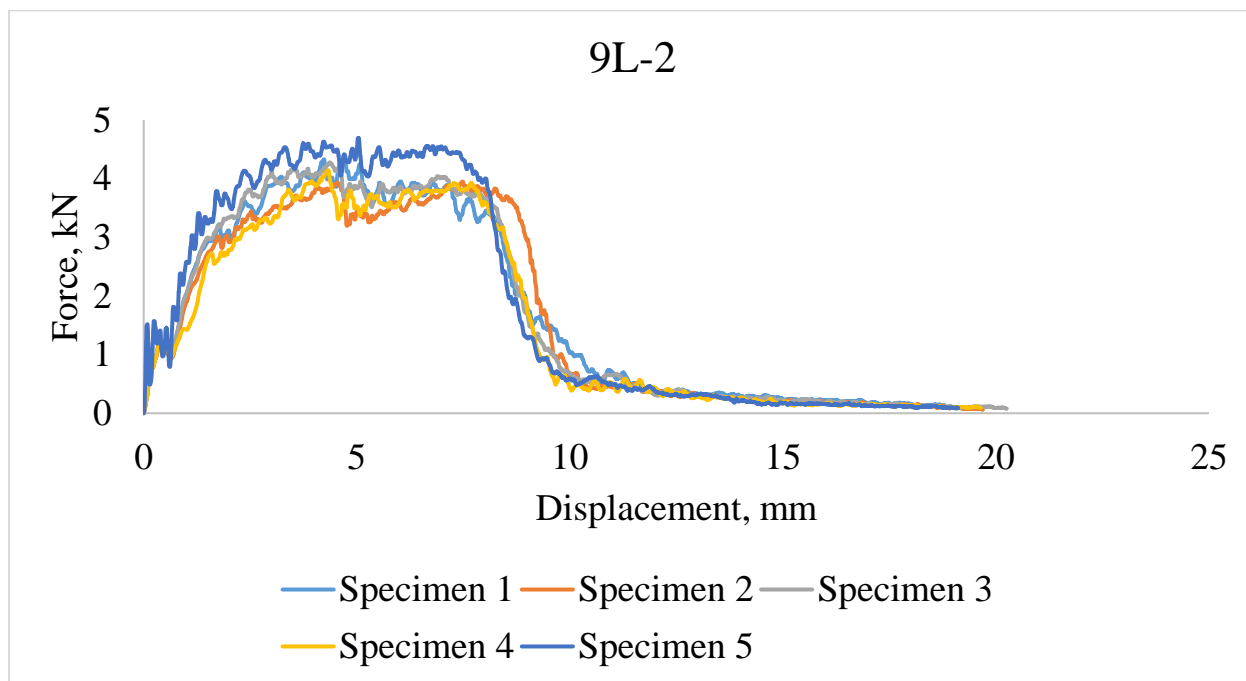


(f)

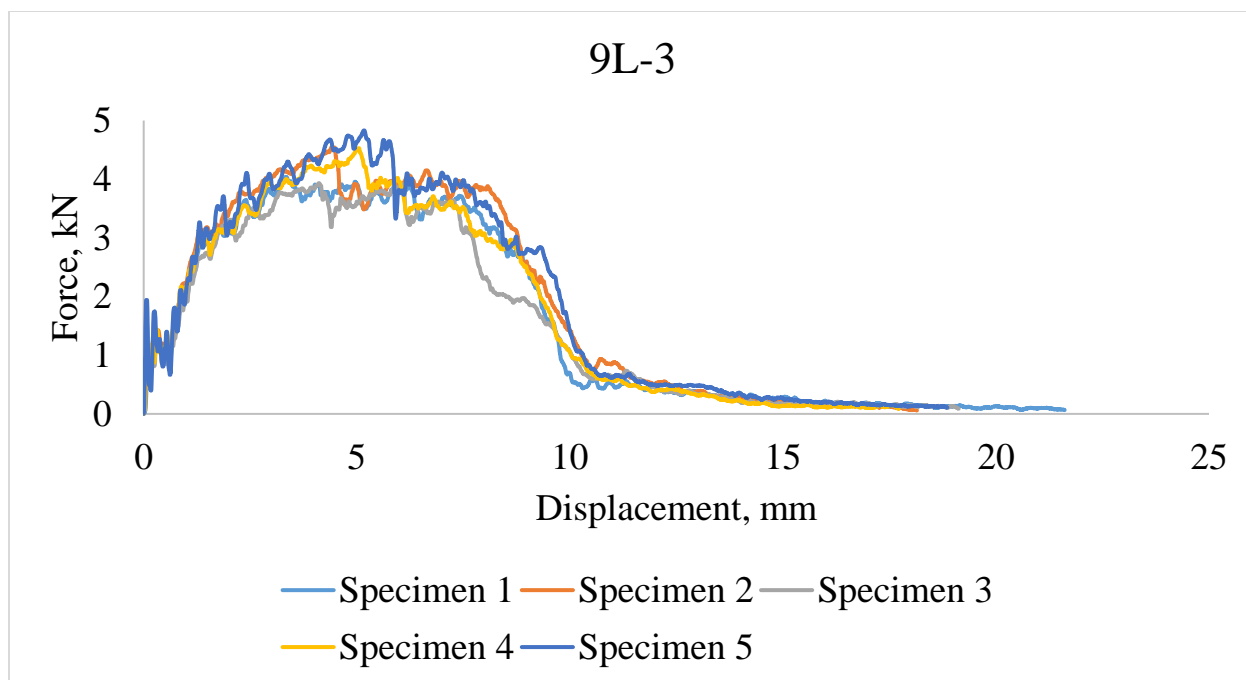
Figure 204. Force- displacement curves of 6 Y-yarn layers 3DOW composites (a) plain and 1:1 Z to Y-yarn ratio, (b) 2x2 warp rib and 1:1 Z to Y-yarn ratio, (c) 3x3 warp rib and 1:1 Z to Y-yarn ratio, (d) plain and 1:3 Z to Y-yarn ratio, (e) 2x2 warp rib and 1:3 Z to Y-yarn ratio, (f) 3x3 warp rib and 1:3 Z to Y-yarn ratio



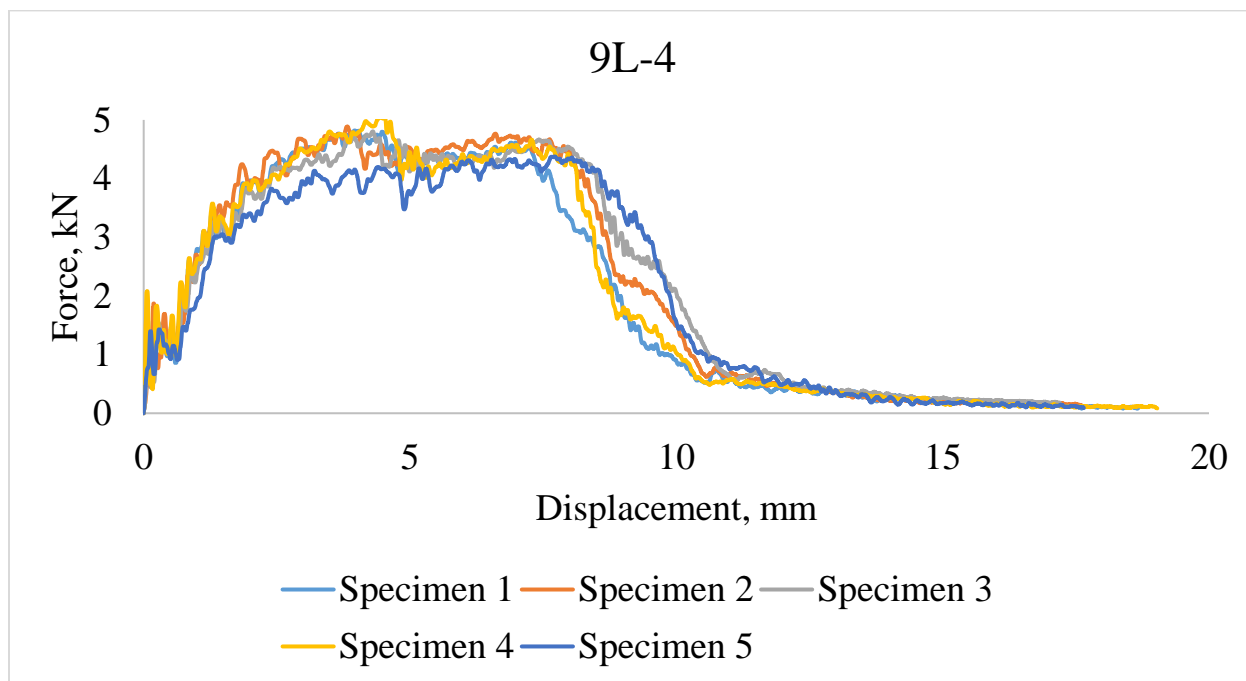
(a)



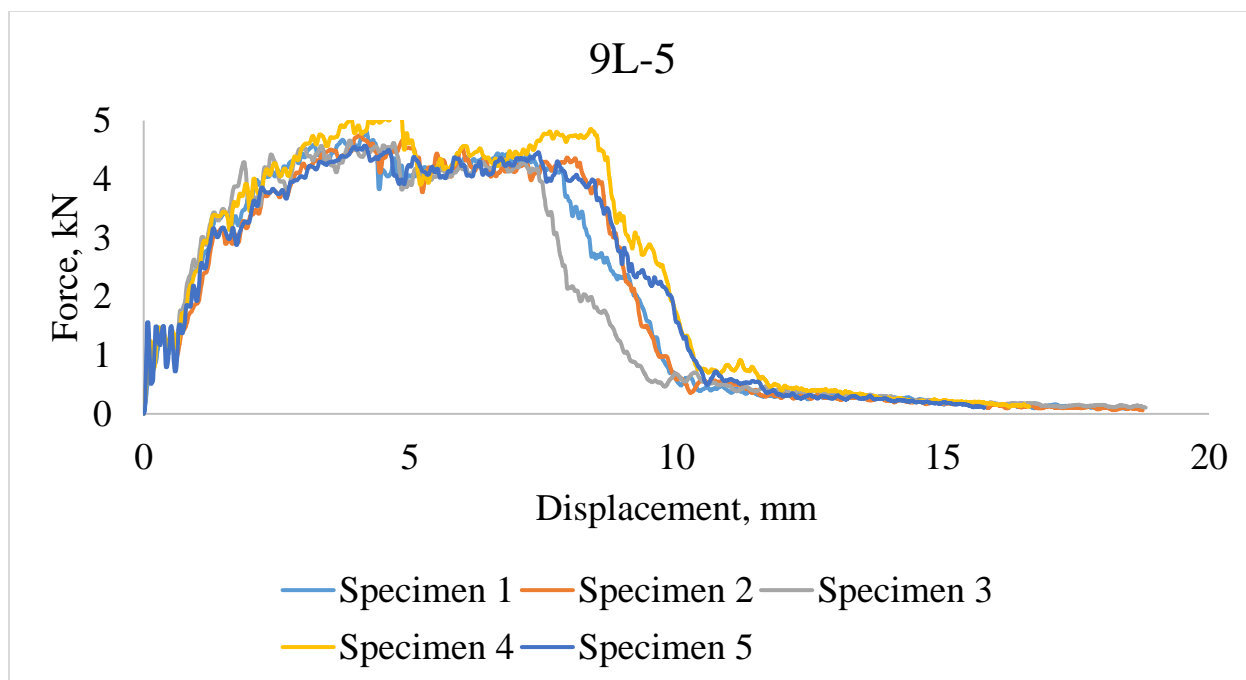
(b)



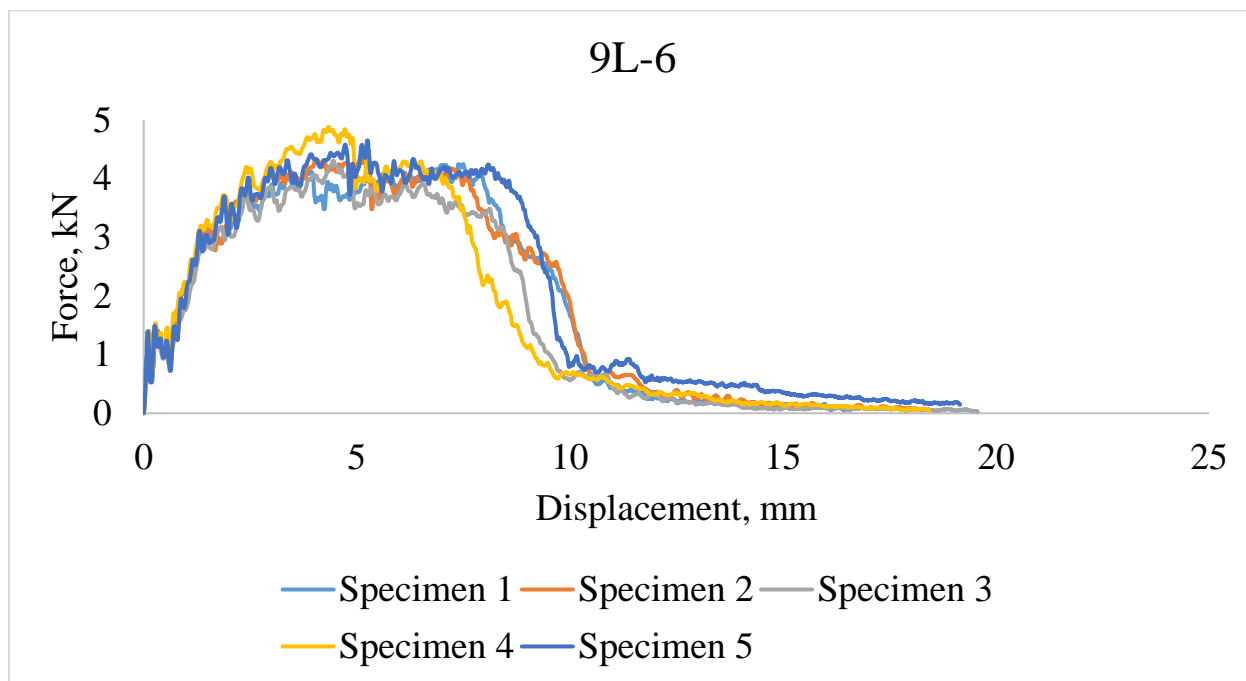
(c)



(d)



(e)

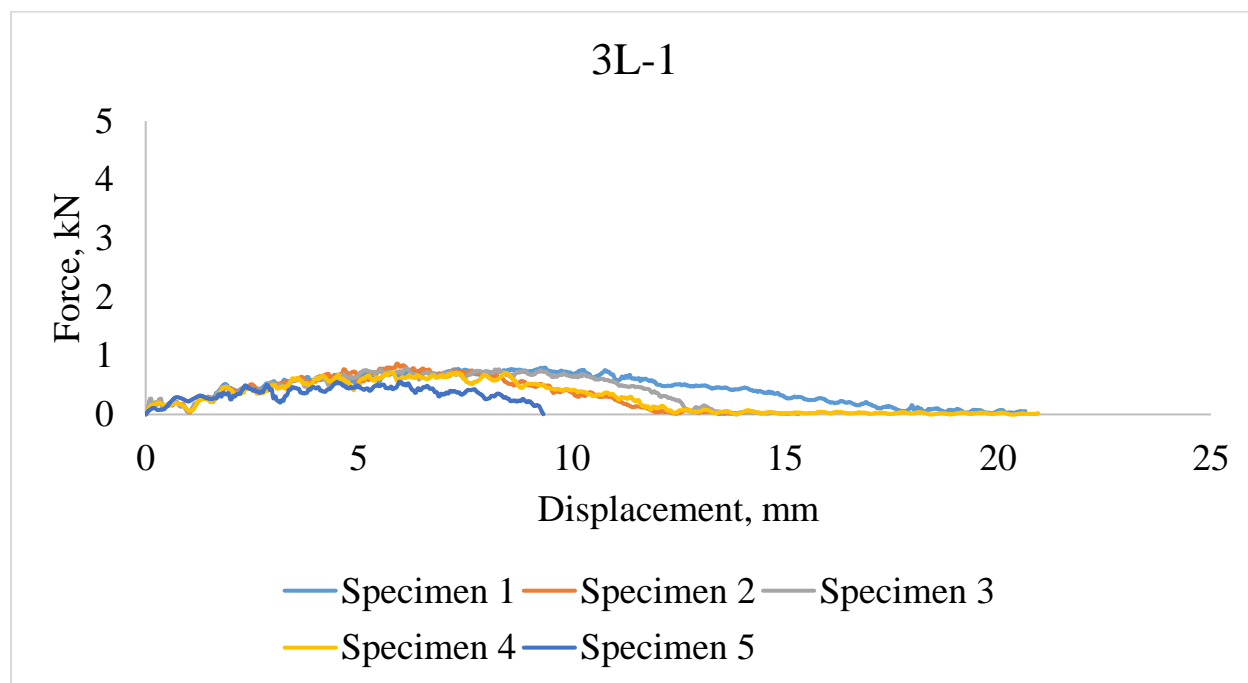


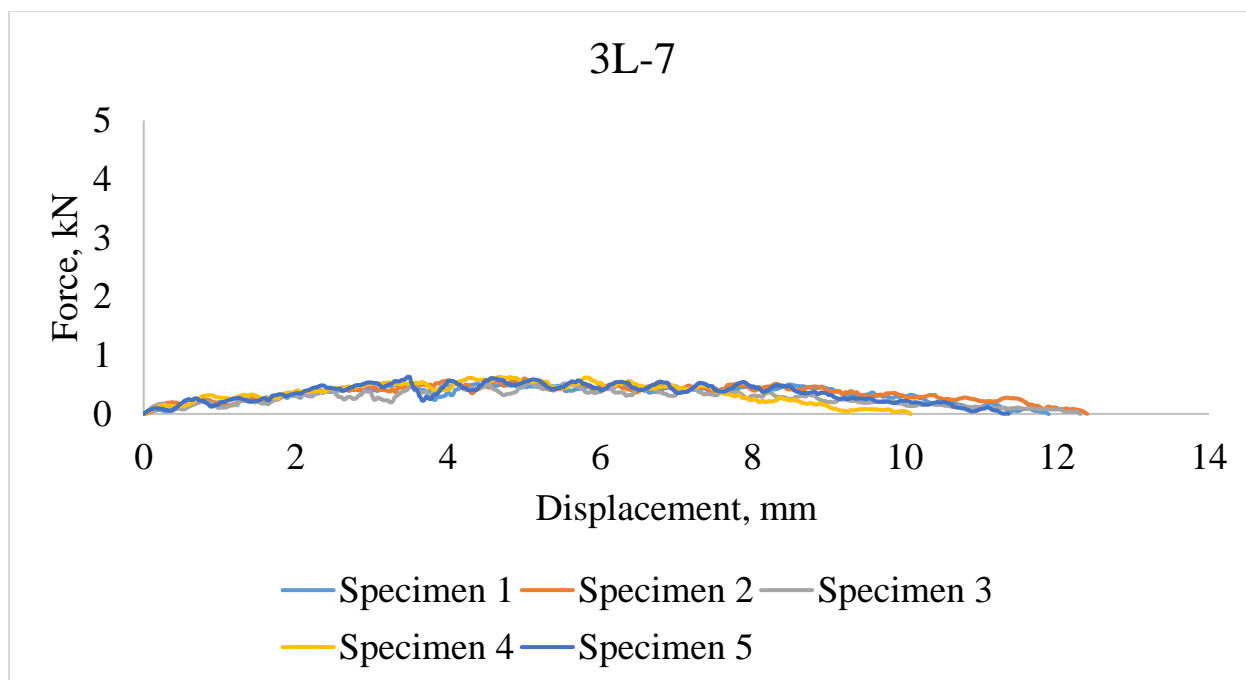
(f)

Figure 205. Force- displacement curves of 9 Y-yarn layers 3DOW composites (a) plain and 1:1 Z to Y-yarn ratio, (b) 2x2 warp rib and 1:1 Z to Y-yarn ratio, (c) 3x3 warp rib and 1:1 Z to Y-yarn ratio, (d) plain and 1:3 Z to Y-yarn ratio, (e) 2x2 warp rib and 1:3 Z to Y-yarn ratio, (f) 3x3 warp rib and 1:3 Z to Y-yarn ratio

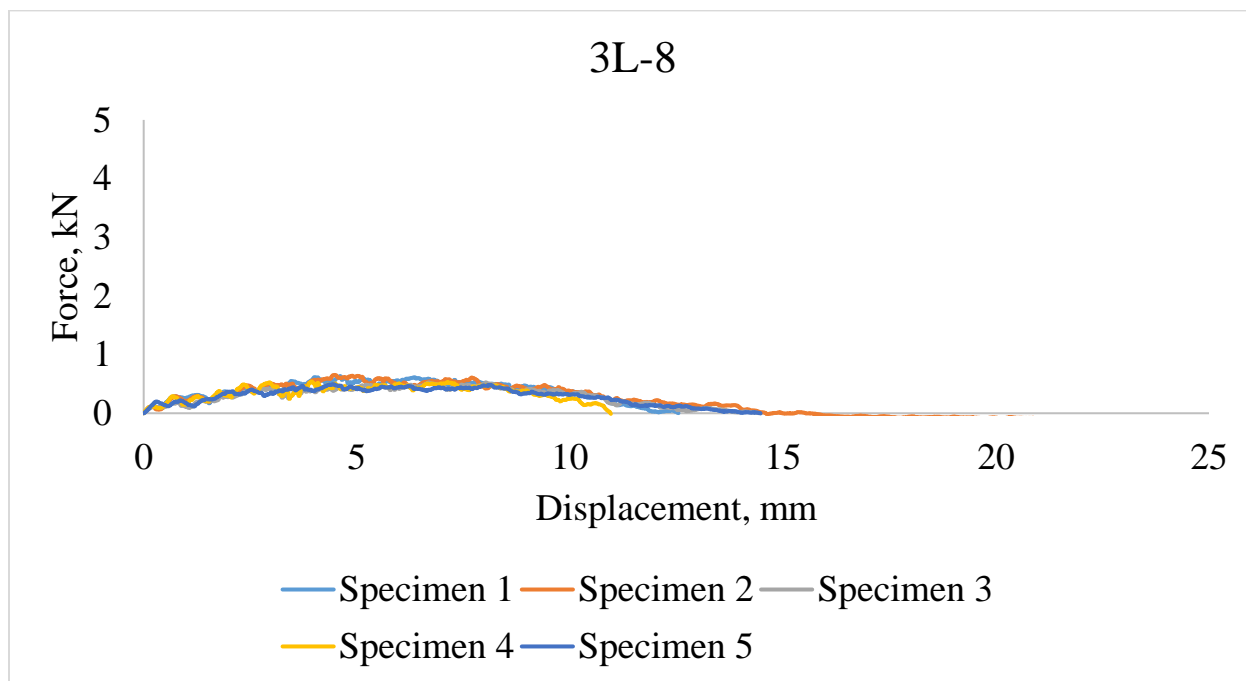
C.4. Force-Displacement Curves of 3DOW Composites of Tup Impact Test-

Experimental Design B

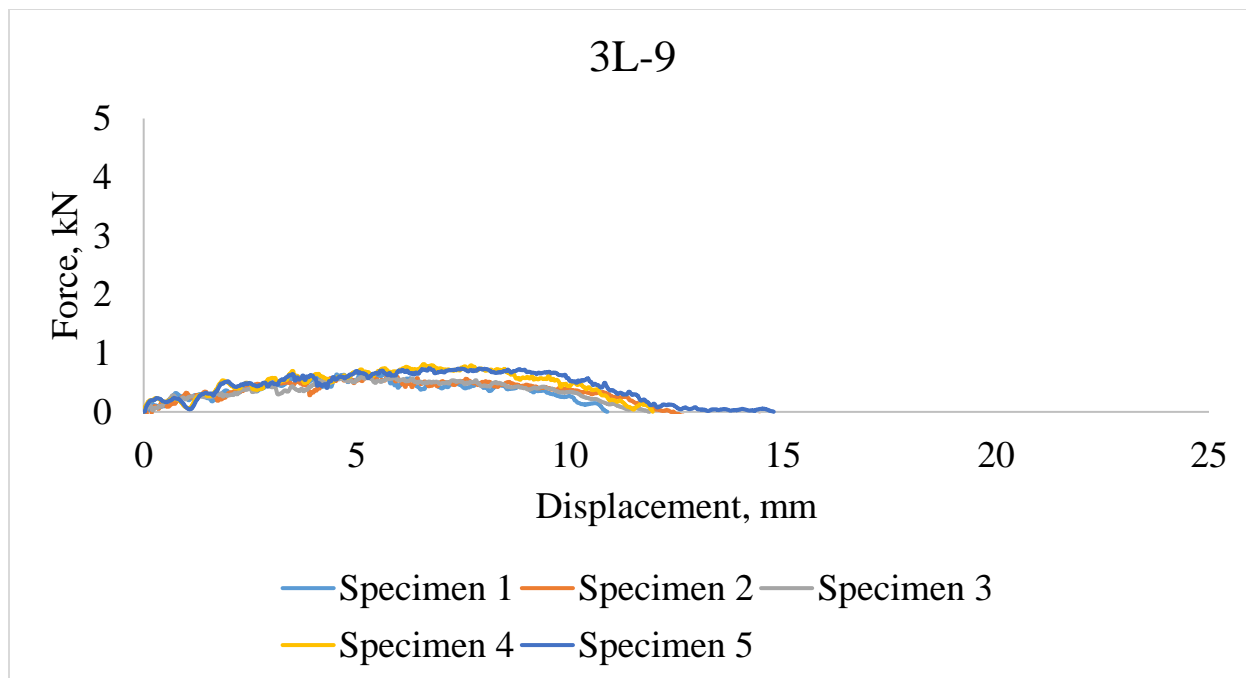




(b)

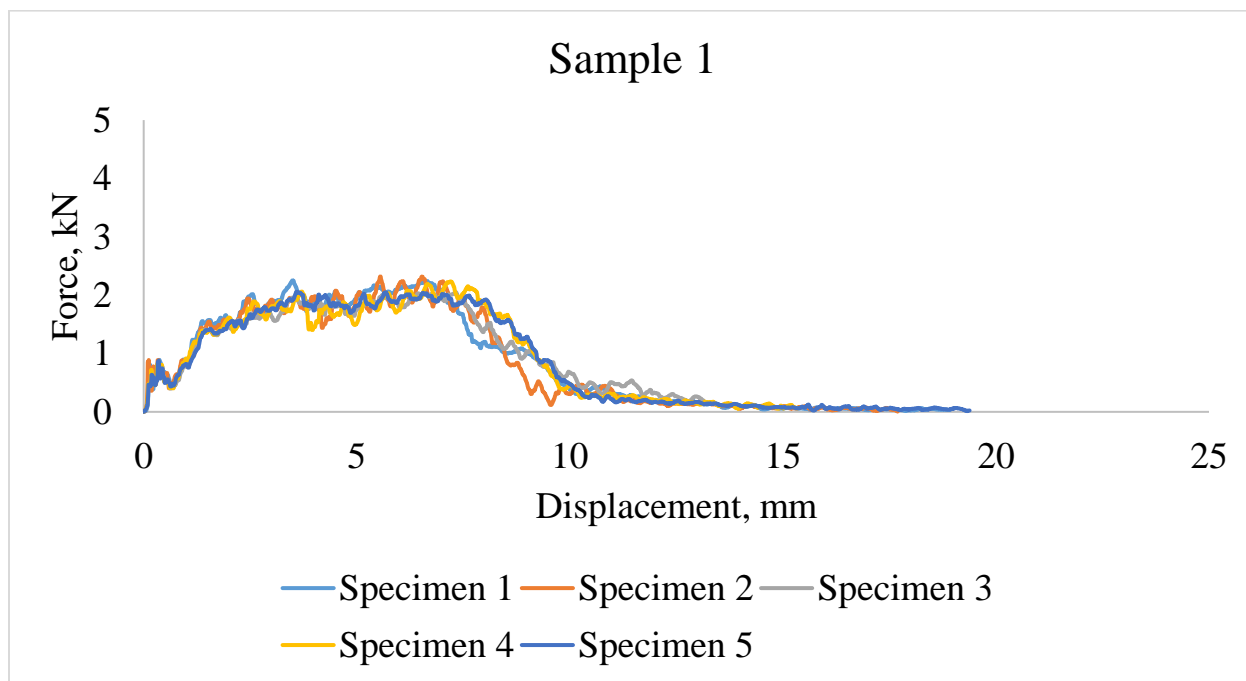


(c)

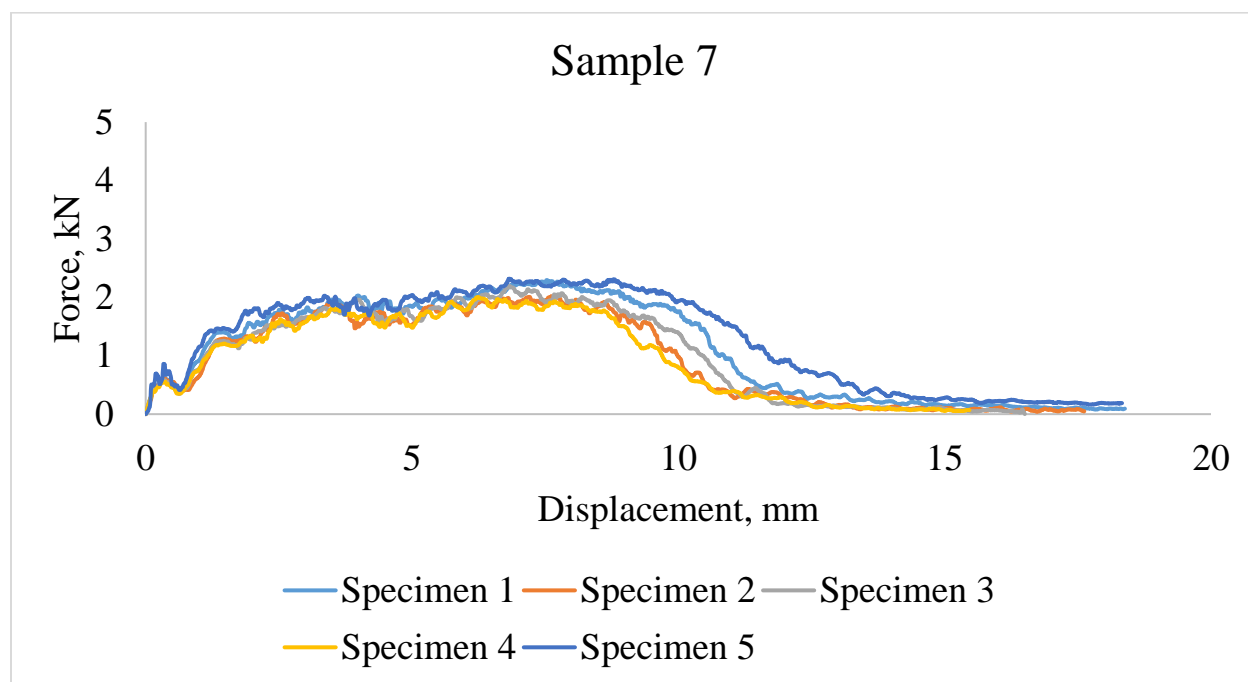


(d)

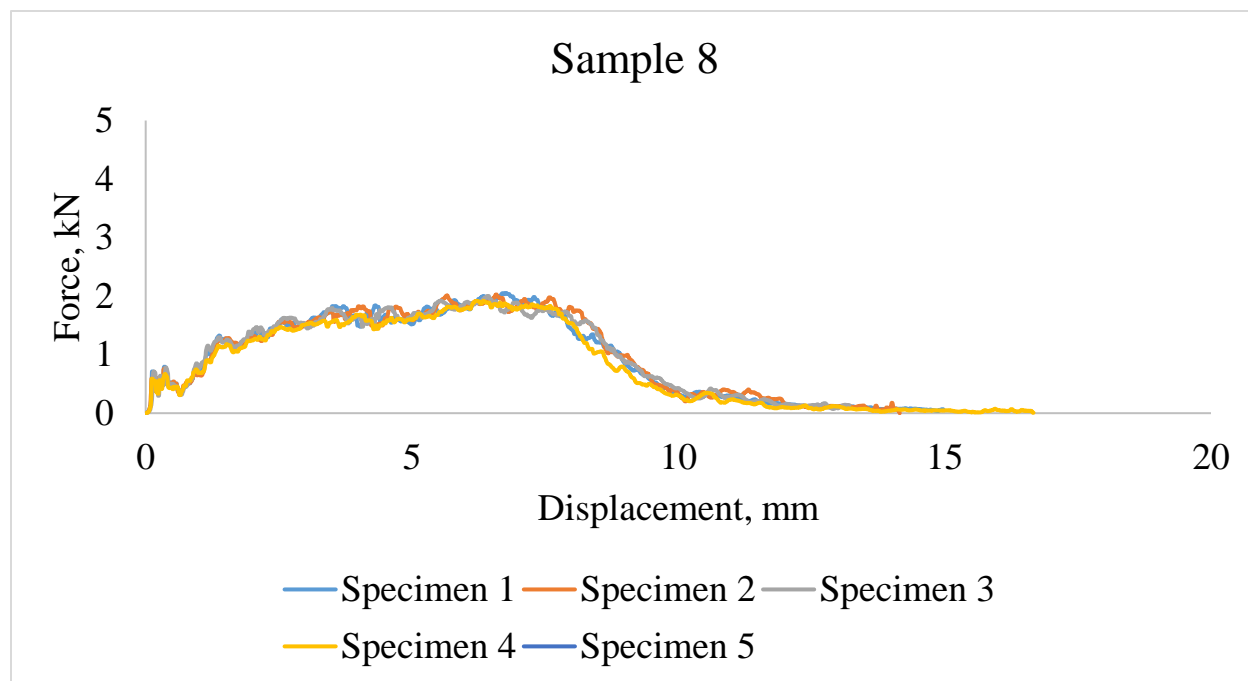
Figure 206. Force- displacement curves of 3 Y-yarn layers 3DOW composites in the X-yarn (filling) (a) bleached flax yarns, (b) BHS flax yarns, (c) HS flax yarns and (d) grey flax yarns



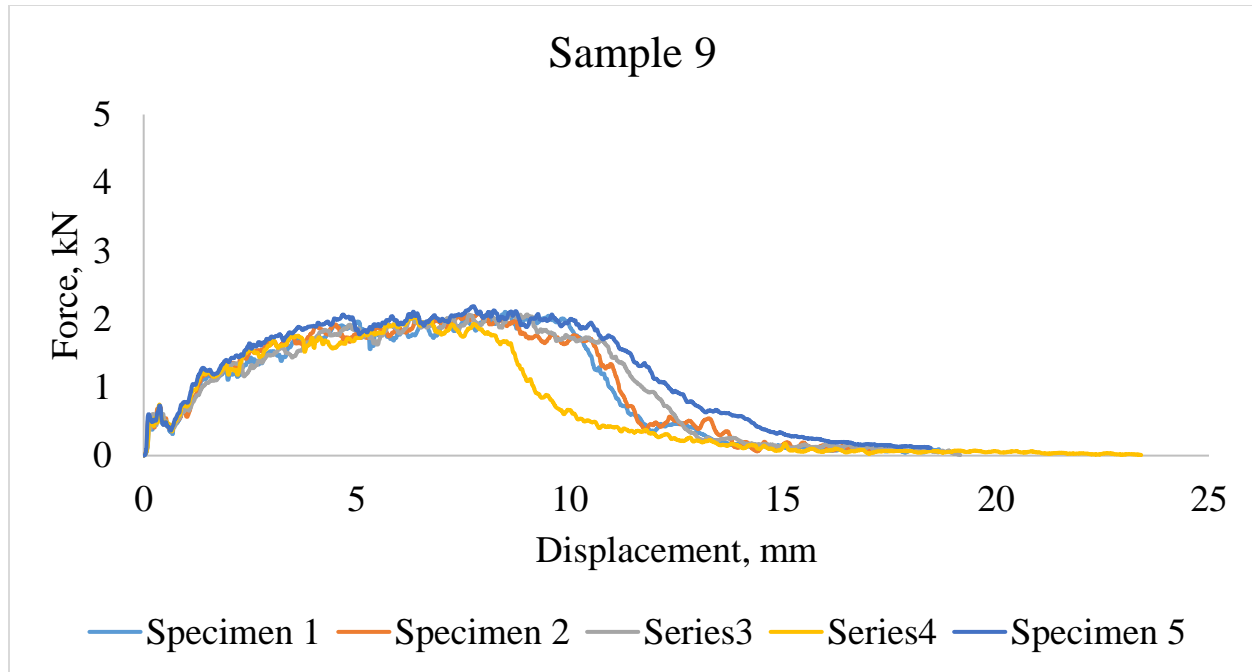
(a)



(b)

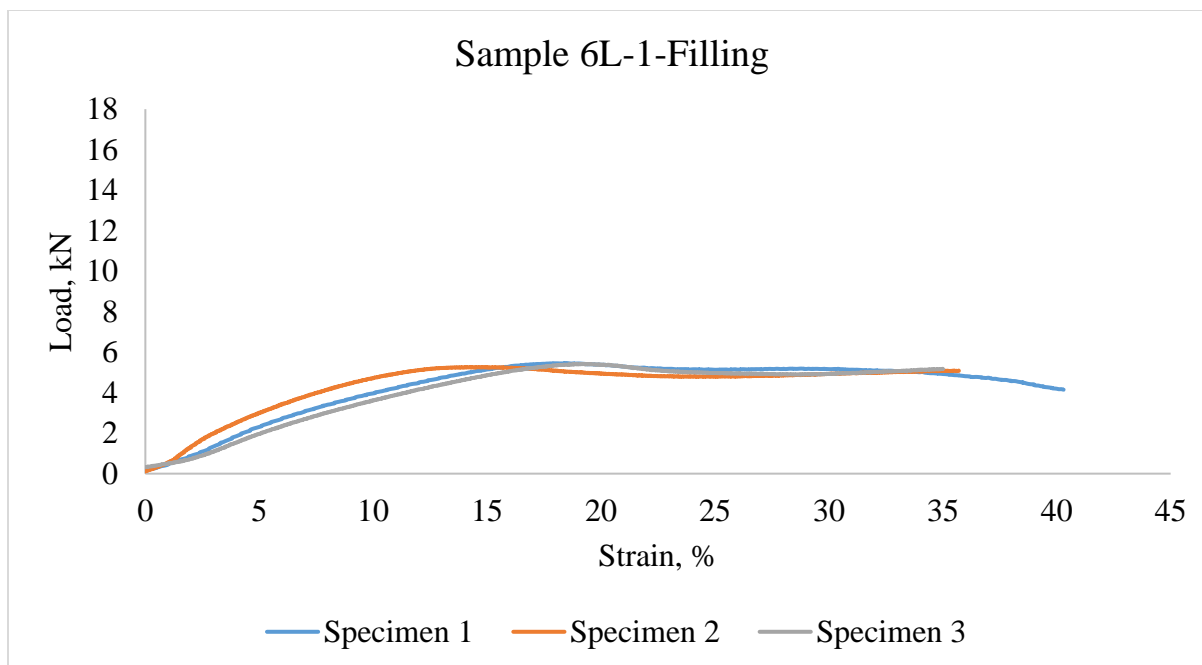
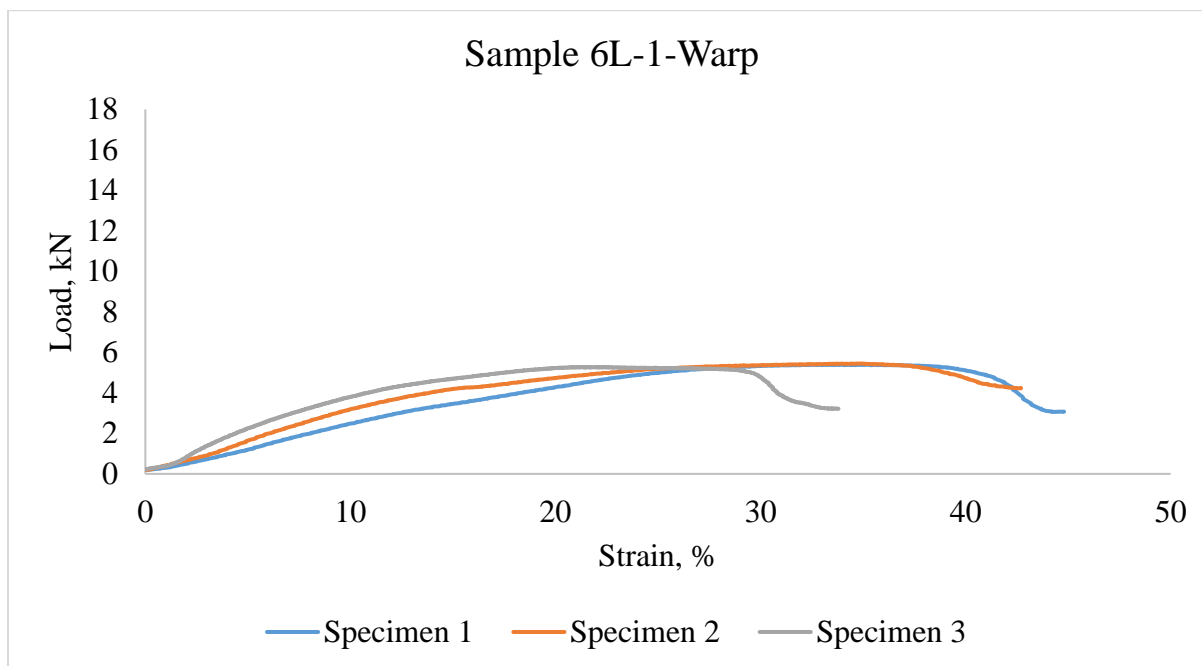


(c)

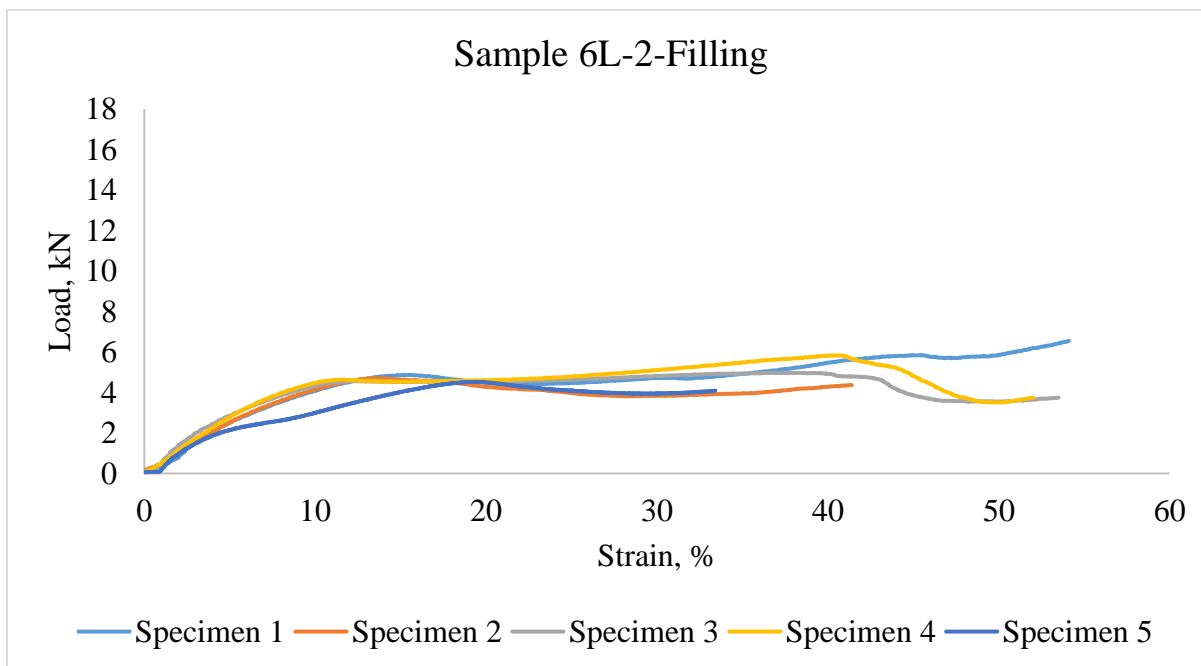
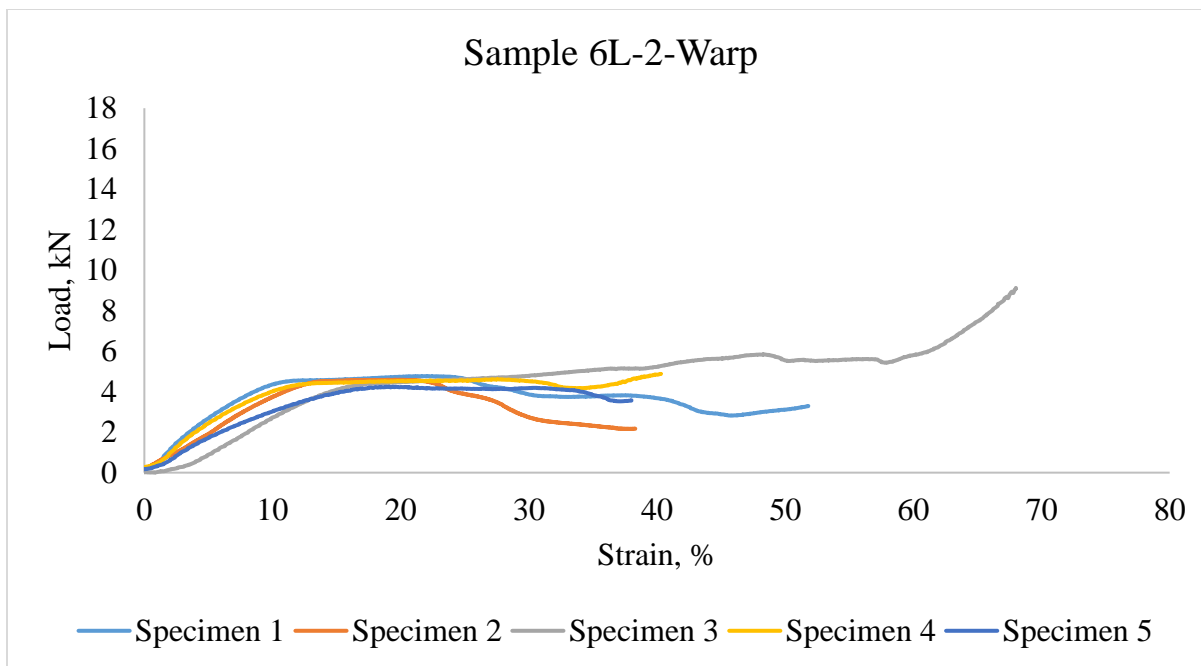


(d)

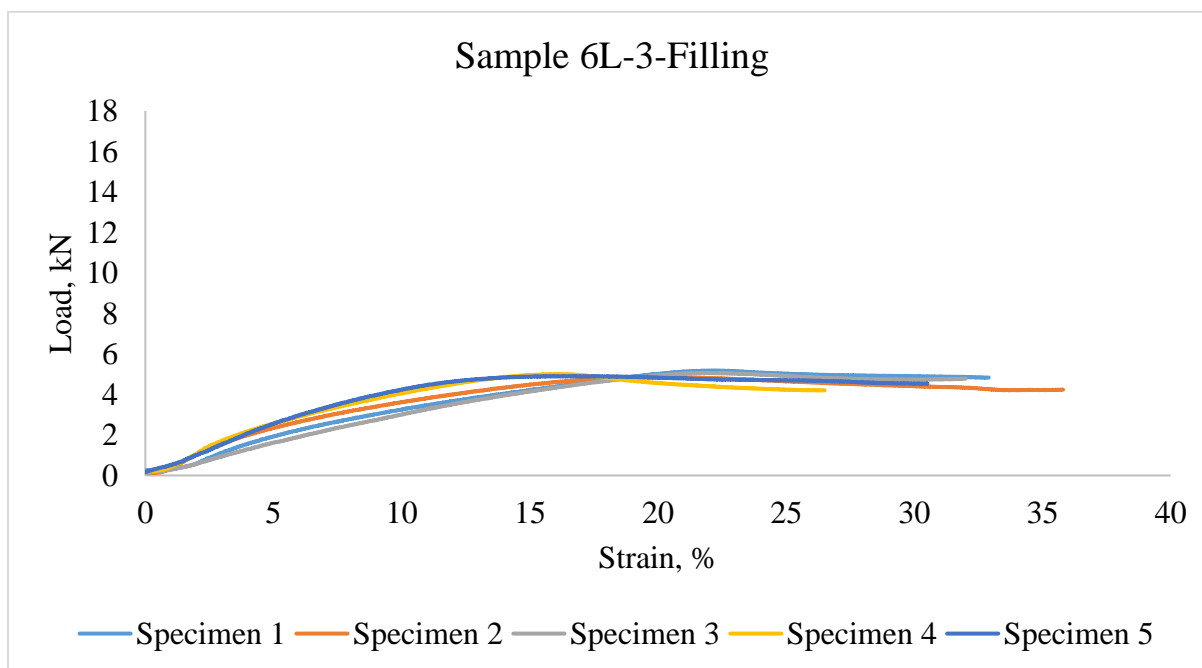
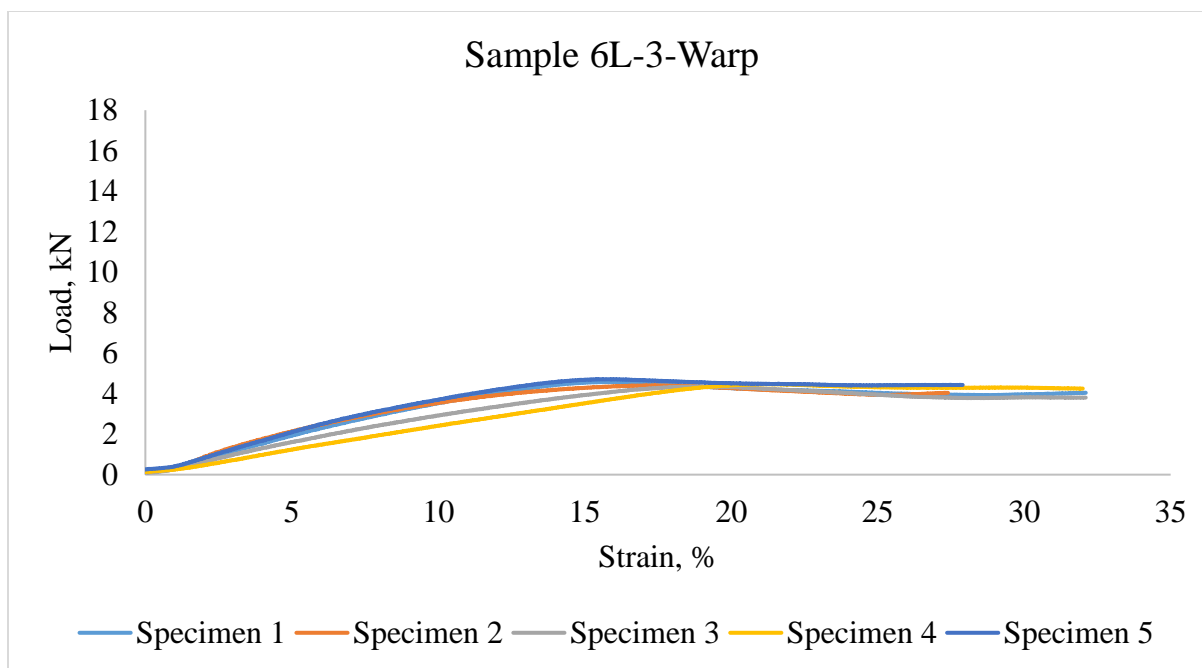
Figure 207. Force- displacement curves of 6 Y-yarn layers 3DOW composites in the X-yarn (filling) (a) bleached flax yarns, (b) BHS flax yarns, (c) HS flax yarns and (d) grey flax yarns

C.5. Typical Compression Curves of 3DOW Composites of Test- Experimental Design**A**

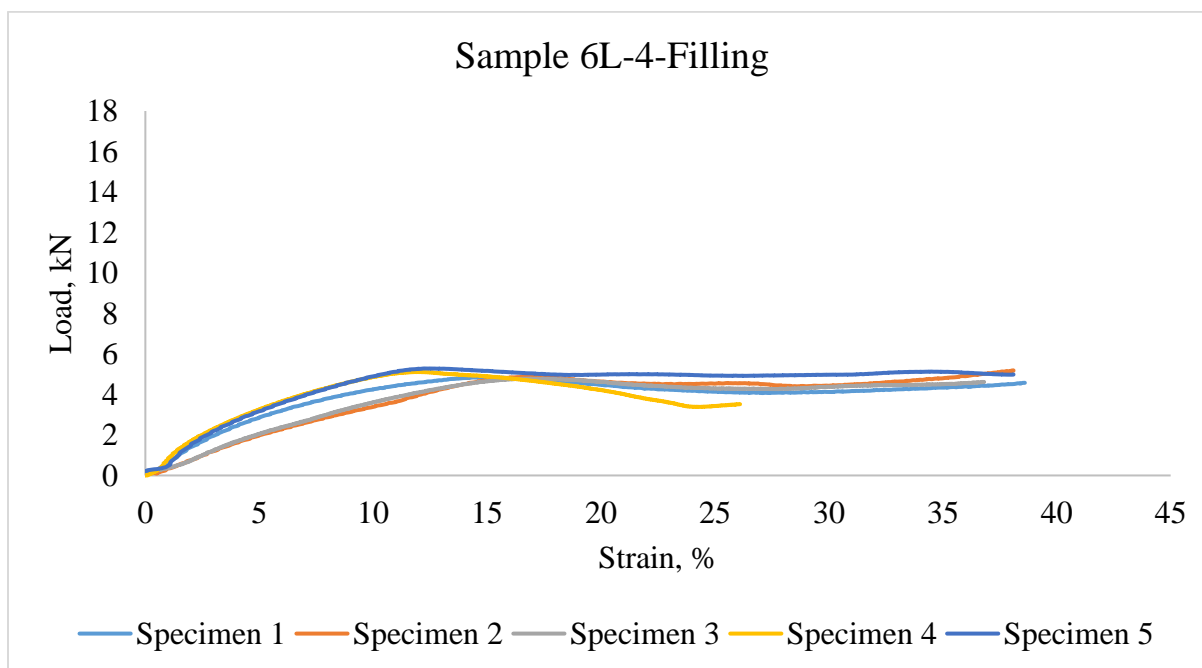
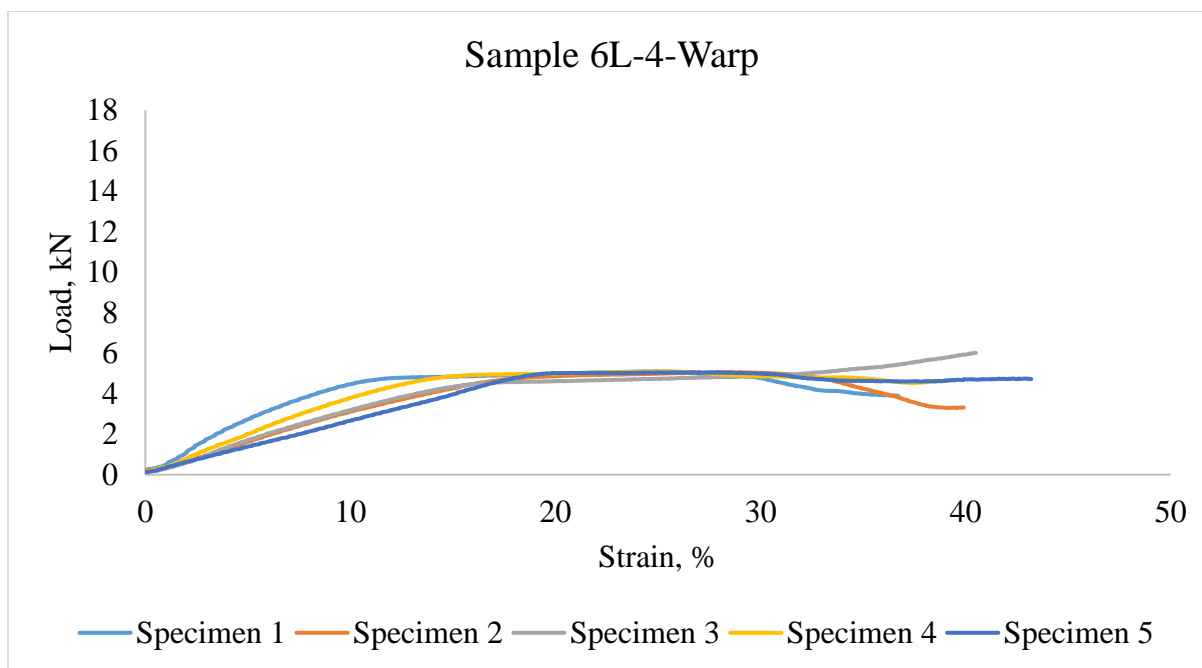
(a)



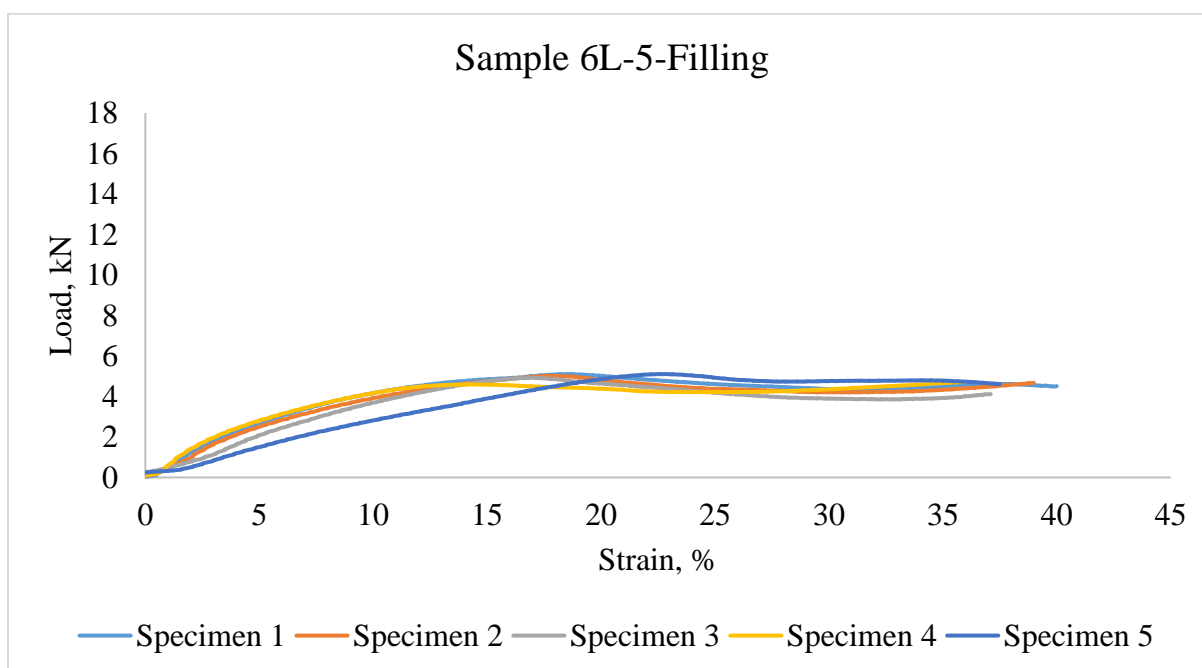
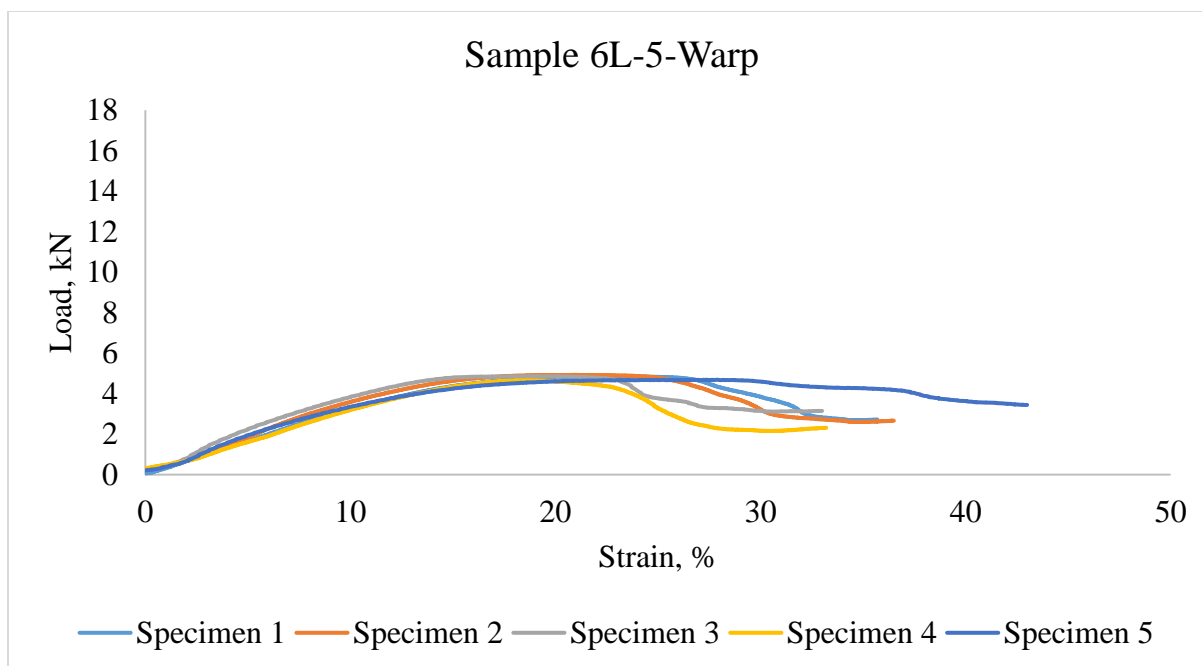
(b)



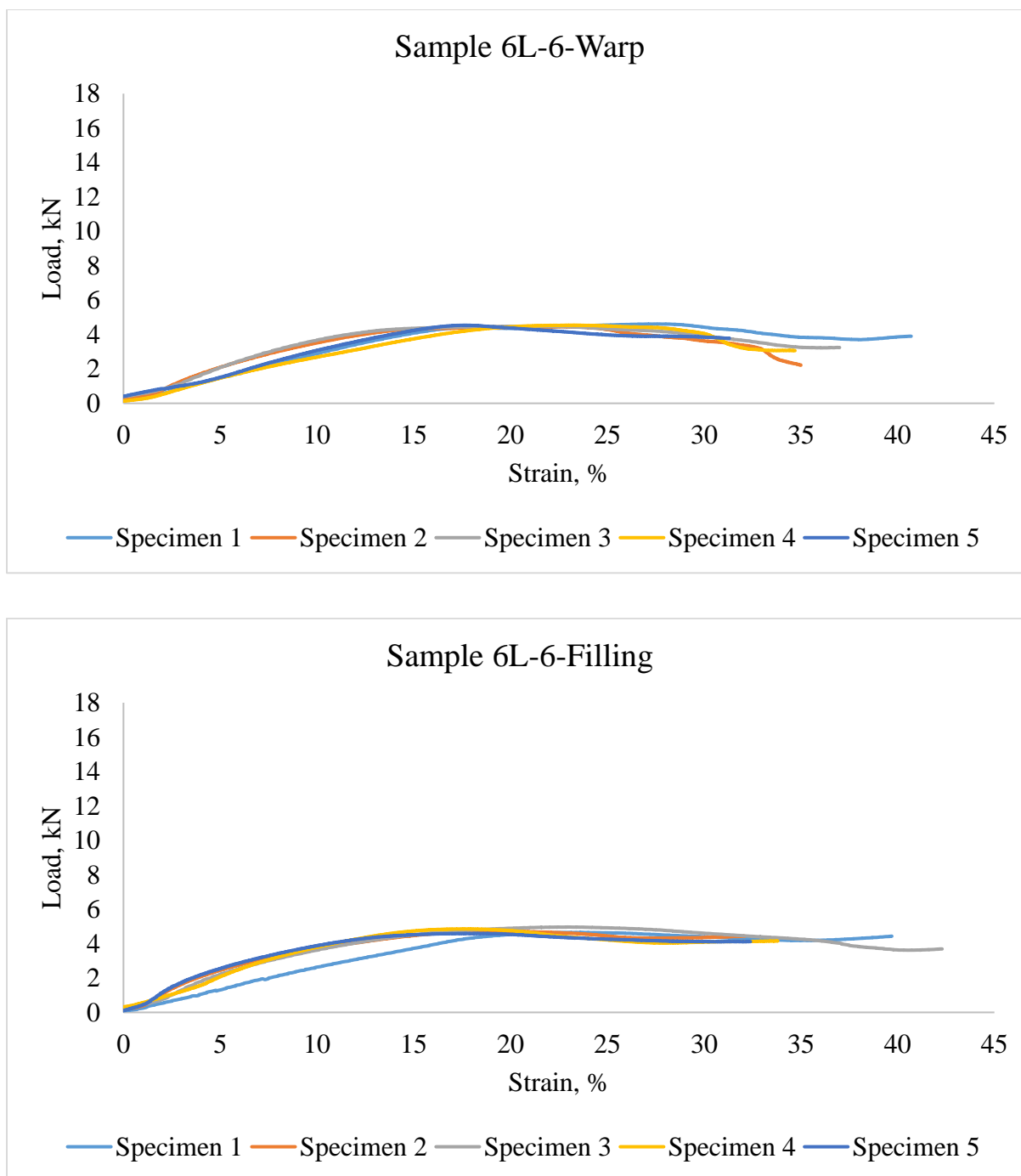
(c)



(d)



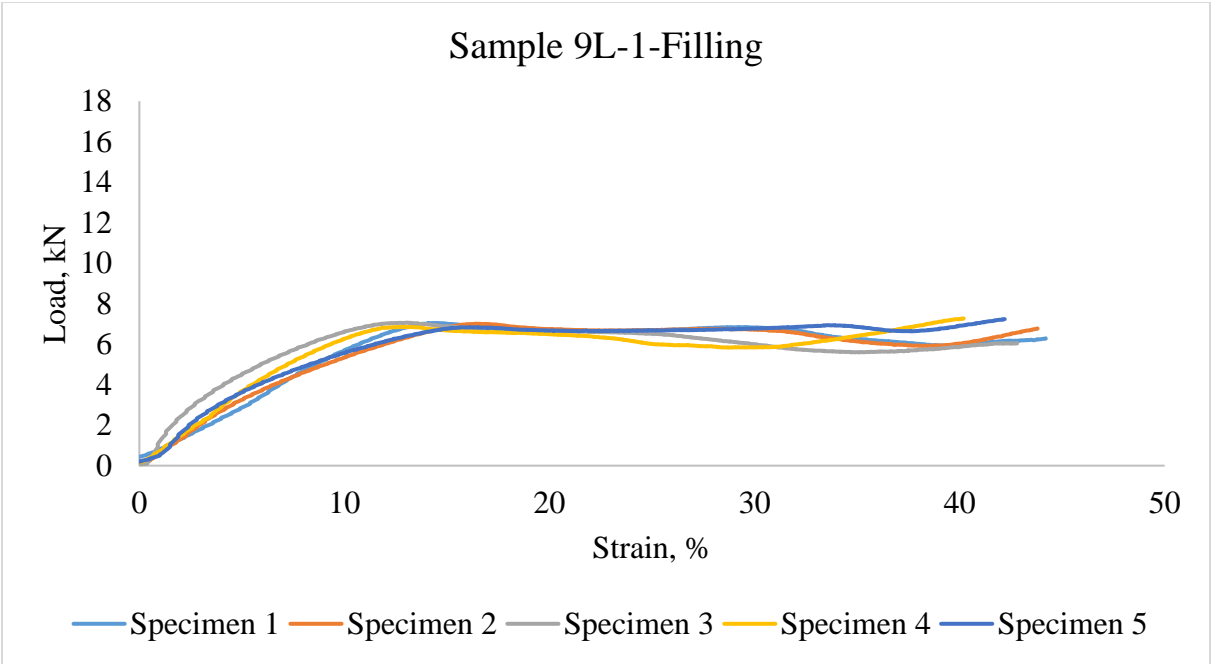
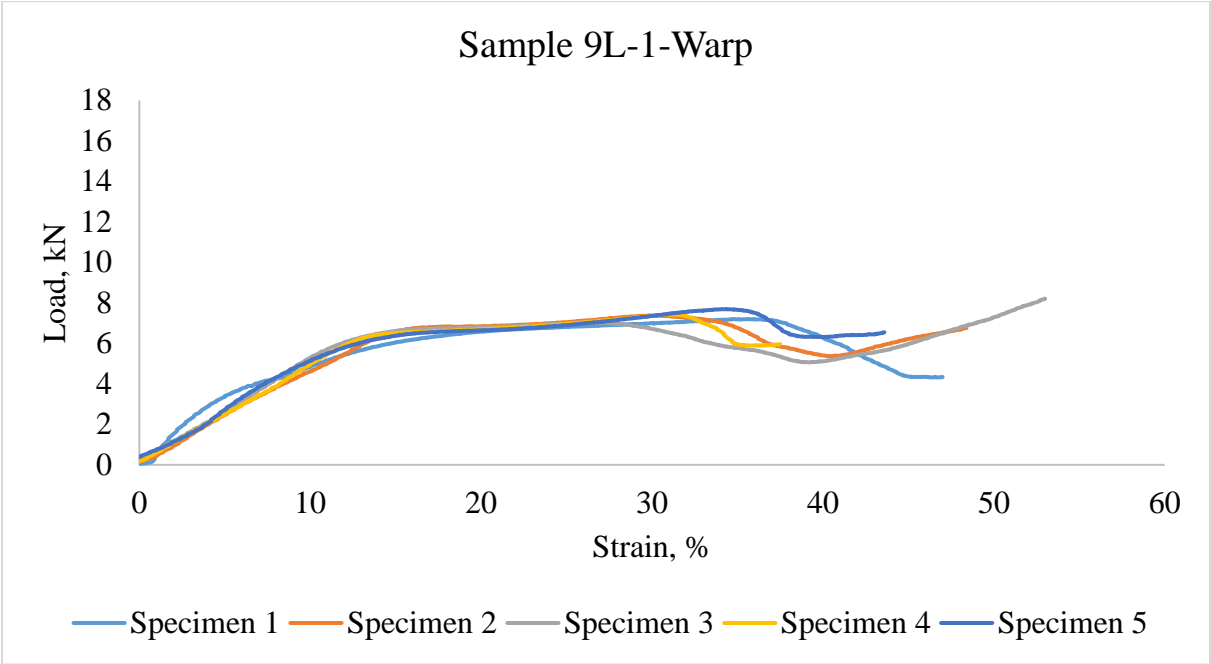
(e)



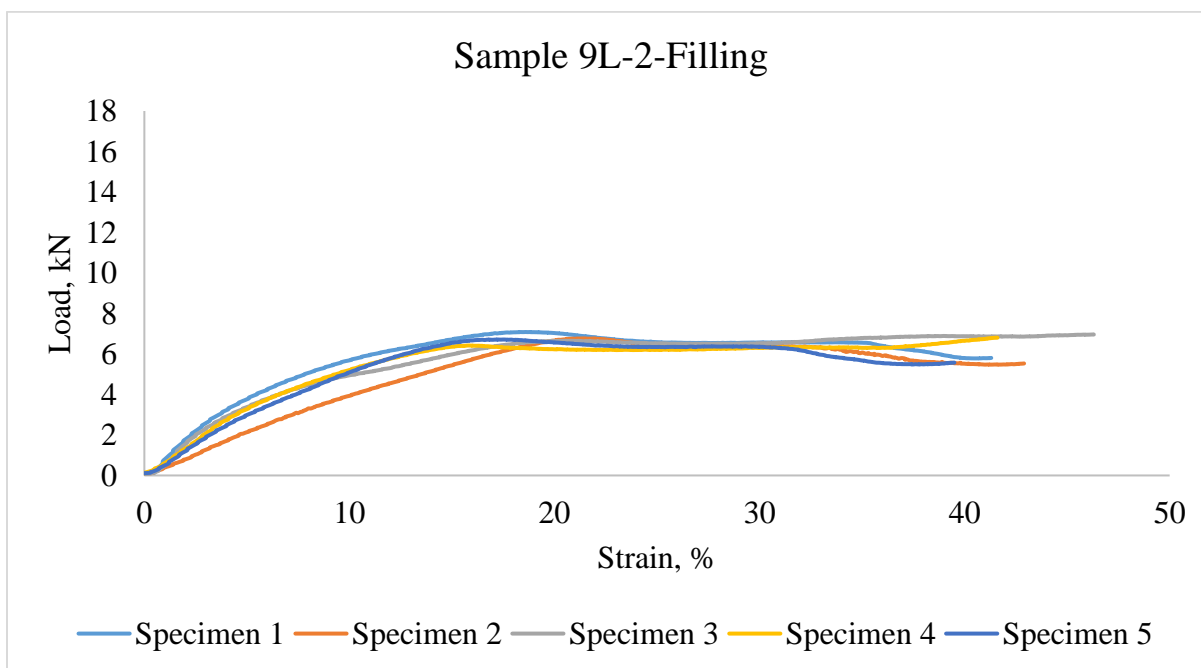
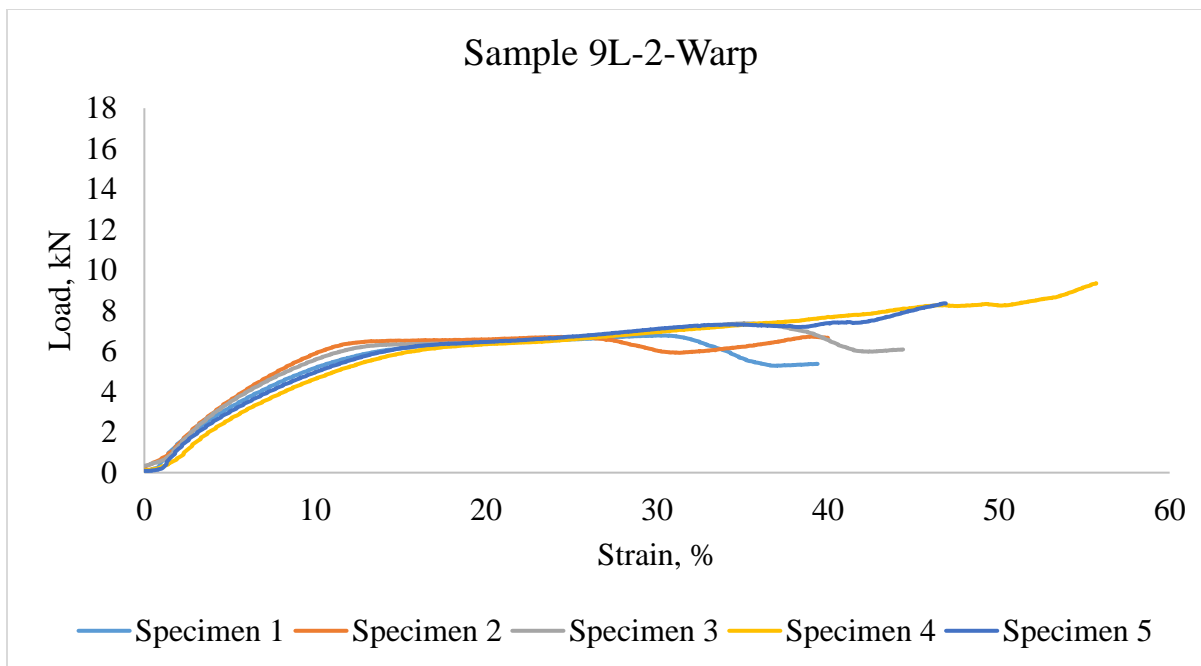
(f)

Figure 208. Typical compression curves of 6 Y-yarn layers 3DOW composites (a) plain and 1:1 Z to Y-yarn ratio, (b) 2x2 warp rib and 1:1 Z to Y-yarn ratio, (c) 3x3 warp rib and 1:1 Z to Y-

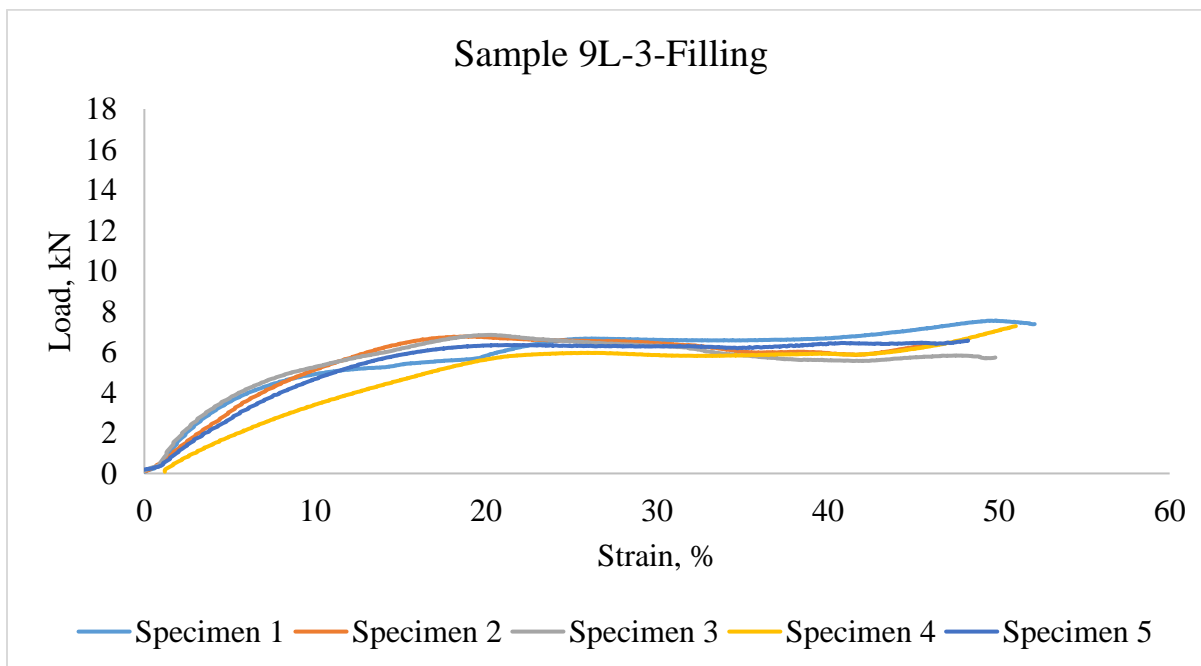
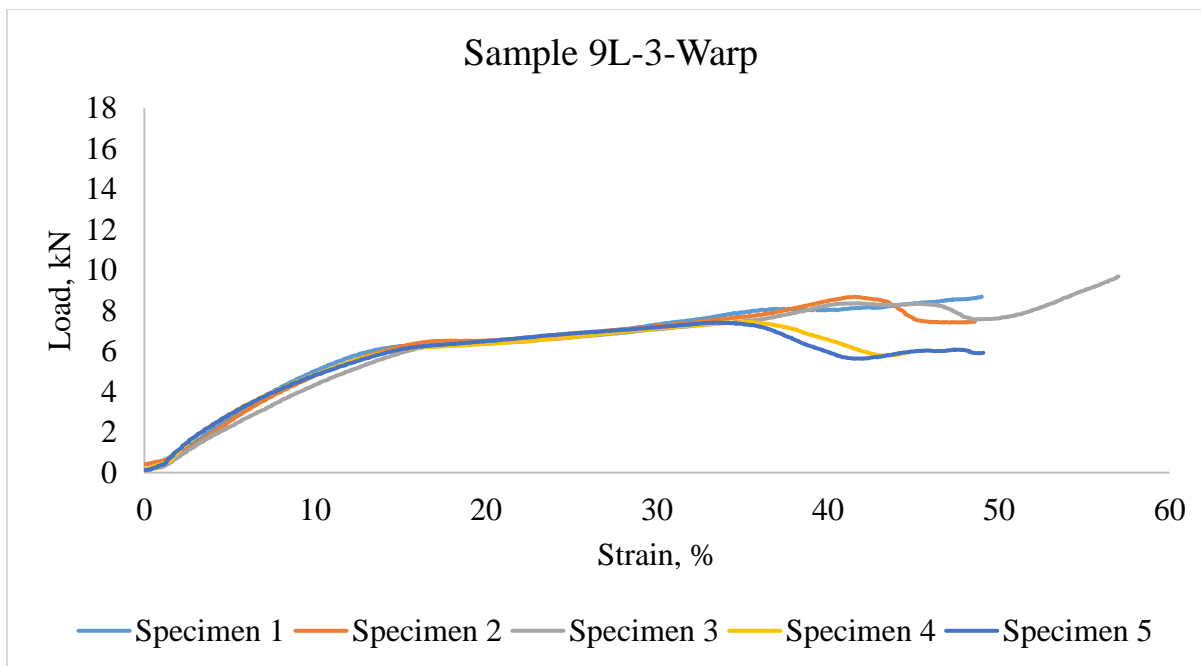
yarn ratio, (d) plain and 1:3 Z to Y-yarn ratio, (e) 2x2 warp rib and 1:3 Z to Y-yarn ratio, (f) 3x3
warp rib and 1:3 Z to Y-yarn ratio



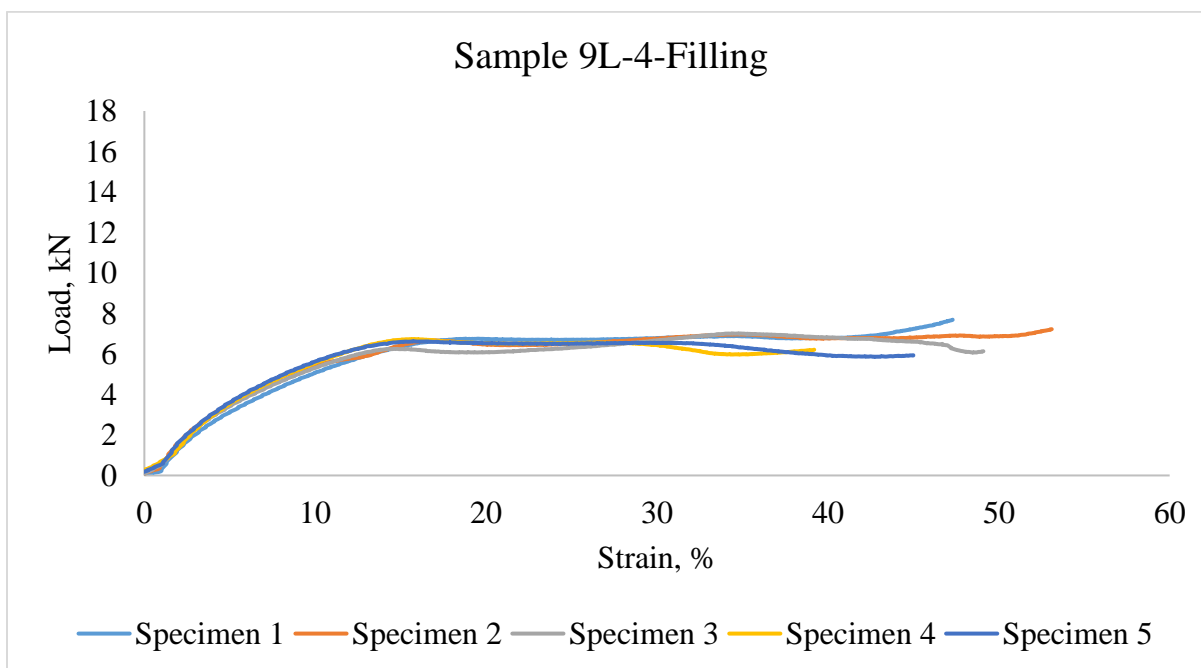
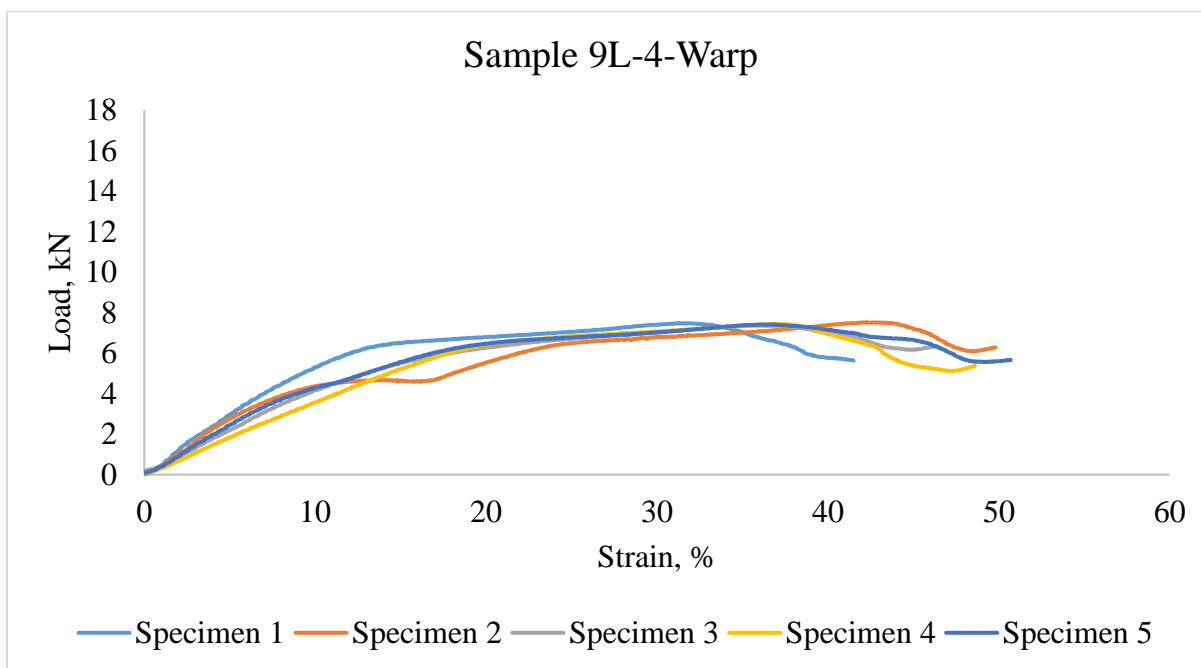
(a)



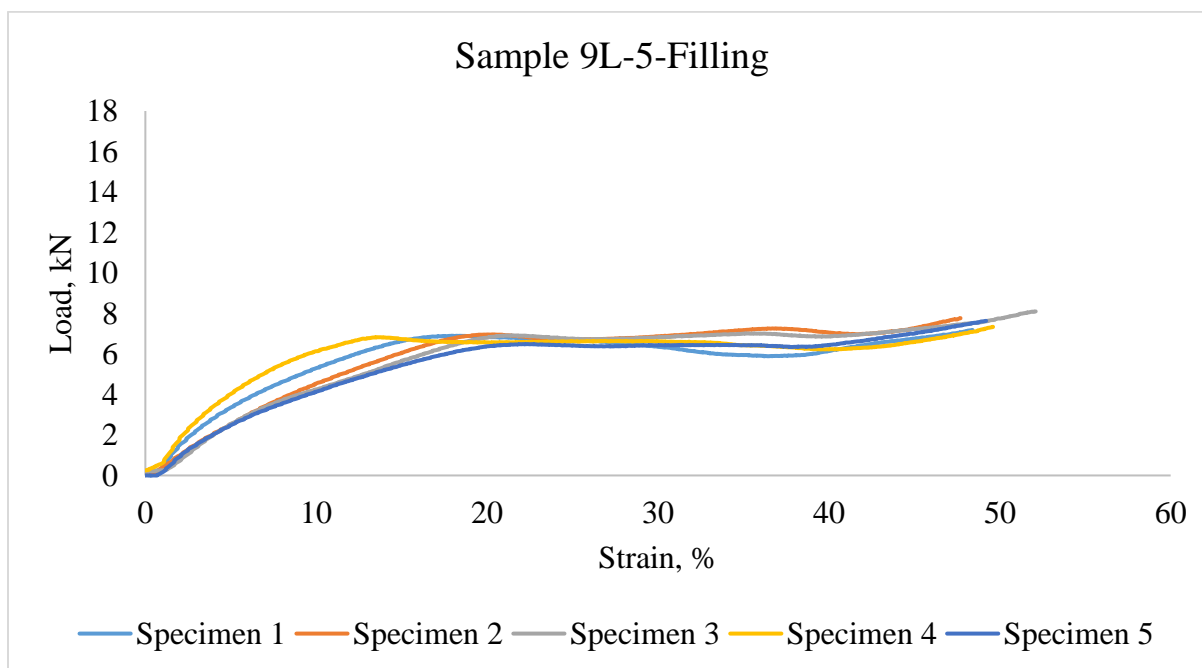
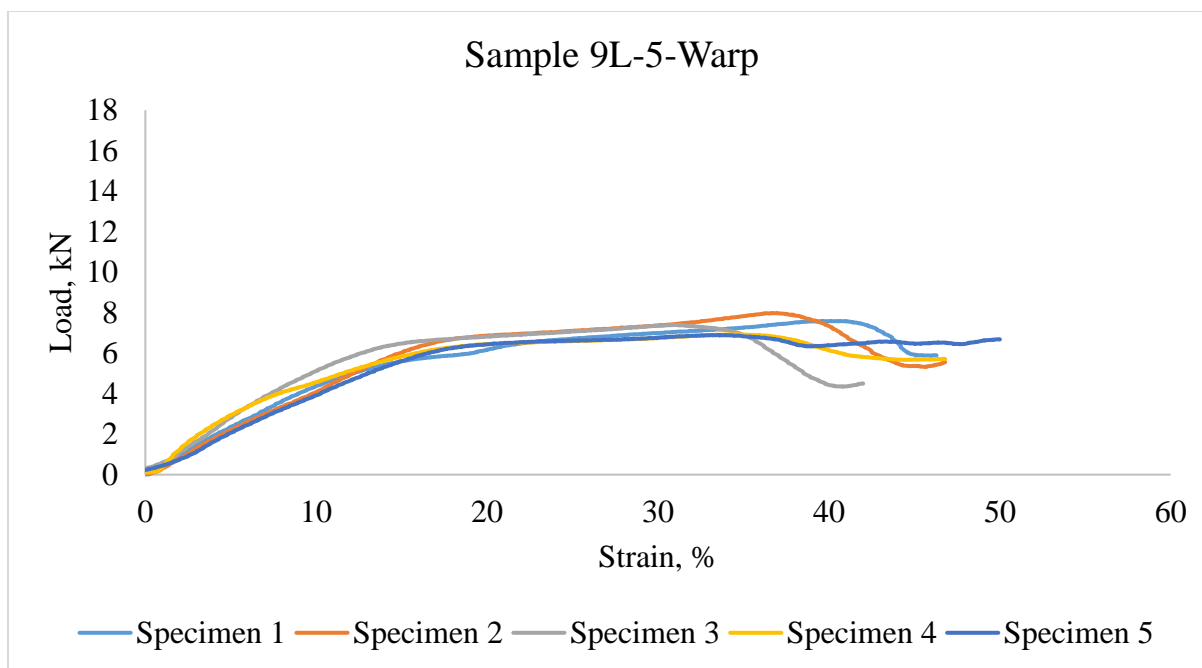
(b)



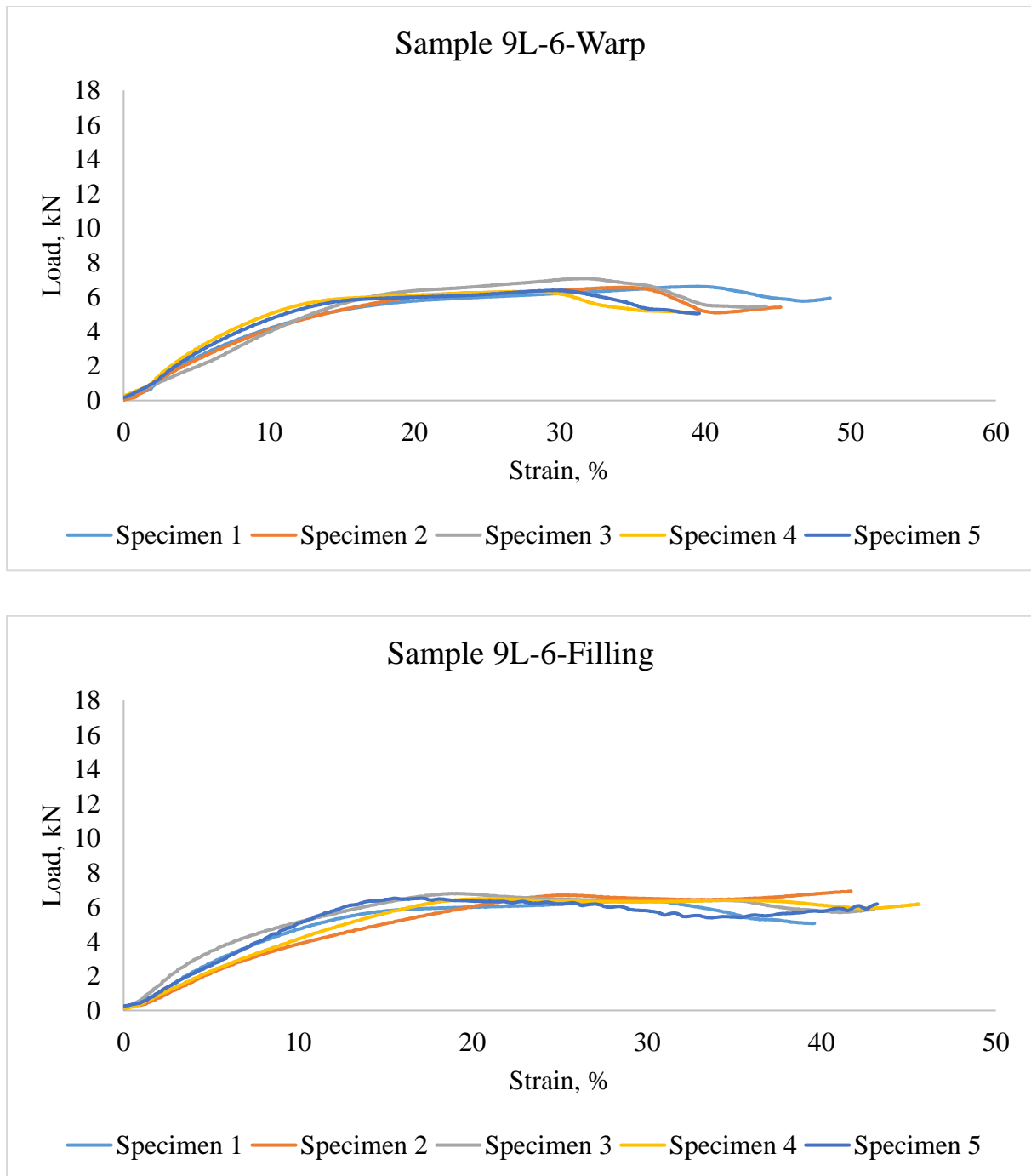
(c)



(d)



(e)



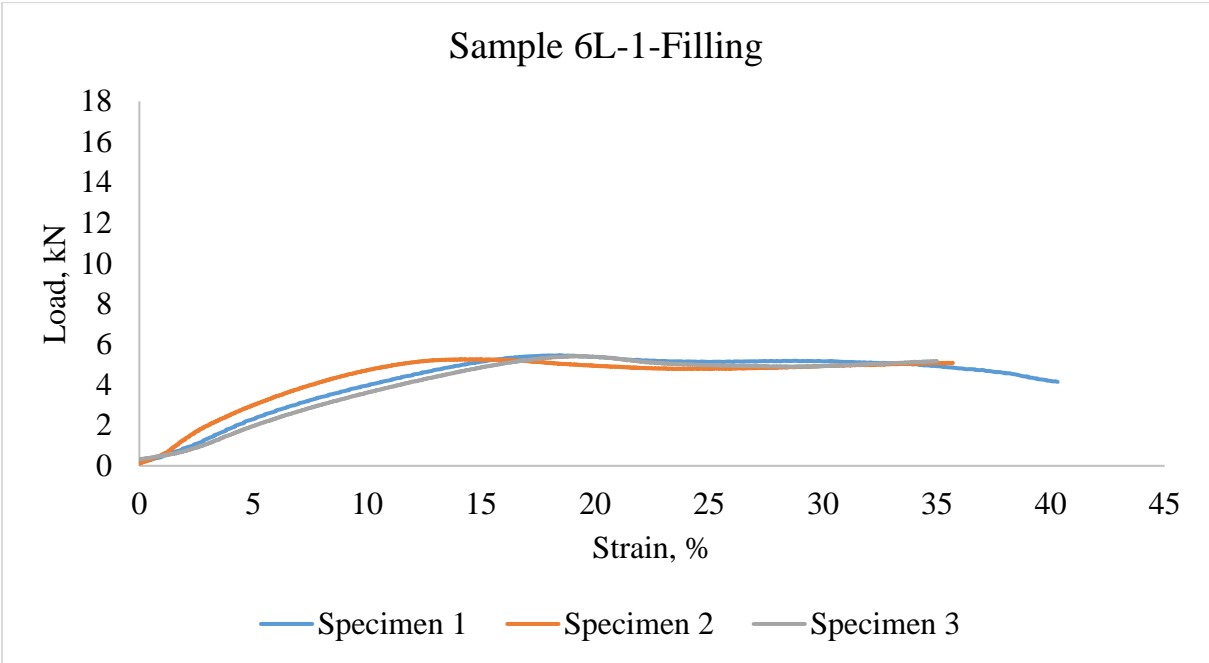
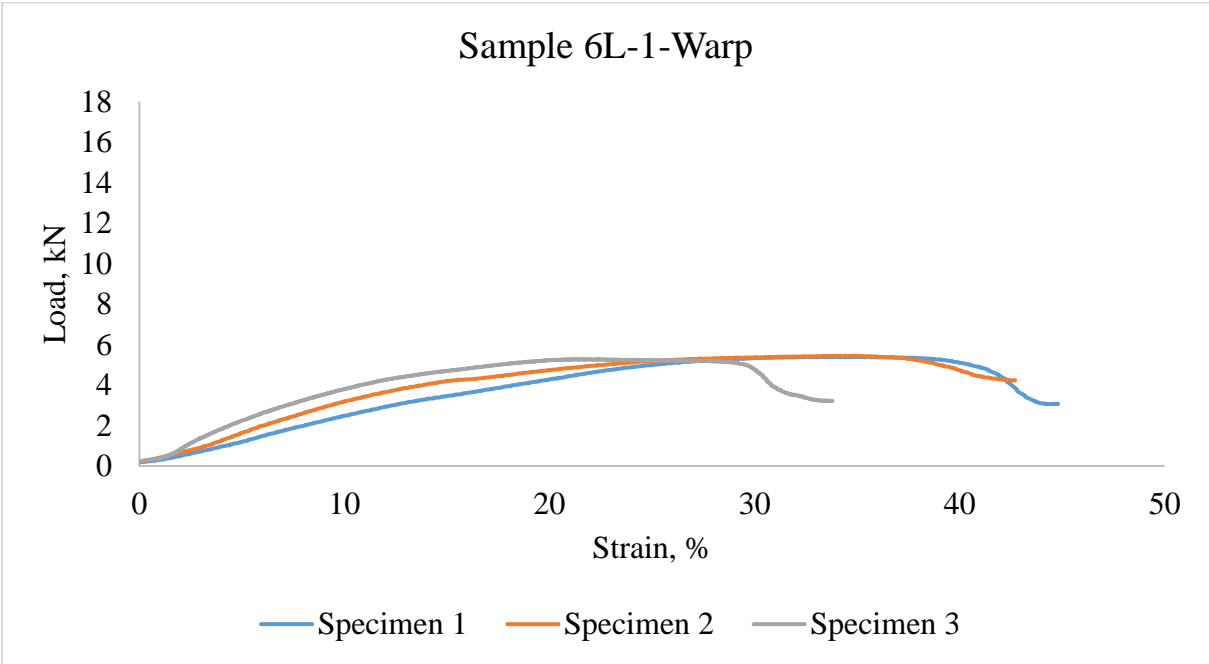
(f)

Figure 209. Typical compression curves of 9 Y-yarn layers 3DOW composites (a) plain and 1:1 Z to Y-yarn ratio, (b) 2x2 warp rib and 1:1 Z to Y-yarn ratio, (c) 3x3 warp rib and 1:1 Z to Y-

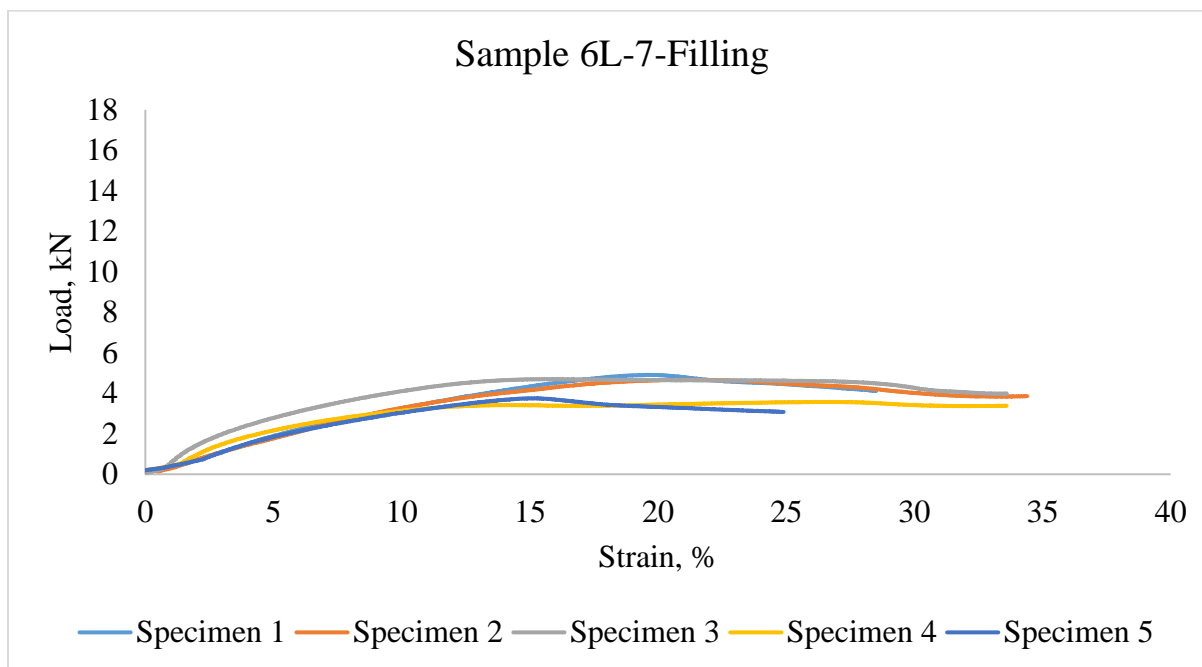
yarn ratio, (d) plain and 1:3 Z to Y-yarn ratio, (e) 2x2 warp rib and 1:3 Z to Y-yarn ratio, (f) 3x3 warp rib and 1:3 Z to Y-yarn ratio

C.6. Typical Compression Curves of 3DOW Composites of Test- Experimental Design

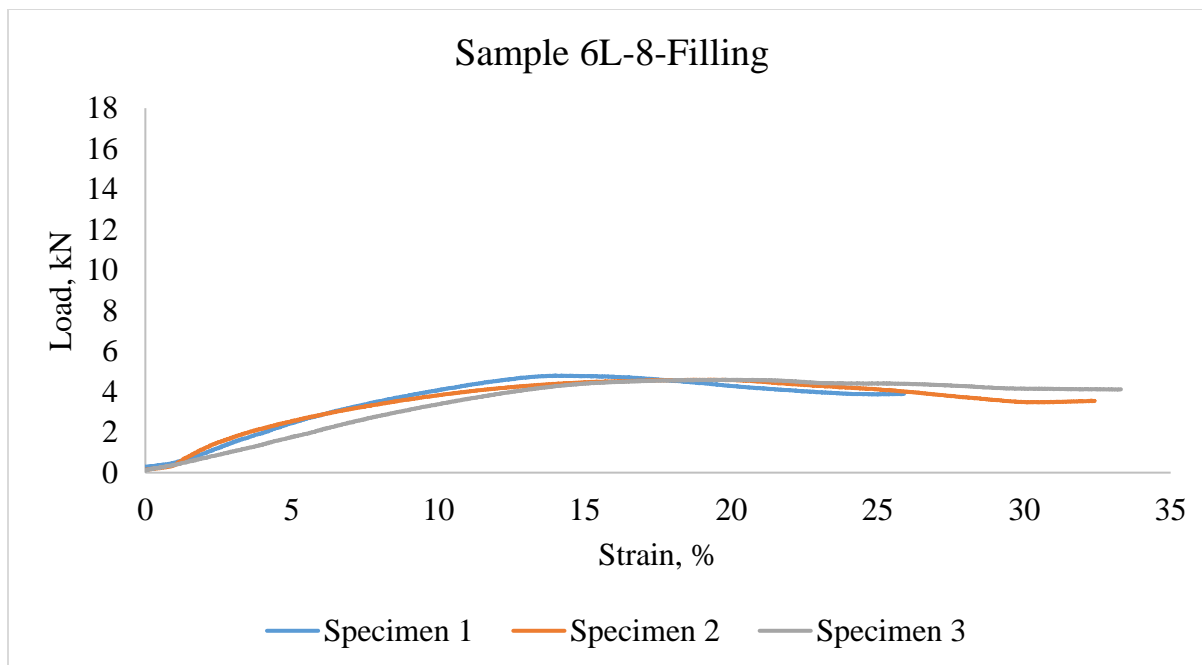
B



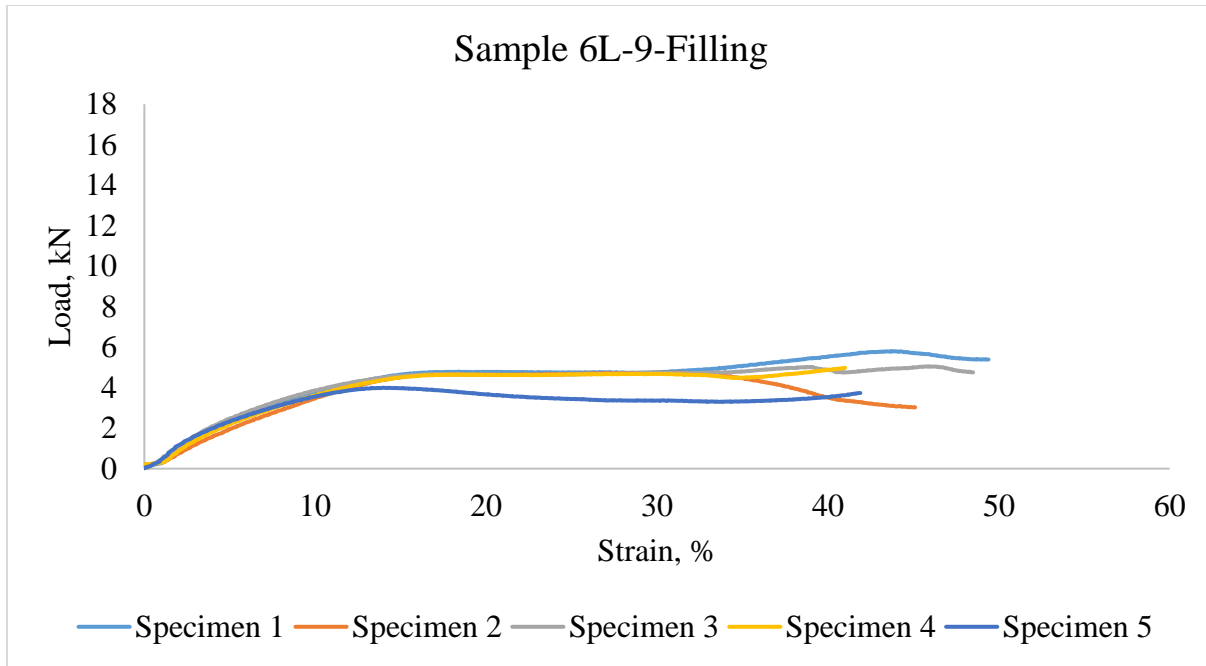
(a)



(b)



(c)



(d)

Figure 210. Force- displacement curves of 6 Y-yarn layers 3DOW composites in the X-yarn (filling) (a) bleached flax yarns, (b) BHS flax yarns, (c) HS flax yarns and (d) grey flax yarns

Appendix D

Table 48. Nomenclature of variables used in statistical analysis

Energy	E
Thickness	t
Load	L
Force	F
Preform	PF.
Composite	Comp.
Arial Density	A. D.
Weaves: 1, 2, 3	Weaves: Plain, 2x2 Warp rib, 3x3 Warp rib
Z/Y Ratio: 1, 0.33	Z/Y Ratio: 1 to 1, 1 to 3

D.1. Statistical Analysis of Experimental Design A

D.1.1. Tensile Test

Summary of Fit					
RSquare			0.96646		
RSquare Adj			0.960723		
Root Mean Square Error			0.537516		
Mean of Response			5.656333		
Observations (or Sum Wgts)			90		
Analysis of Variance					
Source	DF	Sum of Squares	Mean Square	F Ratio	
Model	13	632.72690	48.6713	168.4574	
Error	76	21.95819	0.2889		Prob > F
C. Total	89	654.68509			<.0001*
Parameter Estimates					
Effect Tests					
Source	Nparm	DF	Sum of Squares	F Ratio	Prob > F
Layers	2	2	628.85955	1088.280	<.0001*
Weave	2	2	0.87555	1.5152	0.2263
Z/Y Ratio	1	1	0.00729	0.0252	0.8742
Layers*Weave	4	4	0.16679	0.1443	0.9650
Layers*Z/Y Ratio	2	2	1.15851	2.0049	0.1417
Weave*Z/Y Ratio	2	2	1.65923	2.8714	0.0628

Table 49. ANOVA Results- Tensile (Warp)- Peak load

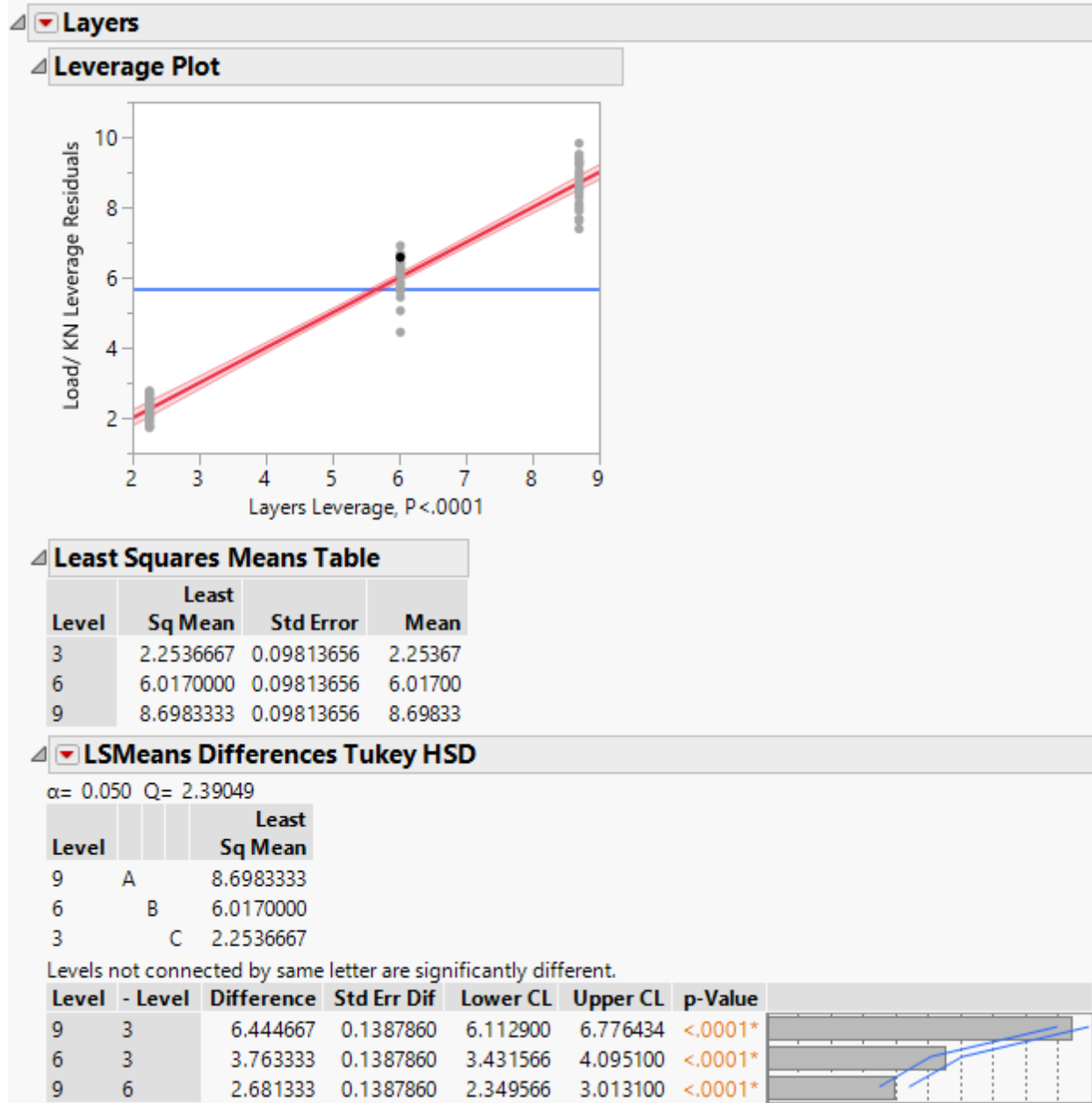


Figure 211. Tukey HSD- Tensile (Warp)- Effect of Layers on Tensile Load

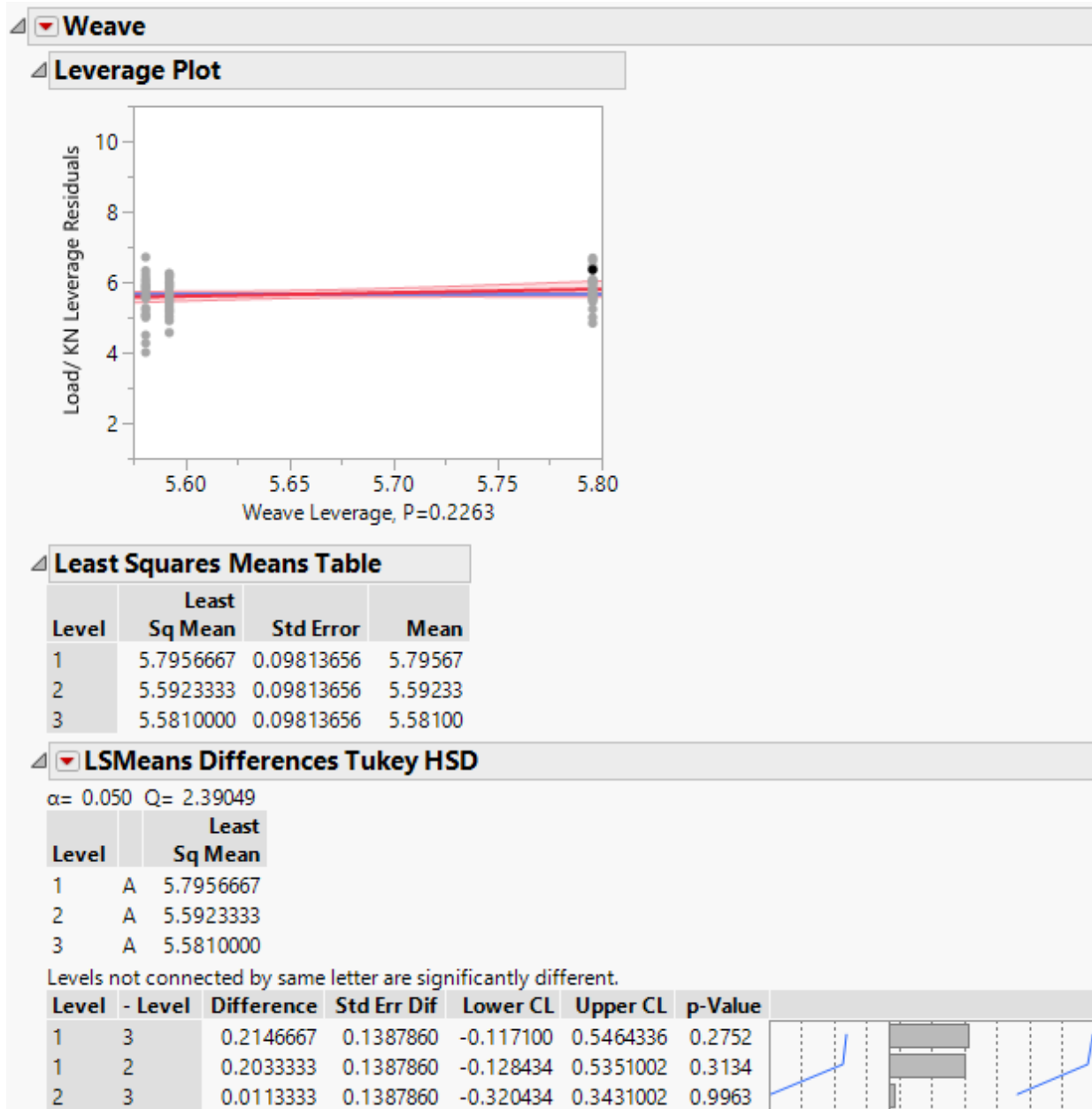


Figure 212. Tukey HSD- Tensile (Warp)- Effect of weave on Tensile Load

Summary of Fit					
RSquare			0.703224		
RSquare Adj			0.65246		
Root Mean Square Error			7.157364		
Mean of Response			65.80444		
Observations (or Sum Wgts)			90		
Analysis of Variance					
Source	DF	Sum of Squares	Mean Square	F Ratio	
Model	13	9225.387	709.645	13.8527	
Error	76	3893.317	51.228		Prob > F
C. Total	89	13118.705			<.0001*
Parameter Estimates					
Effect Tests					
Source	Nparm	DF	Sum of Squares	F Ratio	Prob > F
Layers	2	2	8082.9142	78.8918	<.0001*
Weave	2	2	55.4346	0.5411	0.5844
Z/Y Ratio	1	1	28.3361	0.5531	0.4593
Layers*Weave	4	4	221.6368	1.0816	0.3716
Layers*Z/Y Ratio	2	2	705.4405	6.8853	0.0018*
Weave*Z/Y Ratio	2	2	131.6252	1.2847	0.2827

Table 50. ANOVA Results – Tensile (Warp)- Peak stress

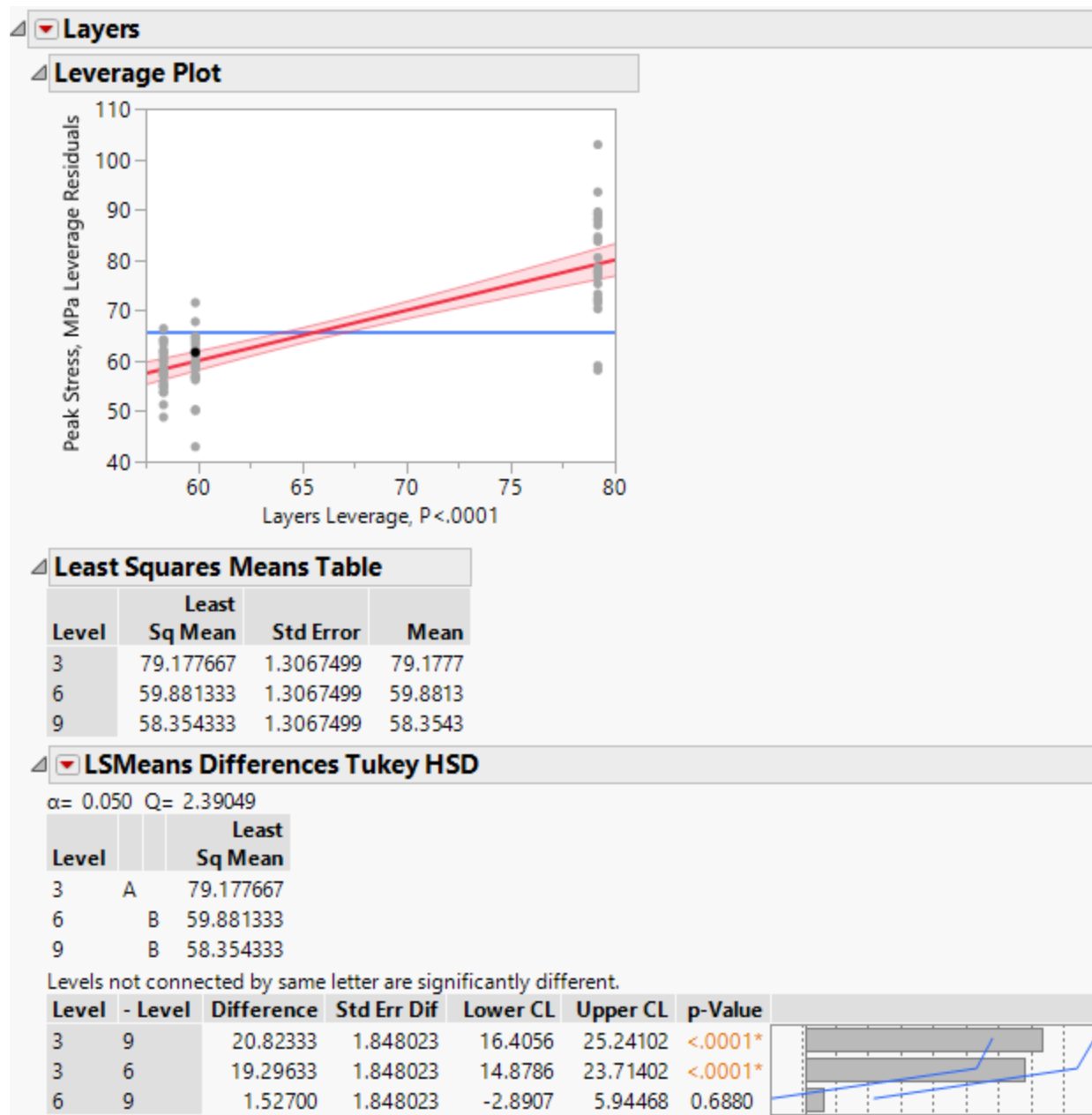


Figure 213. Tukey HSD- Tensile (Warp)- Effect of layers on Tensile stress

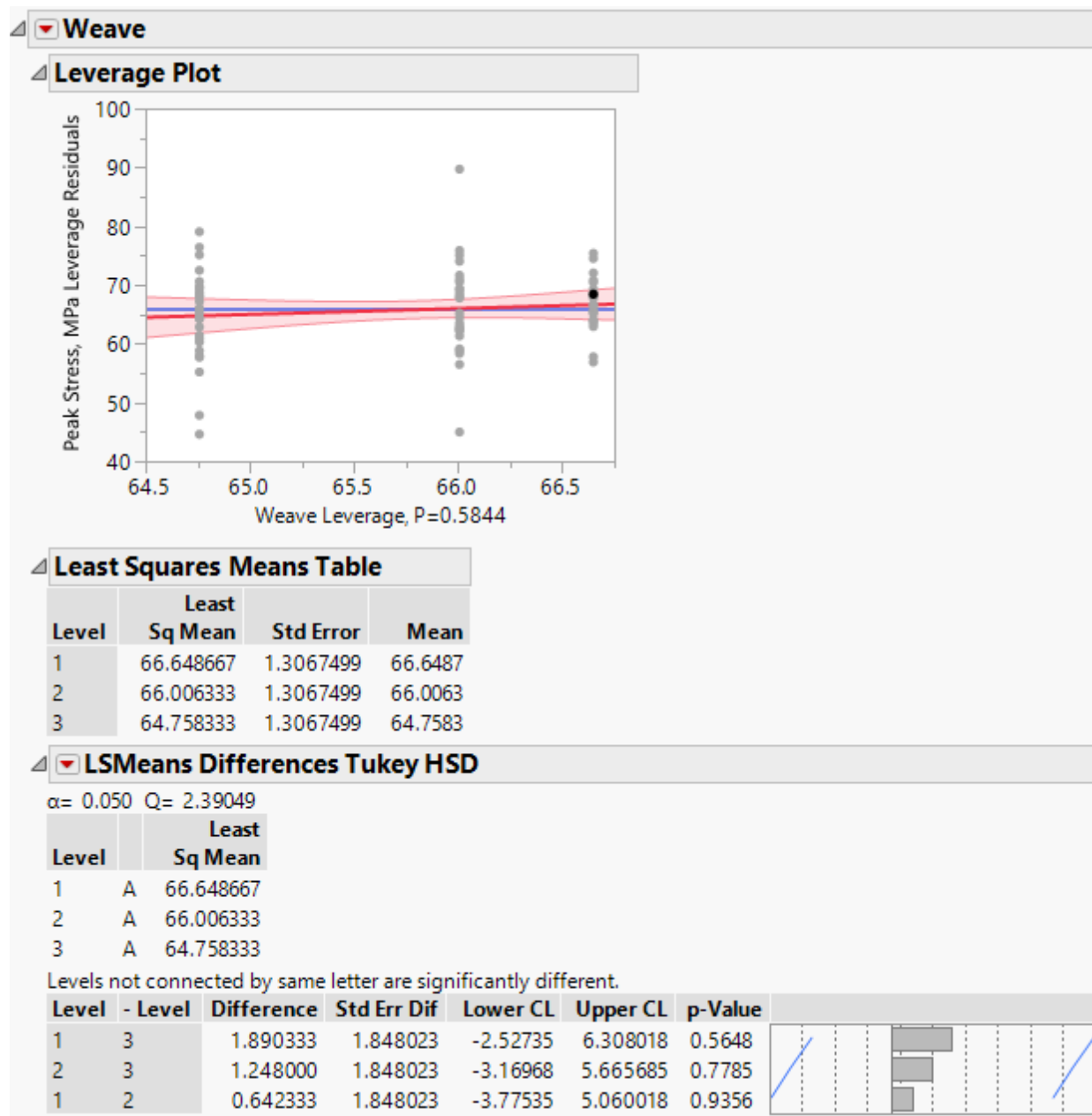


Figure 214. Tukey HSD- Tensile (Warp)- Effect of weave on Tensile stress

Summary of Fit					
RSquare			0.6659		
RSquare Adj			0.608751		
Root Mean Square Error			2.904526		
Mean of Response			29.952		
Observations (or Sum Wgts)			90		
Analysis of Variance					
Source	DF	Sum of Squares	Mean Square	F Ratio	Prob > F
Model	13	1277.8995	98.3000	11.6521	
Error	76	641.1568	8.4363		
C. Total	89	1919.0562			<.0001*
Parameter Estimates					
Effect Tests					
Source	Nparm	DF	Sum of Squares	F Ratio	Prob > F
Layers	2	2	1043.5035	61.8462	<.0001*
Weave	2	2	13.0327	0.7724	0.4655
Z/Y Ratio	1	1	6.5071	0.7713	0.3826
Layers*Weave	4	4	100.8893	2.9897	0.0239*
Layers*Z/Y Ratio	2	2	79.8619	4.7332	0.0116*
Weave*Z/Y Ratio	2	2	34.1049	2.0213	0.1395

Table 51. ANOVA Results – Tensile (Warp)- Tensile Load Normalized by Preform Areal
Density

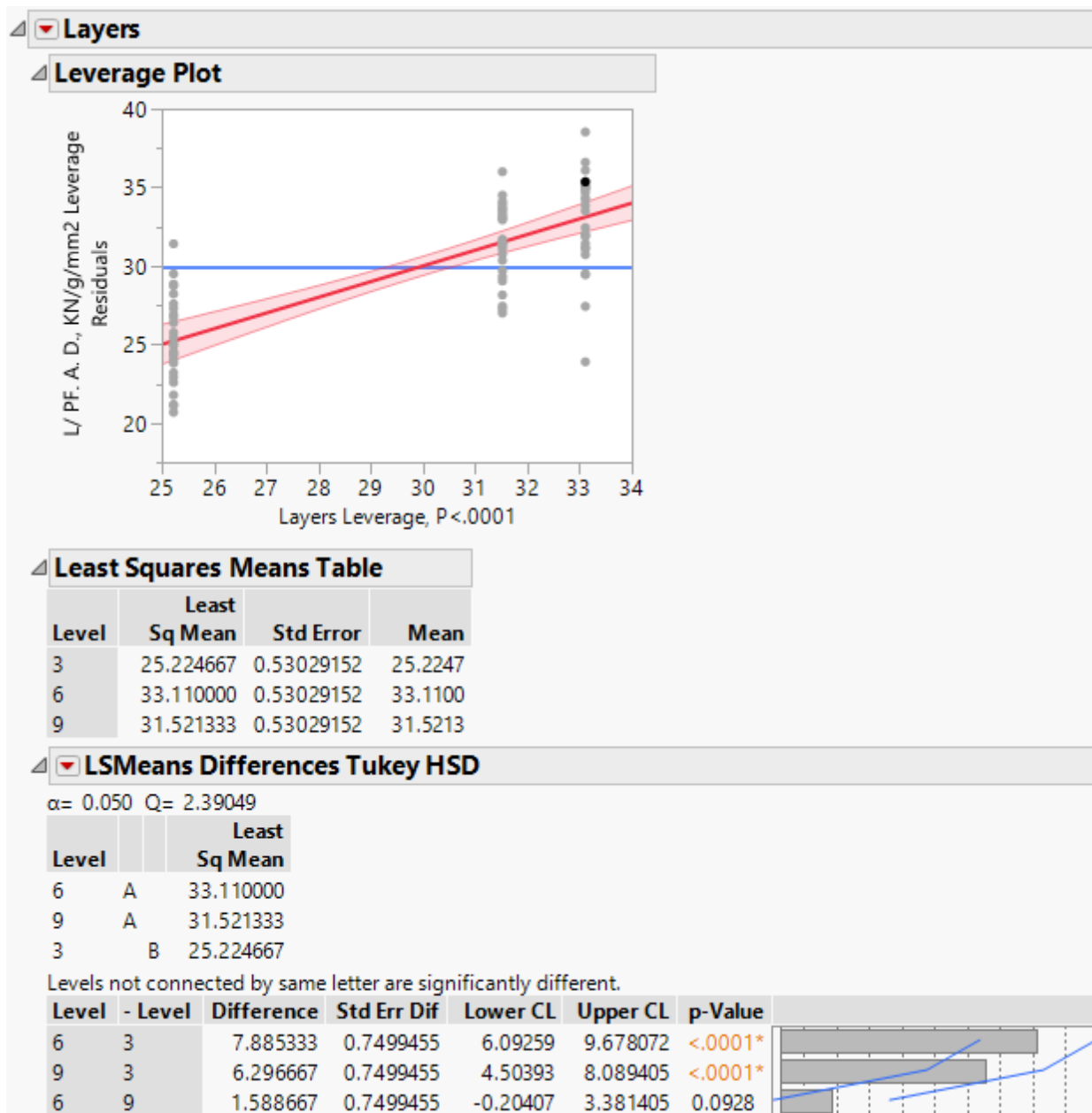


Figure 215. Tukey HSD- Tensile (Warp)- Effect of layers on Tensile Load Normalized by
Preform Areal Density

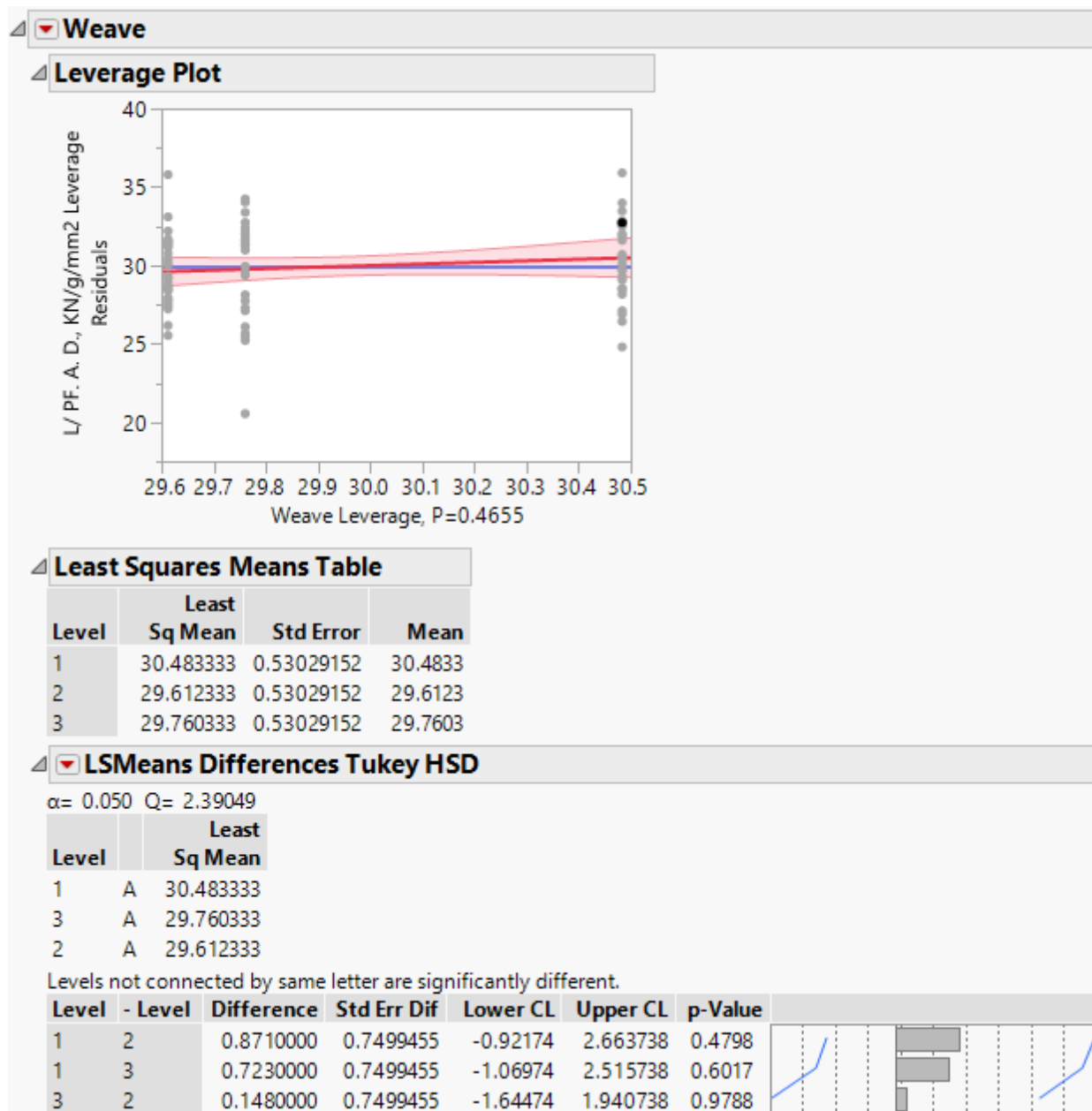


Figure 216. Tukey HSD- Tensile (Warp)- Effect of weave on Tensile Load Normalized by
Preform Areal Density

Summary of Fit					
RSquare			0.400024		
RSquare Adj			0.297397		
Root Mean Square Error			1.08945		
Mean of Response			11.68311		
Observations (or Sum Wgts)			90		
Analysis of Variance					
Source	DF	Sum of Squares	Mean Square	F Ratio	
Model	13	60.14243	4.62634	3.8978	
Error	76	90.20450	1.18690		Prob > F
C. Total	89	150.34693			<.0001*
Parameter Estimates					
Effect Tests					
Source	Nparm	DF	Sum of Squares	F Ratio	Prob > F
Layers	2	2	28.261296	11.9055	<.0001*
Weave	2	2	3.695929	1.5570	0.2174
Z/Y Ratio	1	1	0.109551	0.0923	0.7621
Layers*Weave	4	4	7.274604	1.5323	0.2013
Layers*Z/Y Ratio	2	2	18.266829	7.6952	0.0009*
Weave*Z/Y Ratio	2	2	2.534222	1.0676	0.3489

Table 52. ANOVA Results – Tensile (Warp)- Tensile Load Normalized by Composite Areal
Density

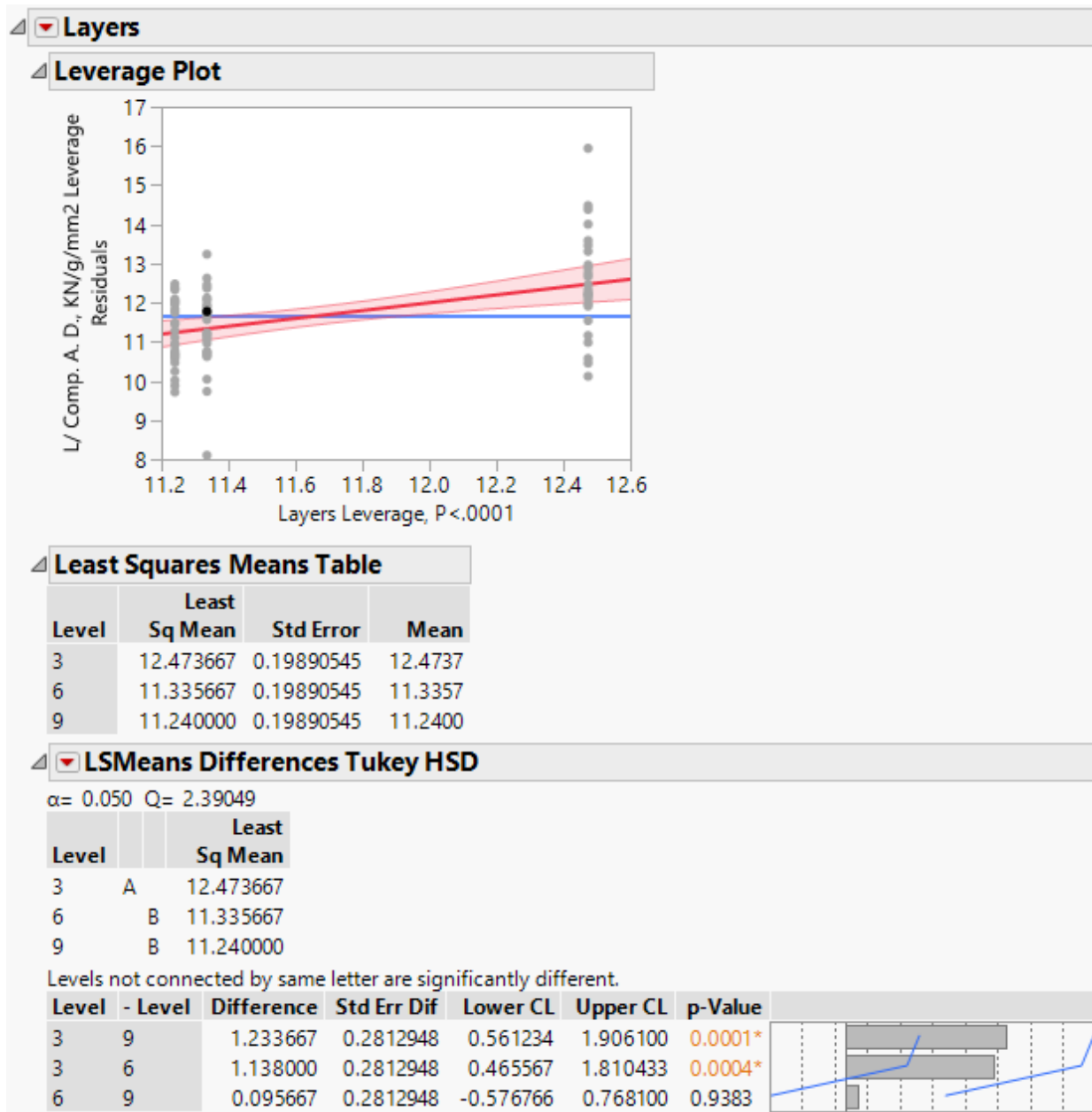


Figure 217. Tukey HSD- Tensile (Warp)- Effect of layers on Tensile Load Normalized by Composite Areal Density

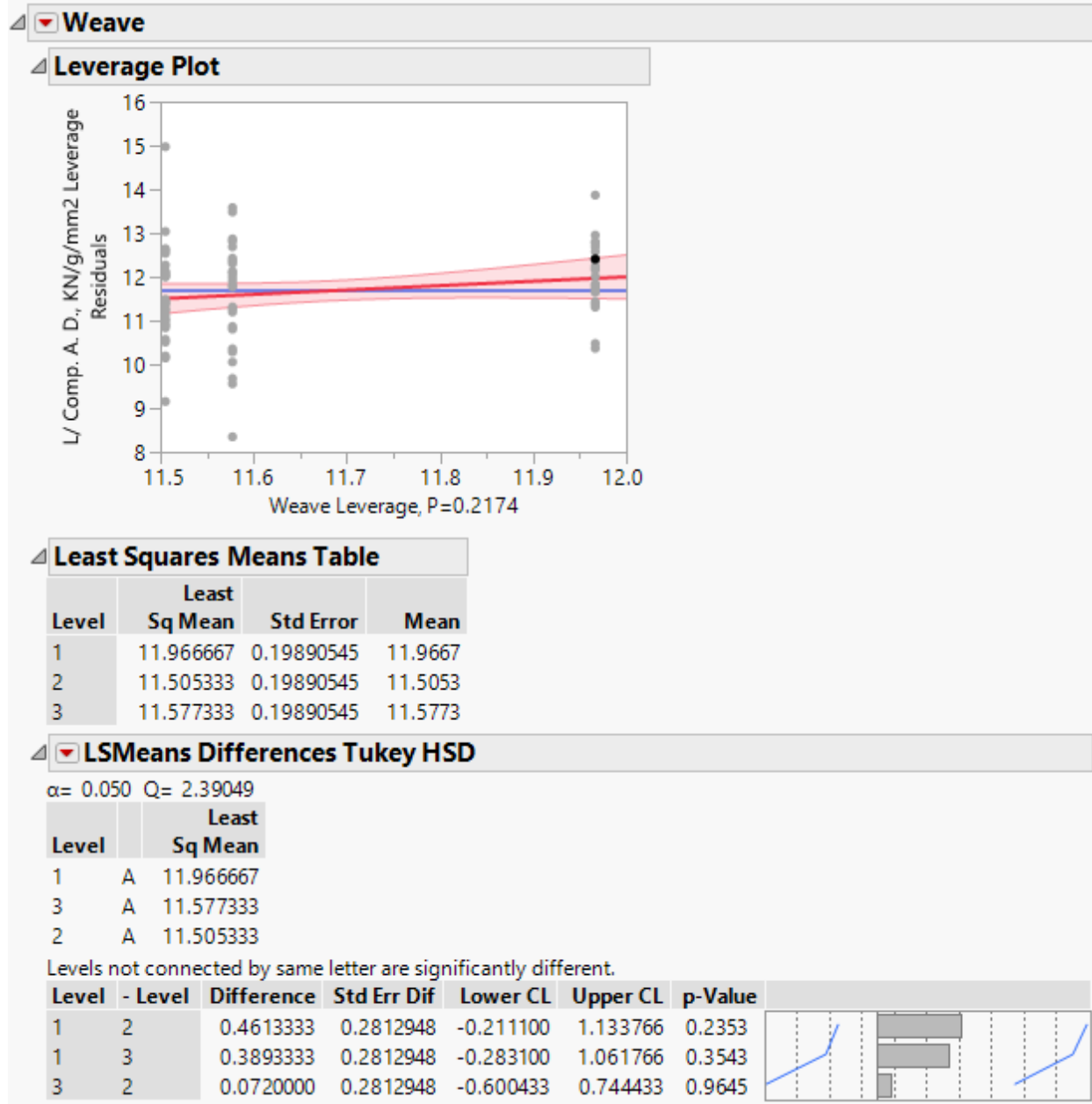


Figure 218. Tukey HSD- Tensile (Warp)- Effect of weave on Tensile Load Normalized by
Composite Areal Density

Summary of Fit					
RSquare			0.975358		
RSquare Adj			0.971143		
Root Mean Square Error			0.852639		
Mean of Response			10.52767		
Observations (or Sum Wgts)			90		
Analysis of Variance					
Source	DF	Sum of Squares	Mean Square	F Ratio	
Model	13	2186.9453	168.227	231.4003	
Error	76	55.2515	0.727		Prob > F
C. Total	89	2242.1968			<.0001*
Parameter Estimates					
Effect Tests					
Source	Nparm	DF	Sum of Squares	F Ratio	Prob > F
Layers	2	2	2101.8587	1445.582	<.0001*
Weave	2	2	50.5685	34.7792	<.0001*
Z/Y Ratio	1	1	0.2122	0.2919	0.5906
Layers*Weave	4	4	30.0043	10.3179	<.0001*
Layers*Z/Y Ratio	2	2	3.4119	2.3466	0.1026
Weave*Z/Y Ratio	2	2	0.8897	0.6119	0.5450

Table 53. ANOVA Results- Tensile (Weft)- Peak load



Figure 219. Tukey HSD- Tensile (Weft)- Effect of Layers on Tensile Load

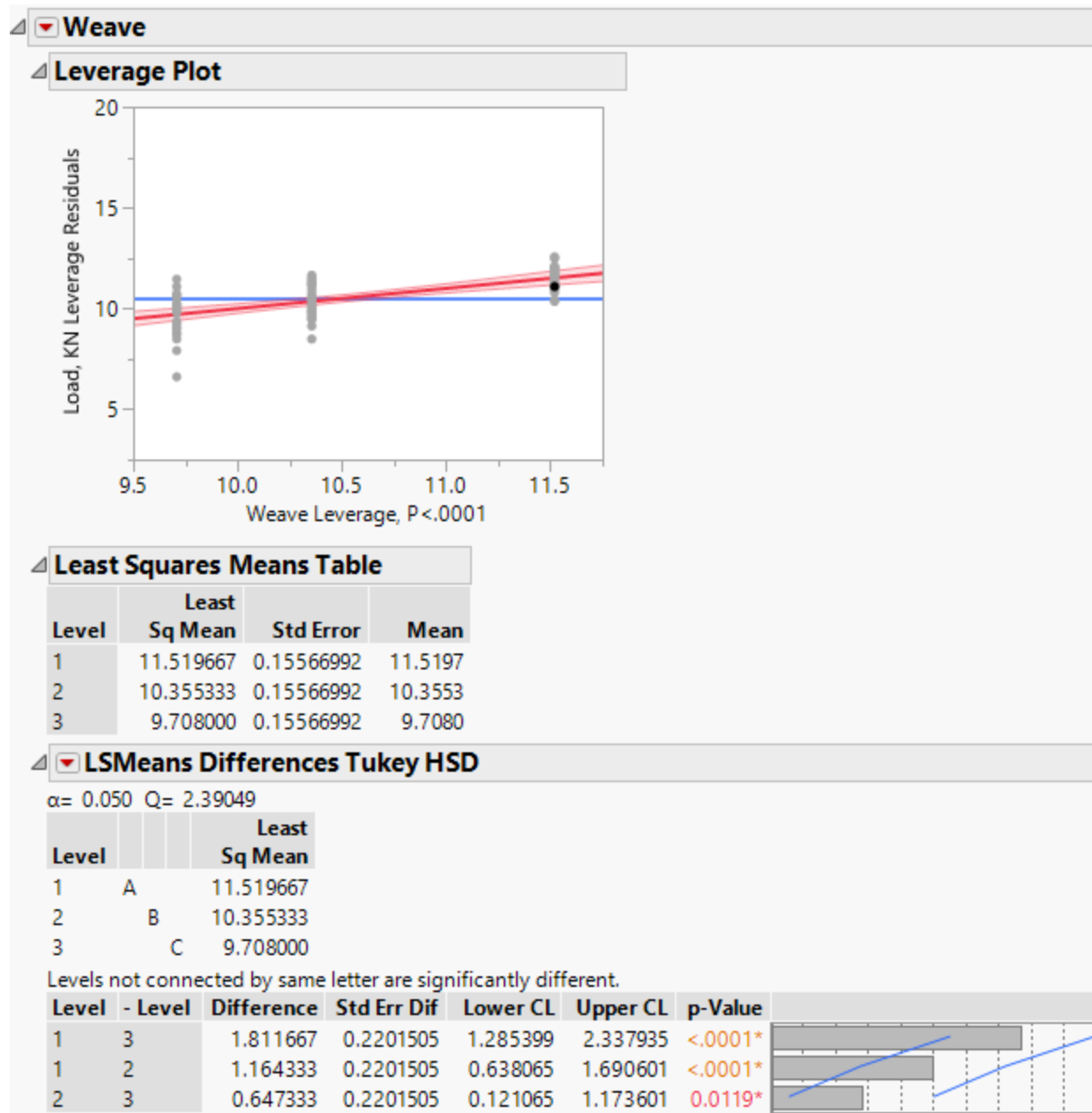


Figure 220. Tukey HSD- Tensile (Weft)- Effect of weave on Tensile Load

Summary of Fit					
RSquare			0.655812		
RSquare Adj			0.596938		
Root Mean Square Error			18.26		
Mean of Response			123.2731		
Observations (or Sum Wgts)			90		
Analysis of Variance					
Source	DF	Sum of Squares	Mean Square	F Ratio	
Model	13	48283.568	3714.12	11.1392	
Error	76	25340.507	333.43		Prob > F
C. Total	89	73624.075			<.0001*
Parameter Estimates					
Effect Tests					
Source	Nparm	DF	Sum of Squares	F Ratio	Prob > F
Layers	2	2	38831.726	58.2311	<.0001*
Weave	2	2	2869.642	4.3032	0.0170*
Z/Y Ratio	1	1	97.011	0.2910	0.5912
Layers*Weave	4	4	5077.862	3.8073	0.0071*
Layers*Z/Y Ratio	2	2	378.131	0.5670	0.5696
Weave*Z/Y Ratio	2	2	1029.196	1.5434	0.2203

Table 54. ANOVA Results – Tensile (Weft)- Peak stress



Figure 221. Tukey HSD- Tensile (Weft)- Effect of layers on Tensile stress

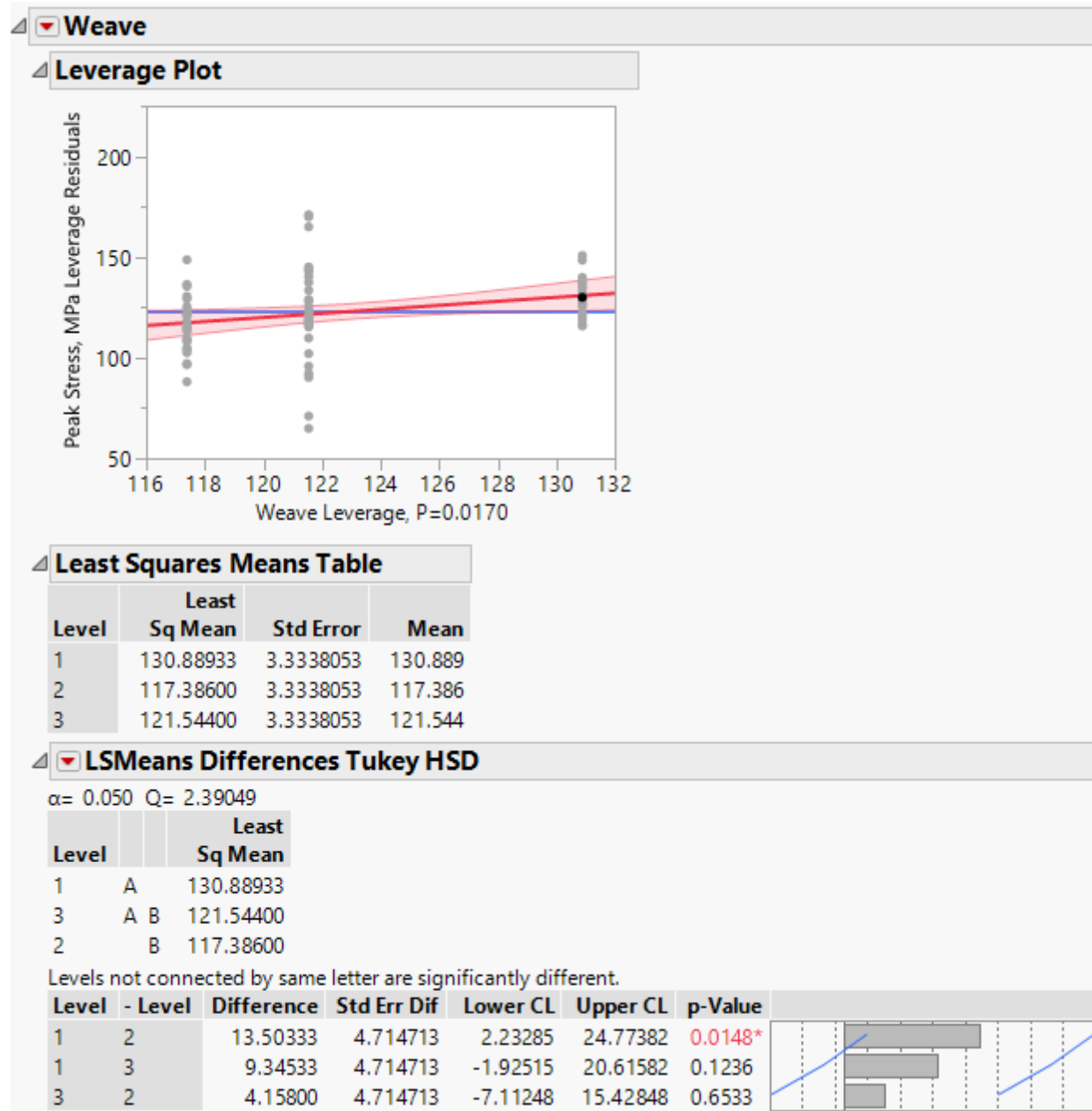


Figure 222. Tukey HSD- Tensile (Weft)- Effect of weave on Tensile stress

Summary of Fit					
RSquare			0.639881		
RSquare Adj			0.578282		
Root Mean Square Error			5.458379		
Mean of Response			56.03133		
Observations (or Sum Wgts)			90		
Analysis of Variance					
Source	DF	Sum of Squares	Mean Square	F Ratio	Prob > F
Model	13	4023.4167	309.494	10.3878	
Error	76	2264.3364	29.794		
C. Total	89	6287.7530			<.0001*
Parameter Estimates					
Effect Tests					
Source	Nparm	DF	Sum of Squares	F Ratio	Prob > F
Layers	2	2	2315.5681	38.8598	<.0001*
Weave	2	2	886.4651	14.8766	<.0001*
Z/Y Ratio	1	1	3.6966	0.1241	0.7256
Layers*Weave	4	4	649.9659	5.4539	0.0006*
Layers*Z/Y Ratio	2	2	15.9765	0.2681	0.7655
Weave*Z/Y Ratio	2	2	151.7445	2.5466	0.0850

Table 55. ANOVA Results – Tensile (Weft)- Tensile Load Normalized by Preform Areal
Density

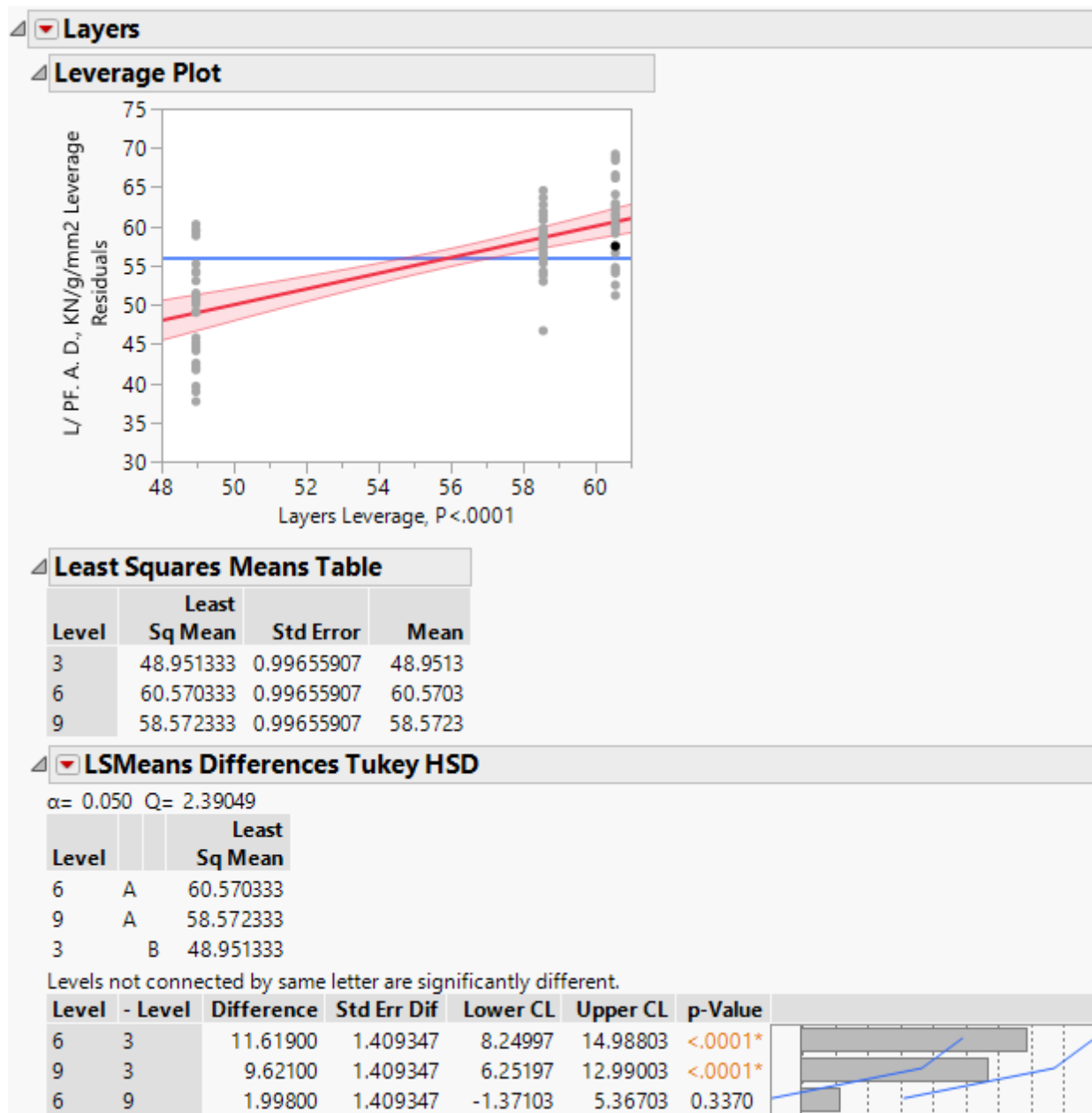


Figure 223. Tukey HSD- Tensile (Weft)- Effect of layers on Tensile Load Normalized by
Preform Areal Density



Figure 224. Tukey HSD- Tensile (Weft)- Effect of weave on Tensile Load Normalized by
Preform Areal Density

Summary of Fit					
RSquare			0.550573		
RSquare Adj			0.473698		
Root Mean Square Error			2.196493		
Mean of Response			21.80478		
Observations (or Sum Wgts)			90		
Analysis of Variance					
Source	DF	Sum of Squares	Mean Square	F Ratio	Prob > F
Model	13	449.18952	34.5530	7.1619	
Error	76	366.66833	4.8246		
C. Total	89	815.85785			<.0001*
Parameter Estimates					
Effect Tests					
Source	Nparm	DF	Sum of Squares	F Ratio	Prob > F
Layers	2	2	215.61296	22.3452	<.0001*
Weave	2	2	109.59800	11.3583	<.0001*
Z/Y Ratio	1	1	2.55025	0.5286	0.4694
Layers*Weave	4	4	89.36373	4.6306	0.0021*
Layers*Z/Y Ratio	2	2	13.66265	1.4159	0.2490
Weave*Z/Y Ratio	2	2	18.40193	1.9071	0.1556

Table 56. ANOVA Results – Tensile (Weft)- Tensile Load Normalized by Composite Areal
Density

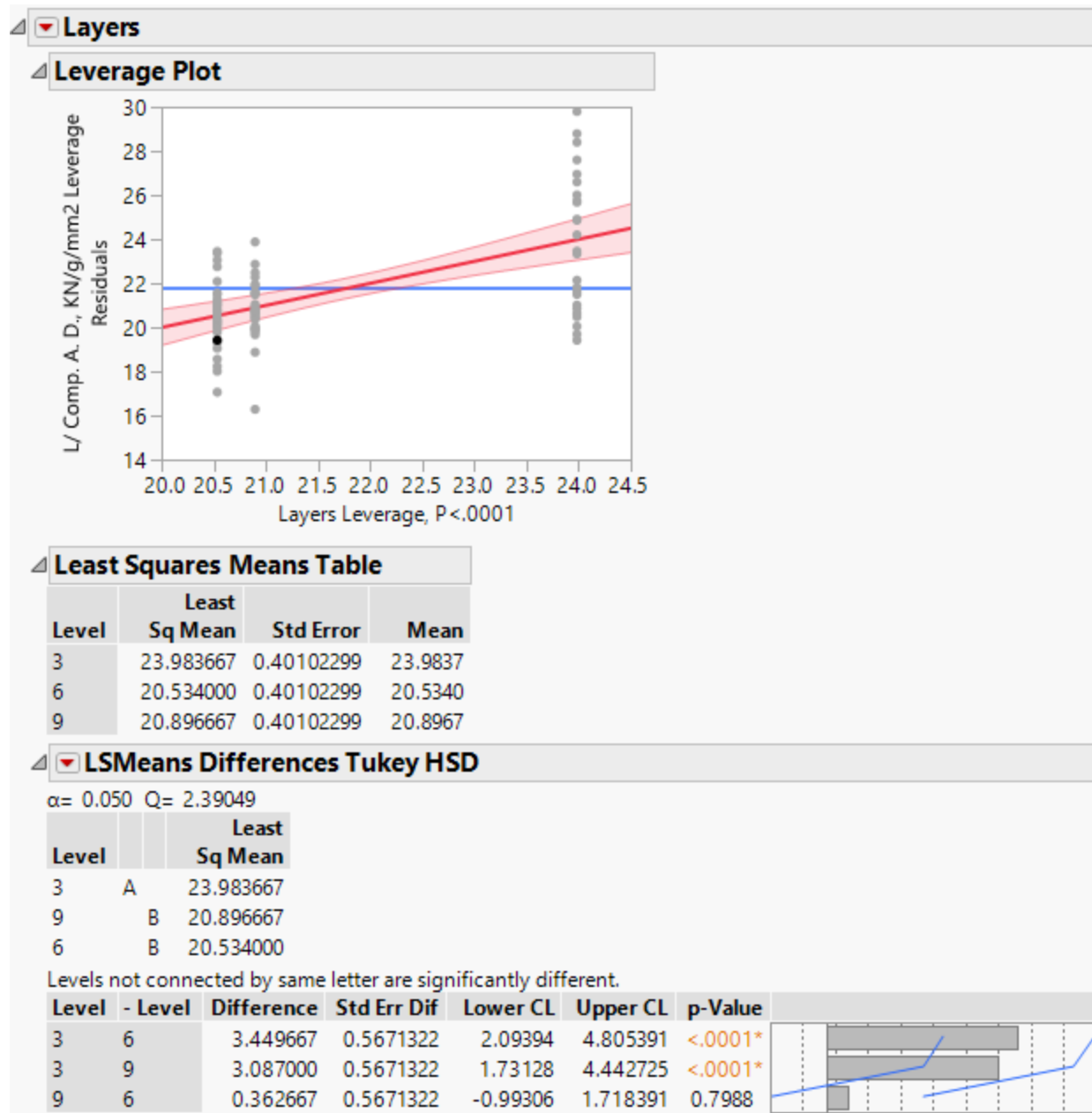


Figure 225. Tukey HSD- Tensile (Weft)- Effect of layers on Tensile Load Normalized by Composite Areal Density

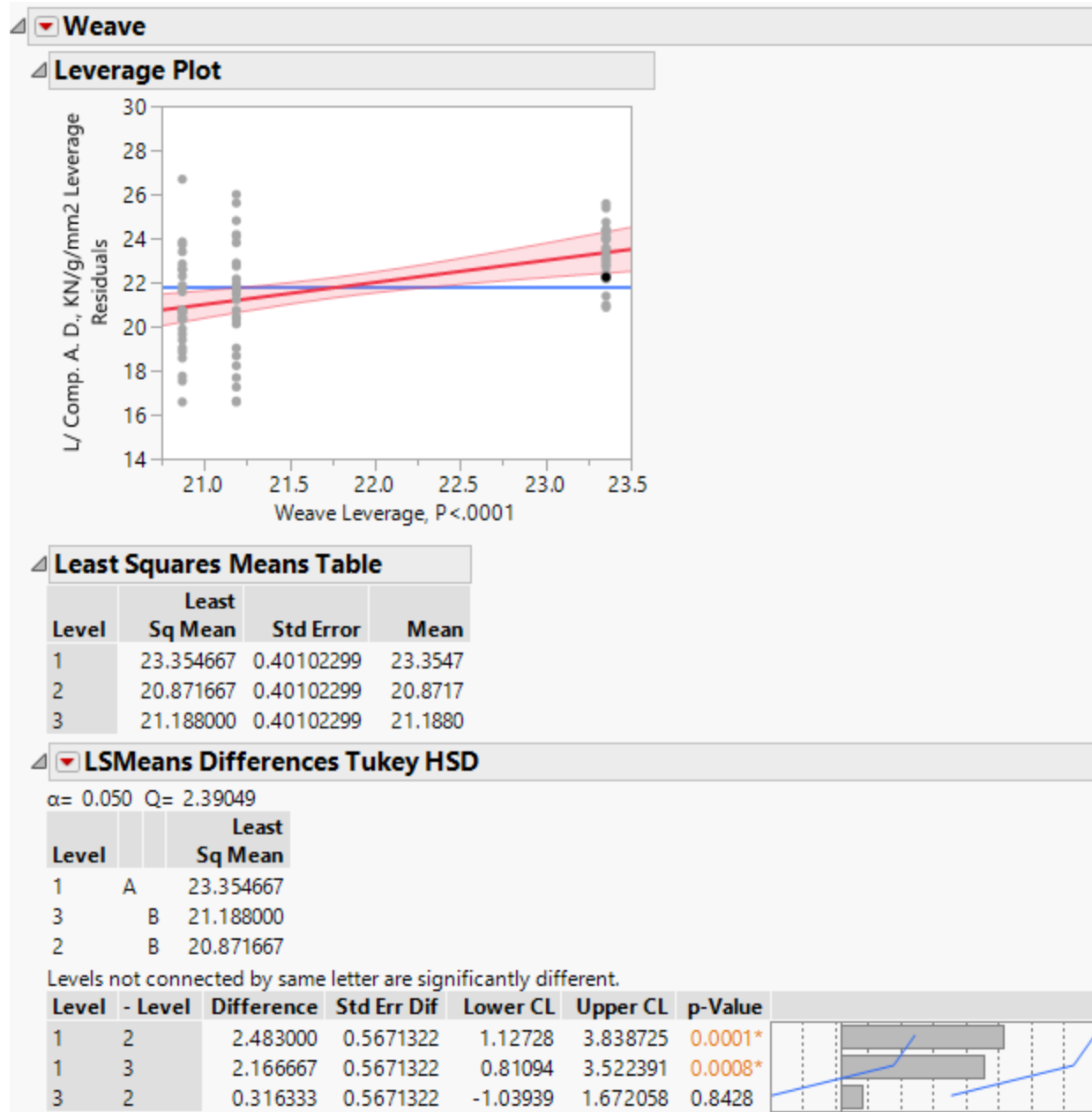


Figure 226. Tukey HSD- Tensile (Weft)- Effect of weave on Tensile Load Normalized by Composite Areal Density

D.1.2. Tup Impact

Summary of Fit					
RSquare			0.985637		
RSquare Adj			0.98318		
Root Mean Square Error			1.745694		
Mean of Response			19.02811		
Observations (or Sum Wgts)			90		
Analysis of Variance					
Source	DF	Sum of Squares	Mean Square	F Ratio	Prob > F
Model	13	15893.871	1222.61	401.1901	
Error	76	231.606	3.05		
C. Total	89	16125.477			<.0001*
Parameter Estimates					
Effect Tests					
Source	Nparm	DF	Sum of Squares	F Ratio	Prob > F
Layers	2	2	15727.070	2580.368	<.0001*
Weave	2	2	64.132	10.5223	<.0001*
Z/Y Ratio	1	1	0.00136111	0.0004	0.9832
Layers*Weave	4	4	62.078	5.0926	0.0011*
Layers*Z/Y Ratio	2	2	20.458	3.3566	0.0401*
Weave*Z/Y Ratio	2	2	20.130	3.3028	0.0421*

Table 57. ANOVA Results – Tup impact- Impact Energy

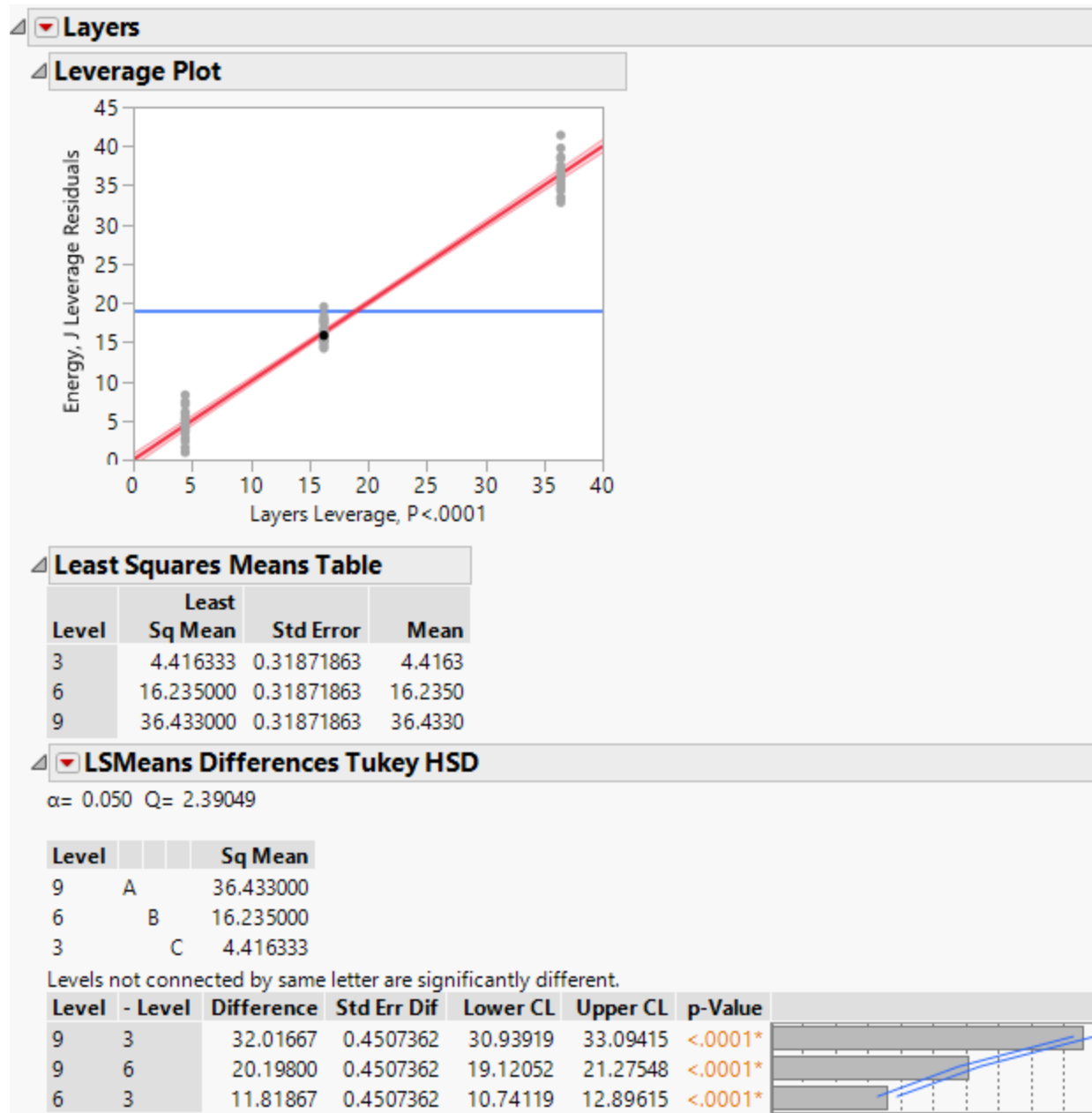


Figure 227. Tukey HSD- Tup impact- Effect of Layers on Impact Energy

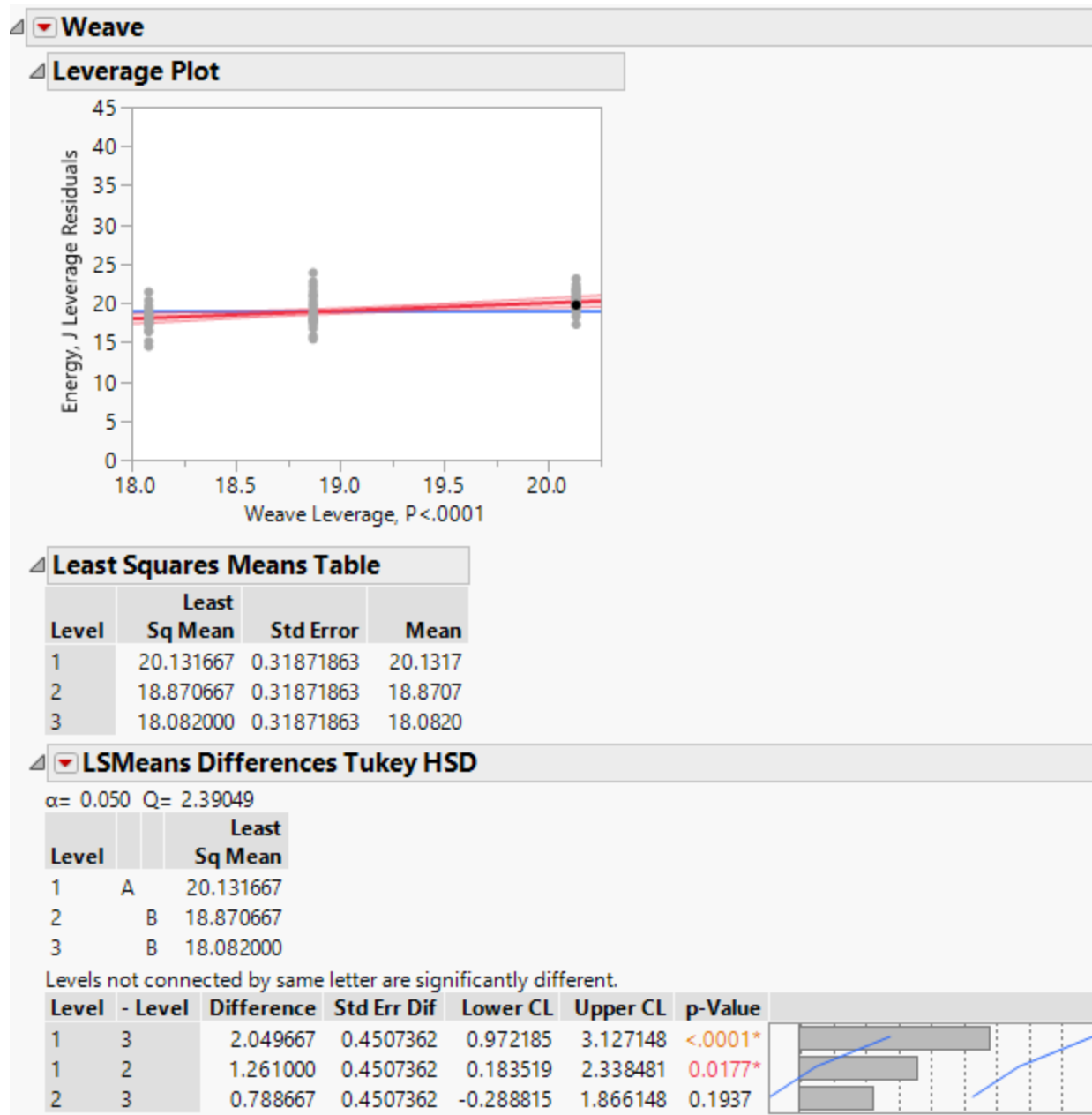


Figure 228. Tukey HSD- Tup impact- Effect of Weave on Impact Energy

Summary of Fit					
RSquare			0.905309		
RSquare Adj			0.889112		
Root Mean Square Error			0.560907		
Mean of Response			4.155222		
Observations (or Sum Wgts)			90		
Analysis of Variance					
Source	DF	Sum of Squares	Mean Square	F Ratio	Prob > F
Model	13	228.60481	17.5850	55.8934	
Error	76	23.91084	0.3146		
C. Total	89	252.51565			<.0001*
Parameter Estimates					
Effect Tests					
Source	Nparm	DF	Sum of Squares	F Ratio	Prob > F
Layers	2	2	220.53170	350.4772	<.0001*
Weave	2	2	2.15303	3.4217	0.0378*
Z/Y Ratio	1	1	0.27005	0.8584	0.3571
Layers*Weave	4	4	2.28681	1.8171	0.1342
Layers*Z/Y Ratio	2	2	2.63128	4.1817	0.0189*
Weave*Z/Y Ratio	2	2	0.73194	1.1632	0.3180

Table 58. ANOVA Results – Tup impact- Impact Energy Normalized by Thickness

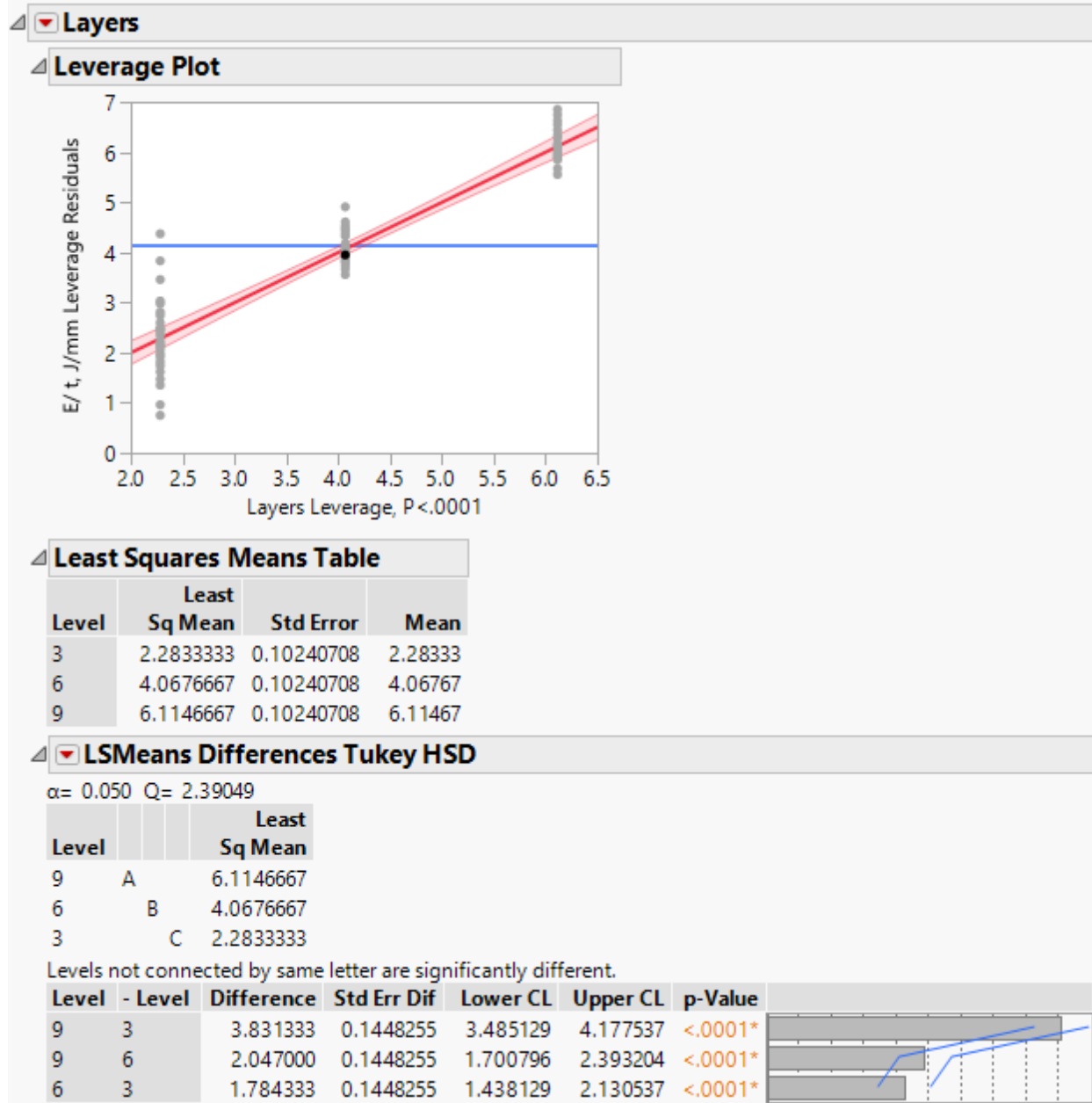


Figure 229. Tukey HSD- Tup impact- Effect of Layers on Impact Energy Normalized by Thickness

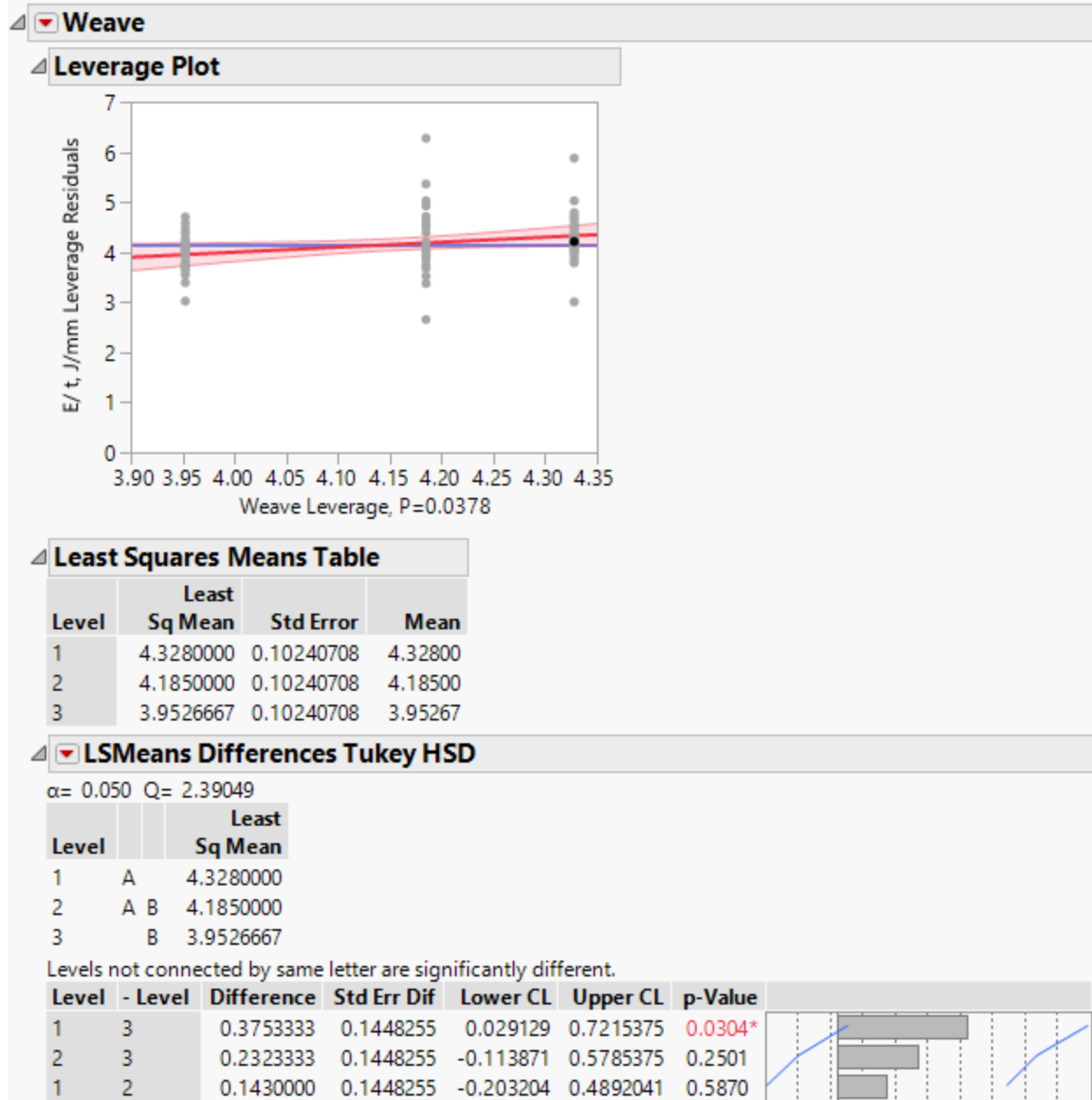


Figure 230. Tukey HSD- Tup impact- Effect of Weave on Impact Energy Normalized by Thickness

Summary of Fit					
RSquare			0.897157		
RSquare Adj			0.879566		
Root Mean Square Error			12.67892		
Mean of Response			90.28789		
Observations (or Sum Wgts)			90		
Analysis of Variance					
Source	DF	Sum of Squares	Mean Square	F Ratio	Prob > F
Model	13	106579.07	8198.39	50.9993	
Error	76	12217.38	160.75		
C. Total	89	118796.45			<.0001*
Parameter Estimates					
Effect Tests					
Source	Nparm	DF	Sum of Squares	F Ratio	Prob > F
Layers	2	2	101703.41	316.3306	<.0001*
Weave	2	2	1066.75	3.3180	0.0415*
Z/Y Ratio	1	1	201.63	1.2543	0.2663
Layers*Weave	4	4	1668.32	2.5945	0.0430*
Layers*Z/Y Ratio	2	2	1357.19	4.2213	0.0183*
Weave*Z/Y Ratio	2	2	581.76	1.8094	0.1707

Table 59. ANOVA Results – Tup impact- Impact Energy Normalized by Preform Areal Density



Figure 231. Tukey HSD- Tup impact- Effect of Layers on Impact Energy Normalized by
Preform Areal Density

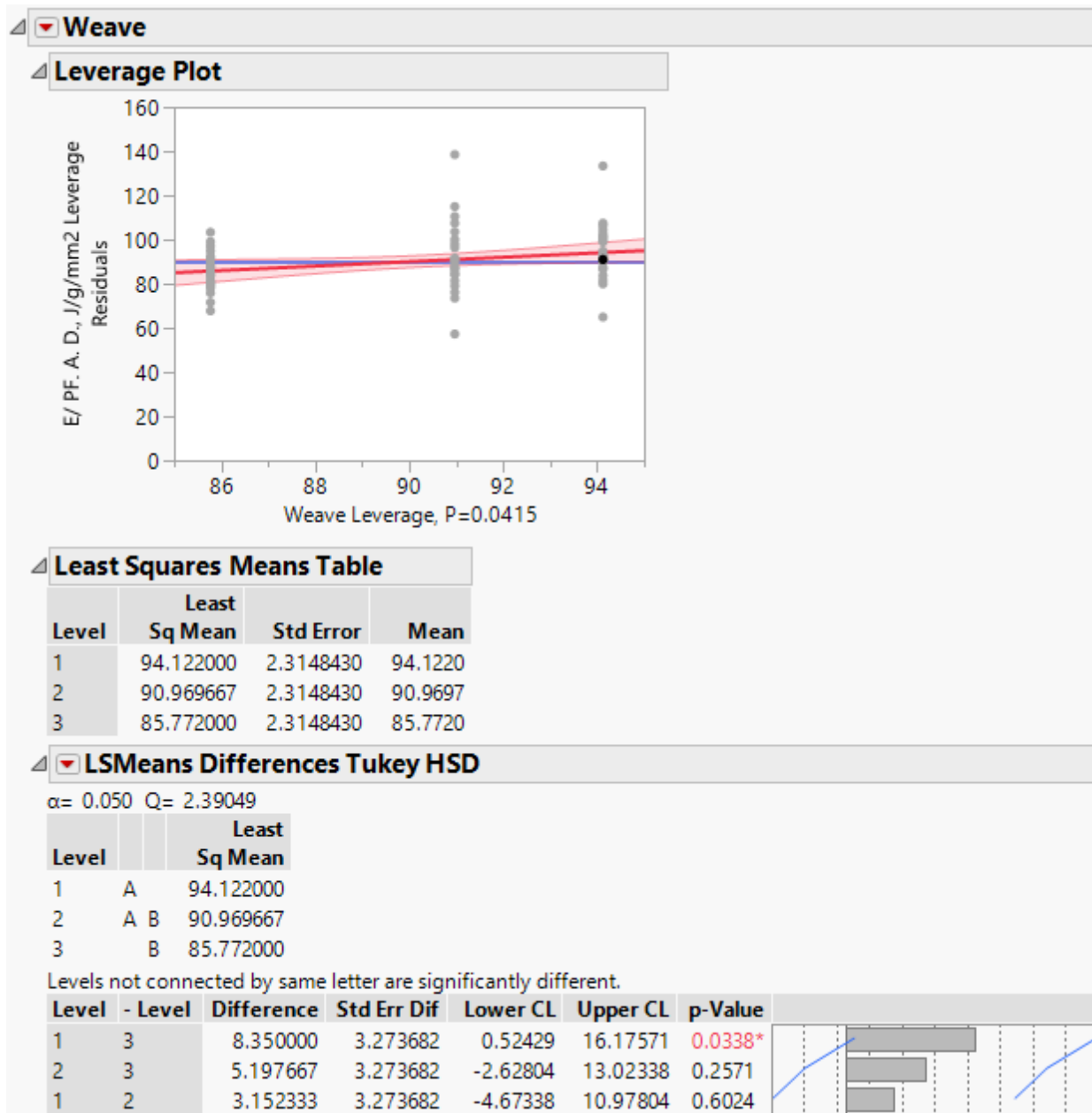


Figure 232. Tukey HSD- Tup impact- Effect of Weave on Impact Energy Normalized by
Preform Areal Density

Summary of Fit					
RSquare			0.780418		
RSquare Adj			0.742858		
Root Mean Square Error			5.813615		
Mean of Response			34.202		
Observations (or Sum Wgts)			90		
Analysis of Variance					
Source	DF	Sum of Squares	Mean Square	F Ratio	Prob > F
Model	13	9129.276	702.252	20.7778	
Error	76	2568.657	33.798		
C. Total	89	11697.933			<.0001*
Parameter Estimates					
Effect Tests					
Source	Nparm	DF	Sum of Squares	F Ratio	Prob > F
Layers	2	2	8409.1354	124.4024	<.0001*
Weave	2	2	192.5322	2.8483	0.0641
Z/Y Ratio	1	1	15.3430	0.4540	0.5025
Layers*Weave	4	4	196.0973	1.4505	0.2257
Layers*Z/Y Ratio	2	2	224.7726	3.3252	0.0413*
Weave*Z/Y Ratio	2	2	91.3956	1.3521	0.2649

Table 60. ANOVA Results – Tup impact- Impact Energy Normalized by Composite Areal
Density

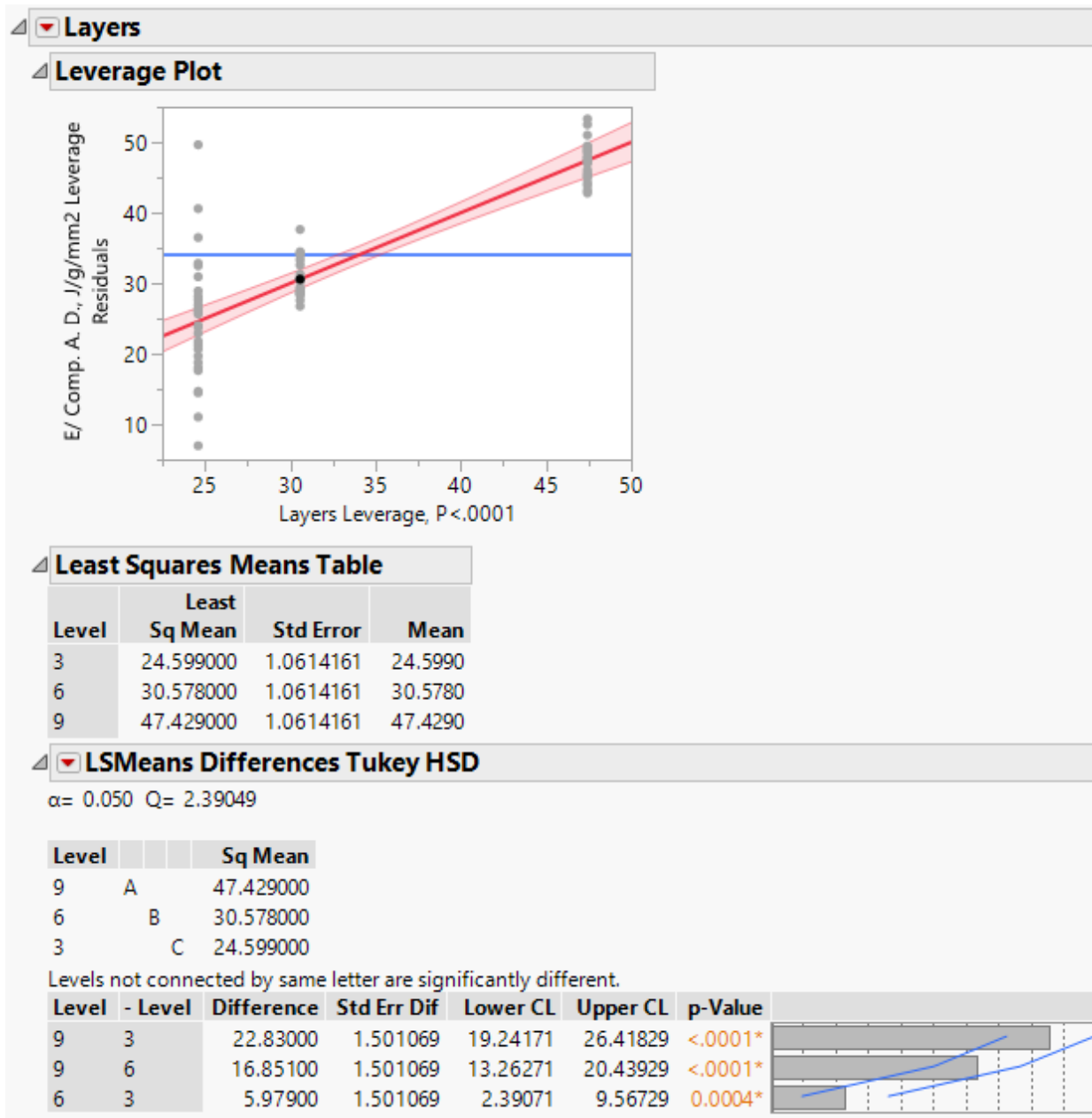


Figure 233. Tukey HSD- Tup impact- Effect of Layers on Impact Energy Normalized by Composite Areal Density

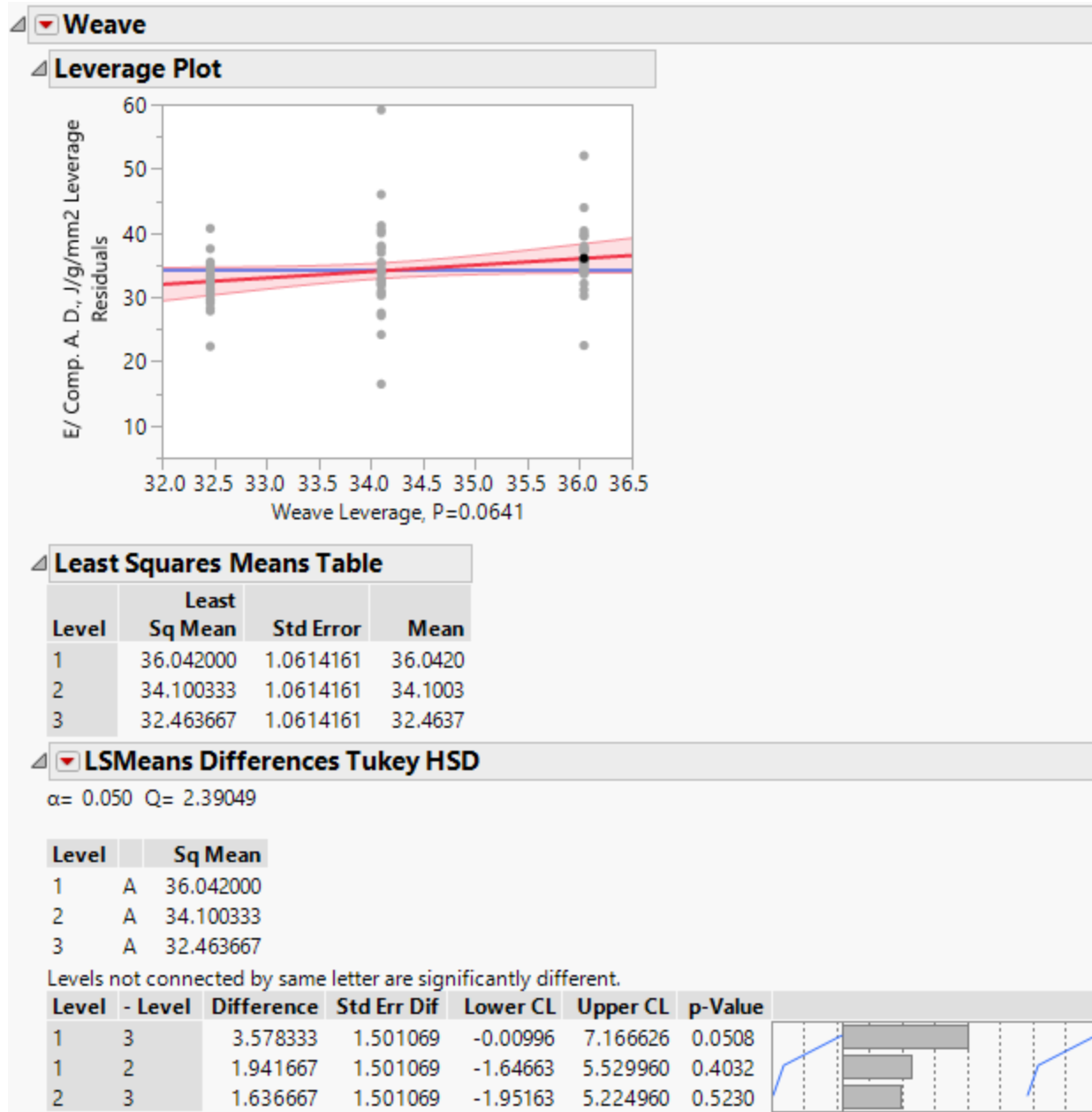


Figure 234. Tukey HSD- Tup impact- Effect of Weave on Impact Energy Normalized by Composite Areal Density

D.1.3. Charpy Impact

Summary of Fit					
RSquare			0.760113		
RSquare Adj			0.719079		
Root Mean Square Error			0.34213		
Mean of Response			1.066333		
Observations (or Sum Wgts)			90		
Analysis of Variance					
Source	DF	Sum of Squares	Mean Square	F Ratio	Prob > F
Model	13	28.188243	2.16833	18.5243	
Error	76	8.896047	0.11705		
C. Total	89	37.084290			<.0001*
Parameter Estimates					
Effect Tests					
Source	Nparm	DF	Sum of Squares	F Ratio	Prob > F
Layers	2	2	20.309147	86.7517	<.0001*
Weave	2	2	1.405527	6.0038	0.0038*
Z/Y Ratio	1	1	0.313290	2.6765	0.1060
Layers*Weave	4	4	3.055967	6.5269	0.0001*
Layers*Z/Y Ratio	2	2	2.084507	8.9041	0.0003*
Weave*Z/Y Ratio	2	2	1.019807	4.3562	0.0162*

Table 61. ANOVA Results – Tup impact (Warp) - Impact Energy

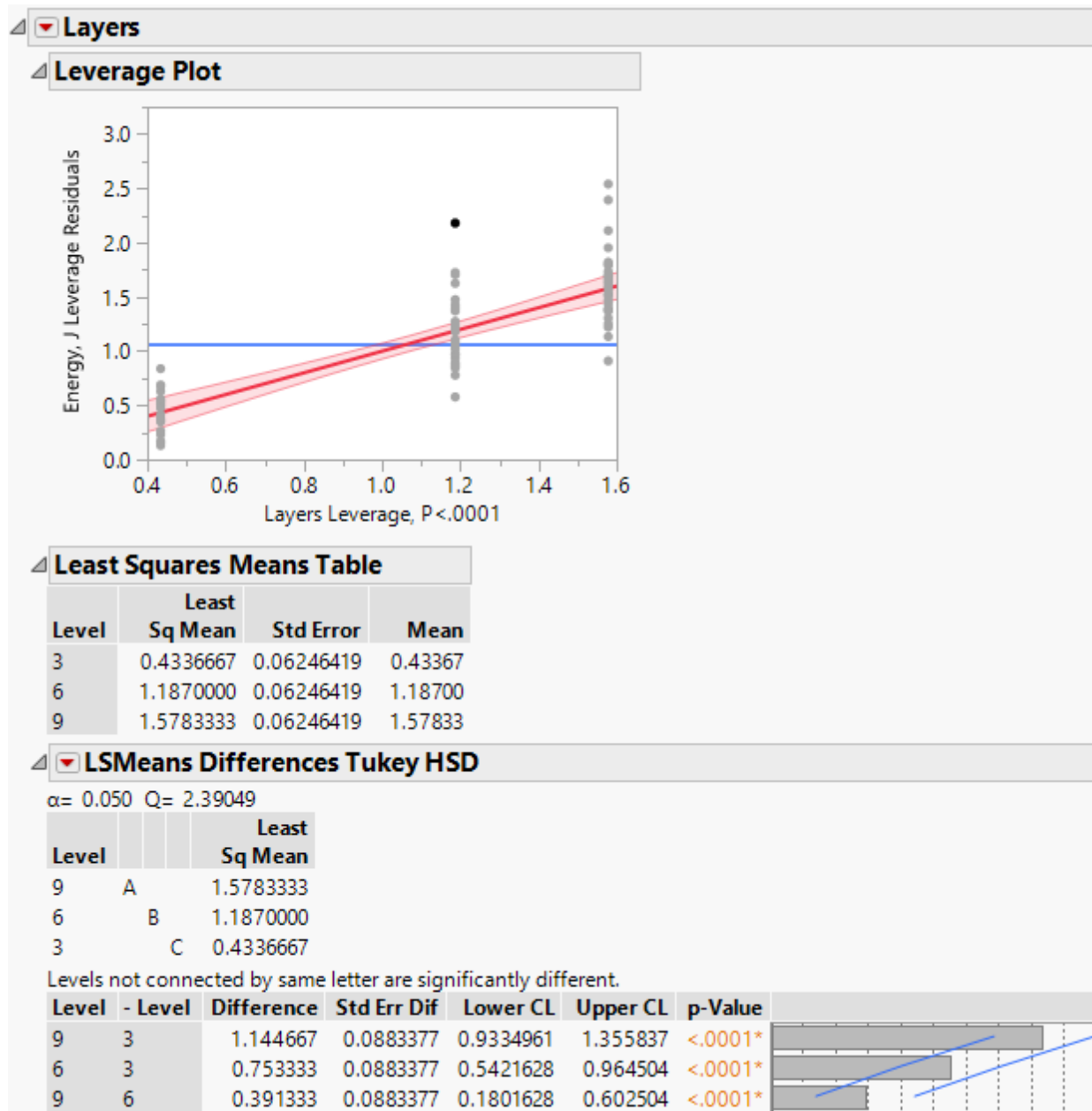


Figure 235. Tukey HSD- Tup impact (Warp) - Effect of Layers on Impact Energy

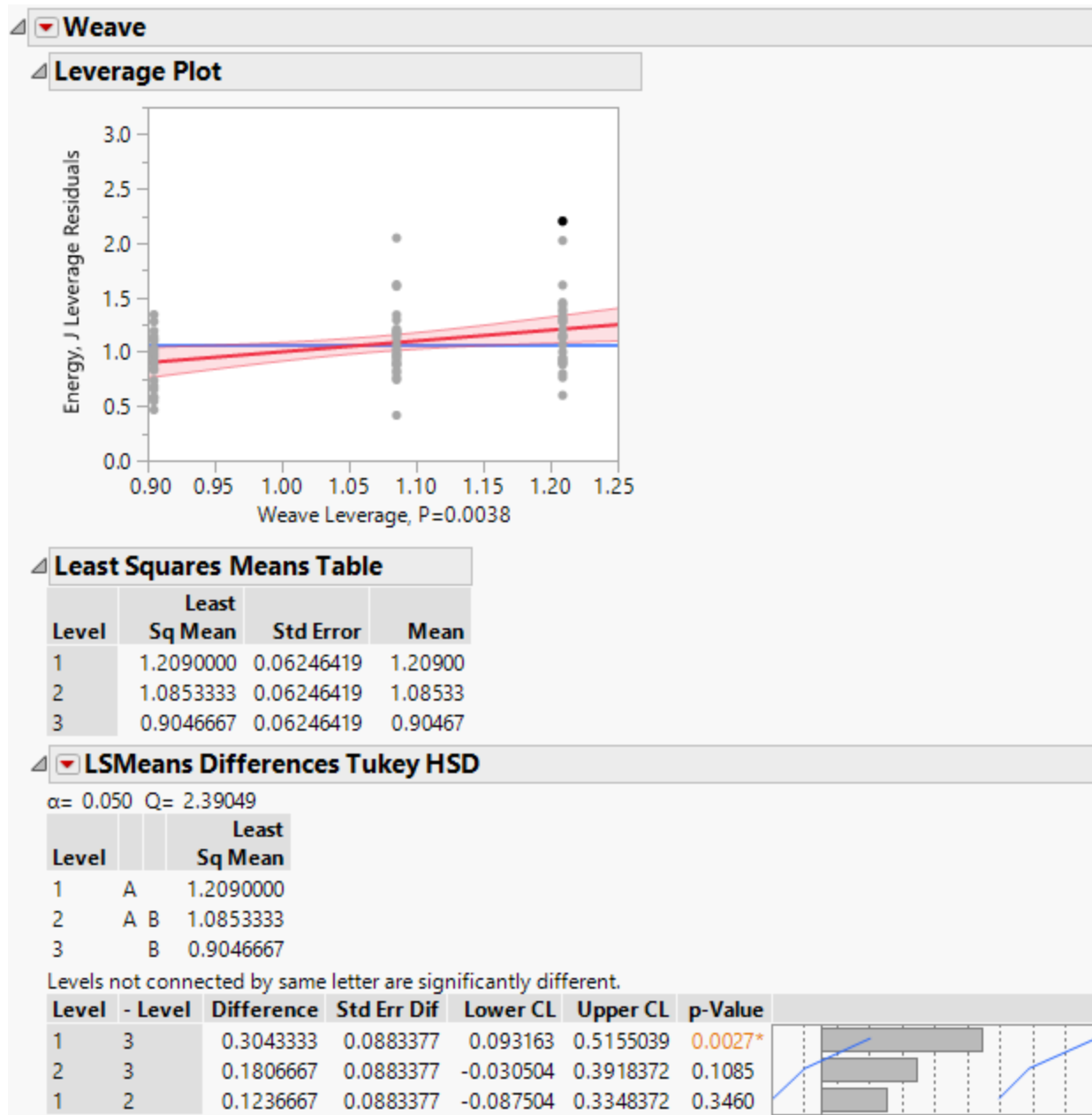


Figure 236. Tukey HSD- Tup impact (Warp) - Effect of Weave on Impact Energy

Summary of Fit					
RSquare			0.462878		
RSquare Adj			0.371002		
Root Mean Square Error			0.080289		
Mean of Response			0.260889		
Observations (or Sum Wgts)			90		
Analysis of Variance					
Source	DF	Sum of Squares	Mean Square	F Ratio	
Model	13	0.42220444	0.032477	5.0381	
Error	76	0.48992444	0.006446		Prob > F
C. Total	89	0.91212889			<.0001*
Parameter Estimates					
Effect Tests					
Source	Nparm	DF	Sum of Squares	F Ratio	Prob > F
Layers	2	2	0.07721556	5.9891	0.0038*
Weave	2	2	0.06869556	5.3282	0.0068*
Z/Y Ratio	1	1	0.01877778	2.9129	0.0920
Layers*Weave	4	4	0.12093778	4.6901	0.0019*
Layers*Z/Y Ratio	2	2	0.10082889	7.8206	0.0008*
Weave*Z/Y Ratio	2	2	0.03574889	2.7728	0.0688

Table 62. ANOVA Results – Tup impact (Warp) - Impact Energy Normalized by Thickness

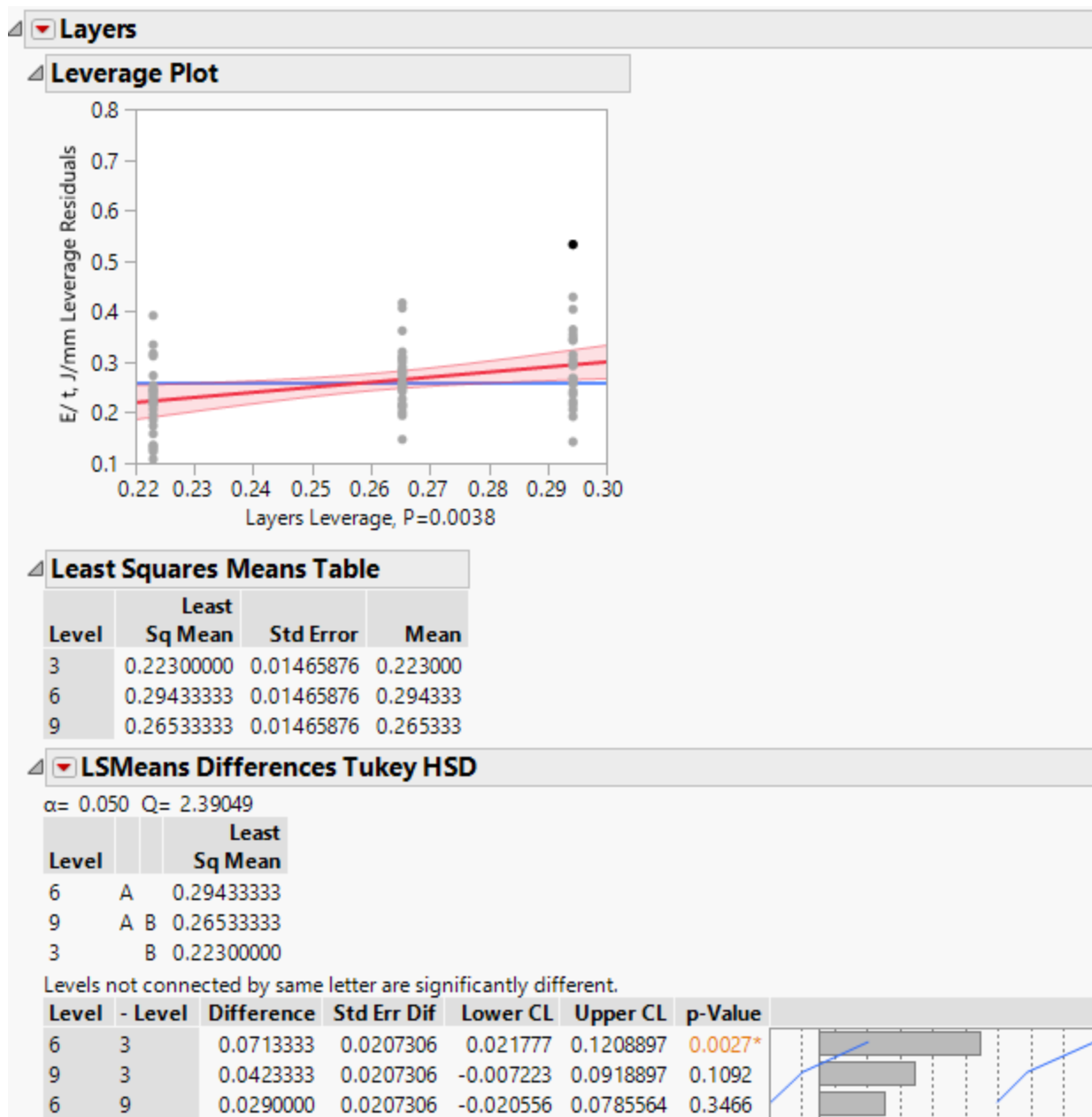


Figure 237. Tukey HSD- Tup impact (Warp) - Effect of Layers on Impact Energy Normalized by Thickness

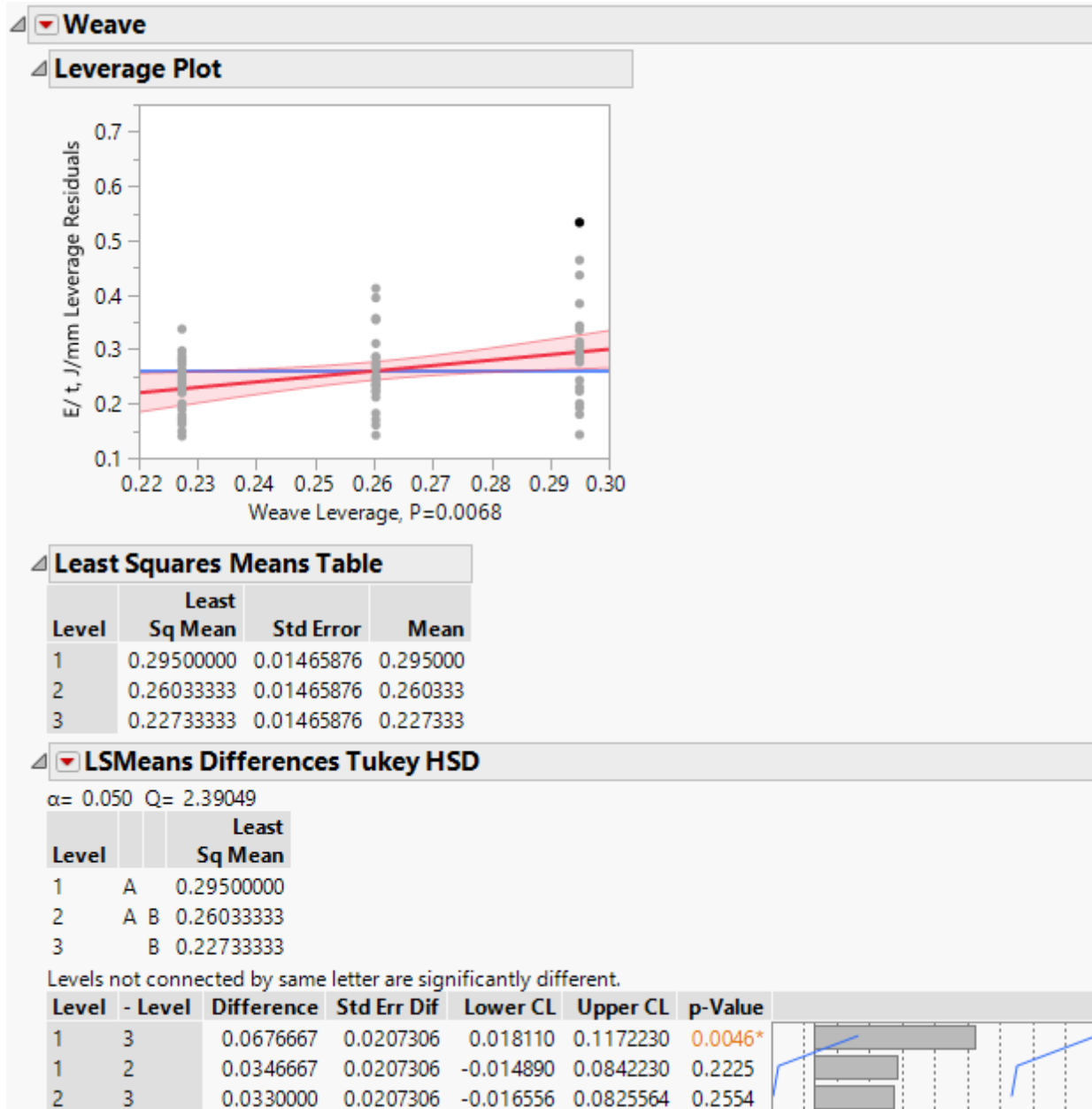


Figure 238. Tukey HSD- Tup impact (Warp) - Effect of Weave on Impact Energy Normalized by Thickness

Summary of Fit					
RSquare			0.496902		
RSquare Adj			0.410846		
Root Mean Square Error			1.736237		
Mean of Response			5.679444		
Observations (or Sum Wgts)			90		
Analysis of Variance					
Source	DF	Sum of Squares	Mean Square	F Ratio	Prob > F
Model	13	226.28176	17.4063	5.7741	
Error	76	229.10351	3.0145		
C. Total	89	455.38527			<.0001*
Parameter Estimates					
Effect Tests					
Source	Nparm	DF	Sum of Squares	F Ratio	Prob > F
Layers	2	2	40.302629	6.6848	0.0021*
Weave	2	2	37.373096	6.1988	0.0032*
Z/Y Ratio	1	1	10.194268	3.3817	0.0698
Layers*Weave	4	4	58.253378	4.8311	0.0016*
Layers*Z/Y Ratio	2	2	57.301242	9.5042	0.0002*
Weave*Z/Y Ratio	2	2	22.857149	3.7912	0.0270*

Table 63. ANOVA Results – Tup impact (Warp) - Impact Energy Normalized by Preform Areal Density

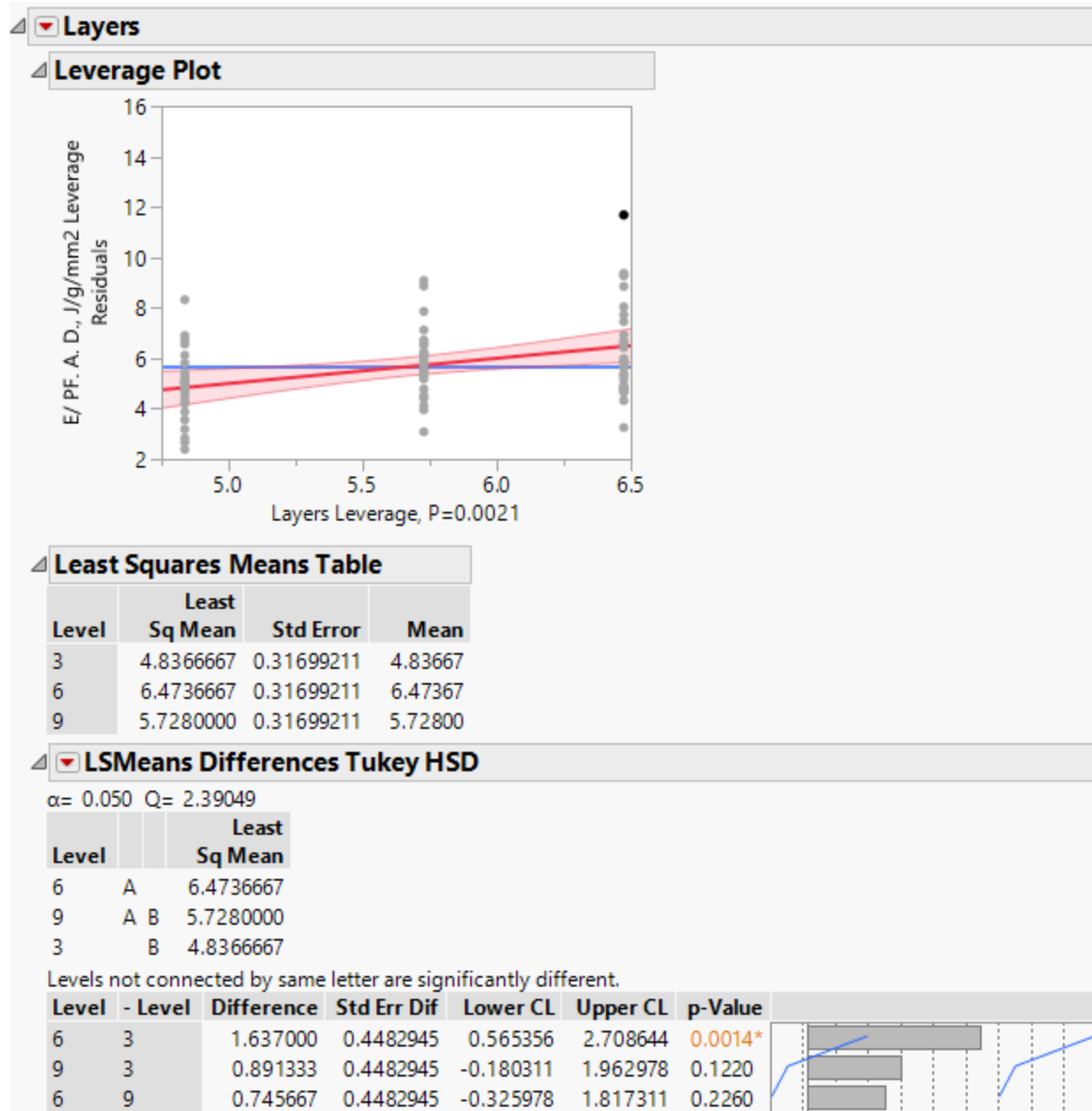


Figure 239. Tukey HSD- Tup impact (Warp) - Effect of Layers on Impact Energy Normalized by Preform Areal Density

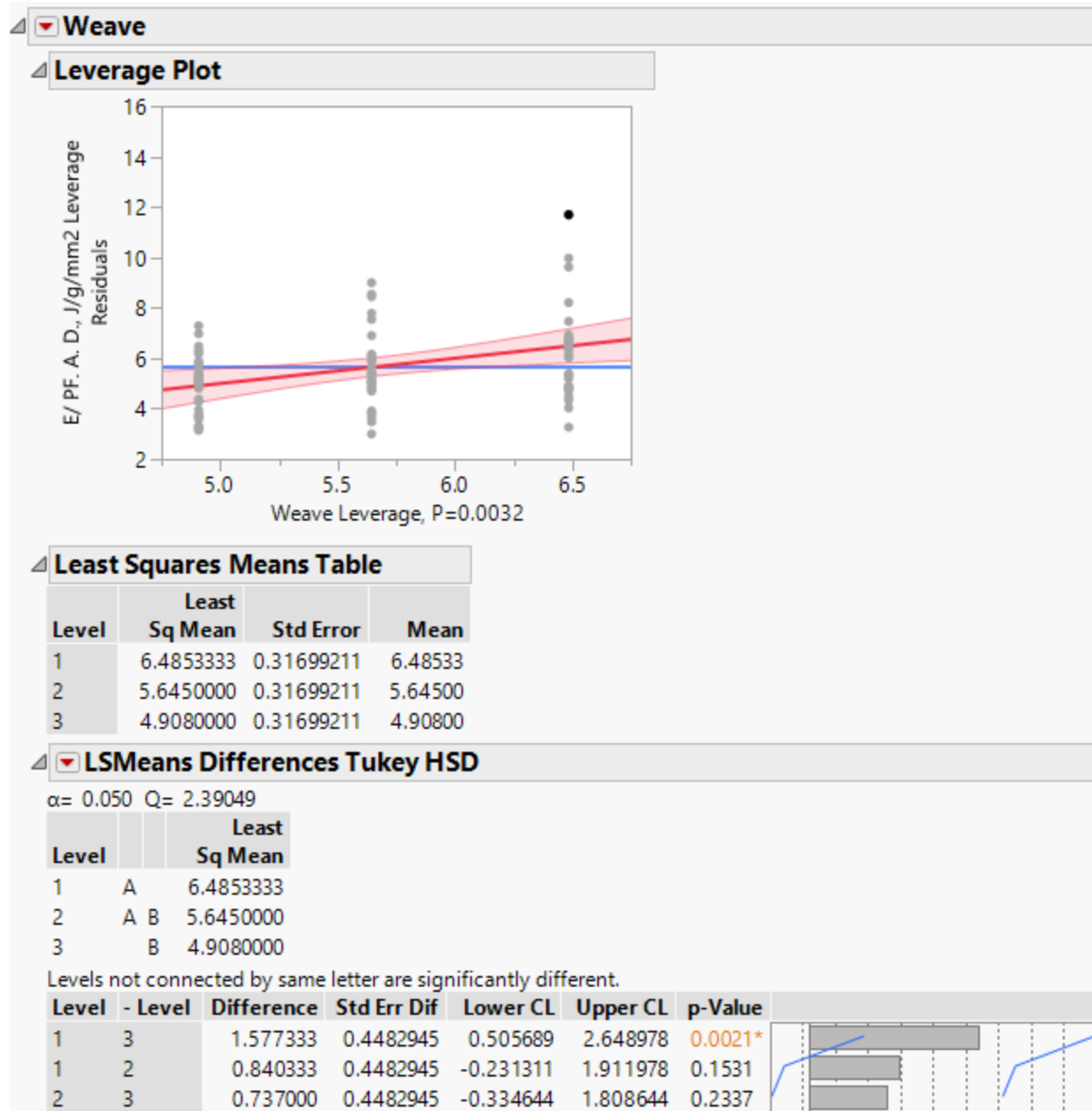


Figure 240. Tukey HSD- Tup impact (Warp) - Effect of Weave on Impact Energy Normalized by Preform Areal Density

Summary of Fit					
RSquare			0.516605		
RSquare Adj			0.433919		
Root Mean Square Error			0.542702		
Mean of Response			1.728667		
Observations (or Sum Wgts)			90		
Analysis of Variance					
Source	DF	Sum of Squares	Mean Square	F Ratio	Prob > F
Model	13	23.921742	1.84013	6.2478	
Error	76	22.383898	0.29452		
C. Total	89	46.305640			<.0001*
Parameter Estimates					
Effect Tests					
Source	Nparm	DF	Sum of Squares	F Ratio	Prob > F
Layers	2	2	5.3771267	9.1285	0.0003*
Weave	2	2	3.6686067	6.2280	0.0031*
Z/Y Ratio	1	1	1.2578844	4.2709	0.0422*
Layers*Weave	4	4	6.1235067	5.1978	0.0009*
Layers*Z/Y Ratio	2	2	5.3072289	9.0098	0.0003*
Weave*Z/Y Ratio	2	2	2.1873889	3.7134	0.0289*

Table 64. ANOVA Results – Tup impact (Warp) - Impact Energy Normalized by Composite Areal Density

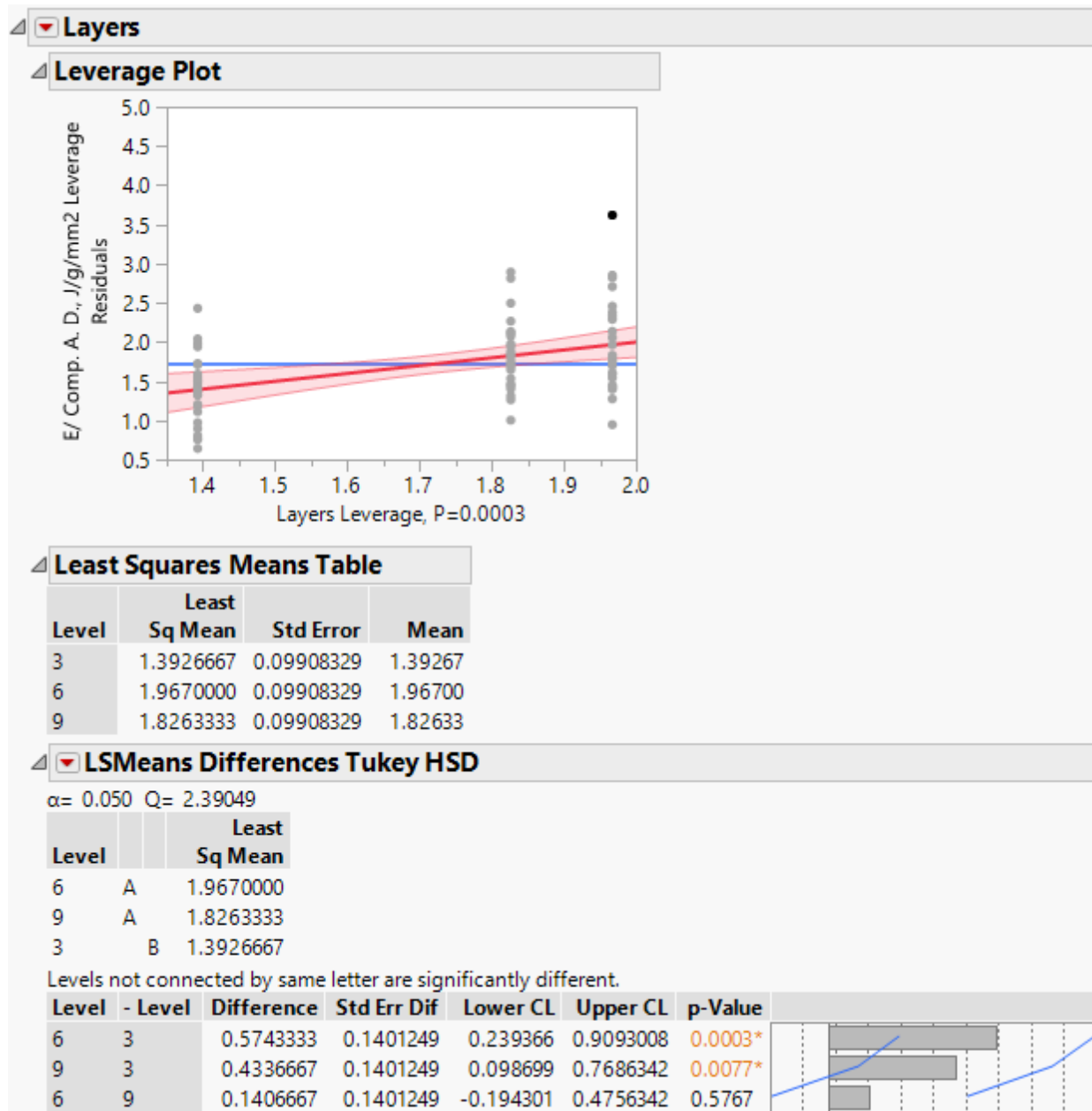


Figure 241. Tukey HSD- Tup impact (Warp) - Effect of Layers on Impact Energy Normalized by Composite Areal Density

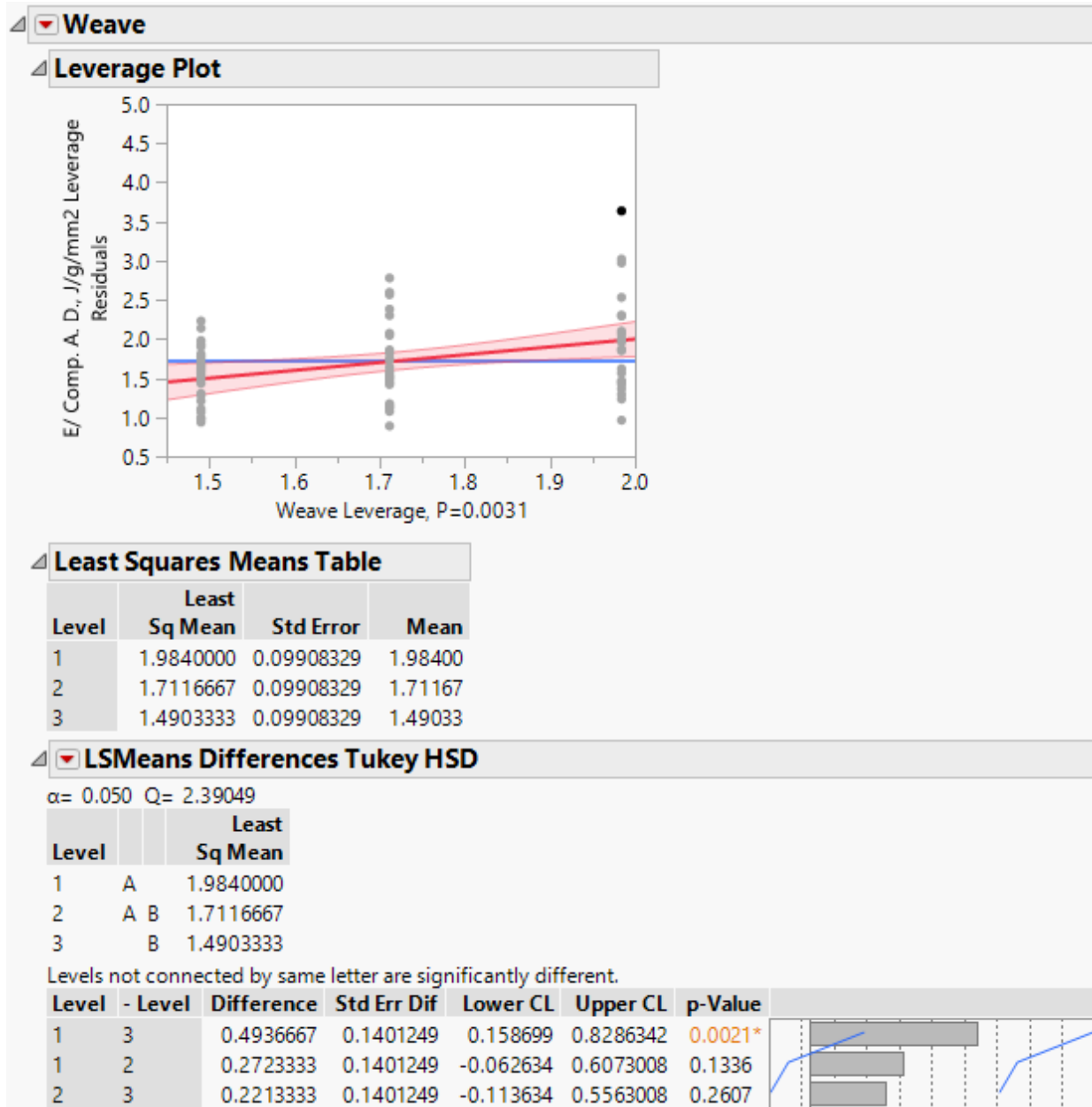


Figure 242. Tukey HSD- Tup impact (Warp) - Effect of Weave on Impact Energy Normalized by Composite Areal Density

Summary of Fit					
RSquare			0.832275		
RSquare Adj			0.803586		
Root Mean Square Error			0.5204		
Mean of Response			2.337222		
Observations (or Sum Wgts)			90		
Analysis of Variance					
Source	DF	Sum of Squares	Mean Square	F Ratio	Prob > F
Model	13	102.13101	7.85623	29.0095	
Error	76	20.58199	0.27082		
C. Total	89	122.71301			<.0001*
Parameter Estimates					
Effect Tests					
Source	Nparm	DF	Sum of Squares	F Ratio	Prob > F
Layers	2	2	98.467709	181.7984	<.0001*
Weave	2	2	1.181262	2.1809	0.1200
Z/Y Ratio	1	1	0.425734	1.5720	0.2138
Layers*Weave	4	4	1.654204	1.5271	0.2028
Layers*Z/Y Ratio	2	2	0.077802	0.1436	0.8664
Weave*Z/Y Ratio	2	2	0.324302	0.5988	0.5521

Table 65. ANOVA Results – Tup impact (Weft) - Impact Energy

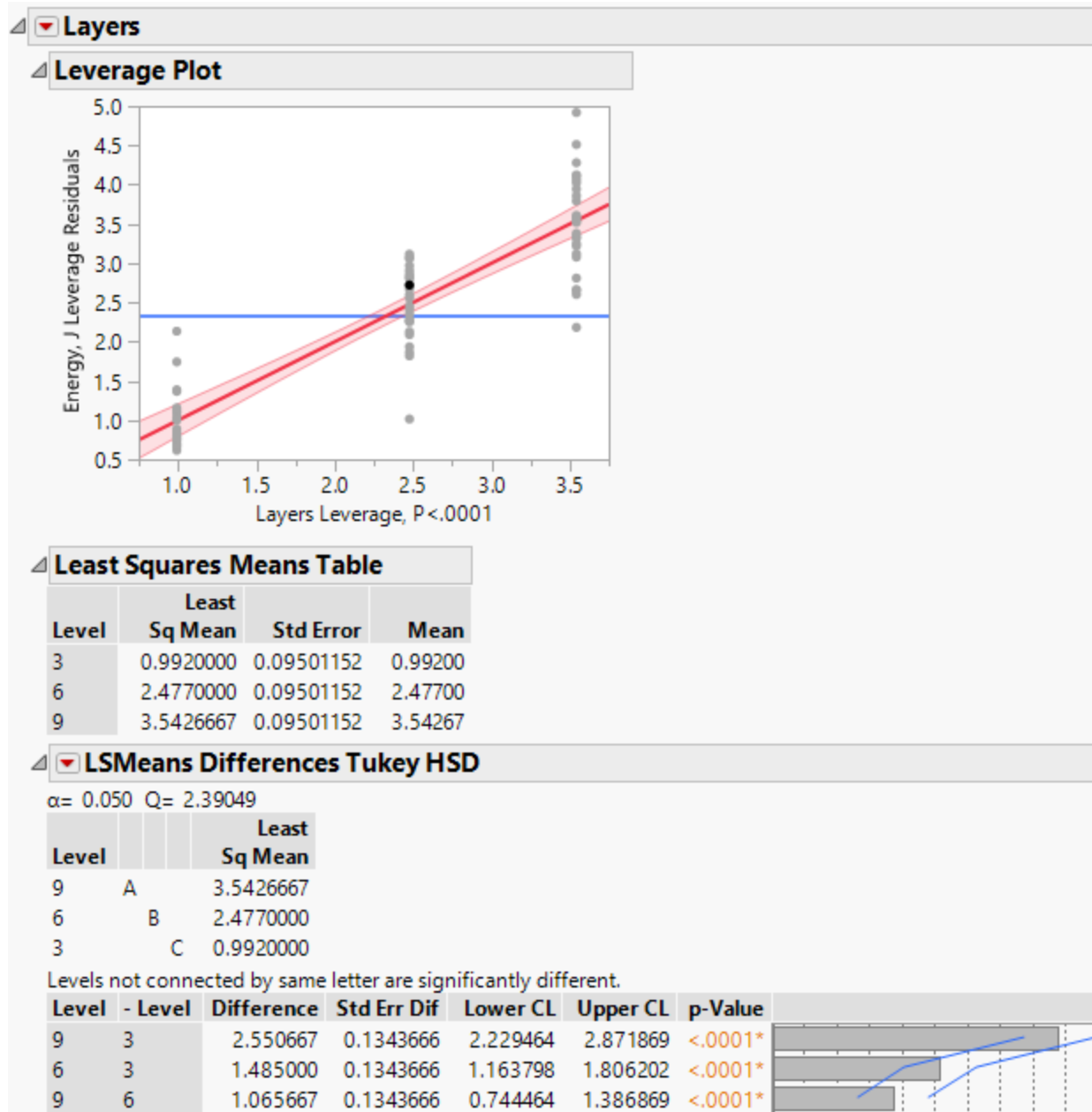


Figure 243. Tukey HSD- Tup impact (Weft) - Effect of Layers on Impact Energy

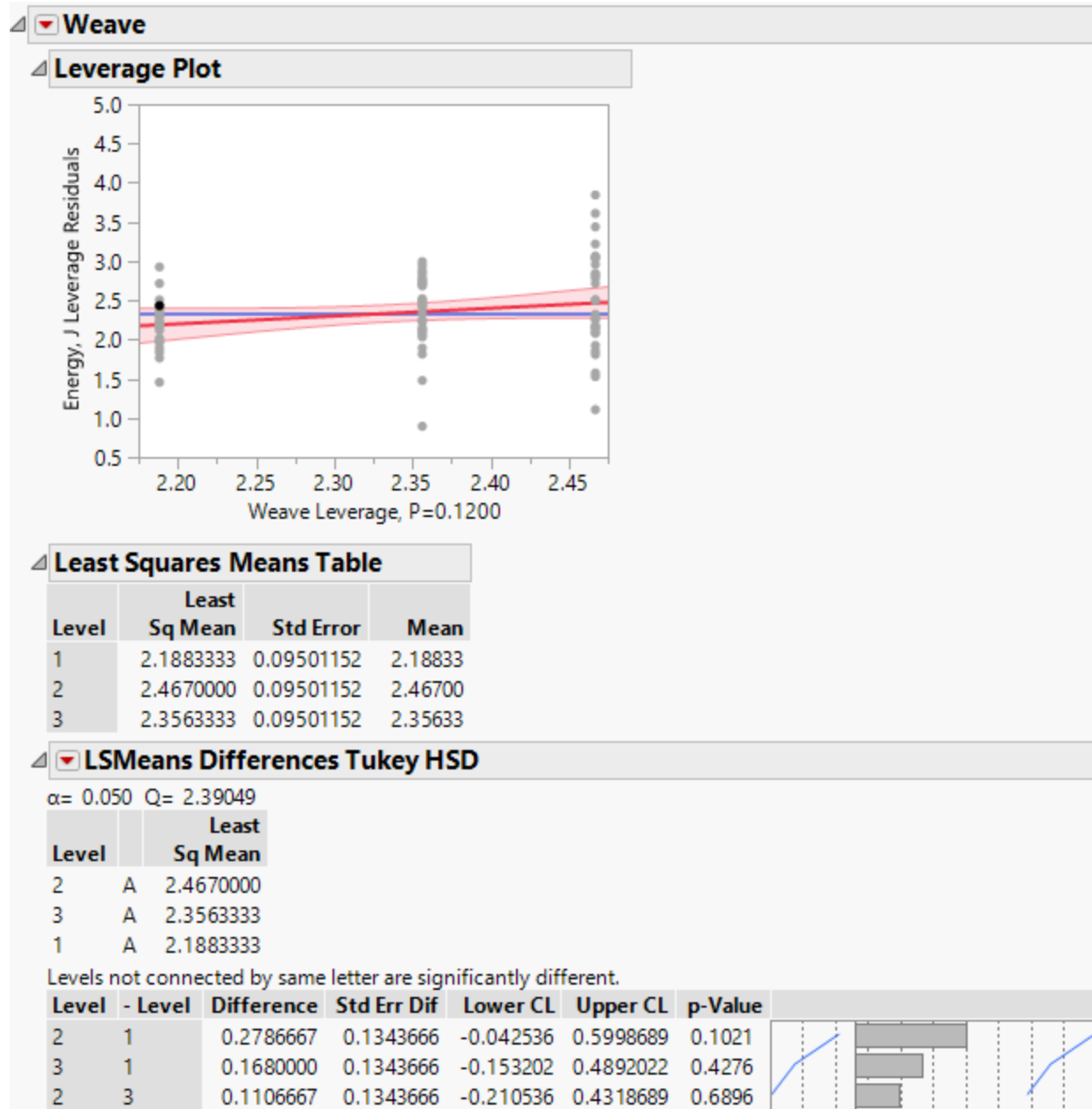


Figure 244. Tukey HSD- Tup impact (Weft) - Effect of Weave on Impact Energy

Summary of Fit					
RSquare			0.276879		
RSquare Adj			0.153188		
Root Mean Square Error			0.137962		
Mean of Response			0.577667		
Observations (or Sum Wgts)			90		
Analysis of Variance					
Source	DF	Sum of Squares	Mean Square	F Ratio	
Model	13	0.5538722	0.042606	2.2385	
Error	76	1.4465378	0.019033		Prob > F
C. Total	89	2.0004100			0.0153*
Parameter Estimates					
Effect Tests					
Source	Nparm	DF	Sum of Squares	F Ratio	Prob > F
Layers	2	2	0.18524667	4.8664	0.0103*
Weave	2	2	0.13100667	3.4415	0.0371*
Z/Y Ratio	1	1	0.04053444	2.1296	0.1486
Layers*Weave	4	4	0.12674667	1.6648	0.1669
Layers*Z/Y Ratio	2	2	0.02873556	0.7549	0.4736
Weave*Z/Y Ratio	2	2	0.04160222	1.0929	0.3405

Table 66. ANOVA Results – Tup impact (Weft) - Impact Energy Normalized by Thickness

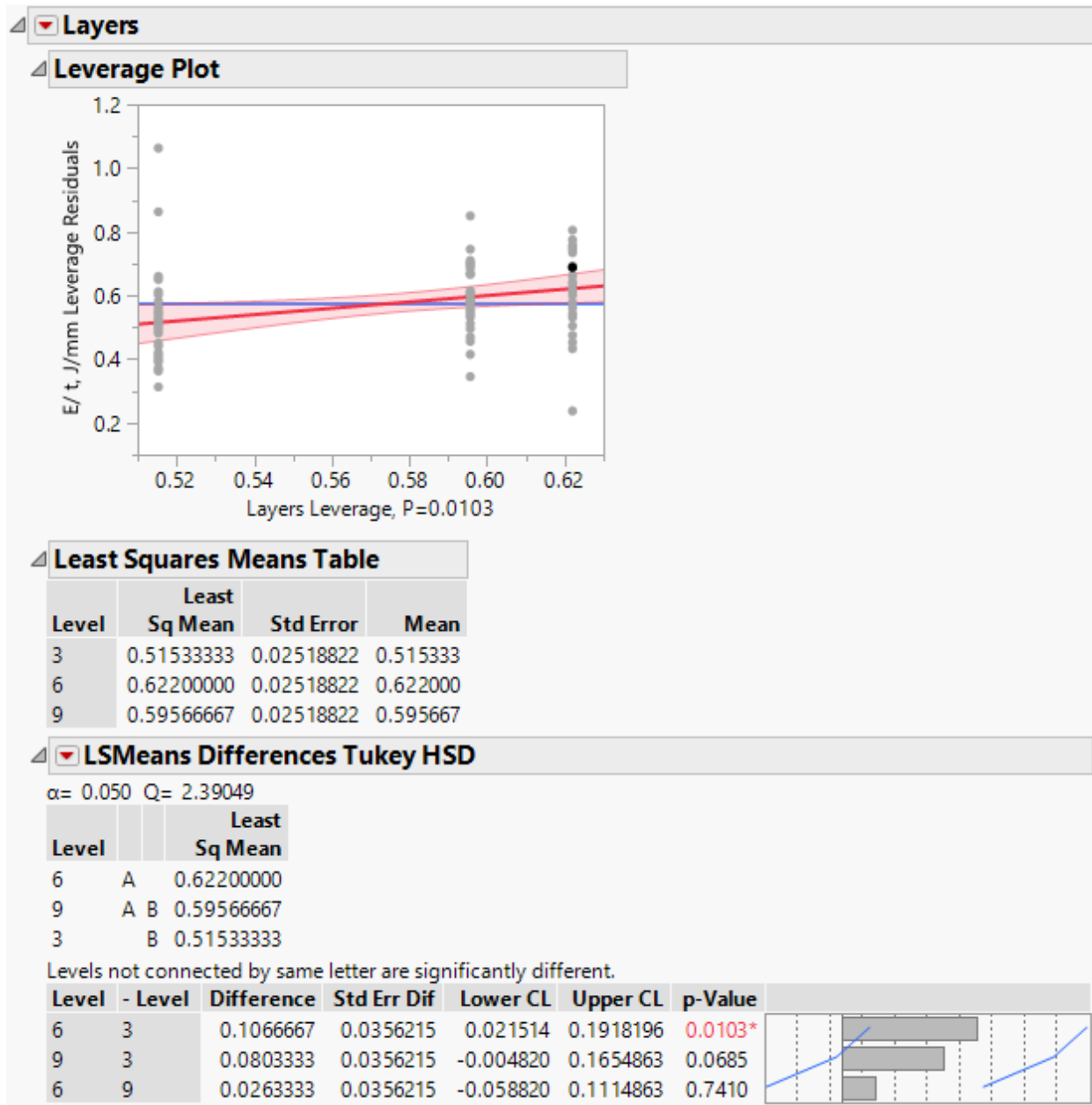


Figure 245. Tukey HSD- Tup impact (Weft) - Effect of Layers on Impact Energy Normalized by Thickness

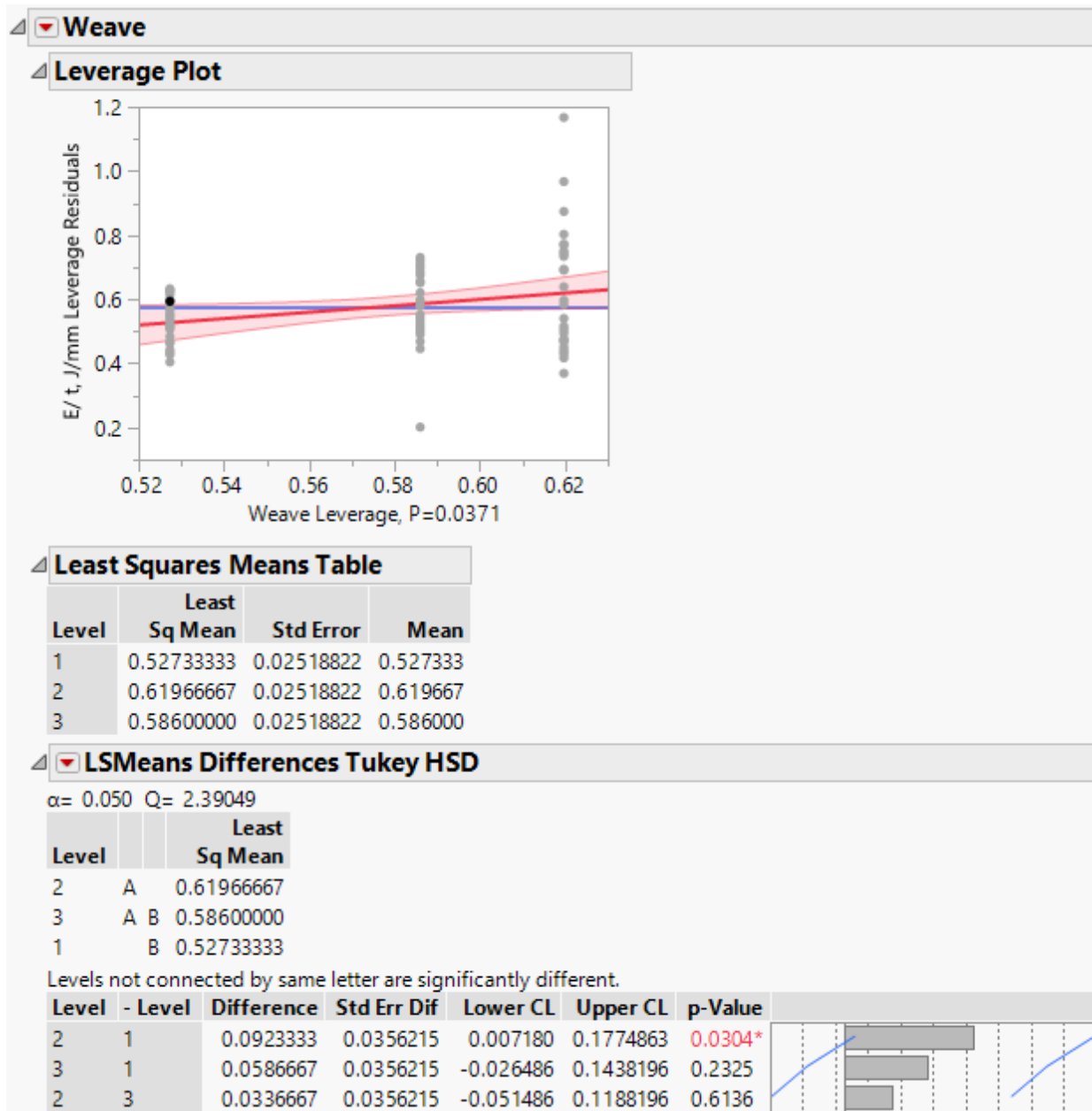


Figure 246. Tukey HSD- Tup impact (Weft) - Effect of Weave on Impact Energy Normalized by Thickness

Summary of Fit					
RSquare			0.279169		
RSquare Adj			0.155869		
Root Mean Square Error			2.970726		
Mean of Response			12.52456		
Observations (or Sum Wgts)			90		
Analysis of Variance					
Source	DF	Sum of Squares	Mean Square	F Ratio	
Model	13	259.76007	19.9815	2.2641	
Error	76	670.71596	8.8252		Prob > F
C. Total	89	930.47603			0.0141*
Parameter Estimates					
Effect Tests					
Source	Nparm	DF	Sum of Squares	F Ratio	Prob > F
Layers	2	2	107.62815	6.0978	0.0035*
Weave	2	2	57.57763	3.2621	0.0437*
Z/Y Ratio	1	1	22.97245	2.6030	0.1108
Layers*Weave	4	4	54.43332	1.5420	0.1986
Layers*Z/Y Ratio	2	2	7.44528	0.4218	0.6574
Weave*Z/Y Ratio	2	2	9.70323	0.5497	0.5794

Table 67. ANOVA Results – Tup impact (Weft) - Impact Energy Normalized by Preform Areal
Density

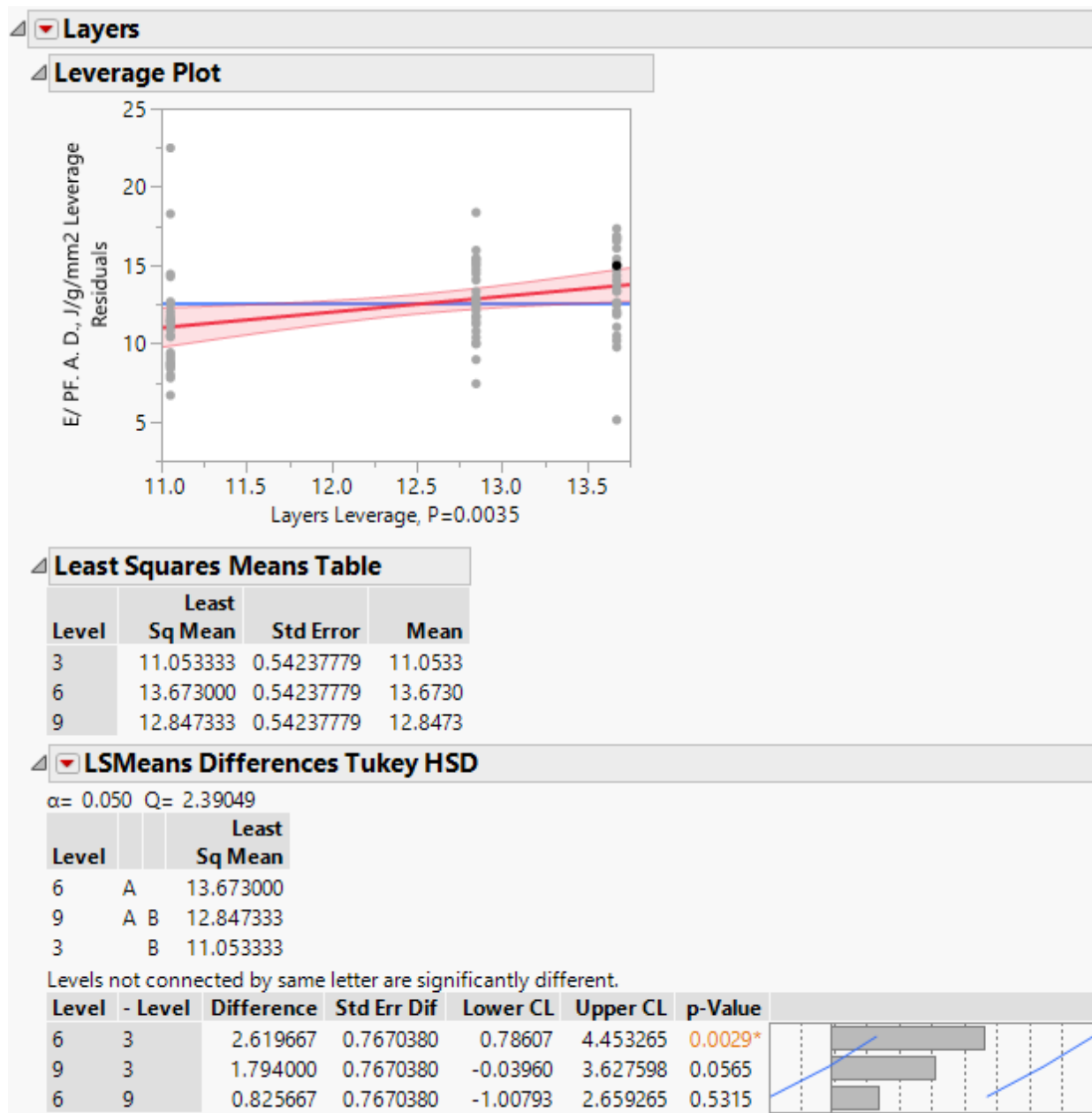


Figure 247. Tukey HSD- Tup impact (Weft) - Effect of Layers on Impact Energy Normalized by Preform Areal Density

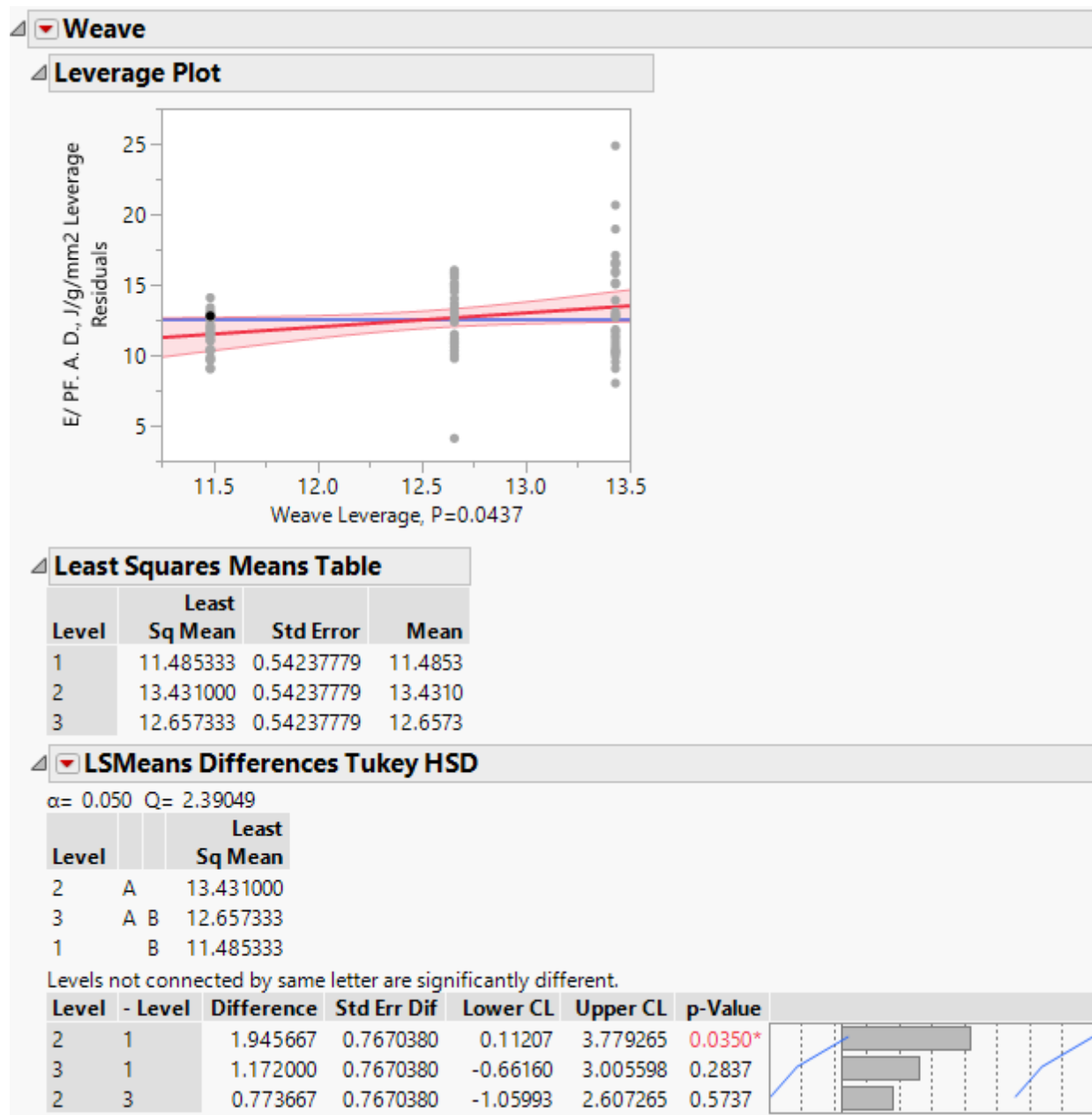


Figure 248. Tukey HSD- Tup impact (Weft) - Effect of Weave on Impact Energy Normalized by Preform Areal Density

Summary of Fit					
RSquare			0.336151		
RSquare Adj			0.222598		
Root Mean Square Error			0.896812		
Mean of Response			3.805444		
Observations (or Sum Wgts)			90		
Analysis of Variance					
Source	DF	Sum of Squares	Mean Square	F Ratio	
Model	13	30.951528	2.38089	2.9603	
Error	76	61.124704	0.80427		Prob > F
C. Total	89	92.076232			0.0015*
Parameter Estimates					
Effect Tests					
Source	Nparm	DF	Sum of Squares	F Ratio	Prob > F
Layers	2	2	16.666469	10.3612	0.0001*
Weave	2	2	4.760749	2.9597	0.0578
Z/Y Ratio	1	1	2.898028	3.6033	0.0615
Layers*Weave	4	4	4.546504	1.4132	0.2377
Layers*Z/Y Ratio	2	2	1.124776	0.6993	0.5001
Weave*Z/Y Ratio	2	2	0.955002	0.5937	0.5548

Table 68. ANOVA Results – Tup impact (Weft) - Impact Energy Normalized by Composite Areal Density

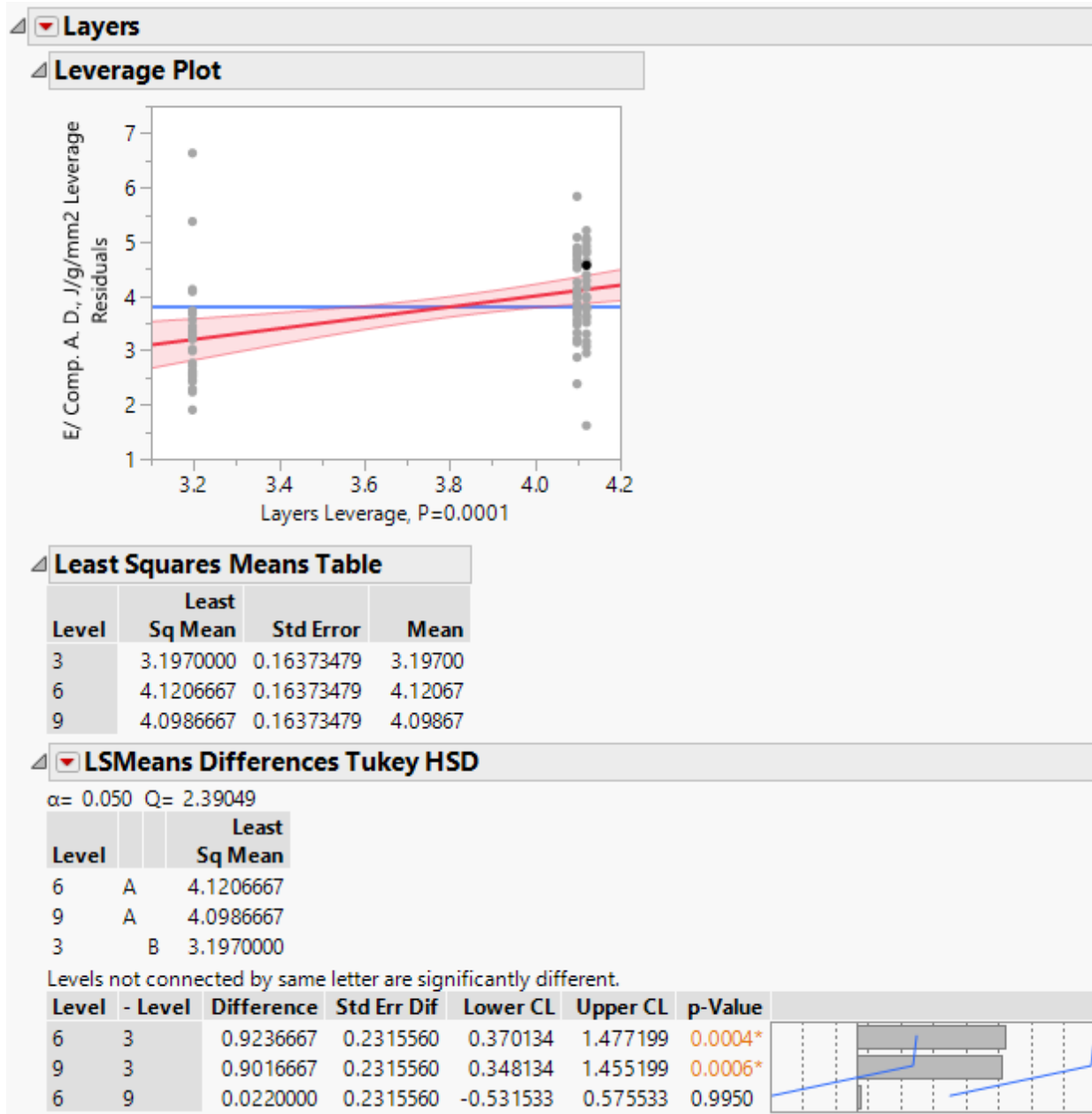


Figure 249. Tukey HSD- Tup impact (Weft) - Effect of Layers on Impact Energy Normalized by Composite Areal Density

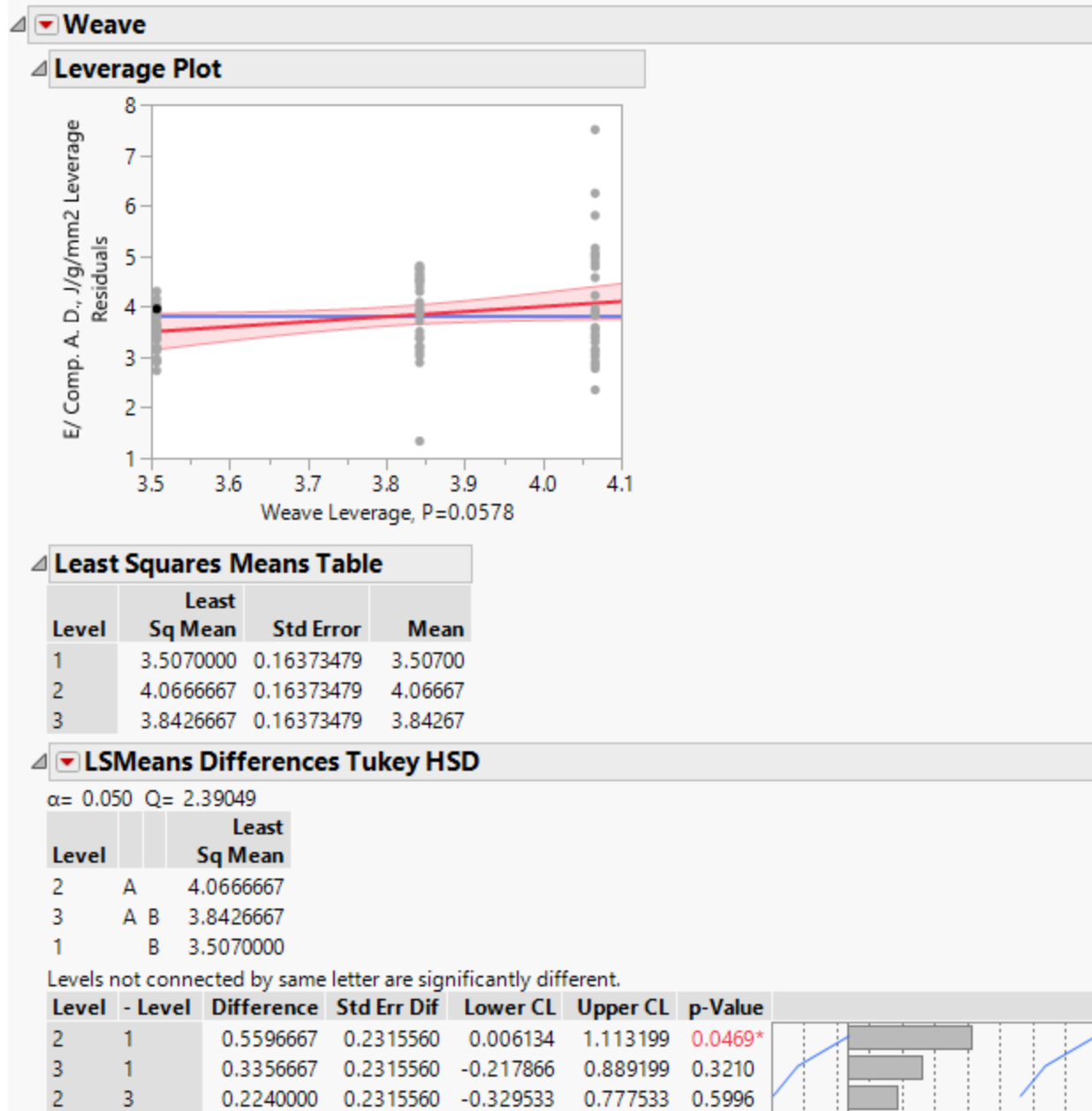


Figure 250. Tukey HSD- Tup impact (Weft) - Effect of Weave on Impact Energy Normalized by Composite Areal Density

D.1.4. Compression Test

Summary of Fit					
RSquare			0.859564		
RSquare Adj			0.834285		
Root Mean Square Error			0.607549		
Mean of Response			7.357667		
Observations (or Sum Wgts)			60		
Analysis of Variance					
Source	DF	Sum of Squares	Mean Square	F Ratio	Prob > F
Model	9	112.96189	12.5513	34.0038	
Error	50	18.45578	0.3691		
C. Total	59	131.41767			<.0001*
Parameter Estimates					
Effect Tests					
Source	Nparm	DF	Sum of Squares	F Ratio	Prob > F
Layers	1	1	107.84323	292.1665	<.0001*
Weave	2	2	0.41754	0.5656	0.5716
Z/Y Ratio	1	1	0.20886	0.5658	0.4554
Layers*Weave	2	2	0.08486	0.1150	0.8916
Layers*Z/Y Ratio	1	1	0.70851	1.9195	0.1721
Weave*Z/Y Ratio	2	2	3.69889	5.0105	0.0104*

Table 69. ANOVA Results- Compression (Warp)- Peak load

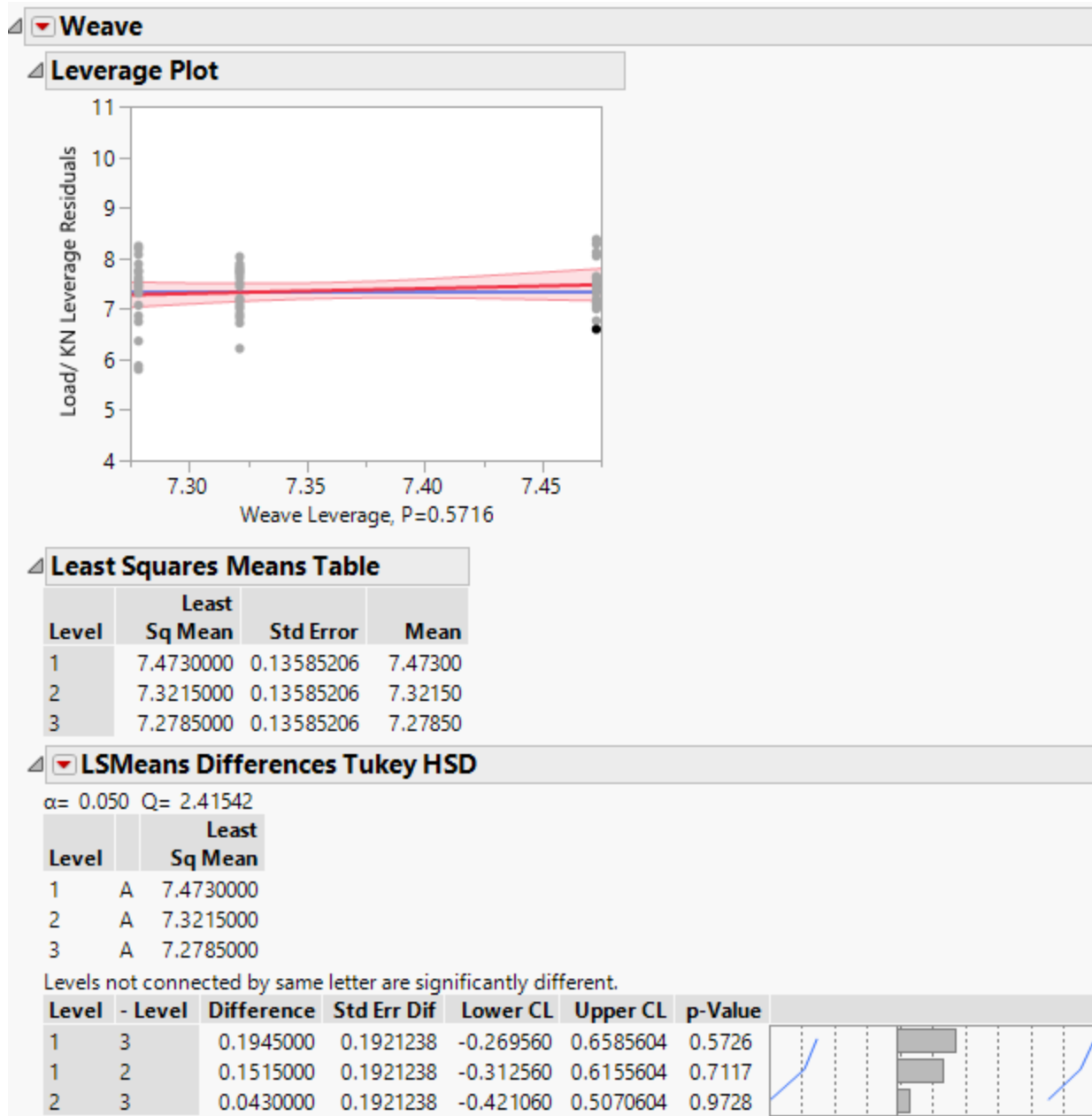


Figure 251. Tukey HSD- Compression (Warp)- Effect of weave on Compression Load

Summary of Fit					
RSquare			0.363746		
RSquare Adj			0.24922		
Root Mean Square Error			4.92697		
Mean of Response			59.11783		
Observations (or Sum Wgts)			60		
Analysis of Variance					
Source	DF	Sum of Squares	Mean Square	F Ratio	
Model	9	693.8999	77.1000	3.1761	
Error	50	1213.7515	24.2750		Prob > F
C. Total	59	1907.6514			0.0041*
Parameter Estimates					
Effect Tests					
Source	Nparm	DF	Sum of Squares	F Ratio	Prob > F
Layers	1	1	34.97593	1.4408	0.2357
Weave	2	2	22.53914	0.4642	0.6313
Z/Y Ratio	1	1	90.06200	3.7101	0.0598
Layers*Weave	2	2	42.98421	0.8854	0.4189
Layers*Z/Y Ratio	1	1	131.09860	5.4006	0.0242*
Weave*Z/Y Ratio	2	2	372.24000	7.6671	0.0012*

Table 70. ANOVA Results – Compression (Warp)- Peak stress

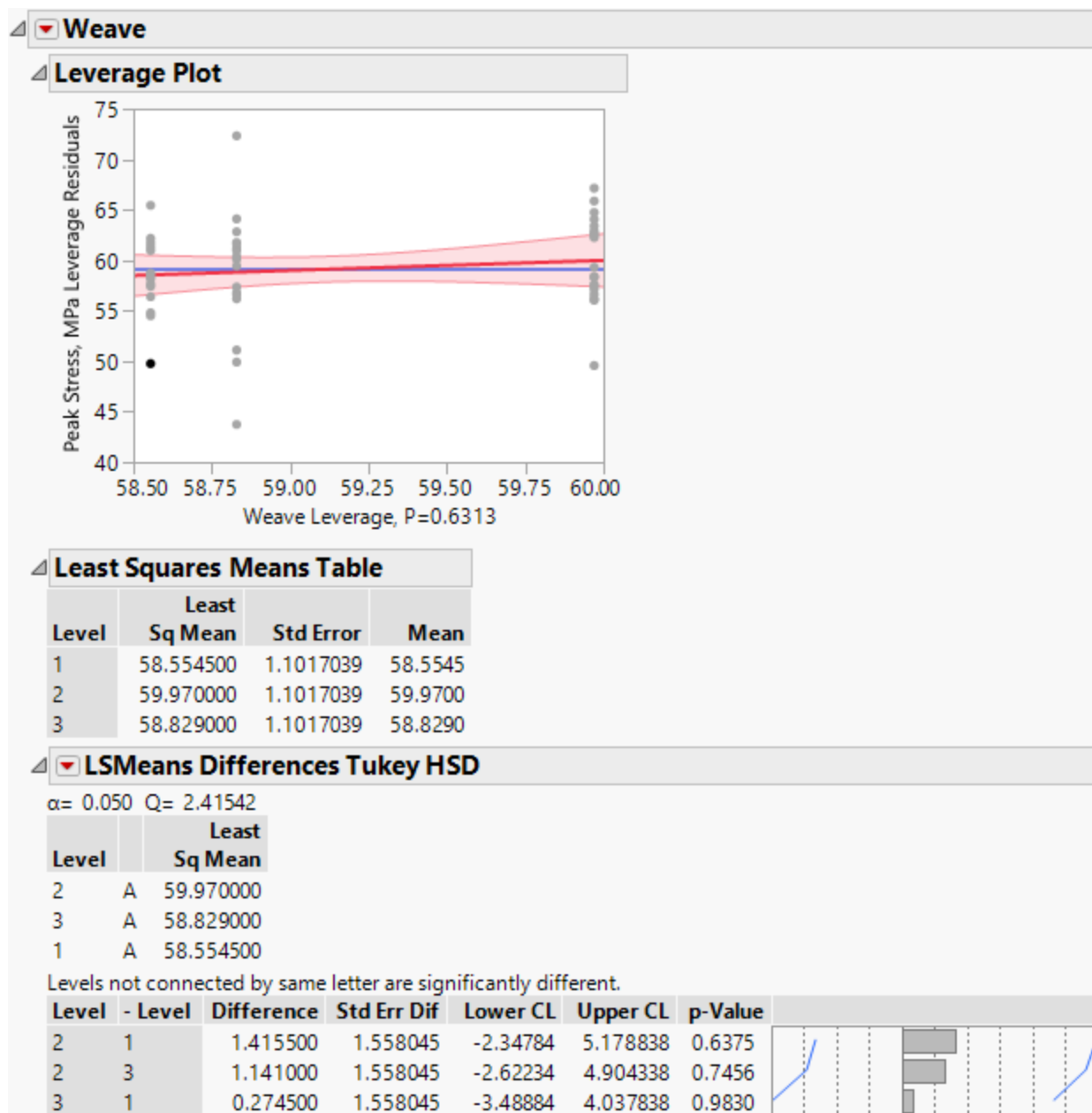


Figure 252. Tukey HSD- Compression (Warp)- Effect of weave on Compression stress

Summary of Fit					
RSquare			0.313494		
RSquare Adj			0.189924		
Root Mean Square Error			2.729277		
Mean of Response			32.31567		
Observations (or Sum Wgts)			60		
Analysis of Variance					
Source	DF	Sum of Squares	Mean Square	F Ratio	
Model	9	170.07919	18.8977	2.5370	
Error	50	372.44768	7.4490		Prob > F
C. Total	59	542.52687			0.0175*
Parameter Estimates					
Effect Tests					
Source	Nparm	DF	Sum of Squares	F Ratio	Prob > F
Layers	1	1	37.85793	5.0823	0.0286*
Weave	2	2	8.01350	0.5379	0.5873
Z/Y Ratio	1	1	7.89163	1.0594	0.3083
Layers*Weave	2	2	0.84444	0.0567	0.9450
Layers*Z/Y Ratio	1	1	8.06667	1.0829	0.3030
Weave*Z/Y Ratio	2	2	107.40502	7.2094	0.0018*

Table 71. ANOVA Results – Compression (Warp)- Compression Load Normalized by Preform Areal Density

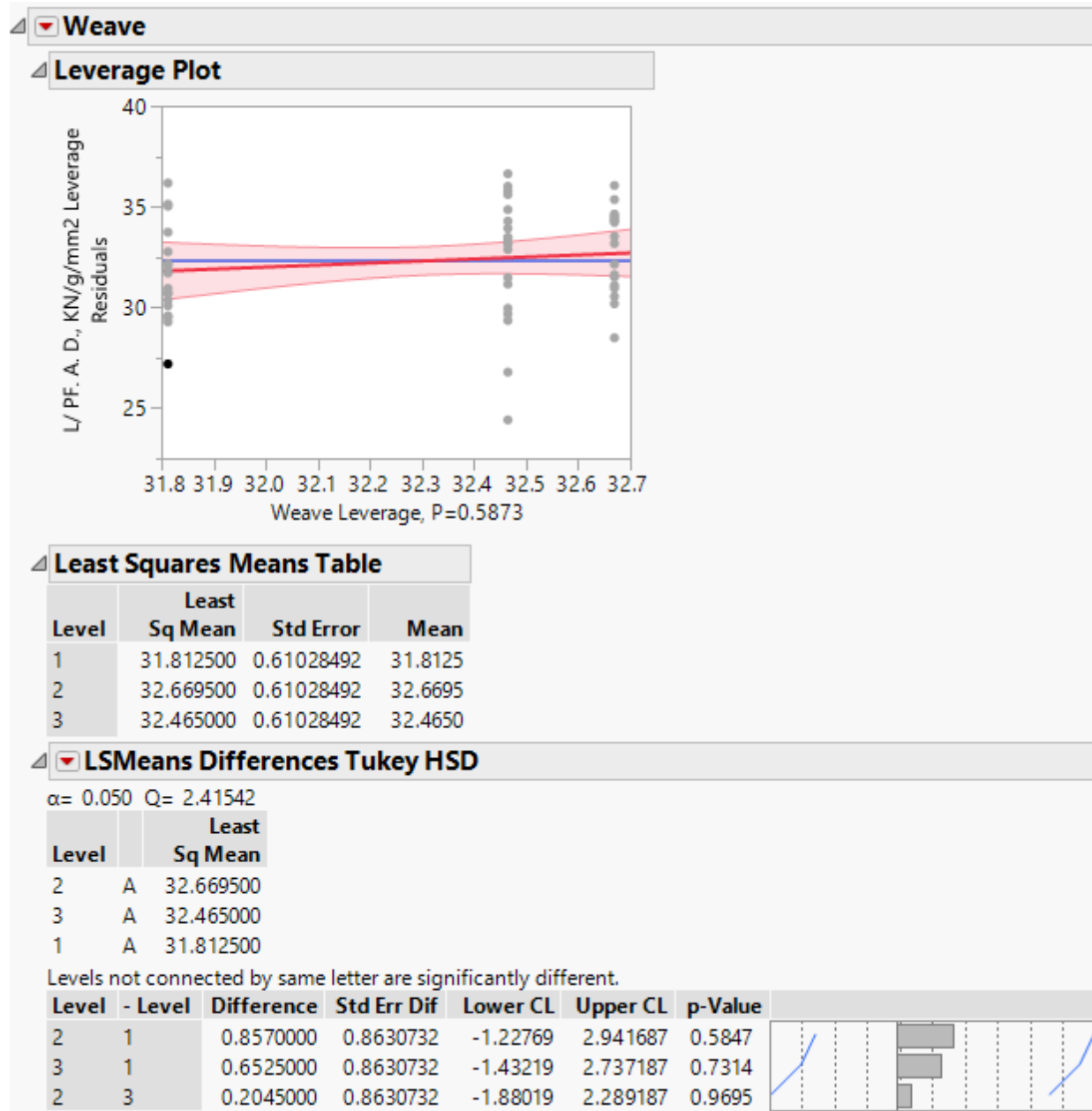


Figure 253. Tukey HSD- Compression (Warp)- Effect of weave on Compression Load

Normalized by Preform Areal Density

Summary of Fit					
RSquare			0.174299		
RSquare Adj			0.025673		
Root Mean Square Error			5.11578		
Mean of Response			39.65017		
Observations (or Sum Wgts)			60		
Analysis of Variance					
Source	DF	Sum of Squares	Mean Square	F Ratio	Prob > F
Model	9	276.2277	30.6920	1.1727	
Error	50	1308.5604	26.1712		
C. Total	59	1584.7881			0.3326
Parameter Estimates					
Effect Tests					
Source	Nparm	DF	Sum of Squares	F Ratio	Prob > F
Layers	1	1	0.71068	0.0272	0.8698
Weave	2	2	6.75190	0.1290	0.8793
Z/Y Ratio	1	1	78.36408	2.9943	0.0897
Layers*Weave	2	2	8.76396	0.1674	0.8463
Layers*Z/Y Ratio	1	1	77.04400	2.9438	0.0924
Weave*Z/Y Ratio	2	2	104.59310	1.9982	0.1463

Table 72. ANOVA Results – Compression (Warp)- Compression Load Normalized by
Composite Areal Density

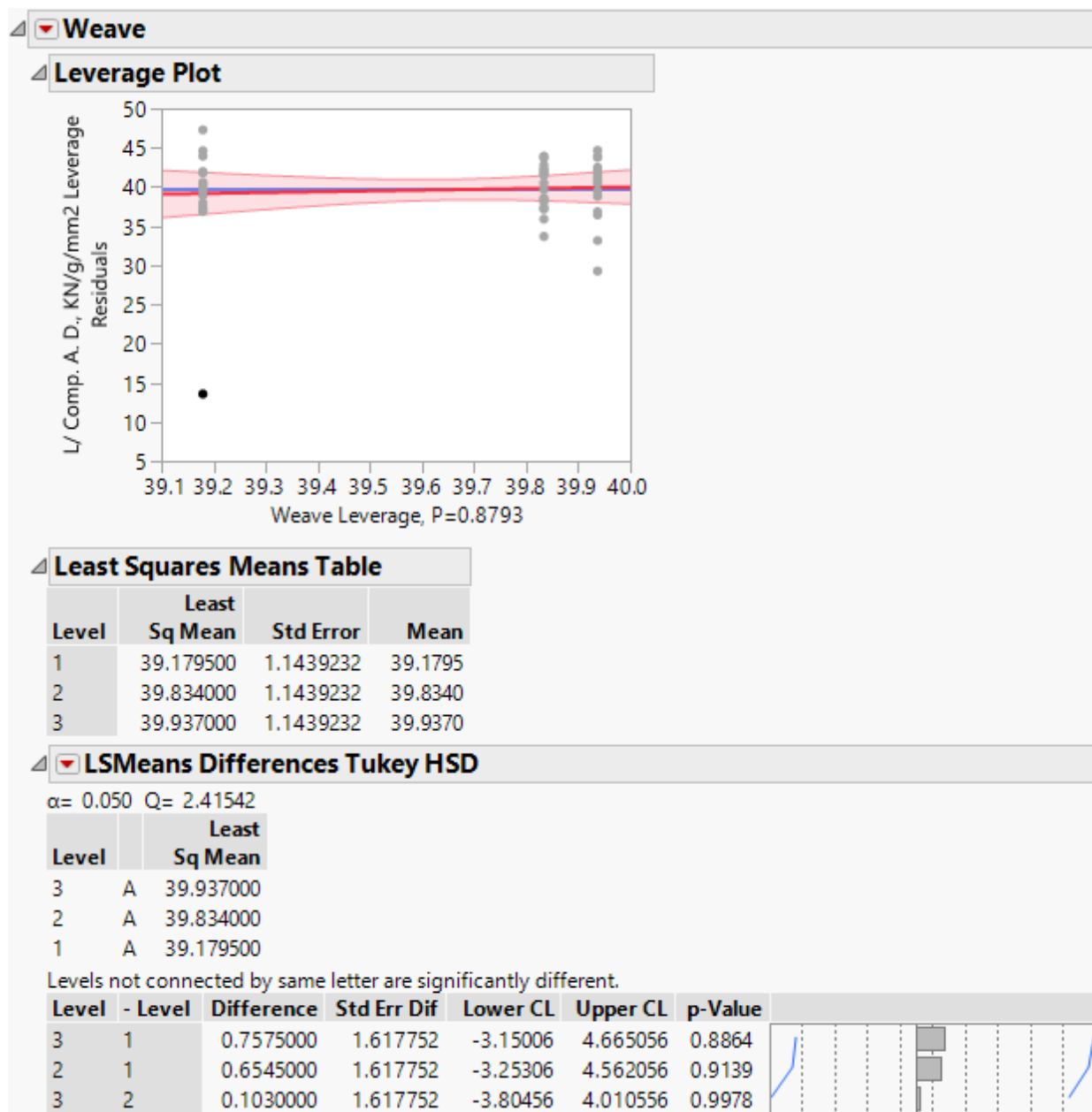


Figure 254. Tukey HSD- Compression (Warp)- Effect of weave on Compression Load
Normalized by Composite Areal Density

Summary of Fit					
RSquare			0.912397		
RSquare Adj			0.896628		
Root Mean Square Error			0.958531		
Mean of Response			13.60467		
Observations (or Sum Wgts)			60		
Analysis of Variance					
Source	DF	Sum of Squares	Mean Square	F Ratio	
Model	9	478.46005	53.1622	57.8617	
Error	50	45.93904	0.9188		Prob > F
C. Total	59	524.39909			<.0001*
Parameter Estimates					
Effect Tests					
Source	Nparm	DF	Sum of Squares	F Ratio	Prob > F
Layers	1	1	397.63153	432.7817	<.0001*
Weave	2	2	66.31974	36.0912	<.0001*
Z/Y Ratio	1	1	0.89793	0.9773	0.3276
Layers*Weave	2	2	10.87814	5.9199	0.0049*
Layers*Z/Y Ratio	1	1	2.43211	2.6471	0.1100
Weave*Z/Y Ratio	2	2	0.30060	0.1636	0.8495

Table 73. ANOVA Results- Compression (Weft)- Peak load

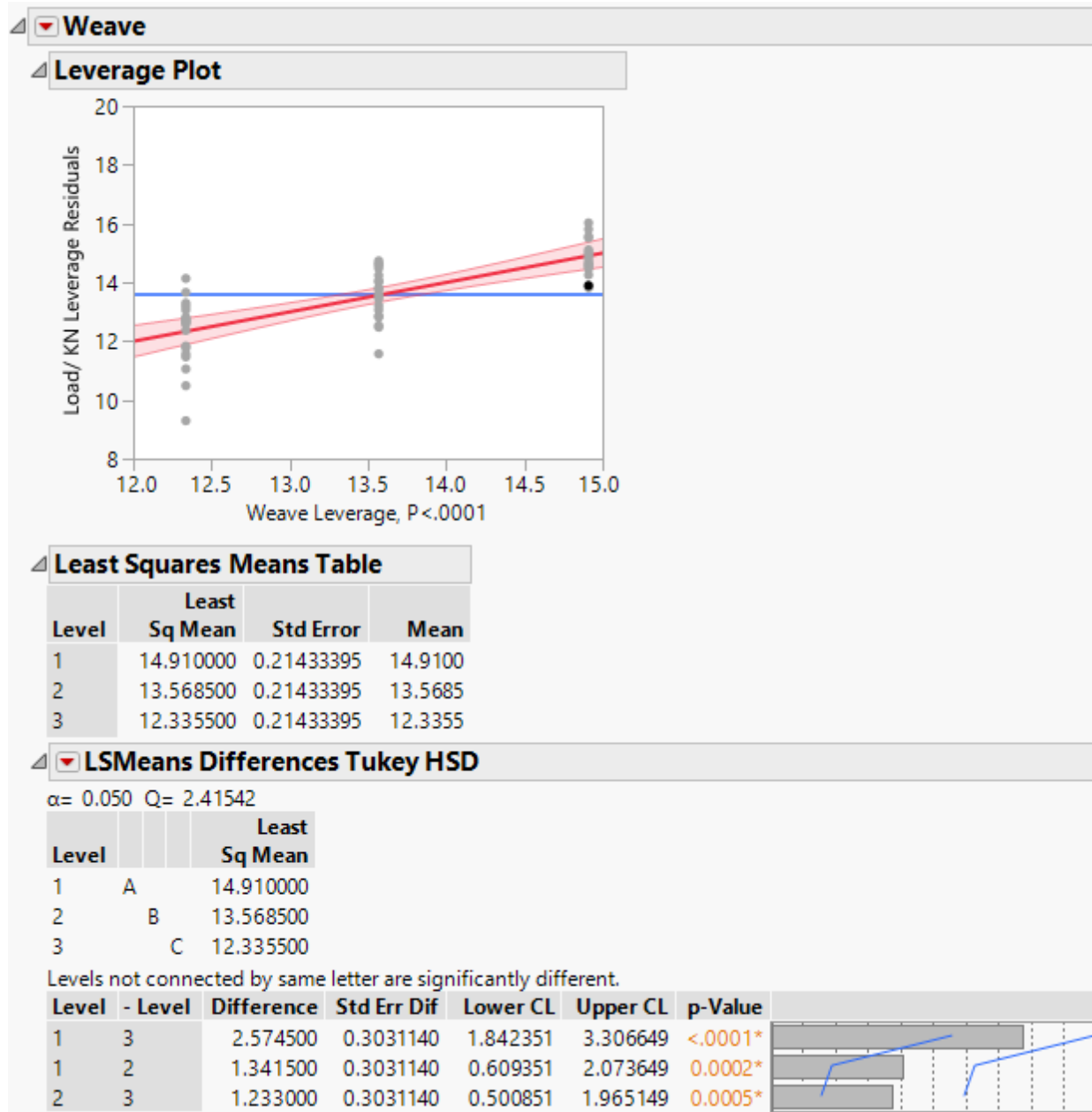


Figure 255. Tukey HSD- Compression (Weft)- Effect of weave on Compression Load

Summary of Fit					
RSquare			0.487023		
RSquare Adj			0.394687		
Root Mean Square Error			8.969818		
Mean of Response			108.5853		
Observations (or Sum Wgts)			60		
Analysis of Variance					
Source	DF	Sum of Squares	Mean Square	F Ratio	
Model	9	3819.3372	424.371	5.2745	
Error	50	4022.8815	80.458		Prob > F
C. Total	59	7842.2187			<.0001*
Parameter Estimates					
Effect Tests					
Source	Nparm	DF	Sum of Squares	F Ratio	Prob > F
Layers	1	1	0.1793	0.0022	0.9625
Weave	2	2	2687.8989	16.7038	<.0001*
Z/Y Ratio	1	1	3.5819	0.0445	0.8337
Layers*Weave	2	2	651.9997	4.0518	0.0234*
Layers*Z/Y Ratio	1	1	264.6840	3.2897	0.0757
Weave*Z/Y Ratio	2	2	210.9934	1.3112	0.2786

Table 74. ANOVA Results – Compression (Weft)- Peak stress



Figure 256. Tukey HSD- Compression (Weft)- Effect of Compression on Tensile stress

Summary of Fit					
RSquare			0.555392		
RSquare Adj			0.475362		
Root Mean Square Error			4.264888		
Mean of Response			59.57133		
Observations (or Sum Wgts)			60		
Analysis of Variance					
Source	DF	Sum of Squares	Mean Square	F Ratio	Prob > F
Model	9	1136.0748	126.231	6.9398	
Error	50	909.4633	18.189		
C. Total	59	2045.5381			<.0001*
Parameter Estimates					
Effect Tests					
Source	Nparm	DF	Sum of Squares	F Ratio	Prob > F
Layers	1	1	59.88006	3.2921	0.0756
Weave	2	2	745.61170	20.4959	<.0001*
Z/Y Ratio	1	1	6.84113	0.3761	0.5425
Layers*Weave	2	2	226.17777	6.2173	0.0039*
Layers*Z/Y Ratio	1	1	12.69600	0.6980	0.4074
Weave*Z/Y Ratio	2	2	84.86816	2.3329	0.1075

Table 75. ANOVA Results – Compression (Weft)- Compression Load Normalized by Preform
Areal Density

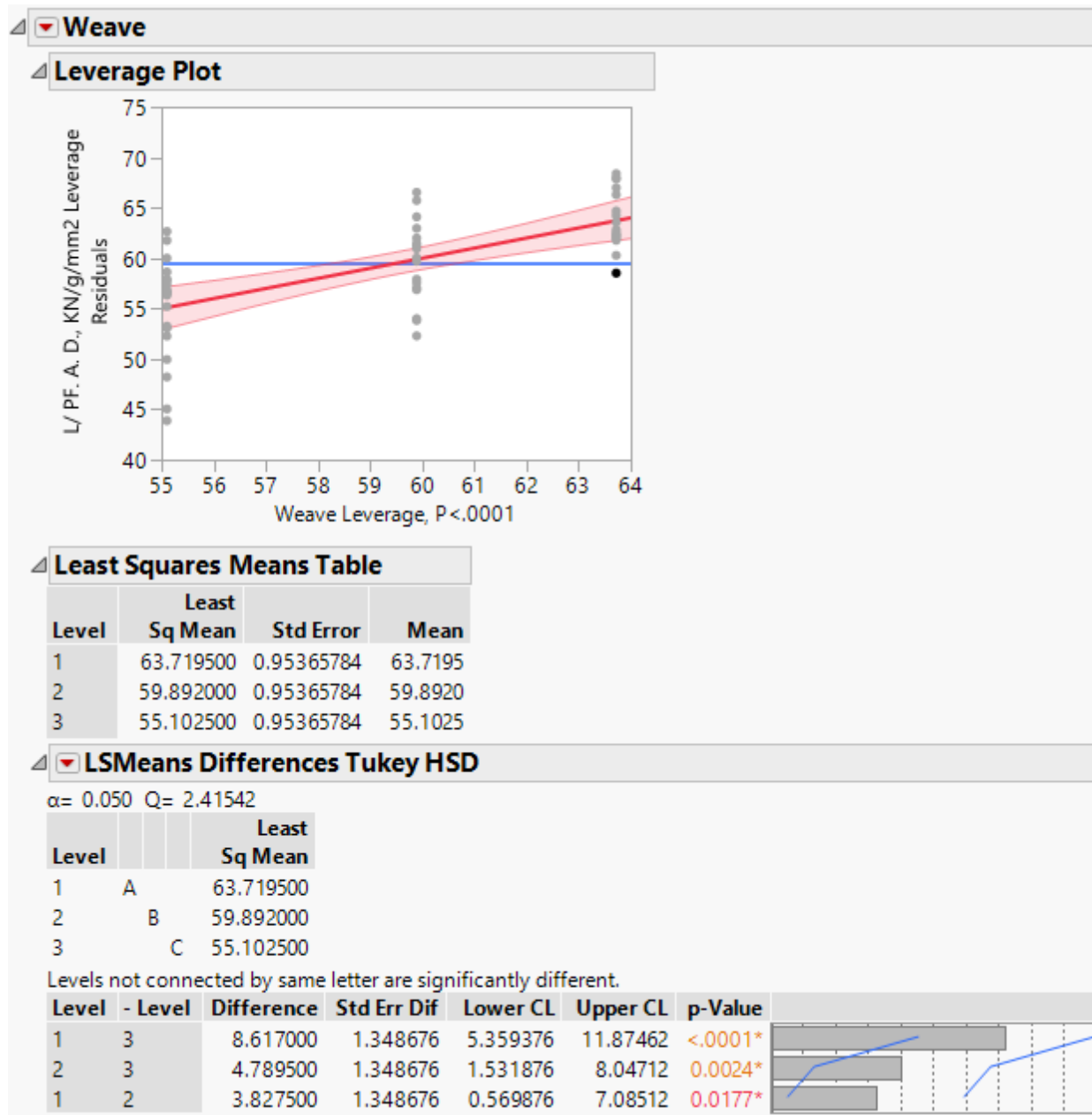


Figure 257. Tukey HSD- Compression (Weft)- Effect of weave on Compression Load

Normalized by Preform Areal Density

Summary of Fit					
RSquare		0.589531			
RSquare Adj		0.515646			
Root Mean Square Error		1.613391			
Mean of Response		22.327			
Observations (or Sum Wgts)		60			
Analysis of Variance					
Source	DF	Sum of Squares	Mean Square	F Ratio	
Model	9	186.92819	20.7698	7.9791	
Error	50	130.15147	2.6030		Prob > F
C. Total	59	317.07966			<.0001*
Parameter Estimates					
Effect Tests					
Source	Nparm	DF	Sum of Squares	F Ratio	Prob > F
Layers	1	1	2.50513	0.9624	0.3313
Weave	2	2	139.53721	26.8028	<.0001*
Z/Y Ratio	1	1	0.21600	0.0830	0.7745
Layers*Weave	2	2	25.34376	4.8681	0.0117*
Layers*Z/Y Ratio	1	1	10.58400	4.0660	0.0491*
Weave*Z/Y Ratio	2	2	8.74209	1.6792	0.1969

Table 76. ANOVA Results – Compression (Weft)- Compression Load Normalized by Composite Areal Density

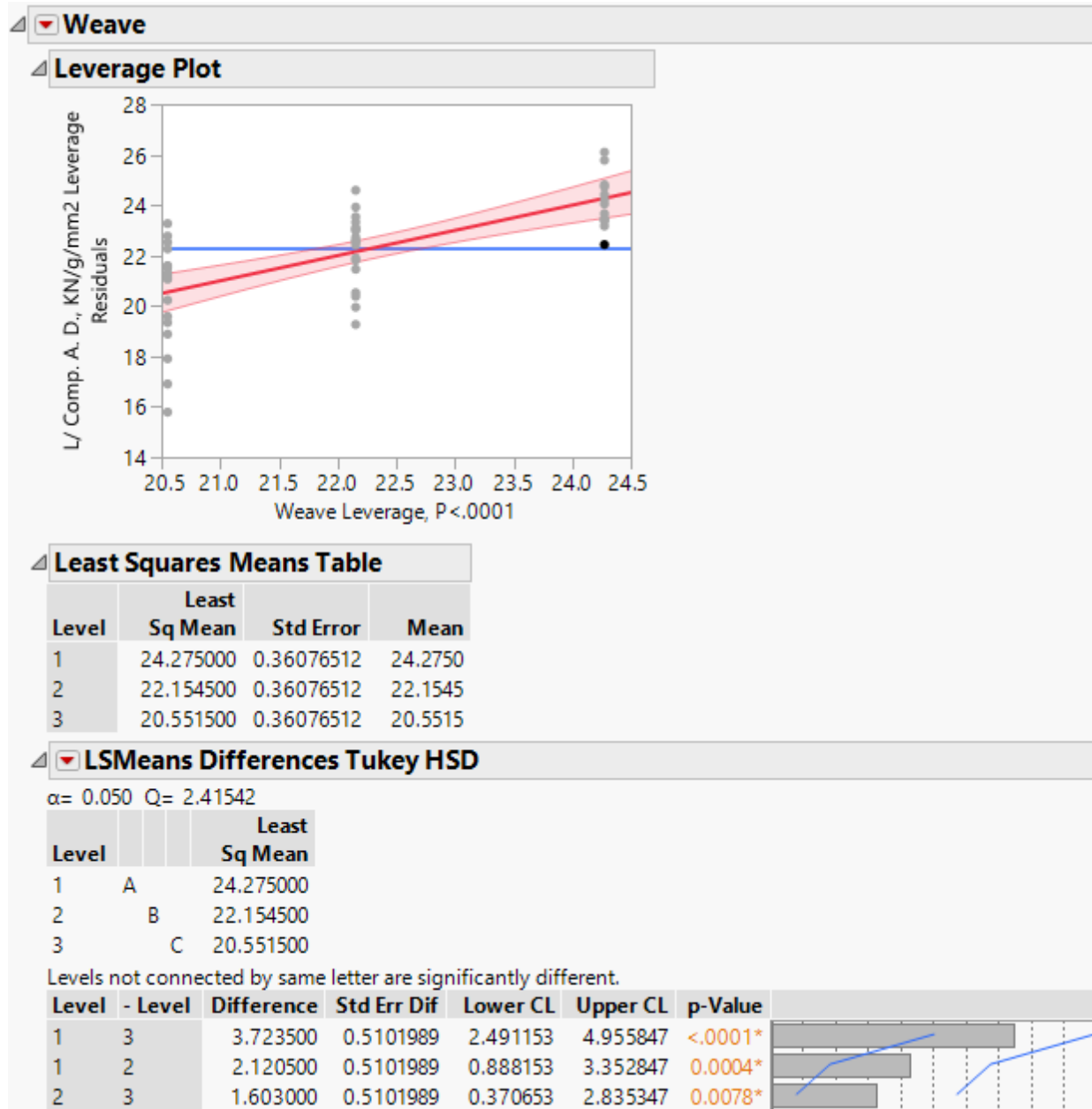


Figure 258. Tukey HSD- Compression (Weft)- Effect of weave on Compression Load

Normalized by Composite Areal Density

D.2. Statistical Analysis of Experimental Design B

D.2.1. Tensile Test

Summary of Fit					
RSquare			0.037617		
RSquare Adj			-0.04258		
Root Mean Square Error			3.621712		
Mean of Response			7.68525		
Observations (or Sum Wgts)			40		
Analysis of Variance					
Source	DF	Sum of Squares	Mean Square	F Ratio	
Model	3	18.45715	6.1524	0.4690	
Error	36	472.20485	13.1168		Prob > F
C. Total	39	490.66200			0.7057
Parameter Estimates					
Effect Tests					
Source	Nparm	DF	Sum of Squares	F Ratio	Prob > F
Yarn Type	3	3	18.457148	0.4690	0.7057

Table 77. ANOVA Results- Tensile (Weft)- Effect of X-yarn type on Peak load

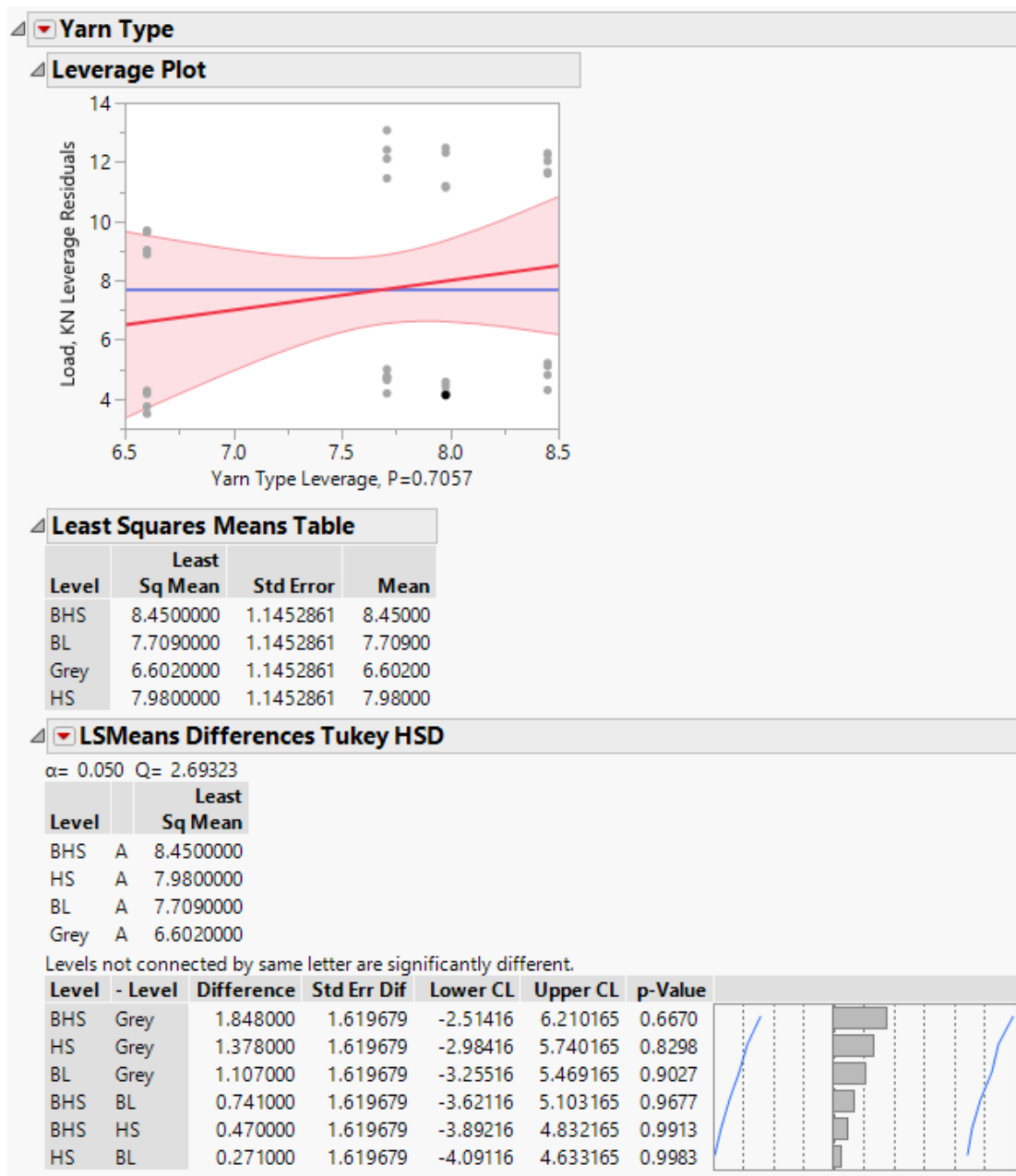


Figure 259. Tukey HSD- Tensile (Weft)- Effect of X-yarn type on Tensile Load

Summary of Fit

RSquare

0.246295

RSquare Adj

0.183486

Root Mean Square Error

23.10415

Mean of Response

130.8525

Observations (or Sum Wgts)

40

Analysis of Variance

Source	DF	Sum of Squares	Mean Square	F Ratio
Model	3	6279.672	2093.22	3.9214
Error	36	19216.863	533.80	Prob > F
C. Total	39	25496.535		0.0161*

Parameter Estimates

Effect Tests

Source	Nparm	DF	Sum of Squares	F Ratio	Prob > F
Yarn Type	3	3	6279.6720	3.9214	0.0161*

Table 78. ANOVA Results- Tensile (Weft)- Effect of X-yarn type on Peak stress

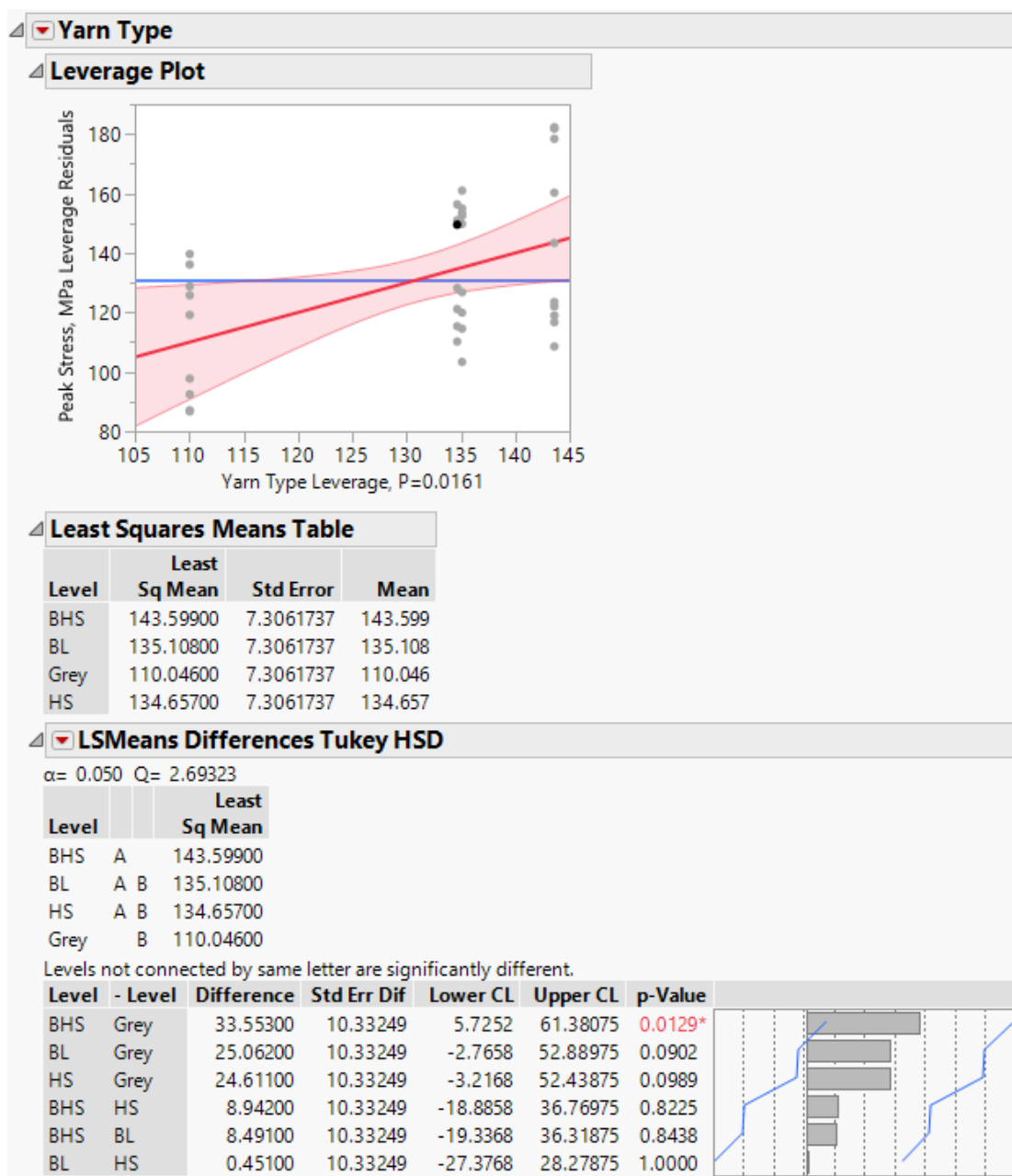


Figure 260. Tukey HSD- Tensile (Weft)- Effect of X-yarn type on peak stress

Summary of Fit					
RSquare			0.396539		
RSquare Adj			0.34625		
Root Mean Square Error			5.843062		
Mean of Response			55.5585		
Observations (or Sum Wgts)			40		
Analysis of Variance					
Source	DF	Sum of Squares	Mean Square	F Ratio	
Model	3	807.6441	269.215	7.8853	
Error	36	1229.0895	34.141		Prob > F
C. Total	39	2036.7335			0.0004*
Parameter Estimates					
Effect Tests					
Source	Nparm	DF	Sum of Squares	F Ratio	Prob > F
Yarn Type	3	3	807.64405	7.8853	0.0004*

Table 79. ANOVA Results- Tensile (Weft)- Effect of X-yarn type on Peak load Normalized by
Preform Areal Density

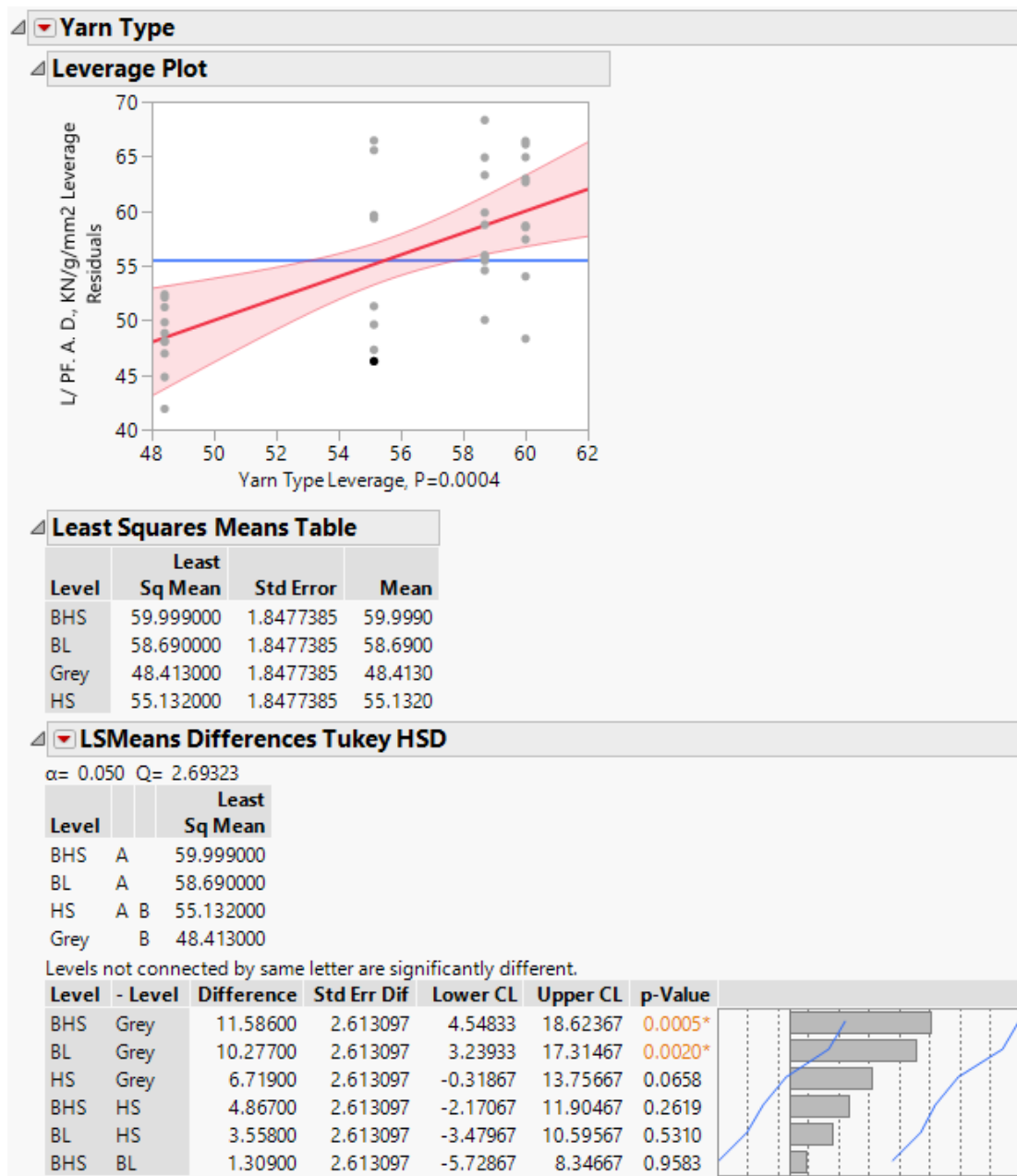


Figure 261. Tukey HSD- Tensile (Weft)- Effect of X-yarn type on Tensile Load Normalized by Preform Areal Density

Summary of Fit					
RSquare			0.499539		
RSquare Adj			0.457834		
Root Mean Square Error			2.202923		
Mean of Response			22.672		
Observations (or Sum Wgts)			40		
Analysis of Variance					
Source	DF	Sum of Squares	Mean Square	F Ratio	
Model	3	174.38174	58.1272	11.9779	
Error	36	174.70330	4.8529		Prob > F
C. Total	39	349.08504			<.0001*
Parameter Estimates					
Effect Tests					
Source	Nparm	DF	Sum of Squares	F Ratio	Prob > F
Yarn Type	3	3	174.38174	11.9779	<.0001*

Table 80. ANOVA Results- Tensile (Weft)- Effect of X-yarn type on Peak load Normalized by
Composite Areal Density

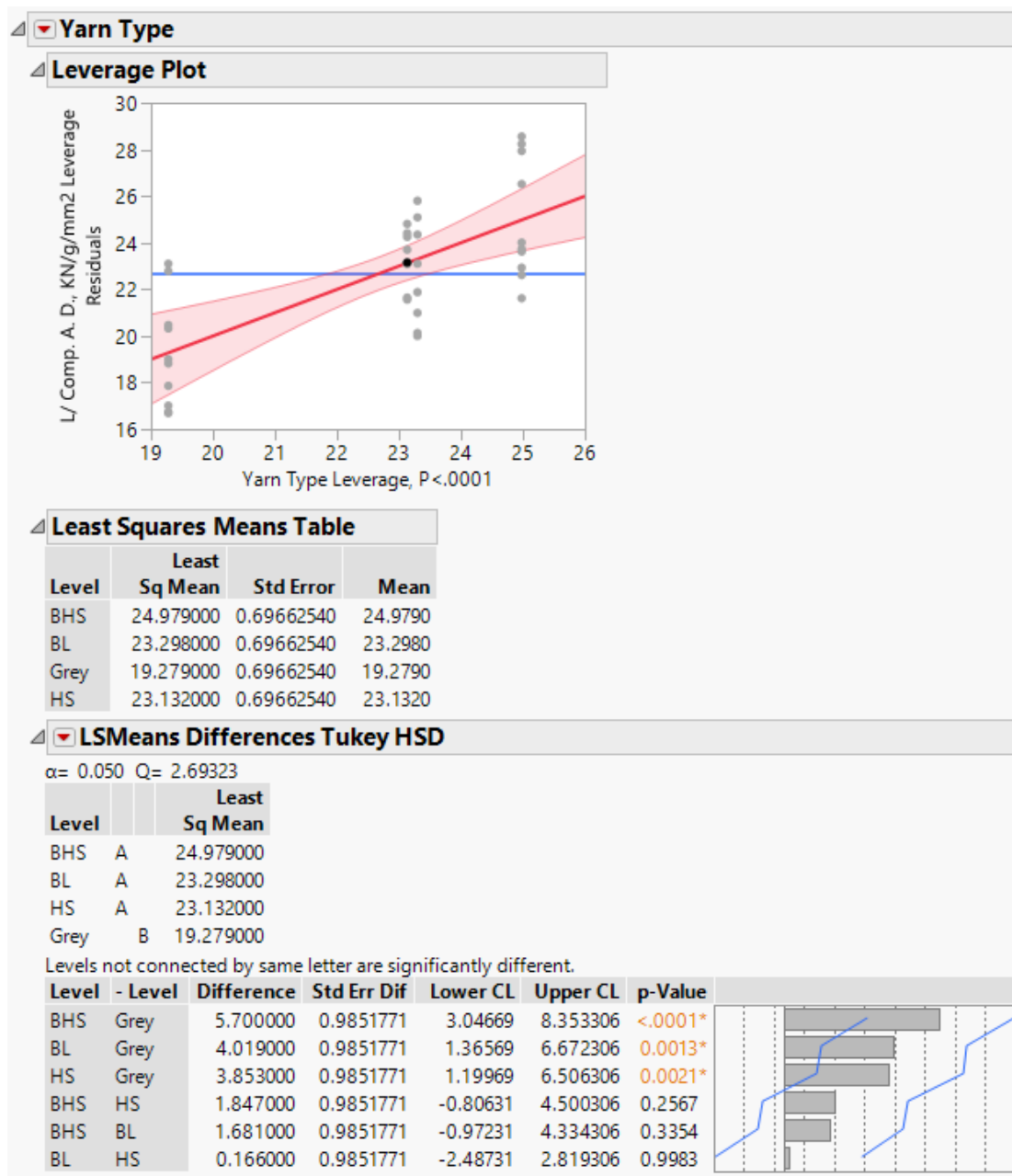


Figure 262. Tukey HSD- Tensile (Weft)- Effect of X-yarn type on Tensile Load Normalized by Composite Areal Density

D.2.2. Tup Impact

Summary of Fit					
RSquare			0.030515		
RSquare Adj			-0.05028		
Root Mean Square Error			6.903557		
Mean of Response			10.80075		
Observations (or Sum Wgts)			40		
Analysis of Variance					
Source	DF	Sum of Squares	Mean Square	F Ratio	
Model	3	54.0037	18.0012	0.3777	
Error	36	1715.7278	47.6591		Prob > F
C. Total	39	1769.7315			0.7696
Parameter Estimates					
Effect Tests					
Source	Nparm	DF	Sum of Squares	F Ratio	Prob > F
Yarn Type	3	3	54.003668	0.3777	0.7696

Table 81. ANOVA Results – Tup impact- Effect of X-yarn type on Impact Energy

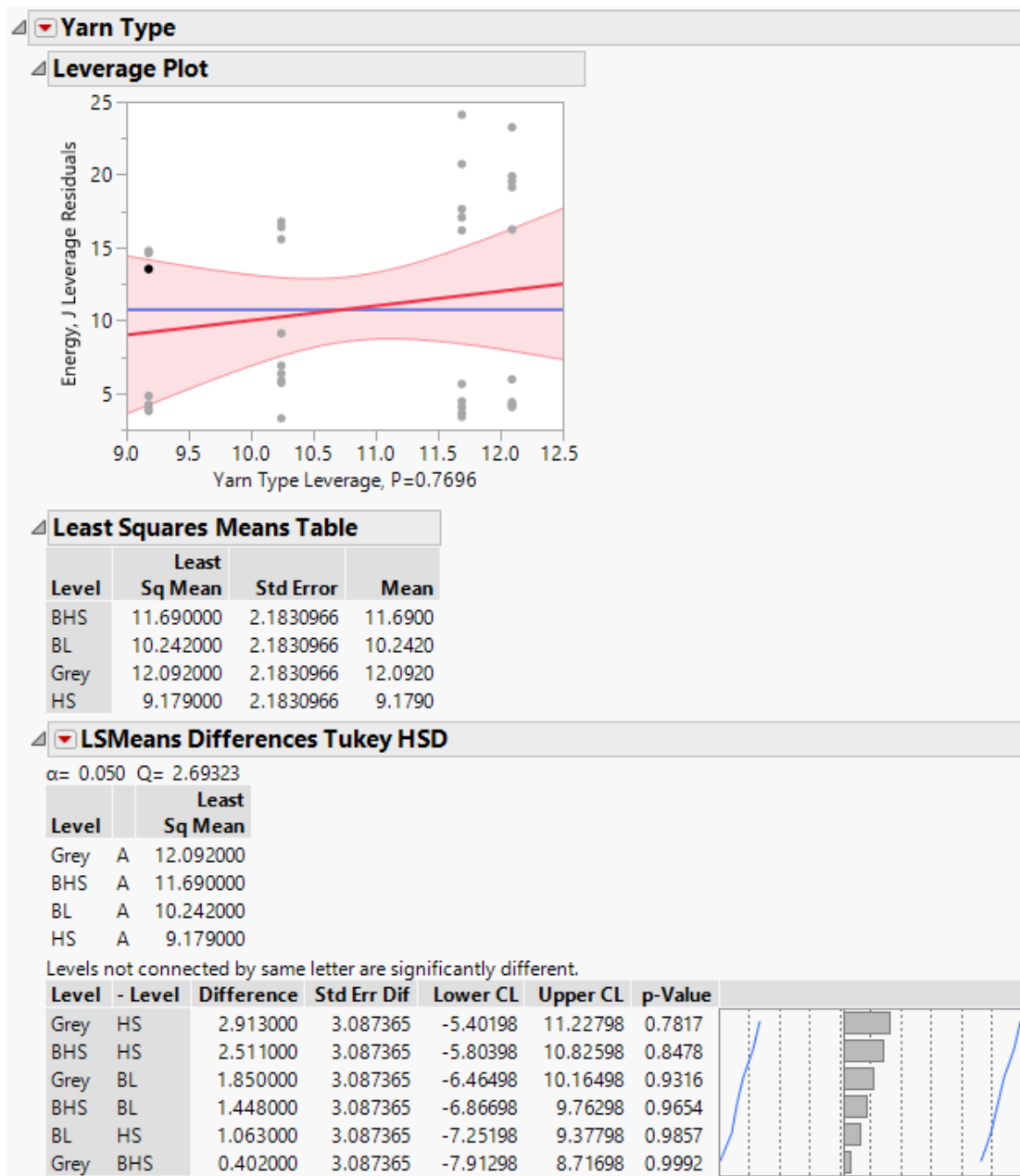


Figure 263. Tukey HSD- Tup impact- Effect of X-yarn type on Impact Energy

Summary of Fit					
RSquare			0.056881		
RSquare Adj			-0.02171		
Root Mean Square Error			1.261441		
Mean of Response			3.334		
Observations (or Sum Wgts)			40		
Analysis of Variance					
Source	DF	Sum of Squares	Mean Square	F Ratio	
Model	3	3.454940	1.15165	0.7237	
Error	36	57.284420	1.59123		Prob > F
C. Total	39	60.739360			0.5444
Parameter Estimates					
Effect Tests					
Source	Nparm	DF	Sum of Squares	F Ratio	Prob > F
Yarn Type	3	3	3.4549400	0.7237	0.5444

Table 82. ANOVA Results – Tup impact- Effect of X-yarn type on Impact Energy Normalized
by Thickness

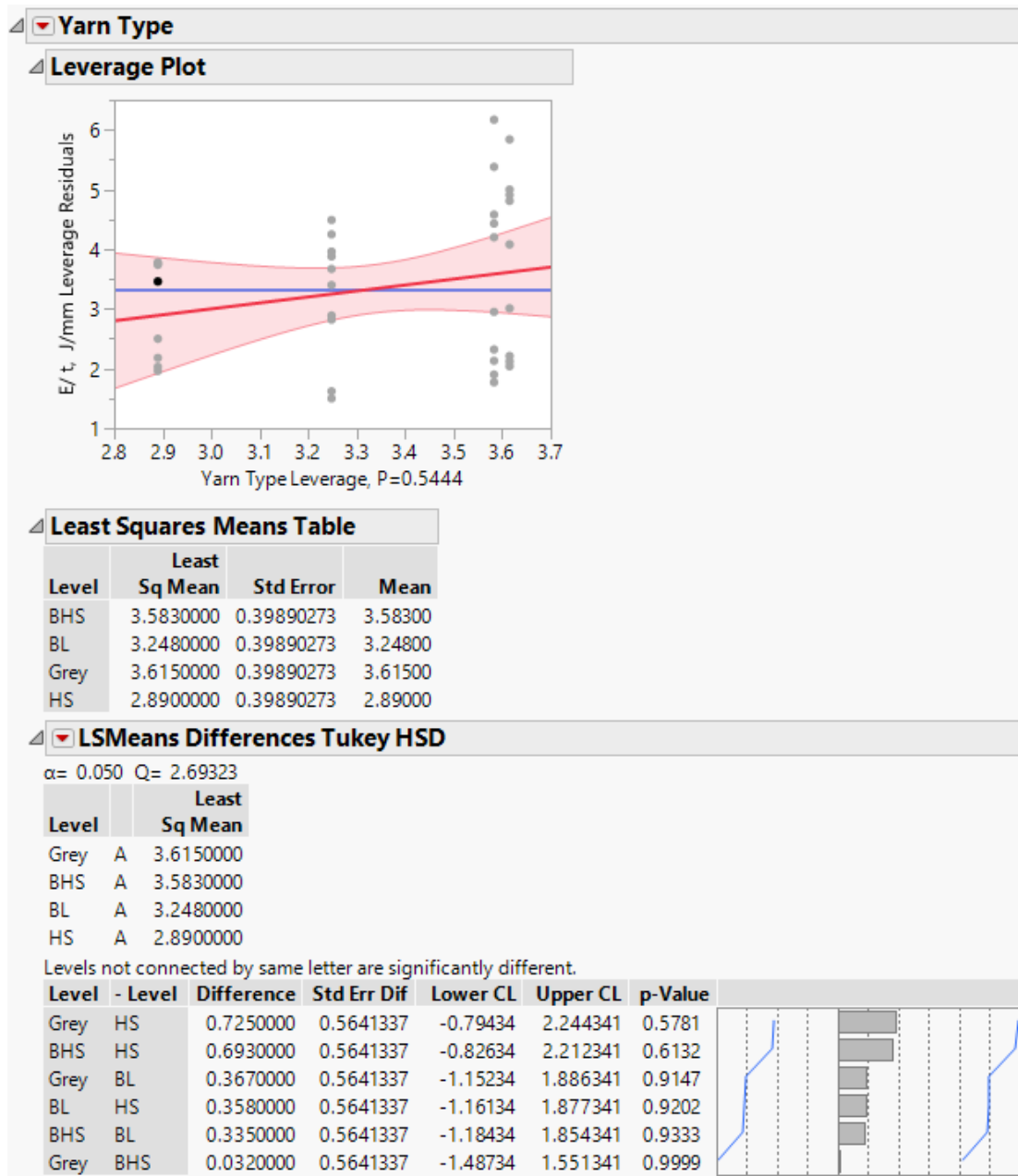


Figure 264. Tukey HSD- Tup impact- Effect of X-yarn type on Impact Energy Normalized by Thickness

Summary of Fit					
RSquare			0.08978		
RSquare Adj			0.013929		
Root Mean Square Error			24.98182		
Mean of Response			73.61525		
Observations (or Sum Wgts)			40		
Analysis of Variance					
Source	DF	Sum of Squares	Mean Square	F Ratio	
Model	3	2216.078	738.693	1.1836	
Error	36	22467.295	624.092		Prob > F
C. Total	39	24683.373			0.3296
Parameter Estimates					
Effect Tests					
Source	Nparm	DF	Sum of Squares	F Ratio	Prob > F
Yarn Type	3	3	2216.0776	1.1836	0.3296

Table 83. ANOVA Results – Tup impact- Effect of X-yarn type on Impact Energy Normalized
by Preform Areal Density

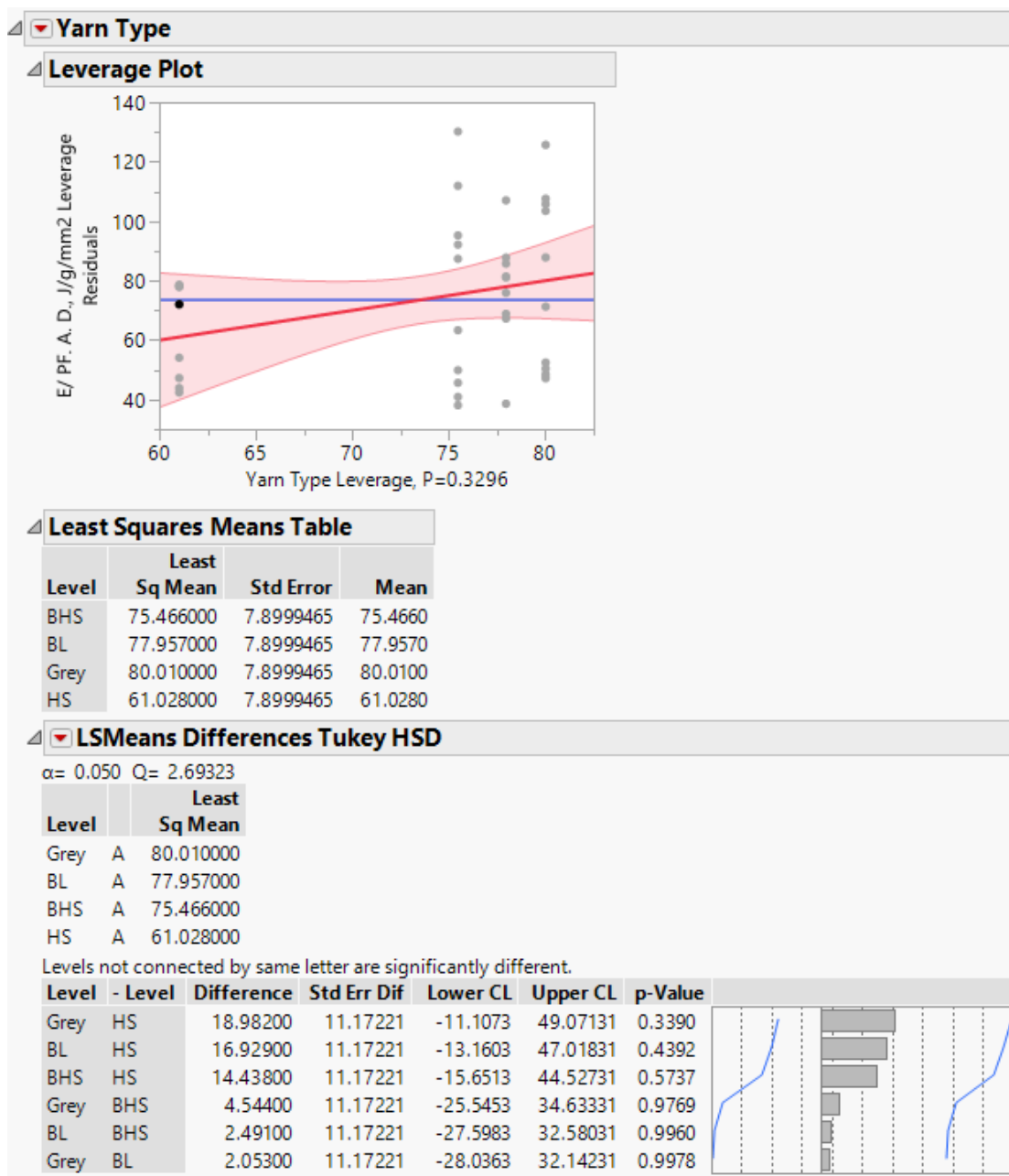


Figure 265. Tukey HSD- Tup impact- Effect of X-yarn type on Impact Energy Normalized by Preform Areal Density

Summary of Fit					
RSquare			0.101774		
RSquare Adj			0.026921		
Root Mean Square Error			7.062299		
Mean of Response			29.407		
Observations (or Sum Wgts)			40		
Analysis of Variance					
Source	DF	Sum of Squares	Mean Square	F Ratio	
Model	3	203.4438	67.8146	1.3597	
Error	36	1795.5383	49.8761		Prob > F
C. Total	39	1998.9820			0.2706
Parameter Estimates					
Effect Tests					
Source	Nparm	DF	Sum of Squares	F Ratio	Prob > F
Yarn Type	3	3	203.44376	1.3597	0.2706

Table 84. ANOVA Results – Tup impact- Effect of X-yarn type on Impact Energy Normalized
by Composite Areal Density

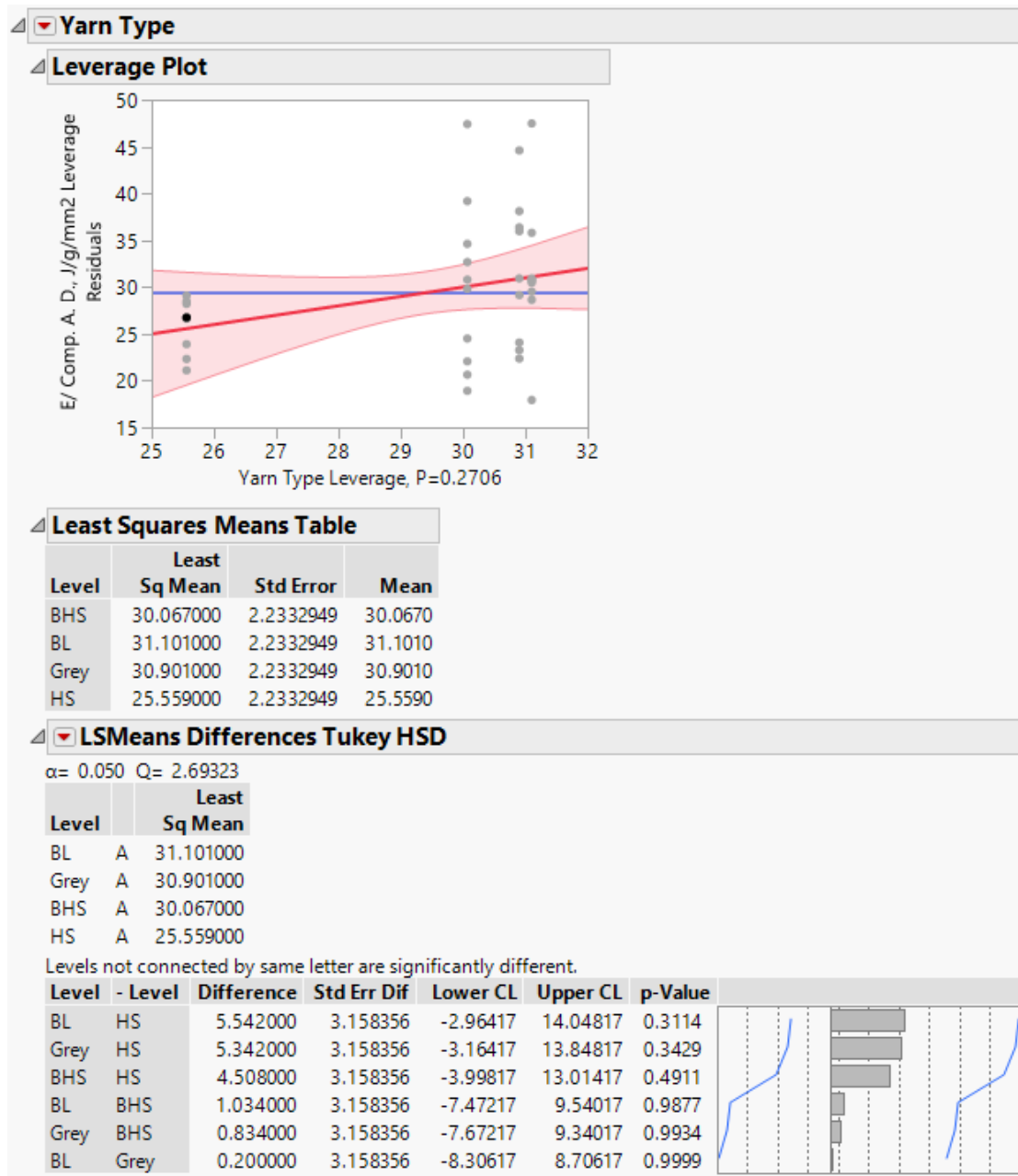


Figure 266. Tukey HSD- Tup impact- Effect of X-yarn type on Impact Energy Normalized by Composite Areal Density

D.2.3. Charpy Impact

Summary of Fit					
RSquare			0.040055		
RSquare Adj			-0.03994		
Root Mean Square Error			0.891885		
Mean of Response			1.6945		
Observations (or Sum Wgts)			40		
Analysis of Variance					
Source	DF	Sum of Squares	Mean Square	F Ratio	
Model	3	1.194890	0.398297	0.5007	
Error	36	28.636500	0.795458		Prob > F
C. Total	39	29.831390			0.6842
Parameter Estimates					
Effect Tests					
Source	Nparm	DF	Sum of Squares	F Ratio	Prob > F
Yarn Type	3	3	1.1948900	0.5007	0.6842

Table 85. ANOVA Results – Charpy impact- Effect of X-yarn type on Impact Energy

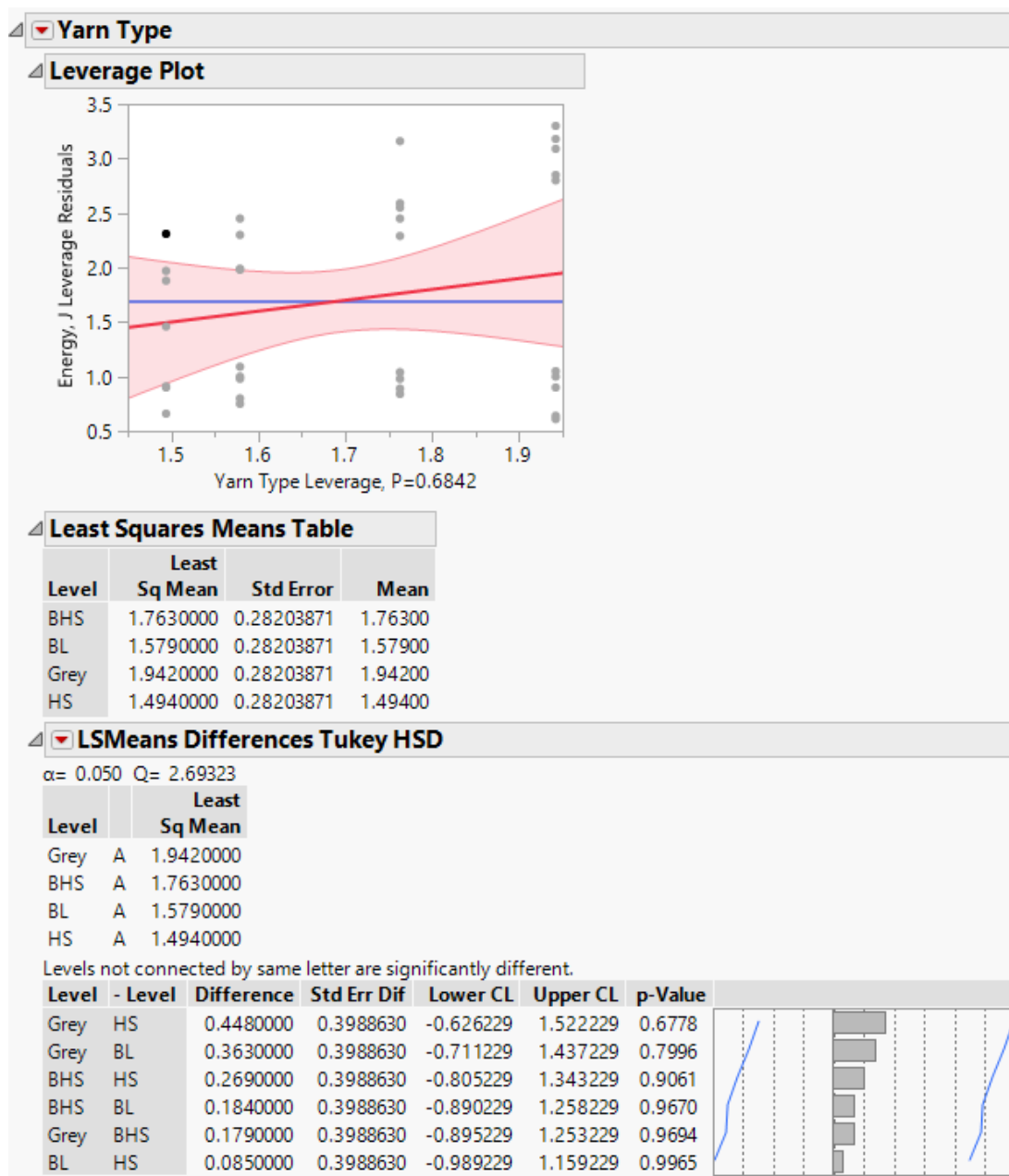


Figure 267. Tukey HSD- Charpy impact- Effect of X-yarn type on Impact Energy

Summary of Fit					
RSquare			0.102004		
RSquare Adj			0.027171		
Root Mean Square Error			0.136639		
Mean of Response			0.54325		
Observations (or Sum Wgts)			40		
Analysis of Variance					
Source	DF	Sum of Squares	Mean Square	F Ratio	
Model	3	0.07634750	0.025449	1.3631	
Error	36	0.67213000	0.018670		Prob > F
C. Total	39	0.74847750			0.2696
Parameter Estimates					
Effect Tests					
Source	Nparm	DF	Sum of Squares	F Ratio	Prob > F
Yarn Type	3	3	0.07634750	1.3631	0.2696

Table 86. ANOVA Results – Charpy impact- Effect of X-yarn type on Impact Energy

Normalized by Thickness

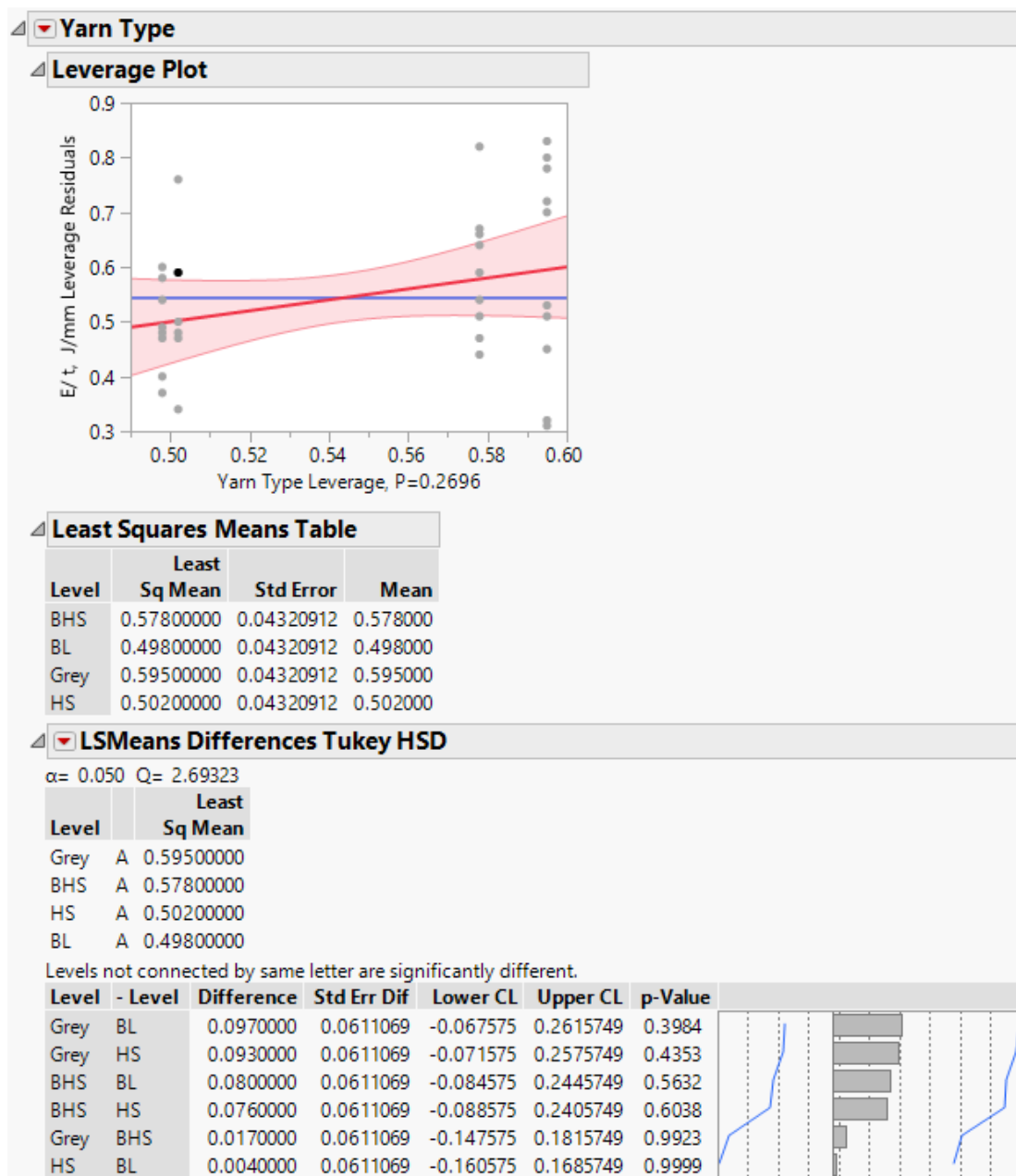


Figure 268. Tukey HSD- Charpy impact- Effect of X-yarn type on Impact Energy Normalized by Thickness

Summary of Fit					
RSquare			0.126527		
RSquare Adj			0.053737		
Root Mean Square Error			2.7133		
Mean of Response			11.84175		
Observations (or Sum Wgts)			40		
Analysis of Variance					
Source	DF	Sum of Squares	Mean Square	F Ratio	
Model	3	38.39105	12.7970	1.7383	
Error	36	265.03193	7.3620		Prob > F
C. Total	39	303.42298			0.1765
Parameter Estimates					
Effect Tests					
Source	Nparm	DF	Sum of Squares	F Ratio	Prob > F
Yarn Type	3	3	38.391047	1.7383	0.1765

Table 87. ANOVA Results – Charpy impact- Effect of X-yarn type on Impact Energy

Normalized by Preform Areal Density

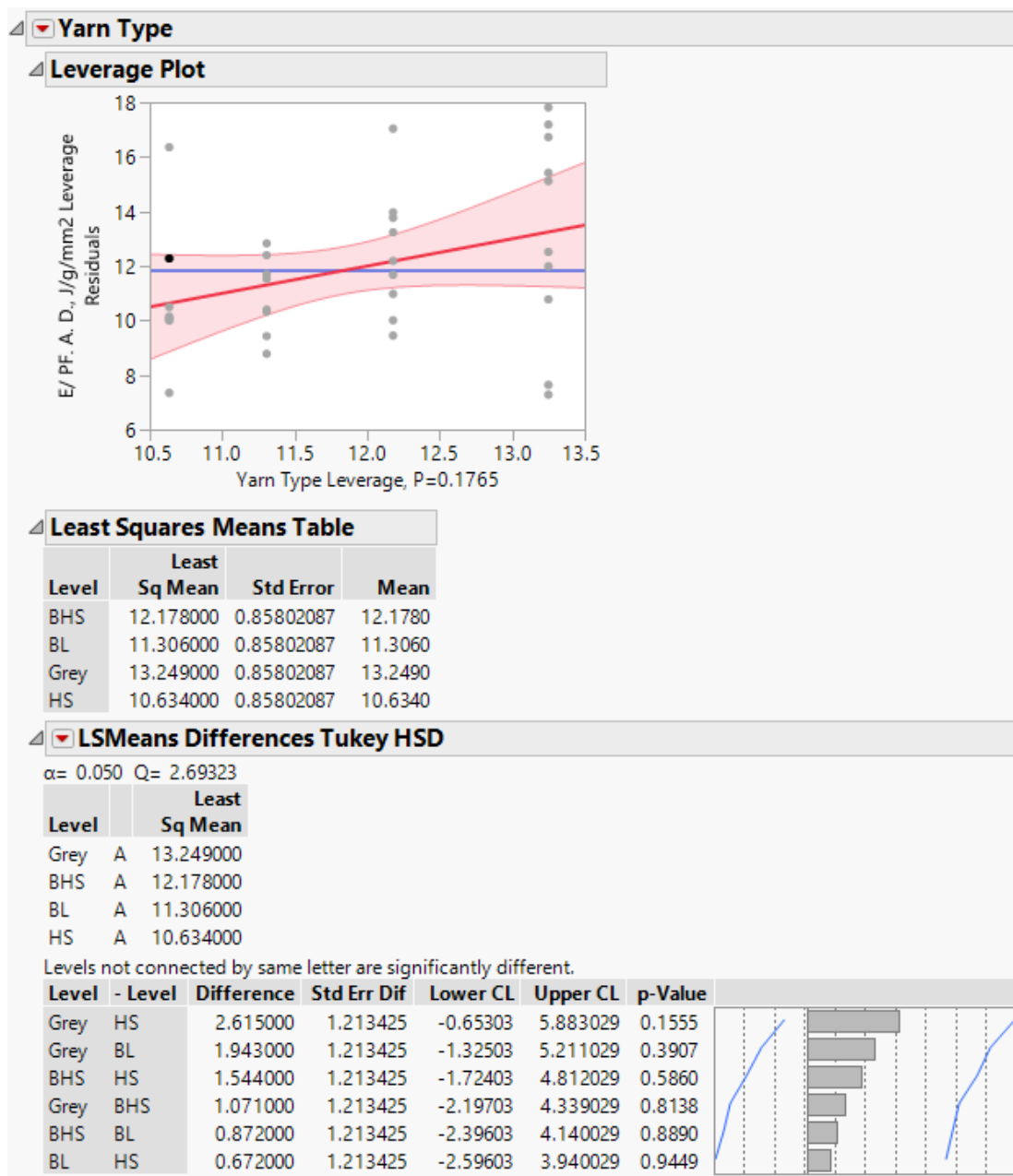


Figure 269. Tukey HSD- Charpy impact- Effect of X-yarn type on Impact Energy Normalized by Preform Areal Density

Summary of Fit					
RSquare			0.070542		
RSquare Adj			-0.00691		
Root Mean Square Error			0.920508		
Mean of Response			3.53475		
Observations (or Sum Wgts)			40		
Analysis of Variance					
Source	DF	Sum of Squares	Mean Square	F Ratio	
Model	3	2.315127	0.771709	0.9107	
Error	36	30.504070	0.847335		Prob > F
C. Total	39	32.819198			0.4454
Parameter Estimates					
Effect Tests					
Source	Nparm	DF	Sum of Squares	F Ratio	Prob > F
Yarn Type	3	3	2.3151275	0.9107	0.4454

Table 88. ANOVA Results – Charpy impact- Effect of X-yarn type on Impact Energy
Normalized by Composite Areal Density

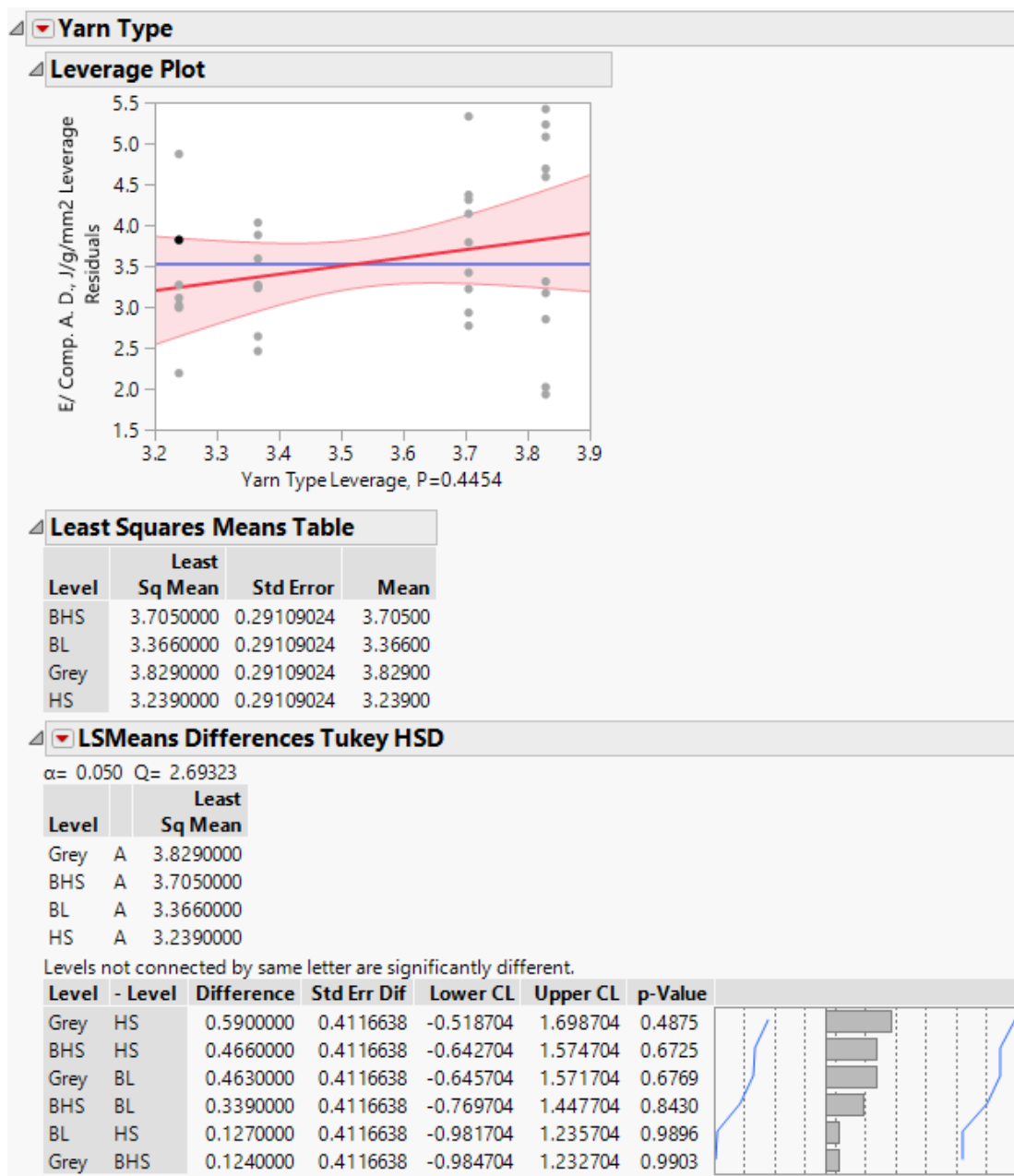


Figure 270. Tukey HSD- Charpy impact- Effect of X-yarn type on Impact Energy Normalized by Composite Areal Density

D.2.4. Compression Test

Summary of Fit					
RSquare			0.871296		
RSquare Adj			0.847164		
Root Mean Square Error			0.514891		
Mean of Response			11.272		
Observations (or Sum Wgts)			20		
Analysis of Variance					
Source	DF	Sum of Squares	Mean Square	F Ratio	
Model	3	28.715920	9.57197	36.1053	
Error	16	4.241800	0.26511		Prob > F
C. Total	19	32.957720			<.0001*
Parameter Estimates					
Effect Tests					
Source	Nparm	DF	Sum of Squares	F Ratio	Prob > F
Yarn Type	3	3	28.715920	36.1053	<.0001*

Table 89. ANOVA Results- Compression (Weft)- Effect of X-yarn type on Compression Load

Peak load

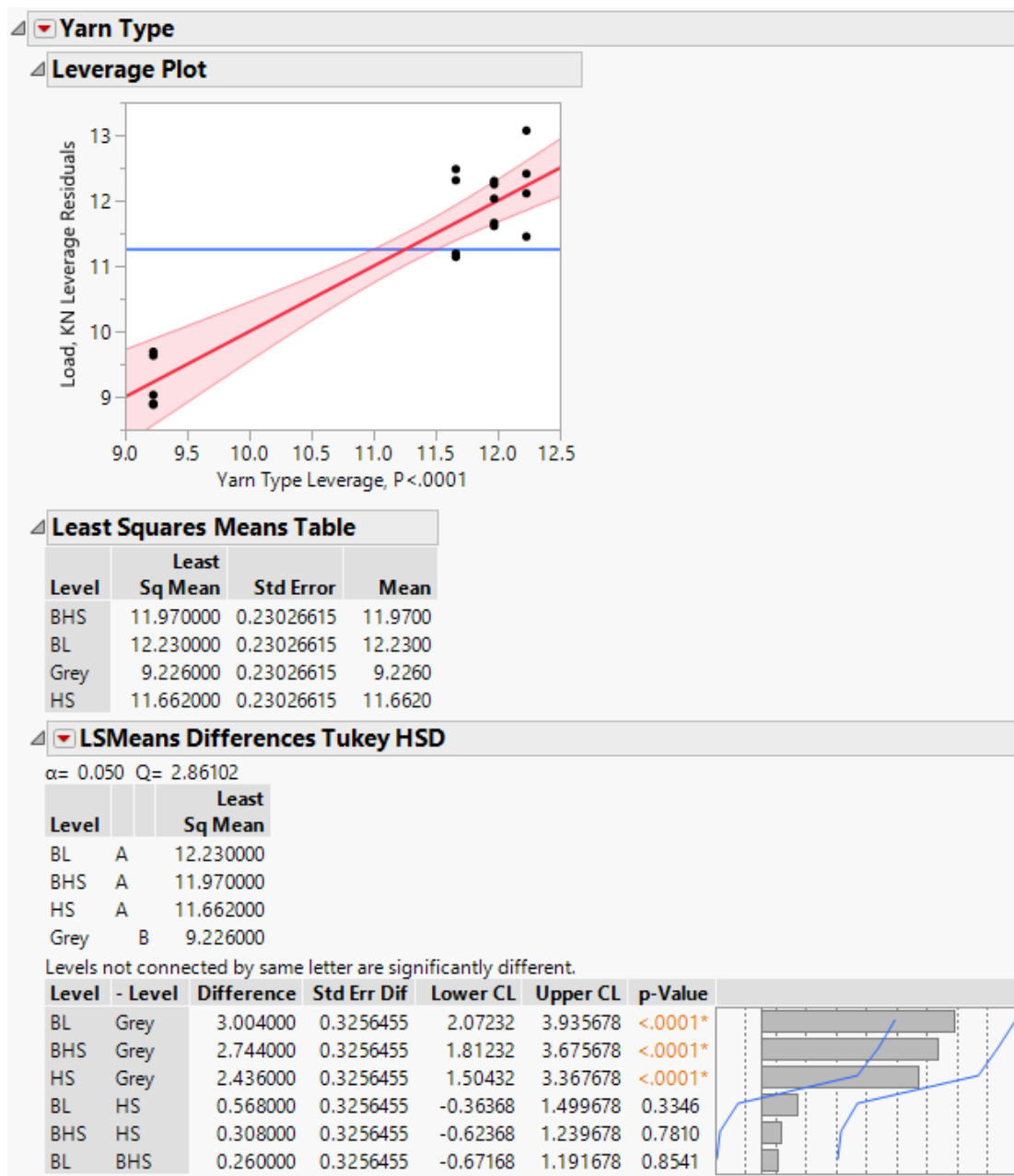


Figure 271. Tukey HSD- Compression (Weft)- Effect of X-yarn type on Compression Load

Summary of Fit					
RSquare			0.823532		
RSquare Adj			0.790444		
Root Mean Square Error			5.97382		
Mean of Response			109.911		
Observations (or Sum Wgts)			20		
Analysis of Variance					
Source	DF	Sum of Squares	Mean Square	F Ratio	
Model	3	2664.6451	888.215	24.8894	
Error	16	570.9844	35.687		Prob > F
C. Total	19	3235.6296			<.0001*
Parameter Estimates					
Effect Tests					
Source	Nparm	DF	Sum of Squares	F Ratio	Prob > F
Yarn Type	3	3	2664.6451	24.8894	<.0001*

Table 90. ANOVA Results- Compression (Weft)- Effect of X-yarn type on Peak stress

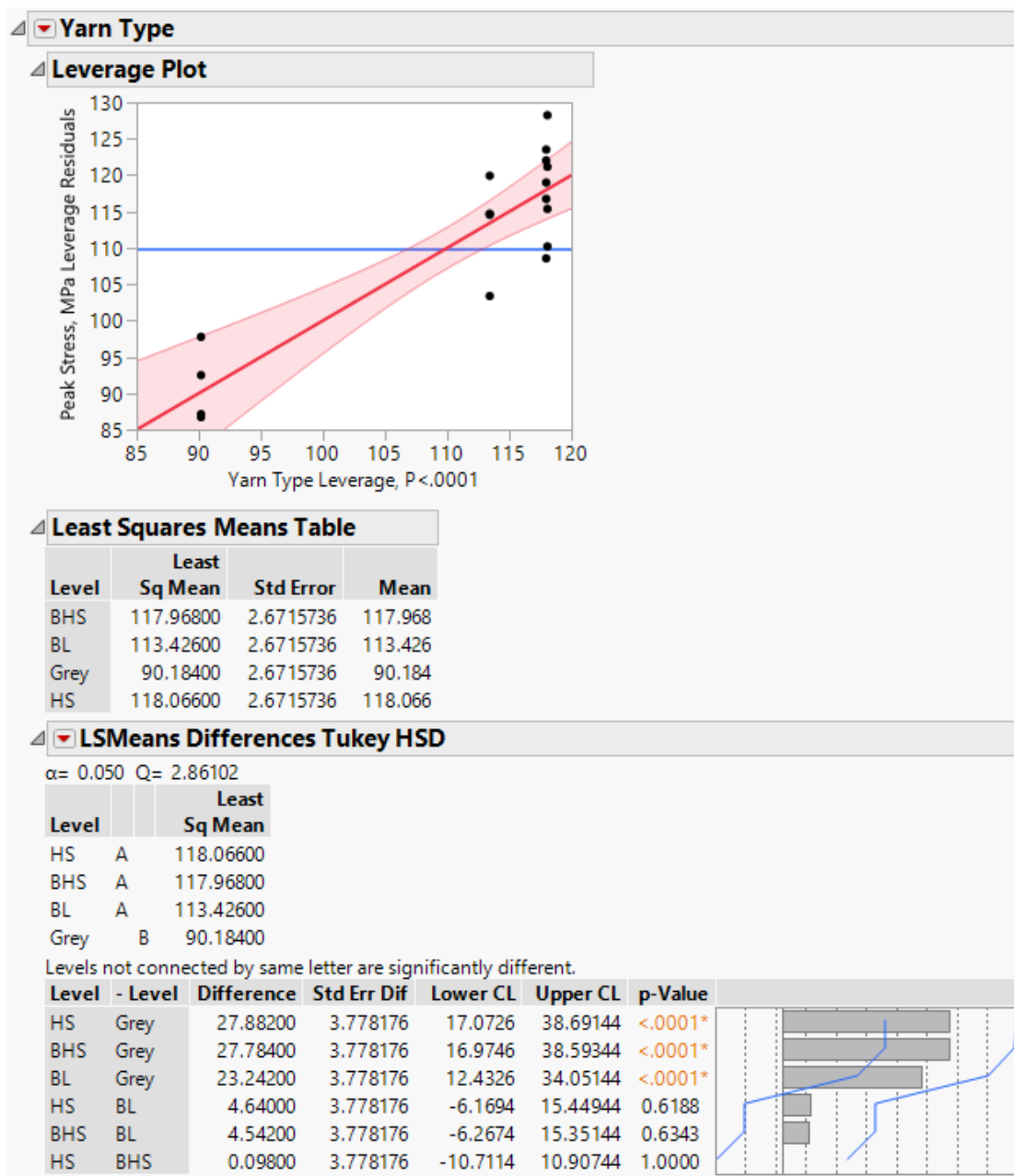


Figure 272. Tukey HSD- Compression (Weft)- Effect of X-yarn type on peak stress

Summary of Fit					
RSquare			0.857442		
RSquare Adj			0.830712		
Root Mean Square Error			2.729899		
Mean of Response			60.137		
Observations (or Sum Wgts)			20		
Analysis of Variance					
Source	DF	Sum of Squares	Mean Square	F Ratio	
Model	3	717.17506	239.058	32.0783	
Error	16	119.23756	7.452		Prob > F
C. Total	19	836.41262			<.0001*
Parameter Estimates					
Effect Tests					
Source	Nparm	DF	Sum of Squares	F Ratio	Prob > F
Yarn Type	3	3	717.17506	32.0783	<.0001*

Table 91. ANOVA Results- Compression (Weft)- Effect of X-yarn type Peak load Normalized
by Preform Areal Density

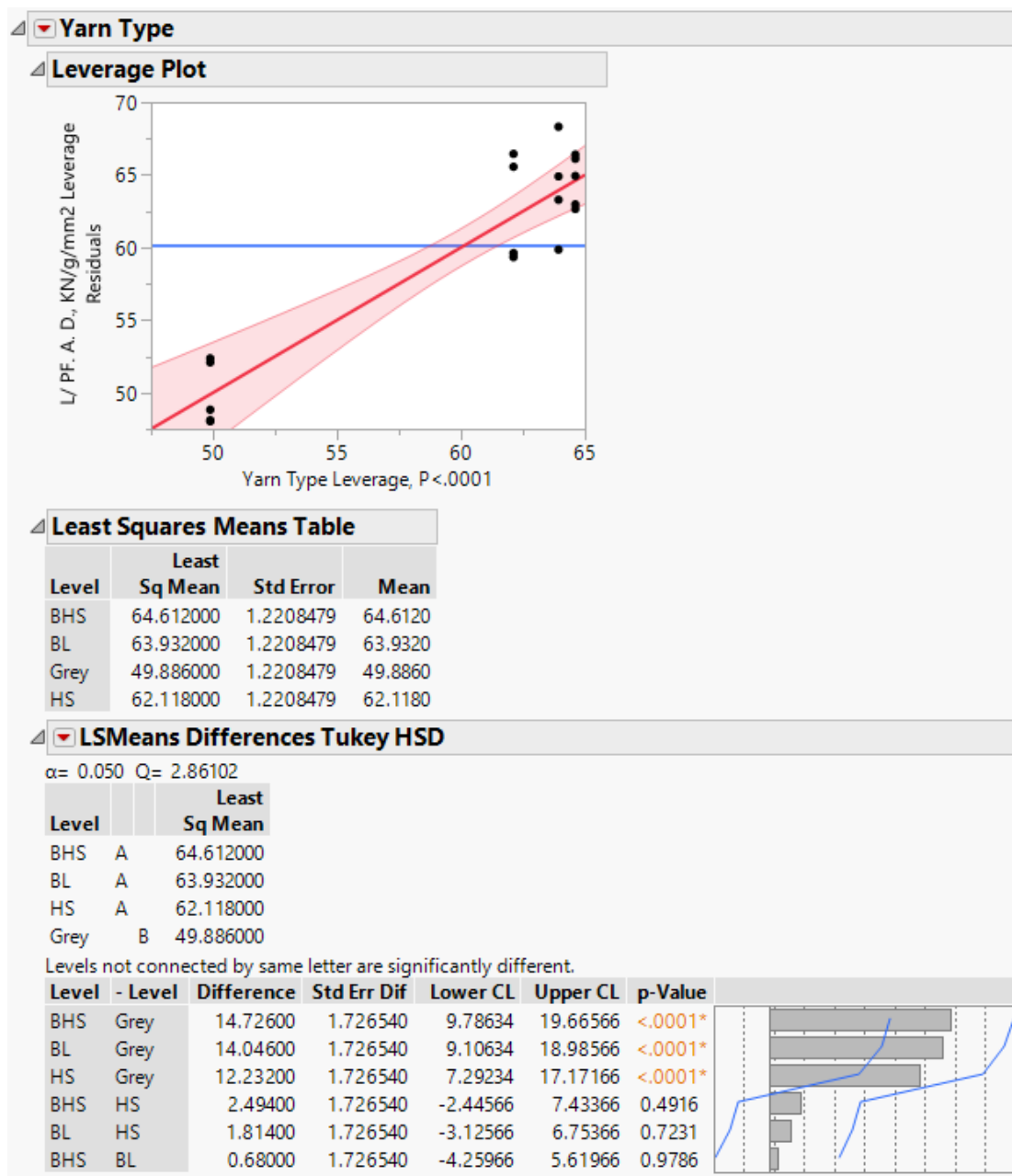


Figure 273. Tukey HSD- Compression (Weft)- Effect of X-yarn type on Compression Load
Normalized by Preform Areal Density

Summary of Fit					
RSquare				0.88029	
RSquare Adj				0.857844	
Root Mean Square Error				1.125143	
Mean of Response				23.3425	
Observations (or Sum Wgts)				20	
Analysis of Variance					
Source	DF	Sum of Squares	Mean Square	F Ratio	
Model	3	148.94642	49.6488	39.2187	
Error	16	20.25516	1.2659		Prob > F
C. Total	19	169.20158			<.0001*
Parameter Estimates					
Effect Tests					
Source	Nparm	DF	Sum of Squares	F Ratio	Prob > F
Yarn Type	3	3	148.94642	39.2187	<.0001*

Table 92. ANOVA Results- Compression (Weft)- Effect of X-yarn type Peak load Normalized
by Composite Areal Density

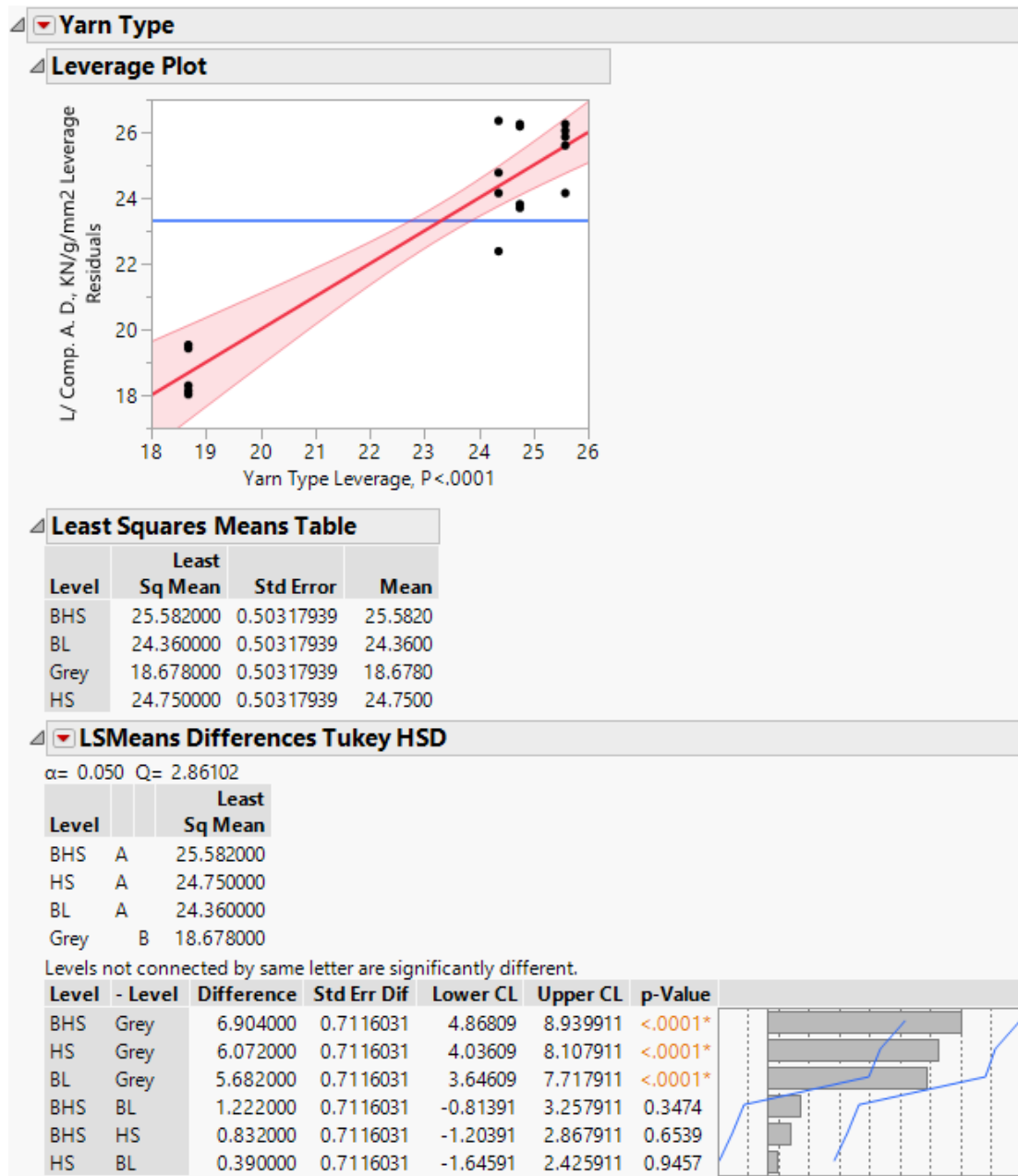


Figure 274. Tukey HSD- Compression (Weft)- Effect of X-yarn type on Compression Load

Normalized by Composite Areal Density